

MODELING AND CONTROL OF  
INTERLINE POWER FLOW CONTROLLER  
FOR POWER SYSTEM STABILITY  
ENHANCEMENT

ALIVELU MANGA PARIMI

DOCTOR OF PHILOSOPHY  
ELECTRICAL AND ELECTRONIC  
ENGINEERING

UNIVERSITI TEKNOLOGI PETRONAS

SEPTEMBER 2011



STATUS OF THESIS

Title of thesis

MODELING AND CONTROL OF INTERLINE POWER FLOW CONTROLLER FOR POWER SYSTEM STABILITY ENHANCEMENT

ALIVELU MANGA PARIMI

hereby allow my thesis to be placed at the Information Resource Center (IRC) of Universiti Teknologi PETRONAS (UTP) with the following conditions:

- 1. The thesis becomes the property of UTP
2. The IRC of UTP may make copies of the thesis for academic purposes only.
3. This thesis is classified as

Confidential

Non-confidential

If this thesis is confidential, please state the reason:

Blank lines for stating reasons if confidential.

The contents of the thesis will remain confidential for years.

Remarks on disclosure:

Blank lines for remarks on disclosure.

Signature of Author

Permanent address: D.No. 8-3-315/12/A, Plot No. 12 Maruthi Nagar, Yusufguda Hyderabad, Andhra Pradesh India-500055.

Date: 19/9/2011

Endorsed by Dr. Irraiyan Elamvazuthi Associate Professor Electrical & Electronics Engineering Department Universiti Teknologi PETRONAS Bandar Seri Iskandar, 31750 Tronoh Perak Darul Ridzuan, MALAYSIA. Tel: 05-366 7882 Fax: 05-365 5905

Name of Supervisor Assoc. Prof. Dr. Irraiyan Elamvazuthi

Date: 19/9/2011

UNIVERSITI TEKNOLOGI PETRONAS  
MODELING AND CONTROL OF INTERLINE POWER FLOW CONTROLLER  
FOR POWER SYSTEM STABILITY ENHANCEMENT

by

ALIVELU MANGA PARIMI

The undersigned certify that they have read, and recommend to the Postgraduate Studies Programme for acceptance of this thesis for the fulfilment of the requirements for the degree stated.

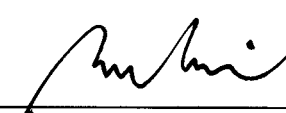
Signature:

  
Dr. Irraivan Elamvazuthi  
Associate Professor  
Electrical & Electronics Engineering Department  
Universiti Teknologi PETRONAS  
Bandar Seri Iskandar, 31750 Tronoh  
Perak Darul Ridzuan, MALAYSIA.  
Tel: 05-366 7882 Fax: 05-365 5905

Main Supervisor:

Assoc. Prof. Dr. Irraivan Elamvazuthi

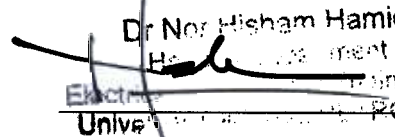
Signature:

  
Dr. Nordin Saad  
Lecturer  
Electrical & Electronics Engineering Program  
Universiti Teknologi PETRONAS  
31750 Tronoh,  
Perak Darul Ridzuan, MALAYSIA

Co-Supervisor:

Assoc. Prof. Dr. Nordin Saad

Signature:

  
Dr. Nor Hisham Hamid  
Head of Department  
Electrical & Electronics Engineering  
Universiti Teknologi PETRONAS

Head of Department:

Assoc. Prof. Nor Hisham Bn Hamid

Date:

19/9/2011

MODELING AND CONTROL OF INTERLINE POWER FLOW CONTROLLER  
FOR POWER SYSTEM STABILITY ENHANCEMENT

By

ALIVELU MANGA PARIMI

A Thesis

Submitted to the Postgraduate Studies Programme

as a Requirement for the Degree of

DOCTOR OF PHILOSOPHY

DEPARTMENT OF ELECTRICAL AND ELECTRONIC ENGINEERING

UNIVERSITI TEKNOLOGI PETRONAS

BANDAR SERI ISKANDAR,

PERAK, MALAYSIA

SEPTEMBER 2011

## DECLARATION OF THESIS

Title of thesis

MODELING AND CONTROL OF INTERLINE POWER FLOW  
CONTROLLER FOR POWER SYSTEM STABILITY  
ENHANCEMENT

I ALIVELU MANGA PARIMI

hereby declare that the thesis is based on my original work except for quotations and citations which have been duly acknowledged. I also declare that it has not been previously or concurrently submitted for any other degree at UTP or other institutions.

Witnessed by



Signature of Author

Permanent address:

D.No. 8-3-315/12/A, Plot No. 12

Maruthi Nagar, Yusufguda

Hyderabad, Andhra Pradesh

India-500055.

Date : 19/9/2011



Signature of Supervisor  
Dr. Irraivan Elamvazuthi  
Associate Professor  
Electrical & Electronics Engineering Department  
Universiti Teknologi PETRONAS  
Bandar Seri Iskandar, 31750 Tronoh  
Perak Darul Ridzuan, MALAYSIA.  
Tel: 05-360 7882 Fax: 05-365 5905

Name of Supervisor

Assoc. Prof. Dr. Irraivan Elamvazuthi

Date : 19/9/2011

*Dedicated to my family*

## ACKNOWLEDGEMENTS

I wish to express sincere gratitude and appreciation to my supervisor Dr. Irraivan Elamvazuthi for his constant support and guidance, consistent encouragement, fruitful comments and advice throughout my PhD program. I am greatly indebted to my advisor Dr. Nirod Chandra Sahoo, for his invaluable instructions and suggestions. His profound knowledge, generous support and guidance have benefited me in accomplishing this work successfully. I express my deepest appreciation and sincere thanks to him.

I would like to thank my Co. supervisor Dr. Nordin Saad for his instruction, guidance, interest and encouragement throughout my stay in UTP.

I would also like to thank particularly Assoc. Prof. Dr. Mohd Noh Bin Karsiti, the Dean of Center of Graduate Studies and Assoc. Prof. Nor Hisham Bin Hamid, the Head of the Electrical and Electronic Department for their support and consideration at crucial time during my studies.

I would like to extend my gratitude to the supporting staff of the Electrical and Electronic Department particularly Mr. Musa B Mohd Yusuf and Mr. Mohd Yasin B Baharudin and Ms. Kamaliah Binti Mohd belonging to the Post Graduate studies Department for their kindness and helping nature.

I wish to thank Prof. K. A. Gopala Rao for his valuable discussion and advices. I would thank my husband, my parents and my son for their affection and encouragement from a distance.

## ABSTRACT

Mitigation of power system oscillations is the problem of concern in the power industry as these oscillations, when exhibiting poor damping; affect the transmission line power transfer capability and power system stability. These oscillations greatly restrict power system operations and, in some cases, can also lead to widespread system disturbances. In this context, the Flexible AC Transmission System (FACTS) device, Interline Power Flow Controller (IPFC) employed to improve the transmission capability can be additionally utilized for damping control of power system oscillations.

IPFC based damping controller design for power system stability requires proper and adequate mathematical representation of power system incorporating the FACTS device. This thesis reports the investigation on the development of steady state model, the dynamic nonlinear mathematical model of the power system installed with the IPFC for stability studies and the linearized extended Phillips Heffron model for the design of control techniques to enhance the damping of the lightly damped oscillations modes.

In this context, the mathematical models of the single machine infinite bus (SMIB) power system and multi-machine power system incorporated with IPFC are established. The controllers for the IPFC are designed for enhancing the power system stability. The eigenvalue analysis and nonlinear simulation studies of the investigations conducted on the SMIB and Multi-machine power systems installed with IPFC demonstrate that the control designs are effective in damping the power system oscillations. The results presented in this thesis would provide useful information to electric power utilities engaged in scheduling and operating with the FACTS device, IPFC.

## ABSTRAK

Pengurangan ayunan sistem kuasa adalah permasalahan yang diberi perhatian dalam industri kuasa kerana ayunan ini, disamping menunjukkan redaman kurang baik, saluran penghantaran mempengaruhi kemampuan pemindahan dan kestabilan system. Ayunan ini menyekat operasi sistem dan dalam beberapa kes, boleh menyebabkan penyebaran gangguan pada sistem. Dalam konteks ini, 'peranti sistem penghantaran AU fleksibel' (FACTS) 'pengawal aliran kuasa antara-talian' (IPFC) yang berfungsi untuk meningkatkan kemampuan penghantaran dapat digunakan untuk meredamkan ayunan sistem kuasa elektrik.

IPFC berasaskan rekabentuk kawalan redaman untuk menstabilkan sistem kuasa memerlukan persamaan matematik yang tepat dan mencukupi untuk mewakili sistem kuasa yang menggabungkan peranti FACTS. Tesis ini melaporkan hasil kajian berkaitan pembangunan model keadaan mantap dan model matematik dinamik tak lurus dari sistem kuasa yang dipasang dengan IPFC untuk kajian kestabilan dan meluruskan model Phillips Heffron untuk merekabentuk teknik kawalan bagi meningkatkan redaman mod ayunan teredam ringan.

Dalam konteks ini, model matematik dari bas mesin tunggal tak terbatas (SMIB) sistem sistem kuasa elektrik dan berbilang-mesin digabungkan dengan IPFC. Pengawal untuk IPFC direka untuk meningkatkan kestabilan sistem kuasa elektrik. Analisis nilai eigen dan kajian simulasi tak lurus dari penyiasatan yang dilakukan pada SMIB dan sistem kuasa MM yang dipasang dengan IPFC menunjukkan bahawa reka bentuk kawalan adalah sangat berkesan dalam mengayunkan sistem tenaga redaman. Penemuan yang dipersembahkan dalam tesis ini dapat memberi maklumat yang berguna untuk pengusaha utiliti kuasa elektrik dalam penjadualan dan pengoperasian sistem menggunakan peranti FACTS, IPFC.

In compliance with the terms of the Copyright Act 1987 and the IP Policy of the university, the copyright of this thesis has been reassigned by the author to the legal entity of the university,

Institute of Technology PETRONAS Sdn Bhd.

Due acknowledgement shall always be made of the use of any material contained in, or derived from, this thesis.

© Aivelu Manga Parimi, 2011

Institute of Technology PETRONAS Sdn Bhd

All rights reserved.

## TABLE OF CONTENTS

Status of Thesis .....	(i)
Approval Page.....	(ii)
Title Page .....	(iii)
Declaration .....	(iv)
Dedication.....	(v)
Acknowledgement.....	(vi)
Abstract .....	(vii)
Abstrak.....	(viii)
Copyright Page.....	(ix)
Table of Contents .....	(x)
List of Tables .....	(xiii)
List of Figures .....	(xv)
Nomenclature .....	(xxi)
Abbreviation .....	(xxxii)

## CHAPTER

1. INTRODUCTION.....	1
1.1 Power System Stability.....	2
1.2 FACTS Devices.....	5
1.3 Interline Power Flow Controller (IPFC) .....	7
1.4 Research Motivation.....	9
1.5 Research Objectives.....	11
1.6 Contributions of Research.....	14
1.7 Thesis Outline.....	15
2. POWER SYSTEM STABILITY: AN OVERVIEW.....	17
2.1 Introduction.....	17
2.2 Power System Oscillations Stability.....	17
2.2.1 Static Var Compensator (SVC) .....	20
2.2.2 Thyristor Controlled Series Capacitor (TCSC) .....	22
2.2.3 Thyristor Controlled Phase Shifter (TCPS) .....	23

2.2.4	Static Synchronous Compensator (STATCOM) .....	25
2.2.5	Static Synchronous Series Compensator (SSSC) .....	26
2.2.6	Unified Power Flow Controller (UPFC) .....	28
2.3	Interline Power Flow Controller.....	31
2.4	Discussion.....	33
2.5	Summary.....	34
3.	MODELING OF INTERLINE POWER FLOW CONTROLLER.....	35
3.1	Introduction.....	35
3.2	Steady State Model.....	35
3.2.1	Load Flow Equations.....	38
3.2.2	Newton-Raphson Method.....	41
3.2.3	The Power Flow Equations Including IPFC.....	44
3.2.4	Newton-Raphson Method for IPFC Buses.....	51
3.2.5	Power Flow Solution of Power System Including IPFC.....	52
3.3	Dynamic Model of IPFC.....	57
3.4	Results.....	66
3.5	Summary.....	68
4.	SINGLE MACHINE INFINITE BUS SYSTEM WITH IPFC.....	69
4.1	Introduction.....	69
4.2	Dynamic Model of SMIB Power System With IPFC.....	70
4.2.1	The Nonlinear Dynamic Model of SMIB Power System With IPFC.....	71
4.2.2	Relationship Between Machine And Synchronous Frame of Reference.....	72
4.2.3	Transforming the Network Equations in $d - q$ Axes Frame..	73
4.3	Linearized Model of Power System.....	75
4.4	State Space Model.....	76
4.5	Modal Analysis of the Power System.....	80
4.6	Power System Stabilizer (PSS).....	84
4.7	Controllers of IPFC.....	87
4.7.1	Power Flow Controller.....	87
4.7.2	DC Voltage Regulator.....	88
4.7.3	IPFC Damping Controller.....	89
4.8	Case Study: SMIB Power System With IPFC.....	91
4.8.1	Disturbance: Step Change in Mechanical Power.....	105
4.8.2	Disturbance: Three Phase Fault.....	109
4.8.3	Disturbance: Change in Power Flow Reference.....	116
4.9	Summary.....	120
5.	MULTIMACHINE POWER SYSTEM.....	123
5.1	Introduction.....	123
5.2	Modeling of Multi-Machine Power System.....	123
5.2.1	Synchronous Generators.....	124
5.2.2	Transmission Network and Loads.....	126

5.2.3	Generator Network Interface.....	129
5.2.4	Method 1 of Transforming Network Equations To Individual Machine Frame.....	130
5.2.4.1	Initial conditions for the dynamic system.....	133
5.2.5	Method 2 of Transforming Network Equations To Individual Machine Frame.....	136
5.2.5.1	Initial conditions for the dynamic system.....	140
5.3	Linearized System of Multi-Machine Power System.....	141
5.4	Case Study: Multi-Machine Power System.....	147
5.5	Summary.....	165
6.	MULTIMACHINE POWER SYSTEM WITH IPFC.....	167
6.1	Introduction.....	167
6.2	Modeling of Multi-Machine Power System Incorporating with IPFC.....	167
6.3	Nonlinear Model of Multi-Machine Power System Installed with IPFC.....	171
6.4	Linearized Phillips-Heffron Model of a Multi-Machine Power System Including IPFC in State Space Form.....	174
6.5	Case Study: Multi-Machine Power System With IPFC.....	181
6.5.1	Disturbance: Step Change in Mechanical Power.....	189
6.5.2	Disturbance: Three Phase Fault.....	194
6.5.3	Disturbance: Change in Power Flow Reference.....	199
6.6	Summary.....	202
7.	CONCLUSION.....	203
7.1	Conclusion.....	203
7.2	Achievements of Research Objectives.....	204
7.3	Contributions of Research.....	206
7.4	Suggestions for Future Work.....	207
	REFERENCES.....	208
	LIST OF PUBLICATIONS.....	219
	APPENDIX A.....	220
	Jacobian Terms of the Power Flow With IPFC.....	221
	APPENDIX B.....	225
	1) Phillips-Heffron Model K Constants of a Single Machine Infinite-Bus Power System Equipped With IPFC.....	226
	2) Multimodal Decomposition.....	231
	APPENDIX C.....	234
	Nonlinear Simulation Of WSCC System Using MATLAB/SIMULINK...	235
	APPENDIX D.....	239
	Nonlinear Simulation Of Wscc System Incorporated With IPFC Using MATLAB/SIMULINK.....	240

## LIST OF TABLES

Table 3.1: Three bus system data.....	67
Table 3.2: Load flow results of three bus system.....	67
Table 3.3: Initial values of the control parameters of IPFC.....	68
Table 4.1: SMIB power system data.....	92
Table 4.2: Load flow results of SMIB power system with IPFC.....	92
Table 4.3: $K$ constants at the operating point of $P_e = 0.8$ p.u. ....	92
Table 4.4: Eigenvalues of the linearized SMIB with IPFC at operating point $P_e = 0.8$ p.u. ....	93
Table 4.5: Eigenvalues of the linearized SMIB with IPFC and controllers at operating point $P_e = 0.8$ p.u.....	94
Table 4.6: Eigenvalues of the system computed at different operating points .....	95
Table 4.7: Controllability indices with different IPFC controllable parameters at operating point $P_e = 0.8$ p.u. ....	97
Table 4.8: Controllability indices with different IPFC controllable parameters at operating point $P_e = 1.2$ p.u. ....	97
Table 4.9: Parameters of the damping controllers designed at operating condition $P_e = 0.8$ p.u. ....	98
Table 4.10: Parameters of the damping controllers designed at operating condition $P_e = 1.2$ p.u. ....	98
Table 4.11: Eigenvalues of the system computed at $P_e = 0.8$ p.u. using the damping controllers designed at $P_e = 0.8$ p.u.....	98
Table 4.12: Eigenvalues of the system computed at $P_e = 1.2$ p.u. using the damping controllers designed at $P_e = 1.2$ p.u.....	99
Table 4.13: Oscillation mode calculation with varying operating conditions with the damping controller $m_1$ designed at operating point $P_e = 0.8$ p.u.....	99

Table 4.14:	Oscillation mode calculation with varying operating conditions with the damping controller $m_1$ designed at operating point $P_e = 1.2$ p.u....	100
Table 4.15:	Eigenvalues of the SMIB power system incorporated with IPFC, with PSS, PI power flow controller, DC voltage regulator and damping controller with speed as input .....	101
Table 5.1:	WSCC power system parameters.....	147
Table 5.2:	Generator and exciter data .....	148
Table 5.3:	The load flow results of the WSCC 3-machine 9-bus system .....	148
Table 5.4:	The power flows in each transmission lines .....	148
Table 5.5:	Initial conditions computed using the first method of transformation..	149
Table 5.6:	Initial conditions computed using the second method of transformation .....	149
Table 5.7:	Eigenvalues of WSCC power system .....	153
Table 5.8:	The normalized participation factors of all the eigenvalues .....	155
Table 5.9:	Dominant states of the eigenvalues.....	156
Table 5.10:	Parameters of the PSS's .....	156
Table 5.11:	Eigenvalues of the power system with PSS's.....	156
Table 6.1:	The load flow results of the WSCC .....	182
Table 6.2:	Initial conditions computed.....	183
Table 6.3:	Eigenvalues of WSCC power system with IPFC.....	185
Table 6.4:	The participation factors of the eigenvalues .....	185
Table 6.5:	Eigenvalues with PSS .....	185
Table 6.6:	Controllability indices with different IPFC controllable parameters....	186
Table 6.7:	Eigenvalues of the linearized WSCC with IPFC and controllers .....	188

## LIST OF FIGURES

Figure 1.1: Schematic diagram of IPFC .....	9
Figure 2.1: Power system stabilizer.....	18
Figure 2.2: SVC employing thyristor switched capacitors and thyristor controlled reactors.....	21
Figure 2.3: TCSC with a thyristor-controlled reactor in parallel with a series capacitor.....	22
Figure 2.4: Schematic diagram of TCPS.....	24
Figure 2.5: Schematic diagram of STATCOM .....	25
Figure 2.6: Schematic diagram of SSSC .....	27
Figure 2.7: Schematic diagram of UPFC .....	29
Figure 3.1: IPFC employing $n$ converters .....	36
Figure 3.2: Basic two-converter IPFC.....	36
Figure 3.3: The phasor diagram for transmission line 1.....	37
Figure 3.4: Power balance at bus $i$ for active and reactive power.....	39
Figure 3.5: Equivalent circuit of IPFC .....	44
Figure 3.6: Flowchart of the power flow solution.....	56
Figure 3.7: Structure of IPFC .....	57
Figure 3.8: Detailed three phase diagram of IPFC .....	58
Figure 3.9: a)Equivalent circuit of phase ‘a’ of coupling transformer and VSC-1 b) Dynamics of DC link capacitor .....	59
Figure 3.10: Three bus system with IPFC .....	66
Figure 4.1: SMIB installed with IPFC.....	70
Figure 4.2: Relationship between machine and synchronous frame of reference.....	73
Figure 4.3: Block diagram of a SMIB .....	78

Figure 4.4: Phillips-Heffron model of SMIB system installed with IPFC .....	80
Figure 4.5: Excitation system with AVR and PSS .....	84
Figure 4.6: Structure of the power flow controller .....	88
Figure 4.7: Structure of the DC voltage regulator .....	88
Figure 4.8: Structure of IPFC based damping controller .....	89
Figure 4.9: Block diagram of the system relating electrical power $\Delta P_e$ and $\Delta U$ .....	91
Figure 4.10: IPFC based damping controller .....	95
Figure 4.11: Damping ratio versus operating condition. ....	96
Figure 4.12: SMIB power system with IPFC and its controllers .....	101
Figure 4.13: Simulink model representing rotor angle and speed .....	102
Figure 4.14: Simulation model representing internal voltage and field voltage .....	103
Figure 4.15: Simulation model representing the DC link capacitor voltage .....	103
Figure 4.16: Simulation model for calculation of electrical power and terminal voltage .....	104
Figure 4.17: Simulation model for calculating the transmission line currents .....	104
Figure 4.18: Rotor angle response with the damping controllers $m_1$ and $m_2$ and PSS with step change in mechanical power .....	106
Figure 4.19: Rotor angle response with the damping controllers $\theta_1$ and $\theta_2$ and PSS with step change in mechanical power .....	106
Figure 4.20: Active power flow response in line 1 in the presence of various damping controllers .....	107
Figure 4.21: DC voltage across the capacitor response in the presence of various damping controllers .....	107
Figure 4.22: Rotor angle response with the damping controller $m_1$ designed at two operating conditions .....	108
Figure 4.23: Electrical power response with the damping controller $m_1$ at various operating conditions .....	108
Figure 4.24: SMIB power system with fault .....	109
Figure 4.25: Electrical power response due to three phase fault .....	110
Figure 4.26: Rotor angle response due to three phase fault .....	111

Figure 4.27: Terminal voltage response due to three phase fault.....	111
Figure 4.28: Rotor speed response due to three phase fault .....	112
Figure 4.29: Real power flow response in line 1 due to three phase fault .....	112
Figure 4.30: Real power flow response in line 2 due to three phase fault .....	113
Figure 4.31: Reactive power flow response in line 1 due to three phase fault.....	113
Figure 4.32: DC capacitor voltage response due to three phase fault .....	114
Figure 4.33: Electrical power response due to three phase fault at varying operating conditions.....	114
Figure 4.34: Damping controller with power deviation as input.....	115
Figure 4.35: Structure of the damping controller with power deviation as input.....	115
Figure 4.36: Reactive power flow controller.....	117
Figure 4.37: Block diagram of SMIB with IPFC and its controllers.....	117
Figure 4.38: Response of the real power flow in transmission line 1 with step change in power reference .....	118
Figure 4.39: Response of the real power flow in transmission line 2 with step change in power reference .....	118
Figure 4.40: Response of the reactive power flow in transmission line 1 with step change in power reference.....	119
Figure 4.41: Response of the DC capacitor voltage with step change in power reference.....	119
Figure 4.42: Response of the rotor angle with step change in power reference.....	120
Figure 5.1: The $i^{th}$ machine in a multi-machine power system network.....	125
Figure 5.2: Lumped parameter $\pi$ equivalent transmission line.....	126
Figure 5.3: Interconnected network of synchronous machines and the loads.....	127
Figure 5.4: Multi-machine generator network interface representation.....	130
Figure 5.5: Transformation for interfacing network reference with machine reference-method 1 .....	131
Figure 5.6: Phasor diagram of stator algebraic variables for computing the rotor angle $\delta_i$ method-1.....	135
Figure 5.7: Transformation for interfacing network reference with machine reference-method 2 .....	137

Figure 5.8: Phasor diagram of stator algebraic variables for computing the rotor angle $\delta_i$ method-2.....	140
Figure 5.9: Block diagram of $i^{\text{th}}$ machine in linearized multi-machine power system .....	146
Figure 5.10: 3-machine 9-bus power system.....	147
Figure 5.11: The reduced power system network .....	151
Figure 5.12: Responses of relative angle and speed during steady state operation...	158
Figure 5.13: The power system network during fault condition. ....	159
Figure 5.14: The reduced power system network during fault condition.....	159
Figure 5.15: The power system network after fault clearance with transmission line 5-7 removed. ....	160
Figure 5.16: Relative angle $\delta_{12}$ response with and without PSSs .....	160
Figure 5.17: Relative angle $\delta_{13}$ response with and without PSSs .....	161
Figure 5.18: Generated power response of each machine with PSSs.....	161
Figure 5.19: Relative angle $\omega_{12}$ response with and without PSSs .....	162
Figure 5.20: Relative angle $\omega_{13}$ response with and without PSSs .....	162
Figure 5.21: Responses of relative angles when three phase fault occurs and line is opened after the clearance of fault .....	163
Figure 5.22: Responses of relative angles with change in mechanical input at machine 1 .....	163
Figure 5.23: Responses of relative angles due to line switching in line 8-9 .....	164
Figure 5.24: Responses of terminal voltages due to line switching in line 8-9.....	165
Figure 6.1: A $n$ -machine power system installed with IPFC .....	168
Figure 6.2: Equivalent model of IPFC installed in $n$ -machine power system .....	168
Figure 6.3: WSCC system with IPFC .....	182
Figure 6.4: Reduced system containing the generator and IPFC buses .....	184
Figure 6.5: POD controller of IPFC .....	187
Figure 6.6: Multi-machine system with IPFC and its controllers .....	187
Figure 6.7: Generated power response at machine 1 with mechanical input disturbance .....	190

Figure 6.8: Generated power response at machine 2 with mechanical input disturbance .....	190
Figure 6.9: Real power flow response in IPFC branch 5 – 7 with mechanical input disturbance.....	191
Figure 6.10: Real power flow response in IPFC branch 8 – 7 with mechanical input disturbance.....	191
Figure 6.11: Relative rotor angle $\delta_{12}$ response with mechanical input disturbance .....	192
Figure 6.12: Relative rotor angle $\delta_{13}$ response with mechanical input disturbance .....	192
Figure 6.13: Relative rotor angle $\omega_{13}$ response with mechanical input disturbance .....	193
Figure 6.14: Relative rotor angle $\omega_{12}$ response with mechanical input disturbance .....	193
Figure 6.15: Real power flow response in IPFC branch 5 – 7 with three phase fault .....	195
Figure 6.16: Real power flow response in IPFC branch 8 – 7 with three phase fault .....	196
Figure 6.17: Relative rotor angle $\delta_{21}$ response with three phase fault .....	196
Figure 6.18: Relative rotor angle $\delta_{31}$ response with three phase fault .....	197
Figure 6.19: Electrical power generated response with three phase fault .....	197
Figure 6.20: DC capacitor voltage response due to three phase fault .....	198
Figure 6.21: Relative rotor angle $\omega_{12}$ response with three phase fault .....	198
Figure 6.22: Real power flow response in IPFC branch 5 – 7 with change in power reference.....	199
Figure 6.23: Reactive power flow response in IPFC branch 5 – 7 with change in power reference.....	200
Figure 6.24: Real power flow response in IPFC branch 8 – 7 with change in power reference.....	200
Figure 6.25: Relative rotor angle $\delta_{21}$ response with change in power reference.....	201
Figure 6.26: Relative rotor angle $\delta_{31}$ response with change in power reference.....	201

Figure B.1: The power system installed with IPFC based damping controller .....	233
Figure C.1: Simulink model of multi-machine power system representing the machine equations and stator algebraic equations along with the PSSs .....	235
Figure C.2: Subsystem 1 .....	236
Figure C.3: Subsystem 4 .....	236
Figure C.4: Subsystem 7 .....	236
Figure C.5: Simulink model of multi-machine power system for calculating the $d - q$ axes currents .....	237
Figure C.6: Simulink model of multi-machine power system for calculating the angles from the admittance matrix.....	238
Figure D.1: Simulink model of multi-machine power system with IPFC representing the machine equations and stator algebraic equations along with the PSSs .....	240
Figure D.2: Subsystem 1 .....	241
Figure D.3: Subsystem 4 .....	241
Figure D.4: Subsystem 7 .....	241
Figure D.5: Simulink model of multi-machine power system with IPFC for calculating the $d - q$ axes currents.....	242
Figure D.6: Simulink model of multi-machine power system with IPFC for calculating the angles from the admittance matrix .....	243
Figure D.7: Simulink model of multi-machine power system with IPFC for calculating the currents in IPFC branches .....	244
Figure D.8: Simulink model of multi-machine power system with IPFC for calculating the voltage across the DC link.....	245

## NOMENCLATURE

$A, B, C$	State, control and output matrices
$C_{dc}$	DC capacitor
$D$	Damping coefficient
$D_i$	$i^{th}$ -machine damping coefficient
$D - Q$	Synchronous network rotating reference frame
$d - q$	Synchronous machine rotating reference frame
$E_{fd}$	Generator field voltage in p.u.
$E_{fdi}$	$i^{th}$ -generator field voltage
$E'_q$	Generator internal voltage in p.u.
$E'_{qi}$	$i^{th}$ -machine internal quadrature-axis voltage
$\mathbf{F}$	Represents a set of $n$ nonlinear equations
$\mathbf{F}_1$	Mismatch vector of the active and reactive power flows of the IPFC buses and the power exchanged between the two VSCs
$\bar{\mathbf{F}}$	Mismatch vector of the system with IPFC
$G_c(s)$	Transfer function of IPFC damping controller
$G_s(s)$	Transfer function of between $\Delta P_e$ and $\Delta U$
$g_{Li}, b_{Li}$	Load conductance and susceptance at bus $i$
$g_{ii}, b_{ii}$	Self conductance and susceptance of bus $i$

$g_{in}, b_{in}, n = j, k$	Conductance and susceptance between bus $i$ and $n$
$g_{nn}, b_{nn}, n = j, k$	Self conductance and susceptance of bus $n$
$H_i$	$i^{\text{th}}$ – machine inertia constant in p.u. ( $M_i = 2H_i$ )
$I_D, I_Q$	$D$ and $Q$ axis components of current
$I_{Di}, I_{Qi} \quad i = 1, 2, \dots, n$	$D - Q$ axis components of generator current $\bar{I}_{Gi}$
$I_{2D}, I_{2Q}$	$D$ and $Q$ axis components of current in line 2 of IPFC branch
$I_d, I_q$	$d$ and $q$ axis components of current
$I_{di}, I_{qi}$	$d - q$ axis components of generator current $I_i$
$I_{d0}, I_{q0}$	Initial values of $I_{di}, I_{qi}$
$I_{dt}, I_{qt}$	$d$ and $q$ axis components of stator current in p.u.
$I_1, (I_2)$	Magnitude of current $\bar{I}_1, (\bar{I}_2)$
$\bar{I}$	Vector of injected currents at each bus in multi-machine system
$\bar{I}_G$	Vector of generator currents in multi-machine system in $D - Q$ axis frame
$\bar{I}_L$	Vector of load currents in multi-machine system in $D - Q$ axis frame
$\bar{I}_i$	Current at bus $i$
$\bar{I}_t$	Current flowing at generator bus in p.u. in $D - Q$ axis
$\bar{I}_{ij}, \bar{I}_{ik}$	IPFC branch currents of branch $i - j$ and $i - k$ leaving bus $i$
$\bar{I}_{ji}, \bar{I}_{ki}$	IPFC branch currents of branch $j - i$ and $k - i$ leaving bus $j$ and $k$ respectively

$\bar{I}_1, \bar{I}_2$	Current flowing through IPFC branches
$I_{ni}^{max} \quad n = j, k$	Current rating of the series converters of IPFC
$i, \quad j, \quad k$	Buses in power network
$it$	Iteration count
$i_{dc}$	Current flowing through the DC capacitor
$i_{1a}, i_{1b}, i_{1c}$	Phase currents of line 1 of IPFC branches
$i_{1dc}, i_{2dc}$	DC currents in VSC 1 and 2
$i_{1u}, i_{2u}, \quad (u = a, b, c)$	Currents flowing in each phase in line 1 and 2 respectively
$i_{2a}, i_{2b}, i_{2c}$	Phase currents of line 2 of IPFC branches
$i_{1d}, i_{1q}$	$d$ , and $q$ axis currents in line 1 of the IPFC branches
$i_{2d}, i_{2q}$	$d$ , and $q$ axis currents in line 2 of the IPFC branches
<b>J</b>	Jacobian matrix of the power system without IPFC
<b>J<sub>1</sub></b>	Jacobian matrix of IPFC branches
<b><math>\bar{J}</math></b>	Jacobian matrix of the power system with IPFC
<b>j</b>	Complex parameter
$K_A$	AVR gain
$K_{Ai}$	$i^{th}$ -machine AVR gain
$K_{PSS}$	PSS gain
$K_{pod}$	Gain of damping controller of IPFC
$k_{dp}, k_{di}$	Proportional and integral gain settings of the DC voltage regulator
$k_{qp}, k_{qi}$	Proportional and integral gain settings of the reactive power PI controller

$k_{pp}, k_{pi}$	Proportional and integral gains of the power flow controller controlling real power in the transmission line 1 of IPFC branches
$k_{kp}, k_{ki}$	Proportional and integral gains of the power flow controller controlling real power in the transmission line 2 of IPFC branches
$M = 2H$	Inertia constant
$m_c$	Number of the lead-lag blocks of damping controller of IPFC
$m_1$	Modulation index of VSC 1
$m_2$	Modulation index of VSC 2
$nb$	Number of buses in power system
$P$	Park's transformation
$PE$	Sum of real power exchanged with the transmission lines by the series VSC's
$P_D$	$P_D = D(\omega - 1)$ , $P_D$ - damping power
$P_{Di} = D_i(\omega_i - 1)$	Damping power of $i^{th}$ -machine
$P_{Gi}, Q_{Gi}$	Real and reactive power outputs of $i^{th}$ generator in multi-machine system without IPFC in $D - Q$ axis frame
$P_{Gl}, Q_{Gl}, l = i, j, k$	Active and reactive power injected by the generator at bus $l$
$P_{Li}, Q_{Li}$	Real and reactive components of the voltage dependent load at bus $i$ in multi-machine system $i = 1, 2, \dots, n$
$P_{Lj}, Q_{Lj}$	Real and reactive power of the load at bus $j, (j = (1, \dots, nb))$
$P_{Ll}, Q_{Ll}, l = i, j, k$	Active and reactive powers drawn by a load at bus $l$

$P_e$	Electrical real power of the generator in p.u.
$P_{ei}$	$i^{th}$ -machine electrical output
$P_{flow1}, Q_{flow1}$	Real and reactive power flows in line 1 in p.u. in SMIB power system
$P_{flow2}$	Real power flow in line 2 in p.u. in SMIB power system
$P_{ji}, Q_{ji}$	Active and reactive power flows of the IPFC branch leaving the bus $j$
$P_{ki}, Q_{ki}$	IPFC branch active and reactive power flows leaving the bus $k$
$P_l, Q_l, l = i, j, k$	Net active and reactive transmitted powers at bus $l$
$P_m$	Mechanical power input to the generator in p.u.
$P_{mi}$	$i^{th}$ – machine mechanical input
$P_{sein}, n = j, k$	Real power exchange between the two VSCs and IPFC transmission lines
$P_{sein}^{max}, n = j, k$	Maximum limit of the VSC equipment rating for active power exchange
$P_i^k, Q_i^k$	Transmitted active and reactive powers from bus $i$ to other buses ( $k = 1, \dots, j, \dots, m$ )
$P_{ji}^{Spec}, P_{ki}^{Spec}$	Real power reference set points in IPFC branches $j - i$ and $k - i$
$\Delta P_l, \Delta Q_l, l = i, j, k$	Mismatch active and reactive power at bus $l$
$\Delta P_{ji}$	Mismatch active power in the IPFC branch $i - j$
$\Delta P_{ki}$	Mismatch active power in the IPFC branch $i - k$

$P_{ki}$	Participation factor of $k^{th}$ state variable in the $i^{th}$ mode
$Q_e$	Reactive power of the generator in p.u.
$Q_{seij}$	Reactive power exchange between the VSC-1 and line $i - j$ of IPFC branch
$Q_{ji}^{Spec}$	Reactive power reference set point in IPFC branch $j - i$
$\Delta Q_{ji}$	Mismatch reactive power in the IPFC branch $i - j$
$\Delta \mathbf{R}$	Represents the mismatch line flows and real power exchanged among the IPFC branches
$R_{ij}, X_{ij}$	Resistance and inductive reactance of the transmission line between bus $i$ and bus $j$
$r_s$	Switch on-state resistance
$r_1 (r_2), l_1 (l_2)$	Per phase resistance and inductance of transformer on line 1 (line 2)
$S_{C1a}, (S'_{C1a})$	Switching function of the switch in phase $a$
$S_i$	Complex power at bus $i$
$T_A$	Time constant of AVR in sec
$T_{Ai}$	$i^{th}$ -machine AVR time constant
$T_w$	Washout filter time constant
$T'_{do}$	Open circuit d axis time constant in sec
$T'_{doi}$	$i^{th}$ -machine open circuit d-axis time constant in sec
$T_1, T_2, T_3, T_4$	Time constants of the phase compensation blocks of PSS
$T_{1dc}, T_{2dc}$	Lead and lag time constants of damping controller

$\mathbf{V}_{IPFC}$	Vector of magnitude of the injected voltages
$V_D, V_Q$	$D$ and $Q$ axis components of voltage
$V_{Dt}, V_{Qt}$	$D$ and $Q$ axis components of terminal voltage in p.u.
$V_{PSS}$	Component of electrical torque from PSS
$V_{ZL1}$	Voltage phasor across $Z_{L1}$
$V_{Zlp}, p = 1, 2$	Voltage drop across $Z_{lp}, p = 1, 2$
$V_d, V_q$	$d$ and $q$ axis components of voltage
$V_{dt}, V_{qt}$	$d$ and $q$ axis components of terminal voltage in p.u.
$V_l, \theta_l$	Magnitude and phase angle of $\bar{V}_l, l = i, j, k \dots$ respectively
$V_{ref}$	Reference voltage in p.u.
$V_{refi}$	$i^{th}$ -generator voltage reference
$V_{se1qI}, V_{se1pI}$	Components of $V_{se1}$ , in quadrature and in phase with line current
$V_{sep}, \theta_p$	Magnitude and phase angle of $\bar{V}_{sep}, p = 1, 2$ respectively
$V_{se1d}, V_{se1q}$	Direct and quadrature components of $V_{se1}$
$V_{se1u}, (u = a, b, c)$	injected voltage by the VSC-1 in phase $u, (u = a, b, c)$
$V_{set1d}, V_{set1q}$	Direct and quadrature components of $V_{set1}$
$V_{set1u}, (u = a, b, c)$	Combined voltage across the transformer impedance and VSC-1 in line 1
$V_{se2d}, V_{se2q}$	Direct and quadrature components of $V_{se2}$
$V_{se2u}, (u = a, b, c)$	Injected voltage by the VSC-2 in each phase $u, (u = a, b, c)$
$V_{set2d}, V_{set2q}$	Direct and quadrature components of $V_{set2}$

$V_{set2u}, (u = a, b, c)$	Combined voltage across the transformer impedance and VSC-2 in line 2
$V_t, I_t$	Voltage and current at generator bus in $d - q$ axis reference frame in SMIB power system
$V_{ii}, I_i$ $i = 1, 2, \dots n$	Generator terminal voltage and current of the $i^{th}$ machine in $d - q$ axis in multi-machine power system
$V_{tDi}, V_{tQi}$ $i = 1, 2, \dots n$	$D - Q$ axis components of generator terminal voltage $\bar{V}_{Gi}$ $n$ is the number of generators
$V_{tdi}, V_{tqi}$	$d - q$ axis components of generator terminal voltage $V_{ti}$
$\bar{V}$	Vector of voltages of each bus in multi-machine system
$\bar{V}_G$	Vector of terminal voltages of the generators in multi-machine system without IPFC in $D - Q$ axis frame
$\bar{V}_{Gi}, \bar{I}_{Gi} \quad i = 1, 2, \dots n$	Generator terminal voltage and current of the $i^{th}$ machine in $D - Q$ axis, $n$ is the number of generators
$\bar{V}_L$	Vector of load bus voltages in multi-machine system without IPFC in $D - Q$ axis frame
$\bar{V}_b$	Infinite bus voltage in p.u.
$\bar{V}_l, l = i, j, k \dots$	$\bar{V}_l$ is the voltage of the bus $l$
$\bar{V}_t$	Terminal voltage of the generator in p.u.
$\bar{V}_{sep}, p = 1, 2$	Voltage injected by each VSC of the IPFC
$\bar{V}_{sep}, p = 1, 2$	Equivalent voltage across the coupling transformer impedance and injected voltage

$V_{sep}^{min}, V_{sep}^{max}, p = 1, 2$	Maximum and minimum voltage limits of the series converter of IPFC
$\bar{V}_1, \bar{I}_1$	Voltage and current at bus 1 in SMIB power system in $D - Q$ axis in p.u.
$v_{dc}$	Voltage of the DC link capacitor
$v_{dc(ref)}$	Reference voltage of DC voltage across the capacitor
$\mathbf{X}$	Vector of $n$ unknown state variables
$\mathbf{X}^{(0)}$	Initial estimate of $\mathbf{X}$
$\mathbf{X}_1$	State vector that includes the voltage phase angles and magnitudes of the IPFC buses and the independent control variables of IPFC
$\bar{\mathbf{X}}$	State vector of the unknown variables of the power system with IPFC
$\mathbf{X}_{IPFC}$	State vector of IPFC variables
$X_{abc}$	Variables in $abc$ reference frame
$X_{dq0}$	Variables in $dq0$ reference frame
$\Delta X^{(it)}$	Correction vector
$\Delta x$	Deviation of the variable
$\dot{x}$	First order derivative
$x_{L1}, x_{L2}$	are the transmission line reactances
$x_d, x'_d$	d-axis reactance and d-axis transient reactance
$x_{di}, x'_{di}$	$i^{th}$ -machine d-axis reactance and transient reactance
$x_q$	Generator q-axis reactance

$x_{qi}$	$q$ - axis reactance of the $i^{th}$ -machine
$x_{t1}, x_{t2}$	Reactances of the series transformers
$\bar{Y}$	Bus admittance matrix in multimachine power system
$\bar{Y}_{Cij} = G_{Cij} + jB_{Cij}$	Shunt admittance representing the line charging capacitance
$\bar{Y}_{ii}$	Self-admittance of the bus $i$
$\bar{Y}_{ij}$	Transmission line admittance between bus $i$ and $j$
$\bar{Y}_{red}$	Reduced admittance matrix of the power system network in multi-machine system without IPFC
$\bar{Y}_{sein}, n = j, k$	Admittance between bus $i$ and bus $n$
$\bar{Y}_t$	Bus admittance matrix in multimachine power system keeping generator nodes and nodes $i, j, k$ .
$Z_{L1}$	Impedance of the transmission line of IPFC branch $i - j$
$Z_{L2}$	Impedance of the transmission line of IPFC branch $i - k$
$Z_{tp}, p = 1, 2$	Coupling transformer impedance of the two VSCs of IPFC
$\bar{Z}_{ij}$	Transmission line impedance between bus $i$ and $j$
$\bar{Z}_{sein}, n = j, k$	The total impedance of transmission line between bus $i$ and bus $n$ of the IPFC branches
$\beta$	Angle of the system transfer function without IPFC
$\gamma$	Angle of the transfer function of the system with IPFC
$\gamma_i$	Current phase angle with respect to $D - Q$ axis
$\delta$	Rotor angle of synchronous generator in electric radians
$\delta_i$	Torque angle of the $i^{th}$ -machine in elec.rad/s

$\zeta$	Damping ratio
$\zeta_{C1a}, (\zeta'_{C1a})$	Represent the switches in phase $a$ arm of VSC-1
$\theta_{\text{IPFC}}$	Vector of phase angles of the injected voltages
$(\theta), (V)$	Bus voltage phase angles and magnitudes
$\theta_i$	Voltage phase angle with respect to $D - Q$ axis
$\theta_1$	Phase angle of control signal of VSC 1
$\theta_2$	Phase angle of control signal of VSC 2
$\lambda_i, i = (1, \dots, n)$	Eigenvalue
$\phi$	Right eigenvector matrix
$\phi_{ki}$	$k^{\text{th}}$ entry of right eigenvector $\phi_i$
$\psi$	Left eigenvector matrix
$\psi_{ik}$	$k^{\text{th}}$ entry of left eigenvector $\psi_i$
$\omega$	Rotor speed in p.u.
$\omega_i$	$i^{\text{th}}$ - machine/generator rotor speed
$\omega_n$	Angular frequency of system oscillation from the mechanical loop
$\omega_0$	Synchronous speed ( $\omega_0 = 2\pi f$ $f$ = frequency in Hz)
*	Complex conjugate

## ABBREVIATIONS

AC	Alternating currents
AVR	Automatic voltage regulator
CSC	Convertible Static Compensator
DC	Direct current
EAT	Eigen-Value-Assignment
FACTS	Flexible AC Transmission System
GTO	Gate turn-off thyristor
HSV	Hankel singular values
IGBT	Insulated gate bipolar transistor
IPFC	Interline power flow controller
ISE	Integral-square-error
ITAE	integral of time-multiplied absolute value of the error
LQR	Linear quadratic regulator
MDI	Maximum Damping Influence
MIMO	Multi-Input Multi-Output
MSV	Minimum singular values
NYPA	New York Power Authority
OTEF	Oscillation transient energy function
p.u.	Per unit
PD	Proportional-plus-derivative
PI	Proportional-integral
PID	Proportional–integral-derivative
POD	Power oscillation damping
PSO	Particle swarm optimization
PSS	Power system stabilizer
PWM	Pulse-Width-Modulation
RBFN	Radial basis function network
RGA	Relative gain array

RHP	Right-half plane
SEP	Stable equilibrium point
SMIB	Single Machine Infinite Bus
SSSC	Static Synchronous Series Compensator
STATCOM	Static Synchronous Compensator
SVC	Static Var Compensator
SVD	Singular value decomposition
SVS	Synchronous voltage sources
TCPS	Thyristor Controlled Phase Shifter
TCR	Thyristor-controlled reactors
TCSC	Thyristor Controlled Series Capacitor
TEF	Transient energy function
TSC	Thyristor-switched capacitors
UPFC	Unified Power Flow Controller
VSC	Voltage source converter
WSCC	Western System Coordinating Council
<i>diag</i>	Diagonal matrix



## CHAPTER 1

### INTRODUCTION

Modern day society's requirement and consumption of energy for use in industry, commerce, agriculture, communications, domestic households, etc., have increased steadily. This rapid and continuous growth in electrical energy use is combined with a greater demand for low cost energy and to improve the reliability of power supply.

To make electric energy generation more economical, the generating stations are sited remotely from the load centers, and closer to the source of power. For example, the primary concern to hydroelectric power plants is the availability of water and benefits of the sites having higher heads with significant water flows, while thermoelectric power stations are situated near to coal mines and the nuclear power plants are located distantly away from the urban centers for safety. Consequently, the transmission lines serve the purpose to pool the generating sites and load centers covering large distances between generation and end-users in order to minimize the total generation capacity and fuel cost.

To enhance the system reliability, the electric power supply systems are widely interconnected, i.e., interlinking the neighboring power supply utilities, which further extend to inter-regional and international connections. Moreover, with the probable unavailability of some generating units, the interconnection lines could force the electric power flows to be redirected through longer routes to provide emergency assistance (e.g., when encountering partial blackouts). As such, transmission interconnections enable taking benefit of diversity of loads, availability of sources and fuel price to provide consistent and uninterrupted service to the loads.

This results in evolved planning, construction and operation of interconnected network of transmission lines. Although the interconnection results in operating economy and increased reliability through mutual assistance, yet they contribute

towards increased complexity of stability problems, increased consequences of instability and more requirements of stringent measures for maintaining adequate system dynamic performance. In this context, this chapter gives the background about the stability problems in the power system followed by brief discussion on Flexible AC Transmission Systems (FACTS) used in the power system to enhance the power system stability, the research motivation and objectives.

## **1.1 Power System Stability**

Power system stability is the ability of the power system to maintain a state of equilibrium for a given operating point or to regain an acceptable equilibrium point after being subjected to disturbances [1], [2]. Power system stability is mainly connected with electromechanical phenomena where in the synchronous operation is to be maintained [3]. Electric power is produced, almost entirely, by means of synchronous three-phase generators (i.e., alternators) driven by steam or water turbines. A necessary condition to maintain stability is that several generators in the power system must operate in synchronism during normal steady state and disturbance conditions. These AC generators produce *synchronizing torques* which depends on the relative angular displacements of their rotors to keep the generators in synchronism.

However, instability in power system may also be encountered due to various disturbances or with changing power demand. Maintaining the synchronism is not the only issue at such an instance. The stability and control of voltage and frequency are also of concern. As power systems are nonlinear, their stability depends on both the initial conditions and the size of a disturbance.

Over the years the power system stability definition has taken different forms being influenced by various factors. Different approaches have been developed to deal with different stability problems and methods are formulated to improve the stability. Therefore, the stability definitions have been classified as follows [2], [3]:

***Rotor angle stability*** is the ability of synchronous machines in interconnected power system to remain in synchronism. This stability problem involves the study of electromechanical oscillations inherent in power systems [2]. These oscillations occur in interconnected power systems as the synchronous generators swing against each other in the event of disturbance. Since the phenomenon involves mechanical oscillations of the rotor and oscillations of the generated electrical power, these oscillations are called electromechanical oscillations.

***Voltage stability*** is the ability of the power system to sustain steady voltages at all buses in the system before and after disturbances.

***Frequency stability*** is the ability of the power system to maintain the frequency in the event of disturbances.

Among several problems in the stressed power network, the major concern of study in stability problems. In this thesis, it is the electromechanical oscillations which come under rotor angle stability. The rotor angle stability is further classified as follows:

***Steady-state or small signal stability*** is the ability of the power system to maintain synchronism in response to small disturbances. The disturbances are in the form of small variations in load conditions and small differences in generator schedules.

***Transient stability*** is the ability to maintain synchronism when the power system is subjected to sudden and severe disturbances. The transient stability depends on the initial operating point and the severity of the disturbance. These disturbances can be of varying degree of severity such as short circuits of different types: phase-to-ground, phase-to-phase-to-ground or three-phase fault. They can occur on transmission lines, buses, or near transformers. The fault is assumed to be cleared by the opening of appropriate breakers to isolate the faulted element.

During small disturbances, the angular difference between generators increases and electrical torque is produced with the help of the excitation system which tries to reduce the angular displacement. As such, the moment of inertia of the generator rotors and the positive synchronizing torques cause the angular displacement of the

generators to oscillate, following a system disturbance. The oscillations of the generator's rotors are reflected in other power system variables such as bus voltage, transmission line active and reactive powers, etc. However, from an operating point of view, oscillations are acceptable as long as they decay. But during large disturbances such as short circuit on a transmission line, i.e., when the generator is subjected to relatively larger angular swings, the system may tend to oscillate causing it to become unstable. Fast excitation systems such as high gain automatic voltage regulators (AVR) were introduced to prevent the generators from losing synchronism. Unfortunately, improving the synchronizing torque affects the damping torque, as negative damping was introduced by these AVRs. Consequently, the net damping torque is insufficient and results in power system oscillations of exponentially increasing amplitude in an overstressed system. In the absence of mitigating means, it leads to instability of the power system. Thus, the stability problem is largely due to insufficient damping of the oscillations.

Electric power systems experience problems with the *low frequency oscillations* (0.1 to 2 Hz) [2], [4] which are a frequent phenomenon in the interconnected power system. The low frequency oscillations are characterized by the electromechanical mode oscillations and are initiated in the system when exposed to sudden small disturbances in load, generation and transmission network configuration and worsen following a large disturbance.

The low frequency oscillations are of two types: The first, known as the *local mode oscillations* is associated with a single generator or a group of generators at a generating station oscillating with respect to the rest of the power system. They have natural frequencies of about 1 to 2 Hz [2], [4]. The characteristics of local area oscillations are well understood and adequate damping of these oscillations can be achieved with help of the Power System Stabilizer (PSS), which provides supplementary control action in the excitation systems of the generators.

The second are the *inter-area mode oscillations*, which associate with the machines in one area of the power system oscillating against the machines in other areas of the power system. Inter-area modes of oscillation have lower natural frequencies in the order of 0.1 to 1 Hz [2], [4]. They are caused by two or more

groups of closely coupled machines that are interconnected by weak tie lines. As such these oscillations may also lead to widespread system disturbances if cascading disturbances (faults and protective relaying operation) on transmission lines occur due to the oscillatory power swings across the tie lines. Such an event occurred during the blackout in western US/Canada interconnected system on August 10, 1996 [5] and a similar blackout occurred on August 14, 2003 in eastern Canada and US by severe 0.4-Hz oscillations in several post-contingency stages [6]. Studies about the relations between inter-area mode and different factors in the power system are quite complicated. The characteristics of these modes are complex as they involve more than one utility and require cooperation of the rest of the utilities to obtain effective and economical solution.

Low frequency oscillations are of concern as these oscillations affect the power transfer capability of the line. Damping of these oscillations plays a significant role in power system stability to secure and increase the supply and transmission capability of the system. In the circumstances due to insufficient damping, damping devices are imperative to dampen these power system oscillations.

Demello and Concordia analyzed the mechanism of low frequency oscillation [7], using the linearized (k constant) model. This model is also known as the linearized Phillips-Heffron model of a power system which explains the relationships between small signal stability, high impedance transmission lines, line loading and high gain fast acting excitation systems. Traditional approaches to assist the damping of power system oscillations include the application of PSS to the generator voltage regulator. PSS are designed based on the linearized model of the power system [8]. However, the pressures of the continuing interconnection of electric networks and increase of line loading have indicated that the PSS alone is not sufficient. Proliferation of controls is considered by prudent use of FACTS technology as needed.

## **1.2 FACTS Devices**

With the advent of high power, high speed power electronics based FACTS, their capability in damping power system oscillations has been explored and

investigated [9]. Flexible Alternating-Current Transmission Systems (FACTS) is defined by the IEEE as “AC transmission systems incorporating power electronics-based and other static controllers to enhance controllability and increase power transfer capability” [10]. The FACTS concept originally came into effect in 1980s to solve operation problems due to the restrictions on the construction of new transmission lines, to improve power system stability margins. It also facilitates power exchange between different generation companies and large power users, thus considerably utilizing the existing transmission network instead of adding new transmission lines for the growing demand of power, as it may be restricted due to economical and environmental problems. Correspondingly, a FACTS controller is defined as “a power electronics-based system or other static equipment that provides control of one or more AC transmission parameters” [10]. The FACTS controllers have been beneficial as they operate very fast and enlarge the safe operating point limits of a transmission system without threatening the stability of the system.

The developments in FACTS technology made it possible to rapidly vary the reactive shunt and series compensation, to accommodate the changes in the transmission lines and maintain the stability margins. Since FACTS elements are already being used in power systems for voltage support and power flow control, they can potentially be applied for damping the oscillations of the power system and improve the overall power system stability. The compensation applied by the FACTS controllers is varied to affect the power flow to obtain reliable and rapid damping of the low frequency oscillations, as well as satisfy the primary requirements of the device.

There are two distinct groups of FACTS controllers based on technical approaches [9], [11-14]. The first group is based on line commutated thyristor devices having no intrinsic turn off ability. The thyristor controlled FACTS controllers consists of Static Var Compensator (SVC), Thyristor Controlled Series Capacitor (TCSC) and Thyristor Controlled Phase Shifter (TCPS) employing reactive impedances or tap changing transformers with thyristor switches as controlled elements [9].

Each of these FACTS devices can control only one parameter: SVC- voltage, TCSC-transmission impedance and TCPS-transmission angle. The major members of this group, the SVC and TCSC, have a general characteristic in that the conventional capacitor or reactor banks generate or absorb the necessary reactive power required for the compensation, and the thyristor switches are used only for the control of the combined reactive impedance these banks present to AC system. TCPS does not supply or absorb the reactive power it exchanges with the AC system.

The second group is based on self-commutated converters which use thyristors/transistors with gate turn-off capability, such as GTO's, IGBT's etc. The converter based FACTS controllers are of two types: voltage sourced converters (VSCs) and current sourced converters. However, from economical point of view, the VSCs seem to be preferred and will be the basis for most of the converter-based FACTS controllers [12]. They have an advantage over the thyristor controlled FACTS controllers compensation methods in providing better performance characteristics and uniform applicability for transmission, effective line impedance and angle control. This approach can provide reactive compensating shunt current that is independent of system voltage, as well as series reactive compensating voltage that is independent of line current, i.e., the applied compensation provided by synchronous voltage sources (SVS) remains largely independent of the network variables (line current, voltage or angle). The SVS also has the capability of executing a bidirectional *real* (active) power flow between its AC and DC terminals. Thus, it becomes possible to couple the DC terminals of two or more SVSs and, thereby, they become capable of exchanging real power with the AC system directly along with providing controllable reactive power compensation independently. This group of FACTS controllers consists of Static Synchronous Compensator (STATCOM), the Static Synchronous Series Compensator (SSSC), the Unified Power Flow Controller (UPFC) and the Interline Power Flow Controller (IPFC).

### **1.3 Interline Power Flow Controller (IPFC)**

The IPFC is a recent member of the converter based family of FACTS controllers [15]. IPFC provides comprehensive power flow control scheme for a *multi-line*

transmission system unlike other FACTS controllers (STATCOM, SSSC, and UPFC) which are developed primarily for the control of a *single line*. In general, the IPFC employs a number of voltage sourced converters (VSCs) with a common DC link, each providing a series reactive compensation for a selected line of the transmission system by injecting a series voltage. Due to the common DC link, any converter of the IPFC is able to transmit real power in between other VSCs and thus, able to assist in real power exchange among the lines of the transmission system. Since each converter is also able to provide series reactive compensation, the IPFC is able to provide real and reactive power compensation, and thereby, optimize the utilization of the transmission system. This ability of IPFC makes it possible to equalize both real and reactive power flow between the lines, transfer power from overloaded to under-loaded lines, compensate against reactive voltage drops and the related reactive line power, and to increase the efficiency of the compensating system against dynamic disturbances (transient stability and power oscillation damping). In other words, the IPFC can potentially provide a highly effective scheme for power transmission management at a multi-line substation.

A basic IPFC consists of two VSCs with a common DC link is shown in Figure 1.1 [12]. Each converter is coupled to a different transmission line via its own series insertion transformer, thus, providing independent series reactive compensation to its own line.

The real power is exchanged by the converters at its AC terminals which is supplied to or absorbed from its DC terminal. The IPFC has all the advantages established for the converter based FACTS controllers: Modular construction from similar building blocks which can be fully decoupled and operated as independent series compensators or reconfigured into shunt compensators or UPFC. The rating of selected individual compensators can be increased by the combination of the individual building blocks.

The IPFC configuration provides a flexible utilization of needed compensation assets without any significant cost addition, and thus, makes this approach attractive for utilities (or other transmission system operators) to solve some of difficult transmission problems they face today.

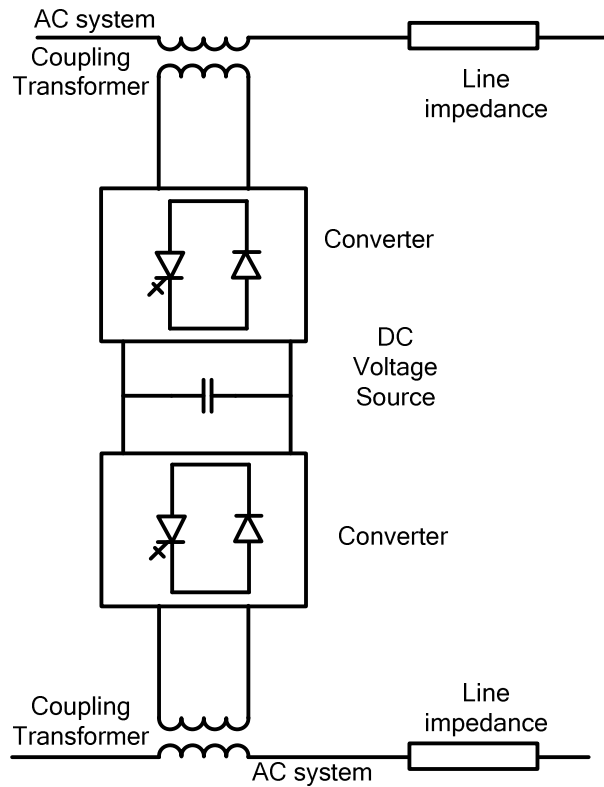


Figure 1.1: Schematic diagram of IPFC

As seen, IPFC is a multivariable controller. The control design of IPFC should be such that it should be able to perform in a stable manner while providing power flow control as well as damping to power system oscillations. If the control system is not designed properly, it could lead to growing oscillations in transmission line power flow and lead to system wide disturbances. In this view the control aspect of an IPFC is an important area of research.

#### 1.4 Research Motivation

The electric utilities are constantly on a lookout for new devices that will enable the power system to have increased power transfer abilities with the transmission lines. The increase in energy exchange within the transmission network further increases the stress of the existing power network entailing enhanced control techniques to ensure power system stability. In the recent research, FACTS devices have been suggested and investigated for improving damping of the power system oscillations. Thus, while performing their primary functions of power flow control; they are also utilized for

enhancing the damping of the oscillation modes. The FACTS-based controllers have been more prospective to stabilize the low frequency oscillations which cannot just be controlled through generator controllers with only local measurements.

The latest FACTS device, IPFC, regulates the power flow in the transmission lines. Consequently, IPFC should not only be able to control the power flow of the concerned transmission lines but also be able to enhance the damping of the power system oscillations present in the system. In this context, greater potential in increasing the oscillations stability with the assistance of the IPFC is perceived. This demands the modeling of IPFC for stability analysis. *However, not much research has been evolved in the modeling of the IPFC for stability analysis and the control aspect of IPFC has also to be investigated.* The power system stability has to be analyzed incorporating the IPFC to consider its effect on the system.

Power system consisting of multiple machines will exhibit multiple modes of oscillations due to a variety of interactions among its components. These oscillations must decay following a system disturbance. If any lightly damped electromechanical mode of oscillation exists, it may increase in amplitude due to inadequate damping torque in some generators. The continuous presence of power system oscillations in the power system can severely restrict system operations. These oscillations are of major concern for the power system operation. Thus, determining the lightly damped modes and their damping are vital for stable operating system.

Tools for analyzing the nature of the system oscillations, in addition to determining the existence of problems are required. It should be able to identify the frequency, damping of the oscillation mode, and factors influencing them, i.e., the variables involved in each of the modes. It should provide information to design efficient oscillation damping controls. Thus, to investigate the problems concerning the low frequency oscillations, the small signal analysis (i.e., modal analysis or eigenvalue analysis) based on linear techniques is suitable. When power system is subjected to a small disturbance, the system will have a small deviation in the neighborhood of a steady state operating point. This allows the system equations to be linearized around the steady state operating point to be permissible for purpose of analysis. System stability is based on eigenvalue analysis. This method characterizes

the system oscillations by assuming a linearized model of the power system about a specific operating point. Since small signal stability is basically viewed as the stability affected by perturbations valid within the boundary of nominal operating point region, the power system model which is linearized, is significant for studies mapped in the domain of small perturbations. The eigenvalues of the state matrix of such model clearly identify the stability of each mode. The eigenvectors give the modeshapes and relationships between the modes and system variables. Performing the eigenvalue analysis, the poorly damped eigenvalues are determined along with their characteristics and sources of the problem which will help in developing mitigating measures.

The nonlinear simulations of the power system will indicate the effects of nonlinearities of the system. Thus, small signal stability analysis along with nonlinear time simulations is the most effective procedure for studying power system oscillations [2], [4], [16], [17].

Considering the facts mentioned the major aim of this research is to develop the dynamic model of the IPFC for stability studies which has to be incorporated into the power system dynamic model. The control methods for the IPFC to control the power flow in the transmission lines and to improve the power system oscillations damping is to be investigated. The power system stability analysis incorporating the IPFC is to be performed through eigenvalue analysis and nonlinear simulations.

## **1.5 Research Objectives**

The ability of IPFC in damping low frequency oscillations in a power system is explored in this research. The design of the controllers for the IPFC requires the power system model incorporated with IPFC. Consequently, modeling of IPFC for steady state stability is initially established which involves the steady state model and dynamic model of the FACTS device. Moreover, the dynamic model of the IPFC involves the DC link dynamics which is a function of the series converter control variables. Modulating these control variables will provide an injected voltage with controllable magnitude and phase angle by the converters which in turn vary the

power flow in the transmission line. Therefore, the main focus of this research is to develop the dynamic model of the *power system incorporated with IPFC*. This model is analyzed for power system stability.

The power system model developed is a nonlinear model consisting of differential state space equations and network algebraic equations, including the dynamics of the IPFC. The nonlinear equations are linearized at an operating point to obtain the linearized Phillips-Heffron state space model of the power system. Consequently, modal analysis is used to identify oscillation modes from the linearized model. The controller is designed based on this linearized system to increase the damping of the un-damped oscillation modes. Design of these controllers to give robust performance under large variations in system parameters and operating conditions is essential. A conventional lead-lag damping controller is designed at a particular operating point based on the linearized Phillips-Heffron model of the system to provide reliable operation.

To understand the basic concepts of the damping contribution of the IPFC controller on the power system, initially a *single-machine-infinite-bus* (SMIB) system is considered. The linearized Phillips-Heffron model of the SMIB power system has been used successfully over the years to provide reliable results as it is quite accurate for studying low frequency oscillations and small signal stability. Based on the insight provided by the model of SMIB installed with IPFC, the dynamic mathematical model of *multi-machine power system* incorporated with IPFC is developed. Further, to illustrate the effectiveness of the proposed IPFC damping controller for multi-machine system, case study is performed: Western System Coordinating Council (WSCC) consisting of three machine and nine buses which presents a poorly damped oscillation modes. The effectiveness of the IPFC on power flow control and on damping power system oscillations is investigated through modal analysis and nonlinear simulations.

The primary function of IPFC is to regulate the power flow in the transmission lines where it has been installed. The series converters of the IPFC control the power flows in the transmission lines. The interaction between the series injected voltage and the transmission line current causes the series inverter to exchange real and

reactive power with the transmission line. The series injected voltage is controlled by the input signals of the IPFC. Thus, controlling the input signals usually with a PI controller, the power flow in the transmission lines is also controlled.

The real power exchange by the series inverter with the transmission line is supplied or absorbed from the other transmission lines through the DC link capacitor. This causes a decrease or increase in the DC capacitor voltage. For proper operation of the IPFC, the *DC capacitor voltage should be regulated* at a specified level. This is the other issue which is focused in this work during the design of the IPFC control system.

The main objective of this research is to design the IPFC based controllers for enhancing the power system stability. This is achieved by:

- a) Establishing the IPFC load flow or the steady-state model, and perform the power flow analysis of the system with the IPFC to obtain the operating point around which the power system is linearized for small changes.
- b) Developing an IPFC dynamic model with its control inputs for dynamic studies.
- c) Deriving of the linearized Phillips-Heffron model of the power system (SMIB and Multi-machine) with IPFC, to be used for analysis and design of controllers.
- d) Designing the conventional lead-lag controller based on the linearized model of the power system incorporated with IPFC. On the basis of this model, the robustness of the commonly used input signals are analyzed, employing transfer function technique and eigenvalue analysis.
- e) Performing nonlinear simulations on SMIB power system and a three-machine nine-bus multi-machine power system. The simulation results demonstrate the effectiveness of the proposed methodologies.

## 1.6 Contributions of Research

FACTS devices are envisaged to play a prominent role in future to maintain the power system stability. IPFC belongs to the second generation type of FACTS devices based on VSCs, provides real and reactive power compensation for multiple transmission lines. This thesis presents the modeling and control strategies for IPFC for enhancement in stability. The contributions of the research:

- The steady state model of IPFC is established for load flow studies which reflect the steady state operation of the FACTS device including all operating limits. The load flow program is developed for the complete power system incorporating IPFC.
- The dynamic model of IPFC is developed including the dynamics of the DC link capacitor which is a function of the control signals of the device. This dynamic model is used to integrate with the power system model for stability analysis.
- Phillips-Heffron model of SMIB incorporated with IPFC is developed by adopting the techniques utilized for other FACTS devices especially the UPFC. The state variables, of the Phillips Heffron model of a SMIB incorporated with IPFC derived, are a function of all the control inputs to indicate their influence.
- The lead-lag controller is designed based on the linearized model of the power system. The output of the controller modulates the input signals of IPFC thus, varying the magnitude and phase angle of the injected voltage into the transmission line. The effect of the input signals on the power system stability is investigated using eigenvalue analysis and detailed simulation studies.
- The mathematical model of the IPFC installed in a multi-machine power system is developed. The linearized Phillips-Heffron model of the multi-machine power system extended with IPFC is developed. From the Phillips-Heffron model, multiple modes in need of damping are identified using modal or eigenvalue analysis.

- The control strategy is devised which enables simultaneous control of power flow on transmission lines to influence the line power, subject to the restriction that real power exchanged with the line via one converter must be balanced by the power exchanged by the other converter, and enhancing the damping of the power system oscillations.

## **1.7 Thesis Outline**

The rest of the thesis is organized as follows:

Chapter 2 provides the theoretical background of power system stability and reviews the modelling procedures, the analysis techniques of the various FACTS devices and the control techniques for enhancement of damping of the power system oscillations.

Chapter 3 presents the steady state model of the IPFC and establishment of the dynamic model of IPFC for small signal stability studies.

Chapter 4 presents the nonlinear model of the SMIB power system equipped with an IPFC. The linearized Phillips-Heffron model of SMIB is developed on which eigenvalue analysis is performed to determine the mode in requirement of damping. Proposed IPFC lead-lag controllers are designed based on the linearized system to dampen the oscillations using local measurements. Their effectiveness on power system stability is investigated through time domain analysis under different system disturbances.

Chapter 5 briefly reviews the nonlinear multi-machine power system model in absence of the FACTS controller. This chapter presents the mathematical models of various components of the multi-machine system. The control scheme involving the PSSs for the power system is presented. To demonstrate the effectiveness of the developed controller, eigenvalue analysis and time simulation (nonlinear simulation) results for the power system are presented.

Chapter 6 presents the application of an IPFC controller for a multi-machine power system. Development of the mathematical model of the multi-machine power system equipped with IPFCs is presented. The control schemes for the power system are presented. To demonstrate the effectiveness of the developed controllers, simulation results for the power system are presented.

Chapter 7 summarizes the findings of the research undertaken and contributions and provides suggestions for future research.

## CHAPTER 2

### POWER SYSTEM STABILITY: AN OVERVIEW

#### **2.1 Introduction**

In this chapter, the relevant literature review of the work related to the problem of damping low frequency oscillations investigated in this thesis is presented. The review is organized in two parts. The first part given in Section 2.2: the work related with improvement of the stability of power system oscillations using FACTS devices is reviewed. Then, the second part covered in Section 2.3, the work related to modeling, control strategy and control systems for IPFC, for damping power system oscillations are discussed.

#### **2.2 Power System Oscillations Stability**

A power system should have the ability to regain the state of equilibrium with most system variables bounded after being subjected to a physical disturbance, i.e., the entire power system should remain intact with no tripping of generators or loads in the other areas, except for those detached by isolation of the faulted elements or purposely tripped to maintain the continuity of operation for the remaining system [2]. The power systems in practice are designed and operated to be stable for a set of designed contingencies which are selected based on their significant possibility of occurrence and severity, given the complexity involving the number of components comprising the power system. However, due to economic and technical limitations, a power system may be guaranteed to be stable for all possible disturbances and contingencies. Power system oscillations are frequent inherent phenomena and are not unexpected, with continually varying load conditions and some slight differences in the design and loading of the generators. The requirement for establishing study procedures and developing tools, for the analysis of system oscillations which determine the existence of the problems and identifying the factors influencing the

problem, provide useful information in developing control measures in mitigation of these oscillations.

The Phillips-Heffron model of a synchronous machine connected to an infinite bus was first presented by Heffron and Phillips [18] and De Mello and Concordia [7] for the analysis of power system oscillation stability. These papers significantly contribute to the required understanding of system damping in the area of small perturbation stability. The linearized Phillips-Heffron model gives insights into effects of machine and system parameters, voltage regulator gain, and stabilizing functions derived from speed and working through the voltage reference of the voltage regulator. Based on this model, the researchers have developed the expressions for torques and revealed the effect of excitation system on stability. It is shown that under many system circumstances, excitation systems can be a major source of negative damping on system oscillations and insufficient damping torque is the cause of oscillation instability necessitating supplementary stabilizing action.

PSS are used for many years to serve the purpose of enhancing the damping of electromechanical oscillations (low frequency oscillations). The basic function of the PSS is to provide additional electrical torque in the excitation system, in phase with the speed variation to increase the damping torque to sustain the power oscillations. Installation of PSS is a simple, effective and economical method. The conventional PSS structure consists of a washout circuit and a cascade of lead-lag networks as shown in Figure 2.1 [2], [8]. The method of damping torque analysis and phase compensation method based on the linearized Phillips-Heffron model were applied to design PSS parameters [2], [8], [19]. The phase compensation is used to compensate the phase lag between the excitation voltage and electrical torque of the synchronous machine.

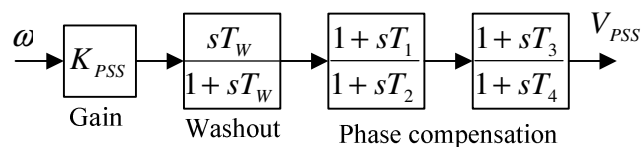


Figure 2.1: Power system stabilizer

A number of input signals to the PSS, such as rotor speed, electric power, and linear combinations of these have been extensively investigated and recommendations regarding different techniques in PSS design have been reported in literature [20]-[27]. PSS is quite suitable in mitigating the local area oscillations. However, its effect is limited in dealing with inter-area oscillations under certain conditions, for the PSS is designed to operate only upon local variables of the associated generators and primarily employed to damp local area oscillations. The PSS, if carefully tuned, may also be effective in damping inter-area modes up to a certain transmission loading. However, this necessitates provision of PSSs on most of the generators and consequently, coordination of tuning among them.

Various techniques have been proposed for the coordination of multiple PSSs installed in multi-machine power systems to suppress multi-mode oscillations. However, it has further been observed that improving damping ratios associated with inter-area modes often adversely affects the damping ratios and also the oscillation frequency associated with local modes [28]. Consequently, oscillation stability analysis and control for these oscillation modes have been important and active subjects in power system research and applications for decades.

Recent appearances of FACTS based stabilizers offer alternative ways to damp power system oscillations. The potential of the FACTS damping function has gained interest in both academic and industrial sectors. Due to fast control actions of the FACTS devices, they have been utilized considerably to improve the power system oscillation damping and also maintain the voltage profile, thus, having an advantage over the PSS. Although the function of the FACTS devices is to control power flow in the transmission lines, their control design enhances the damping characteristics of certain electromechanical modes while satisfying the primary requirements of the device.

These transmission controls to enhance damping of oscillation modes use local input signals near the FACTS device like active and reactive power deviations, bus voltages or currents, since the control devices are located on the transmission lines. Larsen *et al.* [29], presented the general design concepts for the FACTS damping controller based on an approximate multimodal decomposition for systems with

multiple swing modes. This concept is similar to the approach applied to a single-machine model by De Mello and Concordia [7]. Larsen *et al.* [29], suggested that the impact of the synchronizing and damping components of torque on each electromechanical mode of oscillation in a multi-machine system is determined by decomposing the system variables into their modal components. The concepts explained are helpful in developing a set of analytical tools which provide valuable insights to assist the task of designing FACTS controllers to damp power oscillations.

For the study of power system oscillation stability, initially the augmented Phillips-Heffron model of the power system installed with the FACTS devices is established. This model has an advantage due to its systematic configuration and clear demonstration of the control function of the FACTS-based stabilizers. It is convenient for applying the conventional damping torque analysis and using phase compensation method to analyze and design FACTS-based stabilizers. The Phillips-Heffron model of the power system installed with the FACTS-based stabilizers, including SVC - [30], TCSC - [31], TCPS - [32], [33], STATCOM - [34], SSSC- [35] and UPFC - [36]-[38] based stabilizers are established in literature. From the Phillips-Heffron model of the multi-machine power system, a multi-channel model of FACTS-based stabilizers providing damping to oscillation modes in the multi-machine power system can be established [9]. A brief review of each FACTS device, along with their modeling and control strategies is presented in the following sections.

### **2.2.1 Static Var Compensator (SVC)**

The SVC is basically a shunt connected device consisting of thyristor-controlled reactors (TCRs), and thyristor-switched capacitors (TSCs) as shown in Figure 2.2 [9], [12]. The output of the SVC is adjusted to exchange capacitive or inductive current to maintain or control specific power system variable typically, the SVC bus voltage. The main reason for installing a SVC is to improve dynamic voltage control, and thus, increase system loadability. By introducing an additional stabilizing signal superimposed on the voltage control loop of a SVC, by a supplementary control, it can provide damping of system oscillations.

Wang and Swift [30], [39] established an extended Phillips-Heffron model of a SMIB power system to include SVC in 1996. They have analyzed damping torque contribution of the SVC damping control to the power system. The SVC damping control is shown to be effective with variations in the transmission line impedance indicating that the SVC damping control is efficient when the power system is operating at a weaker system connection.

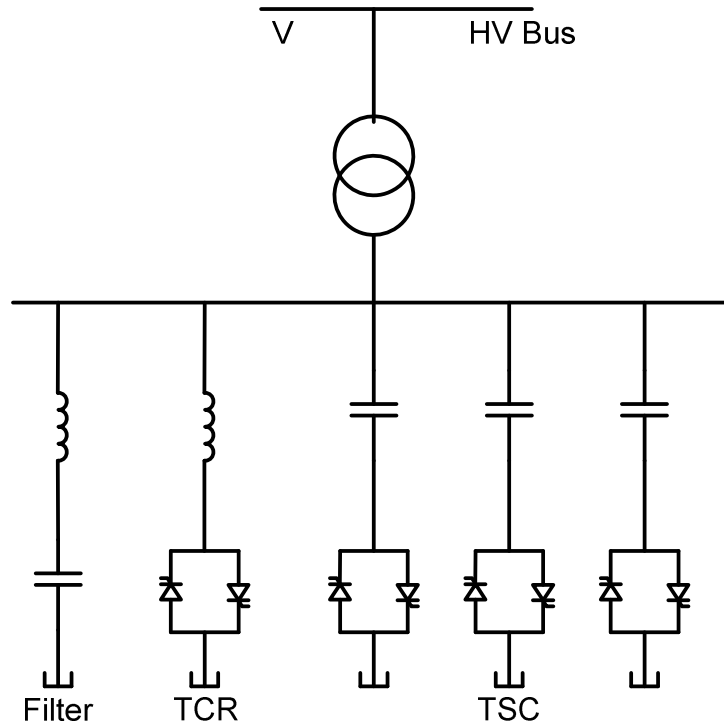


Figure 2.2: SVC employing thyristor switched capacitors and thyristor controlled reactors

Yuan *et al.* [40] designed the SVC supplementary controller whose parameters are designed based on the residue phase compensation method. The authors adopted the synthetic observability and controllability concept to choose the appropriate wide area input signals and for placing the SVCs, based on modal analysis, in the multi-machine power system. The analysis was performed on a 16 machine power system. Farsangi *et al.* [41], suggested the placement of the SVCs in a multi-machine based on the voltage stability utilizing the modal analysis and genetic algorithm. Here, the stabilizing signals for the SVCs are selected using the minimum singular values (MSV), the right-half plane zeros (RHP-zeros), the relative gain array (RGA), and the Hankel singular values (HSV). Larsen [42] considered the locally measured

transmission line current magnitude as the input signal for the SVC for enhancing the damping based on the observability and controllability factors. Similarly line current was used by Zhao and Jiang [43], however, active power [44], [45], generator speed [46] were also used in the stability studies.

### 2.2.2 Thyristor Controlled Series Capacitor (TCSC)

TCSC, a series FACTS controller shown in Figure 2.3 [9], [12] consists of a fixed capacitor in parallel with thyristor controlled reactor, is used to change the equivalent series capacitive reactance of the line dynamically and thereby controlling the real power flow in the lines. In addition to this primary function, TCSC also provides damping in the power system when used along with a supplementary controller which helps in changing the firing angle, thus modulating the effective reactance of a TCSC. This variable series capacitive compensation by TCSC mitigates the low frequency oscillations.

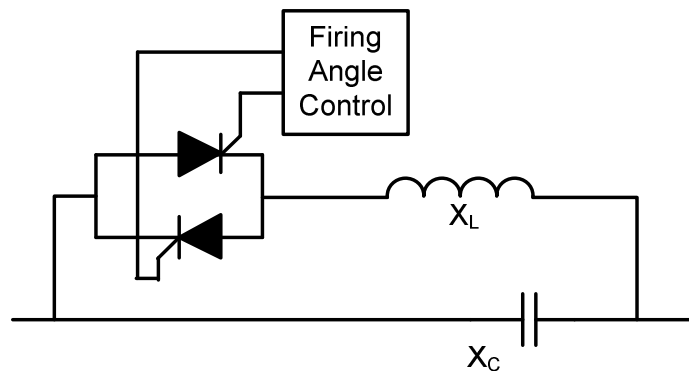


Figure 2.3: TCSC with a thyristor-controlled reactor in parallel with a series capacitor

TCSC with a supplementary controller, utilized for damping inter-area and local area oscillations [47]. A unified model of SMIB power system installed with a TCSC has been developed in [31]-[33]. Sidhartha Panda [48] developed a lead-lag and proportional–integral-derivative (PID) types of TCSC based controllers. The parameters of these controllers are optimized using GA based optimal tuning algorithm for minimizations of integral-square-error (ISE) and integral of time-multiplied absolute value of the error (ITAE). The effectiveness of the lead-lag and

PID structured TCSC controllers are analyzed at different loading conditions and under various disturbance conditions on a SMIB power system and further extended to 3-generator power system.

Kalyan Kumar *et al.* [49] proposed to find a suitable location for TCSC for improving the damping of inter-area mode of oscillations in a multi-machine system. This was achieved by utilizing modal controllability index called line index which is computed by taking set of lines suitable for the TCSC placement (all lines in the system excluding transformer branches) and incorporating their line compensation in the differential algebraic equation model (dynamics of generators included). The feedback signal for the TCSC supplementary controller is taken to be the line real power of the transmission line on which the TCSC is placed. Lin and Lo [50] established a proportional-plus-derivative (PD) control scheme assisted with the use of genetic algorithms for a TCSC on the basis of the linear systems theory to support power system damping performance. The effectiveness of the proposed method is verified through computer simulation using a multi-machine power system associated with a single TCSC. But the authors do not consider the inherent nonlinear character of power systems. Fang *et al.* [51], proposed the oscillation transient energy function (OTEF), to design a TCSC supplementary modulation controller to damp inter-area oscillations. Fuzzy-logic control and adaptive techniques are employed to develop the TCSC damping controller based on OTEF. The OTEF interprets an inter area mode oscillation as the conversion between oscillation kinetic energy and potential energy. The controller achieves oscillation suppression by continuously reducing the OTEF. The proposed controller was implemented on 4-generator 2-area interconnected power system.

### **2.2.3 Thyristor Controlled Phase Shifter (TCPS)**

The TCPS transformer shown in Figure 2.4 [9], [12] is applied to control the power flow in multiple transmission lines by regulating the transmission angle. The phase shifting is obtained by injecting perpendicular variable voltage component in series with the line-to-neutral terminal voltage. The damping controller modulates the phase angle to control power flow so as to provide damping to the oscillations. However, the

tap-changing transformer type phase shifter cannot generate or absorb reactive power and, together with high cost, this type of phase shifter has significant disadvantage in practical applications.

A Phillips-Heffron model of an  $n$ , machine power system installed with a TCPS damping controller was established by Wang *et al.* [52]. The damping torque to the power system by the TCPS damping control is analyzed based on the linearized Phillips-Heffron model of the power system. The authors discussed the robustness of the TCPS damping controller in suppressing the multi-mode oscillations as well as the selection of the controller's location in a multi-machine system. In situations giving rise to multimode oscillations, the TCPS damping control provides some generators in the system with positive damping torque and negative damping torque to other generators.

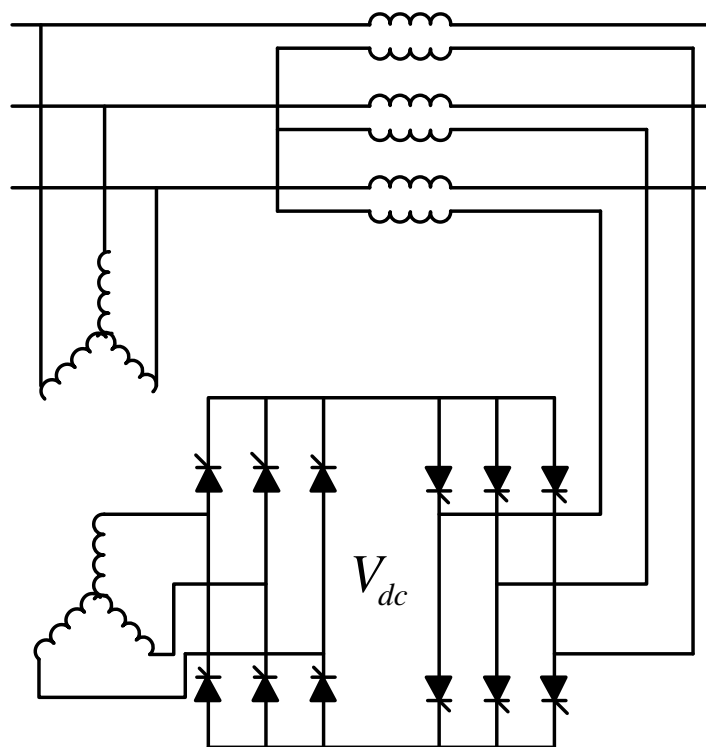


Figure 2.4: Schematic diagram of TCPS

The TCPS damping control may in likelihood have a detrimental influence on other types of oscillation modes, when it is designed only for the suppression of one mode. Co-ordination with other types of controllers is a necessity when using with other controllers such as a PSS, in a multi-machine system.

## 2.2.4 Static Synchronous Compensator (STATCOM)

A STATCOM shown in Figure 2.5 [9], [12] is the static counterpart of rotating synchronous condenser, but without inertia and limited overload capability. It generates a balanced three-phase voltage at the fundamental frequency with controllable amplitude and phase angle. It is a shunt-connected controller used for voltage control and reactive power compensation. The converter can supply real power to the AC system from its DC energy source if the converter output voltage is made to lead the AC system voltage or absorb real power for the DC system if its voltage is lagging behind the AC system voltage. The main function of STATCOM is to regulate the transmission voltage, however it is insufficient to damp all the oscillations modes in the power system thus, entailing the supplementary oscillation damping controller along with the voltage controller.

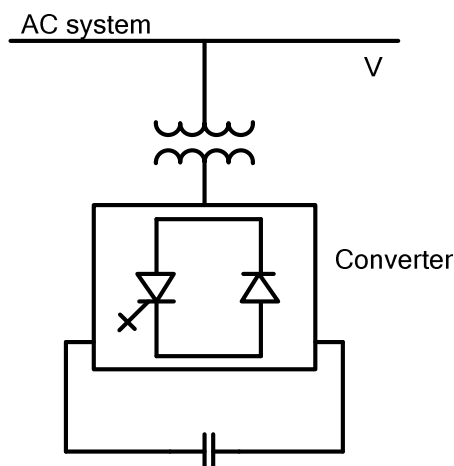


Figure 2.5: Schematic diagram of STATCOM

STATCOM model incorporated into the Phillips-Heffron model of the power system along with its AC/DC voltage regulators controllers interaction has been studied by Wang [34]. A simple lead lag controller was proposed by Wang in [53], and a conventional PI controllers were used in [34]. Bamasak and Abido [54] employed the particle swarm optimization (PSO) algorithm to search for the optimal settings of stabilizer parameters based on the developed linearized model of a SMIB power system equipped with STATCOM-based stabilizer. The singular value decomposition (SVD) based controllability measure is used to identify the effectiveness of each controller input.

The power system oscillation damping via PSS and STATCOM-based stabilizer when applied individually and also through coordinated application was investigated in this paper. The eigenvalue analysis and nonlinear simulation results show the effectiveness and the robustness of the proposed stabilizer in enhancing system stability. Chun *et al.* [55] designed and evaluated the input signals for the STATCOM-based damping controller through controllability, observability and self-interaction gain calculations. Root locus analysis was used to tune the controller gain.

Mak *et al.* [56] presented the power frequency model for STATCOM with conventional controllers. He proposed the fuzzy logic controller to further enhance interconnected power system stability. Simulation tests are conducted on a four-generator test system and results show significant improvement in dynamic behavior of the power system with fuzzy controllers. Gharaveisi [57] presented a novel technique, transient energy function for designing a fuzzy logic controller for STATCOM. The additional damping is provided by increasing the rate of dissipation of transient energy so that the system can reach the stable equilibrium point (SEP) promptly. Energy function and its derivative are given as inputs to the fuzzy logic based STATCOM supplementary controller and the system stability is evaluated by observing the rate of dissipation of the transient energy during post-fault period. Simulations are performed on a four-machine two-area system. Xiaorong *et al.* [58] designed control schemes for STATCOM based on wide-area measurements on reduced-order system model of a large power system. The parameters of the damping control loop are optimized via LQR approach in a multi-machine environment.

### **2.2.5 Static Synchronous Series Compensator (SSSC)**

The SSSC shown in Figure 2.6 [9], [12] is a series compensator whose controllable output voltage is in quadrature with the line current for the purpose of increasing or decreasing the overall reactive voltage drop across the line and thereby controlling the electric power. This controller is similar to the STATCOM except that it is connected in series with the AC system. Due to its ability to modulate the line impedance it can also impart enhanced damping to the power system oscillations.

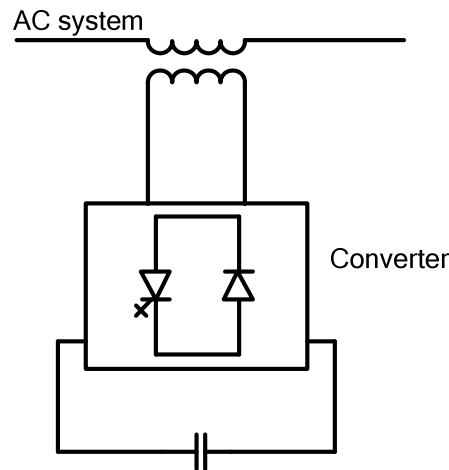


Figure 2.6: Schematic diagram of SSSC

Wang [35], investigated the damping function of the SSSC based on the linearized Phillips-Heffron model of the power system. The SSSC damping controller is designed based on the phase compensation method for a SMIB power system installed with SSSC. An objective function based search algorithm is suggested by the author for designing the controller for multi-machine power systems. The effectiveness of the SSSC damping controller to suppress power system oscillations and its design by the methods proposed for SMIB and multi-machine system was demonstrated in this paper. Pandey [59], presented optimal power oscillation damping (OPOD) controller design using Eigen-Value-Assignment (EAT) with a level of relative stability based on the linearized Phillips-Heffron model of power system installed with SSSC. A two-area power network has been used to demonstrate the capability of the proposed method over a wide range of variations in operating conditions. Juan [60] developed a nonlinear and Multi-Input Multi-Output (MIMO) coordinated model of SSSC and the excitation system of generator, and linearized the nonlinear model by the direct feedback linearization method. The author applied the optimal control theory to design the coordinated nonlinear control scheme between SSSC and the excitation system of the generator to improve power oscillations damping in power system. Chen *et al.* [61] proposed a fuzzy controller to damp power system oscillations by means of series voltage source converter-based FACTS including SSSC. They have been designed devoid of consideration of the interaction between the power loop and DC-link voltage loop.

Ghaisari [62] considered the interactions between the variables and dynamics of the DC-link capacitor voltage. The nonlinear and MIMO model for a SMIB power system employing SSSC is developed. A nonlinear MIMO feedback linearization controller was proposed and used to improve the power oscillations damping in SMIB while maintaining the DC side capacitor voltage constant.

A fuzzy logic based controller for SSSC has been developed to improve transient stability performance of the power system in [63], [64] and for damping power system oscillations in [65]. Ladjavardi and Masoum [66] proposed Genetic Algorithm to optimize the selection of the SSSC based conventional lead-lag damping controller parameters. The objective function based on GA enforces simultaneous improvement of system stability criteria, i.e., damping factor, damping ratio of the eigenvalues, and constraints on the controller parameters. The feedback signal for the damping controller was selected using mode observability. The analysis was conducted on the Phillips-Heffron model of SMIB installed with SSSC. The controller is effective, without deteriorating damping characteristics of other modes in a power system. Haque [67] used the transient energy function (TEF) method to determine the additional damping provided by a SSSC while satisfying the Lyapunov's stability criterion. The proposed control strategy is tested on a SMIB power system with an SSSC. Haque [68] also compared the additional damping provided by STATCOM and SSSC using the TEF method showing better performance of SSSC. However, use of the TEF technique to assess the additional damping provided by various FACTS devices in a multi-machine system especially on the inter-area modes still requires further investigation. Ghaisari [69], developed a multivariable model for a power system installed with a SSSC considering interactions between its variables and power system dynamics. The design of a MIMO PI controller using the diagonal dominance approach was proposed, in addition to DC-link voltage regulation, to sustain power oscillations.

### **2.2.6 Unified Power Flow Controller (UPFC)**

The UPFC is one of the most versatile FACTS controller in a single line transmission system with all encompassing capabilities of voltage regulation, series

compensation and phase shifting. Its main function is to inject a controllable series voltage (controlled magnitude and phase angle with respect to the bus where it is located), thereby modulating the line reactance and controlling both the real and reactive power flow in the transmission line. The UPFC is realized by two VSCs coupled through a DC capacitor. One converter is connected in shunt with the line through a coupling transformer and draws real power from the source and exchanges it to the series converter, i.e., second converter, which is inserted in series with the transmission line through an interface transformer as shown in Figure 2.7 [9], [12]. The power balance between the shunt and series converters is maintained to keep the voltage across the DC link capacitor constant. The UPFC provides effective and efficient power flow control, loop-flow control, enhancement of transient stability, mitigation of low-frequency power system oscillations and voltage (reactive power) regulation. The UPFC is a combination of STATCOM and SSSC which are coupled via a common DC link. The UPFC is able to control the transmission line voltage, impedance and angle or alternatively the real and reactive power in a single line.

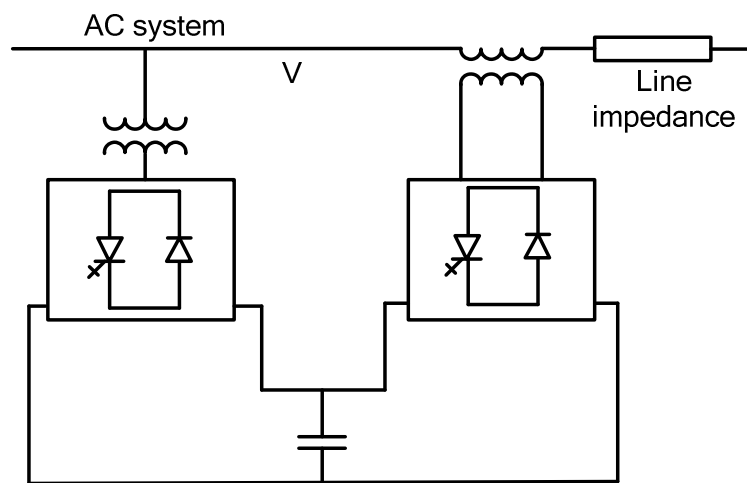


Figure 2.7: Schematic diagram of UPFC

Nabavi-Niaki and Iravani derived the mathematical models of UPFC [70], based on which the Phillips-Heffron model of power system installed with UPFC for an SMIB system and a multi-machine system was developed by Wang [36]-[38]. Wang applied phase compensation method for designing the conventional controller and proposed the criteria for selecting the operating condition of the power system and the input control signal to be superimposed by the UPFC damping function to achieve the

maximum robustness by the damping controller. It has been noted that the damping controller counteracts the negative interaction between the DC link capacitor of the UPFC and the PSS installed in the multi-machine system (three-machine system). Similar results were also presented in [71] and validated by eigenvalue computation and nonlinear simulation. Huang et al. [72] attempted to design a conventional fixed-parameter lead-lag controller for a UPFC installed in the tie-line of a two-area system to damp the inter-area oscillation mode. Tambey and Kothari have presented a comprehensive approach for design of UPFC controllers for a SMIB system [73] and for multi-machine system [74]. Pandey and Singh [75] presented analytical method for selection of the suitable control input signal among the four input signals of UPFC for power oscillation damping (POD) controller utilizing the indices MSV, HSV, direct component of torque (DCT) and residue, for damping of electromechanical modes of oscillation, using the UPFC POD controllers. The damping controllers are designed to produce an electrical torque in phase with the speed deviation. The analysis was performed on a SMIB with variations in loading conditions and was further carried over to two-area system. Eigenvalue analysis technique was used for analyzing oscillatory instability. Chang [76] presented an approach utilizing the root locus method and pole assignment to develop proportional-integral (PI) controller gains for the UPFC control system which included the power flow regulator, shunt current regulator, DC busbar voltage regulator, and AC busbar voltage regulator. The supplementary PI damping controller with integral of active power flow as its input was designed to improve the damping of low-frequency electromechanical mode oscillations.

Abido *et al.* [77] proposed a technique to design simultaneously the UPFC damping controller, the power flow controller and the DC voltage regulator, using the nonlinear model of the power system. Optimization solved with PSO is utilized to design the controllers' parameters settings concurrently. Dhurvey and Chandrakar [78] presented a power oscillation damping controller of the UPFC, whose parameters are optimized by using Nonlinear Control design Block set. The effective control signals for damping oscillations was analyzed by comparing the performance of UPFC in coordination with POD controller and PSS on the linearized SMIB power system installed with UPFC. Chandrakar *et al.* [79] presents a design of PI and RBFN

controllers for the UPFC in SMIB system and multi-machine test system to achieve the increase in line power handling capacity and improvement in transient stability. However, they have not optimized the parameters of POD controller. A Mamdani type fuzzy logic based controller for UPFC was proposed in [80], [81], which was designed based on the linearized Heffron-Philips model of a SMIB power system with UPFC. The fuzzy logic controller was shown to give better damping than the conventional damping controllers. Mok *et al.* [82], [83] designed a fuzzy damping controller for the UPFC where the parameters of the controller are optimized using the gradient descent training method and genetic algorithm. The performance of the fuzzy controller was compared with the conventional controller on a multi-machine interconnected system. A Takagi-Sugeno type nonlinear fuzzy controller was proposed by Mishra *et al.* [84] for UPFC voltage source inverter control for damping inter-area and local mode oscillations in the multi-machine power system. The controller provides variation of control gain and uses linear and nonlinear rules in the subsequent expressions of the fuzzy rule base. However, the initial adjustment of the parameters of the new TS fuzzy controller requires some trial-and-error.

An approach to utilize FACTS controllers to provide a multifunctional power flow management device was proposed in [85]. There are several possibilities of operating configurations by combining two or more converter blocks with flexibility. Among them, there are two operating configurations, namely the Interline Power Flow Controller (IPFC) and the Generalized Unified Power Flow Controller (GUPFC) [15], [85] which are significantly extended to control power flows of multi-lines or a sub-network rather than control power flow of single line. In this thesis the FACTS device IPFC is considered.

### **2.3 Interline Power Flow Controller**

The IPFC, the VSC-based FACTS devices shown in Figure 1.1, was proposed by Gyugyi, Sen and Schauder in 1998 [15]. The IPFC configuration of the Convertible Static Compensator (CSC) was first installed at Marcy 345 kV transmission station by the New York Power Authority (NYPA) [86], [87]. The IPFC consists of two voltage source converters, each of which are coupled in series through transformers to each of

the parallel transmission lines. The modulation index and phase angle of the two voltage source converters can be controlled to inject variable injected voltage into the transmission lines and thus, control the power flow in the lines. The IPFC has more advantage than UPFC since it can control the real and reactive power in more than a single line. The IPFC is thus, used to maximize the use of the existing transmission network and increase power transfer capability.

The controllability of the line power flow and reactive power flow in the transmission lines by IPFC, in the presence of constraints, has been well recognized over the past few years [88]-[95]. However, very limited information is reported concerning the control of the IPFC in providing additional damping during system oscillations.

Modeling of IPFC for power flow analysis has been proposed in references [96]-[99]. The authors present some excellent techniques for power flow modeling of IPFC using the Newton or Newton–Raphson power flow algorithm taking into account the practical operating inequality constraints. The IPFC is modeled as a two controllable series-injected voltage sources with the coupling transformer reactance while including the DC link capacitor dynamics.

Kazemi and Karimi [100] first proposed the dynamic model of the SMIB system with two transmission lines installed with IPFC. The authors established the Phillips–Heffron model of SMIB system integrated with IPFC. The model involves the dynamics of the capacitor. A PI supplementary controller with its input equal to the electrical power of the generator is used to modulate the amplitude modulation ratio of the second voltage source converter. This control action controls the injected voltage in the transmission line in such a way to affect the power transfer such that damping is provided to the power oscillations. Jiang *et al.* [101] discussed the maximum power transfer capability of IPFC under voltage stability condition and also stated that the IPFC can improve small-signal stability by providing damping control supplemental to its regulation control of active power flow in a transmission line. A modal decomposition approach was proposed to determine input signals to the regulator from locally measured signals, including bus voltages, line currents, and line flows based on two indices, i.e., Maximum Damping Influence (MDI) Index, and

Controllability and Observability Gain Product Index. Chen *et al.* [102] proposed a PID controller for oscillation damping enhancement in a SMIB test system.

## 2.4 Discussion

Considerable amount of research has been done in the field of FACTS, where steady-state and dynamic models of the FACTS devices (SVC, TCSC, TCPS, STATCOM, SSSC and UPFC) have been developed [9], [11]. Modeling of the modified linearized Heffron-Phillips models for SMIB system and multi-machine systems installed with various FACTS devices were utilized to design the controllers for enhancing power system stability. Controllers designed using the conventional phase compensation and various other techniques have been discussed and validated by nonlinear simulation. However, very little literature exists with reference to IPFC, being a relatively new device; problems associated with damping of oscillations using IPFC have not been investigated thoroughly.

Stability analysis of power systems with IPFC and design of the IPFC based controller for damping the oscillations require proper modeling of IPFC. This includes both load flow or steady state model and dynamic models. Load flow models are necessary as they form the backbone for any power system dynamic simulations. It is also considered as the essential for power system network calculations. The calculations are required for steady state analysis and dynamic performance of the power systems. Dynamic models are required to capture the interaction between the two series inverters of the IPFC and the system, therefore providing information that would aid in the design of the IPFC based controller. With a proper load flow and dynamic model for IPFC, the impact of IPFC based controllers on power system stability can be analyzed. The power flow model proposed by Zhang [97], [98] is taken into consideration for conducting the load flow studies in this thesis.

The dynamic model of the IPFC with the SMIB power system was proposed in [100]. The injected voltage is shown to be a function of the control signals of IPFC. Accordingly the magnitude and phase angle of the voltage injected are controlled by modulating the control inputs signals of IPFC. However the dynamic model of SMIB

installed with IPFC developed by the authors contains only **one** of the four control inputs of the IPFC. The state space model does not involve the effects of other inputs of the IPFC. Literature survey indicates lack of studies concerning the dynamic modelling of the IPFC in multi-machine system for small signal stability studies.

Regarding the control aspect of IPFC to dampen the power system oscillations, a PI controller was considered in [100] for a SMIB power system: however, the amount of damping introduced by the controller was not investigated through eigenvalue analysis. The modal decomposition method for designing the controller proposed in [101] was on a multi-machine power system, however, it was not equipped with IPFC. The PID controller proposed in [102] is not effective due to the complexity and nonlinearity of the power system and the performance of the damping controller is degraded to a certain extent as stated by the authors.

Motivated by the discussions and literature review in the previous sections, the issues concerning the deficient modeling of IPFC for small signal stability studies are addressed. Appropriate control strategies are devised to dampen the power system oscillations by the IPFC based controller.

## **2.5 Summary**

In the literature survey, a brief review of modeling and control design of various FACTS devices has been conducted. Damping effects of PSS and FACTS controllers designed by phase compensation, and various other methods have been discussed. However, it is found that investigations into modeling of IPFC and damping function of IPFC are limited. Considering these aspects, this research focuses on developing the mathematical models of IPFC incorporated into the power system and studying its control functions. This would be discussed in the next chapter.

## CHAPTER 3

### MODELING OF INTERLINE POWER FLOW CONTROLLER

#### **3.1 Introduction**

The IPFC is installed in the power system to provide comprehensive compensation for real and reactive power flows for some selected transmission lines at a given substation. To examine the stability of the power system when the IPFC is incorporated into a network with transmission lines and generators, an appropriate model is necessary. This includes the steady state model and dynamic model of the IPFC. The steady state model is required to conduct the load flow to obtain initial operating conditions, which is essential for small signal stability studies, whilst the dynamic model of the IPFC is utilized to incorporate it within the power system model and investigate the dynamic stability performance of the overall power system. This chapter presents both steady state and dynamic models of the IPFC.

#### **3.2 Steady State Model**

In general form, the IPFC constitutes of number of VSC's where each one of them is linked together through their DC terminals. Each VSC provides compensation, for a dedicated line with which it is connected in series, as shown in the Figure 3.1 [15]. This configuration facilitates real power compensation from the under utilized transmission lines to the overloaded transmission lines provided that the overall power is balanced at the DC terminal. A basic IPFC scheme under consideration is shown in Figure 3.2 [97], which consists of two back-to-back DC-to-AC converters connected in series with two transmission lines through the transformers. Each VSC injects a series compensating voltage with controllable magnitude and phase angle at the fundamental frequency. The real power is exchanged through the DC link between

the two compensating voltage sources. The IPFC is installed into the network between the buses,  $i - j$ , and  $i - k$  in line 1 and 2 respectively as shown in Figure 3.2.

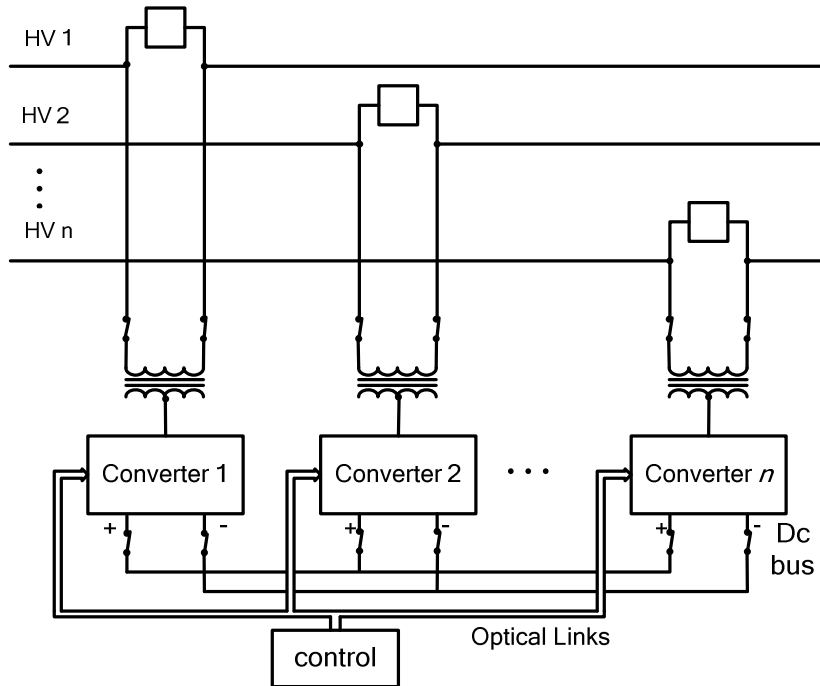


Figure 3.1: IPFC employing  $n$  converters

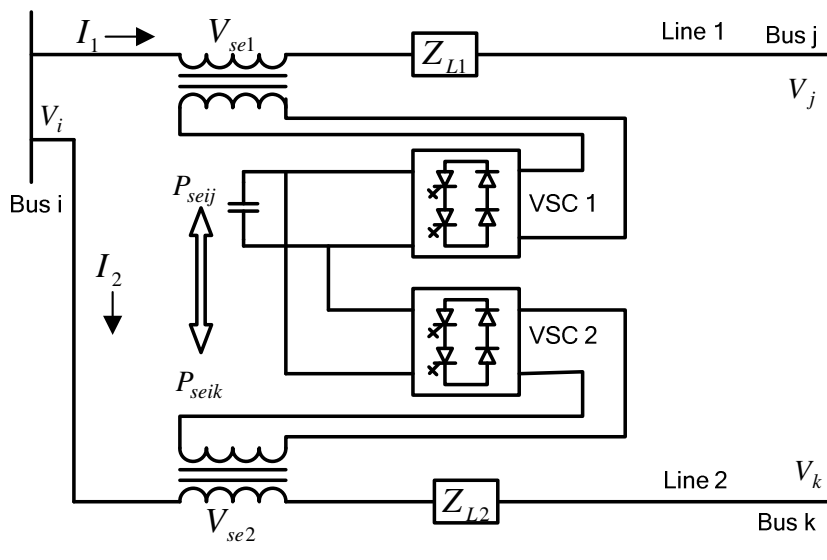


Figure 3.2: Basic two-converter IPFC

The two SVS's with phasors  $V_{se1}$  and  $V_{se2}$  in series with transmission lines 1 and 2 represent the output voltages of two back-to-back DC-to-AC inverters. It can be seen that the sending ends of the two transmission lines are series-connected with the IPFC buses  $j$  and  $k$ , respectively. Transmission line 1 between buses  $i$  and  $j$ , represented by impedance,  $Z_{L1}$ , has a sending-end bus with voltage phasor  $V_i$  and a receiving-end bus with voltage phasor  $V_j$ . The receiving-end voltage phasor of line 2 between buses  $i$  and  $k$ , represented by impedance,  $Z_{L2}$ , is  $V_k$ . The common DC link is represented by a bidirectional link ( $P_{seij} = -P_{seik}$ ) for real power exchange between the two voltage sources. The phasor diagram of the transmission line 1 given in Figure 3.3, shows the relationship between the sending end phasor ' $V_i$ ', receiving end phasor ' $V_j$ ', the voltage phasor across  $Z_{L1}$  ' $V_{ZL1}$ ', and the inserted voltage phasor ' $V_{se1}$ ' with controllable magnitude and varying phase angle [12], [15].

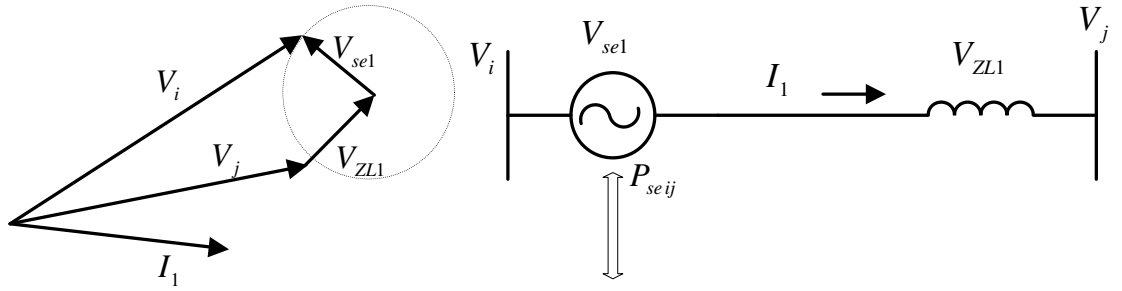


Figure 3.3: The phasor diagram for transmission line 1

The transmission line 1 is arbitrarily chosen to be the primary line for which it is stipulated to have free controllability of both real and reactive line power flow. Line 2 will be the secondary system. The injection of  $V_{se1}$  on line 1 usually results in an exchange of real power  $P_{seij}$  and reactive power  $Q_{seij}$  between converter VSC-1 and the line 1. To establish the transmission relationships, the injected voltage phasor  $V_{se1}$  is decomposed into two components, one  $V_{se1qI}$  in quadrature and second  $V_{se1pI}$  in phase with the line current [12]. The scalar products of these components with the line current give the reactive power  $Q_{seij} = V_{se1qI}I_1$  and real power  $P_{seij} = V_{se1pI}I_1$ . The reactive power  $Q_{seij}$  is generated internally by VSC-1, and provides series reactive compensation for line 1. The real power  $P_{seij}$  gives real power compensation.

However, the real power is attained from the second line through the series-connected VSC-2. Therefore, to satisfy the active power demand of VSC-1, the converter in second line must supply the real power demanded by VSC-1 from line 2, through the common DC link. The VSC-2 injects the series voltage  $V_{se2}$  so as to satisfy the real power demand of VSC-1. Thus, the relationship  $P_{seij} + P_{seik} = 0$  must be satisfied continuously, i.e., the sum of the exchange of real power within the lines should be zero when the converter circuit's losses are ignored. This condition will be fulfilled by controlling VSC-2 to maintain the voltage of the common DC link constant, in the event of varying real power demand. Apparently it is clear that in the primary transmission line controllability of the real and reactive power flow is possible. While in the secondary transmission line, only the real power flow can be controlled within the limits defined by reactive compensation available, whereas the prevailing reactive power will be affected by the real power demand of the primary transmission line. Evidently one degree of freedom is taken from VSC-2. Thus, the operation of VSC-2 is to regulate the DC link voltage by controlling the real component of the injected voltage phasor  $V_{se2}$  and also to control the real power transfer in secondary transmission line by regulating the quadrature component of the injected voltage phasor. Thus, IPFC can control: two independent active and reactive power flows of branch  $i - j$  and one independent active power flow of branch  $i - k$ . In this condition the primary transmission line will have priority over the secondary transmission line in achieving its set-point requirements.

### 3.2.1 Load Flow Equations

The power system network is represented by a set of nonlinear equations. To determine the steady state condition of the power system, power flow is performed to determine the complex voltages and angles at all buses of the network at steady state. From this information the active and reactive power flowing through every transmission line and transformer are computed. Thus, the power flow or the load flow studies establish the operating point or the equilibrium point of the power system about which the nonlinear differential equations are linearized. The nonlinear equations are linearized on the assumption that the disturbance propagated through

the study system is sufficiently small. The basic formulation for power flow is demonstrated through Figure 3.4 [14]. It is a one-line diagram representation of the branches ( $k = 1, \dots, j, \dots, m$ ) connected to bus  $i$ . The voltages  $\bar{V}_i$  and  $\bar{V}_j$  are the voltages of the buses  $i$  and  $j$ ,  $\bar{Z}_{ij}$  is the transmission line impedance between bus  $i$  and  $j$ . The admittance is represented by  $\bar{Y}_{ij} = \frac{1}{\bar{Z}_{ij}} = g_{ij} + j b_{ij}$  and the voltage at bus  $i$  can be represented as  $\bar{V}_i = V_i e^{j\theta_i} = V_i (\cos \theta_i + j \sin \theta_i)$ . The active and reactive power injected by the generator at bus  $i$ , is represented by  $P_{Gi}$  and  $Q_{Gi}$ .  $P_{Li}$  and  $Q_{Li}$  represent the active and reactive powers drawn by a load at bus  $i$ , respectively. The transmitted active and reactive powers from bus  $i$  to other buses ( $k = 1, \dots, j, \dots, m$ ) are denoted by  $P_i^k$  and  $Q_i^k$  respectively.

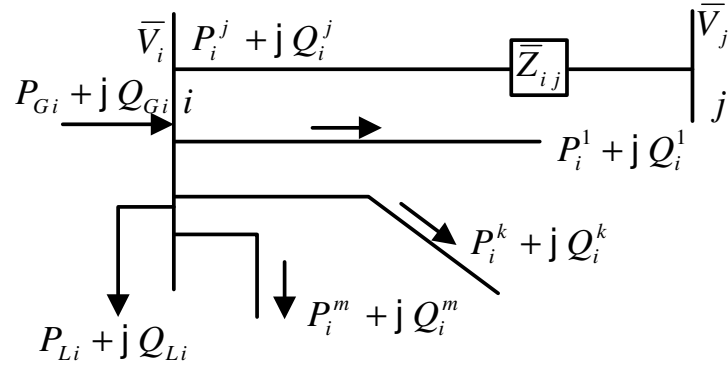


Figure 3.4: Power balance at bus  $i$  for active and reactive power

Based on the Kirchhoff's laws the real and reactive power flow equations for the transmission line element  $i - j$  can be written as [14]:

$$\begin{aligned}
 P_i^j &= V_i^2 g_{ii} + V_i V_j [g_{ij} \cos(\theta_i - \theta_j) + b_{ij} \sin(\theta_i - \theta_j)] \\
 Q_i^j &= -V_i^2 b_{ii} + V_i V_j [g_{ij} \sin(\theta_i - \theta_j) - b_{ij} \cos(\theta_i - \theta_j)]
 \end{aligned}
 \tag{3.1}$$

Equation (3.1) represents the real and reactive powers ( $P_i^j$  and  $Q_i^j$ ) transmitted from bus  $i$  to bus  $j$  through the transmission element. The powers  $P_i^j$  and  $Q_i^j$  are functions of the bus voltages and network admittances.

The net power flow flowing out of the bus  $i$  is the summation of the power flow in each one of the transmission elements connecting bus  $i$  to the other buses ( $k = 1, \dots, j, \dots, m$ ) or to the load. As a result the net active and reactive transmitted powers at bus  $i$  are:

$$\begin{aligned} P_i &= \sum_{k=1}^m P_i^k \\ Q_i &= \sum_{k=1}^m Q_i^k \end{aligned} \quad (3.2)$$

In power flow analysis at each bus, the generated power, load power and power exchanged through the transmission elements connecting to the bus must be zero. This is demonstrated in Figure 3.4 for active and reactive power flow [14]. The injected powers into the bus are taken to be positive and powers leaving the bus are taken to be negative. Thus:

$$\begin{aligned} \Delta P_i &= P_{Gi} - P_{Li} - \sum_{k=1}^m P_i^k = 0 \\ \Delta Q_i &= Q_{Gi} - Q_{Li} - \sum_{k=1}^m Q_i^k = 0 \end{aligned} \quad (3.3)$$

Equations (3.3) are also termed as mismatch power equations. The terms  $\Delta P_i$  and  $\Delta Q_i$  are the mismatch active and reactive power at bus  $i$ , respectively. Each bus is described by four variables, net active power  $P_i$ , net reactive power  $Q_i$ , voltage magnitude  $V_i$ , and voltage phase angle  $\theta_i$ . Two out of the four variables are specified in order to solve Equations (3.3) for each bus. The buses can be classified into the following categories:

**Slack bus:** At a slack bus, the specified quantities are the voltage magnitude and angle whilst the unknown quantities are the active and reactive power injections. The voltage angle of the slack bus is taken as the reference for the angles of all other buses. There is only one slack bus as reference.

**PV Bus:** At a PV bus, the specified quantities are the active power injection and voltage magnitude whilst the unknown quantities are voltage angle and reactive

power injection. Usually buses connected to generators and synchronous condensers are considered as PV buses. For a practical interconnected power system, there may be one or more PV buses.

**PQ Bus:** At a PQ bus, the specified quantities are the active and reactive power injections while the unknown quantities are the voltage magnitude and angle at the bus. Usually a non-generator bus or load bus is considered as a PQ bus. The number of PV or PQ buses depends on the system planner.

Various power flow solution methods have been proposed such as Gauss method, Gauss-Seidel method, decoupled Newton power flow method, Newton-Raphson methods and etc [14]. Among these methods, the Newton-Raphson method has been considered as the efficient power flow solution technique for solving large systems of nonlinear equations [14]. It is an iterative method starting with a reasonable guess for a solution, where the solution represents numerical values of the all the unknown variables. This algorithm verifies how near the solution is; if not, it updates the solution in a direction to improve it. This process is repeated until the verification is satisfied. The following section briefly describes the Newton-Raphson load flow technique.

### 3.2.2 Newton-Raphson Method

The Newton-Raphson approach uses iterative method to solve the set of nonlinear algebraic equations [14]:

$$\left. \begin{array}{l} f_1(x_1, x_2, \dots, x_n) = 0 \\ f_2(x_1, x_2, \dots, x_n) = 0 \\ \vdots \\ f_n(x_1, x_2, \dots, x_n) = 0 \end{array} \right\}, \text{or } \mathbf{F}(\mathbf{X}) = \mathbf{0} \quad (3.4)$$

where  $\mathbf{F}$  represents a set of  $n$  nonlinear equations and  $\mathbf{X}$  is a vector of  $n$  unknown state variables. The method determines the vector of state variables  $\mathbf{X}$  by performing a Taylor series expansion of  $\mathbf{F}(\mathbf{X})$  about the initial estimate  $\mathbf{X}^{(0)}$  neglecting the higher order terms.

$$\mathbf{F}(\mathbf{X}) = \mathbf{F}(\mathbf{X}^{(0)}) + \mathbf{J}(\mathbf{X}^{(0)})(\mathbf{X} - \mathbf{X}^{(0)}) \quad (3.5)$$

where,  $\mathbf{J}(\mathbf{X}^{(0)})$  is the Jacobian matrix. It is a matrix of first-order partial derivatives of  $\mathbf{F}(\mathbf{X})$  with respect to  $\mathbf{X}$  evaluated at  $\mathbf{X} = \mathbf{X}^{(0)}$ . The state vector  $\mathbf{X}$  is calculated from Equation (3.5) assuming that  $\mathbf{X}^{(1)}$  is the value computed by the algorithm at iteration 1 and it is near to the initial estimate  $\mathbf{X}^{(0)}$ . Equation (3.5) can be expanded as follows:

$$\underbrace{\begin{bmatrix} f_1(\mathbf{X}^{(1)}) \\ f_2(\mathbf{X}^{(1)}) \\ \vdots \\ f_n(\mathbf{X}^{(1)}) \end{bmatrix}}_{\mathbf{F}(\mathbf{X}^{(1)})} \approx \underbrace{\begin{bmatrix} f_1(\mathbf{X}^{(0)}) \\ f_2(\mathbf{X}^{(0)}) \\ \vdots \\ f_n(\mathbf{X}^{(0)}) \end{bmatrix}}_{\mathbf{F}(\mathbf{X}^{(0)})} + \underbrace{\begin{bmatrix} \frac{\partial f_1(\mathbf{X})}{\partial x_1} & \frac{\partial f_1(\mathbf{X})}{\partial x_2} & \dots & \frac{\partial f_1(\mathbf{X})}{\partial x_n} \\ \frac{\partial f_2(\mathbf{X})}{\partial x_1} & \frac{\partial f_2(\mathbf{X})}{\partial x_2} & \dots & \frac{\partial f_2(\mathbf{X})}{\partial x_n} \\ \vdots & \vdots & \ddots & \vdots \\ \frac{\partial f_n(\mathbf{X})}{\partial x_1} & \frac{\partial f_n(\mathbf{X})}{\partial x_2} & \dots & \frac{\partial f_n(\mathbf{X})}{\partial x_n} \end{bmatrix}}_{\mathbf{J}(\mathbf{X}^{(0)})} \bigg|_{\mathbf{X}=\mathbf{X}^{(0)}} \underbrace{\begin{bmatrix} X_1^{(1)} - X_1^{(0)} \\ X_2^{(1)} - X_2^{(0)} \\ \vdots \\ X_n^{(1)} - X_n^{(0)} \end{bmatrix}}_{\mathbf{X}^{(1)} - \mathbf{X}^{(0)}} \quad (3.6)$$

In general, the above equation (3.6) can be expressed for the  $it^{th}$  iteration as:

$$\mathbf{F}(\mathbf{X}^{(it)}) = \mathbf{F}(\mathbf{X}^{(it-1)}) + \mathbf{J}(\mathbf{X}^{(it-1)})(\mathbf{X}^{(it)} - \mathbf{X}^{(it-1)}), \quad i = 1, 2, \dots \quad (3.7)$$

If  $\mathbf{X}^{(it)}$  is assumed to be sufficiently close to the solution  $\mathbf{X}^{(*)}$ , then  $\mathbf{F}(\mathbf{X}^{(it)}) \approx \mathbf{F}(\mathbf{X}^{(*)}) = 0$ , henceforth Equation (3.7) becomes,

$$\mathbf{F}(\mathbf{X}^{(it-1)}) + \mathbf{J}(\mathbf{X}^{(it-1)})(\mathbf{X}^{(it)} - \mathbf{X}^{(it-1)}) = 0 \quad (3.8)$$

and, solving for  $\mathbf{X}^{(it)}$  from Equation (3.8) gives;

$$\mathbf{X}^{(it)} = \mathbf{X}^{(it-1)} - \mathbf{J}^{-1}(\mathbf{X}^{(it-1)})\mathbf{F}(\mathbf{X}^{(it-1)}) \quad (3.9)$$

The iterative solution can be expressed as a function of the correction vector  $\Delta\mathbf{X}^{(it)} = \mathbf{X}^{(it)} - \mathbf{X}^{(it-1)}$ , where

$$\Delta\mathbf{X}^{(it)} = -\mathbf{J}^{-1}(\mathbf{X}^{(it-1)})\mathbf{F}(\mathbf{X}^{(it-1)}) \quad (3.10)$$

The initial estimates are updated using;

$$\Delta \mathbf{X}^{(it)} = \mathbf{X}^{(it-1)} + \Delta \mathbf{X}^{(it)} \quad (3.11)$$

This process is repeated until the mismatches  $\Delta \mathbf{X}$  are within a prescribed tolerance (i.e.,  $10^{-12}$ ). Thus, in the power flow problem, the state vector constitutes the unknown bus voltage phase angles  $(\boldsymbol{\theta}) = [\theta_2, \dots, \theta_{nb}]$  and magnitudes  $(\mathbf{V}) = [V_1, \dots, V_{nb}]$ . The initial estimates  $(\boldsymbol{\theta}^{(0)}, \mathbf{V}^{(0)})$  are updated using the following relation:

$$\begin{aligned} \begin{bmatrix} \boldsymbol{\theta} \\ \mathbf{V} \end{bmatrix}^{(it)} &= \begin{bmatrix} \boldsymbol{\theta} \\ \mathbf{V} \end{bmatrix}^{(it-1)} + \underbrace{\begin{bmatrix} \Delta \boldsymbol{\theta} \\ \Delta \mathbf{V} \end{bmatrix}^{(it)}}_{\Delta \mathbf{X}^{(it)}} \\ \Rightarrow \begin{bmatrix} \boldsymbol{\theta} \\ \mathbf{V} \end{bmatrix}^{(it)} &= \begin{bmatrix} \boldsymbol{\theta} \\ \mathbf{V} \end{bmatrix}^{(it-1)} - \underbrace{\begin{bmatrix} \frac{\partial \mathbf{P}}{\partial \boldsymbol{\theta}} & \frac{\partial \mathbf{P}}{\partial \mathbf{V}} \\ \frac{\partial \mathbf{Q}}{\partial \boldsymbol{\theta}} & \frac{\partial \mathbf{Q}}{\partial \mathbf{V}} \end{bmatrix}^{-1}}_{\mathbf{J}^{-1}(\mathbf{X}^{(it-1)})} \underbrace{\begin{bmatrix} \Delta \mathbf{P} \\ \Delta \mathbf{Q} \end{bmatrix}}_{\mathbf{F}(\mathbf{X}^{(it-1)})} \\ & \quad \underbrace{\hspace{10em}}_{\Delta \mathbf{X}^{(it)}} \end{aligned} \quad (3.12)$$

where,  $\Delta \mathbf{P}$  and  $\Delta \mathbf{Q}$  are the mismatch equations. The various matrices in Jacobian may consist of up to  $(nb - 1) \times (nb - 1)$  elements of the form

$$\left. \begin{array}{l} \frac{\partial P_i}{\partial \theta_j}, \frac{\partial P_i}{\partial V_j} \\ \frac{\partial Q_i}{\partial \theta_j}, \frac{\partial Q_i}{\partial V_j} \end{array} \right\} \begin{array}{l} i = 1, \dots, nb - 1 \\ j = 1, \dots, nb - 1 \end{array} \quad (3.13)$$

where  $nb$  is the number of buses. The slack bus entries are omitted in the Jacobian matrix. The rows and columns corresponding to reactive power and voltage magnitude for PV buses are omitted. When buses  $i$  and  $j$  are not directly linked by a transmission element, the corresponding  $i - j$  entry in the Jacobian matrix is null. The power flow solution is started initially with a flat start, i.e., the voltage magnitudes are selected to be 1 p.u. at all PQ buses and voltage phase angles are set to be 0 at all buses. The calculation of Equation (3.12) is repeated until the mismatches are within a

prescribed small tolerance. The result gives the voltage magnitudes and phase angles at each bus and correspondingly the power flows in the transmission lines can be calculated.

When the IPFC is incorporated into the system, the necessary modifications in power flow equations are carried out for the concerned IPFC buses to integrate the IPFC into power flow and obtain the solution when this FACTS device is present in the system. This is explained in the following section.

### 3.2.3 The Power Flow Equations Including IPFC

The equivalent circuit of the IPFC in steady state is shown in Figure 3.5 [97], [98] consisting of two voltage sources in series with the two transmission lines via the transformers and linked together by DC link. The IPFC is installed between buses  $i - j$  and  $i - k$ . Each VSC injects a series voltage  $\bar{V}_{sep} = V_{sep} \angle \theta_p$  ( $p = 1, 2$ ) to provide series compensation to the respective transmission line.  $V_{sep}$  is the magnitude and  $\theta_p$  is the phase angle of  $\bar{V}_{sep}$  ( $p = 1, 2$ ) respectively. The transformer is represented by impedance  $Z_{tp}$ , ( $p = 1, 2$ ) on the two transmission lines. The total impedance of the transmission line between bus  $i$  and bus  $j$  is represented by  $\bar{Z}_{seij}$ , where  $\bar{Z}_{seij} = Z_{L1} + Z_{t1}$ ,  $Z_{L1}$  being the line impedance of the line 1 of the IPFC branches. Similarly  $\bar{Z}_{seik} = Z_{L2} + Z_{t2}$ , represents the total impedance of line 2 (i.e., between bus  $i$  and bus  $k$ ).

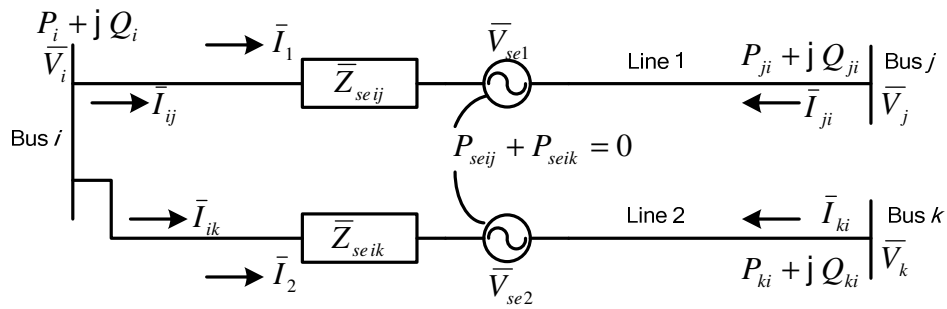


Figure 3.5: Equivalent circuit of IPFC

In Figure 3.5,  $\bar{V}_i = V_i \angle \theta_i$ ,  $\bar{V}_j = V_j \angle \theta_j$ , and  $\bar{V}_k = V_k \angle \theta_k$  are the voltages of the buses  $i, j$  and  $k$ , respectively with  $V_l$  and  $\theta_l$  being the magnitude and phase angle of  $\bar{V}_l$  ( $l = i, j, k$ ).

$P_i, Q_i$  are the sum of the active and reactive power flows leaving the bus  $i$ .  $P_{ji}, Q_{ji}$  are the active and reactive power flows of the IPFC branch leaving the bus  $j$ .  $P_{ki}, Q_{ki}$  are the IPFC branch active and reactive power flows leaving the bus  $k$ .  $\bar{I}_{ij}$  and  $\bar{I}_{ik}$  are the IPFC branch currents of branch  $i - j$  and  $i - k$  leaving bus  $i$ .  $\bar{I}_{ji}$  and  $\bar{I}_{ki}$  are the IPFC branch currents of branch  $j - i$  and  $k - i$  leaving bus  $j$  and  $k$  respectively.  $\bar{I}_{ij}$  is also represented by  $\bar{I}_1$  to indicate the current flowing through the VSC-1 in transmission line 1 of the IPFC branches. Similarly,  $\bar{I}_{ik} = \bar{I}_2$ , the current flowing through VSC-2, in the second transmission line.  $P_{sein}, (n = j, k)$ , is the active power exchange of each converter.

The real power is exchanged between the series converters via the common DC link while the sum of real power exchange at the DC terminal should be balanced. The losses associated with the IPFC operation are ignored and, hence, it neither absorbs nor injects real power with respect to the system during steady-state operation. Thus, total real power injected to the power system by the two voltage sources is equal to zero at steady-state,  $P_{seij} + P_{seik} = 0$ . Physical interpretation of this statement is that the voltage of the DC link capacitor remains constant at the pre-specified value  $v_{dc}$ . The Newton Raphson technique is used to solve the power system load flow to determine the unknown variables which now includes the IPFC variables, i.e.,  $V_{sep}, \theta_p$  ( $p = 1, 2$ ). Buses  $i, j$  and  $k$  are considered to be load buses unless there are PV buses in the load flow analysis. The power flow equations at bus  $i$  can be derived as follows [97]:

The current flowing away from the bus  $i$  is

$$\bar{I}_i = \bar{I}_{ij} + \bar{I}_{ik} \quad (3.14)$$

$$\begin{aligned}
\Rightarrow \bar{I}_i &= \frac{\bar{V}_i - \bar{V}_{se1} - \bar{V}_j}{\bar{Z}_{seij}} + \frac{\bar{V}_i - \bar{V}_{se2} - \bar{V}_k}{\bar{Z}_{seik}} \\
&= (\bar{V}_i - \bar{V}_{se1} - \bar{V}_j)\bar{Y}_{seij} + (\bar{V}_i - \bar{V}_{se2} - \bar{V}_k)\bar{Y}_{seik} \\
&= (\bar{V}_i - \bar{V}_{se1} - \bar{V}_j)(g_{ij} + j b_{ij}) + (\bar{V}_i - \bar{V}_{se2} - \bar{V}_k)(g_{ik} + j b_{ik})
\end{aligned} \tag{3.15}$$

where,  $\bar{Y}_{sein} = \frac{1}{\bar{Z}_{sein}} = g_{in} + j b_{in}$ ,  $n = j, k$

The complex power at bus  $i$  is:

$$S_i = \bar{V}_i \bar{I}_i^* = P_i + j Q_i, \text{ where, } \bar{I}_i^* \text{ is the complex conjugate of } \bar{I}_i. \tag{3.16}$$

Substituting  $\bar{I}_i$  from (3.15) into the complex power Equation (3.16), and separating the real and imaginary parts, the power flows at bus  $i$   $P_i$  and  $Q_i$  are obtained as follows:

$$\begin{aligned}
P_i &= V_i^2 g_{ii} - \sum_{n=j,k} V_i V_n (g_{in} \cos(\theta_i - \theta_n) + b_{in} \sin(\theta_i - \theta_n)) \\
&\quad - \sum_{n=j,k} V_i V_{sep} (g_{in} \cos(\theta_i - \theta_p) + b_{in} \sin(\theta_i - \theta_p))
\end{aligned} \tag{3.17}$$

$$\begin{aligned}
Q_i &= -V_i^2 b_{ii} - \sum_{n=j,k} V_i V_n (g_{in} \sin(\theta_i - \theta_n) - b_{in} \cos(\theta_i - \theta_n)) \\
&\quad - \sum_{n=j,k} V_i V_{sep} (g_{in} \sin(\theta_i - \theta_p) - b_{in} \cos(\theta_i - \theta_p))
\end{aligned} \tag{3.18}$$

where  $g_{ii} = \sum_{n=j,k} g_{in}$        $b_{ii} = \sum_{n=j,k} b_{in}$       and       $p = 1, 2$

Similarly the active and reactive power flows of the IPFC branch  $n - i$  leaving bus ( $n = j, k$ ), are given as,

$$\left. \begin{aligned} P_{ni} &= \text{Re}(\bar{V}_n \bar{I}_{ni}^*) \\ Q_{ni} &= \text{Im}(\bar{V}_n \bar{I}_{ni}^*) \end{aligned} \right\} n = j, k \tag{3.19}$$

which can be written as,

$$P_{ni} = V_n^2 g_{nn} - V_i V_n (g_{in} \cos(\theta_n - \theta_i) + b_{in} \sin(\theta_n - \theta_i)) \\ + V_n V_{sep} (g_{in} \cos(\theta_n - \theta_p) + b_{in} \sin(\theta_n - \theta_p)) \quad (3.20)$$

$$Q_{ni} = -V_n^2 b_{nn} - V_i V_n (g_{in} \sin(\theta_n - \theta_i) - b_{in} \cos(\theta_n - \theta_i)) \\ + V_n V_{sep} (g_{in} \sin(\theta_n - \theta_p) - b_{in} \cos(\theta_n - \theta_p)) \quad (3.21)$$

where  $g_{in} = g_{nn} = \text{Re}[1/\bar{Z}_{sein}]$ ,  $b_{in} = b_{nn} = \text{Im}[1/\bar{Z}_{sein}]$ ,  $n = j, k$ ,  $p = 1, 2$

For the IPFC, the power mismatches at buses  $i, j, k$  should hold

$$\Delta P_l = P_{Gl} - P_{Ll} - P_l = 0 \quad (3.22)$$

$$\Delta Q_l = Q_{Gl} - Q_{Ll} - Q_l = 0 \quad (3.23)$$

where,  $P_{Gl}$ ,  $Q_{Gl}$  ( $l = i, j, k$ ) are the real and reactive power generation entering the bus  $l$  ( $l = i, j, k$ ) respectively.  $P_{Ll}$ ,  $Q_{Ll}$  ( $l = i, j, k$ ) are the real and reactive power load at bus  $l$  respectively.  $P_l$  and  $Q_l$  ( $l = i, j, k$ ) are the sum of real and reactive power flows of the lines connected to bus  $l$ , respectively, which includes the IPFC branches flows. The power flow Equations (3.17-3.21) for the FACTS branches should be taken into account in the calculations of  $P_l$  and  $Q_l$ . According to the operating principles of the IPFC, the operating constraint representing the active power exchange between the series converters via a common DC link assuming the converters are lossless is expressed by Equation (3.24) which also ensure the constancy of DC link capacitor voltage.

$$PE = \sum_{n=j,k} P_{sein} = 0 \quad (3.24)$$

where  $P_{sein}$  ( $n = j, k$ ), in Equation (3.24) is the real power exchanged with the transmission lines by each series VSC's,  $P_{seij} = \text{Re}(\bar{V}_{se1} \bar{I}_{ji}^*)$ , is the real power exchanged by VSC-1 with transmission line  $i - j$ .  $P_{seik} = \text{Re}(\bar{V}_{se2} \bar{I}_{ki}^*)$  is the real power exchanged by VSC-2 with transmission line  $i - k$ .

The sum of the exchanged real powers ‘PE’ should be zero as to ensure the real powers exchanged are balanced.  $\bar{I}_{ni}^*$  is the conjugate of  $\bar{I}_{ni}$ , where  $(n = j, k)$ . Therefore, the equations for  $P_{sein}$  ( $n = j, k$ ), are as follows:

$$P_{sein} = \text{Re} \left[ \bar{V}_{sep} \times \left( \frac{\bar{V}_n + \bar{V}_{se1} - \bar{V}_i}{\bar{Z}_{sein}} \right)^* \right]$$

$$p = 1, 2$$

$$= \text{Re} \{ \bar{V}_{sep} [(\bar{V}_n + \bar{V}_{se1} - \bar{V}_i)(g_{in} + j b_{in})]^* \}$$

The real power exchanged  $P_{sein}$  ( $n = j, k$ ) can be written as:

$$P_{sein} = V_{sep}^2 g_{in} - V_{sep} V_i (\cos(\theta_p - \theta_i) g_{in} + b_{in} \sin(\theta_p - \theta_i))$$

$$+ V_{sep} V_n (\cos(\theta_p - \theta_n) g_{in} + b_{in} \sin(\theta_p - \theta_n)) \quad p = 1, 2 \quad (3.25)$$

The IPFC can control active power flow,  $P_{ji}$ , and reactive power flow,  $Q_{ji}$ , at the receiving end bus  $j$  to the reference set points  $P_{ji}^{Spec}$  and  $Q_{ji}^{Spec}$  in the primary line 1, and only the active power flow  $P_{ki}$  to the set point  $P_{ki}^{Spec}$  on the secondary line 2. Therefore, the control constraints of IPFC in the two lines are represented as follows:

$$P_{ji} - P_{ji}^{Spec} = 0 \quad (3.26)$$

$$Q_{ji} - Q_{ji}^{Spec} = 0$$

$$P_{ki} - P_{ki}^{Spec} = 0 \quad (3.27)$$

where  $P_{ji}^{Spec}$  and  $Q_{ji}^{Spec}$  are the specified active and reactive set points of the line 1 and  $P_{ki}^{Spec}$  is the specified active set point of the line 2 respectively.

### ***Constraints of IPFC operation:***

The IPFC operation is subject to following constraints [11], [97], [98]:

- a) The controllable injected voltage's magnitude and angle of each VSC is constrained by:

$$V_{sep}^{min} \leq V_{sep} \leq V_{sep}^{max}, p = 1,2$$

$$-\pi \leq \theta_p \leq \pi, p = 1,2$$

where  $V_{sep}^{min}$  and  $V_{sep}^{max}$  are maximum and minimum voltage limits of the series converter. The phase angle of the injected voltage  $\theta_p$  can be controlled over a full revolution.

- b) The current flowing through each VSC should be within its current rating

$$I_{ni} \leq I_{ni}^{max}, n = j, k,$$

where,  $I_{ni}^{max}$  is the current rating of the series converter at which level it can operate continuously.

- c) The active power exchanged between the two VSCs via the DC link is constrained by

$$-P_{sein}^{max} \leq P_{sein} \leq P_{sein}^{max}, n = j, k,$$

where,  $P_{sein}^{max}$  is the maximum limit of the VSC equipment rating for active power exchange between the series converter and the DC link.

### ***Initialization of IPFC variables***

The initial values of IPFC variables,  $V_{sep}, \theta_p$  ( $p=1,2$ ), can be obtained from Equation (3.26) and Equation (3.27), while setting bus voltages  $V_i = V_j = V_k = 1.0$ , if buses  $i, j, k$  are not voltage controlled buses and  $\theta_i = \theta_j = \theta_k = 0$  [98].

In the primary line 1, i.e., the  $i - j$  branch, the IPFC can control both real and reactive power flow, henceforth from Equation (3.26):

$$P_{ji} - P_{ji}^{Spec} = 0 \text{ and } Q_{ji} - Q_{ji}^{Spec} = 0 \quad (3.28)$$

Substituting Equation (3.20) and Equation (3.21) for,  $n = j$ , in Equation (3.28) and setting  $\theta_i = \theta_j = \theta_k = 0$  the following equations are obtained:

$$V_j^2 g_{jj} - V_i V_j g_{ij} + V_j V_{se1} (g_{ij} \cos \theta_1 - b_{ij} \sin \theta_1) - P_{ji}^{Spec} = 0 \quad (3.29)$$

$$-V_j^2 b_{jj} + V_i V_j b_{ij} - V_j V_{se1} (g_{ij} \sin \theta_1 + b_{ij} \cos \theta_1) - Q_{ji}^{Spec} = 0 \quad (3.30)$$

The initial values of  $V_{se1}$  and  $\theta_1$  are achieved by solving the above Equations (3.29-3.30):

$$V_{se1} = \frac{1}{V_j} \sqrt{\frac{AA}{(g_{ij}^2 + b_{ij}^2)}} \quad (3.31)$$

$$\theta_1 = \tan^{-1} \left( \frac{P_{ji}^{Spec} - V_j^2 g_{jj} + V_i V_j g_{ij}}{Q_{ji}^{Spec} + V_j^2 b_{jj} - V_i V_j b_{ij}} \right) - \tan^{-1} \left( \frac{g_{ij}}{-b_{ij}} \right) \quad (3.32)$$

where  $AA$  is given by:

$$AA = (P_{ji}^{Spec} - V_j^2 g_{jj} + V_i V_j g_{ij})^2 + (Q_{ji}^{Spec} + V_j^2 b_{jj} - V_i V_j b_{ij})^2$$

For the secondary converter in the  $i - k$  branch, since it can control only the real power, only one equation (3.27) can be used to find the initial values of VSC-2. As such  $V_{se2}$  is set to a value in between  $V_{se2}^{min}$  and  $V_{se2}^{max}$ , and then the initial value of  $\theta_2$  can be attained by solving (3.27), on substitution of  $\theta_i = \theta_j = \theta_k = 0$ , which will be:

$$V_k^2 g_{kk} - V_i V_k g_{ik} + V_k V_{se2} (g_{ik} \cos \theta_2 - b_{ik} \sin \theta_2) - P_{ki}^{Spec} = 0 \quad (3.33)$$

$$\Rightarrow \theta_2 = \sin^{-1} \left( \frac{P_{ki}^{Spec} - V_k^2 g_{kk} + V_i V_k g_{ik}}{V_k V_{se2} \sqrt{(g_{ik}^2 + b_{ik}^2)}} \right) - \tan^{-1} \left( \frac{g_{ik}}{-b_{ik}} \right) \quad (3.34)$$

This section describes the amendments in the power flow equations related to the IPFC buses and the initialization of IPFC variables to obtain the power flow solution. The Newton Raphson method is applied for these IPFC buses to obtain the IPFC

buses voltage magnitudes and angles along with the injected voltage magnitudes and angles of the two VSCs, which is explained in the following section.

### 3.2.4 Newton-Raphson Method for IPFC Buses

The power flow solution is obtained by the Newton-Raphson method for the IPFC buses. The iteration solution equation is expressed as:

$$\mathbf{X}_1^{(it)} = \mathbf{X}_1^{(it-1)} - \mathbf{J}_1^{-1}(\mathbf{X}_1^{(it-1)})\mathbf{F}_1(\mathbf{X}_1^{(it-1)}) \quad (3.35)$$

where  $\mathbf{X}_1$  is the unknown state vector that includes the voltage phase angles and magnitudes of the IPFC buses and the independent control variables of IPFC, i.e.,

$$\mathbf{X}_1 = [\theta_i, V_i, \theta_j, V_j, \theta_k, V_k, \theta_1, V_{se1}, \theta_2, V_{se2}]^T \quad (3.36)$$

The unknown IPFC VSCs variables  $V_{sep}, \theta_p, (p = 1, 2)$  are determined from the power flow Equations (3.20-3.21) of the lines in which the power flows are controlled to a set point or reference values. The active and reactive power flows  $P_{ji}$  and  $Q_{ji}$  on the IPFC branch  $i - j$ , are maintained at their references,  $P_{ji}^{Spec}$  and  $Q_{ji}^{Spec}$  by the series VSC-1. On the branch  $i - k$  only one, the active power flow can be controlled by the VSC-2, while the active power exchange between the series converter should be balanced. Also the active and reactive power balances at buses  $i, j, k$  should also be maintained. Taking all these into considerations, the mismatch vector can be written as

$$\mathbf{F}_1 = [\Delta P_i, \Delta Q_i, \Delta P_j, \Delta Q_j, \Delta P_k, \Delta Q_k, \Delta P_{ji}, \Delta Q_{ji}, \Delta P_{ki}, \Delta PE]^T \quad (3.37)$$

where,  $\mathbf{F}_1$  refers to the mismatch vector of the active and reactive power flows of the IPFC buses and the power exchanged between the two VSCs.  $\Delta P_l$  and  $\Delta Q_l$  for  $l = i, j, k$  is given by Equation (3.22) and Equation (3.23), while,  $\Delta P_{ji} = P_{ji} - P_{ji}^{Spec}$ ,  $\Delta Q_{ji} = Q_{ji} - Q_{ji}^{Spec}$ ,  $\Delta P_{ki} = P_{ki} - P_{ki}^{Spec}$  and  $\Delta PE = -PE$ . The Jacobian matrix for the IPFC branches is given by Equation (3.38).

$$\mathbf{J}_1 = \begin{bmatrix}
\frac{\partial P_i}{\partial \theta_i} & \frac{\partial P_i}{\partial V_i} & \frac{\partial P_i}{\partial \theta_j} & \frac{\partial P_i}{\partial V_j} & \frac{\partial P_i}{\partial \theta_k} & \frac{\partial P_i}{\partial V_k} & \frac{\partial P_i}{\partial \theta_1} & \frac{\partial P_i}{\partial V_{se1}} & \frac{\partial P_i}{\partial \theta_2} & \frac{\partial P_i}{\partial V_{se2}} \\
\frac{\partial Q_i}{\partial \theta_i} & \frac{\partial Q_i}{\partial V_i} & \frac{\partial Q_i}{\partial \theta_j} & \frac{\partial Q_i}{\partial V_j} & \frac{\partial Q_i}{\partial \theta_k} & \frac{\partial Q_i}{\partial V_k} & \frac{\partial Q_i}{\partial \theta_1} & \frac{\partial Q_i}{\partial V_{se1}} & \frac{\partial Q_i}{\partial \theta_2} & \frac{\partial Q_i}{\partial V_{se2}} \\
\frac{\partial P_j}{\partial \theta_i} & \frac{\partial P_j}{\partial V_i} & \frac{\partial P_j}{\partial \theta_j} & \frac{\partial P_j}{\partial V_j} & 0 & 0 & \frac{\partial P_j}{\partial \theta_1} & \frac{\partial P_j}{\partial V_{se1}} & 0 & 0 \\
\frac{\partial Q_j}{\partial \theta_i} & \frac{\partial Q_j}{\partial V_i} & \frac{\partial Q_j}{\partial \theta_j} & \frac{\partial Q_j}{\partial V_j} & 0 & 0 & \frac{\partial Q_j}{\partial \theta_1} & \frac{\partial Q_j}{\partial V_{se1}} & 0 & 0 \\
\frac{\partial P_k}{\partial \theta_i} & \frac{\partial P_k}{\partial V_i} & 0 & 0 & \frac{\partial P_k}{\partial \theta_k} & \frac{\partial P_k}{\partial V_k} & 0 & 0 & \frac{\partial P_k}{\partial \theta_2} & \frac{\partial P_k}{\partial V_{se2}} \\
\frac{\partial Q_k}{\partial \theta_i} & \frac{\partial Q_k}{\partial V_i} & 0 & 0 & \frac{\partial Q_k}{\partial \theta_k} & \frac{\partial Q_k}{\partial V_k} & 0 & 0 & \frac{\partial Q_k}{\partial \theta_2} & \frac{\partial Q_k}{\partial V_{se2}} \\
\frac{\partial P_{ji}}{\partial \theta_i} & \frac{\partial P_{ji}}{\partial V_i} & \frac{\partial P_{ji}}{\partial \theta_j} & \frac{\partial P_{ji}}{\partial V_j} & 0 & 0 & \frac{\partial P_{ji}}{\partial \theta_1} & \frac{\partial P_{ji}}{\partial V_{se1}} & 0 & 0 \\
\frac{\partial Q_{ji}}{\partial \theta_i} & \frac{\partial Q_{ji}}{\partial V_i} & \frac{\partial Q_{ji}}{\partial \theta_j} & \frac{\partial Q_{ji}}{\partial V_j} & 0 & 0 & \frac{\partial Q_{ji}}{\partial \theta_1} & \frac{\partial Q_{ji}}{\partial V_{se1}} & 0 & 0 \\
\frac{\partial P_{ki}}{\partial \theta_i} & \frac{\partial P_{ki}}{\partial V_i} & 0 & 0 & \frac{\partial P_{ki}}{\partial \theta_k} & \frac{\partial P_{ki}}{\partial V_k} & 0 & 0 & \frac{\partial P_{ki}}{\partial \theta_2} & \frac{\partial P_{ki}}{\partial V_{se2}} \\
\frac{\partial PE}{\partial \theta_i} & \frac{\partial PE}{\partial V_i} & \frac{\partial PE}{\partial \theta_j} & \frac{\partial PE}{\partial V_j} & \frac{\partial PE}{\partial \theta_k} & \frac{\partial PE}{\partial V_k} & \frac{\partial PE}{\partial \theta_1} & \frac{\partial PE}{\partial V_{se1}} & \frac{\partial PE}{\partial \theta_2} & \frac{\partial PE}{\partial V_{se2}}
\end{bmatrix} \quad (3.38)$$

The individual Jacobian terms are given in detail in Appendix A. The Newton Raphson algorithm formulation for the IPFC buses can be built into the existing power flow solution of the whole system. This algorithm updates all the variables simultaneously and achieves the solution through quadrature convergence. The following section describes the power flow solution of the complete power system with incorporation of IPFC.

### 3.2.5 Power Flow Solution of Power System Including IPFC

In a power system consisting of  $nb$  buses when an IPFC consisting of  $M$  VSCs is placed, the number of load flow equations will increase by  $2M$  [97], [98]. As such for a simple IPFC consisting of two VSCs, when included in the system, the number of load flow equations increases by 4.

The compact form of Newton power flow equation for the power system including the IPFC is as follows:

$$\Delta \bar{\mathbf{X}}^{(it)} = -\bar{\mathbf{J}}^{-1}(\bar{\mathbf{X}}^{(it-1)})\bar{\mathbf{F}}(\bar{\mathbf{X}}^{(it-1)}) \quad (3.39)$$

where,  $it$  represents the number of iterations and

$$\bar{\mathbf{F}}(\bar{\mathbf{X}}) = [\Delta \mathbf{P}, \Delta \mathbf{Q}, \Delta \mathbf{R}]^T \quad (3.40)$$

$\Delta \mathbf{P} = [\Delta P_1, \Delta P_2, \dots, \Delta P_{nb}]$  and  $\Delta \mathbf{Q} = [\Delta Q_1, \Delta Q_2, \dots, \Delta Q_{nb}]$  are the mismatch equations of the active and reactive power flows at each bus.  $\Delta \mathbf{R} = [\Delta P_{ji}, \Delta P_{ki}, \Delta Q_{ji}, \Delta PE]$ , represents the mismatch line flows and real power exchanged among the IPFC branches.

$$\bar{\mathbf{X}} = [\mathbf{X}, \mathbf{X}_{\text{IPFC}}]^T, \quad (3.41)$$

$$\mathbf{X} = [\boldsymbol{\theta}, \mathbf{V}], \quad \mathbf{X}_{\text{IPFC}} = [\boldsymbol{\theta}_{\text{IPFC}}, \mathbf{V}_{\text{IPFC}}], \quad \boldsymbol{\theta}_{\text{IPFC}} = [\theta_1, \theta_2], \quad \mathbf{V}_{\text{IPFC}} = [V_{se1}, V_{se2}]$$

$$\bar{\mathbf{J}} = \frac{\partial \bar{\mathbf{F}}}{\partial \bar{\mathbf{X}}} = \begin{bmatrix} \frac{\partial \mathbf{P}}{\partial \boldsymbol{\theta}} & \frac{\partial \mathbf{P}}{\partial \mathbf{V}} & \frac{\partial \mathbf{P}}{\partial \boldsymbol{\theta}_{\text{IPFC}}} & \frac{\partial \mathbf{P}}{\partial \mathbf{V}_{\text{IPFC}}} \\ \frac{\partial \mathbf{Q}}{\partial \boldsymbol{\theta}} & \frac{\partial \mathbf{Q}}{\partial \mathbf{V}} & \frac{\partial \mathbf{Q}}{\partial \boldsymbol{\theta}_{\text{IPFC}}} & \frac{\partial \mathbf{Q}}{\partial \mathbf{V}_{\text{IPFC}}} \\ \frac{\partial \mathbf{R}}{\partial \boldsymbol{\theta}} & \frac{\partial \mathbf{R}}{\partial \mathbf{V}} & \frac{\partial \mathbf{R}}{\partial \boldsymbol{\theta}_{\text{IPFC}}} & \frac{\partial \mathbf{R}}{\partial \mathbf{V}_{\text{IPFC}}} \end{bmatrix} \quad (3.42)$$

The Jacobian parameters in Equation (3.42),  $\frac{\partial \mathbf{P}}{\partial \boldsymbol{\theta}_{\text{IPFC}}}$ ,  $\frac{\partial \mathbf{P}}{\partial \mathbf{V}_{\text{IPFC}}}$ ,  $\frac{\partial \mathbf{Q}}{\partial \boldsymbol{\theta}_{\text{IPFC}}}$ ,  $\frac{\partial \mathbf{Q}}{\partial \mathbf{V}_{\text{IPFC}}}$ ,  $\frac{\partial \mathbf{R}}{\partial \boldsymbol{\theta}}$ ,  $\frac{\partial \mathbf{R}}{\partial \mathbf{V}}$ ,  $\frac{\partial \mathbf{R}}{\partial \boldsymbol{\theta}_{\text{IPFC}}}$ ,  $\frac{\partial \mathbf{R}}{\partial \mathbf{V}_{\text{IPFC}}}$  with respect to IPFC branches are computed in reference to Equation (3.38). The Newton Raphson load flow implementation of the power system incorporated with IPFC is summarized in the following steps:

Step 1: The power system data is specified, which includes the generated power by the generators, transmission lines data, transformer impedances, load power, IPFC series transformer impedances.

Step 2: The active and reactive power flows ( $P_{ji}^{Spec}$ ,  $P_{ki}^{Spec}$  and  $Q_{ji}^{Spec}$ ) on the transmission lines in between the IPFC buses are specified.

Step 3: The admittance matrix is formed which also includes the IPFC transformer impedances.

Step 4: The initial values of the bus voltages are set to the value 1 and angles to zero. The initial values of the injected voltage magnitude and angles are set to the computed values from Equations (3.31), (3.32) and (3.34). Set the iteration count to 1.

Step 5: Compute the power flows at all the buses using Equation (3.2). The power flows of the IPFC branches are modified by Equations (3.17-3.18) and Equations (3.20-3.21). The power exchanged between the VSCs of the IPFC is calculated by Equation (3.24).

Step 6: Compute the mismatches at each bus and the mismatches of the power flows in the IPFC connected buses as given in Equation (3.40).

Step 7: If the mismatch is less than the tolerance value then go to step 12 or else go to step 8.

Step 8: Form the conventional Jacobian matrix parameters as in Equation (3.13). The Jacobian matrix parameters are modified and updated to include the IPFC parameters according to Equation (3.42).

Step 9: The IPFC injected voltage magnitudes and angles are updated simultaneously with the bus voltage magnitudes and angles.

Step 10: Check whether all constraints are satisfied. If the constraints are violated set the parameters at the limited values.

Step 11: Increase the iteration count. Go to step 5.

Step 12: The load flow is converged. Calculate the bus power flows with the final results of voltage magnitudes and angles.

Thus, the Newton-Raphson load flow is developed accommodating the IPFC controller configuration. The flow chart for the power flow solution for the power system is given in Figure 3.6. The load flow program is developed in Matlab.

The load flow provides the unknown voltages, angles of the buses, the injected voltage magnitudes and angles of the IPFC VSCs, and the line power flows of the power system network at steady state. These values will be used to compute the initial conditions to linearize the power system dynamic equations around this operating point. The linearized system will be utilized for modal analysis and control design. The following section establishes the dynamic equations of IPFC.

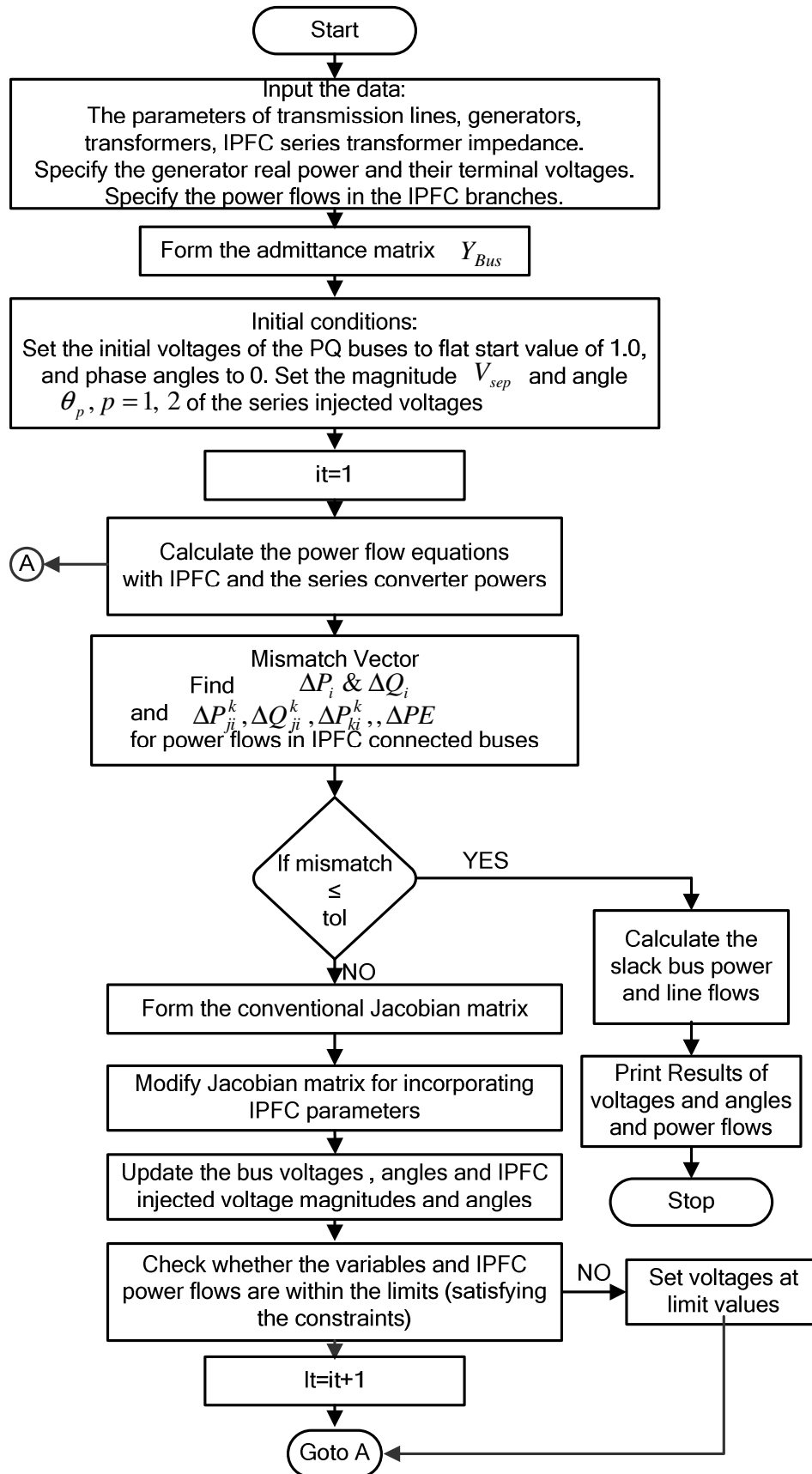


Figure 3.6: Flowchart of the power flow solution.

### 3.3 Dynamic Model of IPFC

The steady state model developed in Section 3.2 provides the basic foundation for conducting the dynamic stability studies. The dynamic model of IPFC includes the DC link capacitor dynamics and the converter control variables. The IPFC structure is shown in Figure 3.7. It consists of two, three-phase, gate turn-off (GTO) based VSCs, each injecting a synchronous voltage with controllable magnitude and angle. The VSCs are linked together at their DC terminals and are connected to the transmission lines through their series coupling transformers in line 1 and line 2.

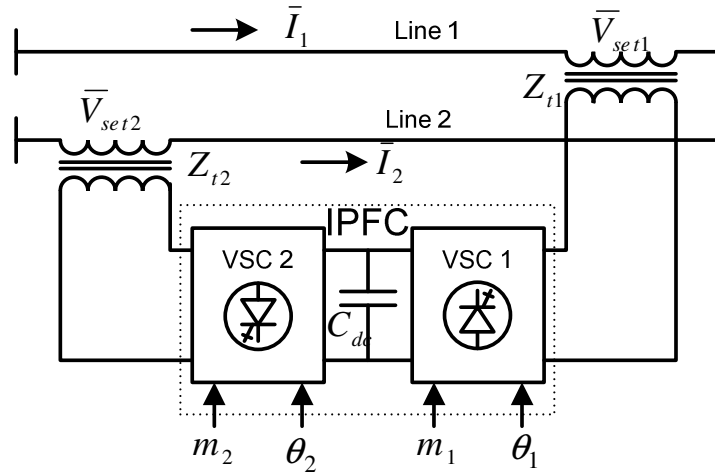


Figure 3.7: Structure of IPFC

$\bar{I}_1$  and  $\bar{I}_2$  are the currents flowing through the line 1 and 2, respectively in Figure 3.7. The voltages injected by the VSCs are represented by  $\bar{V}_{sep}, p=1, 2$  in this model. In the Figure 3.7,  $\bar{V}_{sep}, p=1, 2$  is the equivalent voltage across the coupling transformer impedance  $Z_{tp}, (p=1, 2)$  and injected voltage  $\bar{V}_{sep}, p=1, 2$ , ( $\bar{V}_{setp} = \bar{V}_{sep} + \bar{V}_{ztp}$ , and  $V_{ztp} = Z_{tp} \bar{I}_p, (p=1, 2)$ ). In Figure 3.7,  $m_1, m_2$  and  $\theta_1, \theta_2$  refer to amplitude modulation indices and phase angles constituting the control signals for the VSCs of the IPFC. The modulation index and the phase angle of the series inverters along with the DC link capacitor dynamics are included in developing the model for power system stability studies. IPFC primary function is to control the power flow in multi-transmission lines which is accomplished by the injected voltages

with varying magnitude and angle. The control of the injected voltage is obtained by the control signals of the IPFC.

The detailed three-phase GTO based VSCs and DC link capacitor diagram is shown in Figure 3.8 [70]. The general Pulse-Width-Modulation (PWM) is adopted for the GTO based VSC.  $V_{se1u}, (u = a, b, c)$  is the injected voltage by the VSC-1 in phase  $u, (u = a, b, c)$ , and  $V_{set1u}, (u = a, b, c)$  is the combined voltage across the transformer impedance and VSC-1 in line 1.  $V_{se2u}, (u = a, b, c)$  is the injected voltage by the VSC-2 in each phase  $(u = a, b, c)$  and  $V_{set2u}, (u = a, b, c)$  is the combined voltage across the transformer impedance and VSC-2 in line 2.

In Figure 3.8,  $i_{1u}, i_{2u}, (u = a, b, c)$  are the currents flowing in each phase in line 1 and 2 respectively.  $i_{dc}$  is the current flowing through the capacitor.  $v_{dc}$  is the voltage across the DC capacitor  $C_{dc}$ .  $r_1$  ( $r_2$ ) and  $l_1$  ( $l_2$ ) are the per phase resistance and inductance of transformer on line 1 (line 2). To model the IPFC, phase 'a' of the coupling transformer and VSC-1 arms along with the DC link is considered, as shown in Figure 3.9.  $\zeta_{C1a}$  and  $\zeta'_{C1a}$  represent the switches which can be either on or off respectively in Figure 3.9.  $r_s$  is the switch on-state resistance.  $S_{C1a}, (S'_{C1a})$  is defined as the switching function of the switch  $\zeta_{C1a}, (\zeta'_{C1a})$ .  $S_{C1a}, (S'_{C1a})$  can either be 0 or 1 corresponding to the off or on states of the switch respectively [70].

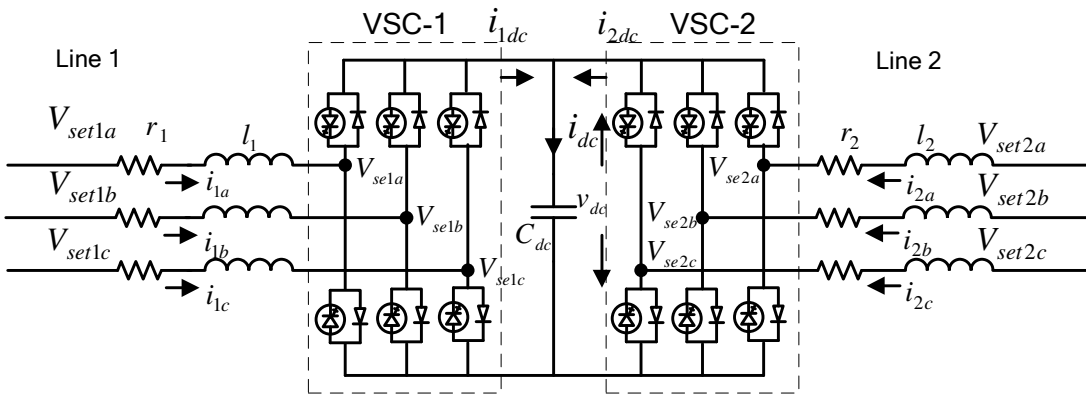


Figure 3.8: Detailed three phase diagram of IPFC

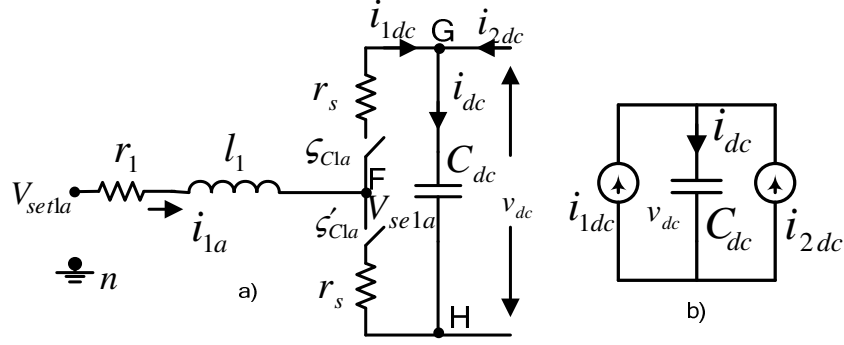


Figure 3.9: a) Equivalent circuit of phase 'a' of coupling transformer and VSC 1, b) Dynamics of DC link capacitor

Based on the principle of VSC,  $S_{C1a}$  and  $S'_{C1a}$  are always complimentary, i.e.,

$$S_{C1a} + S'_{C1a} = 1 \quad (3.43)$$

From Figure 3.9(a),  $V_{se1a}$  can be written as:

$$V_{se1a} = v_{FH} + v_{Hn} \quad (3.44)$$

When  $\zeta_{C1a}$  is on  $S_{C1a} = 1$  and  $S'_{C1a} = 0$ , then  $v_{FH} = (i_{1a}r_s + v_{dc})S_{C1a}$ , and when  $\zeta_{C1a}$  is off,  $S_{C1a} = 0$  and  $S'_{C1a} = 1$ ,  $v_{FH} = (i_{1a}r_s)S'_{C1a}$ . Thus,  $v_{FH}$  can be written as:

$$\begin{aligned} v_{FH} &= (i_{1a}r_s + v_{dc})S_{C1a} + (i_{1a}r_s)S'_{C1a} \\ &= (i_{1a}r_s + v_{dc})S_{C1a} + (i_{1a}r_s)(1 - S_{C1a}) \\ &= i_{1a}r_s + v_{dc}S_{C1a} \end{aligned} \quad (3.45)$$

The behavior of the circuit in Figure 3.9(a) can be written as:

$$l_1 \frac{di_{1a}}{dt} + r_1 i_{1a} = V_{set1a} - V_{se1a} \quad (3.46)$$

Substituting Equation (3.45) in Equation (3.44) and then for  $V_{se1a}$  into Equation (3.46) gives:

$$l_1 \frac{di_{1a}}{dt} + r_1 i_{1a} = V_{set1a} - (i_{1a}r_s + v_{dc}S_{C1a} + v_{Hn}) \quad (3.47)$$

$$\Rightarrow l_1 \frac{di_{1a}}{dt} = -R_1 i_{1a} - v_{dc} S_{C1a} - v_{Hn} + V_{set1a}$$

where,  $R_1 = (r_1 + r_s)$ . Similarly for the other two phases 'b' and 'c';

$$l_1 \frac{di_{1b}}{dt} = -R_1 i_{1b} - v_{dc} S_{C1b} - v_{Hn} + V_{set1b} \quad (3.48)$$

$$l_1 \frac{di_{1c}}{dt} = -R_1 i_{1c} - v_{dc} S_{C1c} - v_{Hn} + V_{set1c} \quad (3.49)$$

The voltage  $v_{Hn}$  can be obtained by adding the equations of the three phases Equations (3.47-3.49) and using  $i_{1a} + i_{1b} + i_{1c} = 0$ , and  $V_{set1a} + V_{set1b} + V_{set1c} = 0$ , is given by:

$$v_{Hn} = -\frac{v_{dc}}{3} \sum_{u=a,b,c} S_{C1u} \quad (3.50)$$

The switching function  $S_{C1u}$  can be expressed in terms of the control signals as follows [70]:

$$\begin{aligned} S_{C1a} &= \frac{m_1}{2} \cos(\omega t + \theta_1) + \frac{1}{2} \\ S_{C1b} &= \frac{m_1}{2} \cos(\omega t + \theta_1 - 120^\circ) + \frac{1}{2} \\ S_{C1c} &= \frac{m_1}{2} \cos(\omega t + \theta_1 - 240^\circ) + \frac{1}{2} \end{aligned} \quad (3.51)$$

Substituting (3.51) into (3.50) gives:

$$v_{Hn} = -\frac{v_{dc}}{2} \quad (3.52)$$

The mathematical model governing the behavior of phase 'a' is obtained by substituting the first equation in Equation (3.51) and Equation (3.52) into Equation (3.47) to give:

$$l_1 \frac{di_{1a}}{dt} = -R_1 i_{1a} - \frac{m_1 v_{dc}}{2} \cos(\omega t + \theta_1) + V_{set1a}$$

$$\Rightarrow \frac{di_{1a}}{dt} = -\frac{R_1}{l_1}i_{1a} - \frac{m_1 v_{dc}}{2l_1} \cos(\omega t + \theta_1) + \frac{1}{l_1} V_{set1a} \quad (3.53)$$

In matrix form the three phase differential equations of the VSC-1 of the IPFC can be written as follows:

$$\begin{aligned} \begin{bmatrix} \frac{di_{1a}}{dt} \\ \frac{di_{1b}}{dt} \\ \frac{di_{1c}}{dt} \end{bmatrix} &= \begin{bmatrix} -\frac{R_1}{l_1} & 0 & 0 \\ 0 & -\frac{R_1}{l_1} & 0 \\ 0 & 0 & -\frac{R_1}{l_1} \end{bmatrix} \begin{bmatrix} i_{1a} \\ i_{1b} \\ i_{1c} \end{bmatrix} - \frac{m_1 v_{dc}}{2l_1} \begin{bmatrix} \cos(\omega t + \theta_1) \\ \cos(\omega t + \theta_1 - 120^\circ) \\ \cos(\omega t + \theta_1 - 240^\circ) \end{bmatrix} \\ &+ \begin{bmatrix} \frac{1}{l_1} & 0 & 0 \\ 0 & \frac{1}{l_1} & 0 \\ 0 & 0 & \frac{1}{l_1} \end{bmatrix} \begin{bmatrix} V_{set1a} \\ V_{set1b} \\ V_{set1c} \end{bmatrix} \end{aligned} \quad (3.54)$$

The mathematical model is similarly derived for VSC-2 in line 2 and is given as:

$$\begin{aligned} \begin{bmatrix} \frac{di_{2a}}{dt} \\ \frac{di_{2b}}{dt} \\ \frac{di_{2c}}{dt} \end{bmatrix} &= \begin{bmatrix} -\frac{R_2}{l_2} & 0 & 0 \\ 0 & -\frac{R_2}{l_2} & 0 \\ 0 & 0 & -\frac{R_2}{l_2} \end{bmatrix} \begin{bmatrix} i_{2a} \\ i_{2b} \\ i_{2c} \end{bmatrix} - \frac{m_2 v_{dc}}{2l_2} \begin{bmatrix} \cos(\omega t + \theta_2) \\ \cos(\omega t + \theta_2 - 120^\circ) \\ \cos(\omega t + \theta_2 - 240^\circ) \end{bmatrix} \\ &+ \begin{bmatrix} \frac{1}{l_2} & 0 & 0 \\ 0 & \frac{1}{l_2} & 0 \\ 0 & 0 & \frac{1}{l_2} \end{bmatrix} \begin{bmatrix} V_{set2a} \\ V_{set2b} \\ V_{set2c} \end{bmatrix} \end{aligned} \quad (3.55)$$

where,  $R_2 = (r_2 + r_s)$ .

The dynamics of the DC link capacitor from Figure 3.9(b) is given by:

$$\frac{dv_{dc}}{dt} = \frac{1}{C_{dc}} i_{dc} \quad (3.56)$$

where,

$$i_{dc} = i_{1dc} + i_{2dc} = \sum_{u=a,b,c} (i_{1u} S_{C1u} + i_{2u} S_{C2u})$$

On substituting the switching functions in terms of the control signals Equation (3.56) can be written as:

$$\begin{aligned} \frac{dv_{dc}}{dt} = \frac{1}{2C_{dc}} & \left[ m_1 \left( \cos(\omega t + \theta_1) i_{1a} + \cos(\omega t + \theta_1 - 120^\circ) i_{1b} + \cos(\omega t + \theta_1 - 240^\circ) i_{1c} \right) \right. \\ & \left. + m_2 \left( \cos(\omega t + \theta_2) i_{2a} + \cos(\omega t + \theta_2 - 120^\circ) i_{2b} + \cos(\omega t + \theta_2 - 240^\circ) i_{2c} \right) \right] \end{aligned} \quad (3.57)$$

Equations (3.54), (3.55) and (3.57) are three-phase time-varying differential equations. These equations are converted to time-invariant differential equations using the Park's transformation. Park's transformation converts the variables from three axes reference frame ( $a, b, c$ ), to new quantities on the  $dqo$  rotating reference frame, where one is along the direct axis of the rotor field winding, called the direct axis, and second along the neutral axis of the field winding called the quadrature axis which is  $90^\circ$  apart from the direct axis, and the third is on a stationary axis [17], [103].

The electrical variables in the  $abc$  reference frame are transformed into a rotating synchronous rotating  $dqo$  reference (or the rotor axis reference frame) using the Park's transformation as:

$$X_{dq0} = T X_{abc} \quad (3.58)$$

where,  $X_{abc} = [i_{1a}, i_{1b}, i_{1c}, i_{2a}, i_{2b}, i_{2c}, v_{dc}]^T$ ,

$$X_{dq0} = [i_{1d}, i_{1q}, i_{10}, i_{2d}, i_{2q}, i_{20}, v_{dc}]^T$$

$$T = \begin{bmatrix} P & 0 & 0 \\ 0 & P & 0 \\ 0 & 0 & I \end{bmatrix} \text{ and}$$

$$P = \frac{2}{3} \begin{bmatrix} \cos \omega t & \cos(\omega t - 120^\circ) & \cos(\omega t + 120^\circ) \\ -\sin \omega t & -\sin(\omega t - 120^\circ) & -\sin(\omega t + 120^\circ) \\ \frac{1}{2} & \frac{1}{2} & \frac{1}{2} \end{bmatrix} \quad (3.59)$$

Equations (3.54), (3.55) and (3.57) are transformed in  $dqo$  axes reference frame and are given in one matrix as follows:

$$\begin{bmatrix} \frac{di_d}{dt} \\ \frac{di_q}{dt} \\ \frac{di_{10}}{dt} \\ \frac{di_{2d}}{dt} \\ \frac{di_{2q}}{dt} \\ \frac{di_{20}}{dt} \\ \frac{dv_{dc}}{dt} \end{bmatrix} = \begin{bmatrix} -\frac{R_1}{l_1} & \omega & 0 & 0 & 0 & 0 & -\frac{m_1}{2l_1} \cos \theta_1 \\ -\omega & -\frac{R_1}{l_1} & 0 & 0 & 0 & 0 & -\frac{m_1}{2l_1} \sin \theta_1 \\ 0 & 0 & -\frac{R_1}{l_1} & 0 & 0 & 0 & 0 \\ 0 & 0 & 0 & -\frac{R_2}{l_2} & \omega & 0 & -\frac{m_2}{2l_2} \cos \theta_2 \\ 0 & 0 & 0 & \omega & -\frac{R_2}{l_2} & 0 & -\frac{m_2}{2l_2} \sin \theta_2 \\ 0 & 0 & 0 & 0 & 0 & -\frac{R_2}{l_2} & 0 \\ \frac{3}{4} \frac{m_1}{C_{dc}} \cos \theta_1 & \frac{3}{4} \frac{m_1}{C_{dc}} \sin \theta_1 & 0 & \frac{3}{4} \frac{m_2}{C_{dc}} \cos \theta_2 & \frac{3}{4} \frac{m_2}{C_{dc}} \sin \theta_2 & 0 & 0 \end{bmatrix} \begin{bmatrix} i_d \\ i_q \\ i_{10} \\ i_{2d} \\ i_{2q} \\ i_{20} \\ v_{dc} \end{bmatrix}$$

$$+ \begin{bmatrix} \frac{1}{l_1} & 0 & 0 & 0 & 0 & 0 & 0 \\ 0 & \frac{1}{l_1} & 0 & 0 & 0 & 0 & 0 \\ 0 & 0 & \frac{1}{l_1} & 0 & 0 & 0 & 0 \\ 0 & 0 & 0 & \frac{1}{l_2} & 0 & 0 & 0 \\ 0 & 0 & 0 & 0 & \frac{1}{l_2} & 0 & 0 \\ 0 & 0 & 0 & 0 & 0 & \frac{1}{l_2} & 0 \\ 0 & 0 & 0 & 0 & 0 & 0 & 0 \end{bmatrix} \begin{bmatrix} V_{set1d} \\ V_{set1q} \\ V_{set10} \\ V_{set2d} \\ V_{set2q} \\ V_{set20} \\ 0 \end{bmatrix}$$

(3.60)

From Equation (3.60) the dynamics of d-axis component of the current in line 1 is given by:

$$\frac{di_{1d}}{dt} = -\frac{R_1}{l_1}i_{1d} + \omega i_{1q} - \frac{m_1 v_{dc}}{2l_1} \cos \theta_1 + \frac{1}{l_1}V_{set1d} \quad (3.61)$$

For the study of power system oscillation stability, the resistance and transients of the transformers and VSCs of the IPFC are neglected, i.e.,

( $R_1 = 0, \frac{di_{1d}}{dt} = \frac{di_{1q}}{dt} = \frac{di_{2d}}{dt} = \frac{di_{2q}}{dt} = 0$ ). The above equation can be written as:

$$0 = \omega i_{1q} - \frac{m_1}{2l_1} \cos \theta_1 v_{dc} + \frac{1}{l_1}V_{set1d} \quad (3.62)$$

$$\Rightarrow V_{set1d} = -\omega l_1 i_{1q} + \frac{m_1 v_{dc}}{2} \cos \theta_1 \quad (3.63)$$

$$\Rightarrow V_{set1d} = -x_{t1} i_{1q} + \frac{1}{2}v_{dc}m_1 \cos \theta_1 \quad (3.64)$$

where,  $x_{t1} = \omega l_1$

Similarly the  $d - q$  components of  $V_{setp}, (p = 1, 2)$ , of the two VSCs can be derived from Equation (3.60) as follows:

$$\begin{bmatrix} V_{set1d} \\ V_{set1q} \end{bmatrix} = \begin{bmatrix} 0 & -x_{t1} \\ x_{t1} & 0 \end{bmatrix} \begin{bmatrix} i_{1d} \\ i_{1q} \end{bmatrix} + \frac{v_{dc}}{2} \begin{bmatrix} m_1 \cos \theta_1 \\ m_1 \sin \theta_1 \end{bmatrix} \quad (3.65)$$

$$\begin{bmatrix} V_{set2d} \\ V_{set2q} \end{bmatrix} = \begin{bmatrix} 0 & -x_{t2} \\ x_{t2} & 0 \end{bmatrix} \begin{bmatrix} i_{2d} \\ i_{2q} \end{bmatrix} + \frac{v_{dc}}{2} \begin{bmatrix} m_2 \cos \theta_2 \\ m_2 \sin \theta_2 \end{bmatrix} \quad (3.66)$$

where  $x_{t1} = \omega l_1, x_{t2} = \omega l_2$  are the reactances of the series transformers. The DC link dynamics in  $d - q$  axes is:

$$\frac{dv_{dc}}{dt} = \frac{3m_1}{4C_{dc}} [\cos \theta_1 \quad \sin \theta_1] \begin{bmatrix} i_{1d} \\ i_{1q} \end{bmatrix} + \frac{3m_2}{4C_{dc}} [\cos \theta_2 \quad \sin \theta_2] \begin{bmatrix} i_{2d} \\ i_{2q} \end{bmatrix} \quad (3.67)$$

The Equations (3.65-3.67) give the voltages and the DC link dynamics on  $d - q$  axis reference frame. The equivalent voltages can be written as:

$$\begin{aligned}\bar{V}_{set1} &= V_{set1d} + j V_{set1q} \\ &= j x_{t1} \bar{I}_1 + \frac{1}{2} v_{dc} m_1 (\cos \theta_1 + j \sin \theta_1) \\ &= j x_{t1} \bar{I}_1 + \bar{V}_{se1}\end{aligned}\quad (3.68)$$

$$\begin{aligned}\bar{V}_{set2} &= V_{set2d} + j V_{set2q} \\ &= j x_{t2} \bar{I}_2 + \frac{1}{2} v_{dc} m_2 (\cos \theta_2 + j \sin \theta_2) \\ &= j x_{t2} \bar{I}_2 + \bar{V}_{se2}\end{aligned}\quad (3.69)$$

$$\text{where, } \bar{I}_1 = i_{1d} + j i_{1q}, \bar{I}_2 = i_{2d} + j i_{2q} \quad (3.70)$$

In Equations (3.68) and (3.69)  $j x_{t1} \bar{I}_1$  and  $j x_{t2} \bar{I}_2$  are the voltage drops across the VSCs transformer reactance.  $\bar{V}_{se1}$  and  $\bar{V}_{se2}$  are the actual values of the voltages injected by the VSCs and are function of the IPFC control parameters, i.e., modulations indices ( $m_1, m_2$ ) and phase angles ( $\theta_1, \theta_2$ ). From Equations (3.68) and (3.69)  $\bar{V}_{se1}$  and  $\bar{V}_{se2}$  can be written as:

$$\begin{aligned}\bar{V}_{se1} &= \frac{1}{2} v_{dc} m_1 (\cos \theta_1 + j \sin \theta_1) \\ &= V_{se1} \angle \theta_1 \\ \bar{V}_{se2} &= \frac{1}{2} v_{dc} m_2 (\cos \theta_2 + j \sin \theta_2) \\ &= V_{se2} \angle \theta_2\end{aligned}\quad (3.71)$$

$$\text{where } V_{se1} = \frac{v_{dc} m_1}{2} \text{ and } V_{se2} = \frac{v_{dc} m_2}{2} \quad (3.72)$$

Equations (3.65-3.67) constitute the dynamic model of the IPFC which will be utilized to incorporate the IPFC model into the power system dynamic model, together developing the dynamic model of the power system *installed* with IPFC, which is used for power system stability analysis.

The following section demonstrates the application of the steady state model and dynamic model of IPFC developed in Section 3.2 and Section 3.3 by taking a three bus system incorporated with IPFC. The steady state model of the power system installed with IPFC will be used to perform the load flow. The load flow results give the steady state operating point of the system along with the VSCs injected voltage magnitudes and angles, which will be used to determine the initial values of IPFC control parameters from the dynamic model.

### 3.4 Results

Consider a three bus power system consisting of two transmission lines with IPFC incorporated as shown in Figure 3.10. The three buses are represented with notation as  $i, j$  and  $k$ . Bus  $i$  is taken as the slack bus, while bus  $j$  and  $k$  are taken as the  $PQ$  buses. The loads  $P_{Lj} + jQ_{Lj}$  and  $P_{Lk} + jQ_{Lk}$  are connected to bus  $j$  and  $k$  respectively. The two VSCs of IPFC are in between buses  $i - j$  and  $i - k$  respectively. The system data is given in Table 3.1 and all the values are given in p.u. The transmission lines are modeled by equivalent  $\pi$  model. For performing the load flow, the bus  $i$  is taken as the slack bus where the voltage is taken as:  $V_i = 1.04$  p.u. Bus  $j$  and  $k$  are considered as the load buses where the loads values are given in Table 3.1. The IPFC variables have been initialized, accordingly computed from the Equations (3.31-3.32) and (3.34).

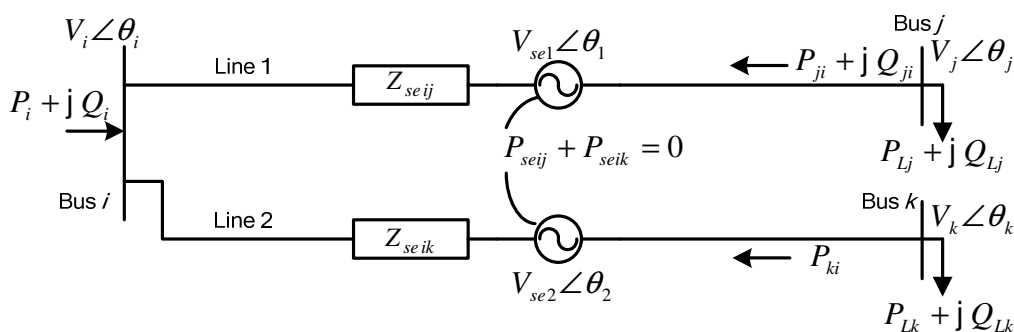


Figure 3.10: Three bus system with IPFC

Table 3.1: Three bus system data

Transmission line data	Resistance	Reactance	$B_c / 2$
$i - j$	0.02	0.04	0.02
$i - k$	0.01	0.025	0.025
Loads	Bus	MW ( $P_L$ )	MVAR ( $Q_L$ )
1	$j$	0.5	0.1
2	$k$	0.5	0.1
VSC transformer		Resistance	Reactance
VSC-1		0	0.015
VSC-2		0	0.015
IPFC DC capacitor parameters			
$v_{dc} = 225 \text{ KV} = 2 \text{ p.u.}$		$C_{dc} = 100 \mu\text{F} = 0.2 \text{ p.u.}$	

In the system the power flows from bus  $i$  to the other two buses  $j$  and  $k$ , which absorb power and this direction of the power flow is taken positive. The power flow on line  $j - i$  and on line  $k - i$  is set to 0.5 p.u. ( $P_{ji}^{Spec} = -0.5, P_{ki}^{Spec} = -0.5$ ) and the set point of reactive power on line  $j - i$ , is specified to 0.08 p.u., ( $Q_{ji}^{Spec} = -0.08$ ). The negative sign indicates the direction of power flow in the lines from bus  $j, k$  to bus  $i$ . The load flow is performed on the system and the results are given in Table 3.2. From Table 3.2 the injected voltages are  $\bar{V}_{se1} = 0.0932 \angle 71.7854^\circ$  and  $\bar{V}_{se2} = 0.0184 \angle -112.5248^\circ$ . Using Equations (3.71) and (3.72) the initial values of control parameters of IPFC are calculated. The results are given in Table 3.3. The initial values given in Table 3.3 are utilized for small signal stability studies and time domain simulations of the power system incorporating IPFC.

Table 3.2: Load flow results of three bus system

Buses	Voltages magnitudes in p.u.	Voltages angles in degrees	Real and reactive powers in p.u.
1	1.0400	0	1.0075 + j0.1663
2	1.0000	-6.4692	-0.5000 - j0.1000
3	1.0394	-0.0835	-0.5000 - j0.1000
Injected voltage		Magnitude in p.u.	Angle in degrees
VSC-1 $\bar{V}_{se1}$		0.0932	71.7854
VSC-2 $\bar{V}_{se2}$		0.0184	-112.5248
The power flows in the IPFC branches			
$P_{ji} = -0.5 \text{ p.u.}$		$P_{ki} = -0.5 \text{ p.u.}$	$Q_{ji} = -0.08 \text{ p.u.}$

Table 3.3: Initial values of the control parameters of IPFC

$m_1$	0.0932
$m_2$	0.0184
$\theta_1$	71.7854
$\theta_2$	-112.5248

### 3.5 Summary

In this chapter the steady state model of an IPFC is presented. The corresponding power flow equations relating to the integration of the IPFC model into load flow studies has been described. The flowchart for power flow solution of the power system with IPFC based on Newton Raphson method is presented. The solution provides the operating point of the power system from which necessary initial conditions are computed for conducting small signal studies and dynamic simulations. The dynamic model of the IPFC in  $d - q$  axis form is established which will be used to develop the integrated power system model added with IPFC. This power system model is utilized for conducting power system analysis and time domain simulations to investigate the dynamic performance of the power system in the presence of, the FACTS device, IPFC. The following chapter presents the incorporation of IPFC dynamic model into the SMIB power system model.

## CHAPTER 4

### SINGLE MACHINE INFINITE BUS SYSTEM WITH IPFC

#### 4.1 Introduction

To understand the dynamic behavior of an electric power system and to design a controller to improve its performance, it is essential to model the power system. The mathematical model of the power system, consisting of the nonlinear differential-algebraic equations of various system components, is developed using the system structure and fundamental physical laws governing the power system elements. A proper and adequate power system model for power system dynamic studies must be chosen to include all significant components, which can reflect the characteristic phenomena of the dynamic behavior.

To study the power system stability, the modeling of various power system components is required, consisting of generators, their control systems including excitation control, automatic voltage regulators, and the transmission system components. The dynamic behavior of the individual components is described by differential algebraic equations. For small signal stability analysis, the equations characterizing the overall power system are linearized around equilibrium point. The small signal stability technique includes load flow computation, state matrix representation and eigenvalue analysis or modal analysis, based on the linearized models of the system dynamics, for studying the power system stability. The power system stability analysis is also investigated by nonlinear simulation of the dynamic model of the power system.

This chapter presents the dynamic model of the Single Machine Infinite Bus (SMIB) power system incorporated with IPFC. The nonlinear model of the system is linearized to develop the Phillips-Heffron model of SMIB including IPFC model. The IPFC based damping controller is designed based on the linearized model.

Consequently the power system is analyzed for the oscillation stability. The performance of the controllers is demonstrated by nonlinear simulation studies.

#### 4.2 Dynamic Model of SMIB Power System With IPFC

A dynamic model for IPFC for stability analysis is developed in section 3.3. The complete power system dynamic model in the presence of IPFC is developed by incorporating it with the models for generator, exciter, etc. in order to form the state equations and to analyze the dynamic stability. The SMIB power system equipped with an IPFC is shown in Figure 4.1.

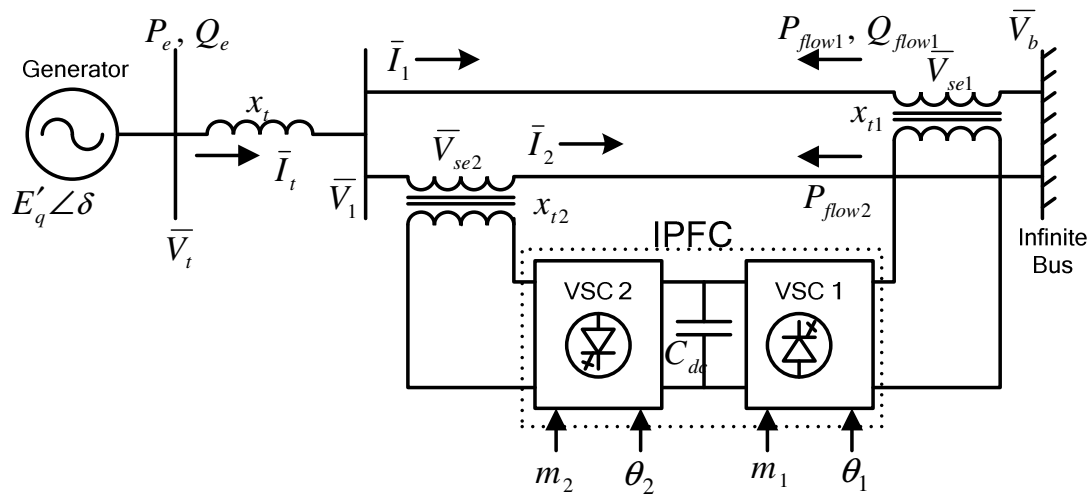


Figure 4.1: SMIB installed with IPFC

Figure 4.1 shows the power system consisting of a generator which is connected to the infinite bus via parallel transmission lines. There is no load at the generator bus. An elementary IPFC consisting of two three-phase GTO based VSCs is installed on the two transmission lines. Each VSC compensates a different transmission line by series voltage injection.

#### 4.2.1 The Nonlinear Dynamic Model of SMIB Power System With IPFC

The nonlinear dynamic model of the SMIB power system with IPFC is developed as follows:

The synchronous machine in the system is represented by the third order model [2], [104], [105]:

$$\dot{\delta} = \omega_0(\omega - 1) \quad (4.1)$$

$$\dot{\omega} = \frac{P_m - P_e - P_D}{M} \quad (4.2)$$

$$\dot{E}'_q = \frac{(-E_q + E_{fd})}{T'_{do}} \quad (4.3)$$

The exciter of the machine is represented by:

$$\dot{E}_{fd} = \frac{-E_{fd} + K_A(V_{ref} - V_t)}{T_A} \quad (4.4)$$

The DC voltage dynamics linking the VSCs of the IPFC is given by:

$$\dot{V}_{dc} = \frac{3m_1}{4C_{dc}}(i_{1d} \cos \theta_1 + i_{1q} \sin \theta_1) + \frac{3m_2}{4C_{dc}}(i_{2d} \cos \theta_2 + i_{2q} \sin \theta_2) \quad (4.5)$$

where the auxiliary equations are given as:

$$P_e = V_{dt} I_{dt} + V_{qt} I_{qt}, \quad E_q = E'_q + (x_d - x'_d) I_{dt} = E'_q + (x_d - x'_d)(i_{1d} + i_{2d})$$

$$V_{qt} = E'_q - x'_d I_{dt} = E'_q - x'_d(i_{1d} + i_{2d}), \quad V_{dt} = x_q I_{qt} = x_q(i_{1q} + i_{2q})$$

$$V_t = (V_{dt}^2 + V_{qt}^2)^{1/2},$$

$$I_t = I_{dt} + j I_{qt}, \quad I_t = I_1 + I_2, \quad I_1 = i_{1d} + j i_{1q}, \quad I_2 = i_{2d} + j i_{2q}$$

$$I_t = i_{1d} + j i_{1q} + i_{2d} + j i_{2q}, \quad I_{dt} = i_{1d} + i_{2d}, \quad I_{qt} = i_{1q} + i_{2q}$$

From Figure 4.1,

$$\bar{V}_t = j x_t \bar{I}_t + \bar{V}_1 \quad (4.6)$$

$$\begin{aligned} \bar{V}_1 &= j x_{L1} \bar{I}_1 + j x_{t1} \bar{I}_1 + \bar{V}_{se1} + \bar{V}_b \\ &= j x_{L2} \bar{I}_2 + j x_{t2} \bar{I}_2 + \bar{V}_{se2} + \bar{V}_b \end{aligned} \quad (4.7)$$

where  $x_{L1}$ ,  $x_{L2}$  are the transmission line reactances, the resistances of the transmission lines are neglected,  $\bar{V}_b$  is the infinite bus voltage. Equations (4.6) and (4.7) represent the network equations of the power system. These equations are in synchronously rotating frame denoted by  $D$  and  $Q$  axes which have to be transformed to the synchronous machine rotor axis frame denoted by  $d - q$  axes [17], [103].

#### 4.2.2 Relationship Between Machine And Synchronous Frame of Reference

The synchronous machine stator and network variables should be transformed to a reference frame that converts balanced three phase sinusoidal variations into constants which is accomplished by the Park's transformation of Equation (3.30). The synchronous rotating frame is transformed into machine reference frame by the following transformation [17], [103]:

$$\begin{aligned} V_{DQO} &= P V_{abc} = P P^{-1} V_{dqo} \\ I_{DQO} &= P I_{abc} = P P^{-1} I_{dqo} \end{aligned} \quad (4.8)$$

where  $P$  is the Park's transformation matrix and  $V$  and  $I$  represents the voltage and current variables. The synchronous frame of reference denoted by  $D$  and  $Q$  axes, are orthogonal in nature as shown in Figure 4.2 [17]. The  $d$  and  $q$  axes of the machine are also shown in the figure. The angle between  $D$  and  $q$  axes is  $\delta$  and the angle between  $D$  and  $d$  axes is  $\frac{\pi}{2} - \delta$ . The currents in the two reference frames are related by:

$$\begin{bmatrix} I_D \\ I_Q \end{bmatrix} = \begin{bmatrix} \sin \delta & \cos \delta \\ -\cos \delta & \sin \delta \end{bmatrix} \begin{bmatrix} I_d \\ I_q \end{bmatrix} \quad (4.9)$$

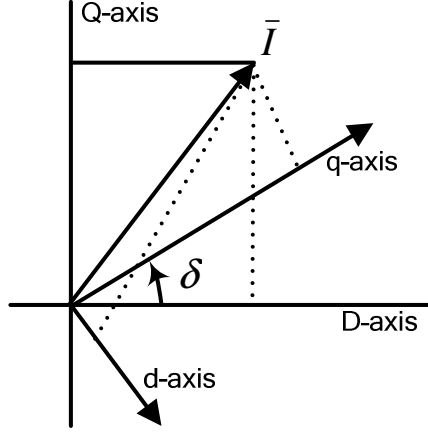


Figure 4.2: Relationship between machine and synchronous frame of reference.

This transformation gives,  $(I_D + j I_Q) = (I_d + j I_q) e^{j(\delta - \pi/2)}$ . Similarly for voltage  $(V_D + j V_Q) = (V_d + j V_q) e^{j(\delta - \pi/2)}$ . Using these relations the network variables are converted to the  $d - q$  reference frame.

#### 4.2.3 Transforming the Network Equations in $d - q$ Axes Frame

The network Equations (4.6-4.7) are transformed to  $d - q$  axes frame as follows:

$$\begin{aligned}
 \bar{V}_t &= jx_t \bar{I}_t + \bar{V}_1 \\
 &= jx_t \bar{I}_t + \bar{V}_{se2} + jx_{L2} \bar{I}_2 + \bar{V}_b \\
 \Rightarrow V_{Dt} + jV_{Qt} &= jx_t \bar{I}_t + \bar{V}_{se2} + j(x_{t2} + x_{L2}) \bar{I}_2 + \bar{V}_b
 \end{aligned} \tag{4.10}$$

$V_{Dt}$  and  $V_{Qt}$  are on the  $D - Q$  axes frame. Multiplying by  $e^{j(\pi/2 - \delta)}$  will transform the above  $D - Q$  axes frame of equations to  $d - q$  axes reference frame as follows:

$$(V_{Dt} + jV_{Qt}) e^{j(\pi/2 - \delta)} = (jx_t \bar{I}_t + \bar{V}_{se2} + j(x_{t1} + x_{L2}) \bar{I}_2 + \bar{V}_b) e^{j(\pi/2 - \delta)} \tag{4.11}$$

Left Hand Side of Equation (4.11) gives:

$$(V_{Dt} + jV_{Qt}) e^{j(\pi/2 - \delta)} = V_{dt} + jV_{qt} = x_q I_{qt} + j(E'_q - x'_d I_{dt}) \tag{4.12}$$

where  $V_{dt} = V_{Dt} e^{j(\pi/2 - \delta)}$ ,  $V_{qt} = V_{Qt} e^{j(\pi/2 - \delta)}$

Right Hand Side of Equation (4.11) gives:

$$\begin{aligned} jx_t(I_{dt} + j I_{qt}) + V_{se2d} + j V_{se2q} + j (x_{L2} + x_{t1})(i_{2d} + j i_{2q}) \\ + V_b \sin \delta + j V_b \cos \delta \end{aligned} \quad (4.13)$$

where

$$\begin{aligned} \bar{I}_t e^{j(\pi/2-\delta)} &= I_t = (I_{dt} + j I_{qt}) \\ \bar{I}_2 e^{j(\pi/2-\delta)} &= (I_{2D} + j I_{2Q}) e^{j(\pi/2-\delta)} = I_2 = (i_{2d} + j i_{2q}) \\ \bar{V}_b e^{j(\pi/2-\delta)} &= V_b \sin \delta + j V_b \cos \delta \end{aligned} \quad (4.14)$$

$$\begin{aligned} \bar{V}_{se2} e^{j(\pi/2-\delta_1)} &= V_{se2} e^{j(\pi/2-\delta+\theta_1)} \\ &= V_{se2} (\sin(\delta - \theta_2) + j \cos(\delta - \theta_2)) \\ &= V_{se2d} + j V_{se2q} \end{aligned}$$

Equation (4.11) becomes

$$\begin{aligned} x_q(i_{1q} + i_{2q}) + j E'_q - j x'_d(i_{1d} + i_{2d}) \\ = j x_t(i_{1d} + i_{2d} + j i_{1q} + j i_{2q}) + V_{se2d} + j V_{se2q} \\ + j (x_{L2} + x_{t1})(i_{2d} + j i_{2q}) + V_b \sin \delta + j V_b \cos \delta \end{aligned} \quad (4.15)$$

Equation (4.7) in  $d - q$  axes reference frame will be

$$\begin{aligned} j (x_{L1} + x_{t1})(i_{1d} + j i_{1q}) + V_{se1d} + j V_{se1q} = \\ j (x_{L2} + x_{t2})(i_{2d} + j i_{2q}) + V_{se2d} + j V_{se2q} \end{aligned} \quad (4.16)$$

Solving Equations (4.15-4.16):

$$\begin{aligned} i_{1d} = x_{11d} E'_q + \frac{1}{2} (x_{12d} - x_{11d}) v_{dc} m_2 \cos(\delta - \theta_2) \\ - \frac{1}{2} x_{12d} v_{dc} m_1 \cos(\delta - \theta_2) - x_{11d} V_b \cos \delta \end{aligned} \quad (4.17)$$

$$i_{2d} = x_{21d} E'_q + \frac{1}{2} (x_{22d} - x_{21d}) v_{dc} m_2 \cos(\delta - \theta_2) - \frac{1}{2} x_{22d} v_{dc} m_1 \cos(\delta - \theta_1) - x_{21d} V_b \cos \delta \quad (4.18)$$

$$i_{1q} = \frac{1}{2} (x_{11q} + x_{12q}) v_{dc} m_2 \sin(\delta - \theta_2) - \frac{1}{2} (x_{12q}) v_{dc} m_1 \sin(\delta - \theta_1) + x_{11q} V_b \sin \delta \quad (4.19)$$

$$i_{2q} = \frac{1}{2} (x_{21q} + x_{22q}) v_{dc} m_2 \sin(\delta - \theta_2) - \frac{1}{2} (x_{22q}) v_{dc} m_1 \sin(\delta - \theta_1) + x_{21q} V_b \sin \delta \quad (4.20)$$

where

$$x_{11d} = x_{iL2} / x_{\Sigma 1}, x_{12d} = (x'_{dt} + x_{iL2}) / x_{\Sigma 1}, x_{21d} = x_{iL1} / x_{\Sigma 1}, x_{22d} = -x'_{dt} / x_{\Sigma 1}$$

$$x_{11q} = x_{iL2} / x_{\Sigma 2}, x_{12q} = -(x'_{qt} + x_{iL2}) / x_{\Sigma 2}, x_{21q} = x_{iL1} / x_{\Sigma 2}, x_{22q} = -x'_{qt} / x_{\Sigma 2}$$

$$x_{iL2} = x_{i2} + x_{L2}, x'_{dt} = x'_d + x_t, x_{iL1} = x_{i1} + x_{L1}, x'_{qt} = x_q + x_t$$

$$x_{\Sigma 1} = (x'_{dt} \cdot x_{iL2}) + (x'_{dt} + x_{iL2})(x_{iL1}), x_{\Sigma 2} = (x'_{qt} \cdot x_{iL2}) + (x'_{qt} + x_{iL2})(x_{iL1})$$

Equations (4.1-4.5) supported by Equations (4.17-4.20) mainly constitute the nonlinear model of SMIB embedded with IPFC.

### 4.3 Linearized Model of Power System

The extended linearized Phillips-Heffron model of SMIB system incorporating IPFC is obtained by linearizing the nonlinear model Equations (4.1-4.5) which are obtained as follows:

$$\Delta \dot{\delta} = \omega_o \Delta \omega \quad (4.21)$$

$$\Delta \dot{\omega} = (\Delta P_m - \Delta P_e - D \Delta \omega) / M \quad (4.22)$$

$$\Delta \dot{E}'_q = (-\Delta E_q + \Delta E_{fd}) / T'_{do} \quad (4.23)$$

$$\Delta \dot{E}_{fd} = (-\Delta E_{fd} + K_A (\Delta V_{ref} - \Delta V_t)) / T_A \quad (4.24)$$

$$\Delta \dot{v}_{dc} = K_7 \Delta \delta + K_8 \Delta E'_q - K_9 \Delta v_{dc} + K_{cm1} \Delta m_1 + K_{c\theta1} \Delta \theta_1 + K_{cm2} \Delta m_2 + K_{c\theta2} \Delta \theta_2 \quad (4.25)$$

where

$$\Delta P_e = K_1 \Delta \delta + K_2 \Delta E'_q + K_{pv} \Delta v_{dc} + K_{pm1} \Delta m_1 + K_{p\theta1} \Delta \theta_1 + K_{pm2} \Delta m_2 + K_{p\theta2} \Delta \theta_2 \quad (4.26)$$

$$\Delta E_q = K_4 \Delta \delta + K_3 \Delta E'_q + K_{qv} \Delta v_{dc} + K_{qm1} \Delta m_1 + K_{q\theta1} \Delta \theta_1 + K_{qm2} \Delta m_2 + K_{q\theta2} \Delta \theta_2 \quad (4.27)$$

$$\Delta V_t = K_5 \Delta \delta + K_6 \Delta E'_q + K_{vv} \Delta v_{dc} + K_{vm1} \Delta m_1 + K_{v\theta1} \Delta \theta_1 + K_{vm2} \Delta m_2 + K_{v\theta2} \Delta \theta_2 \quad (4.28)$$

The model has 28  $K$ -constants which are functions of system parameters and the initial operating condition. The initial operating point is computed from the steady state load flow solution. The detailed derivation of the constants is given in the Appendix B.

#### 4.4 State Space Model

The power system is represented in state space as:

$$\Delta \dot{X} = A \Delta X + B \Delta U \quad (4.29)$$

where the state and control vectors are:

$$\Delta X = [\Delta \delta \quad \Delta \omega \quad \Delta E'_q \quad \Delta E_{fd} \quad \Delta v_{dc}]^T \quad (4.30)$$

$$\Delta U = [\Delta m_1 \quad \Delta \theta_1 \quad \Delta m_2 \quad \Delta \theta_2]^T \quad (4.31)$$

and, state and control matrices are:

$$A = \begin{bmatrix} 0 & \omega_0 & 0 & 0 & 0 \\ -\frac{K_1}{M} & -\frac{D}{M} & -\frac{K_2}{M} & 0 & -\frac{K_{pv}}{M} \\ -\frac{K_4}{T'_{do}} & 0 & -\frac{K_3}{T'_{do}} & \frac{1}{T'_{do}} & -\frac{K_{qv}}{T'_{do}} \\ -\frac{K_A K_5}{T_A} & 0 & -\frac{K_A K_6}{T_A} & -\frac{1}{T_A} & -\frac{K_A K_{vv}}{T_A} \\ K_7 & 0 & K_8 & 0 & -K_9 \end{bmatrix}$$

$$B = \begin{bmatrix} 0 & 0 & 0 & 0 \\ -\frac{K_{pml}}{M} & -\frac{K_{p\theta 1}}{M} & -\frac{K_{pm2}}{M} & -\frac{K_{p\theta 2}}{M} \\ -\frac{K_{qml}}{T'_{do}} & -\frac{K_{q\theta 1}}{T'_{do}} & -\frac{K_{qm2}}{T'_{do}} & -\frac{K_{q\theta 2}}{T'_{do}} \\ -\frac{K_A K_{vml}}{T_A} & -\frac{K_A K_{v\theta 1}}{T_A} & -\frac{K_A K_{vm2}}{T_A} & -\frac{K_A K_{v\theta 2}}{T_A} \\ K_{cm1} & K_{c\theta 1} & K_{cm2} & K_{c\theta 2} \end{bmatrix}$$

and  $\Delta m_1$  is the deviation in pulse-width-modulation index  $m_1$  of voltage of series converter 1 in line 1.  $\Delta m_2$  is the deviation in pulse-width-modulation index  $m_2$  of voltage of series converter 2 in line 2.  $\Delta \theta_1$  is the deviation in phase angle of the injected voltage  $V_{se1}$ .  $\Delta \theta_2$  is the deviation in phase angle of the injected voltage  $V_{se2}$ .

Generally the nonlinear model of SMIB without IPFC is constituted by Equations (4.1-4.4) [104], [105] and the linearized Phillips-Heffron model of SMIB is given by Equations (4.21-4.24) where

$$\Delta P_e = K_1 \Delta \delta + K_2 \Delta E'_q \quad (4.32)$$

$$\Delta E_q = K_4 \Delta \delta + \frac{1}{K_3} \Delta E'_q \quad (4.33)$$

$$\Delta V_t = K_5 \Delta \delta + K_6 \Delta E'_q \quad (4.34)$$

The model has 6  $K$ -constants ( $K_1 - K_6$ ) which are functions of the system operating point and its parameters. The linearized equations of SMIB without IPFC in Laplace domain are given by Equations (4.35-4.38) using which the block diagram of SMIB is formed and given in Figure 4.3 [2].

$$\Delta\delta = \frac{\omega_0 \Delta\omega}{s} \quad (4.35)$$

$$\Delta\omega = \frac{(\Delta P_m - \Delta P_e - D\Delta\omega)}{Ms} = \frac{1}{Ms + D} (\Delta P_m - K_1 \Delta\delta - K_2 \Delta E'_q) \quad (4.36)$$

$$\Delta E'_q = \frac{-\Delta E_q + \Delta E_{fd}}{T'_{do}s} = \frac{K_3}{1 + K_3 T'_{do}s} (-K_4 \Delta\delta + \Delta E_{fd}) \quad (4.37)$$

$$\Delta \dot{E}_{fd} = \frac{K_A}{1 + sT_A} (\Delta V_{ref} - K_5 \Delta\delta - K_6 \Delta E'_q) \quad (4.38)$$

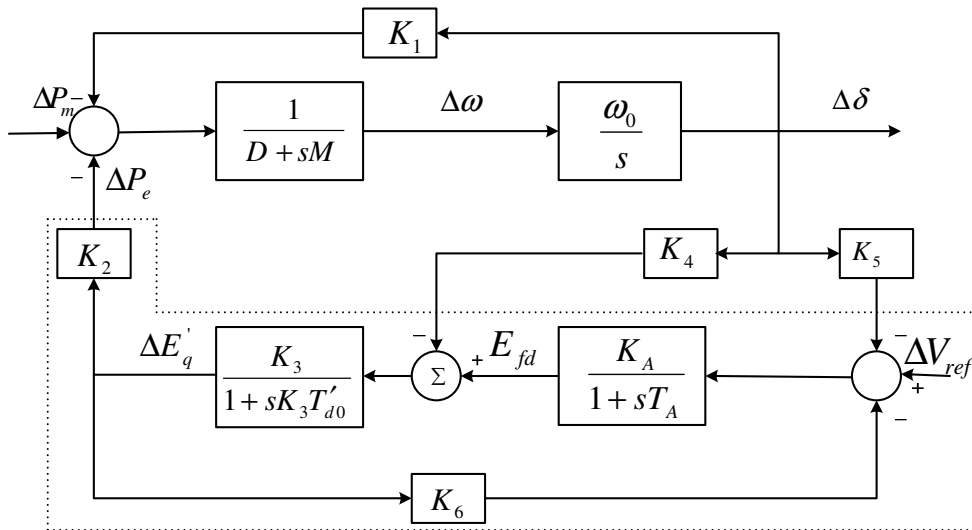


Figure 4.3: Block diagram of a SMIB

With the inclusion of IPFC in SMIB power system, the linearized Equations (4.21-4.25) in Laplace domain are given as follows:

$$\Delta\delta = \frac{\omega_o\Delta\omega}{s} \quad (4.39)$$

$$\begin{aligned} \Delta\omega &= \frac{(\Delta P_m - \Delta P_e - D\Delta\omega)}{Ms} \\ &= \frac{1}{Ms + D} (\Delta P_m - K_1 \Delta\delta - K_2 \Delta E'_q - K_{pv} \Delta v_{dc} - K_p \Delta U) \end{aligned} \quad (4.40)$$

$$\Delta E'_q = \frac{-\Delta E_q + \Delta E_{fd}}{T'_{do} s} = \frac{(\Delta E_{fd} - K_4 \Delta\delta - K_{qv} \Delta v_{dc} - K_q \Delta U)}{K_3 + T'_{do} s} \quad (4.41)$$

$$\Delta \dot{E}_{fd} = \frac{K_A}{1 + sT_A} (\Delta V_{ref} - K_5 \Delta\delta - K_6 \Delta E'_q - K_{vv} \Delta v_{dc} - K_v \Delta U) \quad (4.42)$$

$$\Delta \dot{v}_{dc} = \frac{1}{K_9 + s} (K_7 \Delta\delta + K_8 \Delta E'_q + K_c \Delta U) \quad (4.43)$$

where  $K_p, K_q, K_v$  and  $K_c$  are the row vectors defined as

$$K_p = [K_{pm1} \quad K_{p\theta1} \quad K_{pm2} \quad K_{p\theta2}] \quad (4.44)$$

$$K_q = [K_{qm1} \quad K_{q\theta1} \quad K_{qm2} \quad K_{q\theta2}] \quad (4.45)$$

$$K_v = [K_{vm1} \quad K_{v\theta1} \quad K_{vm2} \quad K_{v\theta2}] \quad (4.46)$$

$$K_c = [K_{cm1} \quad K_{c\theta1} \quad K_{cm2} \quad K_{c\theta2}] \quad (4.47)$$

The Phillips-Heffron model of SMIB with IPFC is shown in Figure 4.4. The model consists of the 28  $K$  constants. From Equation (4.31), it is observed that any one of the four control inputs  $\Delta m_1, \Delta\theta_1, \Delta m_2$  and  $\Delta\theta_2$  can be utilized to exhibit damping characteristics of IPFC. The eigenvalues are calculated from the state matrix of the system using modal analysis or eigenvalue analysis, which is described in the following section, to determine the lightly damped modes.

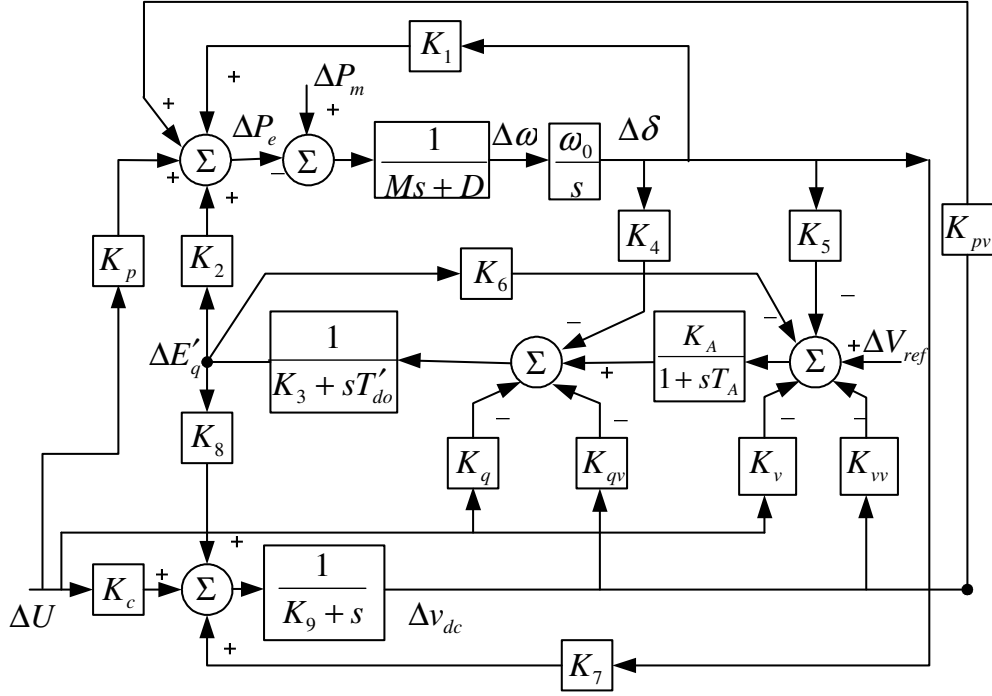


Figure 4.4: Phillips-Heffron model of SMIB system installed with IPFC

#### 4.5 Modal Analysis of the Power System

In general the linearized power system in state space form can be written as [2]:

$$\Delta \dot{X} = A \Delta X + B \Delta U \quad (4.48)$$

$$\Delta Y = C \Delta X + D \Delta U$$

where  $\Delta X$  is the state vector of length equal to number of states  $n$ ,  $\Delta Y$  is the output vector of length  $m$ ,  $\Delta U$  is the input vector of length  $r$ ,  $A$  is the  $(n \times n)$  state matrix,  $B$  is the control or input matrix of size  $(n \times r)$ ,  $C$  is the output vector of size  $(m \times n)$ ,  $D$  is the feed forward matrix of dimension  $(m \times r)$ .

Taking the Laplace transform of Equation (4.48):

$$s \Delta X(s) - X(0) = A \Delta X(s) + B \Delta U(s) \quad (4.49)$$

$$\Delta Y(s) = C \Delta X(s) + D \Delta U(s) \quad (4.50)$$

Rearranging Equations (4.49) and (4.50):

$$(sI - A)\Delta X(s) = X(0) + B\Delta U(s)$$

$$\Delta X(s) = (sI - A)^{-1}[X(0) + B\Delta U(s)]$$

$$= \frac{\text{adj}(sI - A)}{\det(sI - A)}[X(0) + B\Delta U(s)]$$

Correspondingly,

$$\Delta Y(s) = C \frac{\text{adj}(sI - A)}{\det(sI - A)}[X(0) + B\Delta U(s)] + D\Delta U(s) \quad (4.51)$$

The poles of  $\Delta X(s)$  and  $\Delta Y(s)$  are the roots of the equation  $\det(sI - A) = 0$  which is also referred to as the characteristic equation of matrix  $A$ . The values of  $s$  which satisfy the characteristic equation are the eigenvalues of  $A$ . There are a total of  $n$  eigenvalues  $\lambda_i$ ;  $i = 1, 2, \dots, n$ , as  $A$  is an  $n \times n$  matrix. The eigenvalues determine the stability of the power system as follows:

A real eigenvalue in the system corresponds to a non-oscillatory mode. A negative real eigenvalue represents a decaying mode and larger its magnitude value, earlier is its decay. When a real eigenvalue is positive it represents aperiodic instability.

Complex eigenvalues occur in conjugate pairs and each pair corresponds to an oscillatory mode. Thus, for a pair of complex eigenvalues,  $\lambda = \alpha \pm j\beta$ , the time response is of the form  $e^{-\alpha t} \sin(\beta t + \theta)$ . The real part of the eigenvalue gives the damping and imaginary part gives the oscillation frequency,  $f = \beta / 2\pi$ . The damping ratio,  $\zeta = -\alpha / (\sqrt{\alpha^2 + \beta^2})$ , determines the rate of decay of the amplitude of the oscillation. A negative real part in the complex eigenvalue represents a damped oscillation whereas a positive real part represents oscillation of increasing amplitude.

For any eigenvalue  $\lambda_i$ , there is an eigenvector  $\phi_i$  which satisfies the following equation:

$$A\phi_i = \lambda_i\phi_i, \quad i = 1, 2, \dots, n \quad (4.52)$$

where  $\phi_i$  is the right eigenvector of  $A$  associated with the eigenvalue  $\lambda_i$ . Each right eigenvector is a column vector of length  $n$  and has the form:

$$\phi_i = \begin{bmatrix} \phi_{1i} \\ \phi_{2i} \\ \vdots \\ \phi_{ni} \end{bmatrix} \quad (4.53)$$

Similarly, the  $n$ -row vector  $\psi_i$  which satisfies

$$\psi_i A = \lambda_i \psi_i \quad i = 1, 2, \dots, n \quad (4.54)$$

is called the left eigenvector associated with the eigenvalue  $\lambda_i$ , where  $\lambda_i \neq \lambda_j, i \neq j$ .

Expressing the eigenvector in matrices form, they are termed as modal matrices

$$\phi = [\phi_1 \quad \phi_2 \quad \dots \quad \phi_n] \quad (4.55a)$$

$$\psi = [\psi_1^T \quad \psi_2^T \quad \dots \quad \psi_n^T]^T \quad (4.55b)$$

$$\psi\phi = I \quad \psi = \phi^{-1}$$

Equation (4.48) is derived from physical considerations of the power system. The rate of change of each state variable is a linear combination of all the state variables. As a result of cross coupling between the states, it is difficult to isolate those parameters that influence the motion in a significant way. The state variables can be decoupled by expressing the state variables in terms of the modal variables  $Z$ . Consider a new state vector  $Z$  defined by the transformation:

$$\Delta X = \phi \Delta Z \quad (4.56)$$

or

$$\Delta Z = \psi \Delta X \quad (4.57)$$

The original state variables are represented by  $\Delta X_1, \Delta X_2, \dots, \Delta X_n$  and the transformed variables by  $\Delta Z_1, \Delta Z_2, \dots, \Delta Z_n$  which are associated with only one mode. The right eigenvector gives the mode shape, i.e., the extent of the activities of the  $n$  state variables in the  $i^{th}$  mode, and the angles of the elements in the matrix give phase displacements of the state variables with respect to the mode. The left eigenvector identifies which combination of the original state variables displays only in the  $i^{th}$  mode.

Equation (4.48) is transformed into new state equation as:

$$\Delta \dot{Z} = \phi^{-1} A \phi \Delta Z + \phi^{-1} B \Delta U \quad (4.58)$$

$$\Delta Y = C \phi \Delta Z + D \Delta U \quad (4.59)$$

The state equation in decoupled form may therefore be written as

$$\Delta \dot{Z} = \Lambda \Delta Z + B' \Delta U \quad (4.60)$$

$$\Delta Y = C' \Delta Z + D \Delta U \quad (4.61)$$

where  $\Lambda$  is a diagonal matrix consisting of eigenvalues of the state matrix  $A$ .

$$\Lambda = \phi^{-1} A \phi \quad (4.62)$$

$$B' = \phi^{-1} B \quad (4.63)$$

$$C' = C \phi \quad (4.64)$$

The mode controllability and observability matrices are defined by Equations (4.63) and (4.64) respectively. By inspecting the matrices  $B'$  and  $C'$ , one can determine the controllability and observability properties of the modes. If the  $i^{th}$  row of the matrix  $B'$  is zero, the inputs have no effect on the  $i^{th}$  mode. Such a mode is said to be uncontrollable. If the column of  $C'$  matrix is zero, the corresponding mode is unobservable. If the mode is either uncontrollable or unobservable, the feedback between the output and the input has negligible influence on the mode [2].

The eigenvalues are computed as described in this section from the state matrix. The under damped oscillation modes are observed. Additional stabilizer is provided to increase the damping of these oscillation modes. The conventional method of increasing the damping is the Power System Stabilizer (PSS). The PSS is designed based on the linearized model as explained in the following section.

#### 4.6 Power System Stabilizer (PSS)

The structure of the PSS is shown in Figure 4.5 [17], consisting of three blocks: a phase compensation block, a signal washout block and a gain block. The phase compensation block provides the appropriate phase lead characteristic to compensate the phase lag between the exciter input and the generator electrical torque.

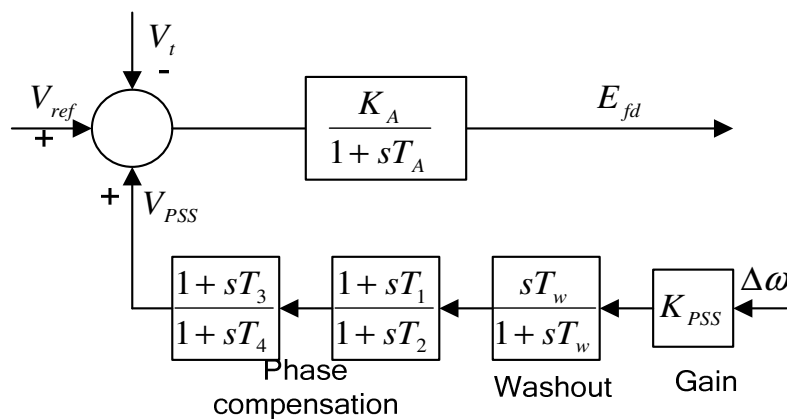


Figure 4.5: Excitation system with AVR and PSS

The signal washout block serves as a high pass filter, with the time constant  $T_w$  high enough to allow signals associated with oscillations in  $\omega$  to pass unchanged and preventing undesirable generator voltage excursions. The stabilizer gain  $K_{PSS}$  determines the amount of damping provided by the PSS. The conventional lead-lag PSS is installed in the feedback loop which produces an electrical torque component  $V_{PSS}$  in phase with the rotor speed deviation. This component is added as a supplementary signal in the excitation control to provide extra damping at the oscillating frequency. In Figure 4.5  $E_{fd}$  is the generator field voltage,  $V_t$  is the

generator output voltage,  $V_{ref}$  is the reference voltage. The block in the forward path represents the voltage regulator that has a time constant of  $T_A$  and a gain of  $K_A$ .

As discussed in [17]: The PSS is usually designed when no FACTS devices exist in the power system. The plant transfer function  $GEP(s)$  can be obtained from Figure 4.3 and is given by:

$$GEP(s) = \frac{\Delta P_e}{\Delta V_{ref}} = \frac{K_2 K_A K_3}{(1 + sK_3 T'_{do})(1 + sT_A) + K_3 K_A K_6} \quad (4.65)$$

Once  $GEP(s)$  is determined, the phase lag of  $GEP(s)$  given by  $\angle GEP(s)$  is determined at the angular frequency of system oscillation from the mechanical loop, i.e.,  $s = j\omega_n$  where  $\omega_n = \sqrt{\frac{K_1 \omega_0}{M}}$ , the undamped natural frequency of the mechanical mode and  $\omega_0 = 2\pi f$  is the system frequency in radians per sec.  $K_1$  is the constant computed in Equation (4.32) for the operating point and given system parameters.  $M$  is the inertia constant in seconds.

The transfer function of PSS is given by:

$$G_{PSS}(s) = K_{PSS} \frac{T_w s (1 + sT_1)(1 + sT_3)}{1 + T_w s (1 + sT_2)(1 + sT_4)} \quad (4.66)$$

The phase of PSS,  $\angle G_{PSS}(s)$  is set to compensate  $\beta = \angle GEP(s)$ , the phase of  $GEP(s)$ , so as to produce a purely damping torque contribution to the generator, i.e.,

$$\angle G_{PSS}(s)|_{s=j\omega_n} + \angle GEP(s)|_{s=j\omega_n} = 0 \quad (4.67)$$

The parameters of the lead-lag block are designed using the phase compensation method. The simplest transfer function of PSS may be chosen in the form of

$$G_{PSS}(s) = K_{PSS} \frac{T_w s}{1 + T_w s} \left( \frac{1 + sT_1}{1 + sT_2} \right)^k, \quad k = 1 \text{ or } 2, \quad T_1 > T_2 \quad (4.68)$$

In Figure 4.5, with  $k = 2$

$$G_{PSS}(s) = K_{PSS} \frac{T_w s}{1 + T_w s} \frac{1 + sT_1}{1 + sT_2} \frac{1 + sT_3}{1 + sT_4}$$

where  $T_3 = T_1, T_4 = T_2$ . The phase compensation provided by each lead-lag block does not exceed a maximum (usually  $60^\circ$ ) [2]. Let,

$$T_1 = aT_2, \text{ and } T_2 = \frac{1}{(\omega_n \sqrt{a})}, \text{ where, } a = \frac{(1 + \sin \beta)}{(1 - \sin \beta)}.$$

The required gain setting of the PSS for the desired damping ratio ' $\zeta$ ' is obtained as [73], [104]:

$$K_{PSS} = \frac{2 \zeta \omega_n M}{|G_{PSS}(s)| |GEP(s)|}, \quad (4.69)$$

where  $|G_{PSS}(s)|$  and  $|GEP(s)|$  are evaluated at  $s = j\omega_n$ . The value of  $T_w$  (the washout filter time constant) is chosen in the range of 10 to 20s [2]. The reasonable choice of  $\zeta$  is between 0.1 and 0.3 [2], [17].

In the actual applications, damping of the electromechanical oscillations is achieved initially with help of the Power System Stabilizers (PSS), which provides supplementary control action in the excitation systems of the generators. The PSS helps to stabilize the rotor angle and speed oscillations.

The IPFC is incorporated in the power system. The primary function of IPFC is to control the power flow in the transmission lines. In this respect, feedback controller is designed for the IPFC to control the active transmission line power. Along with the power flow control, the DC voltage across the capacitor has to be maintained constant simultaneously to ensure safe and efficient operation of IPFC. This is achieved with the use of another feedback controller which controls the DC capacitor voltage to the required constant value. The controllers used for controlling the power and DC voltage may or may not provide additional damping to the oscillations modes. In the event when the oscillations modes have further insufficient damping, supplementary damping controller for IPFC is provided to increase the damping of the oscillations

modes. Taking in view of the above, the IPFC will now be installed with three controllers as explained in the following section.

#### 4.7 Controllers of IPFC

The IPFC is installed with the following controllers:

- (i) Power flow controller
- (ii) DC voltage regulator
- (iii) Damping controller

##### 4.7.1 Power Flow Controller

The power flow controller regulates the power in the transmission lines. The structure of the power flow controller is shown in Figure 4.6 [38]. The power flow controller is of Proportional-Integral (PI) feedback type controller. The proportional and integral gains of the controller are  $k_{pp}$  and  $k_{pi}$ , respectively. The controller in Figure 4.6 regulates the real power in the transmission line 1 to the specified value of  $P_{flow1(ref)}$  in the system. The real power in the transmission line 1 can be controlled by varying the phase angle  $\theta_1$  of the series injected voltage of VSC 1. Generally the input signal  $m_1$  can also be used to regulate the active power of the transmission line, however, the range in which  $m_1$  ( $0 \leq m_1 \leq 1$ ) can be regulated is narrower than that of  $\theta_1$  ( $0 \leq \theta_1 \leq 360^\circ$ ). In Figure 4.6,  $P_{flow1}$  represents the power flow in line 1 and  $P_{flow1(ref)}$  represents the specified power flow in line 1. The error of the active power flow is amplified through the PI block and modulates the input signal  $\theta_1$ . Through PI controller the error is regulated to zero. Modulating the input signal  $\theta_1$ , the currents in both the transmission lines are controlled, as they are function of  $\theta_1$  as seen in Equations (4.17-4.20). Thus, the active and reactive powers in both the lines are modulated.

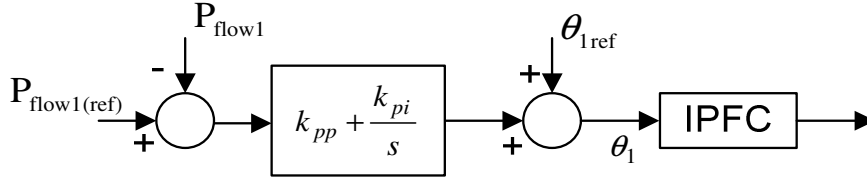


Figure 4.6: Structure of the power flow controller

#### 4.7.2 DC Voltage Regulator

The DC voltage regulator functions by controlling the exchange of active power between the two VSCs and the power system. It has to ensure that the net exchange of real power is zero. This is achieved by maintaining constant voltage across the capacitor. The DC voltage regulator is of PI type as shown in Figure 4.7 [38].  $k_{dp}$  and  $k_{di}$  are the proportional and integral gain settings of the DC voltage regulator respectively. As this regulator is responsible for converting the same amount of real power to replace the power drained by the VSC-1 through the DC link, the regulator is used to modulate the input signal  $\theta_2$ , the phase angle of the injected voltage of VSC 2. In the Figure 4.7  $v_{dc}$  is the DC voltage across the capacitor and  $v_{dc(ref)}$  is the reference voltage. Since the currents flowing in the transmission lines are function of  $\theta_2$  as seen in (4.17-4.20), this controller make sure the net active power exchanged is zero.

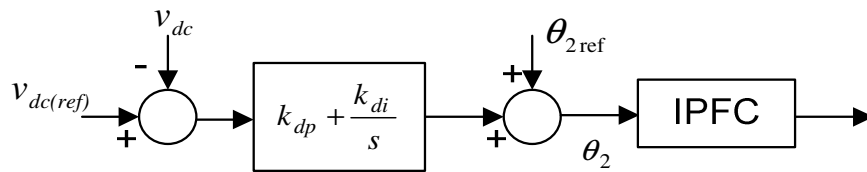


Figure 4.7: Structure of the DC voltage regulator

During power flow control one PI controller may or may not be sufficient to obtain the desired power flows in the transmission lines. It becomes necessary to have additional PI controllers to control the other input signals of IPFC to achieve the preferred power flows in the lines. The reactive power flow in transmission line 1 can be modulated through input signal  $m_1$ , as the input signal  $\theta_1$  is utilized for controlling  $P_{flow1}$  in line 1.

The real power in transmission line 2 can be controlled by input signal  $m_2$ , since apparently the input signal  $\theta_2$ , of VSC-2 is utilized for controlling the DC voltage, The controllers are of PI feedback type controller similar to Figure 4.6, whereas the inputs to these controllers vary corresponding to reactive power flow control in line 1 or real power flow control in line 2.

### 4.7.3 IPFC Damping Controller

The IPFC damping controller is designed to increase the damping of the selected oscillation mode. The structure of the IPFC based damping controller is shown in Figure 4.8 [38], which comprises of the amplification block having gain  $K_{pod}$ , signal washout block and  $m_c$  stages of lead lag compensator blocks.  $K_{pod}$ , is a positive gain, and  $T_w$  is the washout time constant.  $T_{1dc}$  and  $T_{2dc}$  are the lead and lag time constants respectively. The time constants of lead-lag compensator are determined using the phase compensation method [2] to compensate the phase shift between the control input signal  $\Delta U$  and electrical power deviation  $\Delta P_e$ .

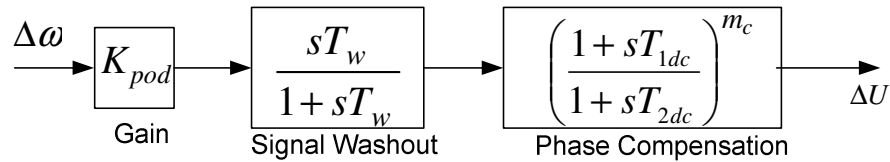


Figure 4.8: Structure of IPFC based damping controller

The steps to determine the damping controller constants are as follows: Compute the natural frequency of oscillation  $\omega_n$  from the mechanical loop as:

$$\omega_n = \sqrt{K_1 \omega_0 / M} \quad (4.70)$$

where  $K_1$  is the synchronizing torque coefficient value determined in Equation (4.26) of the linearized system when IPFC is placed.

Let  $\gamma$  be the angle of the transfer function:

$$G_s(s) = \frac{\Delta P_e}{\Delta U}, \quad (4.71)$$

which gives the phase lag between  $\Delta U$  and  $\Delta P_e$ , at  $s = j\omega_n$  with  $\Delta U$  being one of the inputs ( $\Delta m_1, \Delta \theta_1, \Delta m_2$ , or  $\Delta \theta_2$ ) as shown in Figure 4.9. Figure 4.9 represents the transfer function block diagram of the system relating electrical power  $\Delta P_e$  and  $\Delta U$ . The transfer function of the IPFC based damping controller is represented by:

$$G_c(s) = K_{pod} \frac{sT_w}{1+sT_w} \left( \frac{1+sT_{1dc}}{1+sT_{2dc}} \right)^{m_c} \quad (4.72)$$

The phase compensation limit provided by each lead-lag block is about  $60^\circ$ . The number of the lead-lag blocks  $m_c$  is determined by taking the largest number near to  $\gamma/60$ , where  $\gamma$  is the required phase compensation of the controller at the concerned oscillation mode frequency range.

Assume for the lead-lag network,

$$T_{1dc} = aT_{2dc}, \quad (4.73)$$

where  $a = \frac{(1 + \sin \gamma)}{(1 - \sin \gamma)}$  and  $T_{2dc} = \frac{1}{(\omega_n \sqrt{a})}$ .

The required gain setting of the damping controller for the desired damping ratio ' $\zeta$ ' is obtained as:

$$K_{pod} = \frac{2\zeta\omega_n M}{|G_c(s)||G_s(s)|}, \quad (4.74)$$

where  $|G_s(s)|$  and  $|G_c(s)|$  are evaluated at  $s = j\omega_n$ . The value of  $T_w$  (the washout filter time constant) is chosen in the range of 10 to 20s [2]. The reasonable choice of  $\zeta$  is between 0.1 and 0.3 [17]. The four control parameters,  $m_1, m_2, \theta_1$  and  $\theta_2$  can be modulated to produce the damping torque. The damping controller based on the IPFC

input signal  $m_1$  is termed as the damping controller  $m_1$  and consequently other controller based on input signals  $m_2, \theta_1$  and  $\theta_2$  are termed as damping controller  $m_2$ , damping controller  $\theta_1$  and damping controller  $\theta_2$ .

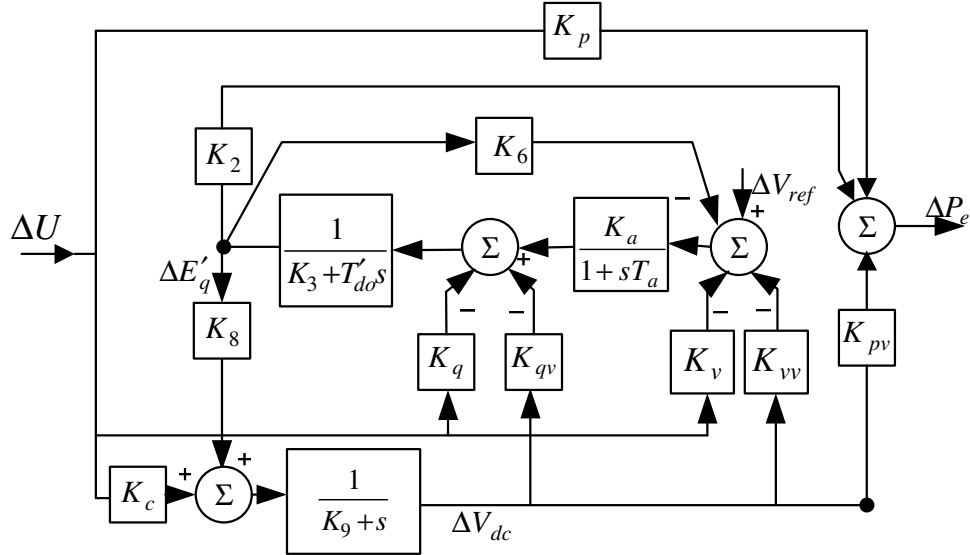


Figure 4.9: Block diagram of the system relating electrical power  $\Delta P_e$  and  $\Delta U$

However, one of the first stages in the design of the stabilizer is the selection of the IPFC input signal parameter upon which the damping signal is superimposed. In order to select the IPFC control parameter most suitable for modulation, by the damping controller, the concept of a controllability index is used. The controllability index is formulated based on an approximate multimodal decomposition approach as explained in Appendix B [29].

#### 4.8 Case Study: SMIB Power System With IPFC

A SMIB power system with IPFC as shown in Figure 4.1 is considered for analysis. The data for the system (in p.u. except where indicated) are given in Table 4.1 [9]. The load flow is performed to find the steady state condition of the system, i.e., the voltages at various buses with their phase angles and the power flows in the transmission lines, the results of which are given in Table 4.2.

Table 4.1: SMIB power system data

$H = 4.0s.$	$D = 0.0$	$T'_{d0} = 5.044s$	$x_d = 1.0$	$x_q = 0.6$	$x'_d = 0.3$
$x_t = 0.01$	$x_{t1} = 0.015$	$x_{t2} = 0.015$	$x_{L1} = 0.05$	$x_{L2} = 0.05$	$K_A = 10.0$
$T_A = 0.01s$	$v_{dc} = 2 \text{ p.u.}$	$P_e = 0.8$	$V_b = 1.0$	$V_t = 1.02$	$C_{dc} = 0.2$

Table 4.2: Load flow results of SMIB power system with IPFC

$P_e = 0.8 \text{ p.u.}$	$Q_e = -1.0223 \text{ p.u.}$	$V_t = 1.02 \text{ p.u.}$	$V_b = 1.0 \text{ p.u.}$
$V_{se1} = 0.0512 \text{ p.u.}$	$V_{se2} = 0.1237 \text{ p.u.}$	$\theta_1 = -77.8458^\circ$	$\theta_2 = -23.8761^\circ$
$\delta = 0.8280 \text{ rad}$	$P_{flow1} = 0.4 \text{ p.u.}$	$Q_{flow1} = 0.2921 \text{ p.u.}$	$P_{flow2} = 0.4 \text{ p.u.}$

Table 4.2 shows the results from the load flow, which gives the power flows in each transmission line represented by  $P_{flow1}$ ,  $Q_{flow1}$  and  $P_{flow2}$ , injected voltages  $V_{se1}$  and  $V_{se2}$ , and their corresponding phase angles  $\theta_1$  and  $\theta_2$  of VSCs of IPFC in each transmission line. The real and reactive power at the generator bus is given by  $P_e$  and  $Q_e$ .  $V_t$  is the terminal voltage of the generator bus.  $V_b$  is the voltage of infinite bus. The numerical values are computed at the nominal operating point of  $P_e = 0.8 \text{ p.u.}$ , i.e., the generator is generating an electrical power of 0.8 p.u. for a 100 MVA base. The nonlinear equations of the power system are linearized around this operating point. The  $K$  constants computed at this operating point are given in Table 4.3. The state, control, and output matrices ( $A, B$  and  $C$ ) are computed and are given by Equations (4.75-4.77). The outputs taken are  $\Delta P_e$  and  $\Delta P_{flow1}$ . The system is found to be controllable and observable from the controllability and observability matrices calculated as described in Section 4.5.

Table 4.3:  $K$  constants at the operating point of  $P_e = 0.8 \text{ p.u.}$

$K_1 = 1.575856$	$K_2 = 2.382711$	$K_3 = 3.043796$	$K_4 = 1.667898$
$K_5 = 0.000299$	$K_6 = 0.082475$	$K_7 = 0.023072$	$K_8 = 0.027127$
$K_9 = 0.004617$	$K_{pv} = 0.036168$	$K_{qv} = -0.005127$	$K_{vv} = 0.029190$
$K_{pm1} = 0.721441$	$K_{p\theta1} = -0.008752$	$K_{pm2} = 0.286143$	$K_{p\theta2} = -0.084596$
$K_{qm1} = 0.590336$	$K_{q\theta1} = -0.042716$	$K_{qm2} = -0.327326$	$K_{q\theta2} = -0.119733$
$K_{vm1} = 0.116607$	$K_{v\theta1} = 0.022488$	$K_{vm2} = 0.423723$	$K_{v\theta2} = 0.020285$
$K_{cm1} = -1.442618$	$K_{c\theta1} = 0.199523$	$K_{cm2} = -4.999133$	$K_{c\theta2} = 0.028017$

$$A = \begin{bmatrix} 0 & 377 & 0 & 0 & 0 \\ -0.1970 & 0 & -0.2978 & 0 & -0.0045 \\ -0.3307 & 0 & -0.6034 & 0.1983 & 0.001 \\ -0.2986 & 0 & -82.4750 & -100 & -29.1897 \\ 0.0231 & 0 & 0.0271 & 0 & -0.0046 \end{bmatrix} \quad (4.75)$$

$$B = \begin{bmatrix} 0 & 0 & 0 & 0 \\ -0.0902 & 0.0011 & -0.0358 & 0.0106 \\ -0.1170 & 0.0085 & 0.0649 & 0.0237 \\ -116.6073 & -22.4884 & -423.7235 & -20.2849 \\ -1.4426 & 0.1995 & -4.9991 & 0.0280 \end{bmatrix} \quad (4.76)$$

$$C = \begin{bmatrix} 1.5759 & 0 & 2.3827 & 0 & 0 & 0.0362 \\ -0.7413 & 0 & -1.0753 & 0 & -0.0182 \end{bmatrix} \quad (4.77)$$

The eigenvalues are computed from the state matrix formed by using the  $K$  constants in Table 4.3. Table 4.4 gives the computed eigenvalues, for the power system with IPFC. The system contains real and one pair of complex eigenvalues and they are stable. The oscillation modes have a damping ratio of 0.0291 and are lightly damped. These undamped modes have an oscillation frequency of 1.3697 Hz. They contribute to local area oscillations (1-2Hz) when the system is subjected to a disturbance. The disturbance can be in the form of change in mechanical input or a three phase fault. The pair of oscillation modes given by complex eigenvalues are contributed by the rotor angle and rotor speed variables of the generator. The real eigenvalues are contributed by the remaining state variables of Equation (4.30).

Table 4.4: Eigenvalues of the linearized SMIB with IPFC at operating point

$$P_e = 0.8 \text{ p.u.}$$

Eigenvalues	Damping Ratio	Frequency
-99.8353	1	0
-0.2503±j 8.6063	0.0291	1.3697
-0.2685	1	0
-0.0037	1	0

The damping of the oscillations modes is increased by placing the PSS in the excitation system of the generator. The PSS is designed as described in Section 4.6.

The PSS parameters are;  $K_{pss} = 1.9889$  ,  $T_1 = 0.33239$  ,  $T_2 = 0.054258$  , and  $T_3 = T_1, T_4 = T_2, T_w = 10$  . The PSS is designed at the operating point  $P_e = 0.8$  p.u. The controllers of IPFC, i.e., the PI power flow controller controlling the real power in transmission line 1 and PI DC voltage regulator, are placed in the system to maintain the powers in the transmission line and maintain the DC voltage constant in the event of disturbance. The parameters of the power flow controller are  $k_{pp} = 1$  and  $k_{pi} = 0.01$  and DC voltage regulator are  $k_{dp} = 4$  and  $k_{di} = 4$ . They have been designed by trial and error using simulation. The effect of controllers on the oscillation mode of the SMIB system incorporated with IPFC is given in Table 4.5. It has been observed that the PSS significantly increases the damping ratio to 0.09. The PI power flow controller and DC voltage regulator have little influence on the oscillation mode. Together they contribute to minor increase in damping ratio.

Table 4.5: Eigenvalues of the linearized SMIB with IPFC and controllers at operating point  $P_e = 0.8$  p.u.

SMIB with IPFC and Controllers	Eigenvalues	Damping Ratio	Frequency
No controllers	$-0.2503 \pm j 8.6063$	0.0291	1.3697
With only PSS	$-0.77508 \pm j 8.5625$	0.090152	1.3628
PSS and Power flow controller	$-0.79007 \pm j 8.5463i$	0.092053	1.3602
PSS and DC voltage regulator	$-0.77262 \pm j 8.5622$	0.08987	1.3627
PSS, power flow controller and DC voltage regulator	$-0.77649 \pm j 8.5758i$	0.090176	1.3649

The IPFC is installed with the damping controller to increase the damping of the oscillation mode present in the system. The structure of the damping controller is shown in Figure 4.10. The input to the controller is the rotor speed. The damping controller contributes a positive damping torque in phase with the speed deviation to the electromechanical oscillation loop of the generator. The parameters of the damping controller are designed as described in Section 4.7.3 using phase compensation technique. The output of the damping controller superimposes and modulates any one of the input signal  $u = (m_1, m_2, \theta_1 \text{ or } \theta_2)$  of IPFC. The controller

is designed to increase the damping ratio of the oscillation mode to a reasonable choice between 0.1 and 0.3 [17].

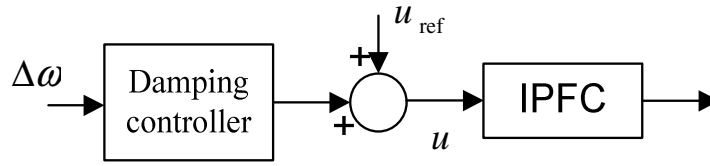


Figure 4.10: IPFC based damping controller

The active power generated by the generator may change in the range from lighter load condition  $P_e = 0.2$  p.u. to heavier load condition  $P_e = 1.2$  p.u. with  $V_t = 1.02$  p.u. ,  $V_b = 1.0$  p.u. to meet the varying requirement of power supply. The effectiveness of damping controller also changes with the variation of power system operating conditions. Therefore, the IPFC based damping controller should be designed at an operating point such that it is robust over a set of know operating conditions. Table 4.6 gives the eigenvalues computed at different operating points without any controllers. Figure 4.11 shows the relationship between the damping ratio of the oscillation mode and the operating point. From Table 4.6 and Figure 4.11, it is observed that the oscillation mode is of poorest damping at operating condition  $P_e = 1.2$  p.u.

Table 4.6: Eigenvalues of the system computed at different operating points

Operating point $P_e$	Eigenvalues	Damping ratio	Frequency
0.2	$-0.42927 \pm j 7.5064$	0.057095	1.1947
0.4	$-0.3456 \pm j 7.683$	0.044937	1.2228
0.6	$-0.26677 \pm j 8.0658$	0.033057	1.2837
0.8	$-0.2503 \pm j 8.6063$	0.029075	1.3697
0.9	$-0.24842 \pm j 8.8303$	0.028122	1.4054
1.0	$-0.24446 \pm j 9.0188$	0.027096	1.4354
1.2	$-0.23165 \pm j 9.3249$	0.024834	1.4841

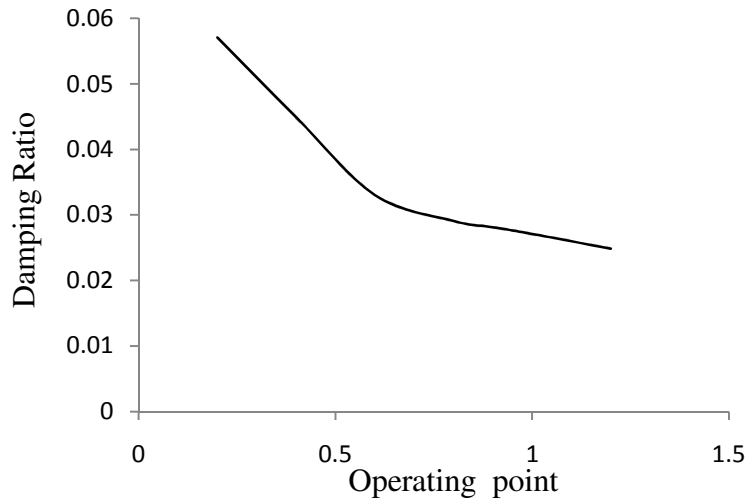


Figure 4.11: Damping ratio versus operating condition.

There are two potential choices of operating conditions for designing the IPFC based damping controller:

- 1) The nominal operating condition  $P_e = 0.8$  p.u , which is the usual active power delivered by the generator.
- 2) The operating point at which the system oscillation mode is of poorest damping  $P_e = 1.2$  p.u.

IPFC based damping controller is designed at the two operating points and its effectiveness is verified over varying operating conditions through eigenvalue analysis. To determine which input signal is significant in providing the damping, the controllability index is calculated. The controllability index is computed based on the linearized model for the electromechanical mode to be damped, taking the control parameters  $(\Delta m_1, \Delta \theta_1, \Delta m_2, \Delta \theta_2)$  into account one at a time. The controllability indices with different IPFC controllable parameters are given in Table 4.7 and Table 4.8 computed at the two operating points  $P_e = 0.8$  p.u and  $P_e = 1.2$  p.u respectively. Observation of Table 4.7 and Table 4.8 reveals that the controllability index corresponding to IPFC control parameter  $m_1$  has higher controllability index

compared to other input signals and thus, is the most efficient signal for damping. The signals  $\theta_1$  and  $\theta_2$  have lesser values of controllability index.

Table 4.7: Controllability indices with different IPFC controllable parameters at operating point  $P_e = 0.8$  p.u

Input signal	Controllability index
$\Delta m_1$	0.090447
$\Delta \theta_1$	0.0011749
$\Delta m_2$	0.035781
$\Delta \theta_2$	0.010632

Table 4.8: Controllability indices with different IPFC controllable parameters at operating point  $P_e = 1.2$  p.u

Input signal	Controllability index
$\Delta m_1$	0.11336
$\Delta \theta_1$	0.0010221
$\Delta m_2$	0.085591
$\Delta \theta_2$	0.0096744

To confirm the prediction, the various damping controllers are designed and installed in the system, to achieve an improvement of the damping ratio of the oscillation mode to around 0.1. The various damping controllers modulating different input signals ( $m_1$ ,  $m_2$ ,  $\theta_1$  and  $\theta_2$ ) are designed at the nominal operating point, i.e.,  $P_e = 0.8$  p.u. and  $P_e = 1.2$  p.u., based on the linearized model to mitigate the oscillations. The parameters of each controller, are given in Table 4.9 designed at the operating point  $P_e = 0.8$  p.u. and in Table 4.10 designed at operating point  $P_e = 1.2$  p.u., which are computed using phase compensation method. From Tables 4.9 and 4.10, it is observed that the damping controllers  $m_1$  and  $m_2$  have only one lead-lag block compared to the other damping controllers  $\theta_1$  and  $\theta_2$ . The gain values of the damping controllers  $m_1$  and  $m_2$  are also comparatively less making them cost efficient. The other two damping controllers  $\theta_1$  and  $\theta_2$  have larger gain values, thus making them less efficient comparatively.

Using these designed damping controllers, the eigenvalues of the system are computed with only damping controllers to observe their contribution towards increase of damping ratio of the oscillation mode. Table 4.11 gives the eigenvalues computed at the operating point  $P_e = 0.8$  p.u. with the damping controllers designed at  $P_e = 0.8$  p.u. whose values are given in Table 4.9. Table 4.12 gives the eigenvalues computed at the operating point  $P_e = 1.2$  p.u. with the damping controllers designed at  $P_e = 1.2$  p.u. whose values are given in Table 4.10.

Table 4.9: Parameters of the damping controllers designed at operating condition  $P_e = 0.8$  p.u.

Damping controller	Parameters of the damping controller				
	Phase angle $\gamma$	$K_{pod}$	$T_{1dc}$	$T_{2dc}$	$m_c$
$m_1$	8.0903	21.974	0.10071	0.1337	1
$\theta_1$	132.11	5005.5	0.024605	0.54728	2
$m_2$	40.087	73.382	0.054004	0.24935	1
$\theta_2$	176.99	5379.1	0.032184	0.41841	3

Table 4.10: Parameters of the damping controllers designed at operating condition  $P_e = 1.2$  p.u.

Damping controller	Parameters of the damping controller				
	Phase angle $\gamma$	$K_{pod}$	$T_{1dc}$	$T_{2dc}$	$m_c$
$m_1$	6.443	18.523	0.095688	0.11988	1
$\theta_1$	63.363	4032	0.025354	0.45243	1
$m_2$	19.479	26.396	0.075722	0.15149	1
$\theta_2$	171.92	4631.6	0.031415	0.36514	3

Table 4.11: Eigenvalues of the system computed at  $P_e = 0.8$  p.u. using the damping controllers designed at  $P_e = 0.8$  p.u.

Input signal	Eigenvalues	Damping ratio	Frequency
$\Delta m_1$	-1.1309 $\pm j$ 8.595	0.13045	1.3679
$\Delta \theta_1$	-0.86263 $\pm j$ 7.9853	0.1074	1.2709
$\Delta m_2$	-1.0711 $\pm j$ 8.689	0.12235	1.3829
$\Delta \theta_2$	-0.81261 $\pm j$ 8.7377	0.092601	1.3906

Table 4.12: Eigenvalues of the system computed at  $P_e = 1.2$  p.u. using the damping controllers designed at  $P_e = 1.2$  p.u.

Input signal	Eigenvalues	Damping ratio	Frequency
$\Delta m_1$	$-1.1813 \pm j 9.3048$	0.12594	1.4809
$\Delta \theta_1$	$-1.1774 \pm j 9.4998$	0.123	1.5119
$\Delta m_2$	$-1.1064 \pm j 9.3423$	0.1176	1.4869
$\Delta \theta_2$	$-0.76049 \pm j 9.4293$	0.080391	1.5007

It is observed at both the operating points that the damping controller  $m_1$  and  $m_2$  provides better damping with lesser gain values and with use of only one lead-lag compensator blocks. However, comparing between  $m_1$  and  $m_2$  damping controllers, the gain value of the damping controller  $m_1$  is much less than damping controller  $m_2$ . As such the damping controller  $m_1$  is the most efficient to provide damping to the oscillation mode. This confirms with the controllability indices calculated in Table 4.7 and Table 4.8. Thus, for providing the damping for the oscillations in SMIB power system, the damping controller  $m_1$  will be considered for further analysis. To investigate the robustness of the damping controller, the operating conditions of the power system are varied and the effect of the controller is observed on the oscillation mode. Table 4.13 and Table 4.14 gives the oscillation modes of the eigenvalues calculated due to the variation in the system operating conditions ( $P_e = 0.2$  to  $1.2$  p.u.) with the IPFC based damping controller  $m_1$  designed at operating point  $P_e = 0.8$  p.u. and  $P_e = 1.2$  p.u. respectively.

Table 4.13: Oscillation modes calculation with the damping controller  $m_1$  designed at operating point  $P_e = 0.8$  p.u.

Op. point	Eigenvalues	Damping ratio	Frequency
0.2	$-0.60792 \pm j 7.206$	0.084064	1.1469
0.4	$-0.85677 \pm j 7.5429$	0.11286	1.2005
0.6	$-0.98889 \pm j 8.0225$	0.12234	1.2768
<b>0.8</b>	<b><math>-1.1309 \pm j 8.595</math></b>	<b>0.13045</b>	<b>1.3679</b>
0.9	$-1.191 \pm j 8.8258$	0.13374	1.4047
1.0	$-1.2402 \pm j 9.0193$	0.13622	1.4355
1.2	$-1.3153 \pm j 9.3321$	0.13956	1.4853

Table 4.14: Oscillation modes calculation with the damping controller  $m_1$  designed at operating point  $P_e = 1.2$  p.u.

Op. point	Eigenvalues	Damping ratio	frequency
0.2	$-0.57547 \pm j 7.2406$	0.079228	1.1524
0.4	$-0.78601 \pm j 7.5472$	0.10359	1.2012
0.6	$-0.8949 \pm j 8.0091$	0.11104	1.2747
0.8	$-1.0193 \pm j 8.574$	0.11805	1.3646
0.9	$-1.0726 \pm j 8.8026$	0.12096	1.401
1.0	$-1.1159 \pm j 8.9945$	0.12312	1.4315
<b>1.2</b>	<b><math>-1.1813 \pm j 9.3048</math></b>	<b>0.12594</b>	<b>1.4809</b>

Both the designs result in effective damping at the operating point selected and quite consistent within neighbouring operating conditions. However a slight difference lies mostly during the lighter load operating condition  $P_e = 0.2$  p.u. Compare the results of Table 4.13 and Table 4.14, (the eigenvalues computed with IPFC based damping controller) with that of Table 4.6, (the eigenvalues computed when no damping controller is used). It is observed that the damping contributed at operating point  $P_e = 0.2$  p.u., by the damping controller designed at  $P_e = 1.2$  p.u. is less compared to the damping controller designed at operating point  $P_e = 0.8$  p.u. However, with increase of its gain value the damping controller designed at  $P_e = 1.2$  p.u. will also be suitable at different operating conditions. For further power system analysis, the damping controller  $m_1$  designed at nominal operating point  $P_e = 0.8$  p.u. is selected.

The various controllers of IPFC (PI real power flow controller, DC voltage regulator and damping controller) along with the PSS are placed in the power system. The schematic diagram representing the SMIB power system with IPFC and its controllers is shown in Figure 4.12. The eigenvalues of the complete closed loop system are computed and are given in Table 4.15. The system is stable and all the oscillation modes are sufficiently damped.

In presence of PSS and damping controller, the oscillation mode damping ratio has increased to 0.2109. The other conjugate pair of eigenvalues have significant higher damping ratio as such they are not of concern in contributing the oscillations.

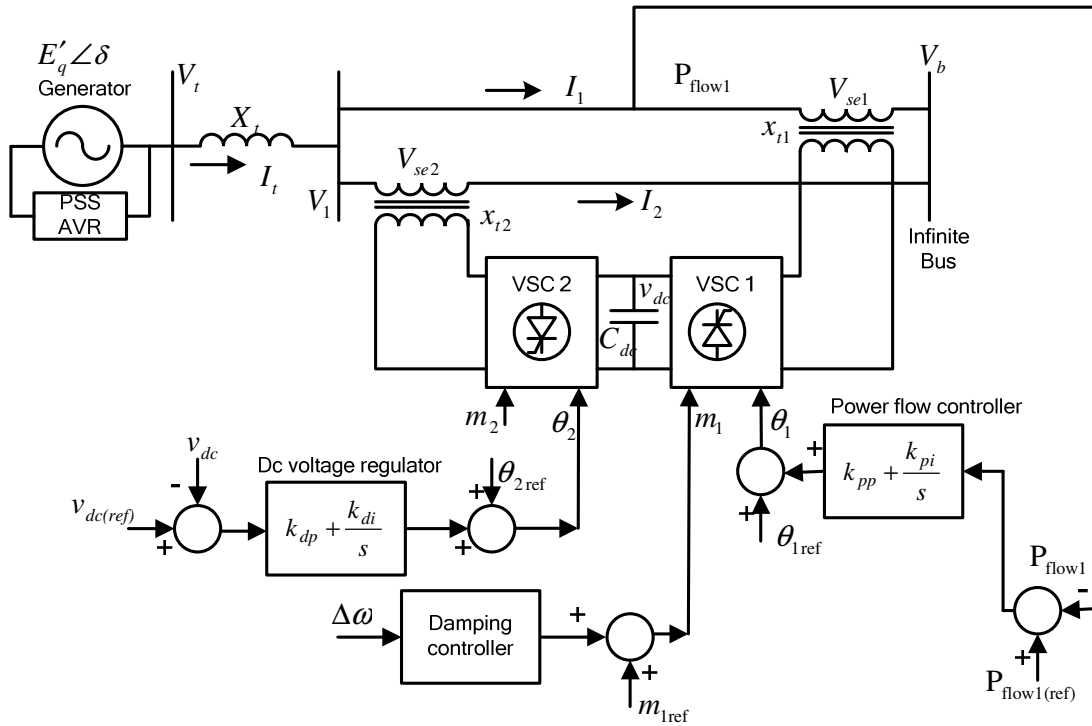


Figure 4.12: SMIB power system with IPFC and its controllers

Table 4.15: Eigenvalues of the SMIB power system incorporated with IPFC, with PSS, PI power flow controller, DC voltage regulator and damping controller with speed as input

Eigenvalues	Damping ratio	frequency
0		
-100.45	1	0
-17.419 ± j 6.1054	0.94371	0.97171
<b>-2.1118 ± j 9.7876</b>	<b>0.21091</b>	<b>1.5577</b>
-7.7599	1	0
-3.0144	1	0
-0.44873 ± j 0.98797	0.41354	0.15724
-0.27731	1	0
-0.09988	1	0
-2.46E-15	1	0
-0.1	1	0

Since the damping controller is designed on the linearized system, its effectiveness is verified on nonlinear power system through nonlinear simulation of the system. The dynamic response of the system is observed with the controllers.

The system response is observed in the time domain simulations for the power system. The nonlinear simulation is conducted through numerical integration and as well as by MATLAB/SIMULINK. Simulation through either method gives the same results. The numerical integration of the differential equations is performed using ode45 functions in Matlab. The MATLAB/SIMULINK block diagram of the nonlinear model of SMIB power system installed with IPFC is developed and is shown in Figures 4.13 –4.17.

Figure 4.13 represents the swing equations: rotor angle Equation (4.1) and speed Equation (4.2) along with the damping controller. The rotor speed is used as input for the damping controller in the SMIB power system as shown. Figure 4.14 represents the generator internal voltage Equation (4.3) and field voltage Equation (4.4). Figure 4.15 shows the simulink model for calculating the DC link capacitor voltage Equation (4.5). Figure 4.16 represents the simulink model for computing the electrical power from the generator and the terminal voltage. Figure 4.17 shows the simulink model for calculating the transmission line currents in d-q axis from Equations (4.17-4.20).

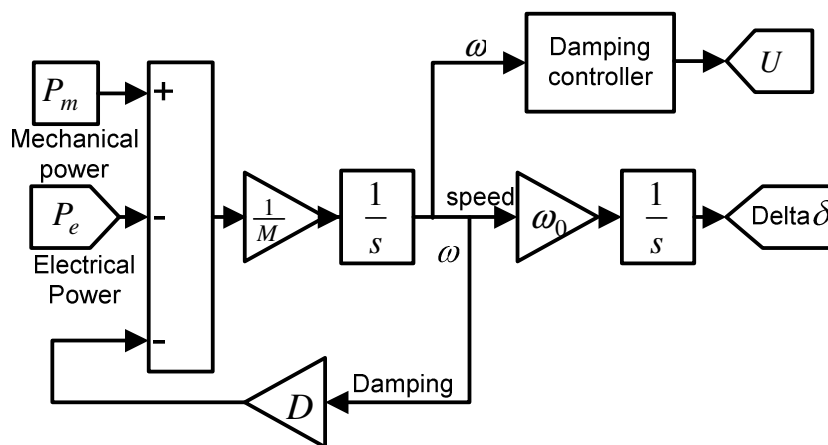


Figure 4.13: Simulink model representing rotor angle and speed

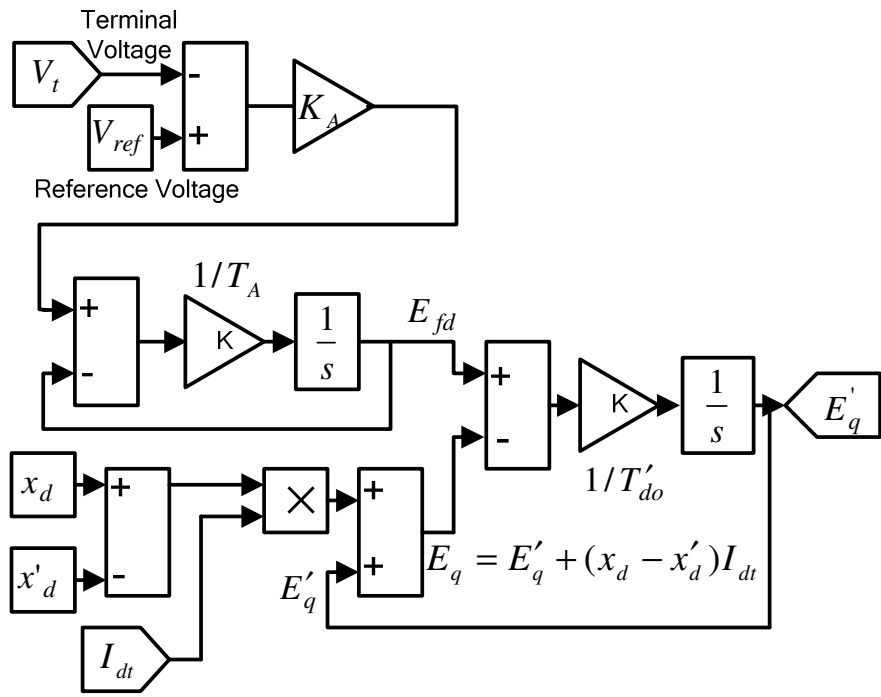


Figure 4.14: Simulation model representing internal voltage and field voltage

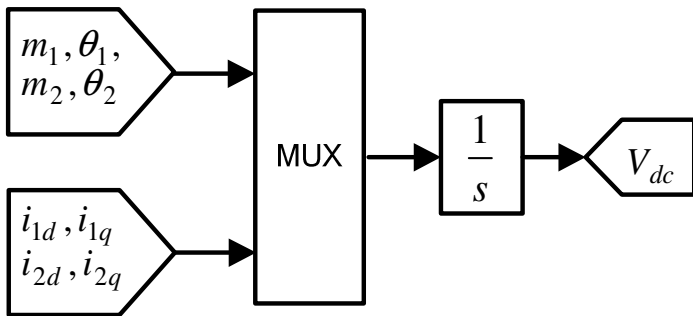


Figure 4.15: Simulation model representing the DC link capacitor voltage

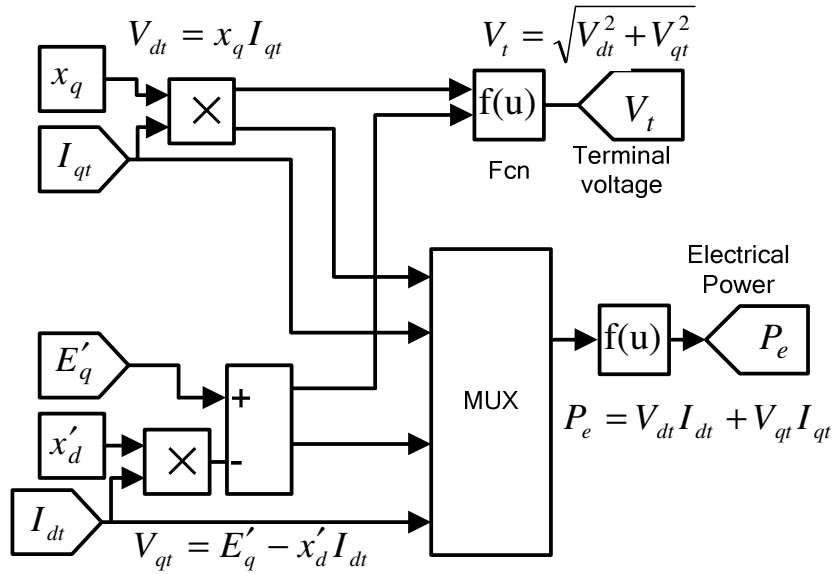


Figure 4.16: Simulation model for calculation of electrical power and terminal voltage

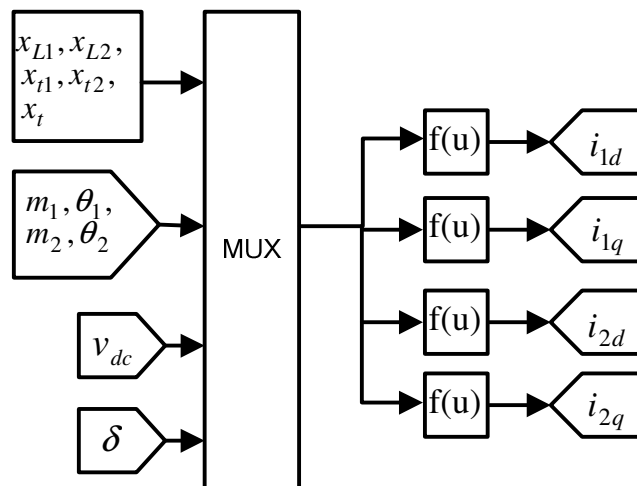


Figure 4.17: Simulation model for calculating the transmission line currents

The system is equipped with the PI power flow controller which controls the active power flow in transmission line 1 at 0.4 p.u. The PI voltage regulator maintains the DC voltage across the capacitor at a constant value of 2 p.u. The system is subjected to various disturbances and the performances of the PSS and damping controllers are investigated.

#### 4.8.1 Disturbance: Step Change in Mechanical Power

A disturbance in the form of a step variation of 0.05 p.u., in mechanical power input  $P_m$ , at 0.5s is applied. Power system oscillations are observed due to this disturbance and are lightly damped. The transmission line power flow is controlled by the injected series voltage such that the rotor angle oscillation is sufficiently damped. The magnitude and phase angle of injected series voltage is controlled by the input signals of the IPFC. The input signals are modulated by the controllers. Ultimately the effectiveness of IPFC damping controller is observed in damping the oscillations.

Figures 4.18 - 4.19 gives the response of the rotor angle at the operating condition  $P_e = 0.8$  p.u., in presence of PSS and damping controllers  $m_1$ ,  $m_2$  and  $\theta_1$ ,  $\theta_2$  respectively. These controllers have been designed at the operating point  $P_e = 0.8$  p.u. The power flow controller and DC voltage regulator are present in the system. The damping controllers  $m_1$ , gives a better performance than the damping controller  $m_2$  as seen in Figure 4.18. The damping controllers  $\theta_1$  and  $\theta_2$  have the least damping effect on the oscillations as seen in Figure 4.19. It is thus shown that the damping controllers  $\theta_1$  and  $\theta_2$  are not suitable signals for providing damping. This is verified with the controllability indices given in Table 4.7.

Figure 4.20 shows the active power flow response on transmission line 1 and Figure 4.21 gives the capacitor voltage  $v_{dc}$  response in the presence of various damping controllers. Figure 4.22 shows the rotor angle response in the presence of damping controller  $m_1$  designed at operating conditions  $P_e = 0.8$  p.u. and  $P_e = 1.2$  p.u. They give similar responses.

Figure 4.23 gives the electrical power  $P_e$  response generated by the generator at various operating conditions with the damping controller  $m_1$  designed at operating condition  $P_e = 0.8$  p.u. The damping controller sufficiently dampens the oscillations.

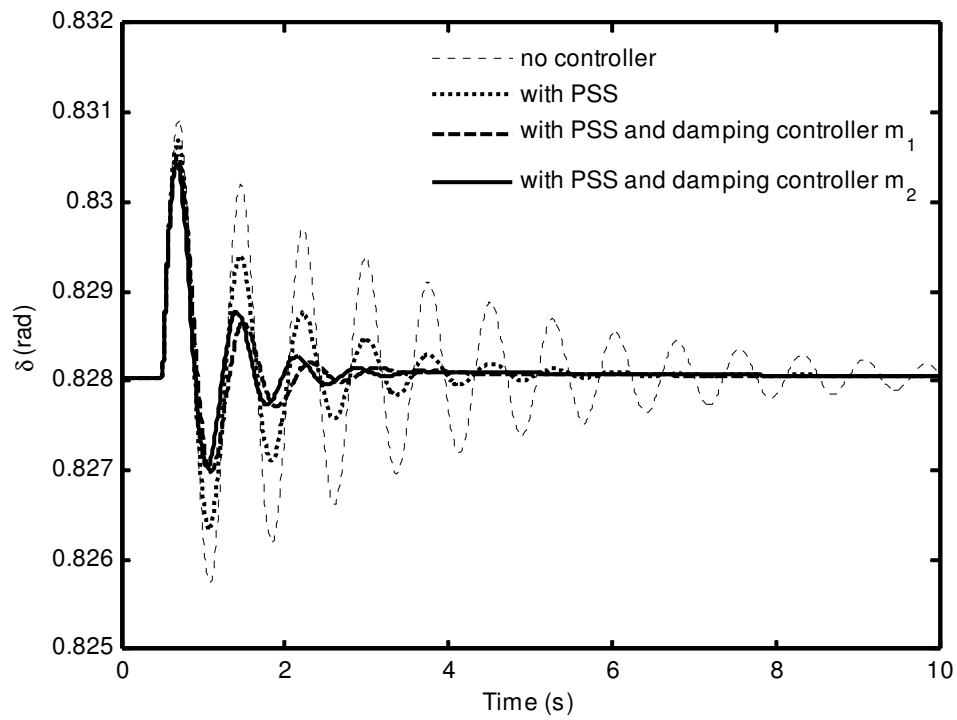


Figure 4.18: Rotor angle response with the damping controllers  $m_1$  and  $m_2$  and PSS with step change in mechanical power

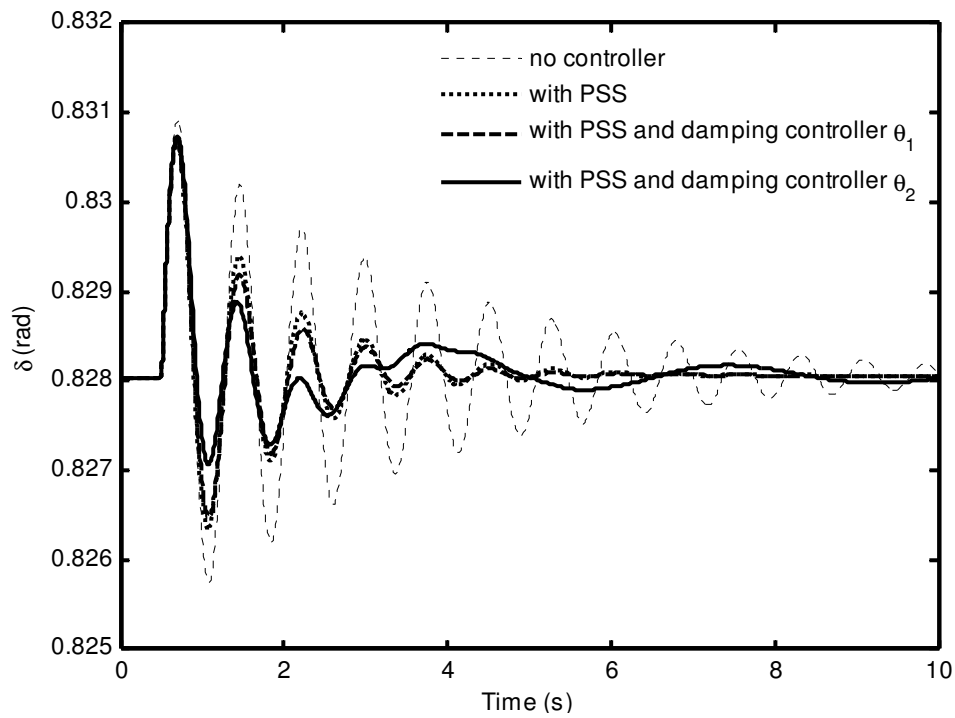


Figure 4.19: Rotor angle response with the damping controllers  $\theta_1$  and  $\theta_2$  and PSS with step change in mechanical power

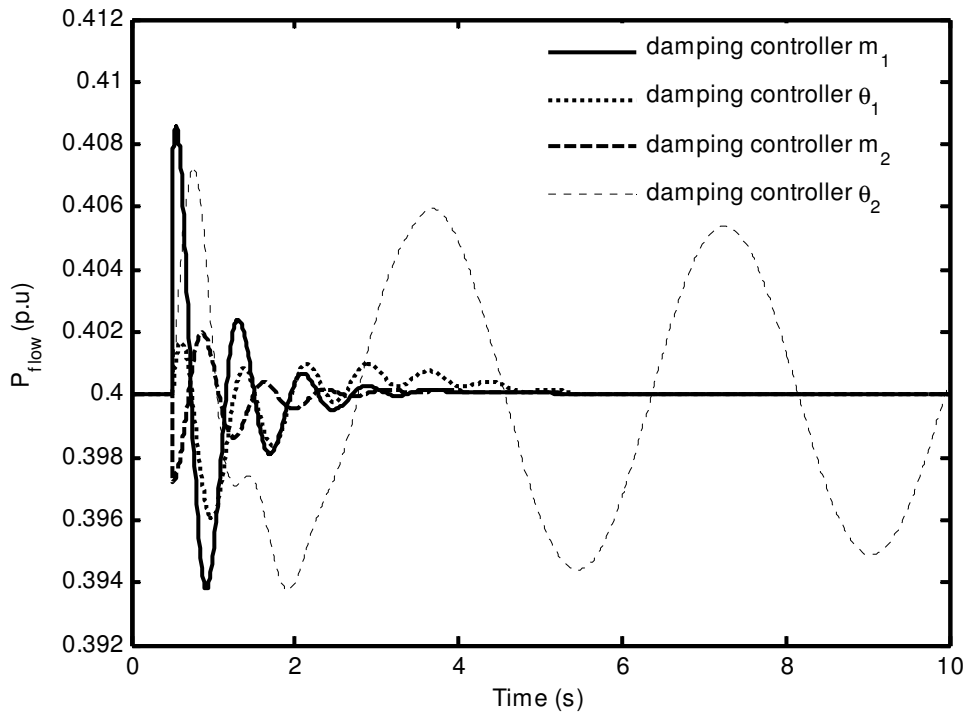


Figure 4.20: Active power flow response in line 1 in the presence of various damping controllers

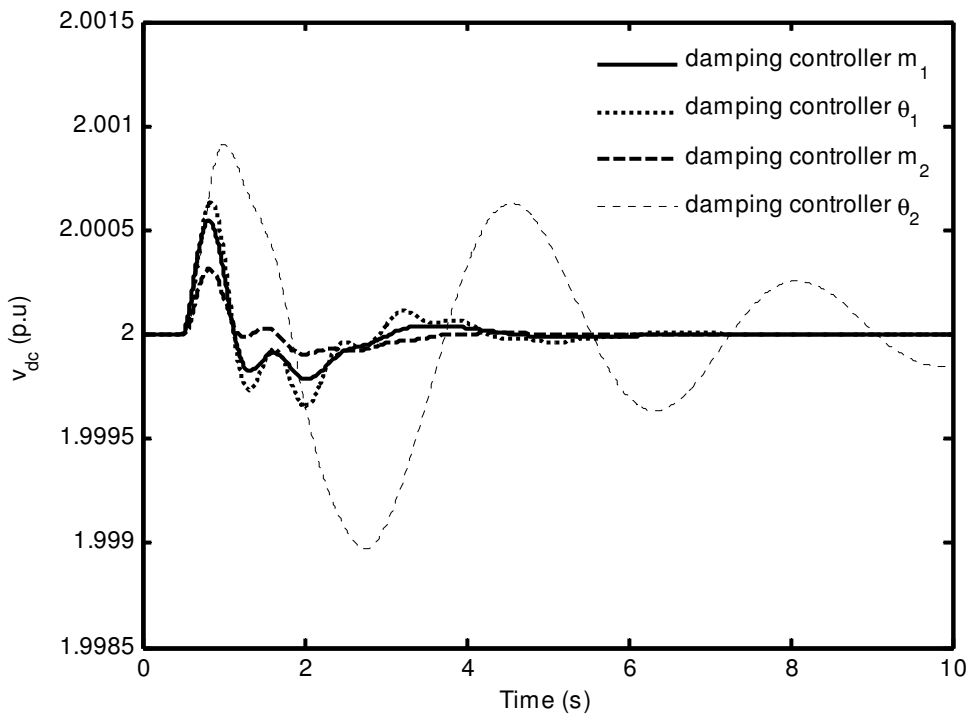


Figure 4.21: DC voltage across the capacitor response in the presence of various damping controllers

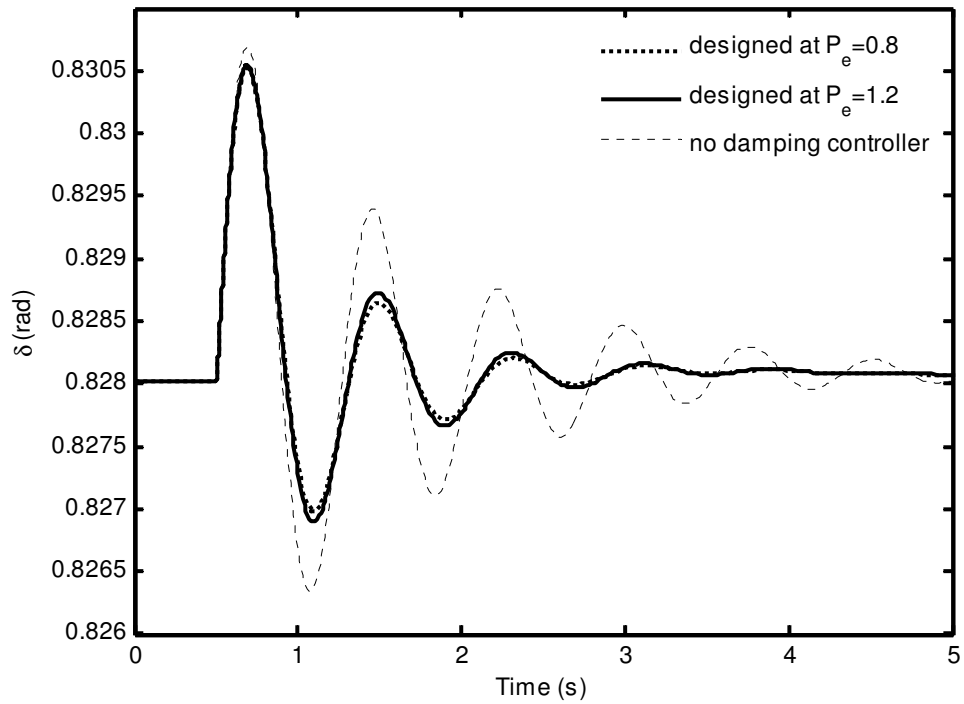


Figure 4.22: Rotor angle response with the damping controller  $m_1$  designed at two operating conditions

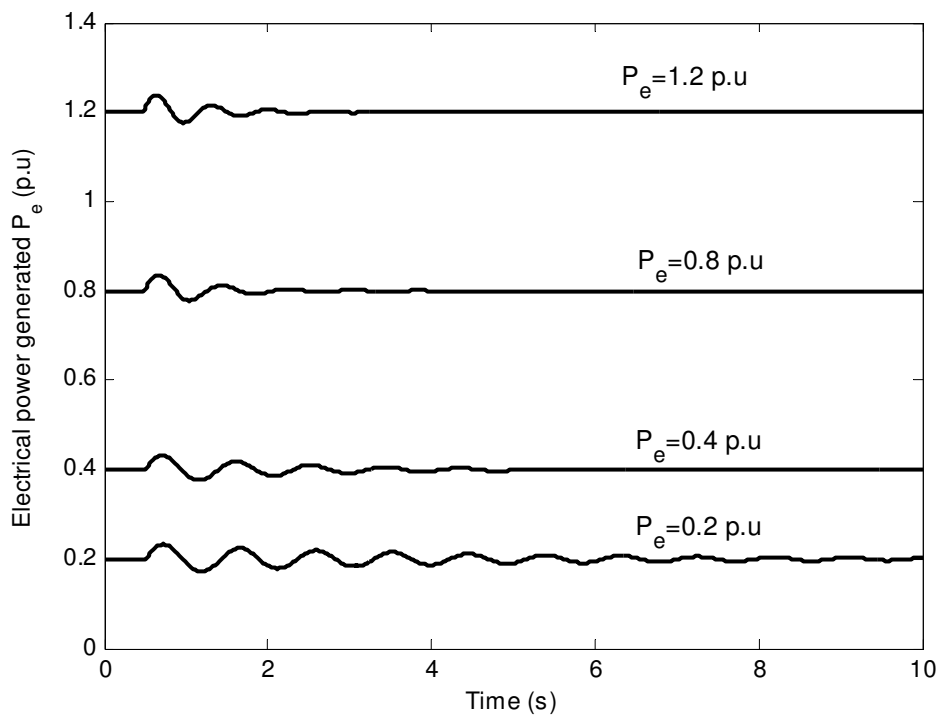


Figure 4.23: Electrical power generated response with the damping controller  $m_1$  at various operating conditions

#### 4.8.2 Disturbance: Three Phase Fault

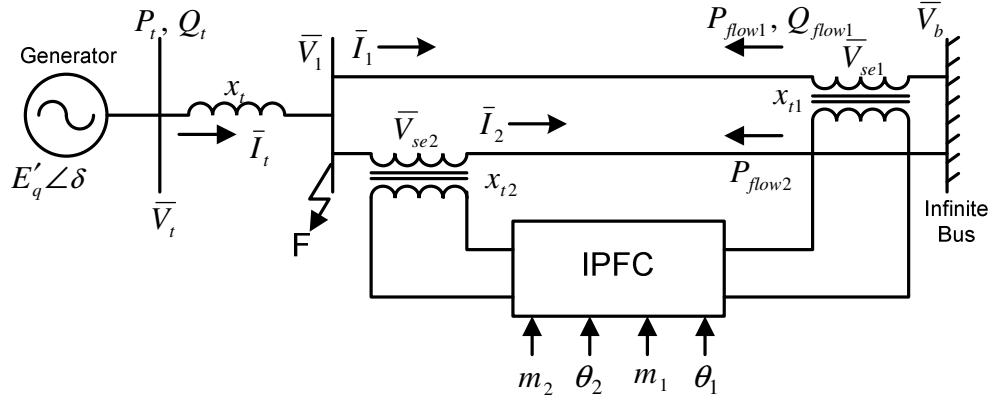


Figure 4.24: SMIB power system with fault

A three-phase fault is applied at bus 1 as shown in Figure 4.24, at  $t=0.5s$  and cleared after 0.1s. The line currents are affected accordingly. Equations (4.17-4.20) represent the line currents for post fault system. During fault, the voltage at the bus becomes zero. Hence, the line currents are modified during fault and are obtained as follows:

$$i_{1d} = y_{11d} E'_q + \frac{1}{2} y_{12d} v_{dc} (m_2 \cos(\delta - \theta_2) - m_1 \cos(\delta - \theta_1)) \quad (4.78)$$

$$i_{2d} = y_{21d} E'_q + \frac{1}{2} y_{22d} v_{dc} (m_2 \cos(\delta - \theta_2) - m_1 \cos(\delta - \theta_1)) \quad (4.79)$$

$$i_{1q} = \frac{1}{2} y_{12q} v_{dc} (m_2 \sin(\delta - \theta_2) - m_1 \sin(\delta - \theta_1)) \quad (4.80)$$

$$i_{2q} = \frac{1}{2} y_{22q} v_{dc} (m_2 \sin(\delta - \theta_2) - m_1 \sin(\delta - \theta_1)) \quad (4.81)$$

where,

$$\begin{bmatrix} y_{11d} & y_{12d} \\ y_{21d} & y_{22d} \end{bmatrix} = \begin{bmatrix} x'_d + x_t & x'_d + x_t \\ x_{L1} + x_{t1} & -(x_{L2} + x_{t2}) \end{bmatrix}^{-1}$$

$$\begin{bmatrix} y_{11q} & y_{12q} \\ y_{21q} & y_{22q} \end{bmatrix} = \begin{bmatrix} x_q + x_t & x_q + x_t \\ -(x_{L1} + x_{t1}) & (x_{L2} + x_{t2}) \end{bmatrix}^{-1}$$

The response of various parameters of the dynamic power system i.e., electrical power generated by the machine, rotor angle, terminal voltage, rotor speed response, power flows in the transmission lines and DC voltage  $v_{dc}$  are shown with and without the damping controller and PSS during three phase fault in Figures 4.25 - 4.32 respectively.

The PI power flow controller and DC voltage regulator are present in the system. The damping controller  $m_1$  mitigates the oscillations efficiently even during the case of three phase fault. The responses given in these figures are at the nominal operating condition  $P_e = 0.8$  p.u. The damping controller and PSS used are designed at operating point  $P_e = 0.8$  p.u.

Figure 4.33 gives the electrical power response at varying operating conditions in the event of three phase fault. It is seen that at the lighter load condition the oscillations take longer time to settle even with the use of the damping controller and PSS.

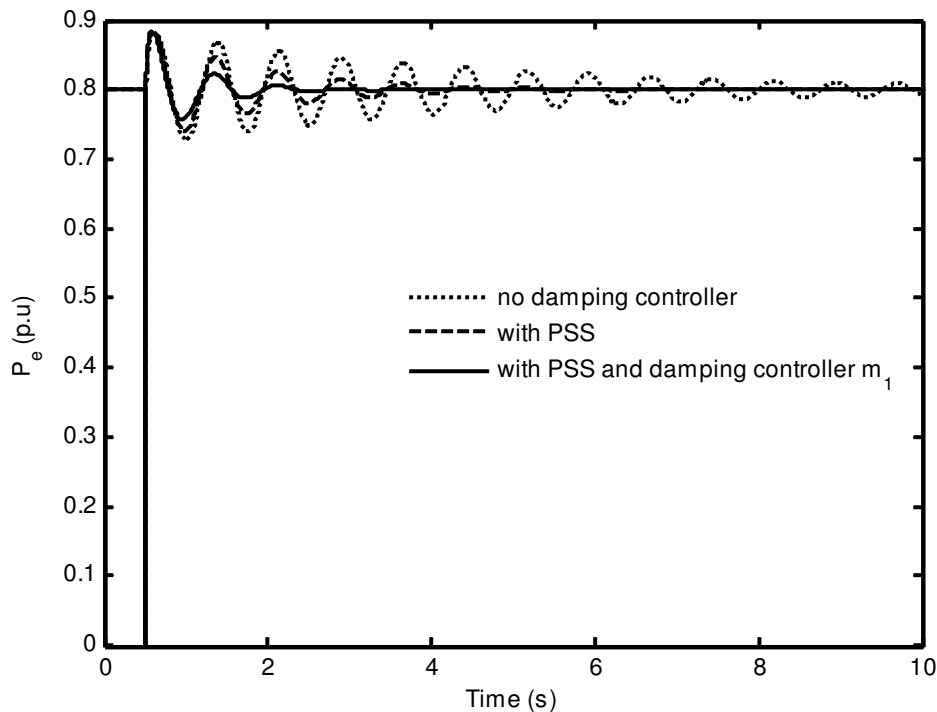


Figure 4.25: Electrical power response due to three phase fault

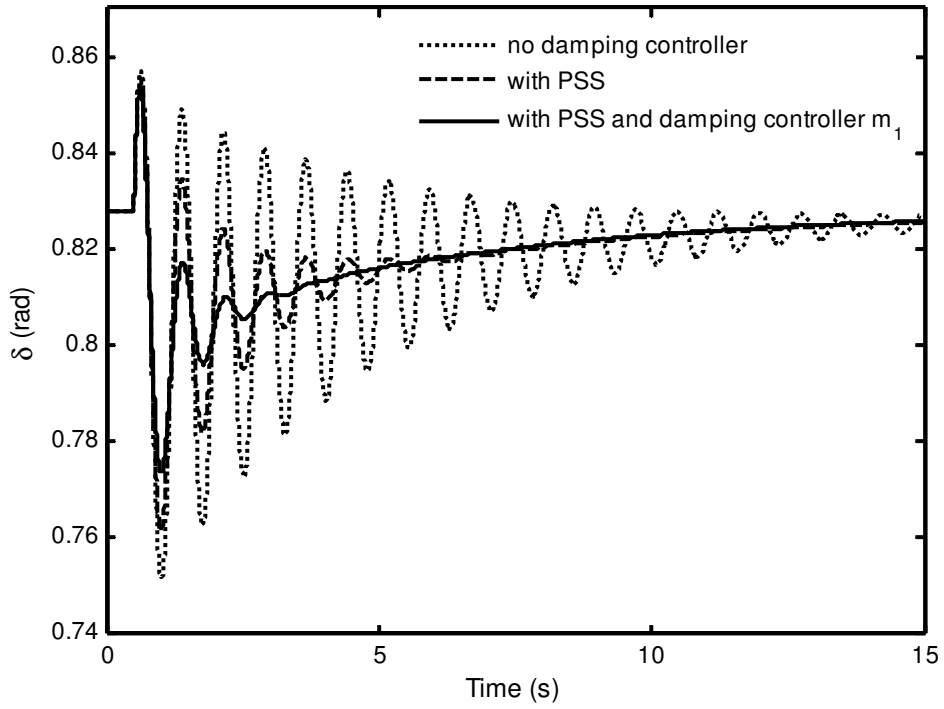


Figure 4.26: Rotor angle response due to three phase fault

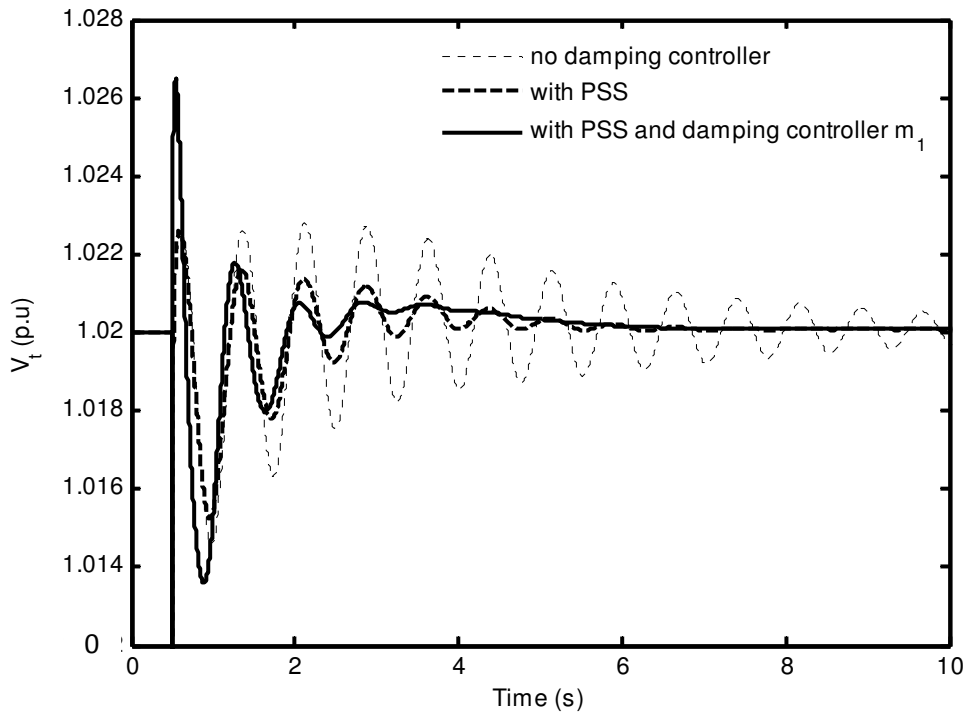


Figure 4.27: Terminal voltage response due to three phase fault

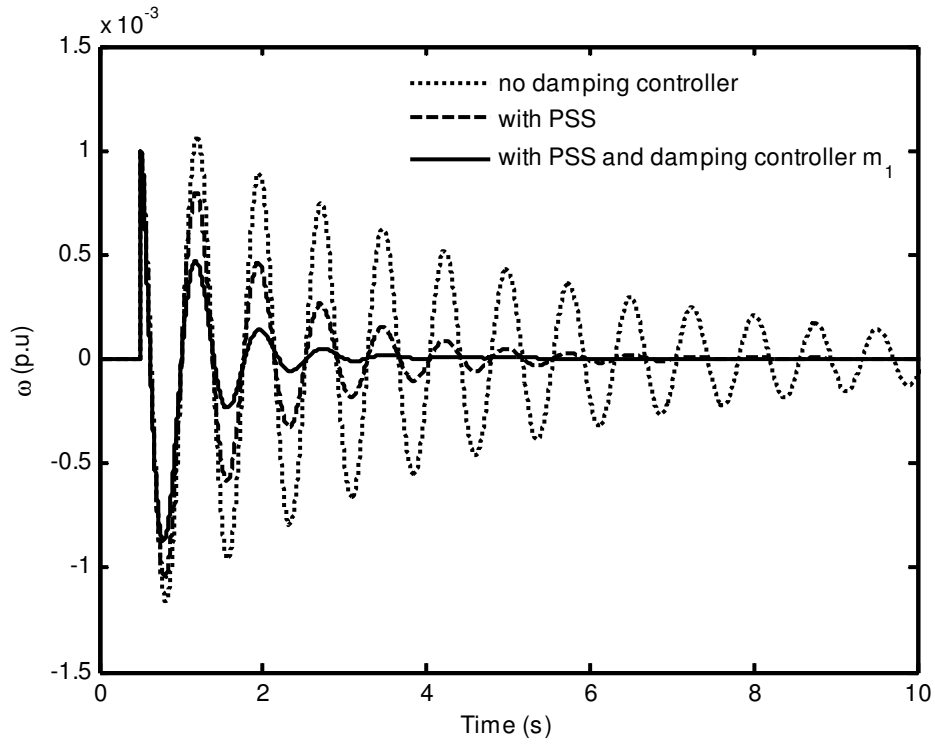


Figure 4.28: Rotor speed response due to three phase fault

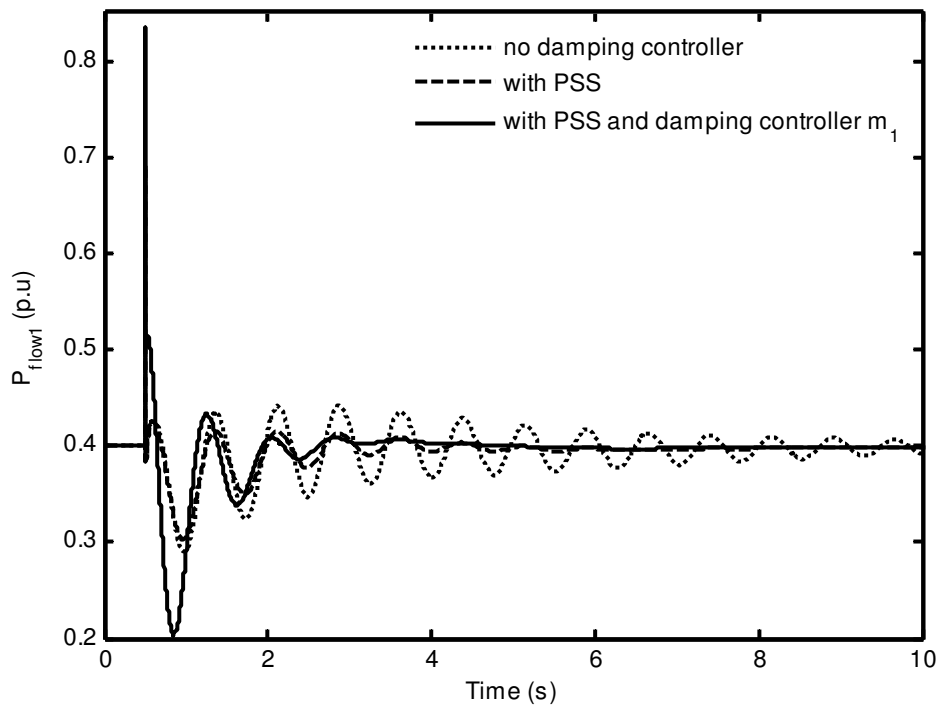


Figure 4.29: Real power flow response in line 1 due to three phase fault

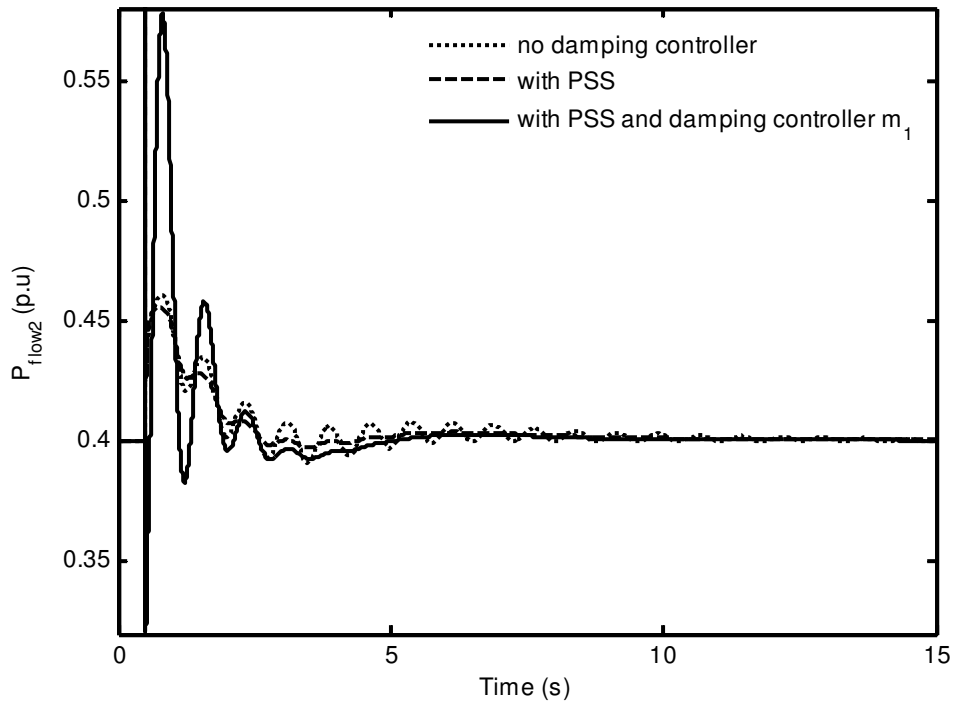


Figure 4.30: Real power flow response in line 2 due to three phase fault

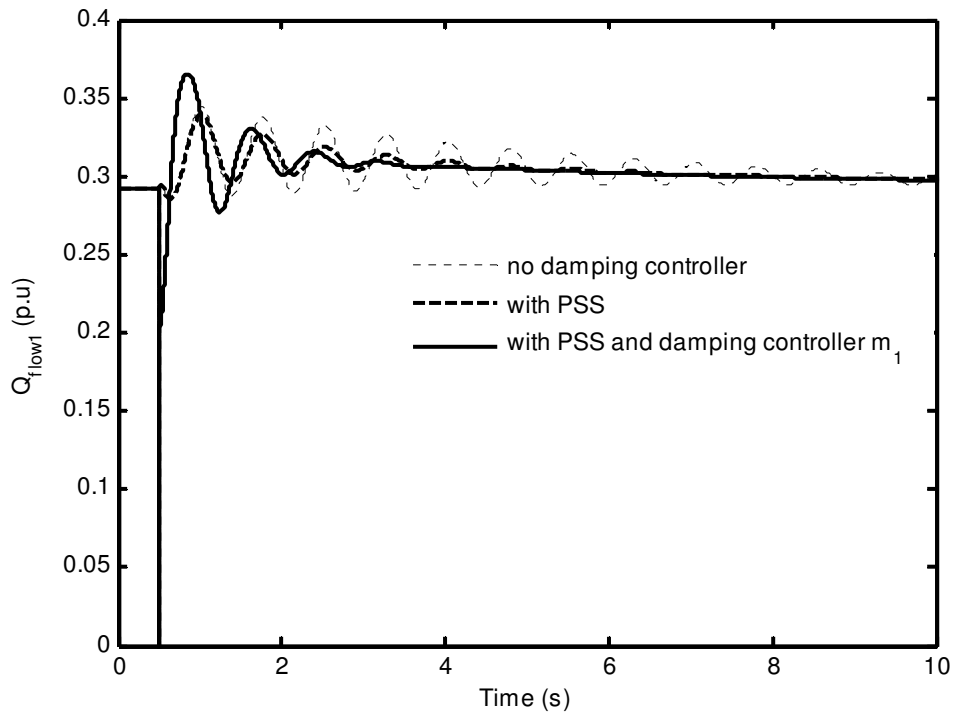


Figure 4.31: Reactive power flow response in line 1 due to three phase fault

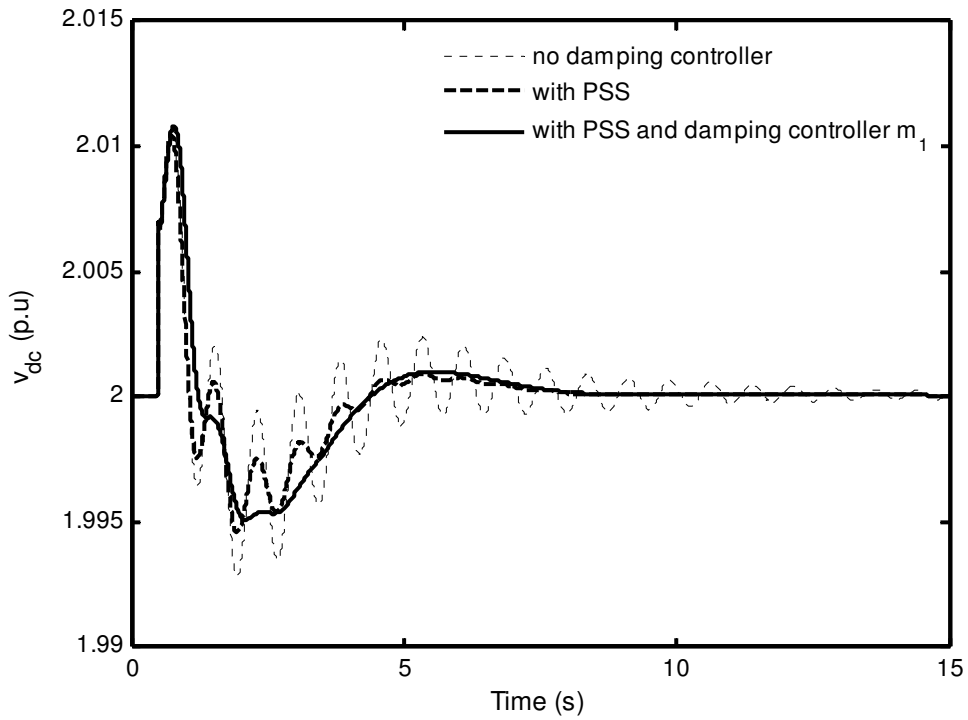


Figure 4.32: DC capacitor voltage response due to three phase fault

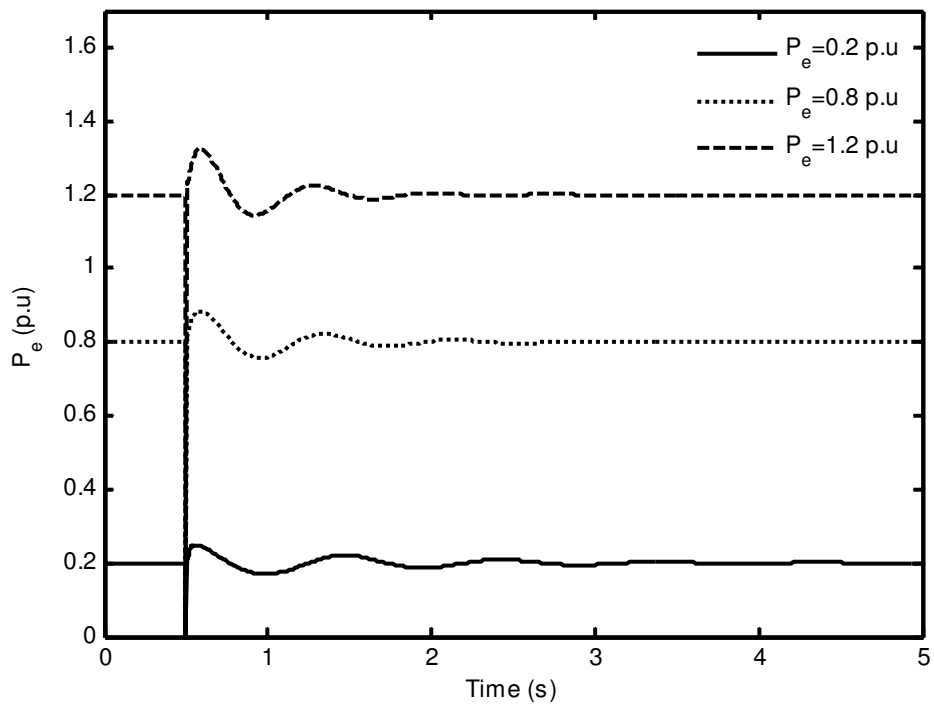


Figure 4.33: Electrical power response due to three phase fault at varying operating conditions

The response of various parameters of the power system in the event of change in mechanical input and three-phase fault disturbance are shown in Figures 4.18-4.33 in the presence of PSS and damping controller. The PI power flow controller and DC voltage regulator are present simultaneously in the system to maintain the power flow and constant DC capacitor voltage. It is to be noted that the input to both PSS and damping controller  $m_1$  is the rotor speed such that the output from these stabilizers is in phase with the rotor speed  $\omega$ .

However, since the FACTS device is incorporated on the transmission lines it is more appropriate to select a signal, given to the damping controller, in its vicinity. Usually the local input signals are always preferred, such as the active or reactive power flow through FACTS device. As such the error signal between the set point and the measured signal of the active power flow will be taken as the input to the damping controller as shown in Figure 4.34. The damping controller output is in phase with the real power flow deviation. This active power has been obtained from the line on which the VSC of IPFC has been installed. The structure of the damping controller is given in Figure 4.35 [38].

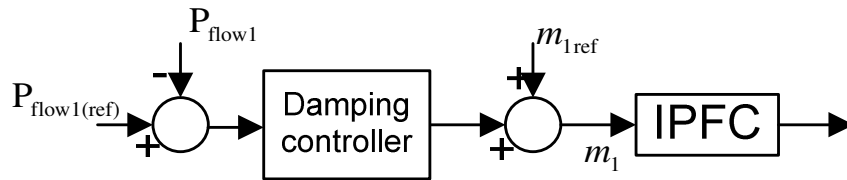


Figure 4.34: Damping controller with power deviation as input

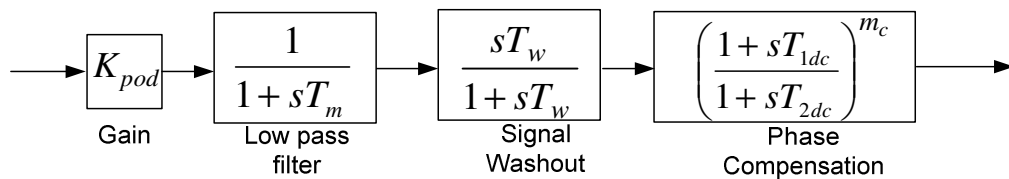


Figure 4.35: Structure of the damping controller with power deviation as input

This damping controller consists of extra block, i.e., the low pass filter, with  $T_m$  being a measurable time constant. This filter attenuates Torsional frequencies.  $T_m$  is chosen to be 0.1s. The damping controller shown in Figure 4.35 will now be termed

as power oscillation damping (POD) controller. The remaining parameters of POD  $m_1$  are unchanged. In the following section the regulation of power in the transmission lines with the control of the input signals of IPFC is discussed.

### 4.8.3 Disturbance: Change in Power Flow Reference

The effect of the power flow controller in controlling the transmission line flow can be observed when new power reference value is given in Figure 4.34. Originally the real power flowing through the two transmission lines is 0.4 p.u. A real power of 0.45 p.u. can be made to flow in the transmission line 1 by changing the power reference  $P_{flow1(ref)}$  to 0.45 p.u. Subsequently the real power flow in transmission line 2 will be 0.35 p.u.

The DC regulator maintains the voltage at a constant value of 2 p.u. The change in power reference is given at 0.5s in the simulation. To obtain the desired power flow, gain scheduling is required and was determined by trial and error on simulation.

The parameters of the power flow controller to obtain this change in power flow in line 1 are  $k_{pp} = 4$  and  $k_{pi} = 15$ . The power flow controller is able to make the desired active power  $P_{flow1}$  of 0.45 p.u., to flow in line 1 and the active power  $P_{flow2}$  in line 2 is reduced to 0.35 p.u., as the difference active power (0.05 p.u.) is made to transfer from transmission line 2 to line 1 through IPFC.

However, the reactive power flow  $Q_{flow1}$  in transmission line 1 has deviated from its reference value. As such another PI controller is installed to regulate the reactive power flow in transmission line 1.

The input signal  $m_1$  is used for controlling the reactive power. The reactive power PI controller is shown in Figure 4.36. The controller parameters are  $k_{qp} = 0.05$  and  $k_{qi} = 0.4$ . The block diagram of the SMIB power system incorporated with IPFC and all the controllers (PSS, PI power flow controllers, POD) is given in Figure 4.37.

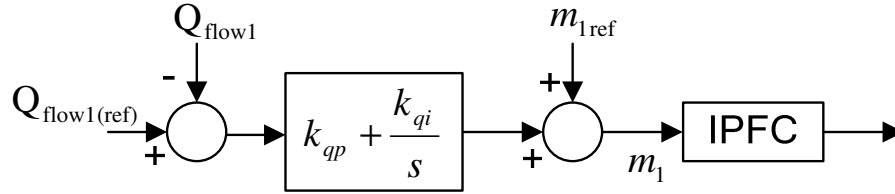


Figure 4.36: Reactive power flow controller

The dynamic response of the system is observed with the controllers with a step change in  $P_{flow1(ref)}$  at 0.5 s. The responses of various parameters (active power flows in line 1 and 2, reactive power flow in line1, DC capacitor voltage and rotor angle) are shown in Figures 4.38-4.42 respectively with PSS and POD. The power flow controller regulates the powers in the transmission lines to the reference values. With the presence of both the PSS and POD the oscillations in power flows settle at the steady state values eventually.

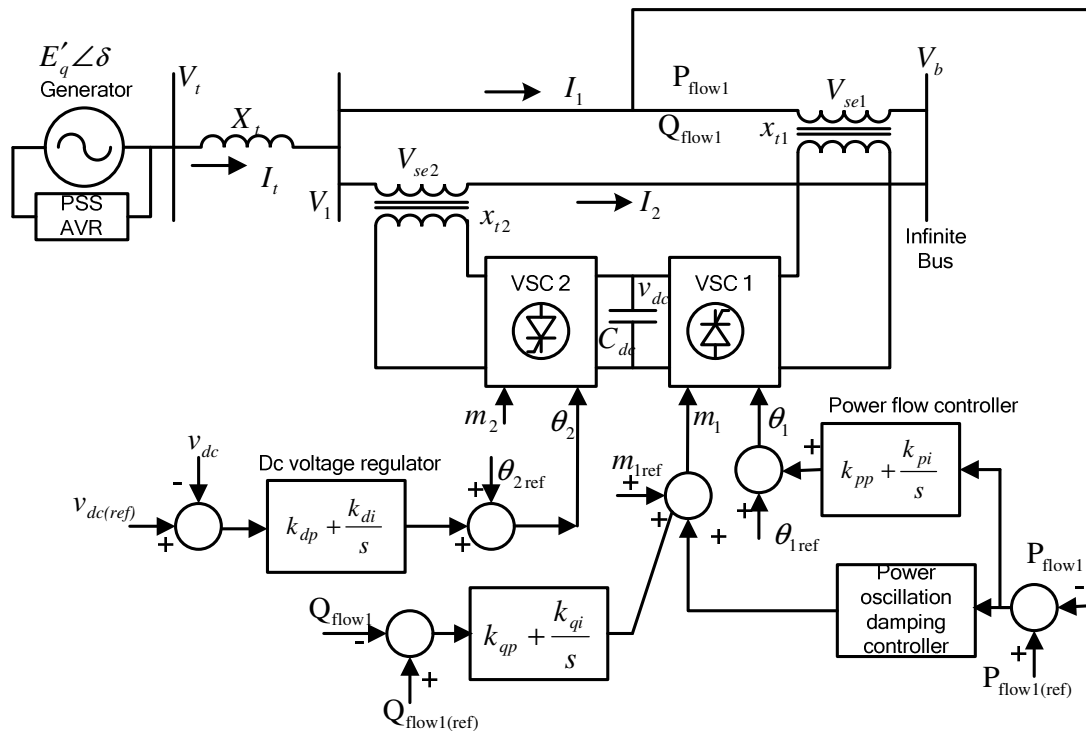


Figure 4.37: Block diagram of SMIB with IPFC and its controllers

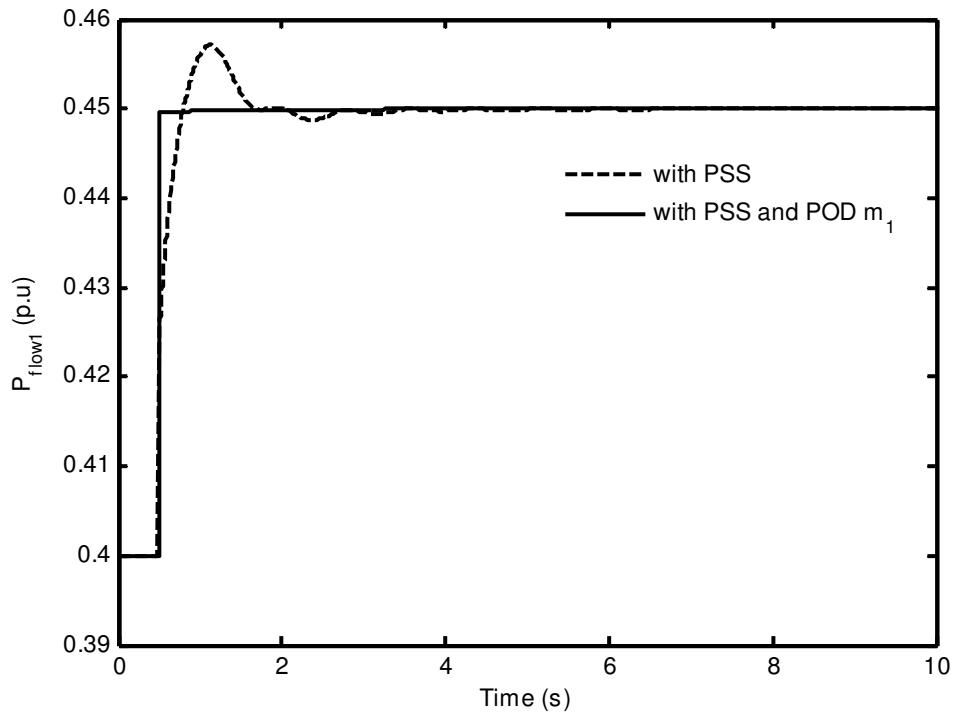


Figure 4.38: Response of the real power flow in transmission line 1 with step change in power reference

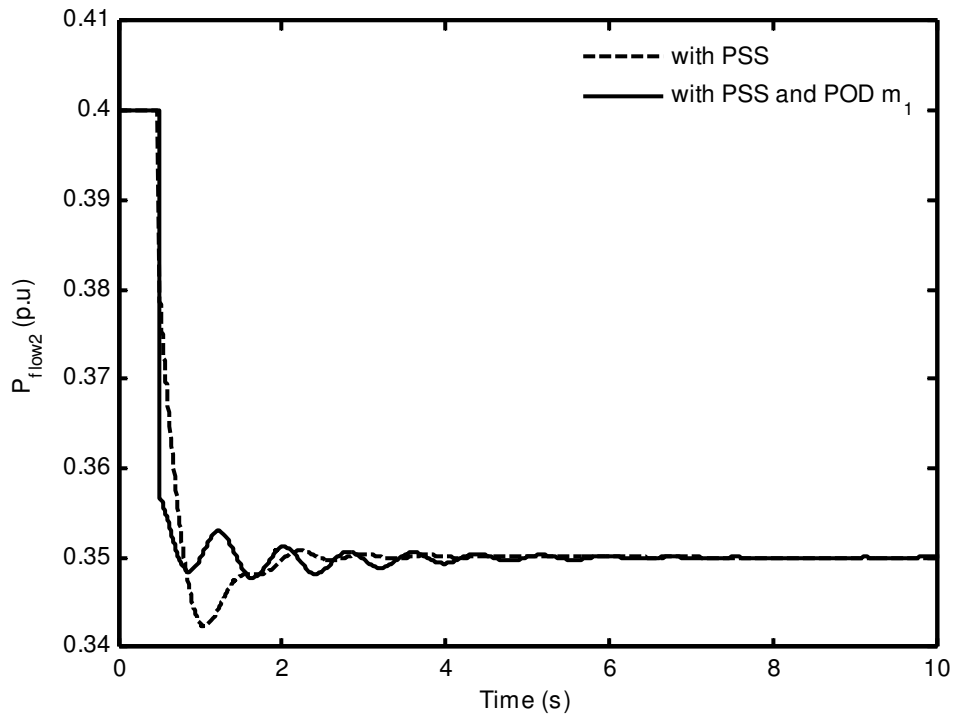


Figure 4.39: Response of the real power flow in transmission line 2 with step change in power reference

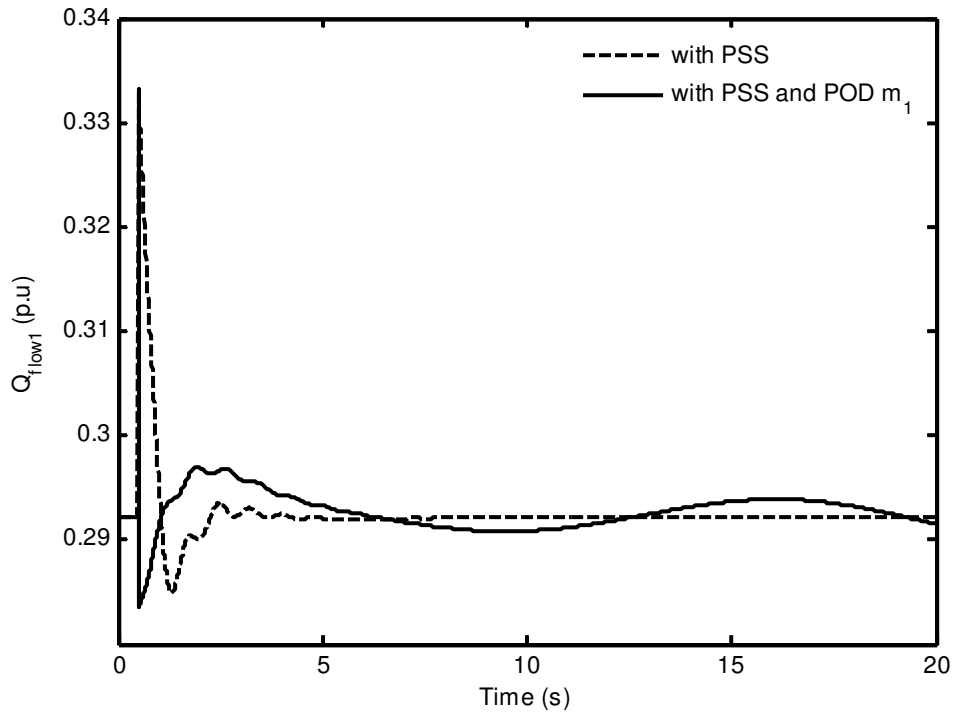


Figure 4.40: Response of the reactive power flow in transmission line 1 with step change in power reference

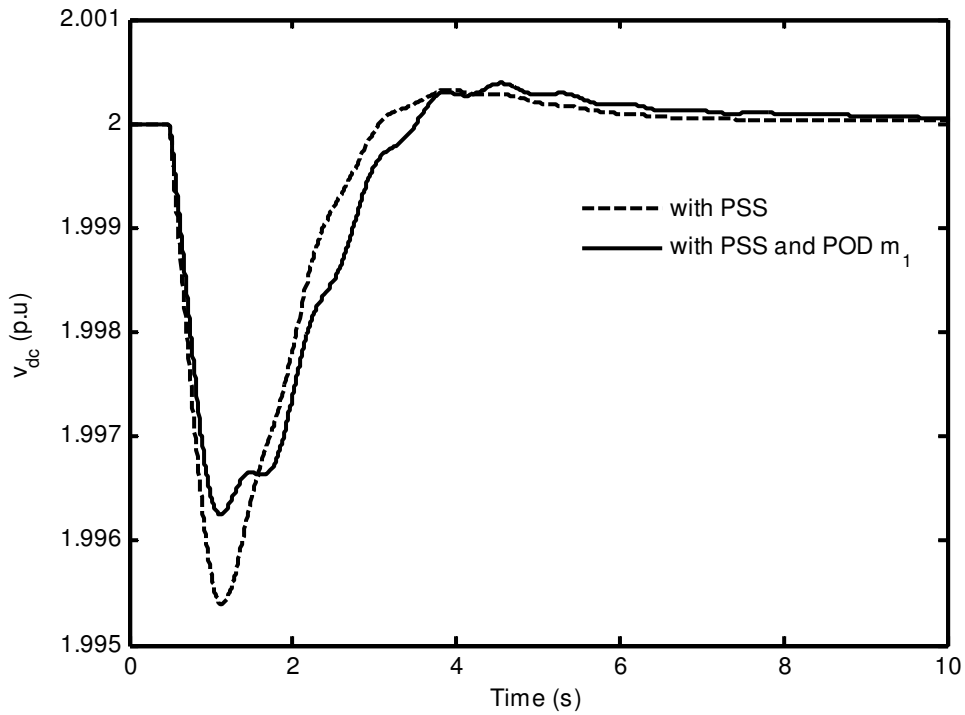


Figure 4.41: Response of the DC capacitor voltage with step change in power reference

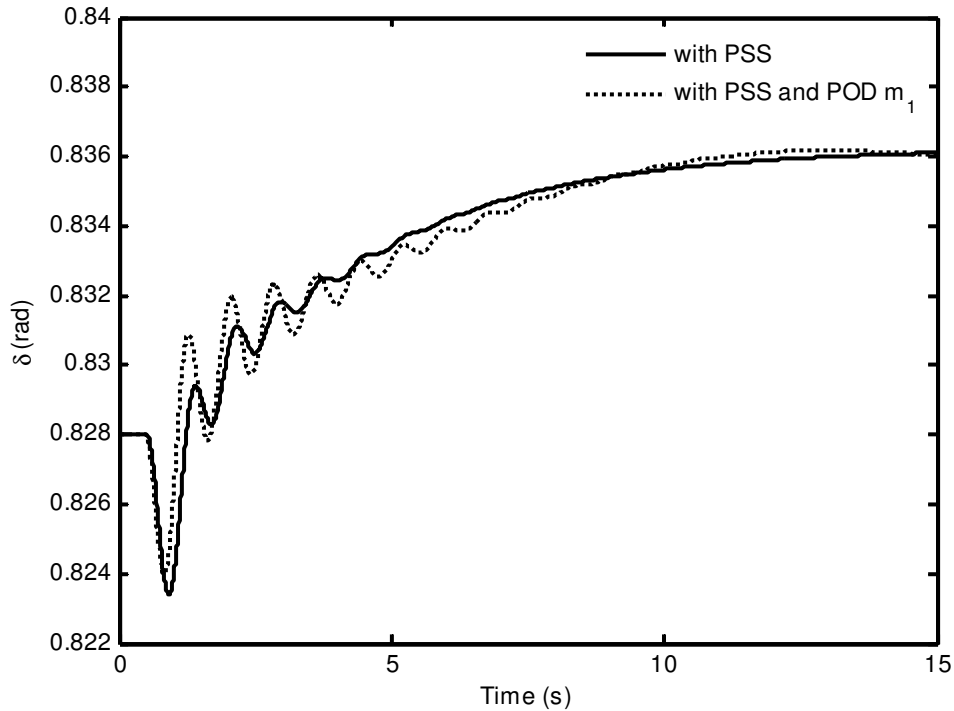


Figure 4.42: Response of the rotor angle with step change in power reference

It is observed from the above figures that all controllers ensure efficient operation of the IPFC in controlling the power flow and mitigating oscillations. The power flow controller only regulates the power in the transmission line and has negligible contribution towards damping of oscillations. The effect is only due to damping controller or the PSS. The effectiveness of the IPFC damping controller in improving the damping of the oscillation mode is investigated through eigenanalysis and nonlinear simulation in this Section 4.8. The effect of the various controllers of the IPFC on the system is investigated.

#### 4.9 Summary

In this chapter, the nonlinear model of the SMIB power system embedded with IPFC has been developed which includes all the inputs of IPFC and DC capacitor dynamics. The linearized model of the power system is established to form the extended Phillips-Heffron model of a SMIB power system incorporated with IPFC. This model is used to study the oscillation stability.

The state model of the power system is formed, from which the eigenvalues are computed using eigenanalysis or the modal analysis. The oscillation mode having low damping ratio is identified. Based on the linearized model, the PSS is designed to increase the damping of the oscillations mode. The power flow controller and DC voltage regulator are also incorporated in the IPFC control to regulate the power flow and to maintain the DC voltage across the DC link.

The damping function of IPFC is also investigated. The IPFC based damping controllers, considering various control signals, are designed to increase the damping of the oscillation modes existing in the system. The parameters of the IPFC damping controller are determined using the phase compensation method. The relative effectiveness of the input control signals  $m_1$ ,  $\theta_1$ ,  $m_2$  and  $\theta_2$  has been determined using the controllability index.

Investigations reveal that control signal  $m_1$  is the most efficient of the input control signals to be used for damping the low frequency oscillations in the power system. The control signals  $\theta_1$  and  $\theta_2$  are not suitable in providing the damping, as they do not provide consistent damping to the oscillations. The effectiveness and robustness of the IPFC damping controllers are validated through eigenanalysis and nonlinear simulation of the power system subjected to various disturbances. The IPFC based damping controller and PSS ensure consistent damping of the low frequency oscillations in the SMIB power system. The following chapter presents the mathematical modeling of mullet-machine power system without FACTS devices.



## CHAPTER 5

### MULTIMACHINE POWER SYSTEM

#### **5.1 Introduction**

Modeling of multi-machine system is quite complex. A typical multi-machine system is composed of synchronous generators, excitation systems, governors, power system stabilizers, transmission lines, transformers, and loads etc. Suitable mathematical models of these devices are required for stability analysis. The dynamics of these models are represented by sets of differential and algebraic equations. These equations are integrated to form the overall system model. In this chapter, the nonlinear, linearized state space form model of multi-machine power system is presented. Power system stability analysis is performed on a case study which utilizes the modeling and stability control techniques.

#### **5.2 Modeling of Multi-Machine Power System**

The nonlinear model of a multi-machine power system is presented in this section. The following assumptions are made to simplify the mathematical model which describes the nonlinear dominant behavior of a multi-machine power system [17], [103], [104].

- 1) Governor and turbine dynamics are neglected. This results in constant input mechanical power.
- 2) The network is in quasi-static state, (i.e., the transient characteristics of the network elements like transmission lines, transformers, etc. are avoided as their effects can be negligible on the electromechanical phenomenon). Network elements are represented by equivalent impedances (or admittances), the value of which are the ones assumed at the equilibrium steady state at

nominal frequency. The problem may be greatly simplified from the analytical and computational point of view, with such a representation in the analysis of power system stability.

- 3) The loads are represented by constant impedance loads (i.e., the dynamics of the load are simplified for the stability studies). This helps in reducing the network to only the generator buses by eliminating load buses as they have zero injection current. When the load buses are eliminated, the network voltage current relationship between the terminal buses of generators is expressed through a reduced bus admittance matrix.

Synchronous generators are the primary sources of electrical energy in power systems. The power system stability problem is basically one of keeping interconnected synchronous machines in synchronism. Hence, an understanding of their characteristics and accurate modeling of their dynamic performance are of fundamental importance to the study of power system stability. In this thesis, the generator represented by a third-order model has been used, which is frequently employed in stability and control analysis due to its simplicity. The dynamic equation of the synchronous generator consists of the swing equations and generator internal voltage equation [2], [16], [17], [104].

### 5.2.1 Synchronous Generators

The nonlinear dynamics for the  $i^{th}$  machine of an  $n$  - machine power system as shown in Figure 5.1 is given as [2], [16], [17], [104]:

The swing equations are written as follows:

$$\dot{\delta}_i = \omega_0(\omega_i - 1) \tag{5.1}$$

$$\dot{\omega}_i = \frac{(P_{mi} - P_{ei} - P_{Di})}{M_i} \tag{5.2}$$

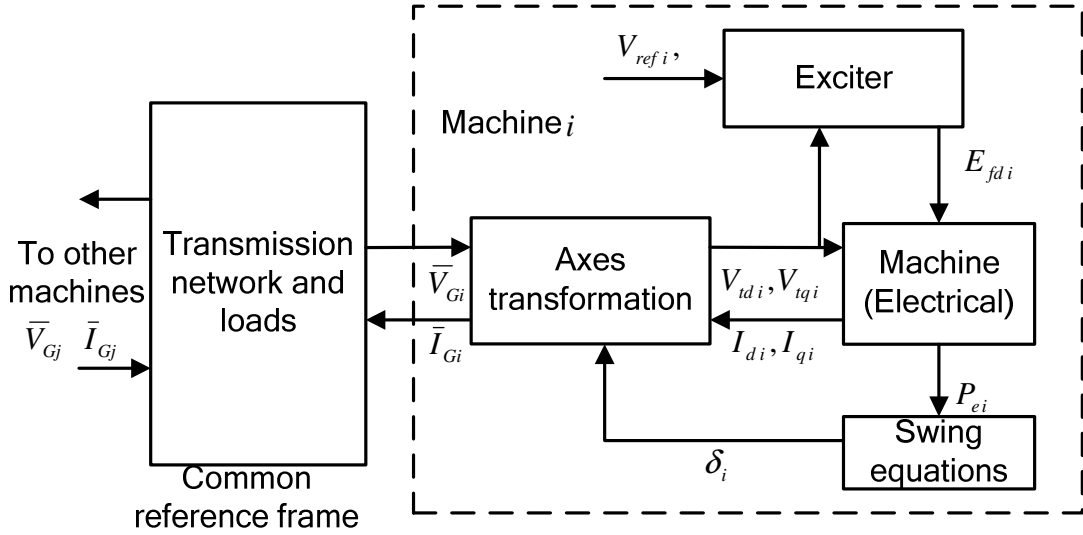


Figure 5.1: The  $i^{th}$  machine in a multi-machine power system network

The internal voltage equation is given by

$$\dot{E}'_{qi} = \frac{1}{T'_{doi}} (E_{fdi} - E'_{qi} - (x_{di} - x'_{di}) I_{di}) \quad (5.3)$$

The excitation system is described by the following equation

$$\dot{E}_{fdi} = \frac{1}{T_{Ai}} (-E_{fdi} + K_{Ai} (V_{ref i} - V_{ti})) \quad (5.4)$$

The auxiliary equations are as follows:

$$\begin{aligned} P_{ei} &= \text{Re}[(I_{di} + j I_{qi}) \times (V_{tdi} + j V_{tqi})] = I_{di} V_{tdi} + I_{qi} V_{tqi} \\ I_i &= I_{di} + j I_{qi}, \quad V_{ti} = V_{tdi} + j V_{tqi}, \quad P_{Di} = D_i (\omega_i - 1), \\ V_{tdi} &= x_{qi} I_{qi}; \quad V_{tqi} = E'_{qi} - x'_{di} I_{di} \end{aligned} \quad (5.5)$$

where,  $i = 1, 2, \dots, n$ ,  $n$  is the number of generators.

### 5.2.2 Transmission Network and Loads

The role of transmission network is to deliver the power produced in generating stations to loads. Thus, nonlinear equations of the synchronous machines are coupled to the network equations that interconnect these machines. In the commonly used models, the network is assumed constantly in steady state and all the transients associated with transmission lines are neglected. The electrical transmission line is represented as an equivalent  $\pi$  model as shown in the Figure 5.2 [14]. In Figure 5.2  $\bar{Z}_{ij} = R_{ij} + jX_{ij}$  represents linear lumped series impedance, where  $R_{ij}$  and  $X_{ij}$  are the resistance and inductive reactance of the transmission line between bus  $i$  and bus  $j$ .  $\bar{Y}_{Cij} = G_{Cij} + jB_{Cij}$  is the shunt admittance representing the line charging capacitance between the two buses. The shunt admittance is evenly distributed in parallel at both ends of the transmission line as shown in Figure 5.2.

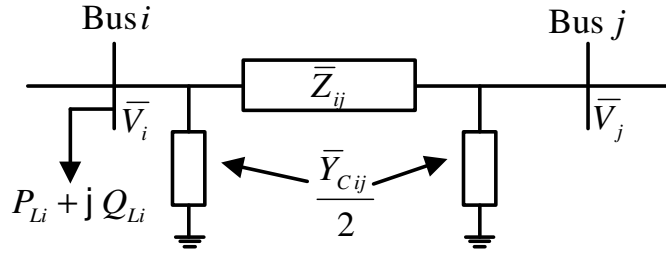


Figure 5.2: Lumped parameter  $\pi$  equivalent transmission line

The load connected to a bus  $i$  in Figure 5.2, is modeled commonly as [2], [17]:

$$P_{Li}(V_i) = P_{Loi}(V_i)^a \quad i = 1, 2, \dots, nb \quad (5.6)$$

$$Q_{Li}(V_i) = Q_{Loi}(V_i)^a \quad i = 1, 2, \dots, nb$$

where  $P_{Li}$  and  $Q_{Li}$  are the real and reactive components of the voltage dependent load connected to the bus  $i$  with  $V_i$  being the magnitude of bus voltage  $\bar{V}_i$ . When  $a = 0, 1$  or  $2$ , the load model given by the above exponential model represents constant power, constant current or constant impedance components. In this thesis for power system analysis, the loads are represented by constant impedances and converted to

equivalent passive admittances. For a bus having a voltage magnitude  $V_i$  to which a load  $P_{Li} + jQ_{Li}$  is connected, this load is represented by the static shunt admittances  $g_{Li}$  and  $b_{Li}$  given by  $\frac{P_{Li}}{V_i^2}$  and  $-\frac{Q_{Li}}{V_i^2}$  respectively [17]. The transformers in the power system are represented by equivalent reactances. Therefore, for an  $n$ -machine  $nb$ -bus interconnected power system, the static network and the loads are shown in Figure 5.3 [17], [103]. Figure 5.3 contains the first  $n$  buses connected to the generators with the local loads and the rest  $n + 1, \dots, nb$  buses are connected to only loads.

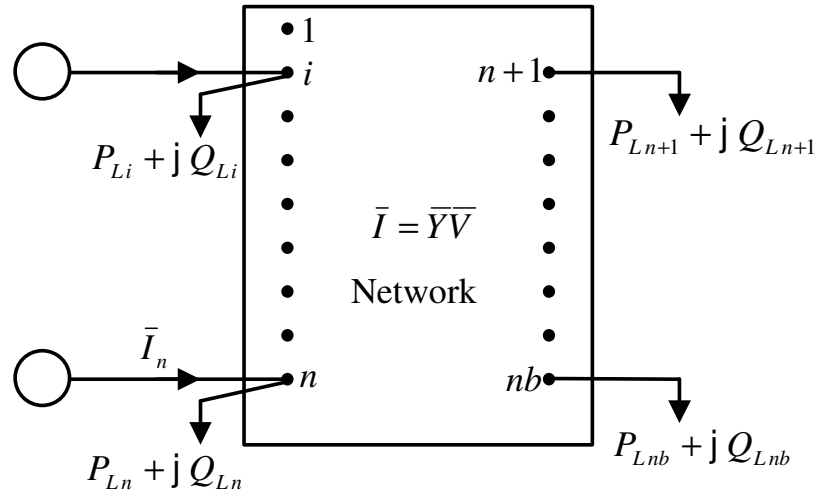


Figure 5.3: Interconnected network of synchronous machines and the loads

The following algebraic equation gives the relationship between the injected currents and bus voltages of the transmission network [17], [103]:

$$\bar{I} = \bar{Y}\bar{V} \quad (5.7)$$

where :

$\bar{I}$  is the vector of injected currents at each bus,  $\bar{I} = \bar{I}_1, \bar{I}_2, \dots, \bar{I}_n, \bar{I}_{n+1}, \dots, \bar{I}_{nb}$

$\bar{V}$  is the vector of voltages of each bus,  $\bar{V} = \bar{V}_1, \bar{V}_2, \dots, \bar{V}_n, \bar{V}_{n+1}, \dots, \bar{V}_{nb}$

$\bar{Y}$  is the bus admittance matrix, where each element is given by  $\bar{Y}_{ij} = \frac{1}{\bar{Z}_{ij}} = g_{ij} + j b_{ij}$ ,  $i = 1, 2, \dots, nb$ ;  $j = 1, 2, \dots, nb$ , and  $\bar{Y}_{ij}$  is the admittance between the bus  $i$  and bus  $j$ . The admittance matrix  $\bar{Y}$  is constructed using the following steps [16], [17]:

- a) The diagonal entries  $\bar{Y}_{ii}$  of the admittance matrix are the sum of all the admittance connected to bus  $i$ , including the shunt admittances.  $\bar{Y}_{ii}$  is known as the self-admittance of the bus  $i$ .

The equivalent shunt admittance for each load of the system is added to the corresponding diagonal entries of the admittance matrix in  $\bar{Y}$  of Equation (5.7), i.e., to the self-admittance of that particular bus.

- b) The off-diagonal entries  $\bar{Y}_{ij}$  of the admittance matrix are the sum of the negatives of all admittance between bus  $i$  and bus  $j$ , known as the transfer admittance between bus  $i$  and bus  $j$ .

Equation (5.7) may be written in partitioned form as [17], [103],

$$\begin{bmatrix} \bar{I}_G \\ \bar{I}_L \end{bmatrix} = \begin{bmatrix} \bar{Y}_{GG} & \bar{Y}_{GL} \\ \bar{Y}_{LG} & \bar{Y}_{LL} \end{bmatrix} \begin{bmatrix} \bar{V}_G \\ \bar{V}_L \end{bmatrix} \quad (5.8)$$

where the subscript ‘ $G$ ’ is used to denote generator buses and the subscript ‘ $L$ ’ is used to denote the remaining load buses.

Equation (5.8) can be written as:

$$\bar{I}_G = \bar{Y}_{GG} \bar{V}_G + \bar{Y}_{GL} \bar{V}_L \quad (5.9)$$

$$\bar{I}_L = \bar{Y}_{LG} \bar{V}_G + \bar{Y}_{LL} \bar{V}_L$$

Since loads are represented by constant impedances, the load buses have zero injection currents, i.e.,  $\bar{I}_L = 0$ ; whereas the generators inject currents into the

generator buses. Thus, eliminating  $\bar{V}_L$  in the above equations, the generator currents can be represented as:

$$\bar{I}_G = (\bar{Y}_{GG} - \bar{Y}_{GL}\bar{Y}_{LL}^{-1}\bar{Y}_{LG})\bar{V}_G$$

$$\bar{I}_G = \bar{Y}_{red}\bar{V}_G \quad (5.10)$$

where  $\bar{Y}_{red} = (\bar{Y}_{GG} - \bar{Y}_{GL}\bar{Y}_{LL}^{-1}\bar{Y}_{LG})$  is the reduced admittance matrix of the power system network and  $\bar{V}_G$  represent the terminal voltages of the generators. Thus, the system admittance matrix is reduced to generator buses and the load buses are eliminated. The stability analysis is performed on the reduced power system containing only the generator buses interconnected to each other.

### 5.2.3 Generator Network Interface

The currents and voltages in Equation (5.10) of the network are in the common reference frame, called the  $D - Q$  axes, which rotates at the synchronous frequency. Equation (5.10) can also be represented as:

$$\begin{bmatrix} I_{D1} + j I_{Q1} \\ \vdots \\ I_{Dn} + j I_{Qn} \end{bmatrix} = \bar{Y}_{red} \begin{bmatrix} V_{iD1} + j V_{iQ1} \\ \vdots \\ V_{iDn} + j V_{iQn} \end{bmatrix} \quad (5.11)$$

where  $\bar{I}_{Gi} = I_{Gi}e^{j\gamma_i} = I_{Di} + j I_{Qi}$ , and  $\bar{V}_{Gi} = V_{Gi}e^{j\theta_i} = V_{iDi} + j V_{iQi}$ ,  $i = 1, 2, \dots, n$ . The generators currents and voltages in Equation (5.11) are in  $D - Q$  axes reference frame. The state equations for each generator of an interconnected power system given in Equations (5.1-5.4) have their own individual  $d_i - q_i$  frame of reference synchronously rotating with its own rotor. In order to study the behavior of a multi-machine system, it is necessary to interface all machines along with the network, as represented in the Figure 5.4 [17]. This is possible either by transforming the generator state variables to the common reference frame or the network equations to the individual machine reference frame.

However, transforming the network equations onto the machine reference frame has an advantage that the generator variables are unchanged and application of control techniques is uncomplicated. There are two methods for transformation of the network Equation (5.10) into the individual machine frame of reference.

### 5.2.4 Method 1 of Transforming Network Equations To Individual Machine Frame

Consider the phasor diagram shown in Figure 5.5 [17]. The common reference frame is represented by the  $D - Q$  axes and the individual machine reference is represented by the  $d_i - q_i$  axes.  $\delta_i$  is the phase angle difference between the  $D$  axis and the  $q_i$  axis.

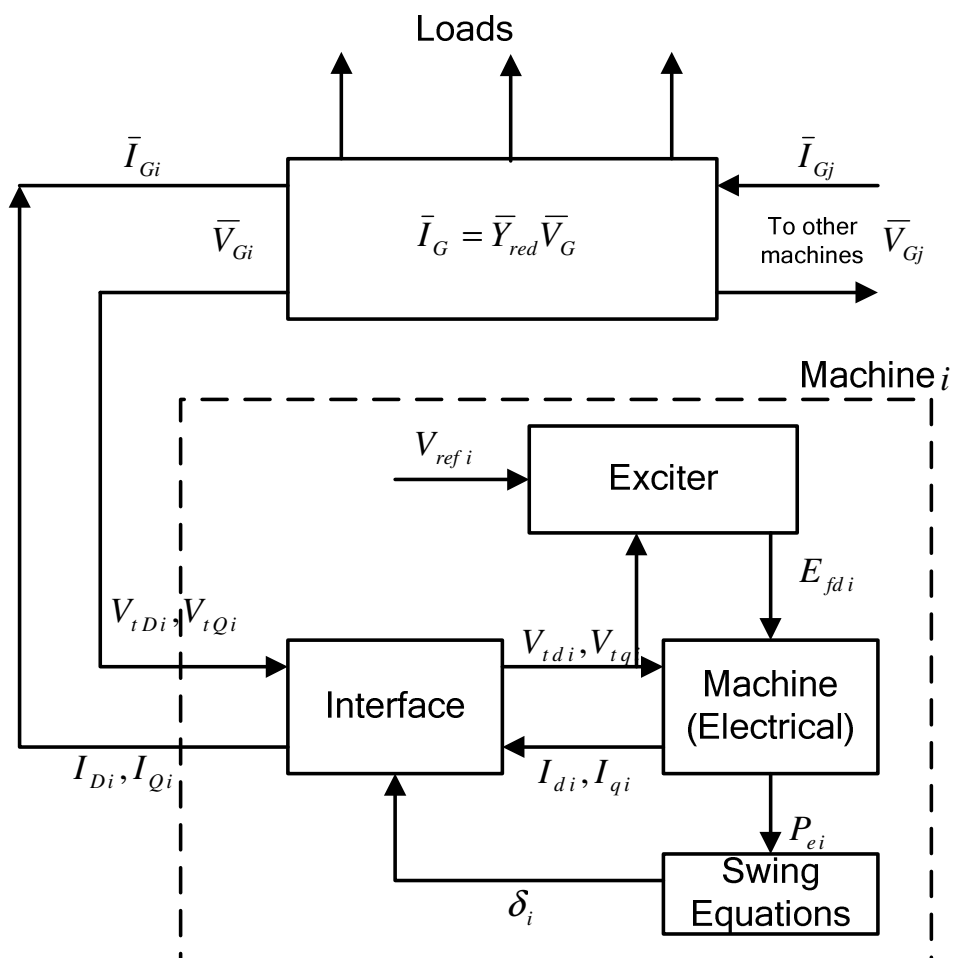


Figure 5.4: Multi-machine generator network interface representation

From Figure 5.5, the relation between the two coordinate axes is obtained as:

$$\begin{bmatrix} V_{tDi} \\ V_{tQi} \end{bmatrix} = \begin{bmatrix} \sin \delta_i & \cos \delta_i \\ -\cos \delta_i & \sin \delta_i \end{bmatrix} \begin{bmatrix} V_{tdi} \\ V_{tqi} \end{bmatrix} \quad (5.12)$$

$$\Rightarrow V_{tDi} + j V_{tQi} = (\sin \delta_i V_{tdi} + \cos \delta_i V_{tqi}) + j (-\cos \delta_i V_{tdi} + \sin \delta_i V_{tqi}) \quad (5.13)$$

$$\Rightarrow V_{tDi} + j V_{tQi} = (V_{tdi} + j V_{tqi}) e^{j(\delta_i - \pi/2)} \quad (5.14)$$

Thus,

$$\begin{aligned} \bar{V}_{Gi} &= V_{Gi} e^{j\theta_i} = V_{tDi} + j V_{tQi} \\ &= (V_{tdi} + j V_{tqi}) e^{j(\delta_i - \pi/2)} = V_{ti} e^{j(\delta_i - \pi/2)} \end{aligned} \quad (5.15)$$

Similarly the current variables can be transformed as:

$$\bar{I}_{Gi} = I_{Gi} e^{j\gamma_i} = I_{Di} + j I_{Qi} = (I_{di} + j I_{qi}) e^{j(\delta_i - \pi/2)} = I_i e^{j(\delta_i - \pi/2)} \quad (5.16)$$

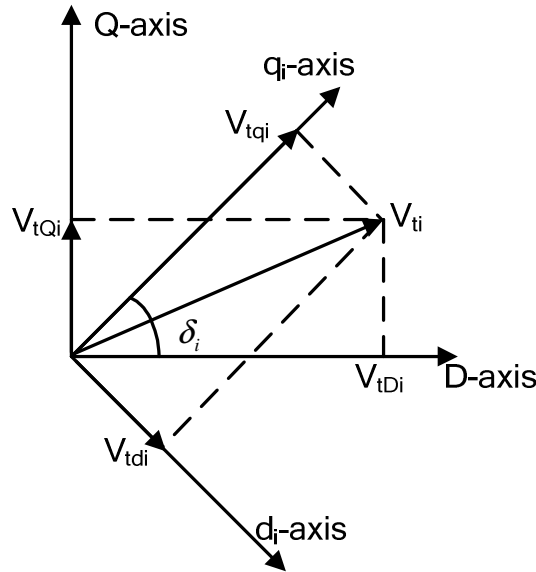


Figure 5.5: Transformation for interfacing network reference with machine reference-method 1

From Equation (5.15)

$$V_{tdi} + j V_{tqi} = (V_{tdi} + j V_{tqi}) e^{j(\delta_i - \pi/2)}$$

Substituting the stator algebraic equations,  $V_{tdi} = x_{qi} I_{qi}$ ;  $V_{tqi} = E'_{qi} - x'_{di} I_{tdi}$  in the above equation, the following is obtained,

$$V_{tdi} + j V_{tqi} = [x_{qi} I_{qi} + j (E'_{qi} - x'_{di} I_{tdi})] e^{j(\delta_i - \pi/2)} \quad (5.17)$$

Substituting  $I_{di} = I_i - j I_{qi}$  in Equation (5.17),

$$\begin{aligned} V_{tdi} + j V_{tqi} &= [x_{qi} I_{qi} + j [E'_{qi} - x'_{di} (I_i - j I_{qi})]] e^{j(\delta_i - \pi/2)} \\ &= E'_{qi} e^{j\delta_i} - j x'_{di} I_i e^{j(\delta_i - \pi/2)} + (x_{qi} - x'_{di}) I_{qi} e^{j(\delta_i - \pi/2)} \end{aligned} \quad (5.18)$$

Replacing  $V_{tdi} + j V_{tqi}$  with  $\bar{V}_{Gi}$  and  $I_i e^{j(\delta_i - \pi/2)}$  with  $\bar{I}_{Gi}$  in Equation (5.18), it can be written in  $D - Q$  axis reference frame as:

$$\bar{V}_{Gi} = E'_{qi} e^{j\delta_i} - j x'_{di} \bar{I}_{Gi} + (x_{qi} - x'_{di}) I_{qi} e^{j(\delta_i - \pi/2)} \quad (5.19)$$

The above equation gives the generator voltages in  $D - Q$  axis reference frame. In matrix form Equation (5.19) can be written as

$$\bar{V}_G = e^{j\delta} E'_q - j x'_d \bar{I}_G + [x_q - x'_d] e^{j(\delta - \pi/2)} I_q \quad (5.20)$$

where,  $\bar{V}_G$ ,  $E'_q$ ,  $\bar{I}_G$ ,  $I_q$  are column matrices and the coefficients  $e^{j\delta}$ ,  $x'_d$ ,  $[x_q - x'_d]$ ,  $e^{j(\delta - \pi/2)}$  are diagonal matrices. Substituting Equation (5.20) in Equation (5.10), the generator current vector becomes:

$$\bar{I}_G = \bar{Y}_{red} [e^{j\delta} E'_q - j x'_d \bar{I}_G + [x_q - x'_d] e^{j(\delta - \pi/2)} I_q],$$

or,

$$\bar{I}_G = (\bar{Y}_{red}^{-1} + j x'_d)^{-1} [e^{j\delta} E'_q + [x_q - x'_d] e^{j(\delta - \pi/2)} I_q] \quad (5.21)$$

Applying the transformation, Equation (5.21) is converted to the  $d_i - q_i$  axes reference frame as follows:

$$e^{j(\pi/2-\delta)} \bar{I}_G = e^{j(\pi/2-\delta)} (\bar{Y}_{red}^{-1} + j x'_d)^{-1} [e^{j\delta} E'_q + [x_q - x'_d] e^{j(\delta-\pi/2)} I_q]$$

$$I = e^{j(\pi/2-\delta)} \bar{Y}_d [e^{j\delta} E'_q + [x_q - x'_d] e^{j(\delta-\pi/2)} I_q] \quad (5.22)$$

where  $\bar{Y}_d = (\bar{Y}_{red}^{-1} + j x'_d)^{-1}$  and  $I = e^{j(\pi/2-\delta)} \bar{I}_G = I_d + j I_q$ . Equation (5.22) can be written in detail as follows:

$$\begin{bmatrix} I_1 \\ \vdots \\ I_n \end{bmatrix} = \begin{bmatrix} I_{d1} + j I_{q1} \\ \vdots \\ I_{dn} + j I_{qn} \end{bmatrix} = \begin{bmatrix} e^{j(\pi/2-\delta_1)} & 0 & 0 \\ 0 & \ddots & 0 \\ 0 & 0 & e^{j(\pi/2-\delta_n)} \end{bmatrix} \begin{bmatrix} \bar{Y}_{d11} & \cdots & \bar{Y}_{d1n} \\ \vdots & \ddots & \vdots \\ \bar{Y}_{dn1} & \cdots & \bar{Y}_{dnn} \end{bmatrix} \times$$

$$\left\{ \begin{bmatrix} e^{j\delta_1} & 0 & 0 \\ 0 & \ddots & 0 \\ 0 & 0 & e^{j\delta_n} \end{bmatrix} \begin{bmatrix} E'_{q1} \\ \vdots \\ E'_{qn} \end{bmatrix} + \begin{bmatrix} x_{q1} - x'_{d1} & 0 & 0 \\ 0 & \ddots & 0 \\ 0 & 0 & x_{qn} - x'_{dn} \end{bmatrix} \times \right.$$

$$\left. \begin{bmatrix} e^{j(\delta_1-\pi/2)} & 0 & 0 \\ 0 & \ddots & 0 \\ 0 & 0 & e^{j(\delta_n-\pi/2)} \end{bmatrix} \begin{bmatrix} I_{q1} \\ \vdots \\ I_{qn} \end{bmatrix} \right\}$$

Therefore, in general, output current of the  $i^{th}$  generator in  $n$  machine power system can be expressed in  $d_i - q_i$  axes as:

$$I_i = I_{di} + j I_{qi} = \sum_{j=1}^n \bar{Y}_{dij} \left[ E'_{qj} e^{j(\pi/2+\delta_{ji})} + (x_{qj} - x'_{dj}) I_{qj} e^{j\delta_{ji}} \right] \quad (5.23)$$

where  $\delta_{ji} = \delta_j - \delta_i$ .

#### 5.2.4.1 Initial conditions for the dynamic system

To perform the power system dynamic analysis, the fixed inputs  $P_{mi}$ ,  $V_{ref i}$  and initial conditions of all the dynamic states are computed [17]:

Step 1: From the load flow, compute the generator's currents:

$$\bar{I}_{Gi} = I_{Gi} e^{j\gamma_i} = \frac{P_{Gi} - jQ_{Gi}}{\bar{V}_{Gi}^*} \quad i = 1, \dots, n \quad (5.24)$$

where  $P_{Gi}$ , and  $Q_{Gi}$ , and are the generator power outputs.  $\bar{V}_{Gi}^*$  is the complex conjugate of  $\bar{V}_{Gi}$ .

Step 2: Compute  $\delta_i$ , which is computed from Equation (5.19) as follows [17];

Equation (5.19) can be written as [17]:

$$\begin{aligned} V_{Gi} e^{j\theta_i} &= E'_{qi} e^{j\delta_i} - jx'_{di} I_{Gi} e^{j\gamma_i} + (x_{qi} - x'_{di}) I_{qi} e^{j(\delta_i - \pi/2)} \\ \Rightarrow V_{Gi} e^{j\theta_i} + jx'_{di} I_{Gi} e^{j\gamma_i} - (x_{qi} - x'_{di}) I_{qi} e^{j(\delta_i - \pi/2)} - E'_{qi} e^{j\delta_i} &= 0 \\ \Rightarrow V_{Gi} e^{j\theta_i} + jx'_{di} (I_{di} + jI_{qi}) e^{j(\delta_i - \pi/2)} - (x_{qi} - x'_{di}) I_{qi} e^{j(\delta_i - \pi/2)} - E'_{qi} e^{j\delta_i} &= 0 \\ \Rightarrow V_{Gi} e^{j\theta_i} + jx'_{di} I_{di} e^{j(\delta_i - \pi/2)} - x_{qi} I_{qi} e^{j(\delta_i - \pi/2)} - E'_{qi} e^{j\delta_i} &= 0 \\ \Rightarrow V_{Gi} e^{j\theta_i} + jx'_{di} I_{di} e^{j(\delta_i - \pi/2)} - jx_{qi} I_{di} e^{j(\delta_i - \pi/2)} &= 0 \\ &+ jx_{qi} I_{di} e^{j(\delta_i - \pi/2)} - x_{qi} I_{qi} e^{j(\delta_i - \pi/2)} - E'_{qi} e^{j\delta_i} = 0 \quad (5.25) \\ \Rightarrow V_{Gi} e^{j\theta_i} + jx_{qi} (I_{di} + jI_{qi}) e^{j(\delta_i - \pi/2)} - E'_{qi} e^{j\delta_i} - j(x_{qi} - x'_{di}) I_{di} e^{j(\delta_i - \pi/2)} &= 0 \\ \Rightarrow V_{Gi} e^{j\theta_i} + jx_{qi} (I_{di} + jI_{qi}) e^{j(\delta_i - \pi/2)} = E'_{qi} e^{j\delta_i} + (x_{qi} - x'_{di}) I_{di} e^{j\delta_i} \end{aligned}$$

Rearrange the terms as follows:

$$V_{Gi} e^{j\theta_i} + jx_{qi} I_{Gi} e^{j\gamma_i} = (E'_{qi} + (x_{qi} - x'_{di}) I_{di}) e^{j\delta_i} \quad (5.26)$$

The Right hand side of Equation (5.26) represents the voltage behind the impedance  $jx_{qi}$  having an angle  $\delta_i$  which can also be computed as angle of

$(V_{Gi}e^{j\theta_i} + x_{qi} I_{Gi}e^{j\gamma_i})$ . The phasor diagram representation of the stator algebraic variables for computing  $\delta_i$  is shown in Figure 5.6.

$$\delta_i = \text{angle of } (V_{Gi}e^{j\theta_i} + x_{qi} I_{Gi}e^{j\gamma_i}), \quad i = 1, \dots, n \quad (5.27)$$

Step 3: Compute  $V_{tdi}, V_{tqi}, I_{di}, I_{qi}$  for the machines from Equations (5.15-5.16) as:

$$V_{Gi}e^{j\theta_i} = (V_{tdi} + j V_{tqi})e^{j(\delta_i - \pi/2)} \quad \text{or} \quad (V_{tdi} + j V_{tqi}) = V_{Gi}e^{j(\theta_i - \delta_i + \pi/2)}, \quad i = 1, \dots, n \quad (5.28)$$

$$I_{Gi}e^{j\gamma_i} = (I_{di} + j I_{qi})e^{j(\delta_i - \pi/2)} \quad \text{or} \quad (I_{di} + j I_{qi}) = I_{Gi}e^{j(\gamma_i - \delta_i + \pi/2)}, \quad i = 1, \dots, n \quad (5.29)$$

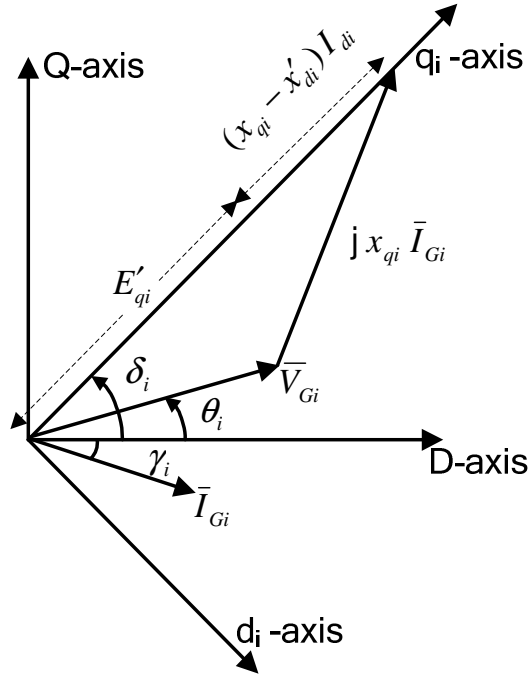


Figure 5.6: Phasor diagram of stator algebraic variables for computing the rotor angle  $\delta_i$  method-1

Step 4: Compute  $E'_{qi}$  as:

$$V_{tqi} = E'_{qi} - x'_{di} I_{di} \quad \text{or} \quad (5.30)$$

$$E'_{qi} = V_{tqi} + x'_{di} I_{di}, \quad i = 1, \dots, n \quad (5.31)$$

Step 5: Compute  $E_{fdi}$  from Equation (5.3) after setting the derivative equal to zero (under steady state).

$$E_{fdi} = E'_{qi} + (x_{di} - x'_{di})I_{di}, \quad i = 1, \dots, n \quad (5.32)$$

Step 6: Compute  $V_{refi}$  from Equation (5.4) after setting the derivative equal to zero.

$$V_{refi} = \frac{E_{fdi}}{K_{Ai}} + V_{ti}, \quad i = 1, \dots, n \quad (5.33)$$

Step 7: The mechanical states  $\omega_i$  and  $P_{mi}$  can be computed from Equations (5.1-5.2) by setting the derivatives equal to zero.

$$\omega_i = 1, \quad i = 1, \dots, n \quad (5.34)$$

$$P_{mi} = P_{ei}, \quad \text{with } P_{Di} = 0$$

$$\begin{aligned} &= I_{di}V_{tdi} + I_{qi}V_{tqi} \\ &= I_{di}x_{qi}I_{qi} + I_{qi}(E'_{qi} - x'_{di}I_{di}) \end{aligned}$$

$$P_{mi} = E'_{qi}I_{qi} + (x_{qi} - x'_{di})I_{di}I_{qi}, \quad i = 1, \dots, n \quad (5.35)$$

This completes the computation of the initial conditions of all the dynamic states using this type of transformation.

## 5.2.5 Method 2 of Transforming Network Equations To Individual Machine Frame

The individual machine coordinates  $d_i - q_i$  may be related to the common system coordinates  $D - Q$  as shown in Figure 5.7 [104], where  $\delta_i$  is the phase angle difference of the  $d_i$  axis with respect to the  $D$  axis or the  $q_i$  axis with respect to the  $Q$  axis.

The orthogonal transformation is given by

$$\begin{bmatrix} V_{tDi} \\ V_{tQi} \end{bmatrix} = \begin{bmatrix} \cos \delta_i & \sin \delta_i \\ -\sin \delta_i & \cos \delta_i \end{bmatrix} \begin{bmatrix} V_{tdi} \\ V_{tqi} \end{bmatrix} \quad (5.36)$$

From Equation (5.36) the relationship between the two coordinate variables is obtained as:

$$V_{tDi} + j V_{tQi} = (V_{tdi} + j V_{tqi}) e^{-j\delta_i} \quad (5.37)$$

Similarly the current variables can be transformed as:

$$I_{Di} + j I_{Qi} = (I_{di} + j I_{qi}) e^{-j\delta_i} \quad (5.38)$$

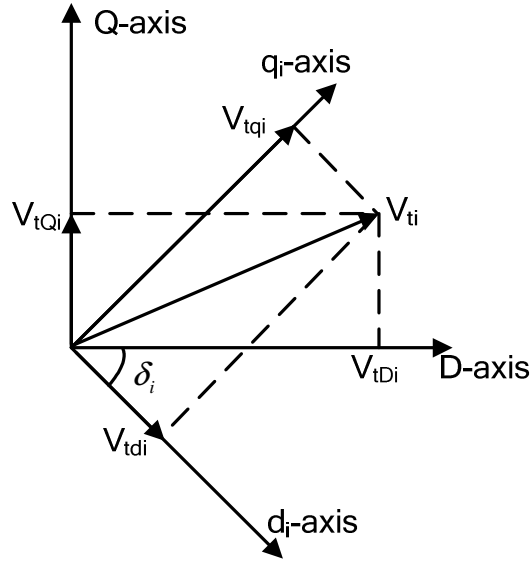


Figure 5.7: Transformation for interfacing network reference with machine reference-method 2

Following the method explained in Section 5.3.1, the generator voltages are derived using this transformation as [104]:

$$\bar{V}_{Gi} = E'_{qi} e^{j(\pi/2 - \delta_i)} - j x'_{di} \bar{I}_{Gi} + (x_{qi} - x'_{di}) I_{qi} e^{-j\delta_i} \quad (5.39)$$

Rewriting the Equation (5.39) as,

$$V_{Gi} e^{j\theta_i} = E'_q e^{j(\pi/2 - \delta_i)} - j x'_d I_{Gi} e^{j\gamma_i} + (x_{qi} - x'_d) I_{qi} e^{-j\delta_i} \quad (5.40)$$

Rearrange the terms in Equation (5.40), by adding and subtracting  $j x_{qi} I_{di} e^{-j\delta_i}$  on right hand side,

$$V_{Gi} e^{j\theta_i} + j x_{qi} I_{Gi} e^{j\gamma_i} = (E'_q + (x_{qi} - x'_d) I_{di}) e^{j(\frac{\pi}{2} - \delta_i)} \quad (5.41)$$

Comparing Equation (5.19) with Equation (5.39) and Equation (5.26) with Equation (5.41), it is observed that the angle between internal quadrature axis voltage and  $D$  axis is  $\delta_i$  with the first transformation whereas it is equal to  $\frac{\pi}{2} - \delta_i$  when using the second transformation.

**Remark:** Since  $\delta_i$  is the angular position of the rotor in electrical radians with respect to the synchronous rotating reference, the rotor angle Equation (5.1) does not differ when using the first transformation as the equation has been developed with the same concept. However, when the second transformation is used, the new angular position is  $\frac{\pi}{2} - \delta_i$ . As such the rotor angle equation is modified as follows:

$$\frac{d\left(\frac{\pi}{2} - \delta_i\right)}{dt} = \omega_0 (\omega_i - 1) \quad (5.42)$$

Equation (5.1) becomes

$$\dot{\delta}_i = -\omega_0 (\omega_i - 1) \quad (5.43)$$

**Note:** When the second transformation is utilized, the rotor angle equation is given by Equation (5.43), and the remaining Equations (5.2-5.4) remain same.

Proceeding, the generator voltage Equation (5.39) can be written in matrix form as,

$$\bar{V}_G = e^{j(\pi/2 - \delta)} E'_q - j x'_d \bar{I}_G + (x_q - x'_d) e^{-j\delta} I_q \quad (5.44)$$

Substituting Equation (5.44) in Equation (5.10) the generator current equation will be:

$$\bar{I}_G = \bar{Y}_{red} [e^{j(\pi/2-\delta)} E'_q - j x'_d \bar{I}_G + (x_q - x'_d) e^{-j\delta} I_q] \quad (5.45)$$

or,

$$\bar{I}_G = (\bar{Y}_{red}^{-1} + j x'_d)^{-1} [e^{j(\pi/2-\delta)} E'_q + (x_q - x'_d) e^{-j\delta} I_q] \quad (5.46)$$

$$\bar{I}_G = \bar{Y}_d [e^{j(\pi/2-\delta)} E'_q + (x_q - x'_d) e^{-j\delta} I_q] \quad (5.47)$$

Applying the transformation, Equation (5.47) is converted onto the  $d_i - q_i$  axes reference frame as follows:

$$I = \bar{I}_G e^{j\delta} = \bar{Y}_d [e^{j(\pi/2-\delta)} E'_q + (x_q - x'_d) e^{-j\delta} I_q] e^{j\delta} \quad (5.48)$$

where  $I = \bar{I}_G e^{j\delta} = I_d + j I_q$

Equation (5.48) can be written as:

$$\begin{aligned} \begin{bmatrix} I_1 \\ \vdots \\ I_n \end{bmatrix} &= \begin{bmatrix} I_{d1} + j I_{q1} \\ \vdots \\ I_{dn} + j I_{qn} \end{bmatrix} = \begin{bmatrix} e^{j\delta_1} & 0 & 0 \\ 0 & \ddots & 0 \\ 0 & 0 & e^{j\delta_n} \end{bmatrix} \begin{bmatrix} \bar{Y}_{d11} & \cdots & \bar{Y}_{d1n} \\ \vdots & \ddots & \vdots \\ \bar{Y}_{dn1} & \cdots & \bar{Y}_{dnn} \end{bmatrix} \times \\ &\left\{ \begin{bmatrix} e^{j(\pi/2-\delta_1)} & 0 & 0 \\ 0 & \ddots & 0 \\ 0 & 0 & e^{j(\pi/2-\delta_n)} \end{bmatrix} \begin{bmatrix} E'_{q1} \\ \vdots \\ E'_{qn} \end{bmatrix} + \right. \\ &\left. \begin{bmatrix} x_{q1} - x'_{d1} & 0 & 0 \\ 0 & \ddots & 0 \\ 0 & 0 & x_{qn} - x'_{dn} \end{bmatrix} \begin{bmatrix} e^{-j\delta_1} & 0 & 0 \\ 0 & \ddots & 0 \\ 0 & 0 & e^{-j\delta_n} \end{bmatrix} \begin{bmatrix} I_{q1} \\ \vdots \\ I_{qn} \end{bmatrix} \right\} \end{aligned} \quad (5.49)$$

From the above equation (5.49) the output current of the  $i^{\text{th}}$  generator is expressed as:

$$I_i = I_{di} + j I_{qi} = \sum_{j=1}^n \bar{Y}_{dij} \left[ E'_{qj} e^{j(\pi/2+\delta_{ij})} + (x_{qj} - x'_{dj}) I_{qj} e^{j\delta_{ij}} \right] \quad (5.50)$$

where  $\delta_{ij} = \delta_i - \delta_j$ .

**Note:** Comparing the two generator currents of Equations (5.23) and (5.50) derived with the two different transformations, the variation lies in the rotor angle difference  $\delta_{ji}$  and  $\delta_{ij}$  between the two equations.

### 5.2.5.1 Initial conditions for the dynamic system

The initial conditions for the dynamic states are computed in a method similar to that explained in Section 5.3.4.1. However, Step 2 and Step 3, i.e., Equations (5.27-5.29) are modified according to the 2<sup>nd</sup> method of transformation.

Step 2: The individual rotor angles  $\delta_i$  are computed from the stator algebraic equation given in Equation (5.41). The phasor diagram representation of the stator algebraic variables for computing  $\delta_i$  in this 2<sup>nd</sup> method of transformation is shown in Figure 5.8.

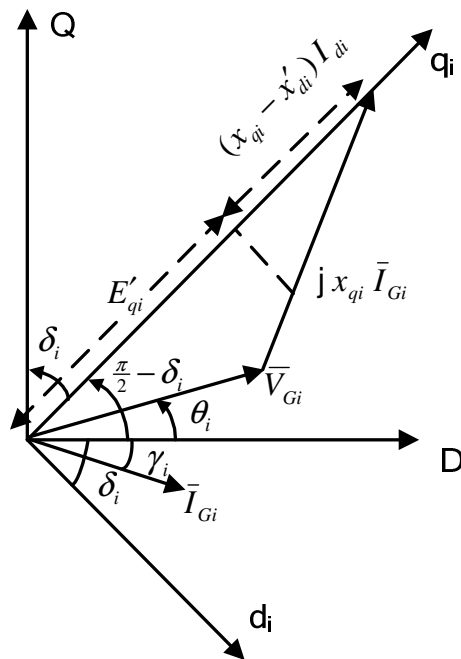


Figure 5.8: Phasor diagram of stator algebraic variables for computing the rotor angle  $\delta_i$  method-2

The Right hand side of Equation (5.41) represents the voltage behind the impedance  $jx_{qi}$  having an angle  $\frac{\pi}{2} - \delta_i$  which is computed as the angle of  $(V_{Gi}e^{j\theta_i} + x_{qi} I_{Gi}e^{j\gamma_i})$ .

$$\frac{\pi}{2} - \delta_i = \text{angle of } (V_{Gi}e^{j\theta_i} + x_{qi} I_{Gi}e^{j\gamma_i}), \text{ or}$$

$$\delta_i = \frac{\pi}{2} - \text{angle of } (V_{Gi}e^{j\theta_i} + x_{qi} I_{Gi}e^{j\gamma_i}), \quad i = 1, \dots, n \quad (5.51)$$

The above equation gives the initial values of the individual machine rotor angles in the 2<sup>nd</sup> method of transformation.

Step 3: Compute  $V_{tdi}, V_{tqi}, I_{di}, I_{qi}$  as follows:

$$V_{Gi}e^{j\theta_i} = (V_{tdi} + j V_{tqi})e^{-j\delta_i} \text{ or } (V_{tdi} + j V_{tqi}) = V_{Gi}e^{j(\theta_i + \delta_i)}, \quad i = 1, \dots, n \quad (5.52)$$

$$I_{Gi}e^{j\theta_i} = (I_{di} + j I_{qi})e^{-j\delta_i} \text{ or } (I_{di} + j I_{qi}) = I_{Gi}e^{j(\gamma_i + \delta_i)}, \quad i = 1, \dots, n \quad (5.53)$$

The rest of the steps for computing the initial values remain unchanged.

### 5.3 Linearized System of Multi-Machine Power System

The linearized Phillips-Heffron model [7], [18] was proposed for the analysis of power system oscillation stability and control. The linearized model for a power system is derived by linearizing the nonlinear equations of the multi-machine power system. The nonlinear equations consist of the differential equations of the mechanical system, electrical equation of the exciter, field winding, and algebraic equations of the stator and network in the multi-machine power system.

The following equations constitute the linearized model of the multi-machine system when the transformation of network variables is performed by first method [17].

$$\Delta \dot{\delta} = \omega_0 \Delta \omega \quad (5.54)$$

$$\Delta \dot{\omega} = M^{-1}(\Delta P_m - \Delta P_e - D\Delta \omega) \quad (5.55)$$

$$\Delta \dot{E}'_q = T_{d0}^{-1}(-\Delta E'_q - (x_d - x'_d)\Delta I_d + \Delta E_{fd}) \quad (5.56)$$

$$\Delta \dot{E}_{fd} = T_A^{-1}(-\Delta E_{fd} + K_A(\Delta V_{ref} - \Delta V_t)) \quad (5.57)$$

where

$$\Delta P_e = I_{q0}\Delta E'_q + I_{q0}(x_q - x'_q)\Delta I_d + E'_q\Delta I_q + I_{d0}(x_q - x'_q)\Delta I_q \quad (5.58)$$

$$\Delta V_{td} = x_q\Delta I_q, \quad \Delta V_{tq} = \Delta E'_q - x'_d\Delta I_d \quad (5.59)$$

and,

$$\Delta \delta = [\Delta \delta_1 \quad \Delta \delta_2 \quad \cdots \quad \Delta \delta_n]^T,$$

$$\Delta \omega = [\Delta \omega_1 \quad \Delta \omega_2 \quad \cdots \quad \Delta \omega_n]^T$$

$$\Delta E'_q = [\Delta E'_{q1} \quad \Delta E'_{q2} \quad \cdots \quad \Delta E'_{qn}]^T,$$

$$\Delta E_{fd} = [\Delta E_{fd1} \quad \Delta E_{fd2} \quad \cdots \quad \Delta E_{fdn}]^T$$

$$\Delta I_d = [\Delta I_{d1} \quad \Delta I_{d2} \quad \cdots \quad \Delta I_{dn}]^T,$$

$$\Delta I_q = [\Delta I_{q1} \quad \Delta I_{q2} \quad \cdots \quad \Delta I_{qn}]^T,$$

$$\Delta V_{td} = [\Delta V_{td1} \quad \Delta V_{td2} \quad \cdots \quad \Delta V_{tdn}]^T,$$

$$\Delta V_{tq} = [\Delta V_{tq1} \quad \Delta V_{tq2} \quad \cdots \quad \Delta V_{tqn}]^T,$$

$$\Delta V_t = [\Delta V_{t1} \quad \Delta V_{t2} \quad \cdots \quad \Delta V_{tn}]^T$$

$$V_{ti} = \sqrt{V_{tdi}^2 + V_{tqi}^2},$$

$$M = \text{diag}(2H_i), D = \text{diag}(D_i), T'_{d0} = \text{diag}(T'_{d0i}),$$

$$x_d = \text{diag}(x_{di}), x_q = \text{diag}(x_{qi}), x'_d = \text{diag}(x'_{di})$$

$$I_{q0} = \text{diag}(I_{q10}, \dots, I_{qn0}), I_{d0} = \text{diag}(I_{d10}, \dots, I_{dn0}),$$

$I_{di0}, I_{qi0}$  are the values of  $I_{di}, I_{qi}$  respectively at the operating point.

$i = 1, \dots, n$ ,  $n$  is the number of generators.

From Equation (5.23) the generator current in  $d - q$  axes is,

$$\begin{aligned} I_i = I_{di} + jI_{qi} &= \sum_{j=1}^n \bar{Y}_{dij} \left[ E'_{qj} e^{j(\pi/2 + \delta_{ji})} + (x_{qj} - x'_{dj}) I_{qj} e^{j\delta_{ji}} \right] \\ &= \sum_{j=1}^n \bar{Y}_{dij} \left[ E'_{qj} e^{j(\pi/2 + \delta_j - \delta_i)} + (x_{qj} - x'_{dj}) I_{qj} e^{j(\delta_j - \delta_i)} \right] \end{aligned} \quad (5.60)$$

Denoting

$$\bar{Y}_{dij} = Y_{dij} e^{j\beta_{dij}}, \quad (5.61)$$

$$I_{di} = \text{real}(\bar{I}_{Gi}), I_{qi} = \text{imag}(\bar{I}_{Gi}) \quad (5.62)$$

$$\delta_{dij} = \delta_j - \delta_i + \beta_{dij} \quad (5.63)$$

Expanding Equation (5.60) into the  $d - q$  axes components,

$$I_{di} = \sum_{j=1}^n Y_{dij} \left[ -E'_{qj} \sin \delta_{dij} + (x_{qj} - x'_{dj}) \cos \delta_{dij} I_{qj} \right] \quad (5.64)$$

$$I_{qi} = \sum_{j=1}^n Y_{dij} \left[ E'_{qj} \cos \delta_{dij} + (x_{qj} - x'_{dj}) \sin \delta_{dij} I_{qj} \right] \quad (5.65)$$

In linearized form Equations (5.64) and (5.65) can be written as,

$$\Delta I_q = C_q \Delta \delta + E_q \Delta E'_q + M_q \Delta I_q \quad (5.66)$$

$$\Delta I_d = C_d \Delta \delta + E_d \Delta E'_q + M_d \Delta I_q \quad (5.67)$$

where,

$$C_{qii} = \sum_{\substack{j=1 \\ j \neq i}}^n Y_{dij} \left[ \sin \delta_{dij} E'_{qj} - (x_{qj} - x'_{dj}) \cos \delta_{dij} I_{qj} \right] \quad i = 1, 2, \dots, n$$

$$C_{qij} = -Y_{dij} \left( \sin \delta_{dij} E'_{qj} + (x_{qj} - x'_{dj}) \cos \delta_{dij} I_{qj} \right) \quad j = 1, 2, \dots, n; \quad i = 1, 2, \dots, n, \quad i \neq j$$
(5.68)

$$E_{qij} = -Y_{dij} \cos \delta_{dij} \quad j = 1, 2, \dots, n; \quad i = 1, 2, \dots, n$$

$$M_{qij} = (Y_{dij} (x_{qj} - x'_{dj}) \sin \delta_{dij}) \quad j = 1, 2, \dots, n; \quad i = 1, 2, \dots, n$$

$$C_{dii} = \sum_{\substack{j=1 \\ j \neq i}}^n Y_{dij} \left[ \cos \delta_{dij} E'_{qj} + (x_{qj} - x'_{dj}) \sin \delta_{dij} I_{qj} \right]$$

$$C_{dij} = -Y_{dij} \left( \cos \delta_{dij} E'_{qj} + (x_{qj} - x'_{dj}) \sin \delta_{dij} I_{qj} \right) \quad j = 1, 2, \dots, n; \quad i = 1, 2, \dots, n, \quad i \neq j$$

$$E_{dij} = -Y_{dij} \sin \delta_{dij} \quad j = 1, 2, \dots, n; \quad i = 1, 2, \dots, n$$

$$M_{dij} = (Y_{dij} (x_{qj} - x'_{dj}) \cos \delta_{dij}) \quad j = 1, 2, \dots, n; \quad i = 1, 2, \dots, n$$
(5.69)

From (5.66)

$$\Delta I_q = D_q \Delta \delta + F_q \Delta E'_q \quad (5.70)$$

where

$$D_q = L_q^{-1} C_q, \quad F_q = L_q^{-1} E_q, \quad \text{and} \quad L_q = 1 - M_q,$$

$$L_{qii} = 1 - Y_{dii} (x_{qi} - x'_{di}) \sin \delta_{dii}, \quad L_{qij} = -Y_{dij} (x_{qj} - x'_{dj}) \sin \delta_{dij} \quad j \neq i$$

Substituting Equation (5.70) into Equation (5.67)  $\Delta I_d$  can be written as:

$$\Delta I_d = D_d \Delta \delta + F_d \Delta E'_q \quad (5.71)$$

where

$$D_d = C_d + M_d D_q, \quad F_d = E_d + M_d F_q$$

Substituting Equations (5.70) and (5.71) into Equations (5.55-5.59), the integrated linearized power system model is formed also known as the Phillips-Heffron model of the multi-machine power system, and in state space form is given in Equation (5.72) while the block diagram for the  $i^{\text{th}}$  machine is represented in Figure 5.9 [104].

$$\begin{bmatrix} \Delta \dot{\delta} \\ \Delta \dot{\omega} \\ \Delta \dot{E}'_q \\ \Delta \dot{E}'_{fd} \end{bmatrix} = \begin{bmatrix} 0 & \omega_0 I & 0 & 0 \\ -M^{-1} K_1 & -M^{-1} D & -M^{-1} K_2 & 0 \\ -T'_{do}{}^{-1} K_4 & 0 & -T'_{do}{}^{-1} K_3 & T'_{do}{}^{-1} \\ -T_A^{-1} K_A K_5 & 0 & -T_A^{-1} K_A K_6 & -T_A^{-1} \end{bmatrix} \begin{bmatrix} \Delta \delta \\ \Delta \omega \\ \Delta E'_q \\ \Delta E'_{fd} \end{bmatrix} \quad (5.72)$$

where,

$$K_1 = I_{q0}(x_q - x'_d)D_d + E'_q D_q + I_{d0}(x_q - x'_d)D_q \quad (5.73)$$

$$K_2 = I_{q0} + I_{q0}(x_q - x'_d)F_q + E'_q F_q + I_{d0}(x_q - x'_d)F_q$$

$$K_4 = (x_d - x'_d)D_d \quad (5.74)$$

$$K_3 = I + (x_d - x'_d)F_d$$

$$K_5 = V_{i0}^{-1} (V_{d0} x_q D_q - V_{q0} x'_d D_d) \quad (5.75)$$

$$K_6 = V_{i0}^{-1} (V_{d0} x_q F_q + V_{q0} - V_{q0} x'_d F_d)$$

The K-constants are the functions of the operating point and system parameters.

The linearized system of equations for the multi-machine, when the network variables are transformed by second method are given by the same set of equations, i.e., Equations (5.54)-(5.75), except Equations (5.54) and (5.63) which are modified according to Equations (5.43) and (5.50) with respect to the second method of transformation and are given as:

$$\Delta \dot{\delta} = -\omega_0 \Delta \omega \quad (5.76)$$

$$\delta_{dij} = \delta_i - \delta_j + \beta_{dij} \quad (5.77)$$

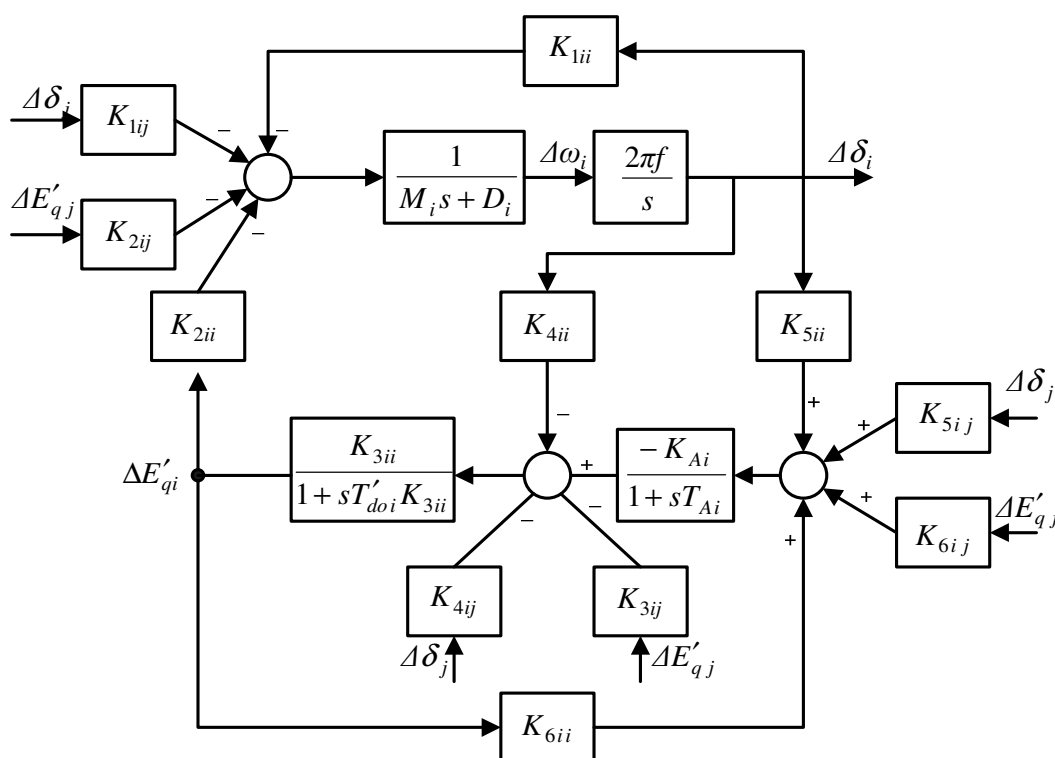


Figure 5.9: Block diagram of  $i^{\text{th}}$  machine in linearized multi-machine power system

The state matrix formed from the  $K$ -constants computed from using either transformation will finally give the same set of eigenvalues. The following section gives the results of the nonlinear simulation of multi-machine power system.

### 5.4 Case Study: Multi-Machine Power System

Consider the 3-machine, 9-bus Western System Coordinating Council (WSCC) power system [17] shown in Figure 5.10. The system parameters are listed in Table 5.1 and the generator and exciter data are given in Table 5.2.

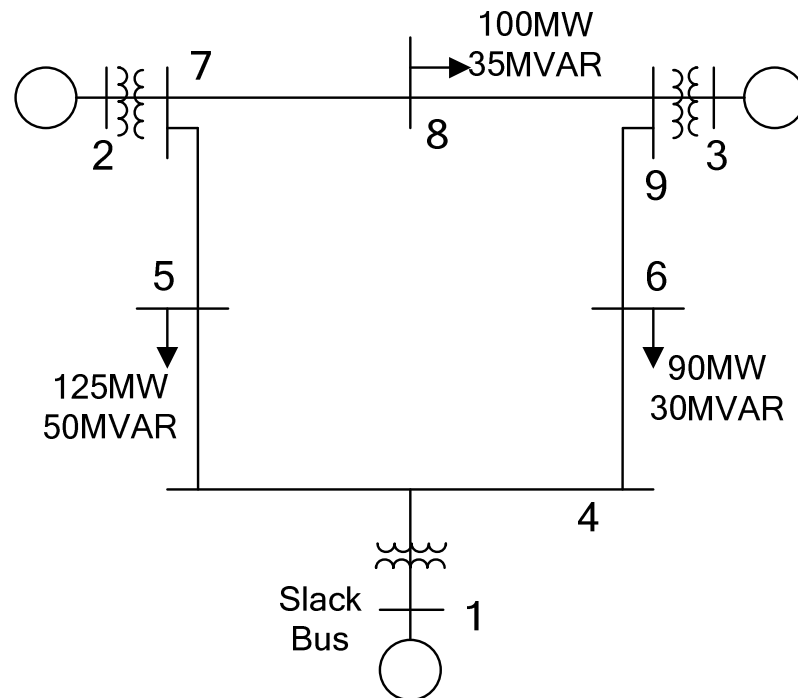


Figure 5.10: 3-machine 9-bus power system

Table 5.1: WSCC power system parameters

	Bus no.	Impedance		
		R	X	$B_c / 2$
Transmission lines		Transformer	reactance	
1	1-4	0	0.0576	
2	2-7	0	0.0625	
3	3-9	0	0.0586	
4	4-5	0.01	0.085	0.088
5	4-6	0.017	0.092	0.079
6	5-7	0.032	0.161	0.153
7	6-9	0.039	0.17	0.179
8	7-8	0.0085	0.072	0.0745
9	8-9	0.0119	0.1008	0.1045
Loads		MW	MVAR	
1	5	125	50	
2	6	90	30	
3	8	100	35	

Table 5.2: Generator and exciter data

Parameters	Generator 1	Generator 2	Generator 3
$H$ (secs)	23.64	6.4	3.01
$D$	0	0	0
$x_d$ (pu)	0.146	0.8958	1.3125
$x'_d$ (pu)	0.0608	0.1198	0.1813
$x_q$ (pu)	0.0969	0.8645	1.2578
$T'_{d0}$ (pu)	8.96	6.0	5.89
$K_A$ (pu)	30	30	10
$T_A$ (sec)	0.05	0.05	0.05

Initially the admittance matrix  $\bar{Y}$  of the power system network is formed which is given by Equation (5.78). The admittance matrix Equation (5.78) includes the admittance due to the loads. The load flow is performed on the system where the results are given in Table 5.3 and the transmission line flows are given in Table 5.4. Bus 1 is taken as the slack (swing) bus for the load flow.

Table 5.3: The load flow results of the WSCC 3-machine 9-bus system

	Bus	Voltage (p.u.)	$P_G$ (p.u.)	$Q_G$ (p.u.)	$-P_L$ (p.u.)	$-Q_L$ (p.u.)
1	(swing)	1.04	0.7164	0.2705		
2	(P-V)	$1.025\angle 9.28^0$	1.6300	0.0665		
3	(P-V)	$1.025\angle 4.665^0$	0.85	- 0.1086		
4	(P-V)	$1.0258\angle - 2.22^0$				
5	(P-Q)	$0.9956\angle -3.99^0$			1.25	0.5
6	(P-Q)	$1.0127\angle -3.7^0$			0.9	0.3
7	(P-Q)	$1.0258\angle 3.72^0$				
8	(P-Q)	$1.0159\angle 0.73^0$			1.0	0.35
9	(P-Q)	$1.0324\angle 1.97^0$				

Table 5.4: The power flows in each transmission lines

Transmission lines	P	Q
1-4	0.7164	0.2705
2-7	1.6300	0.0665
3-9	0.8500	-0.1086
4-5	0.4094	0.2289
4-6	0.3070	0.0103
5-7	-0.8432	- 0.1131
6-9	-0.5946	- 0.1346
7-8	0.7638	- 0.0080
8-9	-0.2410	- 0.2430

$$\bar{Y} = \begin{bmatrix} -j17.3611 & 0 & 0 & j17.3611 & 0 & 0 & 0 & 0 & 0 \\ 0 & -j16.0 & 0 & 0 & 0 & 0 & j16.0 & 0 & 0 \\ 0 & 0 & -j17.0648 & 0 & 0 & 0 & 0 & 0 & j17.0648 \\ j17.3611 & 0 & 0 & 3.3074 & -1.3652 & -1.9422 & 0 & 0 & 0 \\ 0 & 0 & 0 & -j39.3089 & +j11.6041 & +j10.5107 & -1.1876 & 0 & 0 \\ 0 & 0 & 0 & -1.3652 & 3.8138 & 0 & +j5.9751 & 0 & 0 \\ 0 & 0 & 0 & +j11.6041 & -j17.8426 & 4.1018 & 0 & 0 & -1.282 \\ 0 & 0 & 0 & -1.9422 & 0 & -j16.1335 & 2.8047 & -1.6171 & 0 \\ 0 & j16.0 & 0 & 0 & -1.1876 & 0 & -j35.4456 & +j13.6980 & 0 \\ 0 & 0 & 0 & 0 & +j5.9751 & 0 & -1.6171 & 3.7412 & -1.155 \\ 0 & 0 & 0 & 0 & 0 & 0 & +j13.6980 & -j23.6424 & +j9.784 \\ 0 & 0 & j17.0648 & 0 & 0 & -1.2820 & 0 & -1.1551 & 2.437 \\ 0 & 0 & 0 & 0 & 0 & +j5.5882 & 0 & +j9.7843 & -j32.154 \end{bmatrix} \quad (5.78)$$

From the load flow results, the initial operating point is computed. The following two tables give the initial conditions computed as given in Sections 5.2.4.1 and 5.2.5.1 with respect to the two transformations. Table 5.5 gives the initial conditions when the first method of transformation is used. Table 5.6 gives the initial conditions when the second method is used. The values are in p.u. except where mentioned.

Table 5.5: Initial conditions computed using the first method of transformation

State variable	Machine 1	Machine 2	Machine 3
$\delta$ in radians	<b>0.06258</b>	<b>1.06637</b>	<b>0.94486</b>
$E'_q$	1.05636	0.78817	0.76786
$E_{fd}$	1.08215	1.78932	1.40299
$P_m$	0.71641	1.63	0.85
$V_{ref}$	1.07607	1.08464	1.16529

Table 5.6: Initial conditions computed using the second method of transformation

State variable	Machine 1	Machine 2	Machine 3
$\delta$ in radians	<b>1.50821</b>	<b>0.50443</b>	<b>0.62593</b>
$E'_q$	1.05636	0.78817	0.76786
$E_{fd}$	1.08215	1.78932	1.40299
$P_m$	0.71641	1.63	0.85
$V_{ref}$	1.07607	1.08464	1.16529

The power system is reduced to the generator buses by eliminating the load buses as described in Section 5.2.2. The computed reduced admittance matrix  $\bar{Y}_{red}$  of the transmission network is given by Equation (5.79) using which  $\bar{Y}_d$  is calculated from Equation (5.22) and given by Equation (5.80). The reduced system containing only the generator buses is depicted in Figure 5.11.

$$\bar{Y}_{red} = \begin{bmatrix} 1.1051-j 4.6957 & 0.0965+j 2.2570 & 0.0046+j 2.2748 \\ 0.0965+j 2.2570 & 0.7355-j 5.1143 & 0.1230+j 2.8257 \\ 0.0046+j 2.2748 & 0.1230+j 2.8257 & 0.7214-j 5.0231 \end{bmatrix} \quad (5.79)$$

with,

$$\bar{Y}_{GG} = \begin{bmatrix} -j17.3611 & 0 & 0 \\ 0 & -j16.0 & 0 \\ 0 & 0 & -j17.0648 \end{bmatrix}$$

$$\bar{Y}_{GL} = \begin{bmatrix} j17.3611 & 0 & 0 & 0 & 0 & 0 \\ 0 & 0 & 0 & j16.0 & 0 & 0 \\ 0 & 0 & 0 & 0 & 0 & j17.0648 \end{bmatrix}$$

$$\bar{Y}_{LG} = \begin{bmatrix} j17.3611 & 0 & 0 \\ 0 & 0 & 0 \\ 0 & 0 & 0 \\ 0 & j16.0 & 0 \\ 0 & 0 & 0 \\ 0 & 0 & j17.0648 \end{bmatrix}$$

$$\bar{Y}_{LL} = \begin{bmatrix} 3.3074 & -1.3652 & -1.9422 & 0 & 0 & 0 \\ -j 39.3089 & +j 11.6041 & +j 10.5107 & 0 & 0 & 0 \\ -1.3652 & 3.8138 & 0 & -1.1876 & 0 & 0 \\ +j 11.6041 & -j 17.8426 & 0 & +j 5.9751 & 0 & 0 \\ -1.9422 & 0 & 4.1018 & 0 & 0 & -1.2820 \\ +j 10.5107 & 0 & -j 16.1335 & 0 & 0 & +j 5.5882 \\ 0 & -1.1876 & 0 & 2.8047 & -1.6171 & 0 \\ 0 & +j 5.9751 & 0 & -j 35.4456 & +j 13.6980 & 0 \\ 0 & 0 & 0 & -1.6171 & 3.7412 & -1.1551 \\ 0 & 0 & 0 & +j 13.6980 & -j 23.6424 & +j 9.7843 \\ 0 & 0 & -1.2820 & 0 & -1.1551 & 2.4371 \\ 0 & 0 & +j 5.5882 & 0 & +j 9.7843 & -j 32.1539 \end{bmatrix}$$

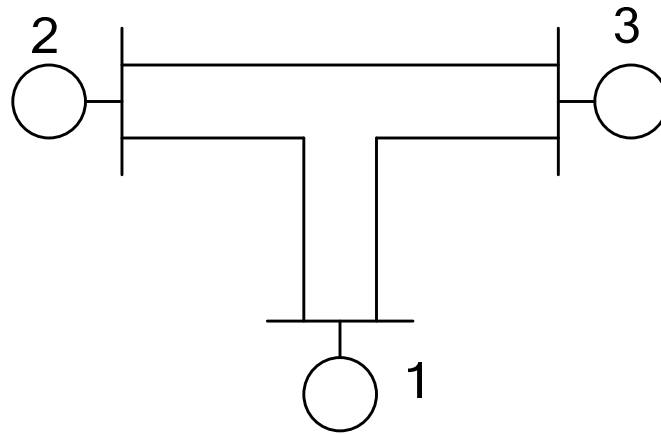


Figure 5.11: The reduced power system network

$$\bar{Y}_d = \begin{bmatrix} 0.8455 - j 2.9883 & 0.2871 + j 1.5129 & 0.2096 + j 1.2256 \\ 0.2871 + j 1.5129 & 0.4200 - j 2.7239 & 0.2133 + j 1.0879 \\ 0.2096 + j 1.2256 & 0.2133 + j 1.0879 & 0.2770 - j 2.3681 \end{bmatrix} \quad (5.80)$$

Each generator in the system has four state variables  $(\Delta\delta, \Delta\omega, \Delta E'_q, \Delta E_{fd})$ . The K-constants are computed and the state matrix is formed. In matrix notation, the differential equations describing the linearized power system is given in Equation (5.81). The numerical values are computed using the initial operating point values listed in Table 5.5.

The state matrix formed, using the values in Table 5.6, is given by Equation (5.82). The two matrices only differ with respect the first six columns. The

magnitudes of the computed values in these columns are same, however, the signs are different. This is due to the difference in the signs of the rotor angle differential equation and  $\delta_{dij}$  as explained in Section 5.3. The values in the other columns remain unchanged.

The dynamic properties of the power system are determined from the nature of the eigenvalues of the state matrix. Consequently the eigenvalues computed from either state matrix give same results. The eigenvalues are listed in Table 5.7. The power system consists of real and complex eigenvalues. The system is stable as all the eigenvalues have negative real part.

$$\begin{bmatrix} \Delta \dot{\delta}_1 \\ \Delta \dot{\delta}_2 \\ \Delta \dot{\delta}_3 \\ \Delta \dot{\omega}_1 \\ \Delta \dot{\omega}_2 \\ \Delta \dot{\omega}_3 \\ \Delta \dot{E}'_{q1} \\ \Delta \dot{E}'_{q2} \\ \Delta \dot{E}'_{q3} \\ \Delta \dot{E}_{fd1} \\ \Delta \dot{E}_{fd2} \\ \Delta \dot{E}_{fd3} \end{bmatrix} = \begin{bmatrix} 0 & 0 & 0 & 377 & 0 & 0 & 0 & 0 & 0 & 0 & 0 & 0 \\ 0 & 0 & 0 & 0 & 377 & 0 & 0 & 0 & 0 & 0 & 0 & 0 \\ 0 & 0 & 0 & 0 & 0 & 377 & 0 & 0 & 0 & 0 & 0 & 0 \\ -0.0501 & 0.0313 & 0.0187 & 0 & 0 & 0 & -0.0527 & 0.02 & 0.0125 & 0 & 0 & 0 \\ 0.1202 & -0.175 & 0.0548 & 0 & 0 & 0 & -0.0843 & -0.2426 & 0.0332 & 0 & 0 & 0 \\ 0.178 & 0.1396 & -0.3176 & 0 & 0 & 0 & -0.0651 & 0.1115 & -0.3926 & 0 & 0 & 0 \\ -0.0031 & 0 & 0.0031 & 0 & 0 & 0 & -0.1314 & 0.0119 & 0.0112 & 0.1116 & 0 & 0 \\ 0.2034 & -0.3174 & 0.114 & 0 & 0 & 0 & 0.0137 & -0.5219 & 0.1285 & 0 & 0.1667 & 0 \\ 0.221 & 0.176 & -0.3969 & 0 & 0 & 0 & 0.0718 & 0.214 & -0.6287 & 0 & 0 & 0.1698 \\ 3.8138 & 5.0469 & -8.8606 & 0 & 0 & 0 & -600.108 & 0.2529 & -0.7747 & -20 & 0 & 0 \\ 34.318 & -16.1255 & -18.1925 & 0 & 0 & 0 & -274.56 & -277.887 & -117.694 & 0 & -20 & 0 \\ 15.2726 & 10.4271 & -25.6997 & 0 & 0 & 0 & -99.6703 & -40.7536 & -85.1017 & 0 & 0 & -20 \end{bmatrix} \begin{bmatrix} \Delta \delta_1 \\ \Delta \delta_2 \\ \Delta \delta_3 \\ \Delta \omega_1 \\ \Delta \omega_2 \\ \Delta \omega_3 \\ \Delta E'_{q1} \\ \Delta E'_{q2} \\ \Delta E'_{q3} \\ \Delta E_{fd1} \\ \Delta E_{fd2} \\ \Delta E_{fd3} \end{bmatrix} \quad (5.81)$$

$$\begin{bmatrix} 0 & 0 & 0 & -377 & 0 & 0 & 0 & 0 & 0 & 0 & 0 & 0 \\ 0 & 0 & 0 & 0 & -377 & 0 & 0 & 0 & 0 & 0 & 0 & 0 \\ 0 & 0 & 0 & 0 & 0 & -377 & 0 & 0 & 0 & 0 & 0 & 0 \\ 0.0501 & -0.0313 & -0.0187 & 0 & 0 & 0 & -0.0527 & 0.02 & 0.0125 & 0 & 0 & 0 \\ -0.1202 & 0.175 & -0.0548 & 0 & 0 & 0 & -0.0843 & -0.2426 & 0.0332 & 0 & 0 & 0 \\ -0.178 & -0.1396 & 0.3176 & 0 & 0 & 0 & -0.0651 & 0.1115 & -0.3926 & 0 & 0 & 0 \\ 0.0031 & 0 & -0.0031 & 0 & 0 & 0 & -0.1314 & 0.0119 & 0.0112 & 0.1116 & 0 & 0 \\ -0.2034 & 0.3174 & -0.114 & 0 & 0 & 0 & 0.0137 & -0.5219 & 0.1285 & 0 & 0.1667 & 0 \\ -0.221 & -0.176 & 0.3969 & 0 & 0 & 0 & 0.0718 & 0.214 & -0.6287 & 0 & 0 & 0.1698 \\ -3.8138 & -5.0469 & 8.8606 & 0 & 0 & 0 & -600.108 & 0.2529 & -0.7747 & -20 & 0 & 0 \\ -34.318 & 16.1255 & 18.1925 & 0 & 0 & 0 & -274.56 & -277.887 & -117.694 & 0 & -20 & 0 \\ -15.2726 & -10.4271 & 25.6997 & 0 & 0 & 0 & -99.6703 & -40.7536 & -85.1017 & 0 & 0 & -20 \end{bmatrix} \quad (5.82)$$

Two zero eigenvalues are obtained due to the redundant state variables [2], [17]. The state matrix formed from the state equations uses absolute changes in machine

rotor angle and speed as state variables, and the system matrix does not contain an infinite bus thus, having no reference for the angles.

Due to the lack of uniqueness of the absolute rotor angle one of the zero eigenvalue is formed. The rotor angle redundancy can be eliminated by choosing one of the machines as a reference and expressing the other machine angles with respect to this reference. With such a formulation the order of the system will be reduced by one. The second zero eigenvalue is associated with zero damping.

The modes having low damping ratio contribute to the power system oscillations in the event of a disturbance. There are two pairs of complex conjugate eigenvalues having low damping ratio. The modes 4 and 5 have low damping ratio of 0.0289 (0.3384/11.7007) with frequency equal to 1.8622 (11.7007/2 $\pi$ ) Hz and similarly the modes 6 and 7 have a low damping ratio of 0.0376 with frequency of 1.3096 Hz. In order to determine which states contribute dominantly to the modes, the participation factors are computed.

Table 5.7: Eigenvalues of WSCC power system

No.	Eigenvalues	Damping Ratio	Frequency
1	-19.5077	1	0
2	-17.0406	1	0
3	-15.6814	1	0
4	-0.3384 + j11.7007	0.0289	1.8622
5	-0.3384 - j 11.7007	0.0289	1.8622
6	-0.3095 + j 8.2283	0.0376	1.3096
7	-0.3095 - j 8.2283	0.0376	1.3096
8	-4.4453	1	0
9	-2.8411	1	0
10	-0.4701	1	0
11	0	-	-
12	0	-	-

Participation factors determine which state variables significantly participate in a selected eigenvalue [2], [17]. The right eigenvectors account for the mode shape, as explained in Section 4.5. The left eigenvectors define the state variable associated exclusively with the mode. The right and left eigenvector are computed as explained in Section 4.5. The participation factors can be seen as right eigenvectors weighted by

left eigenvectors. The participation factor of the  $k^{th}$  state variable in the  $i^{th}$  mode is defined as:  $p_{ki} = \phi_{ki} \psi_{ik}$ ,  $i = 1, \dots, n$ ,  $k = 1, \dots, n$ , where,  $\phi_{ki}$  is the  $k^{th}$  entry of the right eigenvector  $\phi_i$  and  $\psi_{ik}$  is the  $k^{th}$  entry of the left eigenvector  $\psi_i$ .  $\phi_{ki}$  is the measure of the activity of  $k^{th}$  state variable in the  $i^{th}$  mode and  $\psi_{ik}$  weighs the contribution of this activity to the mode. In matrix form the participation matrix is:

$$P = [p_1 \quad p_2 \quad \dots \quad p_n] \quad (5.83)$$

with

$$p_i = \begin{bmatrix} p_{1i} \\ p_{2i} \\ \vdots \\ p_{ni} \end{bmatrix} = \begin{bmatrix} \phi_{1i} \psi_{i1} \\ \phi_{2i} \psi_{i2} \\ \vdots \\ \phi_{ni} \psi_{in} \end{bmatrix}$$

The product  $p_{ki}$  measures the net participation. The participation factor is a dimensionless quantity. The sum of the participation factors associated with any mode  $\sum_{i=1}^n p_{ki}$  or with any state variable  $\sum_{k=1}^n p_{ki}$  is equal to 1. The participation factors can be further normalized by making the largest of all the participation factor values equal to unity. Table 5.8 gives the normalized participation factors of all the eigenvalues and Table 5.9 gives the dominant states of the eigenvalues concluded from the participation factors. On observation of the participation factors in Table 5.8 and Table 5.9, it is noted that the machine 3 rotor angle and speed contribute more to modes 4 and 5, whereas, machine 2 rotor angle and speed contribute mainly to modes 6 and 7.

In this WSCC system, generator 1 is chosen as the slack bus or the reference bus. As such absolute rotor angle and rotor speed state variables of this machine contribute to the zero eigenvalues. This is also indicated while calculating the participation factors as given in Table 5.8. For example, the data given in columns 11 and 12 in Table 5.8 correspond to the eigenvalues 11 and 12 in Table 5.7. The state variables having highest participating factor in these modes are deducted from the respective rows having the value one. Similarly the first eigenvalue -19.5077 in Table 5.7

corresponds to the first column in Table 5.8. The highest normalized participation factor value given by one is in the last row which corresponds to the state variable  $E_{fd3}$ . As such this state variable contributes more to this eigenvalue.

Table 5.8: The normalized participation factors of all the eigenvalues

Eigenvalues												
States	1	2	3	4	5	6	7	8	9	10	11	12
$\delta_1$	0	0	0	0	0	0.4004	0.400	0	0	0	0	1
$\delta_2$	0	0	0	0.1868	0.1868	<b>1</b>	<b>1</b>	0	0	0	0	0.2979
$\delta_3$	0	0	0	<b>1</b>	<b>1</b>	0.1381	0.138	0	0	0	0	0.1548
$\omega_1$	0	0	0	0	0	0.4004	0.400	0	0	0	1	0
$\omega_2$	0	0	0	0.1868	0.1868	<b>1</b>	<b>1</b>	0	0	0	0.2979	0
$\omega_3$	0	0	0	<b>1</b>	<b>1</b>	0.1381	0.138	0	0	0	0.1548	0
$E'_{q1}$	0	0	0.277	0	0	0	0	1	0	0	0	0
$E'_{q2}$	0	0.178	0	0	0	0.1131	0.113	0	1	0.097	0	0
$E'_{q3}$	0	0	0	0.066	0.066	0	0	0	0.1082	1	0	0
$E_{fd1}$	0	0	1	0	0	0	0	0.2795	0	0	0	0
$E_{fd2}$	0.1052	1	0	0	0	0	0	0	0.1564	0	0	0
$E_{fd3}$	1	0.109	0	0	0	0	0	0	0	0	0	0

To increase the damping of these modes, two PSS's are placed at machine 2 and 3 thus, providing a supplementary damping in the excitation of the generators in phase with the rotor speed. The PSS parameters are designed using phase compensation method as explained in Chapter 4, to increase the damping ratio of the concerned modes to 0.1. PSS at machine 2 is designed to increase the damping ratio of the modes 6 and 7, and PSS at machine 3 is designed for increasing the damping ratio of modes 4 and 5. The parameters of the two PSS are given in Table 5.10. The eigenvalues computed when the PSS is included is shown in Table 5.11. Since each PSS contributes three states, the order of system has increased from 12 to 18 when the two PSS's are included in the power system. The damping ratios of the concerned modes have been increased as shown with the PSS's placement in the system. The eigenvalue analysis has been performed on the system with and without the PSS. It is seen that the PSS improves the damping of the concerned modes.

Table 5.9: Dominant states of the eigenvalues

No.	Eigenvalues	Dominant states
1	-19.5077	$E_{fd3}$
2	-17.0406	$E_{fd2}$
3	-15.6814	$E_{fd1}$
4	-0.3384 + j 11.7007	$\omega_3$
5	-0.3384 - j 11.7007	$\delta_3$
6	-0.3095 + j 8.2283	$\omega_2$
7	-0.3095 - j 8.2283	$\delta_2$
8	-4.4453	$E'_{q1}$
9	-2.8411	$E'_{q2}$
10	-0.4701	$E'_{q3}$
11	0	$\omega_1$
12	0	$\delta_1$

Table 5.10: Parameters of the PSS's

	Gain	$T_1$	$T_2$	$T_3$	$T_4$
Machine 2	1.8807	0.3002	0.0492	0.3002	0.0492
Machine 3	3.5843	0.3001	0.0243	0.3001	0.0243

Table 5.11: Eigenvalues of the power system with PSS's

No.	Eigenvalues	Damping Ratio	Frequency	Dominant states
1	-54.6188	1	0	
2	-26.8409	1	0	
3&4	-21.9227 ± j 10.6709	0.8991	1.6983	
5&6	-15.7227 ± j 5.8101	0.938	0.9247	
7	-15.6981	1	0	
8&9	-1.3138 ± j 11.1949	0.1166	1.7817	$\delta_3, \omega_3$
10&11	-0.6606 ± j 8.4186	0.0782	1.3399	$\delta_2, \omega_2$
12	-4.4484	1	0	
13	-2.6394	1	0	
14&15	-0.4258 ± j 0.2684	0.8459	0.0427	
16	-0.1	1	0	
17	0	-	-	
18	0	-	-	

To evaluate the performance of the closed loop system with the designed PSS, nonlinear simulations are conducted. The nonlinear simulation is conducted in the following procedures.

Step 1) Initially the load flow is performed using the generated powers, load powers, and transmission network data, to obtain the steady state operating point.

Step 2) The initial conditions of the dynamic states are computed from the operating point and the machine data.

Step 3) Using the initial conditions the nonlinear dynamic equations of the power system are simulated.

The multi-machine power system is simulated using the nonlinear differential and algebraic equations of the power system of Equations (5.1-5.4) and Equation (5.23) or (5.50). The simulations have been carried out by numerical integration and as well as by MATLAB/SIMULINK. The numerical integration of the differential equations is performed using ode45 functions in Matlab. The program is written in M-file. The MATLAB/SIMULINK block diagram is given in the Appendix C. Both simulations approaches give same results. Under steady state, when no disturbance is present in the system, the responses of relative angles and speeds are given in Figure 5.12. Since the power system has no infinite bus, and, as such no reference, the responses are given relative to each other, and in this study it is with respect to machine 1.

In Figure 5.12,  $\delta_{12} = \delta_1 - \delta_2$ , is the relative angle between machine 1 and 2. Similarly the other parameters,  $\delta_{13}$ ,  $\omega_{12}$ , and  $\omega_{13}$  are defined. Now the disturbance is initiated in the form of three phase fault near bus 7 at the end of line 5-7, of the power system in Figure 5.10. The three phase fault is applied at 0.1s and cleared after 0.1s. During fault, since  $V_7 \equiv 0$ , the rows and columns of the admittance matrix of the prefault system Equation (5.78) corresponding to bus 7 will be deleted [16], [17] and is given by Equation (5.84). Then the load buses are eliminated and the formulated reduced matrix is given by Equation (5.85). The power system network during fault can be visualized as in Figure 5.13 and the reduced system network during fault

containing only the generator buses, in Figure 5.14. These figures are devised from the admittance matrices.

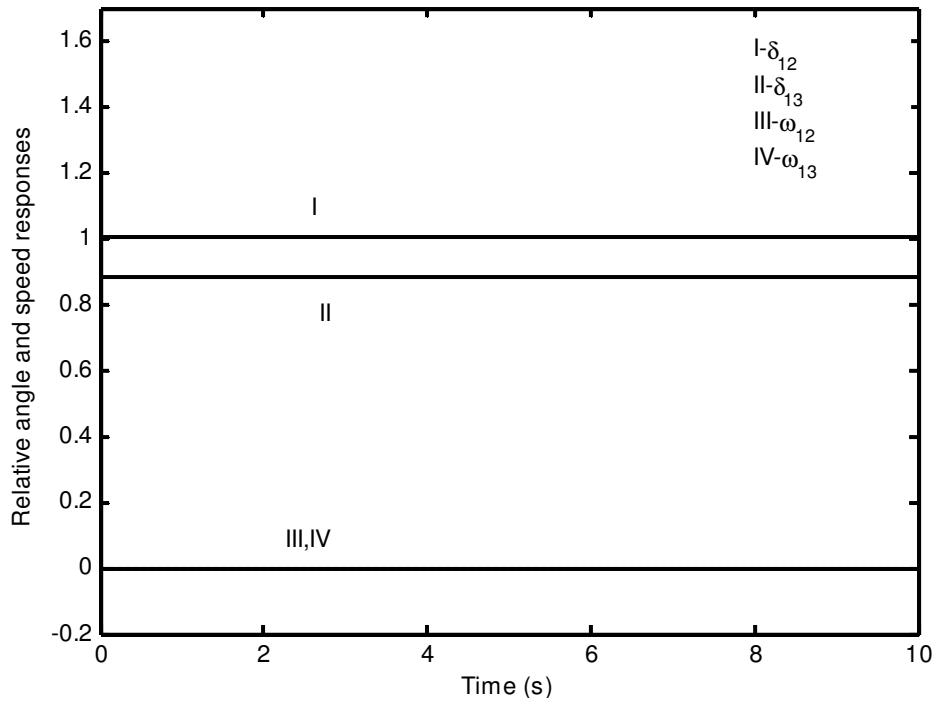


Figure 5.12: Responses of relative angle and speed during steady state operation

$$\bar{Y} = \begin{bmatrix} -j 17.3611 & 0 & 0 & j 17.3611 & 0 & 0 & 0 & 0 \\ 0 & -j 16.0 & 0 & 0 & 0 & 0 & 0 & 0 \\ 0 & 0 & -j 17.0648 & 0 & 0 & 0 & 0 & j 17.0648 \\ j 17.3611 & 0 & 0 & 3.3074 & -1.3652 & -1.9422 & 0 & 0 \\ 0 & 0 & 0 & -j 39.3089 & +j 11.6041 & +j 10.5107 & 0 & 0 \\ 0 & 0 & 0 & -1.3652 & 3.8138 & 0 & 0 & 0 \\ 0 & 0 & 0 & +j 11.6041 & -j 17.8426 & 0 & 0 & 0 \\ 0 & 0 & 0 & -1.9422 & 0 & 4.1018 & 0 & -1.282 \\ 0 & 0 & 0 & +j 10.5107 & 0 & -j 16.1335 & 0 & +j 5.588 \\ 0 & 0 & 0 & 0 & 0 & 0 & 3.7412 & -1.155 \\ 0 & 0 & 0 & 0 & 0 & 0 & -j 23.6424 & +j 9.784 \\ 0 & 0 & j 17.0648 & 0 & 0 & -1.2820 & -1.1551 & 2.437 \\ 0 & 0 & 0 & 0 & 0 & +j 5.5882 & +j 9.7843 & -j 32.154 \end{bmatrix} \quad (5.84)$$

$$Y_{d,duringfault} = \begin{bmatrix} 0.6568 - j 3.8160 & 0 & 0.0701 + j 0.6306 \\ 0 & -j 5.4855 & 0 \\ 0.0701 + j 0.6306 & 0 & 0.1740 - j 2.7959 \end{bmatrix} \quad (5.85)$$

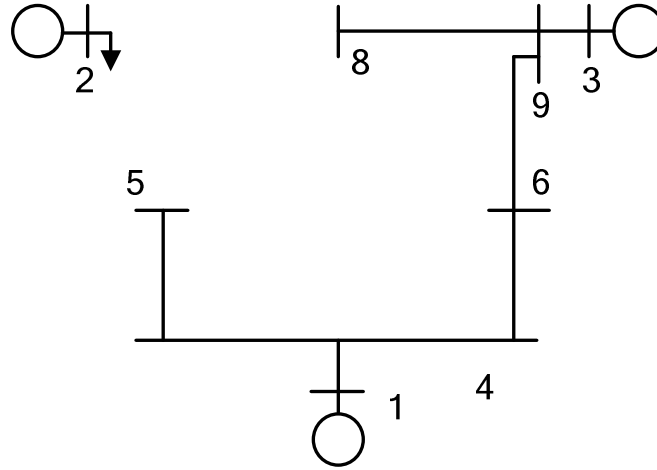


Figure 5.13: The power system network during fault condition.

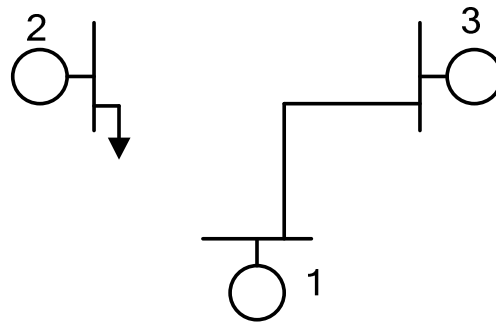


Figure 5.14: The reduced power system network during fault condition

After the fault is cleared, the faulted line is either switched back to service (i.e., the original prefault system is restored) or opened (i.e., postfault system with line 5-7 removed from the network), depending on which the admittance matrix is modified. If the line is removed for the postfault system as shown in Figure 5.15, then the admittance matrix of the network is again computed with the line 5-7 removed and then the reduced admittance matrix is calculated and is given by Equation (5.86). The reduced postfault system network will appear to be similar to Figure 5.11.

$$Y_{d,afterfault} = \begin{bmatrix} 1.1386 - j 2.2966 & 0.1290 + j 0.7063 & 0.1824 + j 1.0637 \\ 0.1290 + j 0.7063 & 0.3744 - j 2.0151 & 0.1921 + j 1.2067 \\ 0.1824 + j 1.0637 & 0.1921 + j 1.2067 & 0.2691 - j 2.3516 \end{bmatrix} \quad (5.86)$$

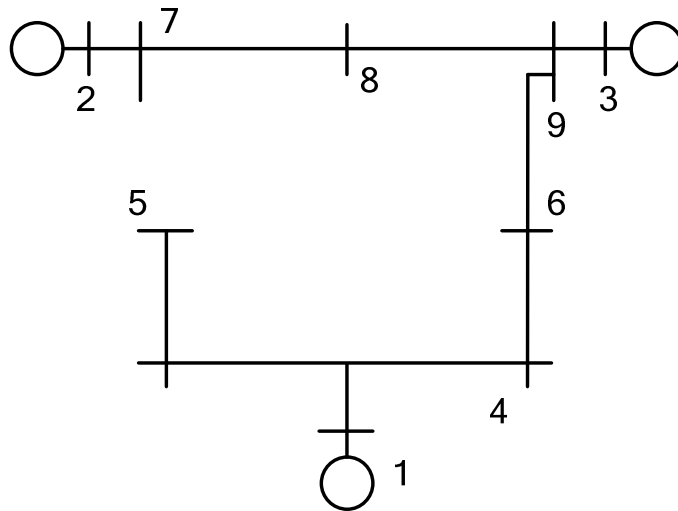


Figure 5.15: The power system network after fault clearance with transmission line 5-7 removed.

The responses for  $\delta_{12}$ ,  $\delta_{13}$ , power generated by the generators,  $\omega_{12}$ , and  $\omega_{13}$  are shown in the following Figures 5.16-5.20, respectively for three-phase fault. The damping control effort provided by the PSS signal is shown clearly in the figures in terms of the overshoot and settling time. The results validate the eigenvalue analysis.

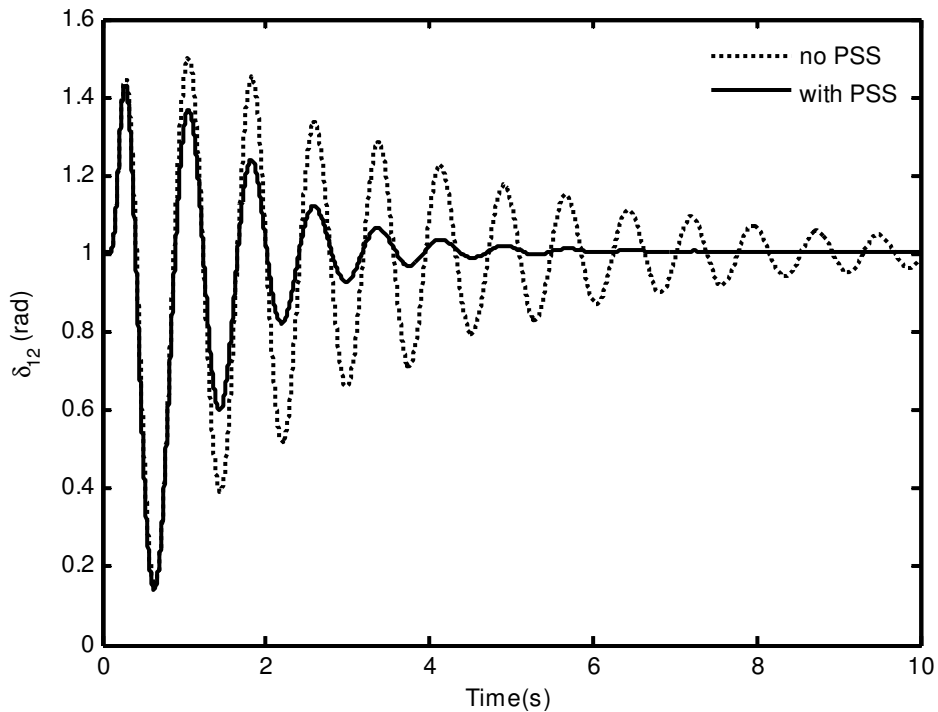


Figure 5.16: Relative angle  $\delta_{12}$  response with and without PSSs

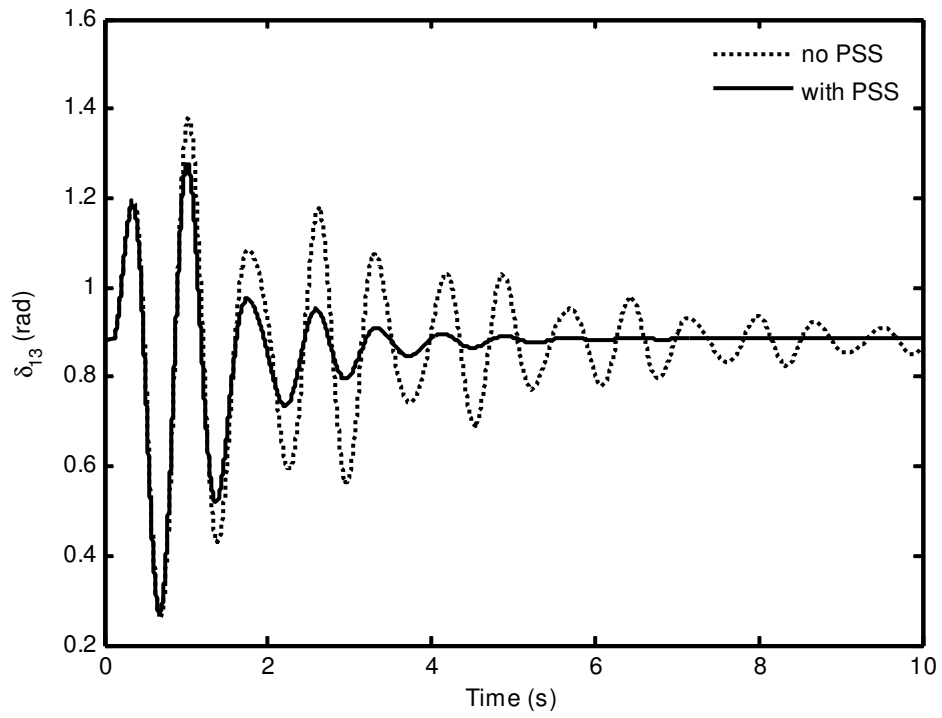


Figure 5.17: Relative angle  $\delta_{13}$  response with and without PSSs

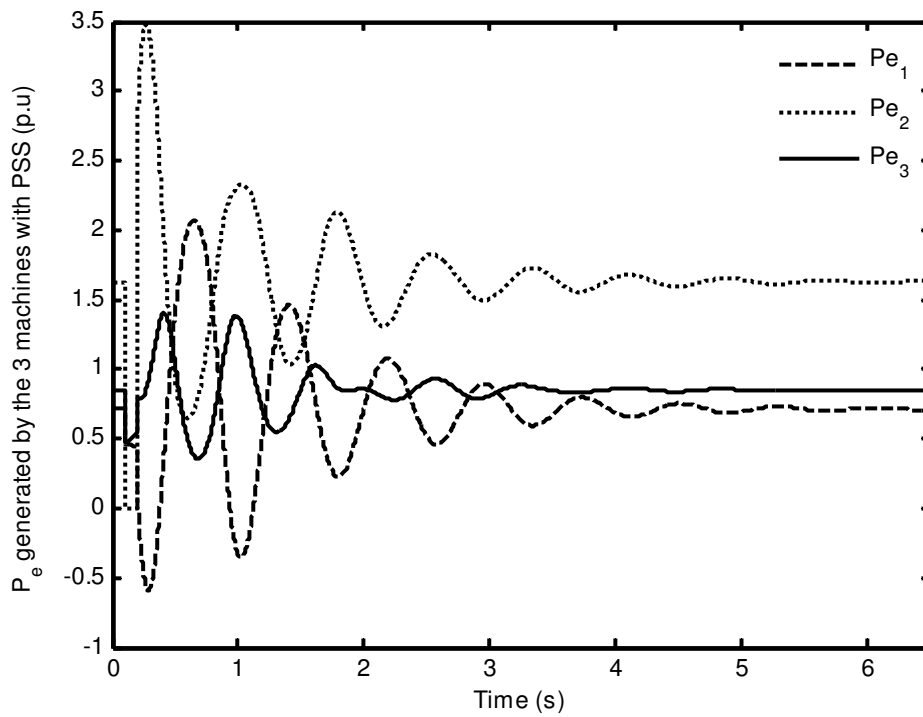


Figure 5.18: Generated power response of each machine with PSSs

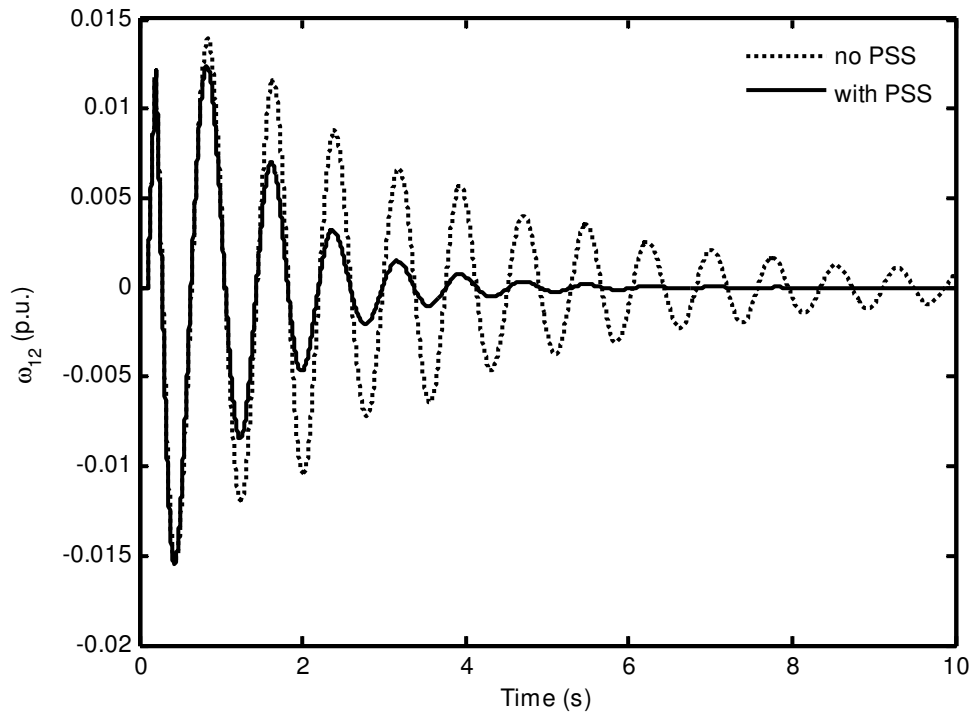


Figure 5.19: Relative angle  $\omega_{12}$  response with and without PSSs

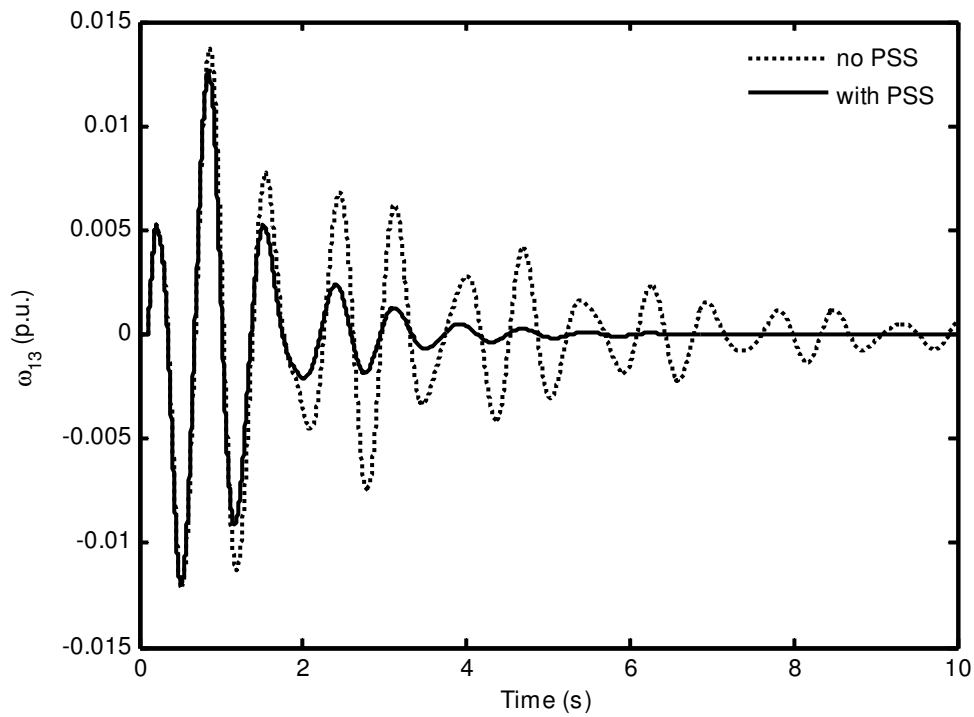


Figure 5.20: Relative angle  $\omega_{13}$  response with and without PSSs

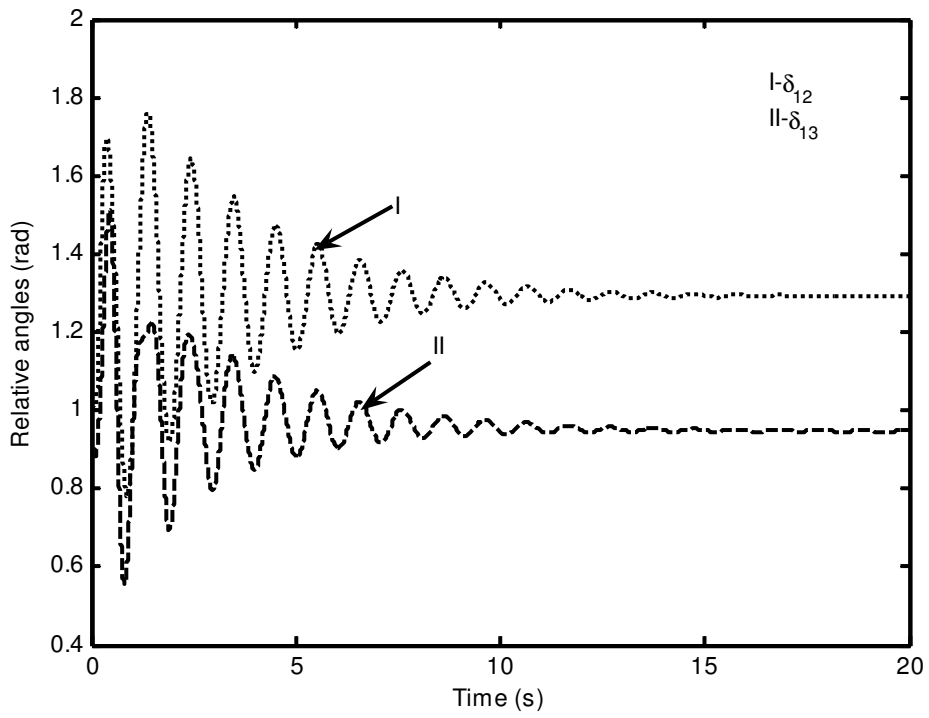


Figure 5.21: Responses of relative angles when three phase fault occurs and line is opened after the clearance of fault

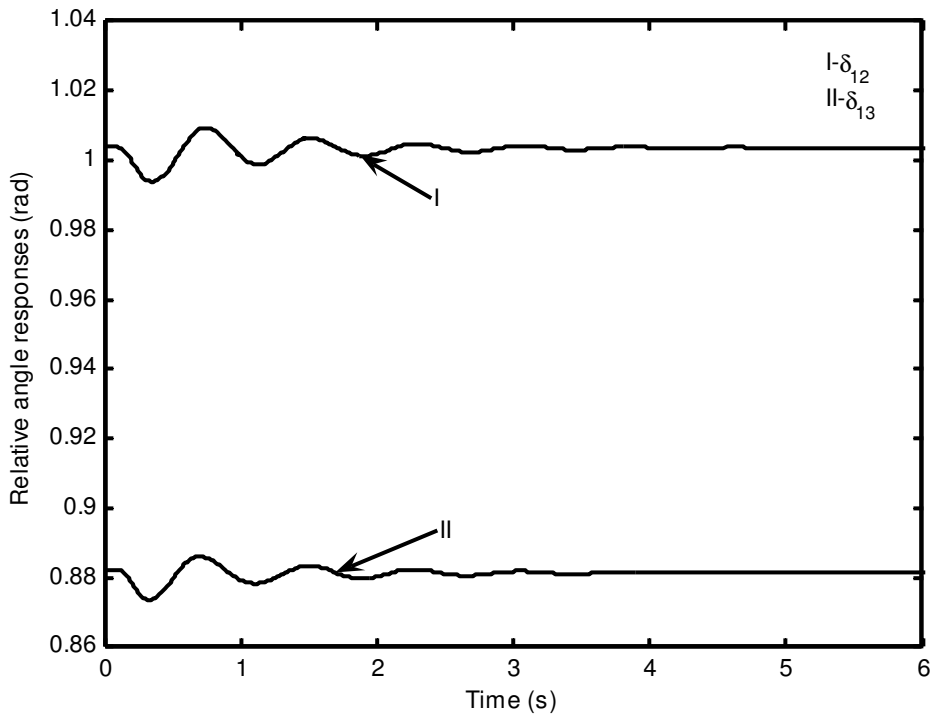


Figure 5.22: Responses of relative angles with change in mechanical input at machine 1

Figures 5.16-5.20 show the responses when a three phase fault occurs at bus 7, and the prefault system is restored after fault clearance. Figure 5.21 shows the  $\delta_{12}$  and  $\delta_{13}$  response when the line 5-7 is opened after fault clearance, in the presence of PSSs. The settling time increases when the postfault system involves the opening of the line compared the responses in Figures 5.16-5.17, when the prefault system is restored.

Figure 5.22 shows the rotor angle responses when the disturbance is in the form of change in mechanical input at machine 1. A step change of 10% is given at mechanical input  $P_{m1}$  for a period of 0.1s. The settling time of the oscillations is less comparatively.

Figure 5.23 gives the responses due to line switching between bus 8 and bus 9 with PSSs. The response of terminal voltages of the three machines due to line switching is given in Figure 5.24. The observation of the responses of the multi-machine power system indicates that the PSS provides sufficient damping to the oscillations.

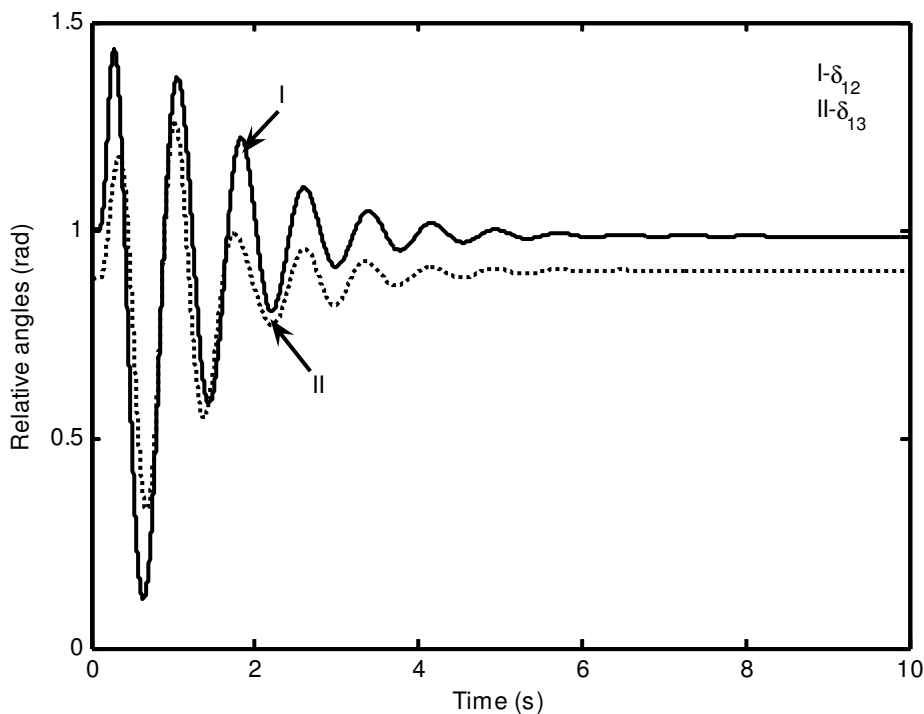


Figure 5.23: Responses of relative angles due to line switching in line 8-9

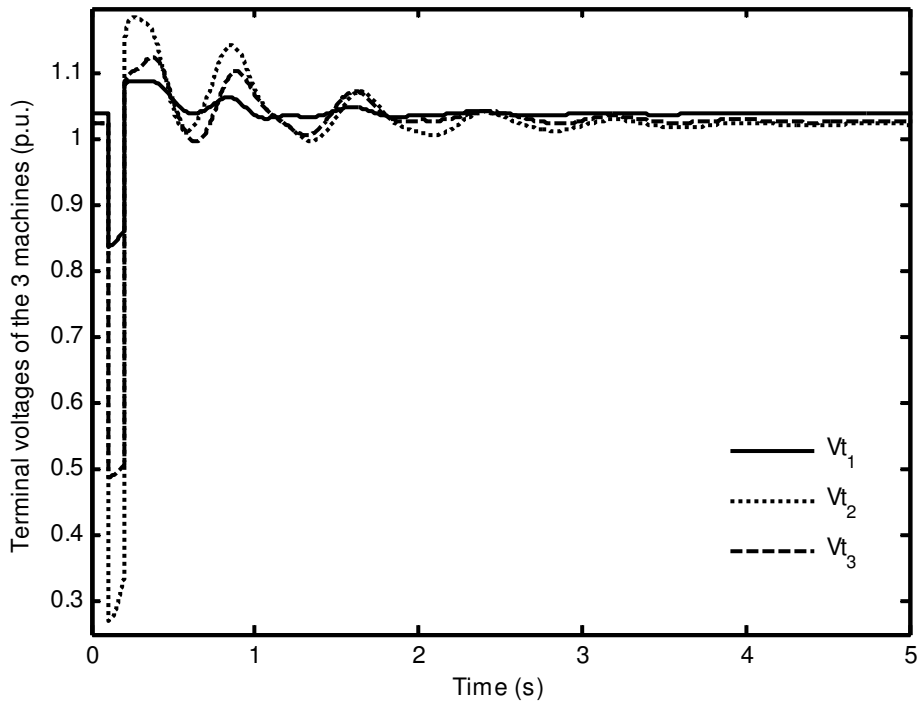


Figure 5.24: Responses of terminal voltages due to line switching in line 8-9

## 5.5 Summary

In this chapter, the multi-machine power system modeling is presented. The third-order synchronous generator model has been used along with the excitation system model for the multi-machine system. Models of load and power balance equations in the network are introduced. The transformation of the network into individual machine reference frame has been discussed.

The linearized Phillips-Heffron model of multi-machine power system is presented. A case study of multi-machine power system is taken to investigate the power system stability. Eigenvalue analysis and nonlinear simulations are carried out to evaluate the effectiveness of the PSS control in enhancing the damping of the oscillatory modes. The following chapter presents the mathematical modeling of multi-machine power system with IPFC.



## CHAPTER 6

### MULTIMACHINE POWER SYSTEM WITH IPFC

#### 6.1 Introduction

Large power systems typically exhibit swing modes which are associated with the dynamics of power transfers and involve groups of machines oscillating relative to each other due to inadequate system damping. Traditionally, PSS's have been designed individually for each generator that is likely to be affected by these oscillations to dampen the oscillations. However, due to the complexity of present day power systems, it experiences multiple modes of oscillations with different frequencies; therefore, the design of an effective PSS has become extremely difficult. In this interest, FACTS devices were installed in the system to improve the transmission capability and additionally utilized for damping of power system swing oscillations.

IPFC based damping controller design requires adequate mathematical representation of power system including the FACTS device for power system stability studies. In this chapter, the dynamic models, both nonlinear and linearized, for multi-machine system installed with IPFC are presented. The effectiveness of the IPFC based controllers, in controlling the power flow and in damping power system oscillations is shown by case studies.

#### 6.2 Modeling of Multi-Machine Power System Incorporating with IPFC

In general, it is assumed that in an  $n$ -machine power system, an IPFC is installed on the branches  $i - j$  and  $i - k$ , as shown in Figure 6.1. Figure 6.2 gives the equivalent model of IPFC in the  $n$ -machine power system.

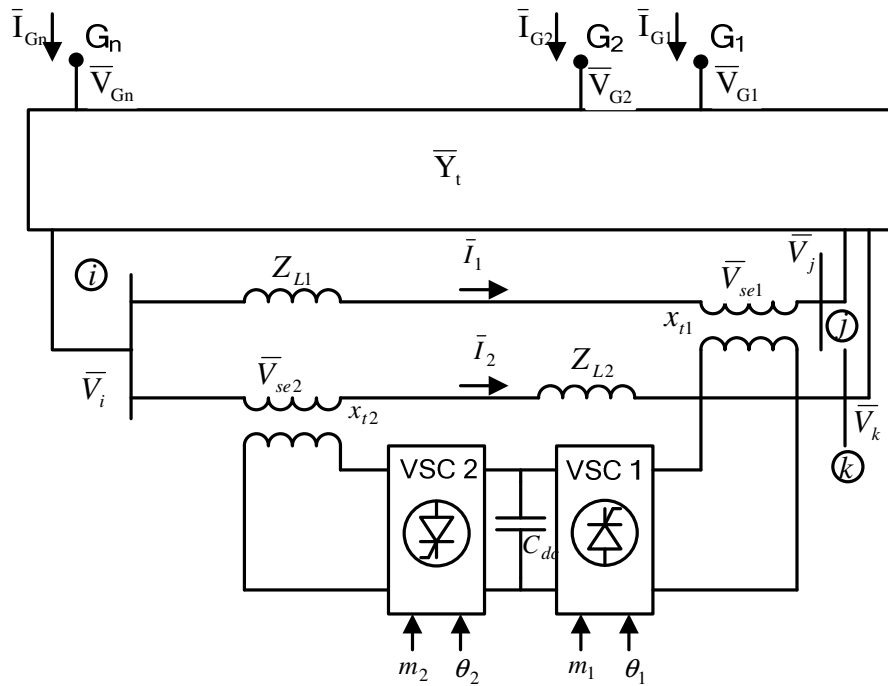


Figure 6.1: A  $n$ -machine power system installed with IPFC

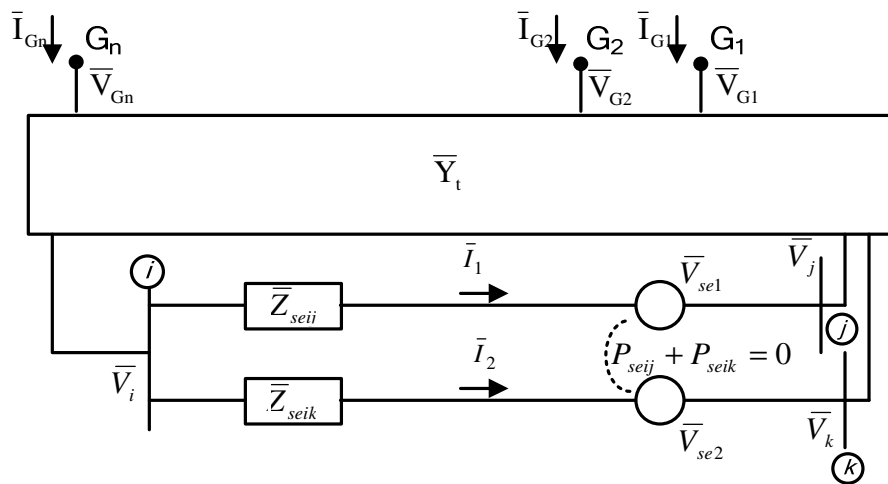


Figure 6.2: Equivalent model of IPFC installed in  $n$ -machine power system

The network admittance  $\bar{Y}_t$  is formed before the IPFC has been installed, keeping  $n$  generator nodes along with the nodes  $i$ ,  $j$ ,  $k$ .

The network equations are given by:

$$\begin{bmatrix} 0 \\ 0 \\ 0 \\ \bar{I}_G \end{bmatrix} = \begin{bmatrix} \bar{Y}_{ii} & \bar{Y}_{ij} & \bar{Y}_{ik} & \bar{Y}_{iG} \\ \bar{Y}_{ji} & \bar{Y}_{jj} & \bar{Y}_{jk} & \bar{Y}_{jG} \\ \bar{Y}_{ki} & \bar{Y}_{kj} & \bar{Y}_{kk} & \bar{Y}_{kG} \\ \bar{Y}_{Gi} & \bar{Y}_{Gj} & \bar{Y}_{Gk} & \bar{Y}_{GG} \end{bmatrix} \begin{bmatrix} \bar{V}_i \\ \bar{V}_j \\ \bar{V}_k \\ \bar{V}_G \end{bmatrix} \quad (6.1)$$

where  $\bar{I}_G = [\bar{I}_{G1} \ \bar{I}_{G2} \ \dots \ \bar{I}_{Gn}]^T$ ,  $\bar{V}_G = [\bar{V}_{G1} \ \bar{V}_{G2} \ \dots \ \bar{V}_{Gn}]^T$ . The dimensions of the vectors  $\bar{Y}_{iG}, \bar{Y}_{jG}, \bar{Y}_{kG}$  are  $1 \times n$  and those of the vectors  $\bar{Y}_{Gi}, \bar{Y}_{Gj}, \bar{Y}_{Gk}$  are  $n \times 1$ , respectively, and  $\bar{Y}_{GG}$  is an  $n \times n$  matrix. With the installation of IPFC between the branches  $i - j$  and  $i - k$ , the network equations are modified as follows:

$$\bar{Y}'_{ii} \bar{V}_i + \bar{I}_1 + \bar{I}_2 + \bar{Y}_{iG} \bar{V}_G = 0 \quad (6.2)$$

$$\bar{Y}'_{jj} \bar{V}_j - \bar{I}_1 + \bar{Y}'_{jk} \bar{V}_k + \bar{Y}_{jG} \bar{V}_G = 0 \quad (6.3)$$

$$\bar{Y}'_{kj} \bar{V}_j + \bar{Y}'_{kk} \bar{V}_k - \bar{I}_2 + \bar{Y}_{kG} \bar{V}_G = 0 \quad (6.4)$$

$$\bar{Y}_{Gi} \bar{V}_i + \bar{Y}_{Gj} \bar{V}_j + \bar{Y}_{Gk} \bar{V}_k + \bar{Y}_{GG} \bar{V}_G = \bar{I}_G \quad (6.5)$$

where  $\bar{Y}'_{ii} = \bar{Y}_{ii} - y_{ij} - y_{ik}$ ,  $\bar{Y}'_{jj} = \bar{Y}_{jj} - y_{ji}$  and  $\bar{Y}'_{kk} = \bar{Y}_{kk} - y_{ki}$

From Figure 6.2, the current in the IPFC branches can be written as:

$$\bar{I}_1 = (\bar{V}_i - \bar{V}_{se1} - \bar{V}_j) / \bar{Z}_{seij} \quad (6.6)$$

$$\bar{I}_2 = (\bar{V}_i - \bar{V}_{se2} - \bar{V}_k) / \bar{Z}_{seik} \quad (6.7)$$

The Equation (6.6) in  $d - q$  axis can be written as follows:

$$\begin{aligned} \bar{I}_1 &= (\bar{V}_i - \bar{V}_{se1} - \bar{V}_j) \bar{Y}_{seij} \\ \Rightarrow \\ i_{1d} + j i_{1q} &= (\bar{V}_i - \bar{V}_{se1} - \bar{V}_j) (g_{ij} + j b_{ij}) = (g_{ij} + j b_{ij}) \left[ V_i e^{j\theta_i} - \frac{m_1 v_{dc}}{2} e^{j\theta_1} - V_j e^{j\theta_j} \right] \end{aligned}$$

$$\begin{aligned} \bar{I}_1 = (g_{ij} + j b_{ij})[V_i(\cos \theta_i + j \sin \theta_i) - \frac{m_1 v_{dc}}{2}(\cos \theta_1 + j \sin \theta_1) \\ - V_j(\cos \theta_j + j \sin \theta_j)] \end{aligned} \quad (6.8)$$

Similarly transforming Equation (6.7) and separating the real and imaginary parts:

$$i_{1d} = g_{ij} \left( V_i \cos \theta_i - \frac{m_1 v_{dc}}{2} \cos \theta_1 - V_j \cos \theta_j \right) + b_{ij} \left( -V_i \sin \theta_i + \frac{m_1 v_{dc}}{2} \sin \theta_1 + V_j \sin \theta_j \right) \quad (6.9)$$

$$i_{1q} = g_{ij} \left( V_i \sin \theta_i - \frac{m_1 v_{dc}}{2} \sin \theta_1 - V_j \sin \theta_j \right) + b_{ij} \left( V_i \cos \theta_i - \frac{m_1 v_{dc}}{2} \cos \theta_1 - V_j \cos \theta_j \right) \quad (6.10)$$

$$i_{2d} = g_{ik} \left( V_i \cos \theta_i - \frac{m_2 v_{dc}}{2} \cos \theta_2 - V_k \cos \theta_k \right) + b_{ik} \left( -V_i \sin \theta_i + \frac{m_2 v_{dc}}{2} \sin \theta_2 + V_k \sin \theta_k \right) \quad (6.11)$$

$$i_{2q} = g_{ik} \left( V_i \sin \theta_i - \frac{m_2 v_{dc}}{2} \sin \theta_2 - V_k \sin \theta_k \right) + b_{ik} \left( V_i \cos \theta_i - \frac{m_2 v_{dc}}{2} \cos \theta_2 - V_k \cos \theta_k \right) \quad (6.12)$$

Substituting the expressions of Equations (6.6) and (6.7), into Equations (6.2-6.4) the IPFC bus voltages  $\bar{V}_i, \bar{V}_j, \bar{V}_k$ , can be written in matrix form as follows:

$$\begin{bmatrix} \bar{V}_i \\ \bar{V}_j \\ \bar{V}_k \end{bmatrix} = -\bar{Y}_t^{-1} \begin{bmatrix} -\frac{1}{Z_{seij}} & -\frac{1}{Z_{seik}} \\ \frac{1}{Z_{seij}} & 0 \\ 0 & \frac{1}{Z_{seik}} \end{bmatrix} \begin{bmatrix} \bar{V}_{se1} \\ \bar{V}_{se2} \end{bmatrix} + \begin{bmatrix} \bar{Y}_{iG} \\ \bar{Y}_{jG} \\ \bar{Y}_{kG} \end{bmatrix} \bar{V}_G \quad (6.13)$$

$$\text{where, } \bar{Y}_t = \begin{bmatrix} \bar{Y}'_{ii} + \frac{1}{Z_{seij}} + \frac{1}{Z_{seik}} & -\frac{1}{Z_{seij}} & -\frac{1}{Z_{seik}} \\ -\frac{1}{Z_{seij}} & \bar{Y}'_{22} + \frac{1}{Z_{seij}} & \bar{Y}_{jk} \\ -\frac{1}{Z_{seik}} & \bar{Y}_{jk} & \bar{Y}'_{33} + \frac{1}{Z_{seik}} \end{bmatrix}$$

Substituting the voltages  $\bar{V}_i, \bar{V}_j, \bar{V}_k$ , from Equation (6.13) into Equation (6.5) and eliminating them the generator currents can be written as follows:

$$\bar{I}_G = \bar{Y}_G \bar{V}_G + \bar{Y}_{se1} \bar{V}_{se1} + \bar{Y}_{se2} \bar{V}_{se2} \quad (6.14)$$

where

$$\bar{Y}_G = \bar{Y}_{GG} - [\bar{Y}_{Gi} \quad \bar{Y}_{Gj} \quad \bar{Y}_{Gk}] \bar{Y}_t^{-1} \begin{bmatrix} \bar{Y}_{iG} \\ \bar{Y}_{jG} \\ \bar{Y}_{kG} \end{bmatrix} \quad (6.15)$$

$$\bar{Y}_{se1} = -[\bar{Y}_{Gi} \quad \bar{Y}_{Gj} \quad \bar{Y}_{Gk}] \bar{Y}_t^{-1} \begin{bmatrix} 1/\bar{Z}_{seij} \\ -1/\bar{Z}_{seij} \\ 0 \end{bmatrix} \quad (6.16)$$

$$\bar{Y}_{se2} = -[\bar{Y}_{Gi} \quad \bar{Y}_{Gj} \quad \bar{Y}_{Gk}] \bar{Y}_t^{-1} \begin{bmatrix} 1/\bar{Z}_{seik} \\ 0 \\ -1/\bar{Z}_{seik} \end{bmatrix} \quad (6.17)$$

The Equations (6.14-6.17) represent the generator currents in terms of the network parameters, terminal voltages and IPFC parameters on common reference frame. Considering the machine dynamics, the nonlinear model of the complete multi-machine power system with IPFC is developed.

### 6.3 Nonlinear Model of Multi-Machine Power System Installed with IPFC

The  $i^{th}$  machine dynamics in  $n$  machine power system is given as:

$$\dot{\delta}_i = \omega_0(\omega_i - 1) \quad (6.18)$$

$$\dot{\omega}_i = \frac{(P_{mi} - P_{ei} - P_{Di})}{M_i} \quad (6.19)$$

$$\dot{E}'_{qi} = \frac{1}{T_{doi}} (E_{fdi} - E'_{qi} - (x_{di} - x'_{di}) I_{di}) \quad (6.20)$$

$$\dot{E}_{fdi} = \frac{1}{T_{Ai}} \left( -E_{fdi} + K_{Ai} (V_{refi} - V_{ti}) \right) \quad (6.21)$$

where,

$$P_{ei} = I_{di} V_{tdi} + I_{qi} V_{tqi} \quad (6.22)$$

$$I_i = I_{di} + j I_{qi}, V_{ti} = V_{tdi} + j V_{tqi}, P_{Di} = D(\omega_i - 1), \quad (6.23)$$

$$V_{tdi} = x_{qi} I_{qi}; V_{tqi} = E'_{qi} - x'_{di} I_{di} \quad (6.24)$$

where,  $i = 1, 2, \dots, n$ ,  $n$  is the number of generators

The dynamics of the IPFC is described by Equations (6.25-6.27) which has been derived in Section 3.3.

The injected voltages are given by:

$$\bar{V}_{se1} = V_{se1} e^{j\theta_1} = \frac{1}{2} v_{dc} m_1 (\cos \theta_1 + j \sin \theta_1) \quad (6.25)$$

$$\bar{V}_{se2} = V_{se2} e^{j\theta_2} = \frac{1}{2} v_{dc} m_2 (\cos \theta_2 + j \sin \theta_2) \quad (6.26)$$

The DC capacitor voltage is given by:

$$\dot{v}_{dc} = \frac{3m_1}{4C_{dc}} (i_{1d} \cos \theta_1 + i_{1q} \sin \theta_1) + \frac{3m_2}{4C_{dc}} (i_{2d} \cos \theta_2 + i_{2q} \sin \theta_2) \quad (6.27)$$

The network equation described by Equation (6.14) which is on the  $D - Q$  axis frame is transformed into the individual machine reference frame  $d_i - q_i$  axis frame using the second type of transformation as explained in Section 5.2.5. Consequently the terminal voltages of the generators for the  $n$  machine power system in common axis frame or  $D - Q$  axis frame is described by Equation (5.44), which is again given in Equation (6.28).

$$\bar{V}_G = e^{j(\pi/2 - \delta)} E'_q - j x'_d \bar{I}_G + (x_q - x'_d) e^{-j\delta} I_q \quad (6.28)$$

Consequently the rotor angle Equation (6.18) is modified as explained in Section 5.2.5 and is given by:

$$\dot{\delta}_i = -\omega_0(\omega_i - 1) \quad (6.29)$$

Substituting Equation (6.28) in Equation (6.14),

$$\bar{I}_G = \bar{Y}'_d [e^{j(\pi/2-\delta)} E'_q + (x_q - x'_d) e^{-j\delta} I_q + \bar{Y}_A \bar{V}_{se1} + \bar{Y}_B \bar{V}_{se2}] \quad (6.30)$$

where,

$$\bar{Y}'_d = [\bar{Y}_G^{-1} + jx'_d]^{-1}, \quad \bar{Y}_A = \bar{Y}_G^{-1} \bar{Y}_{se1}, \quad \bar{Y}_B = \bar{Y}_G^{-1} \bar{Y}_{se2} \quad (6.31)$$

$\bar{Y}'_d$  is an  $n \times n$  dimension matrix,  $\bar{Y}_A$  and  $\bar{Y}_B$  are vectors of size  $n \times 1$ .

In d-q axis form the generator currents Equation (6.30) can be expressed as:

$$I = e^{j\delta} \bar{I}_G = e^{j\delta} \bar{Y}'_d [e^{j(\pi/2-\delta)} E'_q + (x_q - x'_d) e^{-j\delta} I_q + \bar{Y}_A \bar{V}_{se1} + \bar{Y}_B \bar{V}_{se2}] \quad (6.32)$$

$$\begin{aligned} I_i &= I_{di} + j I_{qi} = \bar{I}_{Gi} e^{j\delta_i} \\ &= \sum_{j=1}^n \bar{Y}'_{dij} [E'_{qj} e^{j(\pi/2+\delta_i-\delta_j)} + (x_{qj} - x'_{dj}) e^{j(\delta_i-\delta_j)} + \bar{Y}_{Aj} \bar{V}_{se1} e^{j(\delta_i)} + \bar{Y}_{Bj} \bar{V}_{se2} e^{j(\delta_i)}] \end{aligned} \quad (6.33)$$

Denoting

$$\bar{Y}'_{dij} = Y'_{dij} e^{j(\beta_{dij})} \quad (6.34)$$

$$\bar{Y}_{Aj} = Y_{Aj} e^{j(\beta_{Aj})}, \quad \bar{Y}_{Bj} = Y_{Bj} e^{j(\beta_{Bj})} \quad (6.35)$$

$$\delta_{dij} = \delta_i - \delta_j + \beta_{dij} \quad (6.36)$$

$$\delta_{Aij} = \delta_i + \beta_{dij} + \beta_{Aj} + \theta_1 \quad (6.37)$$

$$\delta_{Bij} = \delta_i + \beta_{dij} + \beta_{Bj} + \theta_2 \quad (6.38)$$

Separating the real and imaginary parts of Equation (6.33) the direct and quadrature components of the generator currents are obtained as follows:

$$I_{di} = \text{real}(I_i), \quad I_{qi} = \text{imag}(I_i)$$

$$I_{di} = \sum_{j=1}^n Y'_{dij} \left[ -E'_{qj} \sin \delta_{dij} + (x_{qj} - x'_{dj}) \cos \delta_{dij} I_{qj} + Y_{Aj} V_{se1} \cos \delta_{Aij} + Y_{Bj} V_{se2} \cos \delta_{Bij} \right] \quad (6.39)$$

$$I_{qi} = \sum_{j=1}^n Y'_{dij} \left[ E'_{qj} \cos \delta_{dij} + (x_{qj} - x'_{dj}) \sin \delta_{dij} I_{qj} + Y_{Aj} V_{se1} \sin \delta_{Aij} + Y_{Bj} V_{se2} \sin \delta_{Bij} \right] \quad (6.40)$$

Equations (6.18-6.27) and Equations (6.39-6.40) together constitute the nonlinear model of the power system installed with IPFC. The nonlinear equations of the system are linearized around the operating point obtained from load flow studies to form the Phillips Heffron model of the multi-machine power system incorporated with IPFC in the following section.

#### 6.4 Linearized Phillips-Heffron Model of a Multi-Machine Power System Including IPFC in State Space Form

The linear dynamic model of the multi-machine power system with IPFC is obtained by linearizing the nonlinear model around an operating point of the power system. The operating point is obtained from load flow analysis. The linearized form of Equations (6.18-6.24) is as follows:

$$\Delta \dot{\delta} = \omega_0 \Delta \omega \quad (6.41)$$

$$\Delta \dot{\omega} = M^{-1} (-\Delta P_e - D \Delta \omega) \quad (6.42)$$

$$\Delta \dot{E}'_q = T_{do}^{-1} (-\Delta E_q + \Delta E_{fd}) \quad (6.43)$$

$$\Delta \dot{E}_{fd} = T_A^{-1}(-\Delta E_{fd} + K_A(-\Delta V_t)) \quad (6.44)$$

where

$$\Delta P_e = I_{q0} \Delta E'_q + I_{q0}(x_q - x'_d) \Delta I_d + E'_q \Delta I_q + I_{d0}(x_q - x'_d) \Delta I_q \quad (6.45)$$

$$\Delta E_q = -\Delta E'_q - (x_d - x'_d) \Delta I_d \quad (6.46)$$

$$\Delta V_{td} = x_q \Delta I_q, \Delta V_{tq} = \Delta E'_q - x'_d \Delta I_d, V_t = V_{td} + j V_{tq} \quad (6.47)$$

and,

$$\Delta \delta = [\Delta \delta_1 \quad \Delta \delta_2 \quad \cdots \quad \Delta \delta_n]^T, \quad \Delta \omega = [\Delta \omega_1 \quad \Delta \omega_2 \quad \cdots \quad \Delta \omega_n]^T,$$

$$\Delta E'_q = [\Delta E'_{q1} \quad \Delta E'_{q2} \quad \cdots \quad \Delta E'_{qn}]^T, \quad \Delta E_{fd} = [\Delta E_{fd1} \quad \Delta E_{fd2} \quad \cdots \quad \Delta E_{fdn}]^T$$

$$\Delta I_d = [\Delta I_{d1} \quad \Delta I_{d2} \quad \cdots \quad \Delta I_{dn}]^T, \quad \Delta I_q = [\Delta I_{q1} \quad \Delta I_{q2} \quad \cdots \quad \Delta I_{qn}]^T,$$

$$\Delta V_{td} = [\Delta V_{td1} \quad \Delta V_{td2} \quad \cdots \quad \Delta V_{tdn}]^T, \quad \Delta V_{tq} = [\Delta V_{tq1} \quad \Delta V_{tq2} \quad \cdots \quad \Delta V_{tqn}]^T,$$

$$\Delta V_t = [\Delta V_{t1} \quad \Delta V_{t2} \quad \cdots \quad \Delta V_{tn}]^T, \quad \Delta V_{ti} = \sqrt{\Delta V_{tdi}^2 + \Delta V_{tqi}^2},$$

$$M = \text{diag}(2H_i), \quad D = \text{diag}(D_i), \quad T'_{d0} = \text{diag}(T'_{d0i}),$$

$$x_d = \text{diag}(x_{di}), \quad x_q = \text{diag}(x_{qi}), \quad x'_d = \text{diag}(x'_{di})$$

$$I_{q0} = \text{diag}(I_{q10}, \dots, I_{qn0}), \quad I_{d0} = \text{diag}(I_{d10}, \dots, I_{dn0}),$$

$I_{di0}, I_{qi0}$  are the values of  $I_{di}, I_{qi}$  respectively at the operating point.

$i = 1, \dots, n$ ,  $n$  is the number of generators.

The  $d - q$  axis components of the generator currents Equations (6.39)-(6.40) are linearized and represented in matrix form as:

$$\begin{aligned} \Delta I_d = & C_d \Delta \delta + E_d \Delta E'_q + M_d \Delta I_q + P_d \Delta v_{dc} + G_{dA} \Delta m_1 + H_{dA} \Delta \theta_1 \\ & + G_{dB} \Delta m_2 + H_{dB} \Delta \theta_2 \end{aligned} \quad (6.48)$$

$$\begin{aligned} \Delta I_q = & C_q \Delta \delta + E_q \Delta E'_q + M_q \Delta I_q + P_q \Delta v_{dc} + G_{qA} \Delta m_1 + H_{qA} \Delta \theta_1 \\ & + G_{qB} \Delta m_2 + H_{qB} \Delta \theta_2 \end{aligned} \quad (6.49)$$

where,

$$\begin{aligned} C_{dii} = & \sum_{\substack{j=1 \\ j \neq i}}^n -Y'_{dij} \left[ \cos \delta_{dij} E'_{qj} + (x_{qj} - x'_{dj}) \sin \delta_{dij} I_{qj} \right] - \frac{1}{2} m_1 v_{dc} \sum_{j=1}^n (Y'_{dij} Y_{Aj} \sin \delta_{Aij}) \\ & - \frac{1}{2} m_2 v_{dc} \sum_{j=1}^n (Y'_{dij} Y_{Bj} \sin \delta_{Bij}) \quad i = 1, 2, \dots, n \end{aligned}$$

$$C_{dij} = Y'_{dij} \left( \cos \delta_{dij} E'_{qj} + (x_{qj} - x'_{dj}) \sin \delta_{dij} I_{qj} \right) \quad i = 1, 2, \dots, n; j = 1, 2, \dots, n; i \neq j$$

$$E_{dij} = -Y'_{dij} \sin \delta_{dij} \quad i = 1, 2, \dots, n; j = 1, 2, \dots, n;$$

$$M_{dij} = (Y'_{dij} (x_{qj} - x'_{dj}) \cos \delta_{dij}) \quad i = 1, 2, \dots, n; j = 1, 2, \dots, n;$$

$$P_{di} = \frac{1}{2} m_1 \sum_{j=1}^n (Y'_{dij} Y_{Aj} \cos \delta_{Aij}) + \frac{1}{2} m_2 \sum_{j=1}^n (Y'_{dij} Y_{Bj} \cos \delta_{Bij}), \quad i = 1, 2, \dots, n$$

$$G_{dAi} = \frac{1}{2} v_{dc} \sum_{j=1}^n (Y'_{dij} Y_{Aj} \cos \delta_{Aij}) \quad i = 1, 2, \dots, n$$

$$H_{dAi} = -\frac{1}{2} m_1 v_{dc} \sum_{j=1}^n (Y'_{dij} Y_{Aj} \sin \delta_{Aij}) \quad i = 1, 2, \dots, n$$

$$G_{dBi} = \frac{1}{2} v_{dc} \sum_{j=1}^n (Y'_{dij} Y_{Bj} \cos \delta_{Bij}) \quad i = 1, 2, \dots, n$$

$$H_{dBi} = -\frac{1}{2} m_2 v_{dc} \sum_{j=1}^n (Y'_{dij} Y_{Bj} \sin \delta_{Bij}) \quad i = 1, 2, \dots, n$$

$$C_{qiq} = \sum_{\substack{j=1 \\ j \neq i}}^n -Y'_{dij} [\sin \delta_{dij} E'_{qj} - (x_{qj} - x'_{dj}) \cos \delta_{dij} I_{qj}] + \frac{1}{2} m_1 v_{dc} \sum_{j=1}^n (Y'_{dij} Y_{Aj} \cos \delta_{Aij}) \\ + \frac{1}{2} m_2 v_{dc} \sum_{j=1}^n (Y'_{dij} Y_{Bj} \cos \delta_{Bij}) \quad i = 1, 2, \dots, n$$

$$C_{qij} = Y'_{dij} (\sin \delta_{dij} E'_{qj} + (x_{qj} - x'_{dj}) \cos \delta_{dij} I_{qj}) \quad j = 1, 2, \dots, n \\ i \neq j$$

$$E_{qij} = -Y'_{dij} \cos \delta_{dij} \quad i = 1, 2, \dots, n; \quad j = 1, 2, \dots, n$$

$$M_{qij} = (Y'_{dij} (x_{qj} - x'_{dj}) \sin \delta_{dij}) \quad i = 1, 2, \dots, n; \quad j = 1, 2, \dots, n$$

$$P_{qi} = \frac{1}{2} m_1 \sum_{j=1}^n (Y'_{dij} Y_{Aj} \sin \delta_{Aij}) + \frac{1}{2} m_2 \sum_{j=1}^n (Y'_{dij} Y_{Bj} \sin \delta_{Bij}), \quad i = 1, 2, \dots, n;$$

$$G_{qAi} = \frac{1}{2} v_{dc} \sum_{j=1}^n (Y'_{dij} Y_{Aj} \sin \delta_{Aij}) \quad i = 1, 2, \dots, n;$$

$$H_{qAi} = \frac{1}{2} m_1 v_{dc} \sum_{j=1}^n (Y'_{dij} Y_{Aj} \cos \delta_{Aij}) \quad i = 1, 2, \dots, n;$$

$$G_{qBi} = \frac{1}{2} v_{dc} \sum_{j=1}^n (Y'_{dij} Y_{Bj} \sin \delta_{Bij}) \quad i = 1, 2, \dots, n;$$

$$H_{qBi} = \frac{1}{2} m_2 v_{dc} \sum_{j=1}^n (Y'_{dij} Y_{Bj} \cos \delta_{Bij}) \quad i = 1, 2, \dots, n;$$

From Equation (6.49)  $\Delta I_q$  can be written as:

$$\Delta I_q = D_q \Delta \delta + F_q \Delta E'_q + N_q \Delta v_{dc} + R_{Aq} \Delta m_1 + S_{Aq} \Delta \theta_1 \\ + R_{Bq} \Delta m_2 + S_{Bq} \Delta \theta_2 \quad (6.50)$$

where

$$D_q = L_q^{-1} C_q, \quad F_q = L_q^{-1} E_q, \quad N_q = L_q^{-1} P_q$$

$$R_{Aq} = L_q^{-1} G_{qA}, \quad S_{Aq} = L_q^{-1} H_{qA}, \quad R_{Bq} = L_q^{-1} G_{qB}, \quad S_{Bq} = L_q^{-1} H_{qB} \quad \text{and}$$

$$L_q = I - M_q, L_{qii} = 1 - Y'_{dii}(x_{qi} - x'_{di}) \sin \delta_{dii}, L_{qij} = -Y'_{dij}(x_{qj} - x'_{dj}) \sin \delta_{dij} \quad j \neq i$$

Substitute  $\Delta I_q$  from Equation (6.50) into Equation (6.48) to get:

$$\begin{aligned} \Delta I_d = & D_d \Delta \delta + F_d \Delta E'_q + N_d \Delta v_{dc} + R_{Ad} \Delta m_1 + S_{Ad} \Delta \theta_1 \\ & + R_{Bd} \Delta m_2 + S_{Bd} \Delta \theta_2 \end{aligned} \quad (6.51)$$

where

$$D_d = C_d + M_d D_q, F_d = E_d + M_d F_q, N_d = P_d + M_d N_q$$

$$R_{Ad} = G_{dA} + M_d R_{Aq}, S_{Ad} = H_{dA} + M_d S_{Aq},$$

$$R_{Bd} = G_{dB} + M_d R_{Bq}, S_{Bd} = H_{dB} + M_d S_{Bq},$$

Substituting Equations (6.50) and (6.51) into Equations (6.45-6.47) the following is obtained:

$$\begin{aligned} \Delta P_e = & K_1 \Delta \delta + K_2 \Delta E'_q + K_{pv} \Delta v_{dc} + K_{pm1} \Delta m_1 + K_{p\theta1} \Delta \theta_1 + \\ & K_{pm2} \Delta m_2 + K_{p\theta2} \Delta \theta_2 \end{aligned} \quad (6.52)$$

$$\begin{aligned} \Delta E_q = & K_4 \Delta \delta + K_3 \Delta E'_q + K_{qv} \Delta v_{dc} + K_{qm1} \Delta m_1 + K_{q\theta1} \Delta \theta_1 + \\ & K_{qm2} \Delta m_2 + K_{q\theta2} \Delta \theta_2 \end{aligned} \quad (6.53)$$

$$\begin{aligned} \Delta V_T = & K_5 \Delta \delta + K_6 \Delta E'_q + K_{vv} \Delta v_{dc} + K_{vm1} \Delta m_1 + K_{v\theta1} \Delta \theta_1 + \\ & K_{vm2} \Delta m_2 + K_{v\theta2} \Delta \theta_2 \end{aligned} \quad (6.54)$$

where

$$K_1 = I_{q0}(x_q - x'_d)D_d + E'_q D_q + I_{d0}(x_q - x'_d)D_q$$

$$K_2 = I_{q0} + I_{q0}(x_q - x'_d)F_d + E'_q F_q + I_{d0}(x_q - x'_d)F_q$$

$$K_{pv} = I_{q0}(x_q - x'_d)N_d + E'_q N_q + I_{d0}(x_q - x'_d)N_q$$

$$K_{pm1} = I_{q0}(x_q - x'_d)R_{Ad} + E'_q R_{Aq} + I_{d0}(x_q - x'_d)R_{Aq}$$

$$K_{p\theta1} = I_{q0}(x_q - x'_d)S_{Ad} + E'_q S_{Aq} + I_{d0}(x_q - x'_d)S_{Aq}$$

$$K_{pm2} = I_{q0}(x_q - x'_d)R_{Bd} + E'_q R_{Bq} + I_{d0}(x_q - x'_d)R_{Bq}$$

$$K_{p\theta2} = I_{q0}(x_q - x'_d)S_{Bd} + E'_q S_{Bq} + I_{d0}(x_q - x'_d)S_{Bq}$$

$$K_4 = (x_d - x'_d)D_d \quad K_3 = I + (x_d - x'_d)F_d$$

$$K_{qv} = (x_d - x'_d)N_d \quad K_{qm1} = (x_d - x'_d)R_{Ad}$$

$$K_{q\theta1} = (x_d - x'_d)S_{Ad} \quad K_{qm2} = (x_d - x'_d)R_{Bd}$$

$$K_{q\theta2} = (x_d - x'_d)S_{Bd} \quad K_5 = V_{t0}^{-1}(V_{d0}x_q D_q - V_{q0}x'_d D_d)$$

$$K_6 = V_{t0}^{-1}(V_{d0}x_q F_q + V_{q0} - V_{q0}x'_d F_d) \quad K_{vv} = V_{t0}^{-1}(V_{d0}x_q N_q - V_{q0}x'_d N_d)$$

$$K_{vm1} = V_{t0}^{-1}(V_{d0}x_q R_{Aq} - V_{q0}x'_d R_{Ad}) \quad K_{v\theta1} = V_{t0}^{-1}(V_{d0}x_q S_{Aq} - V_{q0}x'_d S_{Ad})$$

$$K_{vm2} = V_{t0}^{-1}(V_{d0}x_q R_{Bq} - V_{q0}x'_d R_{Bd}) \quad K_{v\theta2} = V_{t0}^{-1}(V_{d0}x_q S_{Bq} - V_{q0}x'_d S_{Bd})$$

The linearized form of DC capacitor voltage of Equation (6.27) is given by

$$\begin{aligned} \Delta \dot{v}_{dc} = & \frac{3}{4C_{dc}} [m_1 \cos \theta_1 \Delta i_{1d} + m_1 \sin \theta_1 \Delta i_{1q} + m_2 \cos \theta_2 \Delta i_{2d} + m_2 \sin \theta_2 \Delta i_{2q} \\ & + (i_{1d} \cos \theta_1 + i_{1q} \sin \theta_1) \Delta m_1 + m_1 (-\sin \theta_1 i_{1d} + \cos \theta_1 i_{1q}) \Delta \theta_1 \\ & + (i_{2d} \cos \theta_2 + i_{2q} \sin \theta_2) \Delta m_2 + m_2 (-\sin \theta_2 i_{2d} + \cos \theta_2 i_{2q}) \Delta \theta_2] \end{aligned} \quad (6.55)$$

From Equations (6.6) and (6.7)

$$\bar{I}_1 = (\bar{V}_i - \bar{V}_{se1} - \bar{V}_j)(g_{ij} + j b_{ij}) \quad (6.56)$$

$$\bar{I}_2 = (\bar{V}_i - \bar{V}_{se2} - \bar{V}_k)(g_{ik} + j b_{ik}) \quad (6.57)$$

The voltages  $\bar{V}_i, \bar{V}_j, \bar{V}_k$  are written in terms of the terminal voltages of those generator buses to which these IPFC buses are connected. However, if the IPFC buses  $i, j, k$  are the generator buses, then  $\bar{V}_l = V_{dl}, l = i, j, k$ . Then

$$V_{dl} = V_{idl} + j V_{iqd}, \quad l = i, j, k, \quad (\text{IPFC buses}) \quad (6.58)$$

$$V_{idl} = x_{ql} I_{ql}; \quad V_{iqd} = E'_{ql} - x'_{dl} I_{dl}, \quad l = i, j, k \quad (6.59)$$

In linearized form Equation (6.59) can be represented as:

$$\Delta V_{idl} = x_{ql} \Delta I_{ql}; \quad \Delta V_{iqd} = \Delta E'_{ql} - x'_{dl} \Delta I_{dl}, \quad l = i, j, k \quad (6.60)$$

where  $\Delta I_{ql}; \Delta I_{dl}, l = i, j, k$  are obtained from Equations (6.50) and (6.51).

Equation (6.56) in  $d - q$  axis can be written as:

$$i_{1d} + j i_{1q} = ((V_{tdi} + j V_{tqi}) - (V_{se1d} + j V_{se1q}) - (V_{tdj} + j V_{tqj}))(g_{ij} + j b_{ij}) \quad (6.61)$$

$$i_{1d} = g_{ij} \left( V_{tdi} - \frac{m_1 V_{dc}}{2} \cos \theta_1 - V_{tdj} \right) + b_{ij} \left( -V_{tqi} + \frac{m_1 V_{dc}}{2} \sin \theta_1 + V_{tqj} \right) \quad (6.62)$$

$$i_{1q} = g_{ij} \left( V_{tqi} - \frac{m_1 V_{dc}}{2} \sin \theta_1 - V_{tqj} \right) + b_{ij} \left( V_{tdi} - \frac{m_1 V_{dc}}{2} \cos \theta_1 - V_{tdj} \right) \quad (6.63)$$

Substituting Equation (6.59) in Equations (6.62) and (6.63) and the resultant equations are linearized to obtain  $\Delta i_{1d}, \Delta i_{1q}$ . Similarly  $\Delta i_{2d}, \Delta i_{2q}$  are obtained from Equation (6.57) which are finally substituted in Equation (6.55) to get,

$$\Delta \dot{v}_{dc} = K_7 \Delta \delta + K_8 \Delta E'_q - K_9 \Delta v_{dc} + K_{cm1} \Delta m_1 + K_{c\theta1} \Delta \theta_1 + K_{cm2} \Delta m_2 + K_{c\theta2} \Delta \theta_2 \quad (6.64)$$

where  $K_7, K_8$  are  $(1 \times n)$  dimension vectors and the other coefficients in (6.64) are scalars. Substituting Equations (6.52-6.54) in Equations (6.41-6.44), the linearized Phillips Heffron model of the power system installed with IPFC in state space form is given by Equation (6.65). The model involves the DC capacitor dynamics.

$$\begin{aligned}
\begin{bmatrix} \Delta \dot{\delta} \\ \Delta \dot{\omega} \\ \Delta \dot{E}'_q \\ \Delta \dot{E}'_{fd} \\ \Delta \dot{v}_{dc} \end{bmatrix} &= \begin{bmatrix} 0 & \omega_o I & 0 & 0 & 0 \\ -M^{-1}K_1 & -M^{-1}D & -M^{-1}K_2 & 0 & -M^{-1}K_{pv} \\ -T'_{do}{}^{-1}K_4 & 0 & -T'_{do}{}^{-1}K_3 & T'_{do}{}^{-1} & -T'_{do}{}^{-1}K_{qv} \\ -T_A^{-1}K_A K_5 & 0 & -T_A^{-1}K_A K_6 & -T_A^{-1} & -T_A^{-1}K_A K_{vv} \\ K_7 & 0 & K_8 & 0 & -K_9 \end{bmatrix} \begin{bmatrix} \Delta \delta \\ \Delta \omega \\ \Delta E'_q \\ \Delta E'_{fd} \\ \Delta v_{dc} \end{bmatrix} \\
&+ \begin{bmatrix} 0 & 0 & 0 & 0 \\ -M^{-1}K_{pm1} & -M^{-1}K_{p\theta1} & -M^{-1}K_{pm2} & -M^{-1}K_{p\theta2} \\ -T'_{do}{}^{-1}K_{qm1} & -T'_{do}{}^{-1}K_{q\theta1} & -T'_{do}{}^{-1}K_{qm2} & -T'_{do}{}^{-1}K_{q\theta2} \\ -T_a^{-1}K_a K_{vm1} & -T_a^{-1}K_a K_{v\theta1} & -T_a^{-1}K_a K_{vm2} & -T_a^{-1}K_a K_{v\theta2} \\ K_{cm1} & K_{c\theta1} & K_{cm2} & K_{c\theta2} \end{bmatrix} \begin{bmatrix} \Delta m_1 \\ \Delta \theta_1 \\ \Delta m_2 \\ \Delta \theta_2 \end{bmatrix}
\end{aligned} \tag{6.65}$$

The state matrix is utilized to determine the eigenvalues and determine the oscillations modes present in the system. The following section gives the analysis of multi-machine power system with IPFC.

### 6.5 Case Study: Multi-Machine Power System With IPFC

The 3 machine 9-bus (WSCC) power system shown in Figure 5.10 [17] is considered for the stability analysis. The IPFC is placed in the WSCC system and is analyzed with it's the presence. The IPFC is placed in the branches 7-5 and 7-8 as shown in Figure 6.3. In Figure 6.3, IPFC bus sending end  $i$  is bus 7, the receiving end buses  $j$  and  $k$  are represented by buses 5 and 8 respectively. The IPFC is placed to regulate the power flows in its branches at the specified values  $P_{ji} = P_{57} = 0.8432$  p.u.  $P_{ki} = P_{87} = 0.7590$  p.u.,  $Q_{ji} = Q_{57} = 0.1157$  p.u. The load flow is performed and the results are given in Table 6.1.

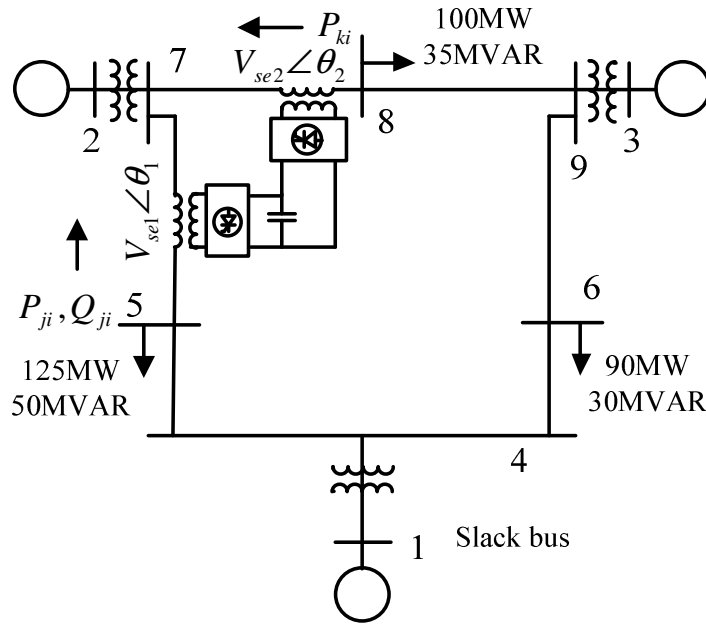


Figure 6.3: WSCC system with IPFC

Table 6.1: The load flow results of the WSCC

Bus	Voltage (p.u.)	$P_G$ (p.u.)	$Q_G$ (p.u.)	$-P_L$ (p.u.)	$-Q_L$ (p.u.)
1 (swing)	1.04	0.7175	0.1576		
2 (P-V)	$1.025 \angle 9.6274^0$	1.63	0.0188		
3 (P-V)	$1.025 \angle 4.9268^0$	0.85	0.0577		
4 (P-V)	$1.0287 \angle 4.08^0$				
5 (P-Q)	$1.0162 \angle -4.02^0$			1.25	0.5
6 (P-Q)	$0.9843 \angle -1.056^0$			0.9	0.3
7 (P-Q)	$1.0229 \angle 2.204^0$				
8 (P-Q)	$1.0133 \angle -3.62^0$			1.0	0.35
9 (P-Q)	$1.032 \angle -2.21^0$				
$V_{se1} = 0.0445$ p.u.		$V_{se2} = 0.0533$ p.u.		$\theta_1 = 172.5895^0$	
$P_{ji} = P_{57} = 0.8432$ p.u.		$P_{ki} = P_{87} = 0.7590$ p.u.		$Q_{ji} = Q_{57} = 0.1157$ p.u.	

Table 6.1 gives the voltages and phase angles at each bus, power flowing through the IPFC branches represented by  $P_{ji}$ ,  $Q_{ji}$ ,  $P_{ki}$  and the injected voltages  $V_{se1}$  and  $V_{se2}$  with their corresponding phase angles  $\theta_1$  and  $\theta_2$  of VSCs of IPFC. The load flow results show the IPFC regulates the power flows to the set points in its branches serving its primary function. The initial operating point is computed from the load flow results and Table 6.2 gives the initial values computed. The values are given in p.u. except where indicated.

Table 6.2: Initial conditions computed

State variable	Machine 1	Machine 2	Machine 3
$\delta$ in radians	1.5075	0.4800	0.7241
$E'_q$	1.0498	0.7719	0.8535
$E_{fd}$	1.0664	1.7644	1.5464
$P_m$	0.7175	1.63	0.85
$V_{ref}$	1.0755	1.0838	1.1796
IPFC parameters			
$v_{dc}$	2	$C_{dc}$	0.2
$m_1$	0.0445	$m_2$	0.0533

The power system is reduced to the generator buses and the IPFC buses by eliminating the load buses and as shown in Figure 6.4. The computed reduced admittance matrix  $\bar{Y}_{red}$  of the transmission network is given by Equation (6.66) using which  $\bar{Y}'_d$ ,  $\bar{Y}_A$  and  $\bar{Y}_B$  are calculated from Equation (6.31) and are given by Equations (6.67-6.69).

$$\bar{Y}_{red} = \begin{bmatrix} 0.699 - j 8.012 & 0 & -0.019 + j 1.12 & 0 & -0.268 + j 6.30 & -0.087 + j 0.641 \\ 0 & -j 16 & 0 & j 16 & 0 & 0 \\ -0.019 + j 1.12 & 0 & 0.63 - j 7.34 & 0 & -0.101 + j 0.747 & -0.295 + j 5.62 \\ 0 & j 16 & 0 & 2.11 - j 32.66 & -1.0 + j 5.50 & -1.112 + j 11.39 \\ -0.268 + j 6.30 & 0 & -0.101 + j 0.75 & -1. + j 5.5 & 2.9 - j 13.155 & -0.108 + j 0.42 \\ -0.087 + j 0.641 & 0 & -0.295 + j 5.62 & -1.11 + j 11.39 & -0.1085 + j 0.422 & 2.75 - j 18.152 \end{bmatrix} \quad (6.66)$$

$$\bar{Y}'_d = \begin{bmatrix} 0.8458 - j 2.9525 & 0.2848 + j 1.4839 & 0.2135 + j 1.2209 \\ 0.2848 + j 1.4839 & 0.4078 - j 2.6697 & 0.2168 + j 1.0604 \\ 0.2135 + j 1.2209 & 0.2168 + j 1.0604 & 0.2864 - j 2.3470 \end{bmatrix} \quad (6.67)$$

$$\bar{Y}_A = \begin{bmatrix} 0.1623 + j 0.0251 \\ -0.4691 + j 0.0570 \\ -0.2024 + j 0.0773 \end{bmatrix} \quad (6.68)$$

$$\bar{Y}_B = \begin{bmatrix} -0.1532 + j 0.0477 \\ -0.5421 + j 0.0207 \\ 0.2065 - j 0.0008 \end{bmatrix} \quad (6.69)$$

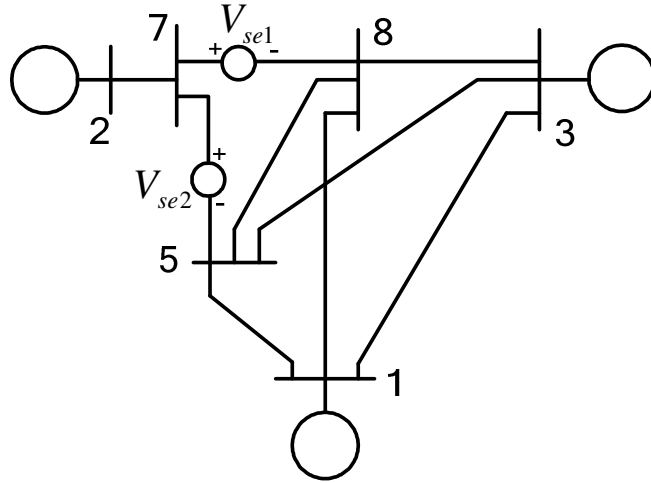


Figure 6.4: Reduced system containing the generator and IPFC buses

The  $K$ -constants are calculated and the eigenvalues are computed and given in Table 6.3. There are a total of 13 eigenvalues with three pair of complex eigenvalues which contribute to oscillations and remaining are real eigenvalues. The participation factors have been computed and the state variables contributing to these oscillation modes have been determined. Table 6.4 gives the normalized participation factors of all the eigenvalues. The oscillations modes 4 & 5 and 6 & 7 have the least damping ratio as seen in Table 6.3. On observation of Table 6.4, it is noted that these oscillations modes 4 & 5 and 6 & 7 are contributed by machine 3 and machine 2, respectively. Compare the results with Table 5.7. It is observed that the power system without IPFC and with IPFC, both have two pair of oscillation modes 4 & 5 and 6 & 7 in which the machine 3 and 2 have highest participation factor. This validates the mathematical model of the power system with IPFC.

To increase the damping of these modes, initially the PSS is installed in the system. The design of PSS and the eigenvalues with PSS of the WSCC system without IPFC are given in Chapter 5. Using those PSS's whose parameters are given in Table 5.10, the WSCC power system is installed with the two PSSs at machine 2 and 3. The eigenvalues of the WSCC system with IPFC in the presence of the two PSS's are given in Table 6.5.

Table 6.3: Eigenvalues of WSCC power system with IPFC

No.	Eigenvalues	Damping ratio	Frequency	Dominant states
1	-19.3	1	0	$E_{fd3}$
2	-17.1802	1	0	$E_{fd2}$
3	-15.6798	1	0	$E_{fd1}$
4&5	$-0.3009 \pm j 11.2735$	0.0267	1.7942	$\delta_3 \ \omega_3$
6&7	$-0.2933 \pm j j \ 8.1607$	0.0359	1.2988	$\delta_2 \ \omega_2$
8	-4.4731	1	0	$E'_{q1}$
9	-2.7315	1	0	$E'_{q2}$
10	-0.6816	1	0	$E'_{q3}$
11&12	$-0.0174 \pm j j \ 0.2109$	0.0823	0.0336	$\delta_1 \ \omega_1$
13	-0.0196	1	0	$v_{dc}$

Table 6.4: The participation factors of the eigenvalues

States	Eigenvalues												
	1	2	3	4	5	6	7	8	9	10	11	12	13
$\delta_1$	0	0	0	0	0	0.427	0.427	0	0	0	1	1	0
$\delta_2$	0	0	0	0.212	0.212	1	1	0	0	0	0.305	0.305	0
$\delta_3$	0	0	0	1	1	0.164	0.164	0	0	0	0.157	0.157	0
$\omega_1$	0	0	0	0	0	0.427	0.427	0	0	0	1	1	0
$\omega_2$	0	0	0	0.212	0.212	1	1	0	0	0	0.305	0.305	0
$\omega_3$	0	0	0	1	1	0.164	0.164	0	0	0	0.157	0.157	0
$E'_{q1}$	0	0	0.277	0	0	0	0	1	0	0	0	0	0
$E'_{q2}$	0	0.168	0	0	0	0.109	0.109	0	1	0.061	0.155	0.155	0
$E'_{q3}$	0	0	0	0.064	0.064	0	0	0	0.125	1	0.366	0.366	0
$E_{fd1}$	0	0	1	0	0	0	0	0.281	0	0	0	0	0
$E_{fd2}$	0.125	1	0	0	0	0	0	0	0.148	0	0	0	0
$E_{fd3}$	1	0.128	0	0	0	0	0	0	0	0	0	0	0
$v_{dc}$	0	0	0	0	0	0	0	0	0	0	0	0	1

The damping ratios of the concerned oscillation modes have increased with the PSS placement in the system as shown in Table 6.5. Complex eigenvalues 11 & 12 in Table 6.3 have an oscillation frequency equal to 0.033 Hz, and they are contributed by machine 1. The damping ratio of these oscillation modes has also been increased with the presence of the two PSSs.

Table 6.5: Eigenvalues with PSS

Eigenvalues	Damping ratio	Frequency	Dominant states
-54.1642	1	0	
-26.8454	1	0	
$-22.1998 \pm j 10.1872$	0.9089	1.6213	
$-15.7747 \pm j 5.8177$	0.9382	0.9259	
-15.6979	1	0	
$-1.1200 \pm j 10.7658$	0.1035	1.7134	$\delta_3 \ \omega_3$
$-0.6599 \pm j 8.3559$	0.0787	1.3299	$\delta_2 \ \omega_2$
-4.4747	1	0	
-2.5057	1	0	
$-0.5183 \pm j 0.2606$	0.8934	0.0415	$\delta_1 \ \omega_1$
$-0.0455 \pm j 0.0864$	0.4654	0.0138	
-0.0198	1	0	
-0.1	1	0	

It is seen that the oscillation modes  $-0.6599 \pm j 8.3559$  still have slightly less damping ratio than 0.1. The damping ratio of this mode can be further increased by IPFC Power Oscillation Damping (POD) controller. The most suitable control signal for providing additional damping is determined from the controllability index computed from the linearized model. The controllability indices are computed and given in Table 6.6, from which it is observed that the input signal  $m_1$  has the highest value, an indicator for the best signal to provide damping.

Table 6.6: Controllability indices with different IPFC controllable parameters

Input signal	Controllability index
$\Delta m_1$	0.0201
$\Delta \theta_1$	0.0036
$\Delta m_2$	0.0070
$\Delta \theta_2$	0.0040

The Power Oscillation Damping (POD) controller is shown in Figure 6.5 having the error signal, of the active power flow of the IPFC branch  $j - i$  or  $5 - 7$ , as its input. The structure of POD controller is given in Figure 4.35. The parameters of the controller are designed using phase compensation technique as described in Section 4.7.3, to compensate the phase shift between the control input signal  $\Delta m_1$  and real

power deviation  $\Delta P_{ji}$ , and improve the damping ratio of the oscillation mode to around 0.1. The POD is designed on the system considering the two PSS.

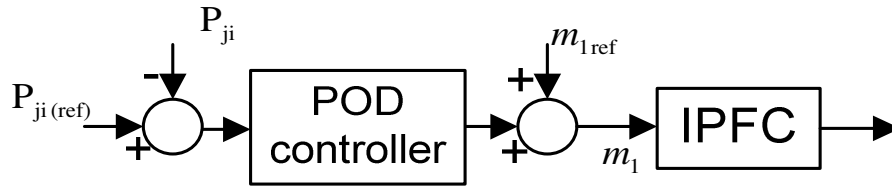


Figure 6.5: POD controller of IPFC

The PI type power flow controllers and DC voltage regulator are present together in the system to maintain the power flow and constant DC capacitor voltage. The block diagram of the complete closed loop system is shown in Figure 6.6.

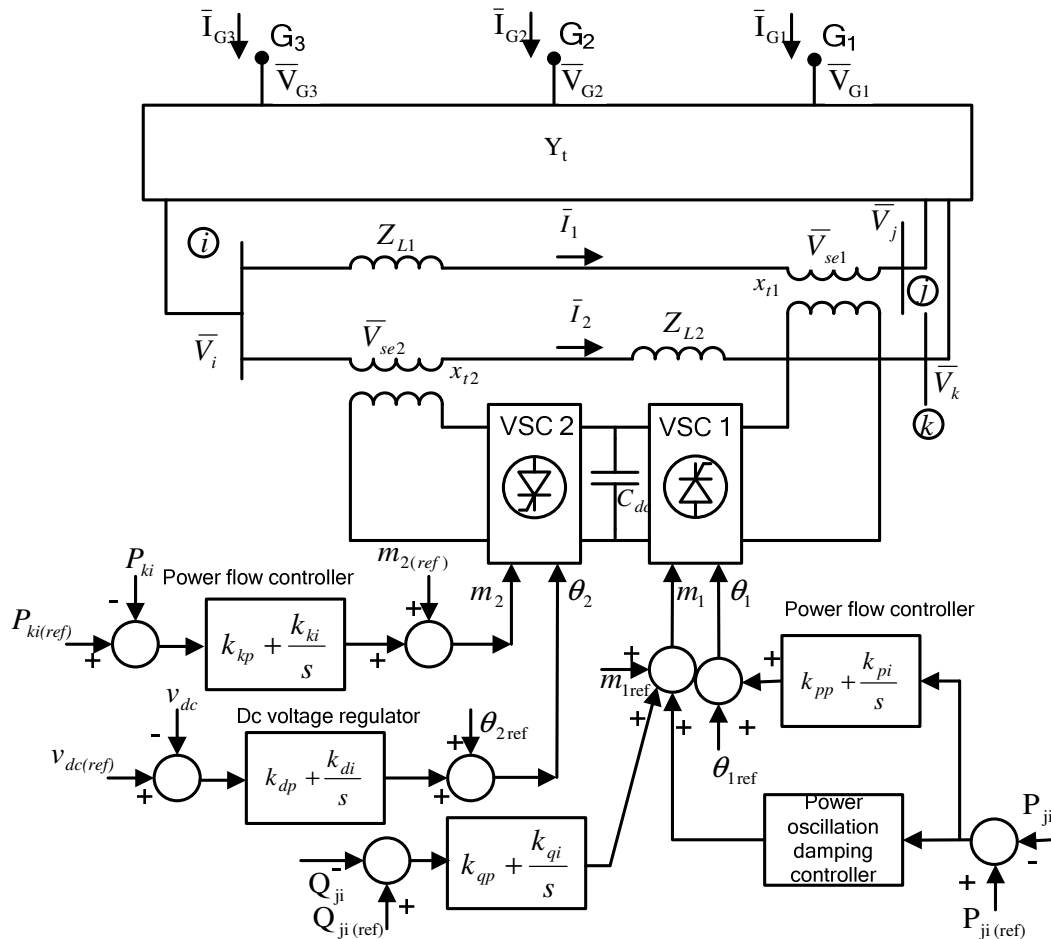


Figure 6.6: Multi-machine system with IPFC and its controllers

Three power flow controllers are placed in the system to control the real and reactive power flow in line  $j - i$  and real power flow in line  $k - i$  respectively. The DC voltage regulator maintains the DC voltage constant. The parameters of the controllers are:  $k_{pp} = 5$ ,  $k_{pi} = 25$ ,  $k_{qp} = 0.06$ ,  $k_{qi} = 0.007$ ,  $k_{kp} = 0.01$ ,  $k_{ki} = 0.01$ ,  $k_{dp} = 10$  and  $k_{di} = 20$ . The parameters of the POD controller are:  $k_{dc} = 0.3554$ ,  $T_w = 10s$ ,  $T_m = 0.01s$ ,  $T_1 = 0.20058$ ,  $T_2 = 0.071407$ ,  $m_c = 1$ . The oscillation modes of the closed loop system are given in Table 6.7. The PI controllers contribute little damping to the oscillation modes. The POD controller significantly increases the damping of the concerned oscillation mode.

The power system incorporating IPFC response is observed in time domain simulations. The nonlinear simulation is conducted through numerical integration and by MATLAB/SIMULINK. The multi-machine power system with IPFC is simulated using the nonlinear differential and algebraic equations of the power system in Equations (6.18-6.24, 6.9-6.12, 6.27, and 6.33). The numerical integration of the differential equations of the power system is performed using ode45 functions in Matlab. The MATLAB/SIMULINK block diagram of the system with IPFC is given in the Appendix D.

Table 6.7: Eigenvalues of the linearized WSCC with IPFC and controllers

WSCC with IPFC and Controllers	Eigenvalues	Damping Ratio	Frequency
No controllers	$-0.3009 \pm j 11.2735$ $-0.2933 \pm j 8.1607$	0.0267 0.0359	1.7942 1.2988
With only PSS	$-1.1200 \pm j 10.7658$ $-0.6599 \pm j 8.3559$	0.1035 0.0787	1.7134 1.3299
PSS and DC voltage regulator	$-1.1252 \pm j 10.7635$ $-0.6585 \pm j 8.3624$	0.104 0.0785	1.7131 1.3309
PSS and Power flow controllers and DC voltage regulator	$-1.1015 \pm j 10.7254$ $-0.6922 \pm j 8.0082$	0.1022 0.0861	1.7070 1.2745
PSS, power flow controller and DC voltage regulator and damping controller	$-1.1055 \pm j 10.7405$ $-0.9752 \pm j 7.0226$	0.1024 0.1376	1.7094 1.1177

The system is equipped with the PI power flow controllers which regulate the real power flow in line  $j - i$  or 5 - 7 at 0.8432 p.u., reactive power at 0.1157 p.u. and real

power flow in line  $k - i$  or 8 - 7 at 0.7590. The DC voltage is maintained at a constant value of 2 p.u. by the voltage regulator. The system is subjected to various disturbances and the performances of the PSS and IPFC damping controller are investigated.

### **6.5.1 Disturbance: Step Change in Mechanical Power**

A disturbance in the form of a step variation of 0.01 p.u. in mechanical power input  $P_{m2}$ , at machine 2 is applied at 0.5s. Oscillations are observed in the system due to the disturbance. The power flow in the transmission line is controlled by the series injected voltage such that oscillations are damped sufficiently. The magnitude and phase angle of the injected series voltages are controlled by the input signals of the IPFC which are modulated by the controllers to effectively control the power flows. The POD controller increases the damping of the oscillations. The responses of various parameters of the power system, i.e., electrical power generated by the machines 1 and 2, active power flow in IPFC branches, relative rotor angles and relative rotor speeds, respectively in the event of change in mechanical input are shown in Figures 6.7-6.14 in the presence of PSSs and POD controller. The PI power flow controllers and DC voltage regulator are present simultaneously in the system to maintain the power flow and constant DC capacitor voltage. The POD controller  $m_1$  mitigates the oscillations efficiently during the mechanical input disturbance. The response of other parameters such as electrical power generated by machine 3 is similar to Figures 6.7 and 6.8 with the initial value at 0.85 p.u. corresponding to its generated power.

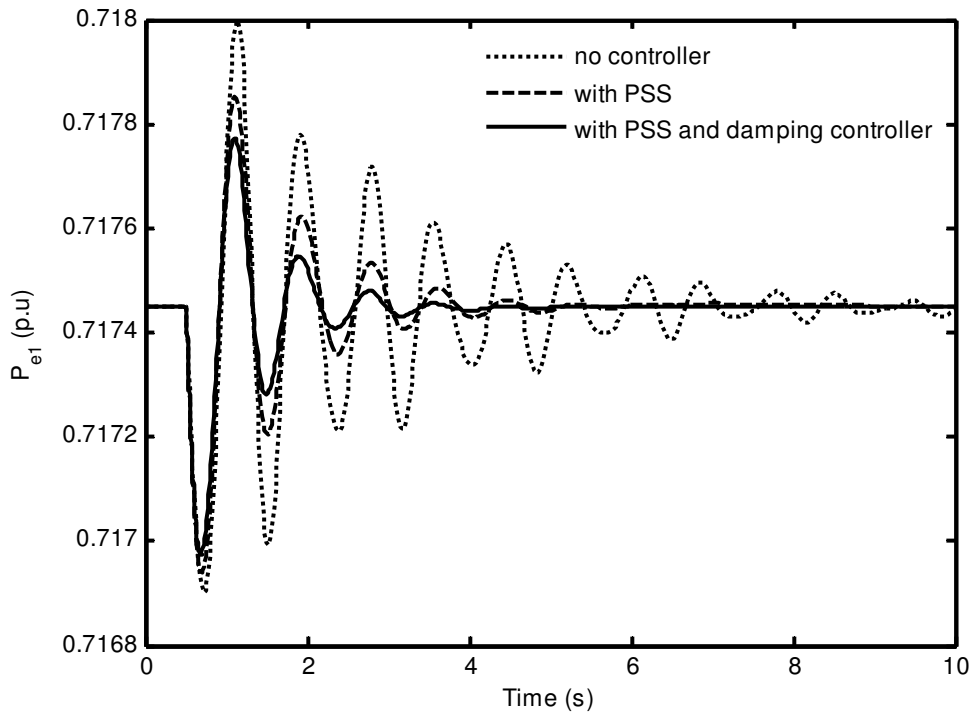


Figure 6.7: Generated power response at machine 1 with mechanical input disturbance

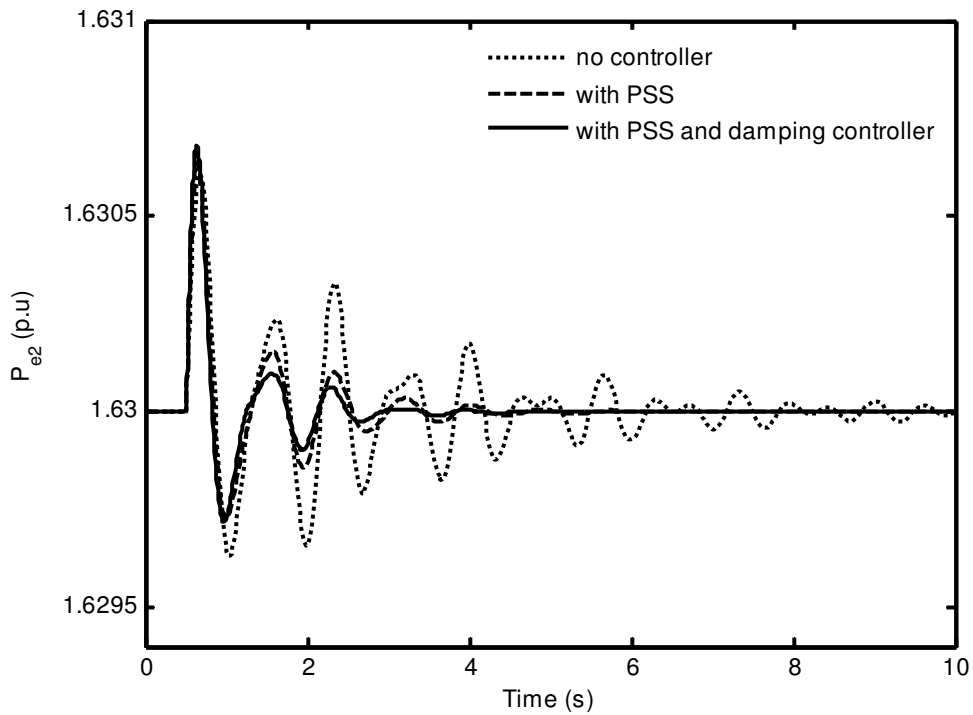


Figure 6.8: Generated power response at machine 2 with mechanical input disturbance

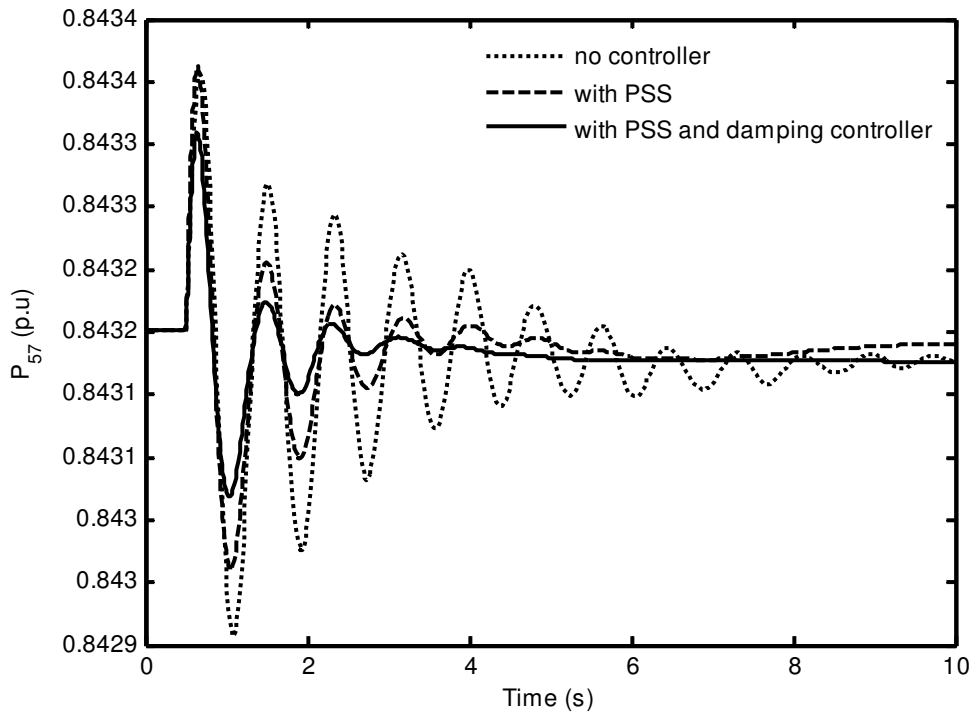


Figure 6.9: Real power flow response in IPFC branch 5 – 7 with mechanical input disturbance

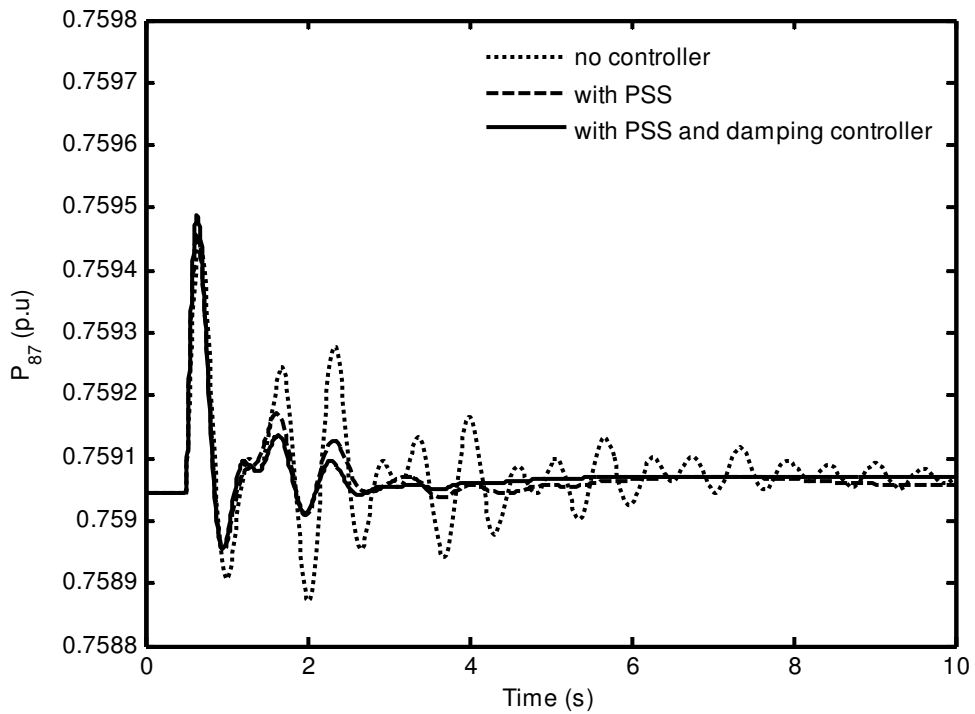


Figure 6.10: Real power flow response in IPFC branch 8 – 7 with mechanical input disturbance

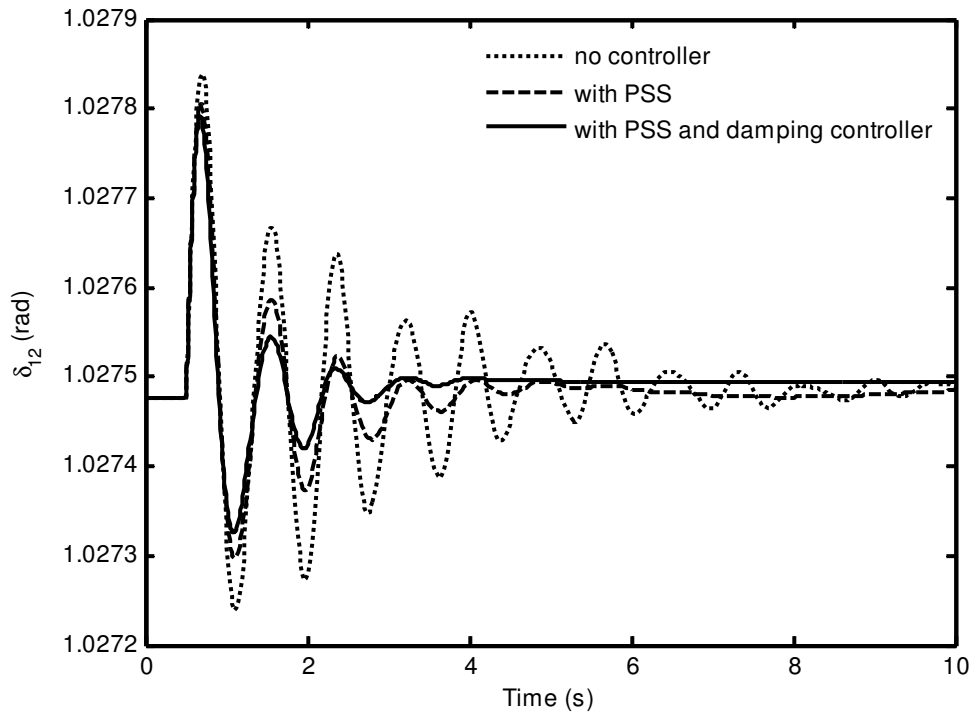


Figure 6.11: Relative rotor angle  $\delta_{12}$  response with mechanical input disturbance

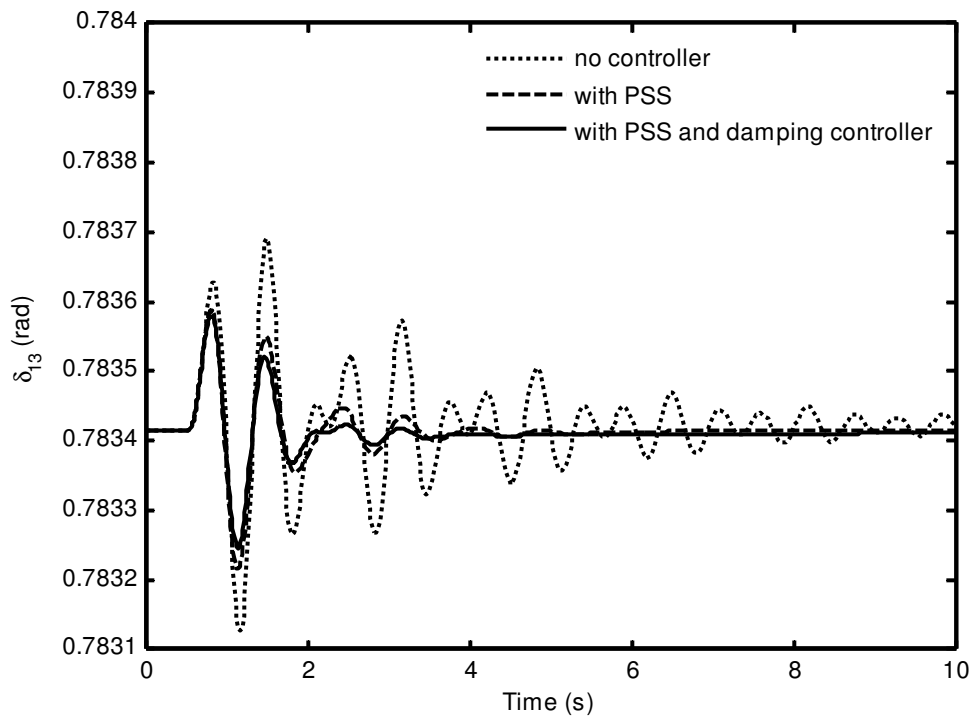


Figure 6.12: Relative rotor angle  $\delta_{13}$  response with mechanical input disturbance

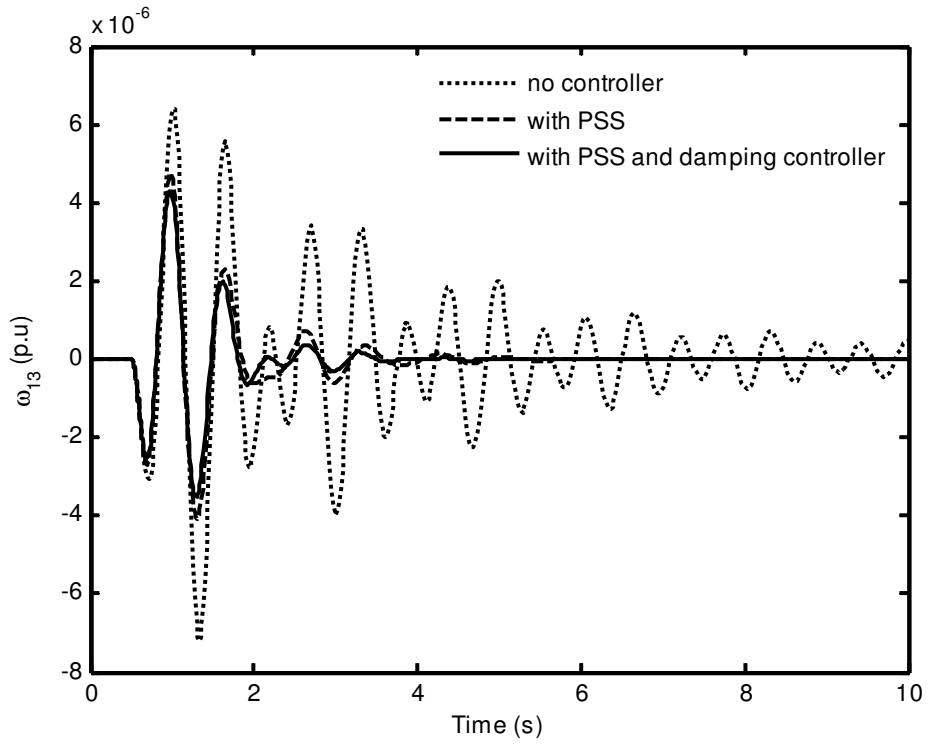


Figure 6.13: Relative rotor angle  $\omega_{13}$  response with mechanical input disturbance

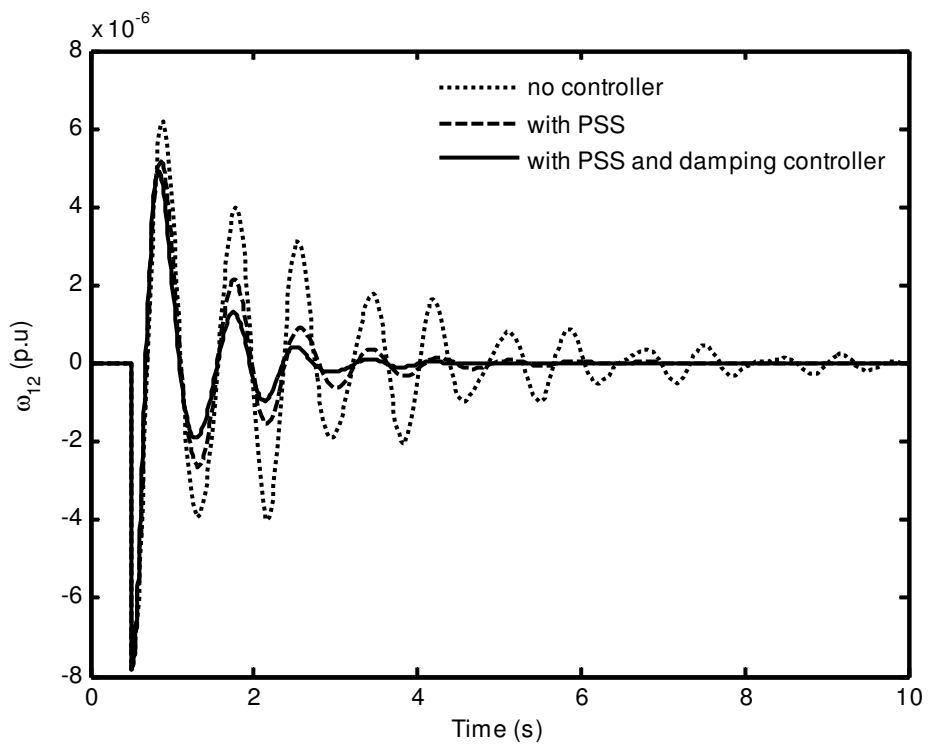


Figure 6.14: Relative rotor angle  $\omega_{12}$  response with mechanical input disturbance

### 6.5.2 Disturbance: Three Phase Fault

The disturbance in the form of three phase fault is initiated near bus 9 at the end of line 6-9, of the power system in Figure 6.3. The three phase fault is applied at 0.5s and cleared after 0.1s. During fault, since  $V_9 \equiv 0$ , the rows and columns of the admittance matrix of the prefault system corresponding to bus 9 will be deleted. Then the load buses are eliminated and the reduced matrix is formulated which given by Equation (6.70), following  $\bar{Y}'_d$ ,  $\bar{Y}_A$  and  $\bar{Y}_B$  are calculated and are given by Equations (6.71-6.73).

$$\bar{Y}_{red} = \begin{bmatrix} 0.7122 - j 8.1398 & 0 & 0 & 0 & -0.2491 + j 6.2195 & 0 \\ 0 & -j 16 & 0 & j 16 & 0 & 0 \\ 0 & 0 & -j 17.0648 & 0 & 0 & 0 \\ 0 & j 16 & 0 & 2.11 - j 32.66 & -1.0 + j 5.50 & -1.112 + j 11.39 \\ -0.2691 + j 6.219 & 0 & 0 & -1 + j 5.5 & 2.9 - j 13.21 & 0 \\ 0 & 0 & 0 & -1.11 + j 11.39 & 0 & 3.299 - j 21.35 \end{bmatrix} \quad (6.70)$$

$$\bar{Y}'_d = \begin{bmatrix} 0.6882 - j 3.7706 & 0.1269 + j 0.7737 & 0 \\ 0.1269 + j 0.7737 & 0.2522 - j 3.2857 & 0 \\ 0 & 0 & -j 4.1684 \end{bmatrix} \quad (6.71)$$

$$\bar{Y}_A = \begin{bmatrix} 0.3218 - j 0.0927 \\ -0.2968 + j 0.0546 \\ 0 \end{bmatrix} \quad (6.72)$$

$$\bar{Y}_B = \begin{bmatrix} -0.3351 + j 0.0991 \\ -0.7333 + j 0.0621 \\ 0 \end{bmatrix} \quad (6.73)$$

The response of various parameters of the dynamic power system i.e., real power flow in IPFC branches, relative rotor angles, electrical power generated by the machines, DC capacitor voltage and relative speed are shown with and without the POD controller and PSS during three phase fault in Figures 6.15 -6.21 respectively. The POD controller  $m_1$  mitigates the oscillations efficiently even during the case of three phase fault. The other parameters responses follow in a similar pattern.

Figure 6.19 gives the electrical power generated by the three machines, where the values are given in p.u. Each generator generates the real power initially as given by the load flow results given in Table 6.1 which is also the steady state operating condition. A disturbance is given at 0.5 s which cause oscillations as seen in the response. The oscillations eventually are dampened with the presence of damping controller and settle at their steady state values.

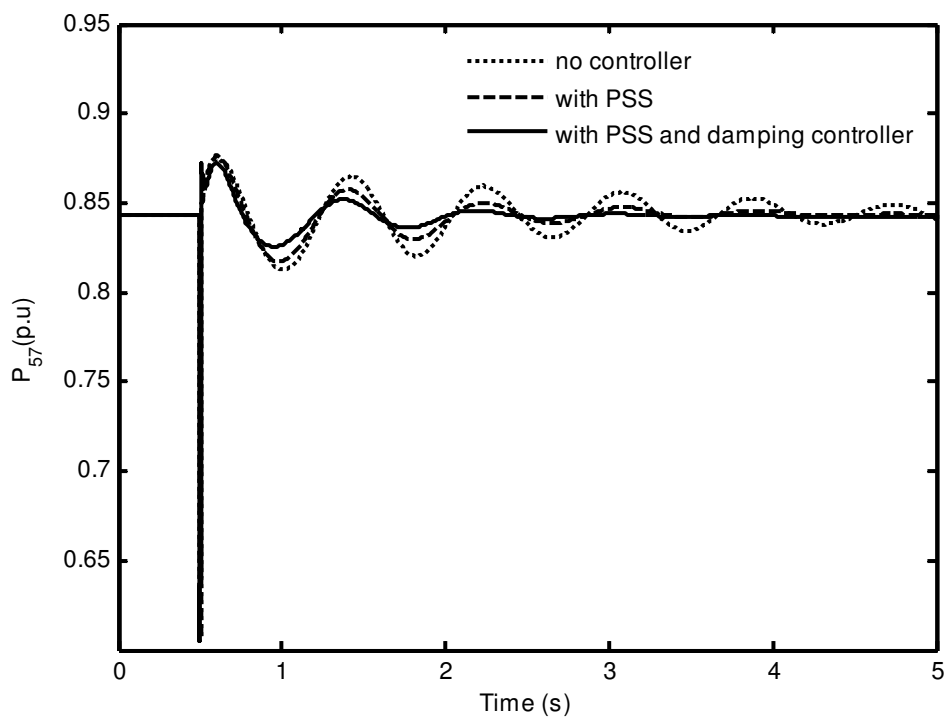


Figure 6.15: Real power flow response in IPFC branch 5 – 7 with three phase fault

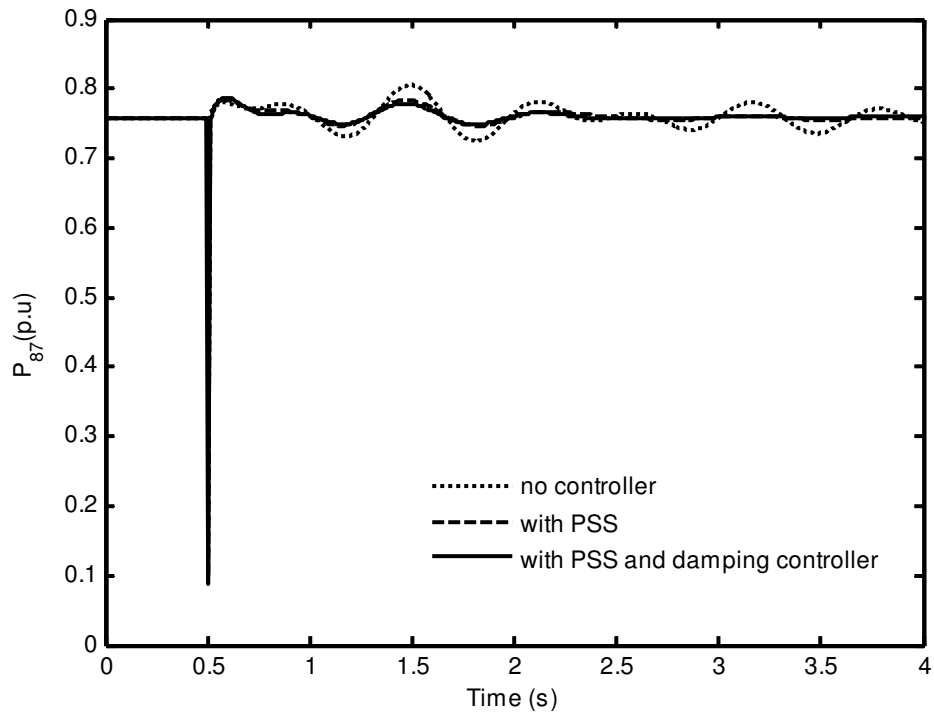


Figure 6.16: Real power flow response in IPFC branch 8 – 7 with three phase fault

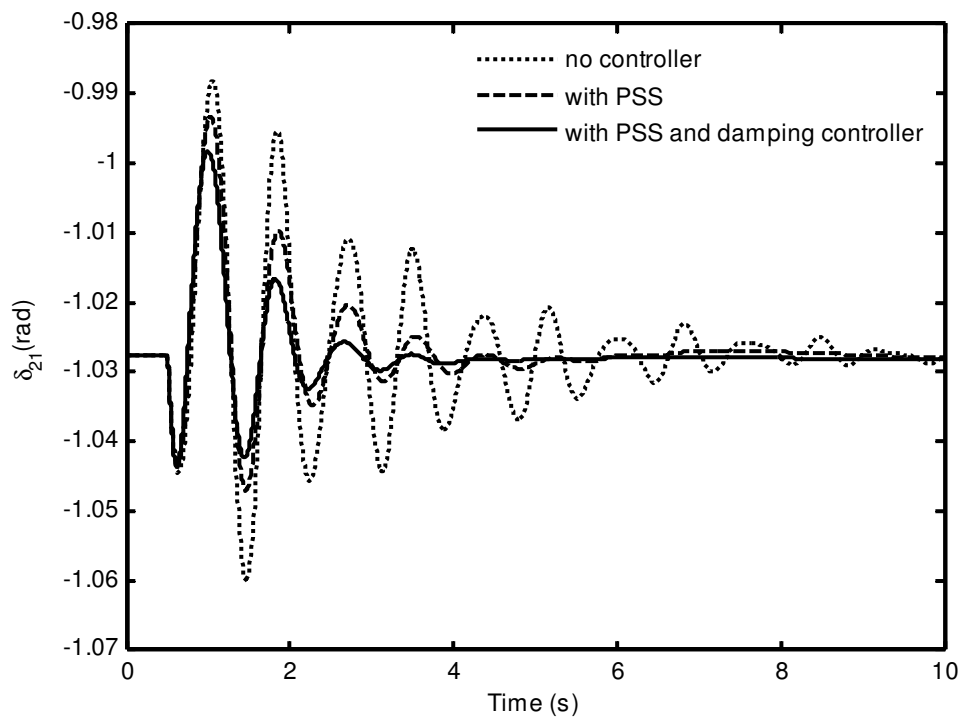


Figure 6.17: Relative rotor angle  $\delta_{21}$  response with three phase fault

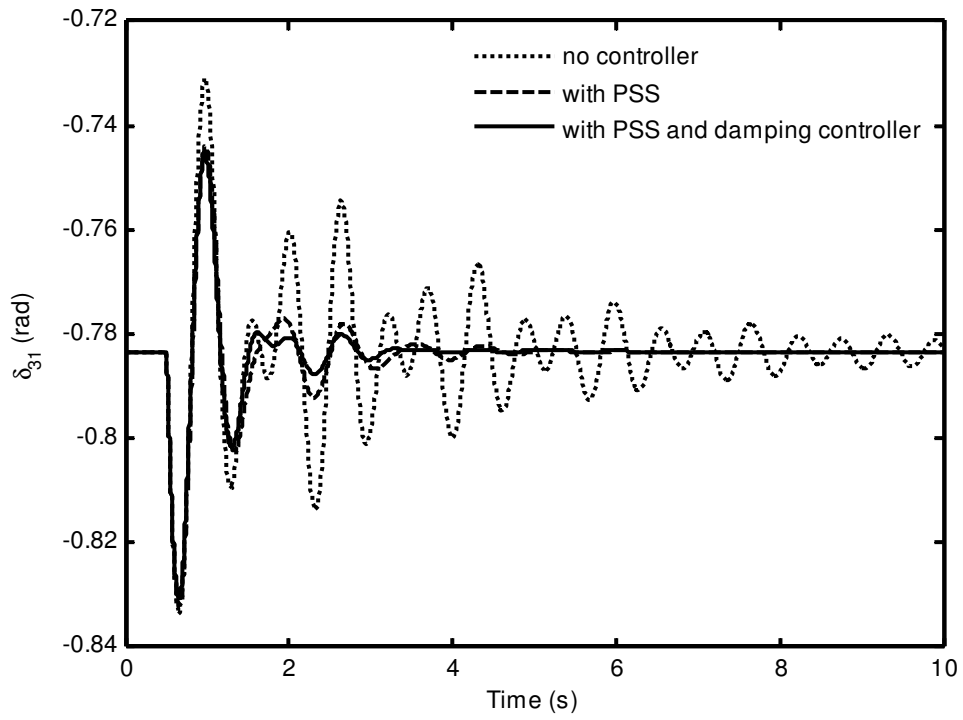


Figure 6.18: Relative rotor angle  $\delta_{31}$  response with three phase fault

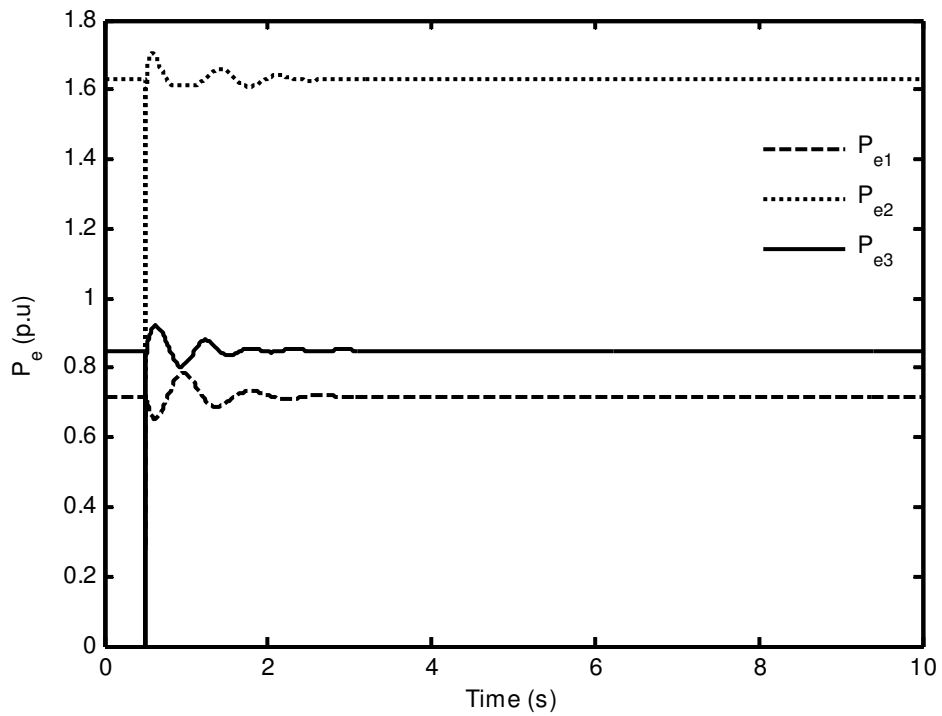


Figure 6.19: Electrical power generated response with three phase fault

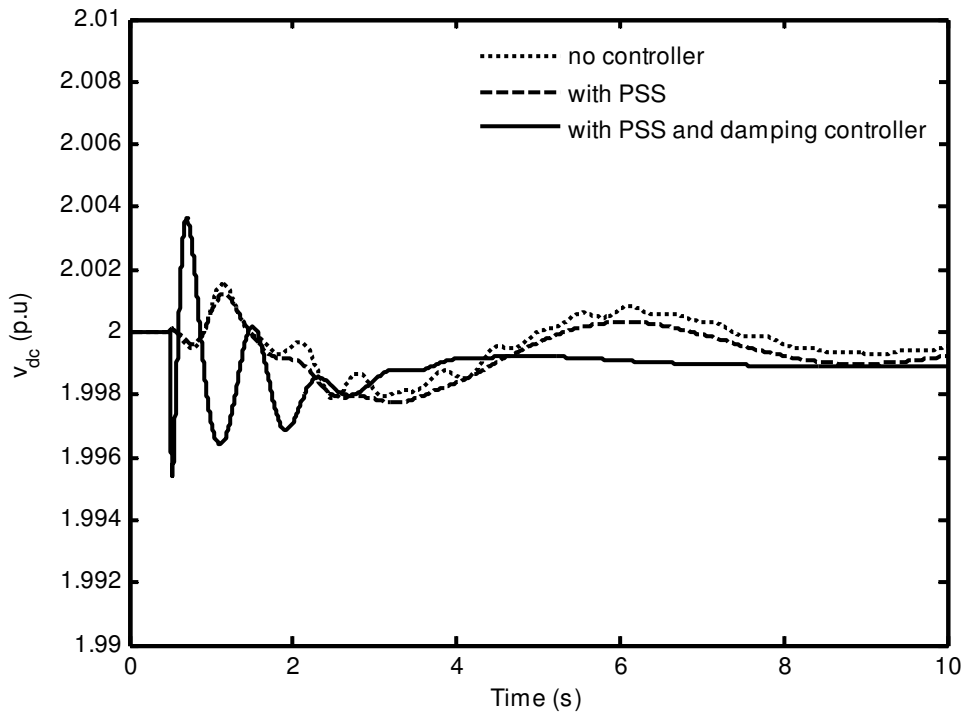


Figure 6.20: DC capacitor voltage response due to three phase fault

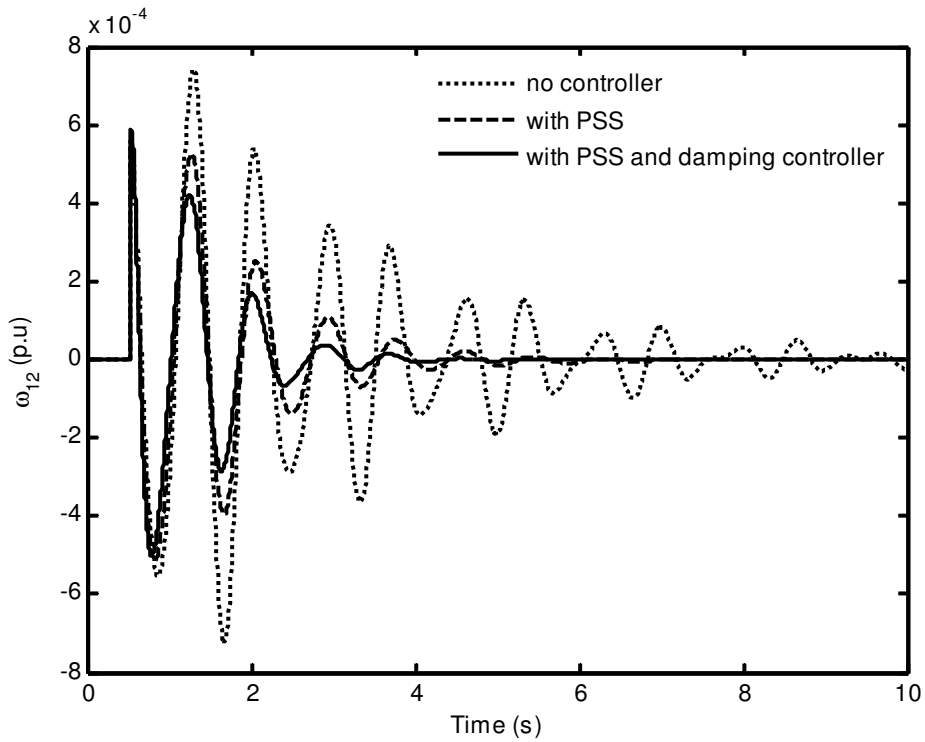


Figure 6.21: Relative rotor angle  $\omega_{12}$  response with three phase fault

### 6.5.3 Disturbance: Change in Power Flow Reference

The transmission line flows in IPFC branches can be controlled by changing the reference set point. Originally the real power flow in line 5 – 7 is 0.8432 p.u. and in line 8 – 7 is 0.7590 p.u. as shown in Table 6.1. An increase of 0.01 p.u. real power, i.e., 0.8532 p.u. can be made to flow in the transmission line 1 by changing the power reference  $P_{ji(ref)}$  to that value. Subsequently the real power flow set point in transmission line 2 is set to  $P_{ki(ref)} = 0.7490$  p.u. The change in power reference is given at 0.5s in the simulation. To obtain the desired power flow, gain scheduling of the concerned PI controller is normally required to achieve the desired change in power level. In the case, when a 0.01 p.u. change in power level is required, the gains  $k_{kp}$ ,  $k_{ki}$  are set to 0.6 and 0.4, respectively. The other parameters remain unchanged. The responses of various parameters (power flows in IPFC branches, relative rotor angles) are shown in Figures 6.22-6.26.

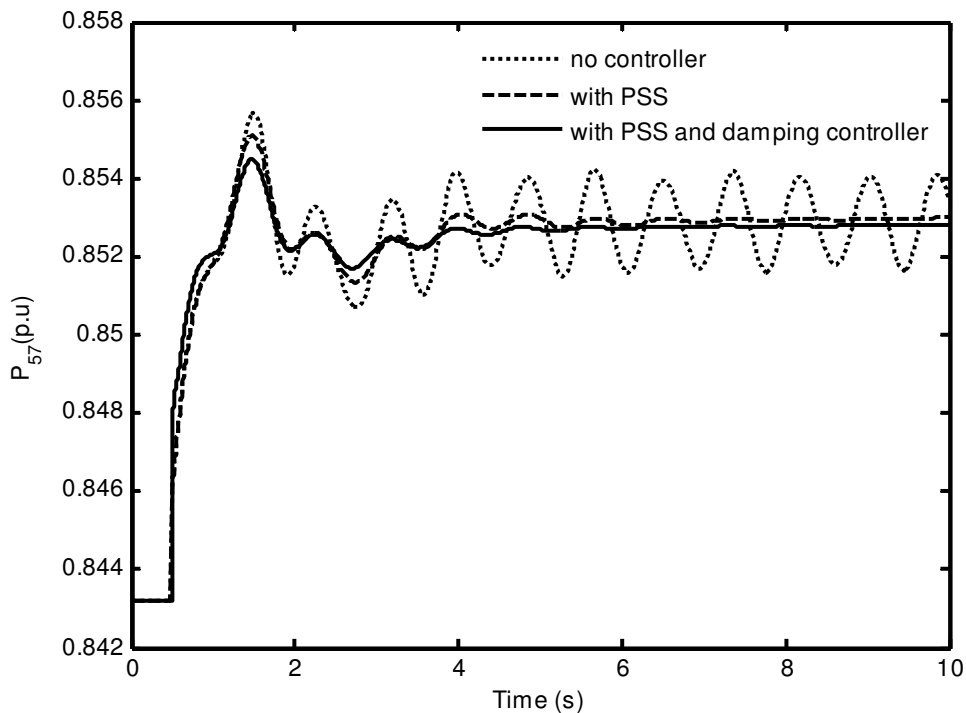


Figure 6.22: Real power flow response in IPFC branch 5 – 7 with change in power reference

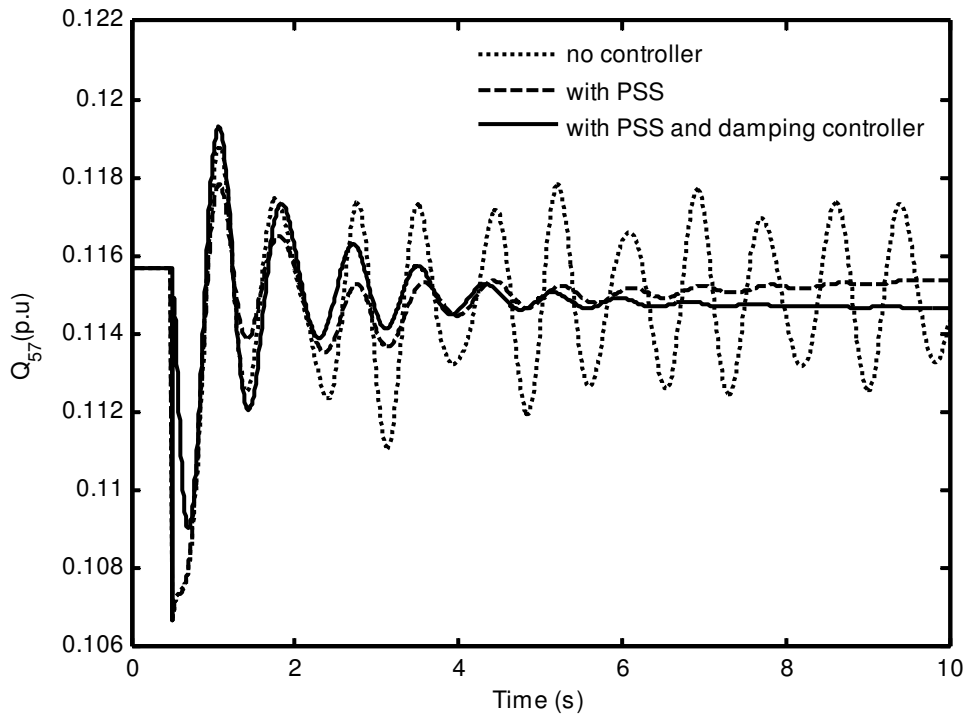


Figure 6.23: Reactive power flow response in IPFC branch 5 – 7 with change in power reference

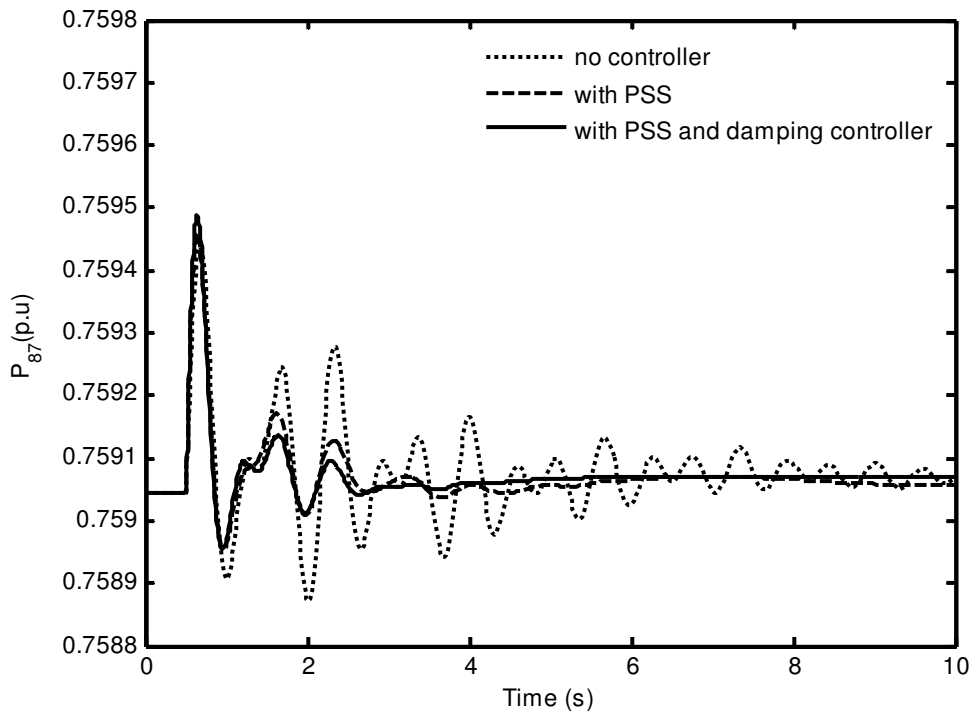


Figure 6.24: Real power flow response in IPFC branch 8 – 7 with change in power reference

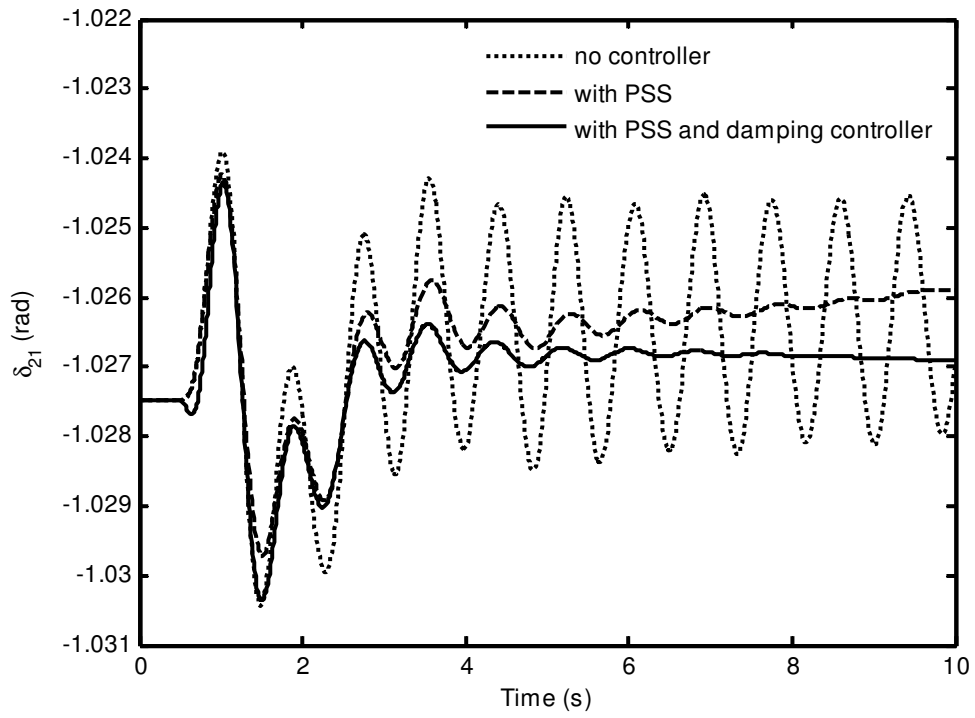


Figure 6.25: Relative rotor angle  $\delta_{21}$  response with change in power reference

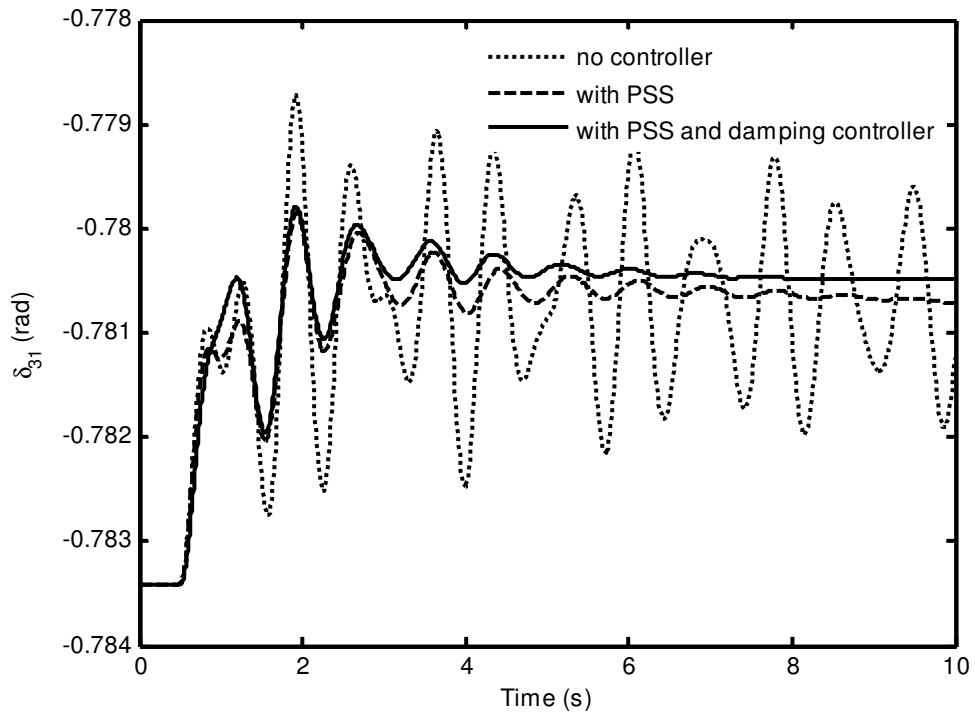


Figure 6.26: Relative rotor angle  $\delta_{31}$  response with change in power reference

It is observed from the above studies that the controllers ensure capable operation of the IPFC in controlling the power flow and damping oscillations in the transmission lines. The power flow controllers regulate the power flows and have minor contribution towards damping of oscillations. The damping is increased by IPFC POD controller.

## **6.6 Summary**

In this chapter, the nonlinear model of the multi-machine power system incorporated with IPFC has been developed. The linearized model of the multi-machine power system with IPFC is developed to form the Phillips-Heffron model. The oscillation modes having low damping ratio are determined by eigenvalue analysis from the Phillips-Heffron model. The IPFC POD controller is designed using the phase compensation method based on the linearized model to increase the damping of the concerned oscillation mode existing in the system.

The power flow controllers and DC voltage controller are incorporated in the IPFC control to regulate the power flow and to maintain the DC voltage across the DC link. The effectiveness and robustness of the IPFC controllers are validated through eigenanalysis and nonlinear simulation of the power system subjected to various disturbances. The IPFC based POD controller and PSS ensure reliable damping of the low frequency oscillations in the multi-machine power system with IPFC. The following chapter gives the thesis conclusions.

## CHAPTER 7

### CONCLUSION

#### **7.1 Conclusion**

Low frequency oscillations are inherent in the modern interconnected power system due to continuous disturbances. These oscillations occur as the synchronous generators oscillate against each other and have the frequency ranging from 0.1 to 2 Hz. These oscillations cause limitations on the amount of power that can be transmitted within the system and can also lead to widespread system disturbances if cascading outages of transmission lines occur due to oscillatory swings. Thus, insufficient damping of these oscillations leads to system instability and requires supplementary damping devices to mitigate them. As such, these oscillations must be considered in planning, operating and designing a power system.

Traditional approach to provide additional damping is with the use of PSS which is placed in the excitation system of the generator. PSS is designed using phase compensation method and taking the local generator speed signal as input. A relatively new solution is to use FACTS devices such as IPFC, for increasing damping of the power system oscillations in addition to performing their primary functions of controlling power flow in the transmission lines. IPFC is a multi-line voltage-sourced converter-based FACTS device. It facilitates both real and reactive power compensation among the transmission lines thus, allowing improved transmission system operation. The primary focus in this thesis is on employing the Interline Power Flow Controller (IPFC) to damp low frequency oscillations.

Several studies are involved in investigating the low frequency oscillations. These include load flow studies, small signal stability studies, and nonlinear simulation. The load flow is used to initialize the nonlinear simulation and small signal stability studies for which the steady state model of the power system with the IPFC is

required. The small signal stability study involves the linearization of nonlinear dynamic model of the power system and eigenvalue analysis. The dynamic model represents the synchronous generators, loads, network and IPFC dynamics by differential and algebraic equations which are linearized at an operating point given by load flow studies. The eigenvalue analysis gives the eigenvalues, eigenvectors, participation factors, natural, damped frequencies, and damping ratio. The oscillation modes with precise indication of oscillation frequency and damping, primarily affecting the stability problem may be identified, with which appropriate action should be taken. The nonlinear simulation of the power system verifies the eigenvalue analysis.

## **7.2 Achievements of Research Objectives**

The steady-state and dynamic models of IPFC have been established in this thesis. For power flow studies, the steady state model of IPFC is incorporated with the power system network. The algorithm given only for IPFC branches is implemented into a full Newton-Raphson load flow program for the complete system incorporated with IPFC. The program is written in Matlab. The solution of the load flow gives the steady state operating point for stability studies. The  $d - q$  axis dynamic model of IPFC has been developed incorporating DC link dynamics for stability studies. This model includes all the four control signals of IPFC.

The overall dynamic model of the power system incorporating IPFC is formulated by augmenting the models of the various components of system, with IPFC and interfacing the network equations with the machine reference frame. Using this approach, the nonlinear dynamic models for a single-machine infinite bus (SMIB) and multi-machine power system incorporating IPFC are developed to study power system oscillations.

Further the linearized Phillips-Heffron model of power system with IPFC is developed. Oscillation modes are identified by eigenvalue analysis. In multi-machine power system, the factors associated with each eigenvalues are revealed by participation factors. This provides valuable information to identify the generators

that may experience oscillations. PSS is placed at the generators according to the participation factors to enhance damping of a system. The dynamic performances of the proposed modeling of power system incorporating IPFC is examined and verified through eigenvalue analysis as well as nonlinear simulations.

The proposed control strategy for IPFC has three major components: first is the control of the real and the reactive power flows on transmission lines where IPFC is located which is the primary function of the FACTS device, the second is that of controlling the DC link capacitor voltage to a constant value to ensure balanced power exchange between the VSCs of IPFC (loss of DC voltage during disturbances could lead to instability) and the third is the damping controller to enhance the damping of the oscillations. PI controllers are used to control the power flow and DC link capacitor voltage. The parameters of PI controllers are determined using simulation response. However, tuning the parameters of the power flow controllers is not the main scope of this work.

A lead-lag damping controller is designed based on the linearized Phillips-Heffron model of the power system to increase damping of the un-damped oscillation modes. The control signal(s) suitable for providing damping is determined using a controllability index. The output of the controller is superimposed on the input signal of IPFC thus, varying the magnitude and phase angle of the injected voltage into the transmission line which controls the power flow in such a way to dampen the power system oscillations. Local measurements such as the real power flow deviation in the transmission line are taken as the input to the damping controller as the IPFC is normally installed on the transmission lines that are away from any generator.

Case studies on SMIB and three-machine nine-bus (WSCC) power system have been carried out. PSS and IPFC based damping controller is designed using phase compensation method. The effectiveness of the controllers in controlling the power flow and in damping the oscillations is examined and verified through eigenvalue analysis and nonlinear simulations under different disturbances.

The work in this thesis includes a complete control system design for IPFC and studying its performance. Power flow calculations and dynamic simulation studies

demonstrate the potential of the IPFC in increasing the power transfer capability of transmission system and enhancing power system stability.

### **7.3 Contributions of Research**

The main contributions of this research are summarized as follows:

- 1) Development of the load flow program in Matlab for load flow analysis of the complete power system incorporating IPFC:

The steady state model of the IPFC is utilized to integrate it into the power system network equations for load flow studies. The load flow program gives the operating point around which the power system nonlinear equations are linearized.

- 2) Modeling of IPFC for dynamic stability studies:

This work demonstrates the steps taken in developing a mathematical model of IPFC for dynamic stability study. This dynamic model of IPFC is used to incorporate it with the power system model to develop one complete dynamic model for stability analysis.

- 3) Modeling of power system incorporated with IPFC:

The nonlinear models of SMIB and multi-machine power system with IPFC have been developed. The nonlinear equations are linearized at an operating point to obtain the linearized Phillips-Heffron state space model of the power system. Eigenvalue analysis is performed to identify oscillation modes from the linearized model.

- 4) Investigations on the control functions of IPFC and its effect on the system oscillations:

A conventional lead-lag damping controller is designed based on linearized model to increase the damping of the oscillations. The performance of the controller to different dynamic states in enhancing the damping of the oscillatory

modes is confirmed through detailed eigenvalue analysis and nonlinear simulation.

#### **7.4 Suggestions for Future Work**

In summary this research work presents the load flow formulation, nonlinear dynamic models, linearized models, damping control design and stability analysis for the power system incorporated with IPFC.

Low frequency oscillations when present in a power system, limits the amount of power transfer on the tie-lines between the regions containing the groups of coherent generators. Damping of these oscillations contributes to the enhancement of the stability limits of the system, signifying greater power transfer through the system. The application of IPFC based damping controller to satisfy different end goals, namely the damping of local *and* inter-area modes over a broad range of operating points in a multi-area power system, has to be investigated. Torsional modes were also not accounted for in the analysis. In modern power systems, apart from a large number of generators and associated controllers, there are many types of load, ranging from a simple resistive load to more complicated loads with electronic controllers. Thus, there are other areas for future research in investigating the control functions of IPFC and their effects on damping power system oscillations considering the facts mentioned above.

PI controllers have been used for power flow control. However the gains of these controllers have been designed at one operating point. It generally requires gain scheduling for different operating conditions in the system. Conventional lead-lag damping controller is proposed in this thesis. Alternative control strategies such as fuzzy logic and adaptive control could be explored for more robust control.

## REFERENCES

- [1] L. L. Grigsby, *Electric Power Engineering Handbook: Power System Stability and Control*, Second ed: CRC Press, Taylor & Francis Group, 2007.
- [2] P. Kundur, *Power System Stability and Control*. New York: McGraw-Hill, 1994.
- [3] J. Machowski, J. W. Bialek, and J. R. Bumby, *Power System Dynamics: Stability and Control*, Second ed: John Wiley & Sons, Ltd., 2008.
- [4] G. Roger, *Power System Oscillations*: Kluwer Academic Publishers, Massachusetts, 2000.
- [5] D. N. Kosterev, C. W. Tylor, and W. A. Mittelstadt, "Model Validation for the August 10, 1996 WSCC System Outage," *IEEE Trans. on Power Systems*, vol. 14, no. 33, pp. 967-979, August 1999.
- [6] "U.S.-Canada Power System Outage Tack Force: Final Report on the August 14, 2003 Blackout in the United States and Canada (on line)," <http://www.pserc.wisc.edu/BlackoutFinal-Web.pdf>.
- [7] F. P. DeMello and C. Concordia, "Concepts of Synchronous Machine Stability as Affected by Excitation Control," *IEEE Trans. on Power Apparatus and Systems*, vol. 88, pp. 316-329, April, 1969.
- [8] E. V. Larsen and D. A. Swann, "Applying Power System Stabilizer, Part I-III," *IEEE Trans on Power Apparatus and Systems*, vol. PAS 100, 1981.
- [9] Y. H. Song and A. T. Johns, *Flexible AC Transmission systems*: IEE Power and Energy series 30, 1999.
- [10] A. A. Edris and et.al., "Proposed terms and definitions for flexible ac transmission system (FACTS)," *IEEE Trans. on Power Delivery*, vol. 12, no. 4, Oct. 1997.
- [11] X.-P. Zhang, C.Rehtanz, and B. Pal, *Flexible AC Transmission Systems: Modelling and Control*: Springer, 2006.
- [12] N. G. Hingorani and L. Gyugyi, *Understanding FACTS Concepts and Technology of Flexible AC Transmission Systems*: Wiley-Interscience, IEEE Press, A John Wiley & Sons, Inc., 2000.

- [13] R. M. Mathur and R. K. Varma, *Thyristor-Based FACTS Controllers for Electrical Transmission Systems*: Wiley Interscience, IEEE Press, A John Wiley & Sons, Inc., 2002.
- [14] E. Acha, C. R. Fuerte-Esquivel, H. Ambriz-Perez, and C. Angeles-Camacho, *FACTS Modelling and Simulation in Power Networks*: John Wiley & Sons, Ltd., 2004.
- [15] L. Gyugyi, K. K. Sen, and C. D. Schauder, "The Interline Power Flow Controller Concept: A New Approach to Power Flow Management in Transmission Systems," *IEEE Trans. on Power Delivery*, vol. 4, No. 3, pp. 115-1123, 1998.
- [16] P. M. Anderson and A. A. Fouad, *Power System Control and Stability*, Second ed: A John Wiley & Sons, Inc., Publication, 2003.
- [17] P. W. Sauer and M. A. Pai, *Power System Dynamics and Stability*. New Jersey: Prentice-Hall, Inc., 1998.
- [18] W. G. Heffron and R. A. Phillips, "Effect of a modern amplidyne voltage regulator on under excited operation of large turbine generator," *AIEE Trans.*, vol. 71, 1952.
- [19] P.Kunder, M.Klein, G.J.Roger, and M.S.Zywno, "Application of power system stabilizers for enhancement of overall system stability," *IEEE Trans. on Power System*, vol. 2, 1989.
- [20] J. H. Chow and J. J. Sanchez-Gasca, "Pole-placement Designs of Power System Stabilizers," *IEEE Trans. on Power Systems*, vol. 4, no. 1, pp. 271-277, 1989.
- [21] R. Gupta, B. Bandyopadhyay, and A. M. Kulkarni, "Design of power system stabilizer for single machine system using robust fast output sampling feedback technique," *Electric Power Systems Research*, vol. 65, pp. 247-257, 2003.
- [22] Hardiansyah, S. Furuya, and J. Irisawa, "A robust  $H_{\infty}$  power system stabilizer design using reduced-order models," *Electrical Power and Energy Systems*, vol. 28, pp. 21-28, 2006.
- [23] H. Guo-qiang, X. Dong-jie, and H. Ren-mu, "Genetic Algorithm Based Design of Power System Stabilizers," in *IEEE International Conference on*

*Electric Utility Deregulation, Restructuring and Power Technologies (DRPT2004)*. Hong Kong, April 2004.

- [24] P. S. Rao and I. Sen, "Robust Tuning of Power System Stabilizers Using QFT," *IEEE Trans. on Control Systems Technology*, vol. 7, no.4, July 1999.
- [25] Z. Barton, "Robust control in a multimachine power system using adaptive neuro-fuzzy stabilisers," *IEE Proc.-Gener. Transm. Distrib.*, vol. 151, March 2004.
- [26] M. Klein, G. J. Rogers, S. Moorthy, and P. Kundur, "Analytical investigation of factors influencing power system stabilizers performance," *IEEE Trans. on Energy Conversion*, vol. 7, no.3, September 1992.
- [27] G. P. Chen, O. P. Malik, Y. H. Qin, and G. Y. Xu, "Optimization Technique for the Design of a linear optimal power system stabilizer," *IEEE Trans. on Energy Conversion*, vol. 7, no. 3, September, 1992.
- [28] M. E. Aboul-Ela, A. A. Sallam, J. D. M. Calley, and A. A. Fouad, "Damping Controller Design for Power System Oscillations Using Global Signals," *IEEE Trans. on Power Systems*, vol. 11, no.2, pp. 767-773, May 1996.
- [29] E. V. Larsen, J. S. Gasca, and J. H. Chow, "Concepts for design of FACTS controllers to damp power swings," *IEEE Trans. on Power System*, vol. 10, no. 2, pp. 948-956, May 1995.
- [30] H.F.Wang and J. F, Swift, "Application of the Phillips-Heffron model in the analysis of the damping torque contribution to power systems by SVC damping control," *Electrical Power and Energy Systems*, vol. 18, no. 5, pp. 307 313, 1996.
- [31] J. F, Swift, H.F.Wang, and, "Application of the Controllable Series Compensator in damping power system oscillations," *IEE Proc. Part C*, No.4, May 1996.
- [32] H.F.Wang and F.J.Swift, "An unified model for the analysis of FACTS devices in damping power system oscillations Part I: single-machine infinite-bus power systems," *IEEE Trans. on Power Delivery*, No.2, 1997.
- [33] H.F.Wang, F.J.Swift, and M. Li, "A unified model for the analysis of FACTS devices in damping power system oscillations part II: multi-machine power systems," *IEEE Trans. on Power Delivery*, No.4, 1998.

- [34] H.F.Wang, "Phillips-Heffron model of power systems installed with STATCOM and applications," *IEE Proc. Part C*, No.5, 1999.
- [35] H.F.Wang, "Design of SSSC Damping Controller to Improve Power System Oscillation Stability," in *AFRICON*, vol. 1, 1999, pp. 495-500.
- [36] H.F.Wang, "Damping function of Unified Power Flow Controller," *IEE Proc. Part C*, No.1, 1999.
- [37] H.F.Wang, "A unified model for the analysis of FACTS devices in damping power system oscillations part III: unified power flow controller," *IEEE Trans. on Power Delivery*, No.3, 2000.
- [38] H.F.Wang, "Applications of modelling UPFC into multi-machine power systems," *IEE Proc. Part C*, No.3, 1999.
- [39] H.F.Wang and F.J.Swift, "Capability of the Static Var Compensator in damping power system oscillations," *IEE Proc-Gener. Transm. Distrib.*, vol. 143, no. 4, July 1996.
- [40] Y. Yuan, L. Cheng, Y. Sun, and G. Li, "Placement of SVCs and Selection of Stabilizing Signals Based on Observability and Controllability," in *Conversion and Delivery of Electrical energy in the 21<sup>st</sup> century: Power and Energy Society General Meeting*, 20-24 July 2008, pp. 1-7.
- [41] M. M. Farsangi, H. Nezamabadi-pour, Y.-H. Song, and K. Y. Lee, "Placement of SVCs and Selection of Stabilizing Signals in Power Systems," *IEEE Trans. on Power Systems*, vol. 22, no. 3, August 2007.
- [42] E. V. Larsen and J. H. Chow, "SVC control design concepts for system dynamic performance," *IEEE Special Publications: Application of Static VAR Systems for System Dynamic Performance*, pp. 36-53, 1987.
- [43] Q. Zhao and J. Jiang, "Robust SVC controller design for improving power system damping," *IEEE Trans. Energy Conversion*, vol. 10, pp. 201-209, June 1995.
- [44] N. Martins and L. T. G. Lima, "Determination of suitable locations for power system stabilizers and Static VAR Compensators for damping electromechanical oscillations in large scale power systems," *IEEE Trans. Power System*, vol. 5, pp. 1455-1469, November 1990.

- [45] P. Pourbeik and M. J. Gibbard, "Damping and synchronizing torques induced on generators by FACTS stabilizers in multimachine power systems," *IEEE Trans. Power System*, vol. 11, pp. 1920-1925, November 1996.
- [46] S. E. M. D. Oliveira, "Synchronizing and damping torque coefficients and power system steady-state stability as affected by static VAR compensators," *IEEE Trans. Power System*, vol. 9, pp. 109-119, February 1994.
- [47] B. Chaudhuri and B. C. Pal, "Robust damping of multi swing modes employing global stabilizing signals with a TCSC," *IEEE Trans. on Power Systems*, vol. 19, no. 1, pp. 499-505, February 2004.
- [48] S. Panda, "Differential evolutionary algorithm for TCSC-based controller design," *Simulation Modelling Practice and Theory*, vol. 17, pp. 1618-1634, 2009.
- [49] B. K. Kumar, S. N. Singh, and S. C. Srivastava, "A Modal Controllability Index for Optimal Placement of TCSC to Damp Inter-Area Oscillations," in *IEEE Power Engineering Society General Meeting*, vol. 2, 112-116 June, 2005.
- [50] Y. J. Lin and K. L. Lo, "Improvement of power systems damping using genetic algorithms aided proportional plus derivative output feedback for TCSC," *The International Journal for Computation and Mathematics in Electrical and Electronic Engineering*, vol. 21, no. 2, pp. 208-222, 2002.
- [51] D. Z. Fang, Y. Xiaodong, S. Wennan, and H. F. Wang, "Oscillation transient energy function applied to the design of a TCSC fuzzy logic damping controller to suppress power system interarea mode oscillations," *IEE Proc.-Gener.Transm. Distrib.*, vol. 150, no 2, March 2003.
- [52] H. F. Wang, F. J. Swift, and M. Li, "Analysis of thyristor-controlled phase shifter applied in damping power system oscillations," *Electrical Power and Energy Systems*, vol. 19, no. 1, pp. 1-9, 1997.
- [53] H.F.Wang and F. Li, "Design of STATCOM multivariable sampled regulator," in *IEEE conference on Electric Utility Deregulation and Restructuring and Power Technologies*, 4-7 April 2000, pp. 1-6.
- [54] S. M. Bamasak and M. A. Abido, "Robust coordinated design of PSS & STATCOM controllers for damping power system oscillation," in *15th Power System Computation Conference*. Liege, August 2005, pp. 22-26.

- [55] L. Chun, J. Qirong, and W. Zhonghong, "Study of STATCOM Control for Power Swings Damping Improvement," in *International Conference on Power System Technology, PowerCon*, 4-7 Dec., 2000, pp. 535-540.
- [56] L. O. Mak, Y. X. Ni, and C. M. Shen, "STATCOM with fuzzy controllers for interconnected power systems," *Electric Power Systems Research*, vol. 55, pp. 87-95, 2000.
- [57] A.A.Gharaveisi, A. Hakimi, and S. M. R. Rafiei, "Power System Stability Enhancement via STATCOM Supplementary Control Based on Fuzzy Energy Function," in *IEEE Bucharest Power Tech Conference*. Bucharest, Romania, 2009.
- [58] X. Xie, J. Li, J. Xiao, and Y. Han, "Inter-Area Damping Control of STATCOM using Wide-Area Measurements," in *IEEE International Conference on Electric Utility Deregulation, Restructuring and Power Technologies (DWT2004)*, April 2004, Hong Kong.
- [59] R. K. Pandey and N. K. Singh, "Optimal Power Oscillation Damping with SSSC," in *IEEE Region 10 Conference, TENCON*, 2008.
- [60] L. Juan, D. Sheng, and Z. Xingfu, "A nonlinear control approach to increase power oscillations damping by SSSC," in *International Conference on Computer and Electrical Engineering: IEEE Computer Society* Washington DC, USA, 2008.
- [61] J. Chen, T. T. Lie, and D. M. Vilathgamuwa, "Enhancement of power system damping using VSC-based series connected FACTS controllers," *IEE Proc. Gener. Transm. Distrib*, vol. 150, no.3, pp. 353-359, May 2003.
- [62] J. Ghaisari, A. Bakhshai, and P. K. Jain, "A Nonlinear Control Approach to Increase Power Oscillations Damping by Means of the SSSC," in *IEEE, Power Engineering Society General Meeting*, vol. 2, 2005, pp. 1601-1608.
- [63] V. K. Chandrasekhar and A. G. Kothari, "Fuzzy logic based static synchronous series compensator (SSSC) for transient stability improvement," in *IEEE International Conference on Electric Utility Deregulation, Restructuring and Power Technologies, (DRPT2004)*, vol. 1, 5-8 April, 2004, pp. 240-245.

- [64] B. Geethalakshmi, T. Hajmunnisa, and P. Dananjayan, "A Fuzzy Logic Controller for Enhancing the Transient Stability of 48-Pulse Inverter Based SSSC," *Elektrika*, vol. 10, no.2, pp. 53-58, 2008.
- [65] S.Kannan, S.Jayaram, and M.M.A.SaLma, "Fuzzy Logic based supplementary controller for Static Synchronous Series Compensator," in *IEEE Canadian Conference on Electrical and Computer Engineering (CCECE)*, 1998, vol. 2. Waterloo, Ont., Canada, 24-28 May 1998, pp. 489-492.
- [66] M. Ladjavardi and M. A. S. Masoum, "Application of Multi-Objective Genetic Algorithm for Optimal Design of SSSC Based Robust Damping Controllers to Improve Small Signal Stability," in *Power Systems Conference and Exposition, PSCE: IEEE PES*, 2006, pp. 2124-2130.
- [67] M. H. Haque, "Determination of Additional Damping Provided by a SSSC through Evaluation of Rate of Dissipation of Transient Energy," in *International Conference on Power System Technology - POWERCON 2004*. Singapore, 21-24 November 2004.
- [68] M. H. Haque, "Damping improvement by FACTS devices: A comparison between STATCOM and SSSC," *Electric Power Systems Research*, vol. 76, pp. 865-872, 2006.
- [69] J. Ghaisari, A. Bakhshai, and P. K. Jain, "Power oscillations damping by means of the SSSC: A multivariable control approach," in *Canadian Conference on Electrical and Computer Engineering on Power Systems*. Saskatoon, May 2005, pp. 2249-2252.
- [70] A. Nabavi-Niaki and M. R. Iravam, "Steady-state and dynamic models of unified power flow controller (UPFC) for power system studies," *IEEE Trans. on Power Systems*, vol. 4, no.11, pp. 1937-1943, 1996.
- [71] M. R. Meshkatoddini, M. Majidi, M. Sadeghierad, and H. Lesani, "Comparison of UPFC-Based Stabilizer and PSS Performances on Damping of Power System Oscillations," *American Journal of Applied Sciences*, vol. 6, no. 3, pp. 401-406, 2009.
- [72] H. Zhengyu, N. Yinxin, C. M. Shen, F. F. Wu, C. Shousun, and Z. Baolin, "Application of unified power flow controller in interconnected power systems-modeling, interface, control strategy, and case study," *IEEE Trans. Power Systems*, vol. 15, no. 2, pp. 817-824, May 2000.

- [73] N. Tambey and M. L. Kothari, "Damping of power system oscillations with unified power flow controller (UPFC)," *IEE Proc. Gen. Tran. & Distr.*, vol. 150, no.2, pp. 129-140, 2003.
- [74] M. L. Kothari and N. Tambey, "Design of UPFC Controllers for a Multimachine System," *IEEE Power Systems Conference and Exposition*, 10-13 October 2004, pp. 1483-1488.
- [75] R. K. Pandey and N. K. Singh, "UPFC control parameter identification for effective power oscillation damping," *Electrical Power and Energy Systems*, vol. 31, pp. 269-276, 2009.
- [76] C.-T. Chang and Y.-Y. Hsu, "Design of UPFC controllers and supplementary damping controller for power transmission control and stability enhancement of a longitudinal power system," *IEE Proc. Gener. Transm. Distrib.*, vol. 149, no. 4, July 2002.
- [77] M. A. Abido, A. T. Al-Awami, and Y. L. Abdel-Magid, "Simultaneous Design of Damping Controllers and Internal Controllers of a Unified Power Flow Controller," *IEEE Power Engineering Society General Meeting*, 2006.
- [78] S. N. Dhurvey and V. K. Chandrakar, "Performance Comparison Of UPFC In Coordination With Optimized POD And PSS On Damping Of Power System Oscillations," *WSEAS Trans. on Power Systems*, vol. 3, May 2008.
- [79] V.K.Chandrakar and A.G.Kothari, "RBFN Based Unified Power Flow Controller (UPFC) for Improving transient stability performance," *WSEAS Trans. on power systems*, vol. 2, no. 1, pp. 1-6, Jan, 2007.
- [80] A. M. Dejamkho, M. Banejad, and N. Talebi, "Fuzzy Logic Based UPFC Controller for Damping Low Frequency Oscillations of Power Systems," in *2nd IEEE International Conference on Power and Energy (PECON 08)*. Johor Baharu, Malaysia, December 1-3, 2008.
- [81] A. A. Eldamaty, S. O. Faried, and S. Aboreshaid, "Damping power system oscillations using a fuzzy logic based unified power flow controller," in *IEEE Candian Conference on Electrical and Computer Engineering*, 1-4 May 2005, pp. 1950-1953.
- [82] T. K. Mok, H. Liu, Y. Ni, F. F. Wu, and R. Hui, "Tuning the fuzzy damping controller for UPFC through genetic algorithm with comparison to the

- gradient descent training," *Electrical Power and Energy Systems*, vol. 27, pp. 275-283, 2005.
- [83] T. K. Mok, Y. Ni, and F. F. Wu, "Design of Fuzzy Damping Controller of UPFC through Genetic Algorithm," in *IEEE Power Engineering Society Summer Meeting*, vol. 3. Seattle, WA, USA, 2000, pp. 1889-1894.
- [84] S.Mishra, P. K.Dash, and G.Panda, "TS-fuzzy controller for UPFC in a multimachine power system," *IEE Proc.-Gener. Transm. Distrib.*, vol. 147, no.1, January 2000.
- [85] B. Fardanesh, M. Henderson, B. Shperling, S. Zelingher, L. Gyugyi, C. Schauder, B. Lam, J. Moundford, R. Adapa, and A. Edris, "Convertible static compensator: Application to the New York transmission system," presented at CIGRE, Paris, France, September 1998.
- [86] B. Fardanesh and A. Schuff, "Dynamic Studies of the NYS Transmission System With the Marcy CSC in the UPFC and IPFC Configurations," *IEEE Transmission and Distribution Conference and Exhibition*, vol. 3, pp. 1175-1179, 2003.
- [87] L. T. Hochberg, M. R. Graham, and L. Hopkins, "NYPA Marcy FACTS Project - Phase II Convertible Static Compensator (CSC) Marcy Inter-line Power Flow Controller (IPFC) Stability Study," NEW YORK POWER AUTHORITY OPERATIONS PLANNING, February 12, 2003.
- [88] V. Diez-Valencia, U. D. Annakkage, D. Jacobson, A. M. Gole, and P. Demchenlko, "Interline power flow controller (IPFC) steady state operation," *IEEE Canadian Conference on Electrical and Computer Engineering (CCECE)*, vol. 1, pp. 280 - 284, 12-15 May 2002.
- [89] J. Chen, T. T. Lie, and D. M. Vilathgamuwa, "Basic Control of Interline Power Flow Controller," in *IEEE Power Engineering Society Winter Meeting*, vol. 1, 2002, pp. 521-525.
- [90] S. Sankar and S. Ramareddy, "Simulation of series and shunt compensated IPFC system," in *IET-UK International Conference on Information and Communication Technology in Electrical Sciences (ICTES 2007)*, Dec. 20-22, 2007, pp. 485-488.

- [91] R. Strzelecki, G. Benysek, and Z. Fedyczak, "Interline power flow controller-probabilistic approach," in *IEEE 33rd Annual Power Electronics Specialists Conference*, vol. 2, 23-27, June 2002, pp. 1037 - 1042.
- [92] S. Teerathana and A. Yokoyama, "An optimal power flow control method of power system using interline power flow controller (IPFC)," in *TENCON 2004. IEEE Region 10 Conference*, vol. 3, 21-24 Nov. 2004, pp. 343 - 346.
- [93] X. Wei, J. H. Chow, B. Fardanesh, and A.-A. Edris, "A common modeling framework of voltage-sourced converters for loadflow, sensitivity, and dispatch analysis," in *IEEE Power Engineering Society General Meeting*, vol. 4, July 2003, pp. 13-17.
- [94] X. Wei, J. H. Chow, B. Fardanesh, and A. A. Edris, "A dispatch strategy for an interline power flow controller operating at rated capacity," in *IEEE Power Systems Conference and Exposition*, vol. 3, 10-13 Oct. 2004, pp. 1459 - 1466.
- [95] J. Zhang and A. Yokoyama, "A Comparison between the UPFC and the IPFC in Optimal Power Flow Control and Power Flow Regulation," *38th North American Power Symposium( NAPS)*, 2006., pp. 339 - 345, Sept. 2006.
- [96] X. Wei, J. H. Chow, B. Fardanesh, and A. Edris, "A common modeling framework of voltage sourced converters for load flow, sensitivity and dispatch analysis," *IEEE Trans. Power System*, vol. 19, no.2, pp. 934-941, May 2004.
- [97] X. P. Zhang, " Modelling of the interline power flow controller and generalized unified power flow controller in Newton power flow," *IEE Proc-Generation Transm. Distrib.*, vol. 150, pp. 268-274, 2003.
- [98] X. P. Zhang, "Robust modeling of the interline power flow controller and the generalized unified power flow controller with small impedances in power flow analysis," *Electrical Engineering*, vol. 89, pp. 1-9, 2006.
- [99] Z. Yankui, Z. Yan, and C. Chen, "A Novel Power Injection Model of IPFC for Power Flow Analysis Inclusive of Practical Constraints," *IEEE Trans. on Power Systems*, vol. 21, no. 4, pp. 1550-1556, Nov. 2006.
- [100] A. Kazemi and E. Karimi, "The Effect of Interline Power Flow Controller (IPFC) on Damping Inter-area Oscillations in the Interconnected Power Systems," *IEEE International Symposium Industrial Electronics, 2006*, vol. 3, pp. 1911 - 1915, July 2006.

- [101] X. Jiang, X. Fang, J. H. Chow, A.-A. Edris, and E. Uzunovic, "Regulation and Damping Control Design for Interline Power Flow Controllers," *IEEE Power Engineering Society General Meeting*, June 2007, pp.1-8.
- [102] J. Chen, T. T. Lie, and D. M. Vilathgamuwa, "Design of an interline power flow controller.," in *14<sup>th</sup> Power Systems Computation Conference*. Sevilla Spain, 24-28, June 2002.
- [103] M. A. Pai, D. P. Sen Gupta, and K. R. Padiyar, *Small Signal Analysis of Power Systems*. U.K: Alpha Science International Ltd., 2004.
- [104] Y. N. Yu, *Electric Power System Dynamics*: Academic Press, 1983.
- [105] P. Kundur and L. Wang, "Small signal stability analysis: experience, achievements, and challenges," in *International Conference on Power System Technology Proceedings*, vol. 1, 2002, pp. 6 -12.

## LIST OF PUBLICATIONS

### Journal Paper

- 1) A. M. Parimi, I. Elamvazuthi, N. Saad, “Interline Power Flow Controller Application for Low Frequency Oscillations Damping”, *WSEAS Trans. on Systems*, Issue 5, vol. 9, May 2010, pp. 511-527.

### Conference Papers

- 2) A. M. Parimi, I. Elamvazuthi, N. Saad, “Interline Power Flow Controller (IPFC) based damping controllers for damping low frequency oscillations in a power system,” *IEEE International Conference on Sustainable Energy Technologies*, 24-27, Nov. 2008, pp. 334 – 339.
- 3) A. M. Parimi, I. Elamvazuthi, N. Saad, “Damping of inter area oscillations using Interline Power Flow Controller based damping controllers,” *IEEE 2nd International Power and Energy Conference*, 1-3 Dec. 2008, pp. 67 – 72.
- 4) A. M. Parimi, N. C. Sahoo, I. Elamvazuthi, N. Saad, “Dynamic modeling of Interline Power Flow Controller for small signal stability” *IEEE International Conference on Power and Energy*, 2010, pp. 583 – 588.
- 5) A. M. Parimi, N. C. Sahoo, I. Elamvazuthi, N. Saad, “Transient Stability Enhancement and Power Flow Control in a Multi-Machine Power System Using Interline Power Flow Controller” accepted in *IEEE International Conference on Energy, Automation and Signal*, Dec. 2011.

## APPENDIX A

## APPENDIX A

### JACOBIAN TERMS OF THE POWER FLOW WITH IPFC

$$\begin{aligned}
 \frac{\partial P_{ji}}{\partial \theta_1} &= V_j V_{se1} (g_{ij} \sin(\theta_j - \theta_1) - b_{ij} \cos(\theta_j - \theta_1)) \\
 \frac{\partial P_{ji}}{\partial V_{se1}} &= V_j (g_{ij} \cos(\theta_j - \theta_1) + b_{ij} \sin(\theta_j - \theta_1)) \\
 \frac{\partial P_{ji}}{\partial \theta_i} &= -V_j V_i (g_{ij} \sin(\theta_j - \theta_i) - b_{ij} \cos(\theta_j - \theta_i)) \\
 \frac{\partial P_{ji}}{\partial V_i} &= -V_j (g_{ij} \cos(\theta_j - \theta_i) + b_{ij} \sin(\theta_j - \theta_i)) \\
 \frac{\partial P_{ji}}{\partial \theta_j} &= V_j V_i (g_{ij} \sin(\theta_j - \theta_i) - b_{ij} \cos(\theta_j - \theta_i)) \\
 &\quad - V_j V_{se1} (g_{ij} \sin(\theta_j - \theta_1) - b_{ij} \cos(\theta_j - \theta_1)) \\
 &= -Q_{ji} - V_j^2 b_{ij} \\
 \frac{\partial P_{ji}}{\partial V_j} &= 2V_j g_{ij} + V_{se1} (g_{ij} \cos(\theta_j - \theta_1) + b_{ij} \sin(\theta_j - \theta_1)) \\
 &\quad - V_j (g_{ij} \cos(\theta_j - \theta_i) + b_{ij} \sin(\theta_j - \theta_i)) \\
 &= \frac{P_{ji}}{V_j} + V_j g_{ij} \\
 \frac{\partial P_{ji}}{\partial V_j} V_j &= P_{ji} + V_j^2 g_{ij} \\
 \frac{\partial Q_{ji}}{\partial \theta_1} &= -V_j V_{se1} (g_{ij} \cos(\theta_j - \theta_1) + b_{ij} \sin(\theta_j - \theta_1)) \\
 \frac{\partial Q_{ji}}{\partial V_{se1}} &= V_j (g_{ij} \sin(\theta_j - \theta_1) - b_{ij} \cos(\theta_j - \theta_1)) \\
 \frac{\partial Q_{ji}}{\partial \theta_i} &= V_i V_j (g_{ij} \cos(\theta_j - \theta_i) + b_{ij} \sin(\theta_j - \theta_i)) \\
 \frac{\partial Q_{ji}}{\partial V_i} &= -V_j (g_{ij} \sin(\theta_j - \theta_i) - b_{ij} \cos(\theta_j - \theta_i)) \\
 \frac{\partial Q_{ji}}{\partial \theta_j} &= -V_j V_i (g_{ij} \cos(\theta_j - \theta_i) + b_{ij} \sin(\theta_j - \theta_i)) \\
 &\quad + V_j V_{se1} (g_{ij} \cos(\theta_j - \theta_{se1}) + b_{ij} \sin(\theta_j - \theta_{se1})) \\
 &= P_{ji} + V_j^2 g_{ij}
 \end{aligned}$$

$$\frac{\partial Q_{ji}}{\partial V_j} = -2V_j b_{ij} + V_{se1} (g_{ij} \sin(\theta_j - \theta_{se1}) - b_{ij} \cos(\theta_j - \theta_{se1}))$$

$$-V_j (g_{ij} \sin(\theta_j - \theta_i) - b_{ij} \cos(\theta_j - \theta_i))$$

$$\frac{\partial Q_{ji}}{\partial V_j} V_j = Q_{ji} - V_j^2 b_{ij}$$

$$\frac{\partial P_{ki}}{\partial \theta_2} = V_k V_{se2} (g_{ik} \sin(\theta_k - \theta_2) - b_{ik} \cos(\theta_k - \theta_2))$$

$$\frac{\partial P_{ki}}{\partial V_{se2}} = V_k (g_{ik} \cos(\theta_k - \theta_2) + b_{ik} \sin(\theta_k - \theta_2))$$

$$\frac{\partial P_{ki}}{\partial \theta_i} = -V_k V_i (g_{ik} \sin(\theta_k - \theta_i) - b_{ik} \cos(\theta_k - \theta_i))$$

$$\frac{\partial P_{ki}}{\partial V_i} = -V_k (g_{ik} \cos(\theta_k - \theta_i) + b_{ik} \sin(\theta_k - \theta_i))$$

$$\frac{\partial P_{ki}}{\partial \theta_k} = V_k V_i (g_{ik} \sin(\theta_k - \theta_i) - b_{ik} \cos(\theta_k - \theta_i))$$

$$-V_k V_{se2} (g_{ik} \sin(\theta_k - \theta_{se2}) - b_{ik} \cos(\theta_k - \theta_{se2}))$$

$$= -Q_{ki} - V_k^2 b_{ik}$$

$$\frac{\partial P_{ki}}{\partial V_k} = 2V_k g_{ik} + V_{se2} (g_{ik} \cos(\theta_k - \theta_{se2}) + b_{ik} \sin(\theta_k - \theta_{se2}))$$

$$-V_i (g_{ik} \cos(\theta_k - \theta_i) + b_{ik} \sin(\theta_k - \theta_i))$$

$$\frac{\partial P_{ki}}{\partial V_k} V_k = P_{ki} + V_k^2 g_{ik}$$

$$PE = \sum_n P_{sein} = P_{seij} + P_{seik}$$

$$\frac{\partial PE}{\partial \theta_1} = V_{se1} V_i (-g_{ij} \sin(\theta_1 - \theta_i) + b_{ij} \cos(\theta_1 - \theta_i)) - V_{se1} V_j (-g_{ij} \sin(\theta_1 - \theta_j) \dots$$

$$+ b_{ij} \cos(\theta_1 - \theta_j)) = -Q_{seij} + V_{se1}^2 b_{ij}$$

$$\frac{\partial PE}{\partial V_{se1}} = -2V_{se1} g_{ij} + V_i (g_{ij} \cos(\theta_1 - \theta_i) + b_{ij} \sin(\theta_1 - \theta_i))$$

$$-V_j (g_{ij} \cos(\theta_1 - \theta_j) + b_{ij} \sin(\theta_1 - \theta_j))$$

$$\frac{\partial PE}{\partial V_{se1}} V_{se1} = -V_{se1}^2 g_{ij} + P_{seij}$$

$$\frac{\partial PE}{\partial \theta_{se2}} = V_{se2} V_i (-g_{ik} \sin(\theta_{se2} - \theta_i) + b_{ik} \cos(\theta_{se2} - \theta_i))$$

$$-V_{se2} V_k (-g_{ik} \sin(\theta_{se2} - \theta_k) + b_{ik} \cos(\theta_{se2} - \theta_k)) = -Q_{seik} + V_{se2}^2 b_{ik}$$

$$\begin{aligned}
\frac{\partial PE}{\partial V_{se2}} &= -2V_{se2} g_{ik} + V_i (g_{ij} \cos(\theta_2 - \theta_i) + b_{ij} \sin(\theta_2 - \theta_i)) \\
&\quad - V_k (g_{ik} \cos(\theta_2 - \theta_k) + b_{ik} \sin(\theta_2 - \theta_k)) \\
\frac{\partial PE}{\partial V_{se2}} V_{se2} &= -V_{se2}^2 g_{ik} + P_{seik} \\
\frac{\partial PE}{\partial \theta_i} &= V_{se1} V_i (g_{ij} \sin(\theta_1 - \theta_i) - b_{ij} \cos(\theta_1 - \theta_i)) \\
&\quad + V_{se2} V_i (g_{ik} \sin(\theta_2 - \theta_i) - b_{ik} \cos(\theta_2 - \theta_i)) \\
\frac{\partial PE}{\partial V_i} &= V_{se1} (g_{ij} \cos(\theta_1 - \theta_i) + b_{ij} \sin(\theta_1 - \theta_i)) \\
&\quad + V_{se2} (g_{ik} \cos(\theta_2 - \theta_i) + b_{ik} \sin(\theta_2 - \theta_i)) \\
\frac{\partial PE}{\partial \theta_j} &= -V_{se1} V_j (g_{ij} \sin(\theta_1 - \theta_j) - b_{ij} \cos(\theta_1 - \theta_j)) \\
\frac{\partial PE}{\partial V_j} &= -V_{se1} (g_{ij} \cos(\theta_1 - \theta_j) + b_{ij} \sin(\theta_1 - \theta_j)) \\
\frac{\partial PE}{\partial \theta_k} &= -V_{se2} V_k (g_{ik} \sin(\theta_2 - \theta_k) - b_{ik} \cos(\theta_2 - \theta_k)) \\
\frac{\partial PE}{\partial V_k} &= -V_{se2} (g_{ik} \cos(\theta_2 - \theta_k) + b_{ik} \sin(\theta_2 - \theta_k)) \\
\frac{\partial P_i}{\partial \theta_{se1}} &= -V_i V_{se1} (g_{ij} \sin(\theta_i - \theta_1) - b_{ij} \cos(\theta_i - \theta_1)) \\
\frac{\partial P_i}{\partial V_{se1}} &= -V_i (g_{ij} \cos(\theta_i - \theta_1) + b_{ij} \sin(\theta_i - \theta_1)) \\
\frac{\partial P_i}{\partial \theta_{se2}} &= -V_i V_{se2} (g_{ik} \sin(\theta_i - \theta_2) - b_{ik} \cos(\theta_i - \theta_2)) \\
\frac{\partial P_i}{\partial V_{se2}} &= -V_i (g_{ik} \cos(\theta_i - \theta_{se2}) + b_{ik} \sin(\theta_i - \theta_{se2})) \\
\frac{\partial P_i}{\partial \theta_i} &= \sum_{n=j,k} V_i V_{sep} (g_{in} \sin(\theta_i - \theta_p) - b_{in} \cos(\theta_i - \theta_p)) \\
&\quad + \sum_{n=j,k} V_i V_n (g_{in} \sin(\theta_i - \theta_n) - b_{in} \cos(\theta_i - \theta_n)) = -Q_i - V_i^2 (b_{ij} + b_{ik}) \\
&\quad p = 1, 2 \\
\frac{\partial P_i}{\partial V_i} &= -2V_i (g_{ij} + g_{ik}) - \sum_{n=j,k} V_{sep} (g_{in} \cos(\theta_i - \theta_p) + b_{in} \sin(\theta_i - \theta_p)) \\
&\quad - \sum_{n=j,k} V_n (g_{in} \cos(\theta_i - \theta_n) + b_{in} \sin(\theta_i - \theta_n)) \\
\frac{\partial P_i}{\partial V_i} V_i &= V_i^2 (g_{ij} + g_{ik}) + P_i \\
\frac{\partial P_i}{\partial \theta_j} &= -V_i V_j (g_{ij} \sin(\theta_i - \theta_j) - b_{ij} \cos(\theta_i - \theta_j))
\end{aligned}$$

$$\begin{aligned}
\frac{\partial P_i}{\partial V_j} &= -V_i (g_{ij} \cos(\theta_i - \theta_j) + b_{ij} \sin(\theta_i - \theta_j)) \\
\frac{\partial P_i}{\partial \theta_k} &= -V_i V_k (g_{ik} \sin(\theta_i - \theta_k) - b_{ik} \cos(\theta_i - \theta_k)) \\
\frac{\partial P_i}{\partial V_k} &= -V_i (g_{ik} \cos(\theta_i - \theta_k) + b_{ik} \sin(\theta_i - \theta_k)) \\
\frac{\partial Q_i}{\partial \theta_1} &= V_i V_{se1} (b_{ij} \sin(\theta_i - \theta_1) + g_{ij} \cos(\theta_i - \theta_1)) \\
\frac{\partial Q_i}{\partial V_{se1}} &= V_i (b_{ij} \cos(\theta_i - \theta_1) - g_{ij} \sin(\theta_i - \theta_1)) \\
\frac{\partial Q_i}{\partial \theta_2} &= V_i V_{se2} (b_{ik} \sin(\theta_i - \theta_2) + g_{ik} \cos(\theta_i - \theta_2)) \\
\frac{\partial Q_i}{\partial V_{se2}} &= V_i (b_{ik} \cos(\theta_i - \theta_2) - g_{ik} \sin(\theta_i - \theta_2)) \\
\frac{\partial Q_i}{\partial \theta_i} &= - \sum_{n=j,k} V_i V_{sep} (b_{in} \sin(\theta_i - \theta_p) + g_{in} \cos(\theta_i - \theta_p)) \\
&\quad - \sum_{n=j,k} V_i V_n (b_{in} \sin(\theta_i - \theta_n) + g_{in} \cos(\theta_i - \theta_n)) = P_i - V_i^2 (g_{ij} + g_{ik}) \\
&\hspace{15em} p = 1,2 \\
\frac{\partial Q_i}{\partial V_i} &= -2V_i (b_{ij} + b_{ik}) + \sum_{n=j,k} V_{sep} (b_{in} \cos(\theta_i - \theta_p) - g_{in} \sin(\theta_i - \theta_p)) \\
&\quad + \sum_{n=j,k} V_n (b_{in} \cos(\theta_i - \theta_n) - g_{in} \sin(\theta_i - \theta_n)) \\
\frac{\partial Q_i}{\partial V_i} V_i &= -V_i^2 (b_{ij} + b_{ik}) + Q_i \\
\frac{\partial Q_i}{\partial \theta_j} &= V_i V_j (b_{ij} \sin(\theta_i - \theta_j) + g_{ij} \cos(\theta_i - \theta_j)) \\
\frac{\partial Q_i}{\partial V_j} &= V_i (b_{ij} \cos(\theta_i - \theta_j) - g_{ij} \sin(\theta_i - \theta_j)) \\
\frac{\partial Q_i}{\partial \theta_k} &= V_i V_k (b_{ik} \sin(\theta_i - \theta_k) + g_{ik} \cos(\theta_i - \theta_k)) \\
\frac{\partial Q_i}{\partial V_k} &= V_i (b_{ik} \cos(\theta_i - \theta_k) - g_{ik} \sin(\theta_i - \theta_k))
\end{aligned}$$

## APPENDIX B

## APPENDIX B

### 1) PHILLIPS-HEFFRON MODEL K CONSTANTS OF A SINGLE MACHINE INFINITE-BUS POWER SYSTEM EQUIPPED WITH IPFC

$$K_1 = \frac{1}{2}(x_q - x'_d)x_{1d}x_{2a}v_{dc}v_b \sin \delta \cos \theta_2 m_2 - \frac{1}{2}(x_q - x'_d)x_{1d}x_{2b}m_1v_{dc}v_b \cos \theta_1 \sin \delta +$$

$$(x_q - x'_d)x_{1d}x_{2c}v_b^2 \sin^2 \delta + E'_q(1 + (x_q - x'_d)x_{1a})x_{2c}v_b \cos \delta +$$

$$\frac{1}{2}(x_q - x'_d)x_{1b}x_{2c}m_2v_{dc}v_b \sin \theta_2 \cos \delta - \frac{1}{2}(x_q - x'_d)x_{1c}x_{2c}m_1v_{dc}v_b \sin \theta_1 \cos \delta -$$

$$(x_q - x'_d)x_{1d}x_{2c}v_b^2 \cos^2 \delta$$

$$K_2 = \frac{1}{2}(1 + (x_q - x'_d)x_{1a})x_{2a}v_{dc}m_2 \cos \theta_2 - \frac{1}{2}(1 + (x_q - x'_d)x_{1a})x_{2b}v_{dc}m_1 \cos \theta_1$$

$$+ (1 + (x_q - x'_d)x_{1a})x_{2c}v_b \sin \delta$$

$$K_{pv} = \frac{1}{2}(x_q - x'_d)x_{1b}x_{2a}v_{dc}m_2^2 \sin \theta_2 \cos \theta_2 - \frac{1}{2}(x_q - x'_d)x_{1b}x_{2b}m_1m_2v_{dc} \cos \theta_1 \sin \theta_2$$

$$+ \frac{1}{2}(x_q - x'_d)x_{1b}x_{2c}m_2v_b \sin \theta_2 \sin \delta - \frac{1}{2}(x_q - x'_d)x_{1c}x_{2a}m_1m_2v_{dc} \sin \theta_1 \cos \theta_2$$

$$+ \frac{1}{2}(x_q - x'_d)x_{1c}x_{2b}v_{dc}m_1^2 \sin \theta_1 \cos \theta_1 - \frac{1}{2}(x_q - x'_d)x_{1c}x_{2c}m_1v_b \sin \theta_1 \sin \delta$$

$$+ \frac{1}{2}E'_q(1 + (x_q - x'_d)x_{1a})x_{2a}m_2 \cos \theta_2 - \frac{1}{2}E'_q(1 + (x_q - x'_d)x_{1a})x_{2b}m_1 \cos \theta_1$$

$$- \frac{1}{2}(x_q - x'_d)x_{1d}x_{2a}m_2v_b \cos \theta_2 \cos \delta + \frac{1}{2}(x_q - x'_d)x_{1d}x_{2b}m_1v_b \cos \theta_1 \cos \delta$$

$$K_{pm1} = -\frac{1}{4}(x_q - x'_d)x_{1c}x_{2a}v_{dc}^2m_2 \sin \theta_1 \cos \theta_2 + \frac{1}{2}(x_q - x'_d)x_{1c}x_{2b}v_{dc}^2m_1 \sin \theta_1 \cos \theta_1$$

$$- \frac{1}{2}(x_q - x'_d)x_{1c}x_{2c}v_{dc}v_b \sin \theta_1 \sin \delta - \frac{1}{2}E'_q(1 + (x_q - x'_d)x_{1a})x_{2b}v_{dc} \cos \theta_1$$

$$- \frac{1}{4}(x_q - x'_d)x_{1b}x_{2b}v_{dc}^2m_2 \cos \theta_1 \sin \theta_2 + \frac{1}{2}(x_q - x'_d)x_{1d}x_{2b}v_{dc}v_b \cos \theta_1 \cos \delta$$

$$K_{p\theta 1} = -\frac{1}{4}(x_q - x'_d)x_{1c}x_{2a}v_{dc}^2m_1m_2 \cos \theta_1 \sin \theta_2 + \frac{1}{4}(x_q - x'_d)x_{1c}x_{2b}v_{dc}^2m_1^2 \cos^2 \theta_1$$

$$- \frac{1}{2}(x_q - x'_d)x_{1c}x_{2c}v_{dc}m_1v_b \cos \theta_1 \sin \delta + \frac{1}{2}E'_q(1 + (x_q - x'_d)x_{1a})x_{2b}v_{dc}m_1 \sin \theta_1$$

$$\begin{aligned}
& +\frac{1}{4}(x_q - x'_d)x_{1b}x_{2b}v_{dc}^2m_1m_2 \sin \theta_1 \sin \theta_2 - \frac{1}{4}(x_q - x'_d)x_{1c}x_{2b}v_{dc}^2m_1^2 \sin^2 \theta_1 \\
& - \frac{1}{2}(x_q - x'_d)x_{1d}x_{2b}v_{dc}m_1v_b \sin \theta_1 \cos \delta
\end{aligned}$$

$$\begin{aligned}
K_{pm2} &= \frac{1}{2}(x_q - x'_d)x_{1b}x_{2a}v_{dc}^2m_2 \sin \theta_2 \cos \theta_2 - \frac{1}{4}(x_q - x'_d)x_{1b}x_{2b}v_{dc}^2m_1 \sin \theta_2 \cos \theta_1 \\
& + \frac{1}{2}(x_q - x'_d)x_{1b}x_{2c}v_{dc}v_b \sin \theta_2 \sin \delta + \frac{1}{2}E'_q(1 + (x_q - x'_d)x_{1a})x_{2a}v_{dc} \cos \theta_2 \\
& - \frac{1}{4}(x_q - x'_d)x_{1c}x_{2a}v_{dc}^2m_1 \cos \theta_2 \sin \theta_1 - \frac{1}{2}(x_q - x'_d)x_{1d}x_{2a}v_{dc}v_b \cos \theta_2 \cos \delta
\end{aligned}$$

$$\begin{aligned}
K_{p\theta2} &= \frac{1}{4}(x_q - x'_d)x_{1b}x_{2a}v_{dc}^2m_2^2 \cos^2 \theta_2 - \frac{1}{4}(x_q - x'_d)x_{1b}x_{2b}v_{dc}^2m_1m_2 \cos \theta_1 \cos \theta_2 \\
& + \frac{1}{2}(x_q - x'_d)x_{1b}x_{2c}v_{dc}m_2v_b \cos \theta_2 \sin \delta - \frac{1}{2}E'_q(1 + (x_q - x'_d)x_{1a})x_{2b}v_{dc}m_2 \sin \theta_2 \\
& - \frac{1}{4}(x_q - x'_d)x_{1b}x_{2a}v_{dc}^2m_2^2 \sin^2 \theta_2 + \frac{1}{4}(x_q - x'_d)x_{1c}x_{2a}v_{dc}^2m_1m_2 \sin \theta_1 \sin \theta_2 \\
& + \frac{1}{2}(x_q - x'_d)x_{1d}x_{2a}v_{dc}m_2v_b \sin \theta_2 \cos \delta
\end{aligned}$$

$$K_3 = (1 + (x_d - x'_d)x_{1a})$$

$$K_4 = (x_d - x'_d)x_{1d} \sin \delta$$

$$K_{qv} = \frac{1}{2}(x_d - x'_d)x_{1b}m_2 \sin \theta_2 - \frac{1}{2}(x_d - x'_d)x_{1c}m_1 \sin \theta_1$$

$$K_{qm1} = -\frac{1}{2}(x_d - x'_d)x_{1c}v_{dc} \sin \theta_1$$

$$K_{q\theta1} = -\frac{1}{2}(x_d - x'_d)x_{1c}v_{dc}m_1 \cos \theta_1$$

$$K_{qm2} = \frac{1}{2}(x_d - x'_d)x_{1b}v_{dc} \sin \theta_2$$

$$K_{q\theta2} = \frac{1}{2}(x_d - x'_d)x_{1b}v_{dc}m_2 \cos \theta_2$$

$$\begin{aligned}
v_t = \text{sqr}t \left[ \frac{1}{4} x_q^2 x_{2a}^2 v_{dc}^2 m_2^2 \cos^2 \theta_2 + \frac{1}{4} x_q^2 x_{2b}^2 v_{dc}^2 m_1^2 \cos^2 \theta_1 + x_q^2 x_{2c}^2 v_b^2 \sin^2 \delta - \right. \\
\frac{1}{2} x_q^2 x_{2a} x_{2b} v_{dc}^2 m_1 m_2 \cos \theta_1 \cos \theta_2 - x_q^2 x_{2b} x_{2c} m_1 v_{dc} v_b \cos \theta_1 \sin \delta + \\
x_q^2 x_{2a} x_{2c} m_2 v_{dc} v_b \cos \theta_2 \sin \delta + E_q'^2 (1 - x_d' x_{1a})^2 + \frac{1}{4} x_d'^2 x_{1b}^2 v_{dc}^2 m_2^2 \sin^2 \theta_2 + \\
\frac{1}{4} x_d'^2 x_{1c}^2 v_{dc}^2 m_1^2 \sin^2 \theta_1 + x_d'^2 x_{1d}^2 v_b^2 \cos^2 \delta - E_q' (1 - x_d' x_{1a}) x_d' x_{1b} v_{dc} m_2 \sin \theta_2 + \\
E_q' (1 - x_d' x_{1a}) x_d' x_{1c} v_{dc} m_1 \sin \theta_1 + 2E_q' (1 - x_d' x_{1a}) x_d' x_{1d} v_b \cos \delta - \\
\left. \frac{1}{2} x_d'^2 x_{1b} x_{1c} v_{dc}^2 m_1 m_2 \sin \theta_2 \sin \theta_1 - x_d'^2 x_{1b} x_{1d} v_{dc} v_b m_2 \sin \theta_2 \cos \delta + \right. \\
\left. x_d'^2 x_{1c} x_{1d} v_{dc} v_b m_1 \sin \theta_1 \cos \delta \right]
\end{aligned}$$

$$\begin{aligned}
K_5 = \frac{1}{2} v_t^{-1} ( x_q^2 x_{2a} x_{2c} v_{dc} v_b m_2 \cos \theta_2 \cos \delta - x_q^2 x_{2b} x_{2c} v_{dc} v_b m_1 \cos \theta_1 \cos \delta \\
+ 2x_q^2 x_{2c}^2 v_b^2 \cos \delta \sin \delta - 2E_q' (1 - x_d' x_{1a}) x_d' x_{1d} v_b \sin \delta \\
+ x_d'^2 x_{1b} x_{1d} v_{dc} v_b m_2 \sin \theta_2 \sin \delta - x_d'^2 x_{1c} x_{1d} v_{dc} v_b m_1 \sin \theta_1 \sin \delta \\
- 2x_d'^2 x_{1d}^2 v_b^2 \cos \delta \sin \delta )
\end{aligned}$$

$$\begin{aligned}
K_6 = \frac{1}{2} v_t^{-1} ( 2E_q' (1 - x_d' x_{1a})^2 + x_d' x_{1b} (1 - x_d' x_{1a}) v_{dc} m_2 \sin \theta_2 + \\
(1 - x_d' x_{1a}) x_d' x_{1c} v_{dc} m_1 \sin \theta_1 + 2(1 - x_d' x_{1a}) x_d' x_{1d} v_b \cos \delta )
\end{aligned}$$

$$\begin{aligned}
K_{vv} = \frac{1}{2} v_t^{-1} \left[ \frac{1}{2} x_q^2 x_{2a}^2 v_{dc}^2 m_2^2 \cos^2 \theta_2 - \frac{1}{2} x_q^2 x_{2a} x_{2b} v_{dc} m_1 m_2 \cos \theta_1 \cos \theta_2 + \right. \\
x_q^2 x_{2a} x_{2c} m_2 v_b \cos \theta_2 \sin \delta - \frac{1}{2} x_q^2 x_{2a} x_{2b} v_{dc} m_1 m_2 \cos \theta_1 \cos \theta_2 \\
+ \frac{1}{2} x_q^2 x_{2b}^2 v_{dc} m_1^2 \cos^2 \theta_1 - x_q^2 x_{2b} x_{2c} m_1 v_b \cos \theta_1 \sin \delta \\
+ E_q' (1 - x_d' x_{1a}) x_d' x_{1c} m_1 \sin \theta_1 - \frac{1}{2} x_d'^2 x_{1b} x_{1c} v_{dc} m_1 m_2 \sin \theta_1 \sin \theta_2 \\
+ \frac{1}{2} x_d'^2 x_{1c}^2 m_1^2 v_{dc} \sin^2 \theta_1 + x_d'^2 x_{1c} x_{1d} v_b m_1 \cos \delta \sin \theta_1 \\
- E_q' (1 - x_d' x_{1a}) x_d' x_{1b} m_2 \sin \theta_2 + \frac{1}{2} x_d'^2 x_{1b}^2 m_2^2 v_{dc} \sin^2 \theta_2 \\
\left. - \frac{1}{2} x_d'^2 x_{1b} x_{1c} v_{dc} m_1 m_2 \sin \theta_1 \sin \theta_2 - x_d'^2 x_{1b} x_{1d} v_b m_2 \cos \delta \sin \theta_2 \right]
\end{aligned}$$

$$K_{vm1} = \frac{1}{2} v_t^{-1} \left[ -\frac{1}{2} x_q^2 x_{2a} x_{2b} v_{dc}^2 m_2 \cos \theta_1 \cos \theta_2 + \frac{1}{2} x_q^2 x_{2b}^2 v_{dc}^2 m_1 \cos^2 \theta_1 \right. \\ \left. - x_q^2 x_{2b} x_{2c} v_{dc} v_b \cos \theta_1 \sin \delta - E'_q (1 - x'_d x_{1a}) x'_d x_{1c} v_{dc} \sin \theta_1 - \right. \\ \left. \frac{1}{2} x_d'^2 x_{1b} x_{1c} v_{dc}^2 m_2 \sin \theta_1 \sin \theta_2 + \frac{1}{2} x_d'^2 x_{1c}^2 m_1 v_{dc}^2 \sin^2 \theta_1 + \right. \\ \left. x_d'^2 x_{1c} x_{1d} v_b v_{dc} \cos \delta \sin \theta_1 \right]$$

$$K_{v\theta1} = \frac{1}{2} v_t^{-1} \left[ \frac{1}{2} x_q^2 x_{2a} x_{2b} v_{dc}^2 m_1 m_2 \sin \theta_1 \cos \theta_2 - \frac{1}{2} x_q^2 x_{2b}^2 v_{dc}^2 m_1^2 \sin \theta_1 \cos \theta_1 \right. \\ \left. + x_q^2 x_{2b} x_{2c} v_{dc} v_b \sin \theta_1 \sin \delta + E'_q (1 - x'_d x_{1a}) x'_d x_{1c} v_{dc} m_1 \cos \theta_1 - \right. \\ \left. \frac{1}{2} x_d'^2 x_{1b} x_{1c} v_{dc}^2 m_1 m_2 \cos \theta_1 \sin \theta_2 + \frac{1}{2} x_d'^2 x_{1c}^2 m_1^2 v_{dc}^2 \sin \theta_1 \cos \theta_1 + \right. \\ \left. x_d'^2 x_{1c} x_{1d} v_b v_{dc} \cos \delta \cos \theta_1 \right]$$

$$K_{vm2} = \frac{1}{2} v_t^{-1} \left[ \frac{1}{2} x_q^2 x_{2a}^2 v_{dc}^2 m_2 \cos^2 \theta_2 - \frac{1}{2} x_q^2 x_{2a} x_{2b} v_{dc}^2 m_1 \cos \theta_1 \cos \theta_2 + \right. \\ \left. x_q^2 x_{2a} x_{2c} v_{dc} v_b \cos \theta_2 \sin \delta - E'_q (1 - x'_d x_{1a}) x'_d x_{1b} v_{dc} \sin \theta_2 - \right. \\ \left. \frac{1}{2} x_d'^2 x_{1b} x_{1c} v_{dc}^2 m_1 \sin \theta_1 \sin \theta_2 + \frac{1}{2} x_d'^2 x_{1b}^2 m_2 v_{dc}^2 \sin^2 \theta_2 - \right. \\ \left. x_d'^2 x_{1b} x_{1d} v_b v_{dc} \cos \delta \sin \theta_2 \right]$$

$$K_{v\theta2} = \frac{1}{2} v_t^{-1} \left[ \frac{1}{2} x_q^2 x_{2a} x_{2b} v_{dc}^2 m_1 m_2 \sin \theta_2 \cos \theta_1 - \frac{1}{2} x_q^2 x_{2a}^2 v_{dc}^2 m_2^2 \sin \theta_2 \cos \theta_2 \right. \\ \left. - x_q^2 x_{2a} x_{2c} v_{dc} v_b \sin \theta_2 \sin \delta - E'_q (1 - x'_d x_{1a}) x'_d x_{1b} v_{dc} m_2 \cos \theta_2 - \right. \\ \left. \frac{1}{2} x_d'^2 x_{1b} x_{1c} v_{dc}^2 m_1 m_2 \cos \theta_2 \sin \theta_1 + \frac{1}{2} x_d'^2 x_{1b}^2 m_2^2 v_{dc}^2 \sin \theta_2 \cos \theta_2 - \right. \\ \left. \frac{1}{2} x_d'^2 x_{1b} x_{1d} m_2 v_b v_{dc} \cos \delta \cos \theta_2 \right]$$

$$K_7 = \frac{3}{4C_{dc}} [x_{11d} m_1 v_b \cos \theta_1 \sin \delta + x_{11q} m_1 v_b \sin \theta_1 \cos \delta \\ + x_{21d} m_2 v_b \cos \theta_2 \sin \delta + x_{21q} m_2 v_b \sin \theta_2 \cos \delta]$$

$$K_8 = \frac{3}{4C_{dc}} [x_{11d} m_1 \cos \theta_1 + x_{21d} m_2 \cos \theta_2]$$

$$K_9 = \frac{3}{4C_{dc}} \left[ \frac{1}{2}(x_{12d} - x_{11d})m_1m_2 \cos \theta_1 \sin \theta_2 - \frac{1}{2}x_{12d}m_1^2 \sin \theta_1 \cos \theta_1 \right. \\ \left. + \frac{1}{2}(x_{11q} + x_{12q})m_1m_2 \sin \theta_1 \cos \theta_2 - \frac{1}{2}x_{12q}m_1^2 \cos \theta_1 \sin \theta_1 \right. \\ \left. + \frac{1}{2}(x_{22d} - x_{21d})m_2^2 \sin \theta_2 \cos \theta_2 - \frac{1}{2}x_{22d}m_1m_2 \sin \theta_1 \cos \theta_2 + \right. \\ \left. + \frac{1}{2}(x_{21q} + x_{22q})m_2^2 \cos \theta_2 \sin \theta_2 - \frac{1}{2}x_{22q}m_1m_2 \cos \theta_1 \sin \theta_2 \right]$$

$$K_{cm1} = \frac{3}{4C_{dc}} \left[ -\frac{1}{2}x_{12d}m_1v_{dc} \cos \theta_1 \sin \theta_1 - \frac{1}{2}x_{12q}m_1v_{dc} \cos \theta_1 \sin \theta_1 \right. \\ \left. \frac{1}{2}(x_{11q} + x_{12q})v_{dc}m_2 \sin \theta_1 \cos \theta_2 + x_{11q}v_b \sin \theta_1 \sin \delta - \frac{1}{2}x_{12q}v_{dc}m_1 \cos \theta_1 \sin \theta_1 \right. \\ \left. x_{11d}E'_q \cos \theta_1 + \frac{1}{2}(x_{12d} - x_{11d})v_{dc}m_2 \cos \theta_1 \sin \theta_2 - \frac{1}{2}x_{12d}v_{dc}m_1 \sin \theta_1 \cos \theta_1 \right. \\ \left. -x_{11d}v_b \cos \theta_1 \cos \delta - \frac{1}{2}x_{22d}v_{dc}m_2 \sin \theta_1 \cos \theta_2 - \frac{1}{2}x_{22q}v_{dc}m_2 \sin \theta_2 \cos \theta_1 \right]$$

$$K_{c\theta1} = \frac{3}{4C_{dc}} \left[ -\frac{1}{2}x_{12d}v_{dc}m_1^2 \cos^2 \theta_1 + \frac{1}{2}x_{12q}v_{dc}m_1^2 \sin^2 \theta_1 + \right. \\ \left. \frac{1}{2}(x_{11q} + x_{12q})v_{dc}m_1m_2 \cos \theta_1 \cos \theta_2 + x_{11q}v_b m_1 \cos \theta_1 \sin \delta - \frac{1}{2}x_{21q}v_{dc}m_1^2 \cos^2 \theta_1 \right. \\ \left. -x_{11d}E'_q m_1 \sin \theta_1 - \frac{1}{2}(x_{12d} - x_{11d})v_{dc}m_1m_2 \sin \theta_1 \sin \theta_2 - \frac{1}{2}x_{12d}v_{dc}m_1^2 \sin^2 \theta_1 \right. \\ \left. x_{11d}v_b m_1 \sin \theta_1 \cos \delta - \frac{1}{2}x_{22d}v_{dc}m_1m_2 \cos \theta_1 \cos \theta_2 + \frac{1}{2}x_{22q}v_{dc}m_1m_2 \sin \theta_1 \sin \theta_2 \right]$$

$$K_{cm2} = \frac{3}{4C_{dc}} \left[ \frac{1}{2}(x_{12d} - x_{11d})v_{dc}m_1 \cos \theta_1 \sin \theta_2 - \frac{1}{2}(x_{11q} + x_{12q})v_{dc}m_1 \sin \theta_1 \cos \theta_2 \right. \\ \left. + \frac{1}{2}(x_{22d} - x_{21d})v_{dc}m_2 \sin \theta_2 \cos \theta_2 + \frac{1}{2}(x_{21q} + x_{22q})v_{dc}m_2 \sin \theta_2 \cos \theta_2 + \right. \\ \left. x_{21q}v_b \sin \theta_2 \sin \delta - \frac{1}{2}x_{22q}v_{dc}m_1 \cos \theta_1 \sin \theta_2 + x_{21d}E'_q \cos \theta_2 - \right. \\ \left. \frac{1}{2}(x_{22d} - x_{21d})v_{dc}m_2 \sin \theta_2 \cos \theta_2 - \frac{1}{2}x_{22d}v_{dc}m_1 \sin \theta_1 \cos \theta_2 \right. \\ \left. -x_{21d}v_b \cos \theta_2 \cos \delta \right]$$

$$\begin{aligned}
K_{c\theta 2} = & \frac{3}{4C_{dc}} \left[ \frac{1}{2}(x_{12d} - x_{11d})v_{dc}m_1m_2 \cos \theta_1 \cos \theta_2 - \frac{1}{2}(x_{11q} + x_{12q})v_{dc}m_1m_2 \sin \theta_1 \sin \theta_2 \right. \\
& + \frac{1}{2}(x_{22d} - x_{21d})v_{dc}m_2^2 \cos^2 \theta_2 - \frac{1}{2}(x_{21q} + x_{22q})v_{dc}m_2^2 \sin^2 \theta_2 + \\
& \frac{1}{2}(x_{21q} + x_{22q})v_{dc}m_2^2 \cos^2 \theta_2 + x_{21q}v_b m_2 \cos \theta_2 \sin \delta - \frac{1}{2}x_{22q}v_{dc}m_1m_2 \cos \theta_1 \cos \theta_2 \\
& - x_{21d}E'_q m_2 \sin \theta_2 - \frac{1}{2}(x_{22d} - x_{21d})v_{dc}m_2^2 \sin^2 \theta_2 + \frac{1}{2}x_{22d}v_{dc}m_1m_2 \sin \theta_1 \sin \theta_2 \\
& \left. + x_{21d}v_b m_2 \sin \theta_2 \cos \delta \right]
\end{aligned}$$

## 2) MULTIMODAL DECOMPOSITION

This method is applicable for multi-machine power system having  $n$  machines [29]. For a SMIB power system,  $n = 1$ . The state space model of the linearized power system with IPFC is given by:

$$\begin{aligned}
\Delta \dot{X} &= A\Delta X + B\Delta U \\
\Delta Y &= C\Delta X + D\Delta U
\end{aligned} \tag{B.1}$$

$$\text{where } \Delta X = [\Delta \delta_1, \Delta \delta_2, \dots, \Delta \delta_n, \Delta \omega_1, \Delta \omega_2, \dots, \Delta \omega_n, \Delta Z^T]^T, \tag{B.2}$$

and  $\Delta \delta$ 's and  $\Delta \omega$ 's represent the generator angles and speeds respectively.  $\Delta Z$  represents the remaining state variables. The system matrices  $A$  and  $B$  can be written in this form:

$$A = \begin{bmatrix} 0 & \omega_0 I & 0 \\ A_{21} & A_{22} & A_{23} \\ A_{31} & A_{32} & A_{33} \end{bmatrix}, B = \begin{bmatrix} 0 \\ B_2 \\ B_3 \end{bmatrix} \tag{B.3}$$

The transformation  $\Delta X_m = u^{-1}\Delta X$  is applied to (B.1) where  $u = \begin{bmatrix} V & 0 & 0 \\ 0 & V & 0 \\ 0 & 0 & I \end{bmatrix}$  and

$V$  is the right eigenvector matrix of  $A_{21}$ , and the matrix  $A_{21}$  relates the generator angles and the derivative of the speeds, representing the synchronizing effects

independent of other state variables. The system equations after transformation will become:

$$\begin{aligned}\Delta\dot{X}_m &= u^{-1}Au\Delta X_m + u^{-1}B\Delta U = A_m\Delta X_m + B_m\Delta U \\ \Delta Y &= Cu\Delta X_m + D\Delta U = C_m\Delta X_m + D\Delta U\end{aligned}\quad (B.4)$$

The angles and speeds in (B.4) represent the modal variables. For the oscillation mode  $\lambda_i$  with modal frequency  $\omega_n$ , the state variables are arranged in the form such that the modal angle  $\Delta\delta_{mi}$  and speed  $\Delta\omega_{mi}$  corresponding to  $\lambda_i$  will become the first and second state variables resulting in the system representation as follows:

$$\begin{bmatrix} \Delta\dot{\delta}_{mi} \\ \Delta\dot{\omega}_{mi} \\ \Delta\dot{Z}_1 \end{bmatrix} = \begin{bmatrix} 0 & \omega_o & 0 \\ -k_{mi} & -d_{mi} & A_{d23} \\ A_{d31} & A_{d32} & A_{d33} \end{bmatrix} \begin{bmatrix} \Delta\delta_{mi} \\ \Delta\omega_{mi} \\ \Delta Z_1 \end{bmatrix} + \begin{bmatrix} 0 \\ -B_{d2} \\ B_{d3} \end{bmatrix} \Delta U \quad (B.5)$$

$$\Delta Y = [C_{d1} \quad C_{d2} \quad C_{d3}] \begin{bmatrix} \Delta\delta_{mi} \\ \Delta\omega_{mi} \\ \Delta Z_1 \end{bmatrix} + D\Delta U \quad (B.6)$$

where,  $\Delta Z_1$  represents all other state variables,  $k_{mi}$  and  $d_{mi}$  represent the modal synchronizing and damping coefficients. The modal frequency is given by  $\omega_n = \sqrt{\omega_o k_{mi}}$  rad/s. This approach is known as single mode evaluation as only one mode is focused at a time. The above system can also be expressed in the frequency domain given in (B.7) and the block diagram of the above single mode power system is constructed using its transfer functions as shown in Figure B.1 [9, 29].

$$\begin{aligned}s\Delta\omega_{mi}(s) &= -(\omega_o / s)K_{mi}(s)\Delta\omega_{mi}(s) - K_{Ci}(s)\Delta U(s) \\ \Delta Y(s) &= K_{Oi}(s)\Delta\omega_{mi}(s) + K_{Ii}(s)\Delta U(s)\end{aligned}\quad (B.7)$$

where,

$$K_{Ci}(s) = A_{d23}(sI - A_{d33})^{-1}B_{d3} + B_{d2} \quad (B.8)$$

$$K_{Oi}(s) = C_{d3}(sI - A_{d33})^{-1}(A_{d31}\frac{\omega_o}{s} + A_{d32}) + (\frac{\omega_o}{s}C_{d1} + C_{d2}) \quad (B.9)$$

$$K_{ILi}(s) = C_{d3}(sI - A_{d33})^{-1}B_{d3} + D \quad (\text{B.10})$$

$$K_{mi}(s) = k_{mi} + \frac{s}{\omega_0}d_{mi} + A_{d23}(sI - A_{d33})^{-1}(A_{d31} + \frac{s}{\omega_0}A_{d32}) \quad (\text{B.11})$$

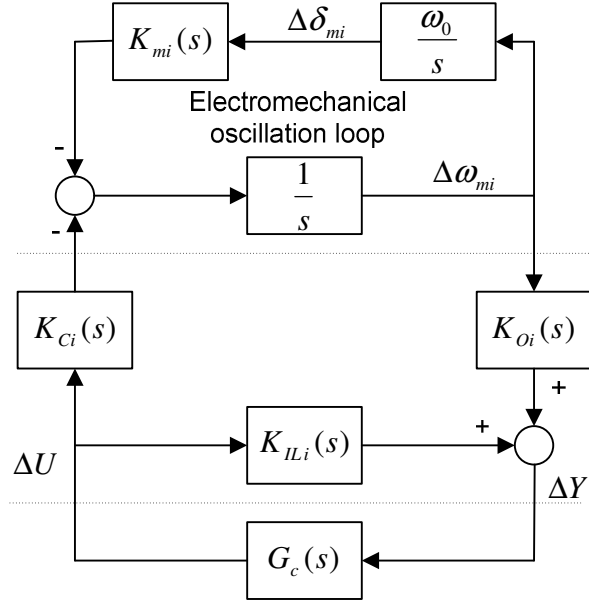


Figure B.1: The power system installed with IPFC based damping controller

Figure B.1 represents the linearized model of the closed loop power system installed with the IPFC and its damping controller.  $K_{Ci}$ ,  $K_{Oi}$ ,  $K_{ILi}$ , and  $K_{mi}$  are the controllability, observability, inner loop and modal transfer functions, respectively. These transfer functions are evaluated at the concerned electromechanical mode of oscillation,  $s = j\omega_n$ .  $G_c(s)$  is the transfer function of the damping controller. When evaluated at  $s = j\omega_n$ ,  $K_{Ci}(j\omega_n)$  provides a measure of how controllable the mode is by the control signal  $\Delta U$ .

## APPENDIX C

## APPENDIX C

### NONLINEAR SIMULATION OF WSCC SYSTEM USING MATLAB/SIMULINK

Simulink model of the multi-machine power system

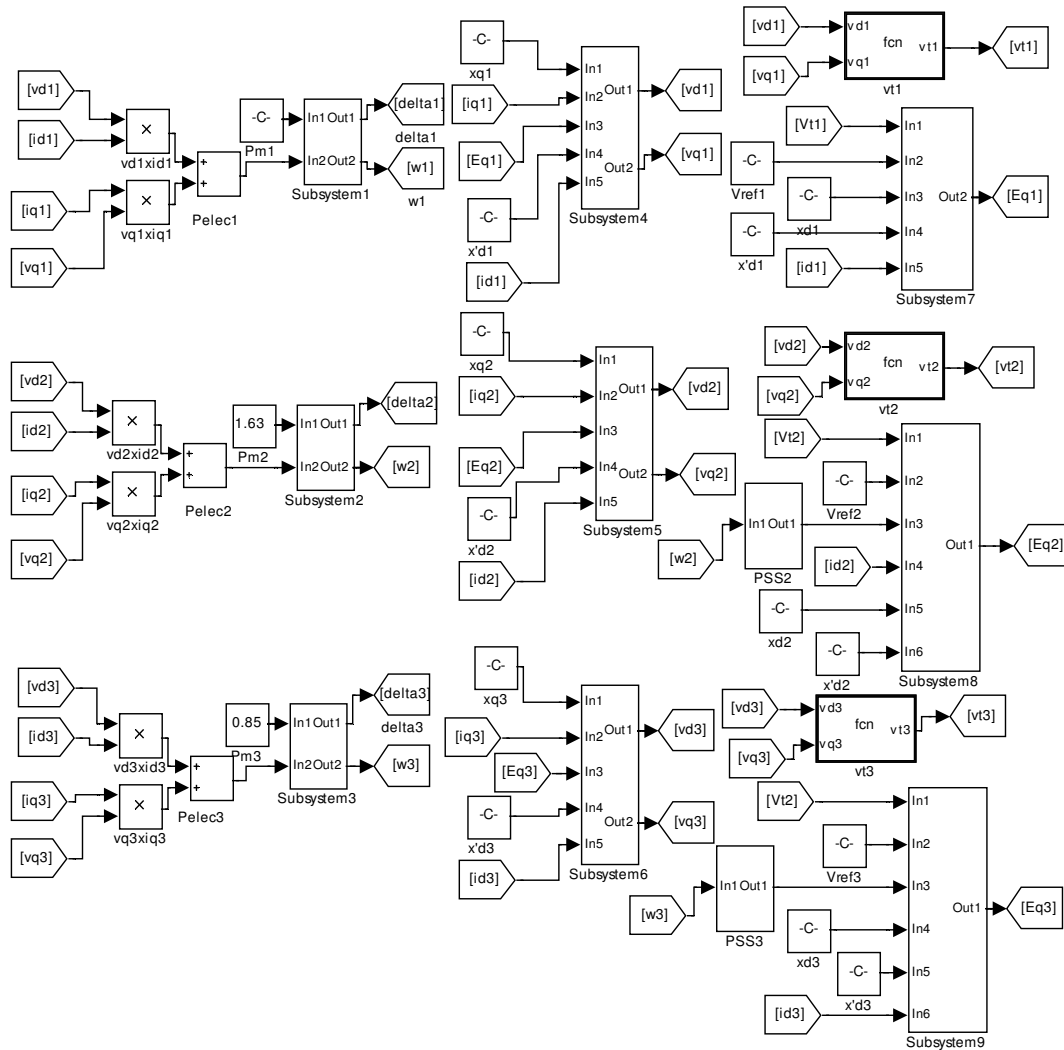


Figure C.1: Simulink model of multi-machine power system representing the machine equations and stator algebraic equations along with the PSSs

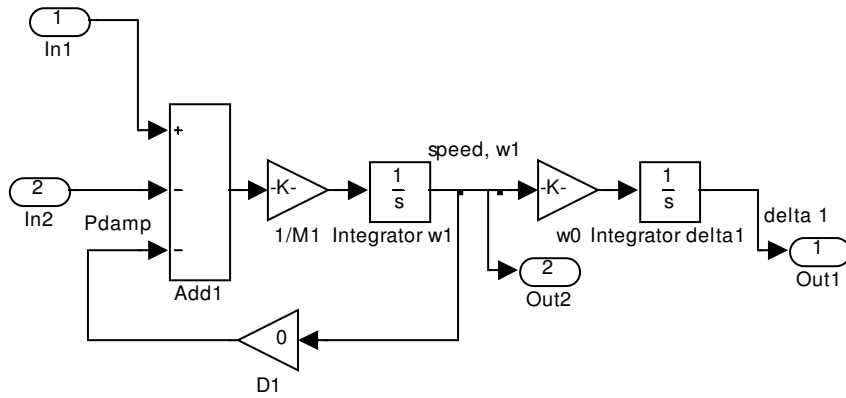


Figure C.2: Subsystem 1

The subsystems 2 and 3 are similar to Figure C.2

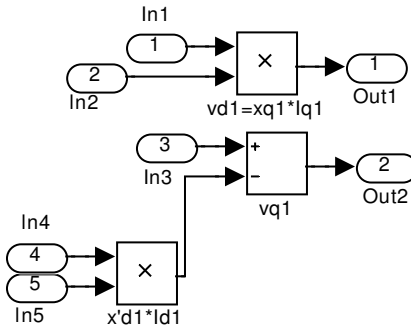


Figure C.3: Subsystem 4

The subsystems 5 and 6 are similar to Figure C.3

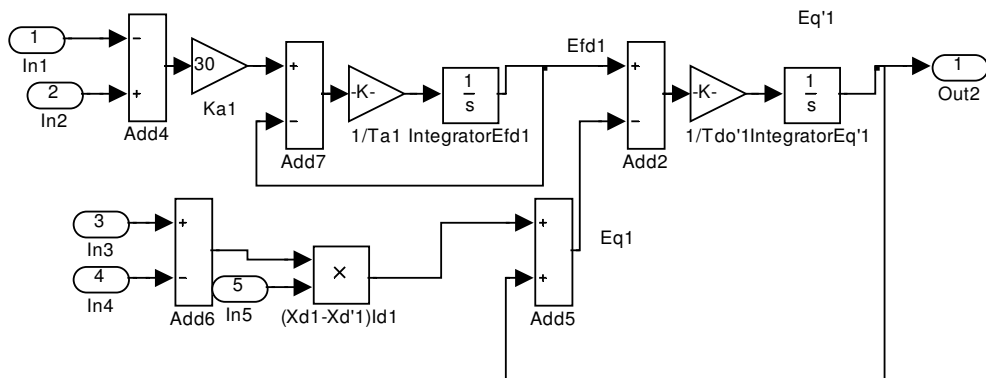


Figure C.4: Subsystem 7

Subsystems 8 and 9 are similar to Figure C.4

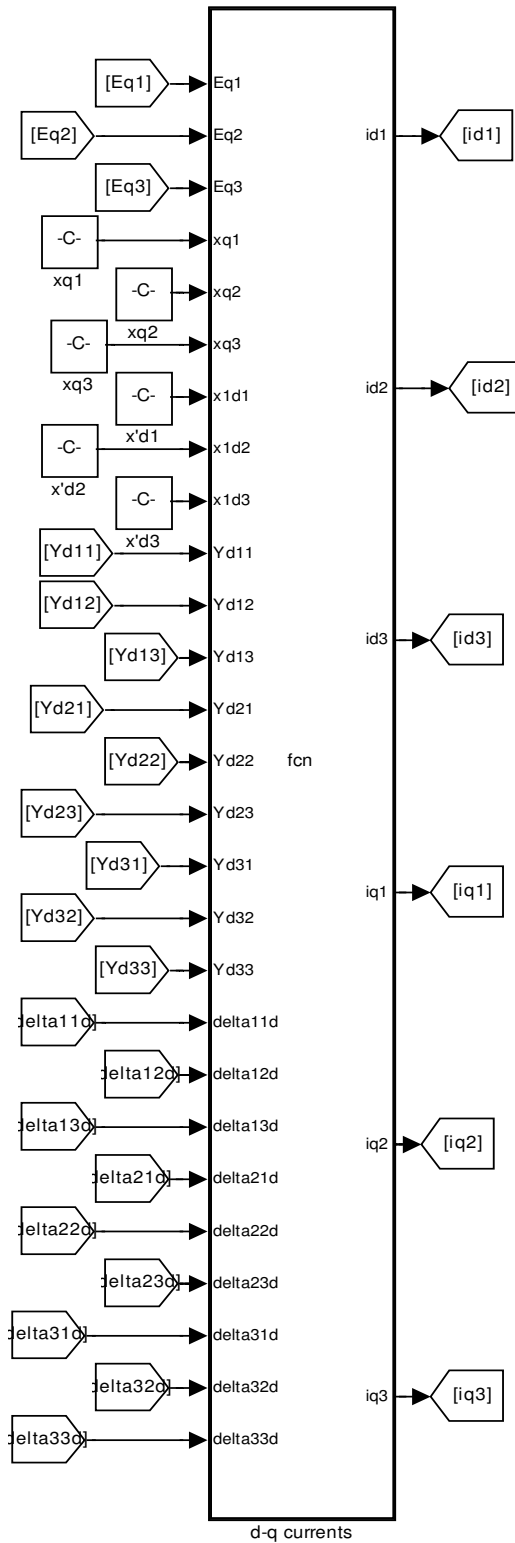


Figure C.5: Simulink model of multi-machine power system for calculating the  $d - q$  axes currents

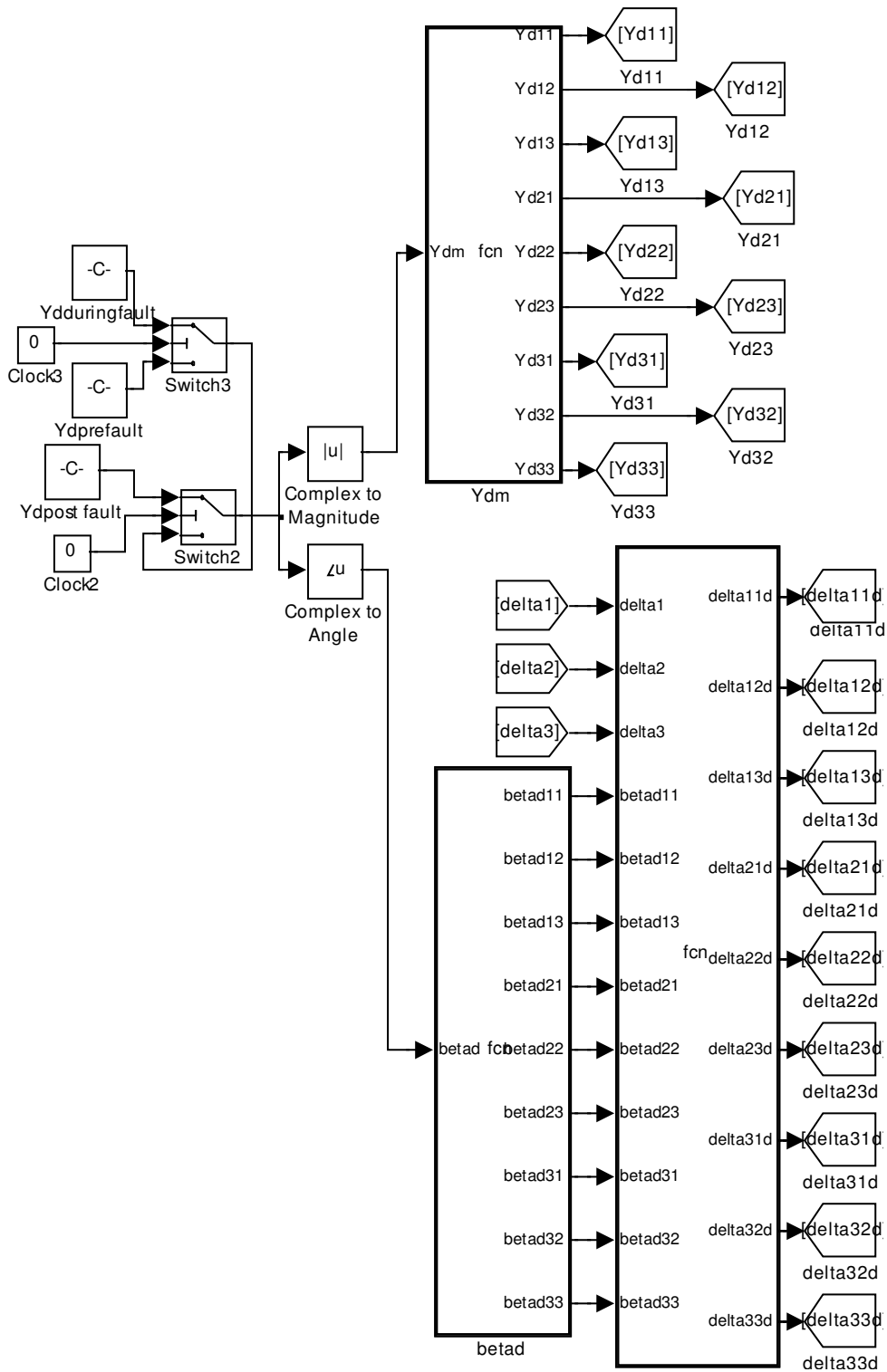


Figure C.6: Simulink model of multi-machine power system for calculating the angles from the admittance matrix

## APPENDIX D

## APPENDIX D

### NONLINEAR SIMULATION OF WSCC SYSTEM INCORPORATED WITH IPFC USING MATLAB/SIMULINK

Simulink model of the multi-machine power system with IPFC

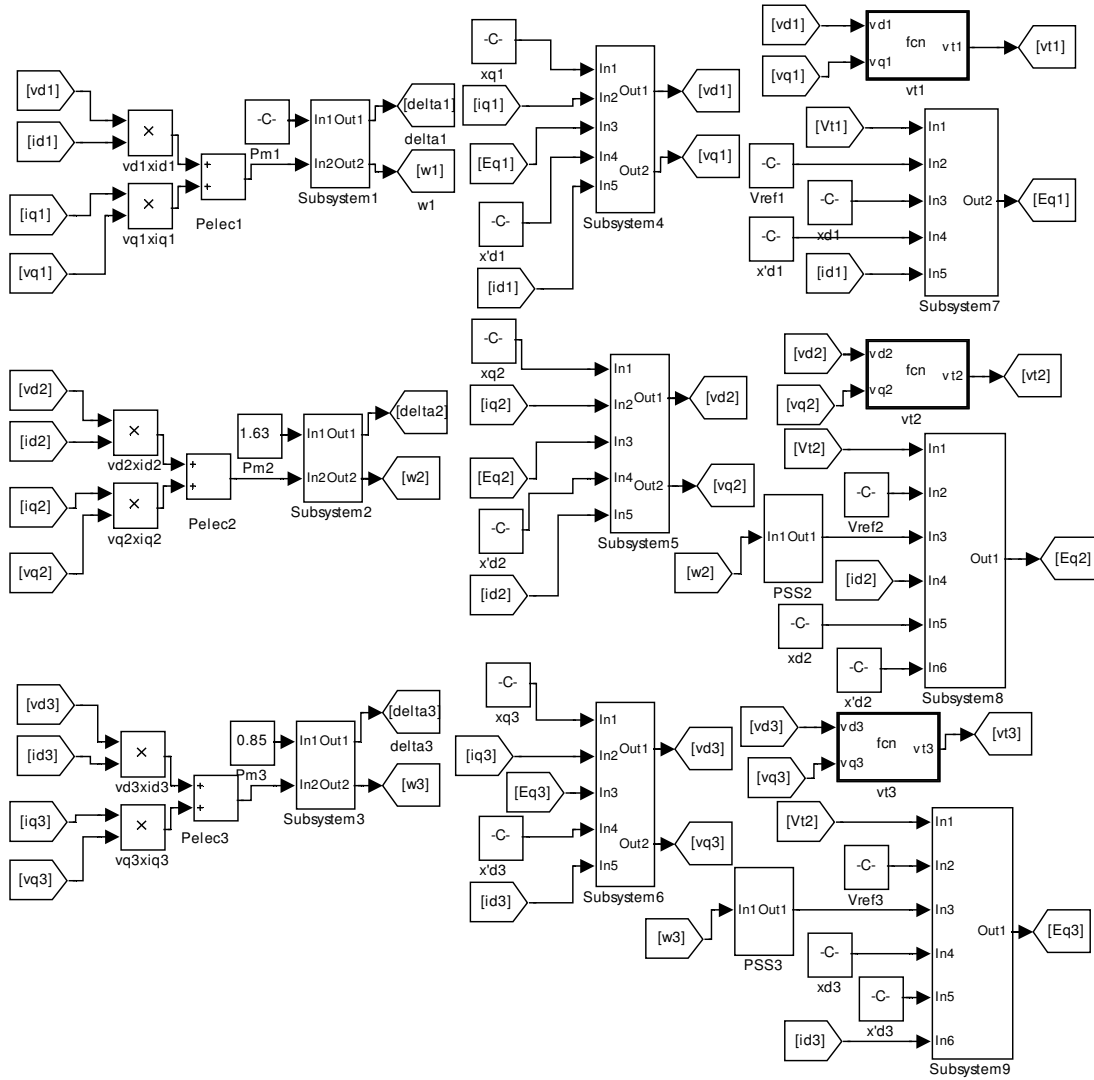


Figure D.1: Simulink model of multi-machine power system with IPFC representing the machine equations and stator algebraic equations along with the PSSs

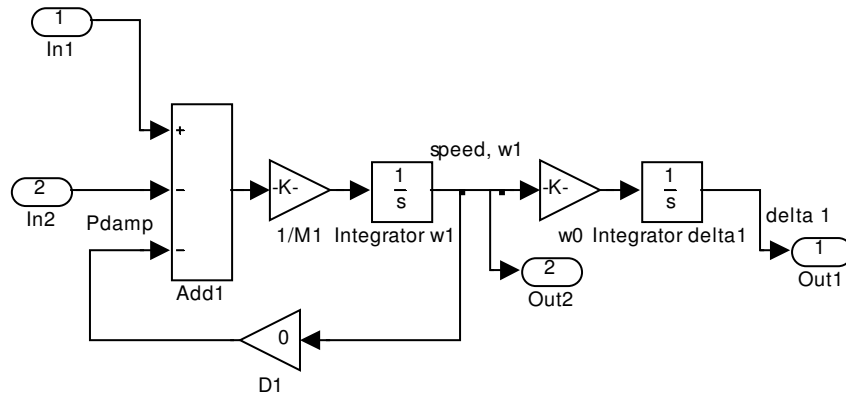


Figure D.2: Subsystem 1

The subsystems 2 and 3 are similar to Figure D.2

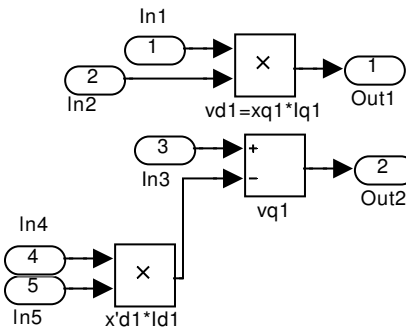


Figure D.3: Subsystem 4

The subsystems 5 and 6 are similar to Figure D.3

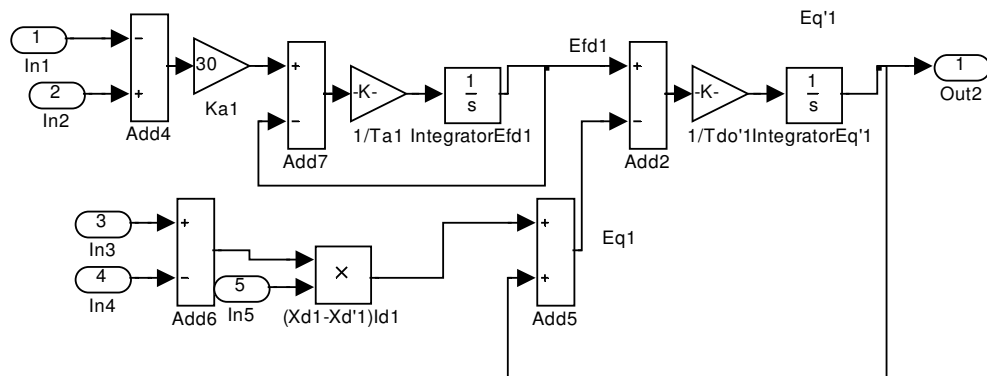


Figure D.4: Subsystem 7

Subsystems 8 and 9 are similar to Figure D.4

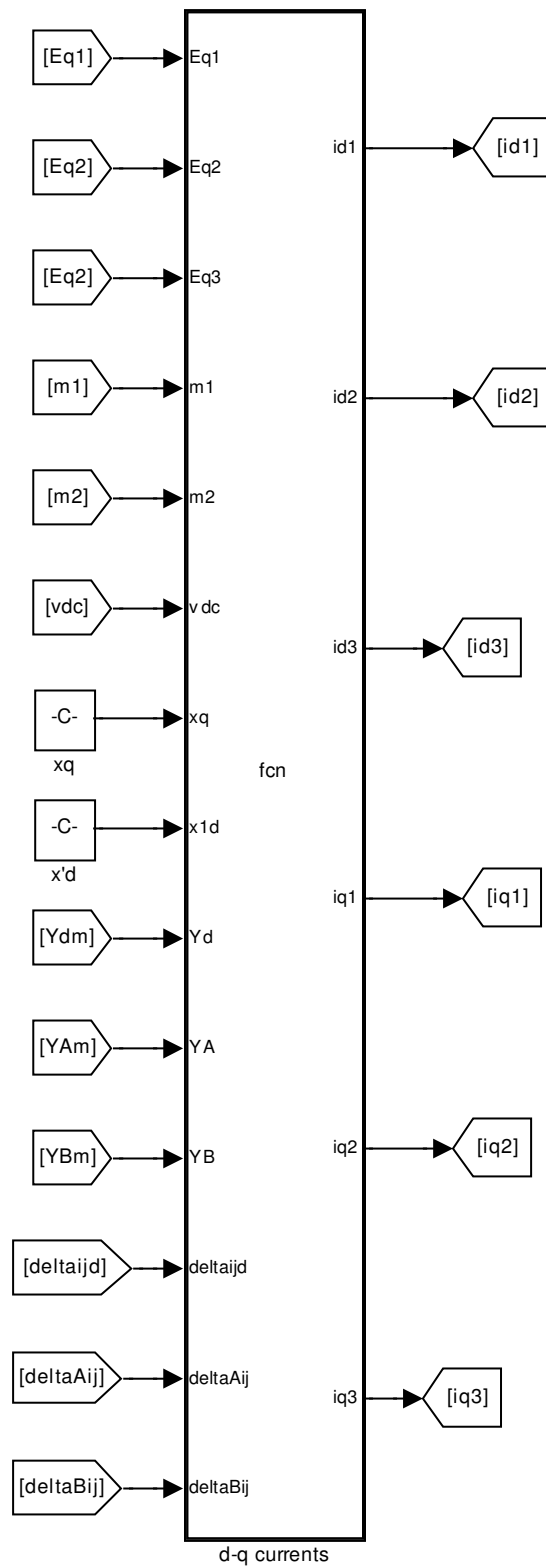


Figure D.5: Simulink model of multi-machine power system with IPFC for calculating the  $d - q$  axes currents

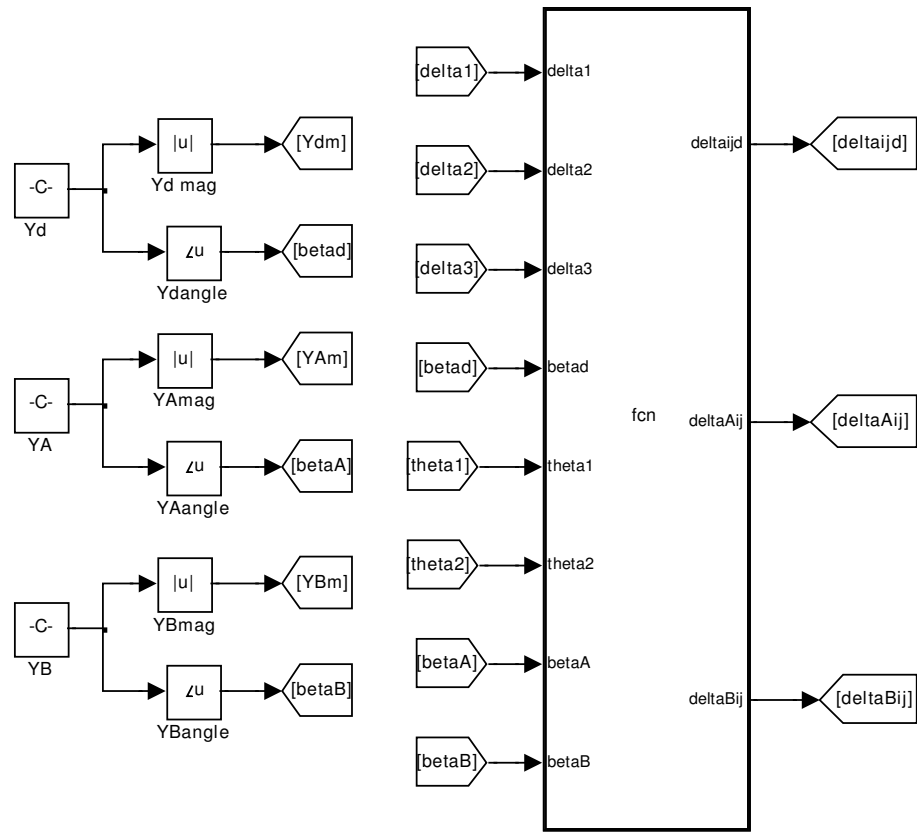


Figure D.6: Simulink model of multi-machine power system with IPFC for calculating the angles from the admittance matrix

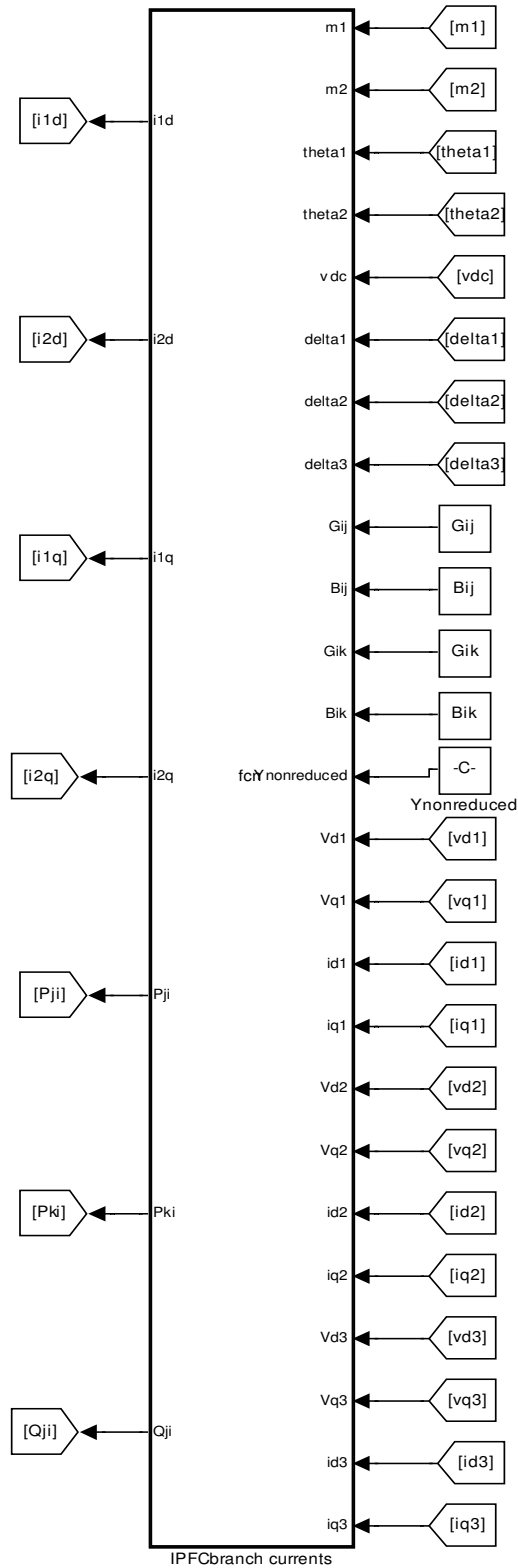


Figure D.7: Simulink model of multi-machine power system with IPFC for calculating the currents in IPFC branches

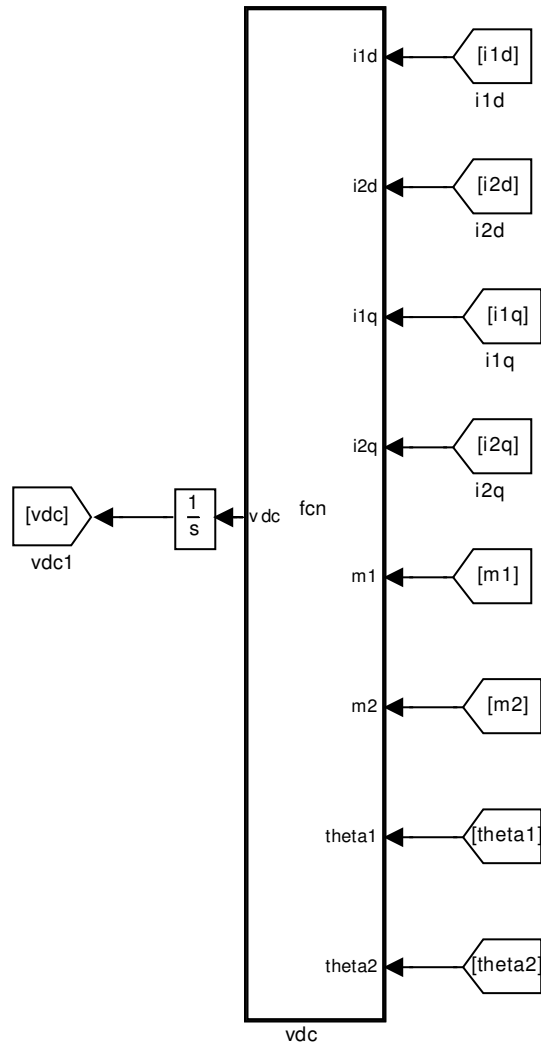


Figure D.8: Simulink model of multi-machine power system with IPFC for calculating the voltage across the DC link

# Interline Power Flow Controller Application for Low Frequency Oscillations Damping

ALIVELU, M. PARIMI      IRRIVAN ELAMVAZUTHI      NORDIN SAAD

Department of Electrical and Electronic Engineering

Universiti Teknologi Petronas

Bandar Seri Iskander, 31750, Tronoh, Perak

MALAYSIA

alivelup@yahoo.co.in, irraivan\_elamvazuthi@petronas.com.my, nordiss@petronas.com.my

*Abstract:* This paper presents the modeling of the power system installed with the Interline Power Flow Controller (IPFC), the latest proposed Flexible AC Transmission System (FACTS) controller. The IPFC is modeled in d-q axis form, and the dynamic model of a single machine infinite bus (SMIB) power system installed with IPFC is developed. Further, the linearized Phillips-Heffron model of the power system is established to study the oscillation stability. The damping controllers considering the various control signals are designed based on the linearized model. The power oscillation stability is investigated with the use of eigenvalue analysis and by nonlinear simulation of the dynamic model of the power system. Studies reveal that the most effective input signal of IPFC utilized for damping the low frequency oscillations is found to be the input signal  $m_2$ , providing robust performance under different operating conditions.

*Key-Words:* - FACTS, Interline power flow controller, Modelling, Phillips Heffron model, Power oscillation stability

## 1 Introduction

The phenomenon that is of great interest and vital concern in the power industry is the stability of electromechanical oscillations, i.e., the low frequency oscillations having an oscillation frequency in the range of 0.2 Hz to 2 Hz. These oscillations limit the maximum amount of power that can be transferred over the transmission lines and sometimes may have disastrous consequences to the interconnected systems stability, leading to partial or total collapses (black-outs). Therefore, equipment and procedures to enhance the damping of these oscillations become mandatory for the safe system operation, and to allow a better use of the existent transmission network. The traditional approaches to aid the damping of a power system oscillations is by adding a Power System Stabilizer (PSS) in the excitation system of the generator for which much experience and insight exist in the industry [1]-[3]. In the recent years, the rapid growth of power electronics has made Flexible AC Transmission Systems (FACTS) controllers very important in terms of controller application in power system damping in addition to their primary purpose of reactive power support, controlling line power flows etc. Major contributions have been made in

[4]-[12], in damping of power system oscillations where universal approaches are proposed for the analysis of the FACTS devices such as Thyristor Controlled Series Capacitor (TCSC), Static Var Compensator (SVC), Static Synchronous Compensator (STATCOM), Static Synchronous Series Capacitor (SSSC), Unified Power Flow Controller (UPFC).

Interline Power Flow Controller (IPFC), is the latest representative of the Voltage Source Converter (VSC) based FACTS devices, and was proposed by Gyugyi with Sen and Schauder [13]. Like the UPFC, the IPFC is a combined compensator, consisting of at least two or more VSCs with a common dc link. This dc link provides the device with an active power transfer path among the converters, thereby facilitating real power transfer among the lines of the transmission system which enables the IPFC to compensate multiple transmission lines at a given substation. Each converter also provides reactive power compensation independently on its own transmission line. Thus, the IPFC provides the real and reactive power compensation to the system. The controllability of the line power flow by IPFC has been well recognized [14]-[16]. However, very limited information is reported [17]-[19] concerning

the control of the IPFC to provide additional damping during system oscillations. The damping function of the IPFC has not been investigated thoroughly. Chen *et. al.* [17, 18], proposed a PID controller for oscillation damping enhancement in a SMIB test system. However, due to the complexity and nonlinearity of the power system the performance of the damping controller is degraded to a certain extent. Kazemi *et. al* [19] proposed a PI supplementary controller with its input equal to the electrical power of the generator for oscillation damping. However, they have not optimized the parameters of the controller.

In the view of this, the primary object of this paper is to develop a dynamic model for IPFC for small signal stability analysis and examine its damping function in mitigating the power system oscillations. The rest of the paper is organized as follows: Firstly the mathematical model has been developed for IPFC in d-q axis form in section 2. Secondly a small signal linearized Phillips–Heffron model of a power system installed with an IPFC is derived in section 3. Thirdly the IPFC based damping controller is designed on the basis of linearized system model, using the phase compensation method as described in section 4. Lastly the relative effectiveness of the IPFC control signals on which the damping function of the IPFC is superimposed is examined and analyzed on single machine infinite bus power system (SMIB). The performance of IPFC based controllers in achieving the damping of low frequency oscillations of the power system is compared. The effectiveness of the controllers under wide variations in operating conditions is studied. The ability of the damping controllers during various disturbances is examined with nonlinear simulation of the dynamic model of the power system. The simulation results are given in section 5.

## 2 Modeling of IPFC

The schematic diagram of IPFC is shown in Fig. 1. It consists of two three phase Gate turn-off (GTO) based VSCs, each providing series reactive compensation for the two lines. The VSCs are linked together at their dc terminals and are connected to the transmission lines through their series coupling transformers. The converters can transfer the real power between them via their common dc terminal. In Fig. 1,  $m_1, m_2$  and  $\delta_1, \delta_2$  refer to amplitude modulation index and phase-angle of the control signal of each VSC, respectively, which are the input control signals to

the IPFC. To model the IPFC, consider phase ‘a’ of the coupling transformer and the VSC 1, arms along with the dc link, as shown in Fig. 2.  $C_{dc}$  is the dc link capacitor.  $r_1$  and  $l_1$  are the per phase resistance and inductance of transformer on line 1.  $\zeta_{C1a}$  and  $\zeta'_{C1a}$  represent the bidirectional switches which can be either on or off in Fig. 2.  $r_s$  is the switch on state resistance.

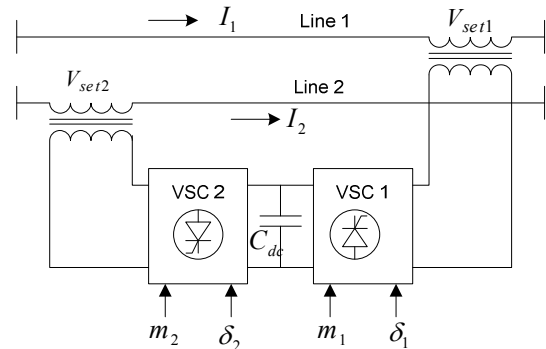


Fig. 1. Schematic diagram of IPFC

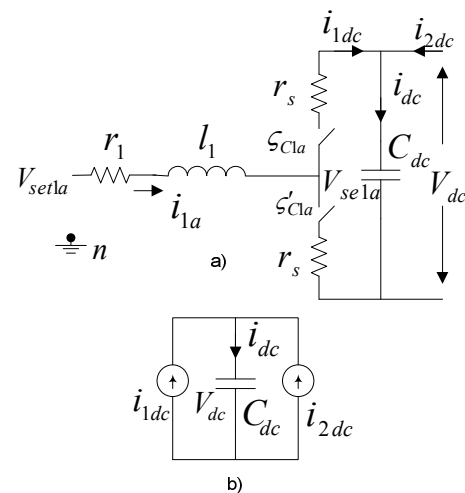


Fig. 2. a) Equivalent circuit of phase ‘a’ of coupling transformer and VSC 1. b) Dynamics of dc link capacitor.

The mathematical model for each phase *a*, *b* and *c* for both the VSC’s are obtained similar to the approach in [20]. The three phase differential equations of the IPFC are:

$$\begin{bmatrix} \frac{di_{1a}}{dt} \\ \frac{di_{1b}}{dt} \\ \frac{di_{1c}}{dt} \end{bmatrix} = \begin{bmatrix} -\frac{R_1}{l_1} & 0 & 0 \\ 0 & -\frac{R_1}{l_1} & 0 \\ 0 & 0 & -\frac{R_1}{l_1} \end{bmatrix} \begin{bmatrix} i_{1a} \\ i_{1b} \\ i_{1c} \end{bmatrix} - \frac{m_1 v_{dc}}{2l_1} \times$$

$$\begin{bmatrix} \cos(\omega t + \delta_1) \\ \cos(\omega t + \delta_1 - 120^\circ) \\ \cos(\omega t + \delta_1 - 240^\circ) \end{bmatrix} + \begin{bmatrix} \frac{1}{l_1} & 0 & 0 \\ 0 & \frac{1}{l_1} & 0 \\ 0 & 0 & \frac{1}{l_1} \end{bmatrix} \begin{bmatrix} V_{set1a} \\ V_{set1b} \\ V_{set1c} \end{bmatrix} \quad (1)$$

$$\begin{bmatrix} \frac{di_{2a}}{dt} \\ \frac{di_{2b}}{dt} \\ \frac{di_{2c}}{dt} \end{bmatrix} = \begin{bmatrix} -\frac{R_2}{l_2} & 0 & 0 \\ 0 & -\frac{R_2}{l_2} & 0 \\ 0 & 0 & -\frac{R_2}{l_2} \end{bmatrix} \begin{bmatrix} i_{2a} \\ i_{2b} \\ i_{2c} \end{bmatrix} - \frac{m_2 v_{dc}}{2l_2} \times \begin{bmatrix} \frac{1}{l_2} & 0 & 0 \\ 0 & \frac{1}{l_2} & 0 \\ 0 & 0 & \frac{1}{l_2} \end{bmatrix} \begin{bmatrix} V_{set2a} \\ V_{set2b} \\ V_{set2c} \end{bmatrix} \quad (2)$$

where  $R_1 = r_1 + r_s$ . The dc link capacitor voltage is:

$$\begin{aligned} \frac{dv_{dc}}{dt} &= \frac{m_1}{2C_{dc}} [\cos(\omega t + \delta_1) \cos(\omega t + \delta_1 - 120^\circ) \\ &\cos(\omega t + \delta_1 + 120^\circ)] \begin{bmatrix} i_{1a} \\ i_{1b} \\ i_{1c} \end{bmatrix} + \frac{m_2}{2C_{dc}} [\cos(\omega t + \delta_2) \\ &\cos(\omega t + \delta_2 - 120^\circ) \cos(\omega t + \delta_2 + 120^\circ)] \begin{bmatrix} i_{2a} \\ i_{2b} \\ i_{2c} \end{bmatrix} \end{aligned} \quad (3)$$

### 2.2 IPFC modeled in d-q axis form

By applying the Park's transformation, the equations (1-3) are developed into the rotating reference ( $d-q-o$  axis) frame as:

$$\begin{bmatrix} \frac{di_{1d}}{dt} \\ \frac{di_{1q}}{dt} \\ \frac{di_{10}}{dt} \end{bmatrix} = \begin{bmatrix} -\frac{R_1}{l_1} & \omega & 0 \\ -\omega & -\frac{R_1}{l_1} & 0 \\ 0 & 0 & -\frac{R_1}{l_1} \end{bmatrix} \begin{bmatrix} i_{1d} \\ i_{1q} \\ i_{10} \end{bmatrix} + \begin{bmatrix} \frac{1}{l_1} & 0 & 0 \\ 0 & \frac{1}{l_1} & 0 \\ 0 & 0 & \frac{1}{l_1} \end{bmatrix} \begin{bmatrix} v_{set1d} \\ v_{set1q} \\ v_{set10} \end{bmatrix} - \frac{m_1 v_{dc}}{2l_1} \begin{bmatrix} \cos\delta_1 \\ \sin\delta_1 \\ 0 \end{bmatrix} \quad (4)$$

$$\begin{bmatrix} \frac{di_{2d}}{dt} \\ \frac{di_{2q}}{dt} \\ \frac{di_{20}}{dt} \end{bmatrix} = \begin{bmatrix} \frac{R_2}{l_2} & \omega & 0 \\ -\omega & \frac{R_2}{l_2} & 0 \\ 0 & 0 & -\frac{R_2}{l_2} \end{bmatrix} \begin{bmatrix} i_{2d} \\ i_{2q} \\ i_{20} \end{bmatrix} + \begin{bmatrix} \frac{1}{l_2} & 0 & 0 \\ 0 & \frac{1}{l_2} & 0 \\ 0 & 0 & \frac{1}{l_2} \end{bmatrix} \begin{bmatrix} v_{set2d} \\ v_{set2q} \\ v_{set20} \end{bmatrix} - \frac{m_2 v_{dc}}{2l_2} \begin{bmatrix} \cos\delta_2 \\ \sin\delta_2 \\ 0 \end{bmatrix} \quad (5)$$

$$\begin{aligned} \frac{dv_{dc}}{dt} &= \frac{3m_1}{4C_{dc}} [\cos\delta_1 \sin\delta_1 \ 0] \begin{bmatrix} i_{1d} \\ i_{1q} \\ i_{10} \end{bmatrix} \\ &+ \frac{3m_2}{4C_{dc}} [\cos\delta_2 \sin\delta_2 \ 0] \begin{bmatrix} i_{2d} \\ i_{2q} \\ i_{20} \end{bmatrix} \end{aligned} \quad (6)$$

Equations (4-6) represent the three phase dynamic differential equations of the IPFC on the rotor axis frame. Neglecting the resistance and transients of series converter transformers the dynamic model of IPFC (4-6) can be written as:

$$\begin{bmatrix} V_{set1d} \\ V_{set1q} \end{bmatrix} = \begin{bmatrix} 0 & -x_{t1} \\ x_{t1} & 0 \end{bmatrix} \begin{bmatrix} i_{1d} \\ i_{1q} \end{bmatrix} + \frac{v_{dc}}{2} \begin{bmatrix} m_1 \cos\delta_1 \\ m_1 \sin\delta_1 \end{bmatrix} \quad (7)$$

$$\begin{bmatrix} v_{set2d} \\ v_{set2q} \end{bmatrix} = \begin{bmatrix} 0 & -x_{t2} \\ x_{t2} & 0 \end{bmatrix} \begin{bmatrix} i_{2d} \\ i_{2q} \end{bmatrix} + \frac{v_{dc}}{2} \begin{bmatrix} m_2 \cos\delta_2 \\ m_2 \sin\delta_2 \end{bmatrix} \quad (8)$$

$$\begin{aligned} \frac{dv_{dc}}{dt} &= \frac{3m_1}{4C_{dc}} [\cos\delta_1 \ \sin\delta_1] \begin{bmatrix} i_{1d} \\ i_{1q} \end{bmatrix} \\ &+ \frac{3m_2}{4C_{dc}} [\cos\delta_2 \ \sin\delta_2] \begin{bmatrix} i_{2d} \\ i_{2q} \end{bmatrix} \end{aligned} \quad (9)$$

where  $x_{t1} = \omega l_1$ ,  $x_{t2} = \omega l_2$  are the reactances of the series transformers.

## 3 System Model

### 3.1 Non Linear Model

Fig. 3 shows a Single machine infinite bus (SMIB) power system equipped with an IPFC. The system consists of a generator which is connected to the infinite bus through the two parallel transmission lines. An elementary IPFC consisting of two three-phase GTO based VSCs, each compensating a

different transmission line by series voltage injection is installed on the two transmission lines.

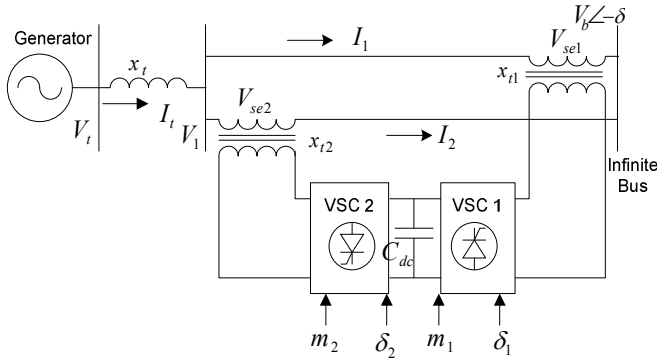


Fig. 3. An IPFC installed in a single machine infinite bus system

The VSCs are linked together at their DC terminals facilitating real power transfer among the transmission lines. The nonlinear dynamic model of the power system of Fig. 3 is derived as follows:

$$\dot{\delta} = \omega_0(\omega - 1) \quad (10)$$

$$\dot{\omega} = \frac{P_m - P_e - P_D}{M} \quad (11)$$

$$\dot{E}'_q = \frac{(-E_q + E_{fd})}{T'_{do}} \quad (12)$$

$$\dot{E}_{fd} = \frac{-E_{fd} + K_a(V_{ref} - V_t)}{T_a} \quad (13)$$

$$\dot{v}_{dc} = \frac{3m_1}{4C_{dc}}(i_{1d} \cos \delta_1 + i_{1q} \sin \delta_1) + \frac{3m_2}{4C_{dc}}(i_{2d} \cos \delta_2 + i_{2q} \sin \delta_2) \quad (14)$$

where

$$P_e = P_1 + P_2 = v_{dt} i_{dt} + v_{qt} i_{qt}$$

$$E_q = E'_q + (x_d - x'_d) i_{dt} = E'_q + (x_d - x'_d)(i_{1d} + i_{2d})$$

$$v_{qt} = E'_q - x'_d i_{dt} = E'_q - x'_d(i_{1d} + i_{2d})$$

$$v_{dt} = x_q i_{qt} = x_q(i_{1q} + i_{2q})$$

$$v_t = (v_{dt}^2 + v_{qt}^2)^{1/2},$$

$$i_t = i_{dt} + j i_{qt}, \quad i_t = i_1 + i_2$$

$$i_{dt} = i_{1d} + i_{2d}, \quad i_{qt} = i_{1q} + i_{2q}$$

$P_1, P_2$  are the power flow in each of the transmission lines and  $\delta$ , is the rotor angle of synchronous generator in radians,  $\omega$  is rotor speed

in rad/sec,  $V_t$  is the terminal voltage of the generator,  $E'_q$  is generator internal voltage,  $E_{fd}$  is the generator field voltage,  $v_{dc}$  is the voltage at DC link.  $I_1$  and  $I_2$  are the line currents flowing the transmission lines.

From the Fig. 3, we obtain:

$$V_t = jx_t I_t + V_1 \quad (15)$$

$$\begin{aligned} V_1 &= V_{se1} + jx_{L1} I_1 + V_b \\ &= V_{se2} + jx_{L2} I_2 + V_b \end{aligned} \quad (16)$$

where  $x_{L1}, x_{L2}$  are the transmission line reactances, therefore,

$$\begin{aligned} V_t &= jx_t I_t + V_{se1} + jx_{L2} I_2 + V_b \\ v_{dt} + jv_{qt} &= x_q(i_{1q} + i_{2q}) + jE'_q - jx'_d(i_{1d} + i_{2d}) \\ &= jx_t(i_{1d} + i_{2d} + j i_{1q} + j i_{2q}) + v_{se2td} \\ &\quad + jv_{se2tq} + j(x_{L2})(i_{2d} + j i_{2q}) \\ &\quad + V_b \sin \delta + jV_b \cos \delta \end{aligned} \quad (17)$$

Solving the equations we get:

$$\begin{aligned} i_{1d} &= x_{11d} E'_q + \frac{1}{2}(x_{12d} - x_{11d})v_{dc} m_2 \sin \delta_2 \\ &\quad - \frac{1}{2}x_{12d} v_{dc} m_1 \sin \delta_1 - x_{11d} v_b \cos \delta \end{aligned} \quad (18)$$

$$\begin{aligned} i_{2d} &= x_{21d} E'_q + \frac{1}{2}(x_{22d} - x_{21d})v_{dc} m_2 \sin \delta_2 \\ &\quad - \frac{1}{2}x_{22d} v_{dc} m_1 \sin \delta_1 - x_{21d} v_b \cos \delta \end{aligned} \quad (19)$$

$$\begin{aligned} i_{1q} &= \frac{1}{2}(x_{11q} + x_{12q})v_{dc} m_2 \cos \delta_2 \\ &\quad - \frac{1}{2}(x_{12q})v_{dc} m_1 \cos \delta_1 + x_{11q} v_b \sin \delta \end{aligned} \quad (20)$$

$$\begin{aligned} i_{2q} &= \frac{1}{2}(x_{21q} + x_{22q})v_{dc} m_2 \cos \delta_2 \\ &\quad - \frac{1}{2}(x_{22q})v_{dc} m_1 \cos \delta_1 + x_{21q} v_b \sin \delta \end{aligned} \quad (21)$$

where

$$x_{11d} = x_{tL2} / x_{\Sigma 1}, \quad x_{12d} = (x'_{dt} + x_{tL2}) / x_{\Sigma 1}$$

$$x_{21d} = x_{tL1} / x_{\Sigma 1}, \quad x_{22d} = -x'_{dt} / x_{\Sigma 1}$$

$$x_{11q} = x_{tL2} / x_{\Sigma 2}, \quad x_{12q} = -(x'_{qt} + x_{tL2}) / x_{\Sigma 2}$$

$$x_{21q} = x_{tL1} / x_{\Sigma 2}, \quad x_{22d} = -x'_{qt} / x_{\Sigma 2}$$

$$x_{iL2} = x_{t2} + x_{L2}, x'_{dt} = x'_d + x_t$$

$$x_{iL1} = x_{t1} + x_{L1}, x'_{qt} = x_q + x_t$$

$$x_{\Sigma 1} = (x'_{dt} \cdot x_{iL2}) + (x'_{dt} + x_{iL2})(x_{iL1})$$

$$x_{\Sigma 2} = (x'_{qt} \cdot x_{iL2}) + (x'_{qt} + x_{iL2})(x_{iL1})$$

### 3.2 Linearized model

The linear Heffron-Phillips model of SMIB system installed with IPFC is obtained by linearizing the non linear model equations (10-21) which is obtained as follows:

$$\Delta \dot{\delta} = \omega_o \Delta \omega \quad (22)$$

$$\Delta \dot{\omega} = \frac{(\Delta P_m - \Delta P_e - D \Delta \omega)}{M} \quad (23)$$

$$\Delta \dot{E}'_q = \frac{-\Delta E_q + \Delta E_{fd}}{T'_{do}} \quad (24)$$

$$\Delta \dot{E}_{fd} = \frac{-\Delta E_{fd} + K_a (\Delta V_{ref} - \Delta V_t)}{T_a} \quad (25)$$

$$\begin{aligned} \Delta \dot{v}_{dc} = & K_7 \Delta \delta + K_8 \Delta E'_q - K_9 \Delta v_{dc} + K_{cm1} \Delta m_1 \\ & + K_{c\delta 1} \Delta \delta_1 + K_{cm2} \Delta m_2 + K_{c\delta 2} \Delta \delta_2 \end{aligned} \quad (26)$$

where

$$\begin{aligned} \Delta P_e = & K_1 \Delta \delta + K_2 \Delta E'_q + K_{pv} \Delta v_{dc} + K_{pm1} \Delta m_1 \\ & + K_{p\delta 1} \Delta \delta_1 + K_{pm2} \Delta m_2 + K_{p\delta 2} \Delta \delta_2 \end{aligned} \quad (27)$$

$$\begin{aligned} \Delta E_q = & K_4 \Delta \delta + K_3 \Delta E'_q + K_{qv} \Delta v_{dc} + K_{qm1} \Delta m_1 \\ & + K_{q\delta 1} \Delta \delta_1 + K_{qm2} \Delta m_2 + K_{q\delta 2} \Delta \delta_2 \end{aligned} \quad (28)$$

$$\begin{aligned} \Delta V_t = & K_5 \Delta \delta + K_6 \Delta E'_q + K_{vv} \Delta v_{dc} + K_{vm1} \Delta m_1 \\ & + K_{v\delta 1} \Delta \delta_1 + K_{vm2} \Delta m_2 + K_{v\delta 2} \Delta \delta_2 \end{aligned} \quad (29)$$

The model has 28 K-constants which are functions of system parameters and the initial operating condition.

### 3.3 State Space Model

The power system is represented in state space as:

$$\dot{X} = AX + BU \quad (30)$$

where the state vector and control vector are:

$$X = [\Delta \delta \quad \Delta \omega \quad \Delta E'_q \quad \Delta E_{fd} \quad \Delta v_{dc}]^T$$

$$U = [\Delta m_1 \quad \Delta \delta_1 \quad \Delta m_2 \quad \Delta \delta_2]^T \quad (31)$$

and, state and control matrix are:

$$A = \begin{bmatrix} 0 & \omega_o & 0 & 0 & 0 \\ -\frac{K_1}{M} & -\frac{D}{M} & -\frac{K_2}{M} & 0 & -\frac{K_{pv}}{M} \\ -\frac{K_4}{T'_{do}} & 0 & -\frac{K_3}{T'_{do}} & \frac{1}{T'_{do}} & -\frac{K_{qv}}{T'_{do}} \\ -\frac{K_a K_5}{T_a} & 0 & -\frac{K_a K_6}{T_a} & -\frac{1}{T_a} & -\frac{K_a K_{vv}}{T_a} \\ K_7 & 0 & K_8 & 0 & -K_9 \end{bmatrix}$$

$$B = \begin{bmatrix} 0 & 0 & 0 & 0 \\ \frac{K_{pm1}}{M} & \frac{K_{p\delta 1}}{M} & \frac{K_{pm2}}{M} & \frac{K_{p\delta 2}}{M} \\ \frac{K_{qm1}}{T'_{do}} & \frac{K_{q\delta 1}}{T'_{do}} & \frac{K_{qm2}}{T'_{do}} & \frac{K_{q\delta 2}}{T'_{do}} \\ \frac{K_a K_{vm1}}{T_a} & \frac{K_a K_{v\delta 1}}{T_a} & \frac{K_a K_{vm2}}{T_a} & \frac{K_a K_{v\delta 2}}{T_a} \\ K_{cm1} & K_{c\delta 1} & K_{cm2} & K_{c\delta 2} \end{bmatrix}$$

and  $\Delta m_1$  is the deviation in pulse width modulation index  $m_1$  of voltage series converter 1 in line 1.  $\Delta m_2$  is the deviation in pulse width modulation index  $m_2$  of voltage series converter 2 in line 2.  $\Delta \delta_1$  is the deviation in phase angle of the injected voltage  $V_{se1}$ .  $\Delta \delta_2$  is the deviation in phase angle of the injected voltage  $V_{se2}$ .

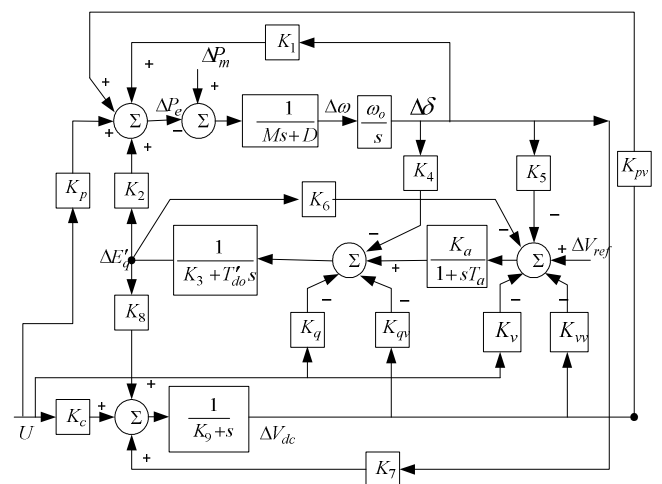


Fig. 4. Phillips-Heffron model of SMIB system installed with IPFC

The extended Phillips-Heffron model of SMIB system installed with IPFC (30) is shown as a block diagram in Fig. 4. It should be noted that  $K_p, K_q, K_v$  and  $K_c$  in Fig. 4 are the row vectors defined as

$$\begin{aligned} K_p &= [K_{pm1} \quad K_{p\delta_1} \quad K_{pm2} \quad K_{p\delta_2}] \\ K_q &= [K_{qm1} \quad K_{q\delta_1} \quad K_{qm2} \quad K_{q\delta_2}] \\ K_v &= [K_{vm1} \quad K_{v\delta_1} \quad K_{vm2} \quad K_{v\delta_2}] \\ K_c &= [K_{cm1} \quad K_{c\delta_1} \quad K_{cm2} \quad K_{c\delta_2}] \end{aligned}$$

From (31), we observe that any of the four inputs control signals  $\Delta m_1, \Delta \delta_1, \Delta m_2$  and  $\Delta \delta_2$  can be utilized to superimpose on the damping function of IPFC.

#### 4 IPFC Damping Controller

The damping controller is designed to contribute a positive damping torque in phase with the speed deviation to the electromechanical oscillation loop of the generator. The structure of the IPFC based damping controller is shown in Fig. 5, which comprises of gain  $K_{dc}$ , signal washout block and ‘n’ lead lag compensator blocks.

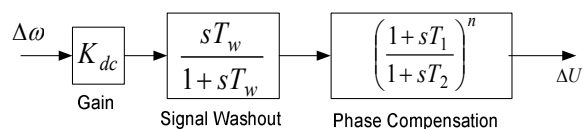


Fig. 5. Structure of IPFC based damping controller

The time constants of lead lag compensator are determined using the phase compensation method [21] to compensate the phase shift between the control input signal  $\Delta U$  and electrical power deviation  $\Delta P_e$ . The gain setting  $K_{dc}$  of the damping controller is chosen to achieve a required damping ratio of the electromechanical mode and the value of  $T_w$  (the washout filter time constant) is chosen in the range of 10 to 20s. The four control parameters,  $m_1, m_2, \delta_1$  and  $\delta_2$  can be modulated to produce the damping torque. The damping controller based on the IPFC input signal  $m_1$  is termed as the damping controller  $m_1$  and consequently other controller based on input signals  $m_2, \delta_1$  and  $\delta_2$  are termed as damping controller  $m_2$ , damping controller  $\delta_1$  and damping controller  $\delta_2$ .

#### 5 Simulation Results

A single machine infinite bus power system installed with IPFC is considered for analysis, parameters of which are given in Appendix A. The system is operated with various different load conditions, i.e., from  $P_e = 0.1$  pu to  $P_e = 1.5$  pu, and  $V_t = 1.02$  pu,  $V_b = 1.0$  pu. The linearized model is obtained at each varying condition and eigenvalue analysis is performed. The values of the  $K$  constants of the system at the one operating point  $P_e = 0.8$  pu is given in the Appendix B. Eigenvalues for the power system at this operating point are shown in Table 1. The system contains a pair of complex eigenvalues having low damping ratio of 0.0084952. A controller is designed to tune the gain  $K_{dc}$  to achieve a damping ratio of 0.1. The various damping controllers are designed at the operating point  $P_e = 0.8$  pu, where the parameters of each controller is given in the Appendix C.

Table 1: Eigenvalues of the linearized SMIB at operating point  $P_e = 0.8$  pu.

Eigenvalues	Damping Ratio	Frequency
-100.09	1	0
-0.09782 ± j11.514	0.0084952	1.8325
-0.31442	1	0
-0.0023063	1	0

The dynamic performance of the system is examined using the alternative damping controllers with varying operating conditions. The responses are shown for the operating conditions  $P_e = 0.8$  pu the nominal condition,  $P_e = 0.2$  pu light load condition and  $P_e = 1.4$  pu the heavy load condition.

##### 5.1 Operating point $P_e = 0.8$ pu

The effectiveness of IPFC damping controllers at the nominal operating condition  $P_e = 0.8$  pu at which they are designed is observed. The power system performance in the presence of the controllers is investigated with the non linear simulation of the system modelled by the nonlinear differential equations (10-21). A three phase fault occurs at 1.0 sec at the starting end of the transmission line and cleared after 100 ms. The response of the system without the controller (marked by ‘no controller’) is shown with dotted line and the responses with IPFC controller is shown with solid line marked by the arrow “with controller”.

**5.1.1 Damping Controller  $m_1$**

The system eigenvalues in the presence of the damping controller  $m_1$  is shown in Table 2.

Table 2: Eigenvalues of the linearized SMIB at operating point  $P_e = 0.8$  pu with damping controller  $m_1$

Eigenvalues	Damping Ratio	Frequency
0	-	0
-100.01	1	0
$-1.2986 \pm j11.531$	0.11191	1.8353
-6.5463	1	0
-0.37662	1	0
-0.095395	1	0
-0.0023062	1	0

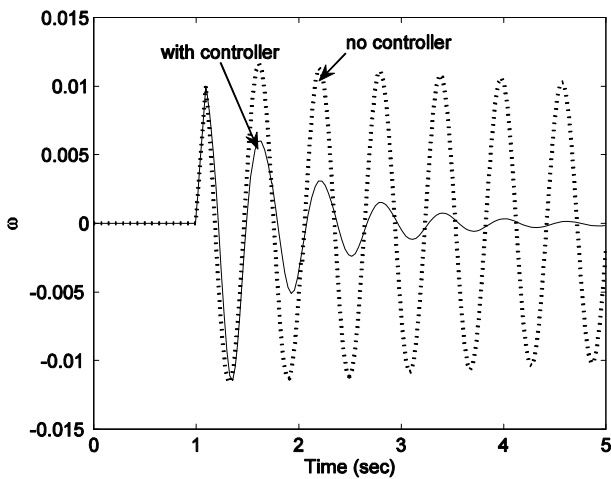


Fig.6. Rotor Speed response with and without damping controller  $m_1$  at  $P_e = 0.8$  pu

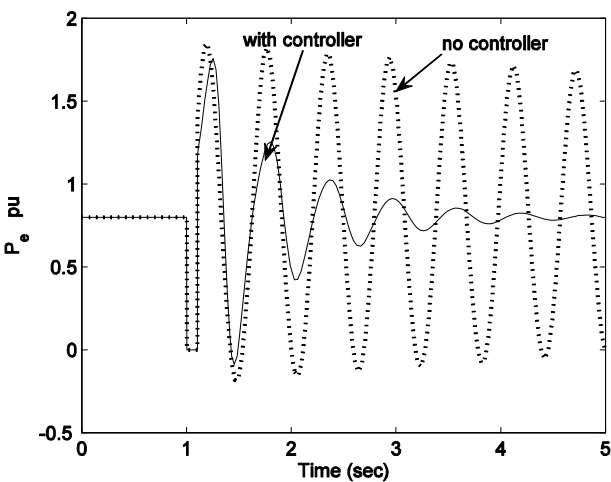


Fig. 7. Electrical Power response with and without damping controller  $m_1$  at  $P_e = 0.8$  pu.

The complex eigenvalue pair's damping ratio has increased to approximately 0.11 as desired. The rotor speed and electrical power response during and after the fault clearance, with and without the controller is shown in Fig. 6 and Fig. 7 respectively. It is clear from these Figures that, the system is oscillating without the controller due to the poor damping of the oscillation modes and as such power system oscillations are clearly observed. It is also seen, that the use of the proposed IPFC damping controller  $m_1$  the oscillations are suppressed in about 4.5 sec. after the fault is cleared i.e at 5.5sec, simulation time.

**5.1.2 Damping Controller  $m_2$**

Table 3 gives the eigenvalues of the system in the presence of the damping controller  $m_2$ . The damping ratio of the pair of complex eigenvalues has increased to 0.10877 with the use of this

Table 3: Eigenvalues of the linearized SMIB at operating point  $P_e = 0.8$  pu with damping controller  $m_2$

Eigenvalues	Damping Ratio	Frequency
0	-	0
-100.08	1	0
$-1.2541 \pm j11.461$	0.10877	1.8241
-11.003	1	0
-0.0023052	1	0
-0.1	1	0
-0.31631	1	0

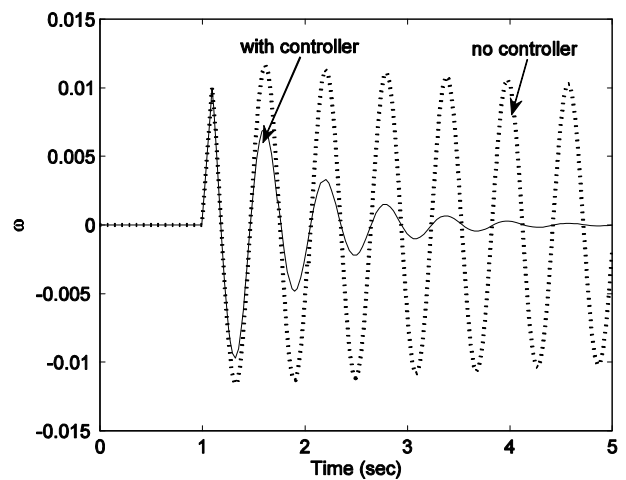


Fig. 8. Rotor Speed response with and without damping controller  $m_2$  at  $P_e = 0.8$  pu

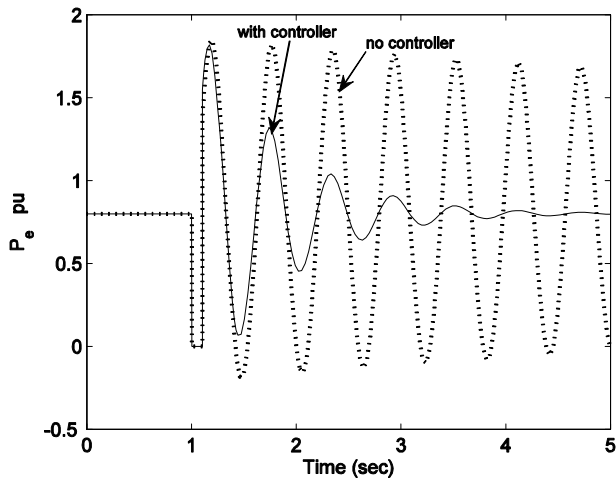


Fig. 9. Electrical Power response with and without damping controller  $m_2$  at  $P_e = 0.8$  pu

damping controller at the operating point  $P_e = 0.8$  pu as per the designed requirement. Fig. 8 and Fig. 9 show the rotor speed and electrical power response in the presence of the damping controller  $m_2$  from the nonlinear simulation. The oscillations occurring due to the fault are mitigated at the time of 4.5 sec i.e around 3.5 sec after the fault clearance. The controller  $m_2$  is comparatively better than the damping controller  $m_1$  and also, in the value of the gain  $K_{dc}$  required by the controllers to achieve same performance. The gain of the controller  $m_1$  is much higher (equal to 182.12) compared to the gain of the damping controller  $m_2$  which is equal to 15.235. As such the damping controller  $m_2$  is much more effective than damping controller  $m_1$ .

### 5.1.3 Damping Controller $\delta_1$

The eigenvalues of the system with the damping controller  $\delta_1$  is given in the Table 4. The controller achieves the damping ratio of 0.10189 for the pair of

Table 4: Eigenvalues of the linearized SMIB at operating point  $P_e = 0.8$  pu with damping controller  $\delta_1$

Eigenvalues	Damping Ratio	Frequency
0	-	0
$-22.599 \pm j94.966$	0.23151	15.114
-105.84	1	0
$-1.139 \pm j11.12$	0.10189	1.7698
-0.31395	1	0
-0.10005	1	0
-0.0023063	1	0

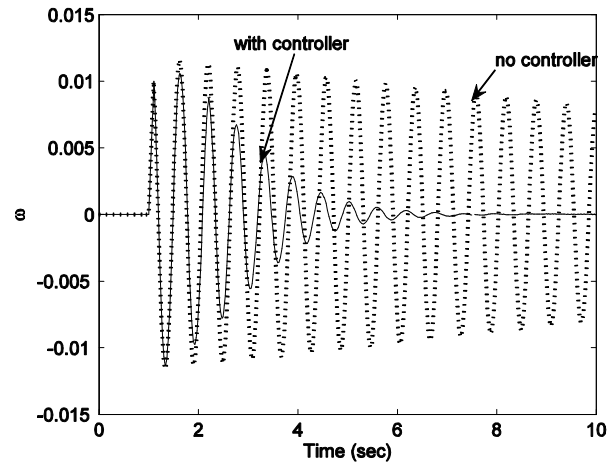


Fig. 10. Rotor Speed response with and without damping controller  $\delta_1$  at  $P_e = 0.8$  pu

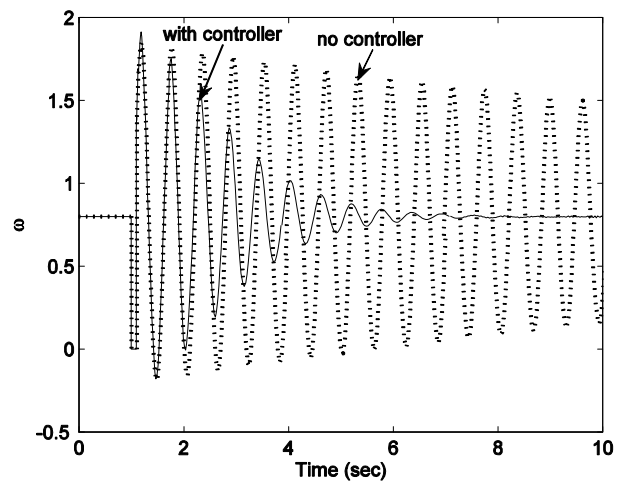


Fig. 11. Electrical Power response with and without damping controller  $\delta_1$  at  $P_e = 0.8$  pu

complex eigenvalues and phase is compensated by two lead lag compensator blocks ( $n = 2$ ) as compared to controllers  $m_1$  and  $m_2$  which require only one lead lag block. The rotor speed response  $\omega$  and electrical power  $P_e$  is shown in Fig. 10 and Fig. 11 respectively. It is observed from the responses that the oscillations are sustained around 7.5 sec. The damping controller  $\delta_1$  is less effective compared to the other two controllers  $m_1$  and  $m_2$  as it requires more time to dampen the oscillations.

### 5.1.4 Damping Controller $\delta_2$

Table 5 shows the eigenvalues of the system with the damping controller  $\delta_2$ . However, this controller does not contribute much to the damping of the oscillation mode as seen from the eigenvalues,

damping ratio in Table 5, although the gain of the damping controller is significantly large.

Table 5: Eigenvalues of the linearized SMIB at operating point  $P_e = 0.8$  pu with damping controller  $\delta_2$

Eigenvalues	Damping Ratio	Frequency
0	-	0
-100.09	1	0
$-0.15569 \pm j10.191$	0.015275	1.622
$-0.1734 \pm j0.21481$	0.62812	0.034188
-0.10615	1	0
-0.05592	1	0
-0.0023054	1	0

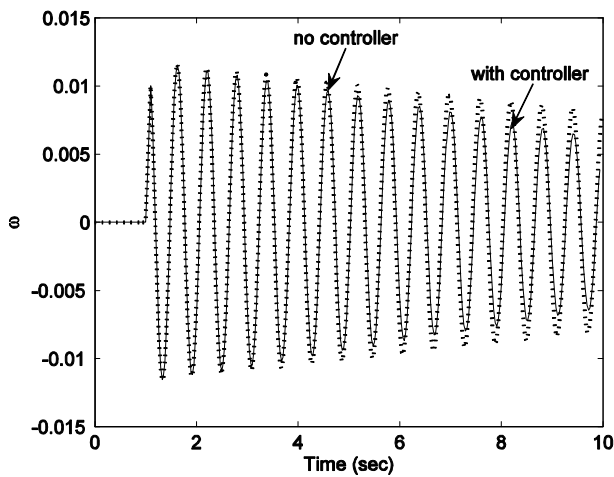


Fig. 12. Rotor Speed response with and without damping controller  $\delta_2$  at  $P_e = 0.8$  pu

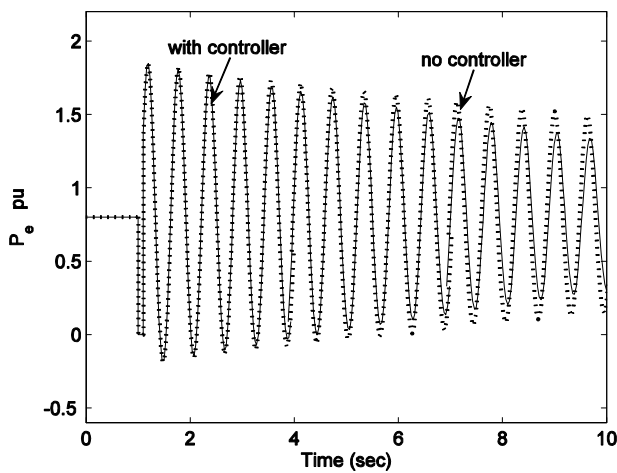


Fig. 13. Electrical Power response with and without damping controller  $\delta_2$  at  $P_e = 0.8$  pu

Further increase of the gain of the controller only pushes the system to instability as the eigenvalues are forced into the RHS of the S plane. The responses of the rotor speed and electrical power of the system with the damping controller  $\delta_2$  is shown in Fig. 12 and Fig. 13 respectively. It is seen that the effect of the controller on the oscillations is negligible and inferior compared to the other three controllers.

### 5.2 Operating point $P_e = 0.2$ pu (light load condition)

The performance of the controllers at different load condition, i.e, at a lighter load condition  $P_e = 0.2$  pu is examined other than the operating point whether the controllers have been designed.

#### 5.2.1 Damping Controller $m_1$

The eigenvalues of the power system at  $P_e = 0.2$  pu with the damping controller  $m_1$  is given in Table 6.

Table 6: Eigenvalues of the linearized SMIB at operating point  $P_e = 0.2$  pu with damping controller  $m_1$

Eigenvalues	Damping Ratio	Frequency
0	-	0
-100.18	1	0
$-8.7464 \pm j15.604$	0.48895	2.4835
-3.4176	1	0
-0.00077924	1	0
-0.10315	1	0
-0.34957	1	0

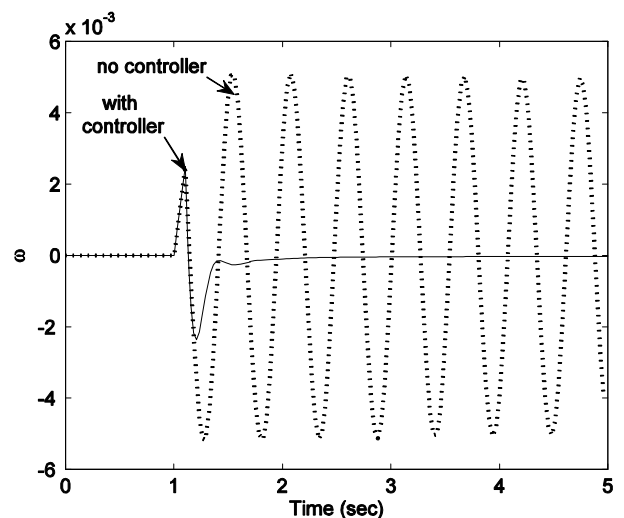


Fig. 14. Rotor Speed response with and without damping controller  $m_1$  at  $P_e = 0.2$  pu.

The damping controller is very effective at lighter load condition as it increases the damping ratio to a higher value of 0.48895 as seen from Table 6. Fig. 14 and Fig. 15 show the rotor speed and electrical power response with and without the damping controller at  $P_e = 0.2$  pu. The damping controller  $m_1$  is able to sustain the oscillations at a faster rate approximately within 1.0 sec. after the fault occurrence as compared to Fig. 6 and Fig., where the settling time is 4.5 sec. It is thus observed that the damping controller  $m_1$  contributes more damping for lighter load conditions.

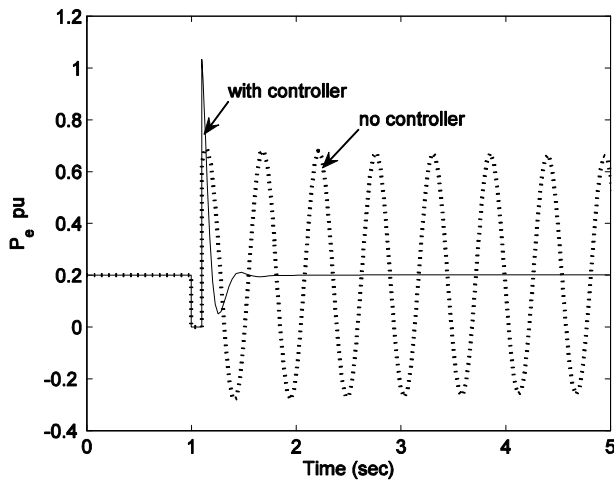


Fig. 15. Electrical Power response with and without damping controller  $m_1$  at  $P_e = 0.2$  pu

### 5.2.2 Damping Controller $m_2$

Table 7 shows the eigenvalues of the system with the damping controller  $m_2$  at the operating point  $P_e = 0.2$  pu. The damping controller increases the damping of the oscillation mode slightly at lighter load condition. This is also observed in the response of the rotor speed and electrical power in Fig. 16

Table 7: Eigenvalues of the linearized SMIB at operating point  $P_e = 0.2$  pu with damping controller  $m_2$

Eigenvalues	Damping Ratio	Frequency
0	-	0
-100.19	1	0
$-1.4903 \pm j12.232$	0.12094	1.9468
-10.987	1	0
-0.00077932	1	0
-0.10031	1	0
-0.34438	1	0

and Fig. 17 respectively. The damping of the oscillation is at 3.5 sec, improving by one sec when compared to Fig 8 and Fig. 9 at the operating point of  $P_e = 0.8$  pu .

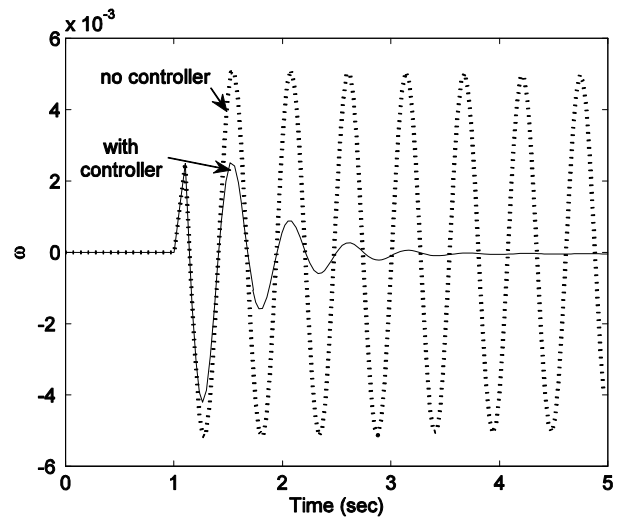


Fig. 16. Rotor Speed response with and without damping controller  $m_2$  at  $P_e = 0.2$  pu.

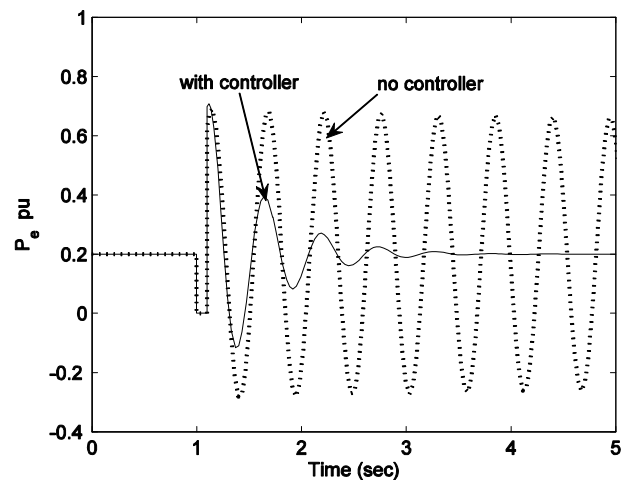


Fig. 17. Electrical Power response with and without damping controller  $m_2$  at  $P_e = 0.2$  pu

### 5.2.3 Damping Controller $\delta_1$

The eigenvalues of the power system with the damping controller  $\delta_1$  is given in Table 8. The damping contributed by this controller is less as compared to damping controllers  $m_1$  and  $m_2$  at this operating point. The damping ratio of the oscillation mode is only 0.034505 which is very less than the required 0.1 value. Fig. 18 and Fig. 19 show the response of the rotor speed and electrical power

Table 8: Eigenvalues of the linearized SMIB at operating point  $P_e = 0.2$  pu with damping controller  $\delta_1$ .

Eigenvalues	Damping Ratio	Frequency
0	-	0
$-71.472 \pm j64.643$	0.74165	10.288
-100.81	1	0
$-0.42678 \pm j12.361$	0.034505	1.9673
-0.34466	1	0
-0.1	1	0
-0.00077932	1	0

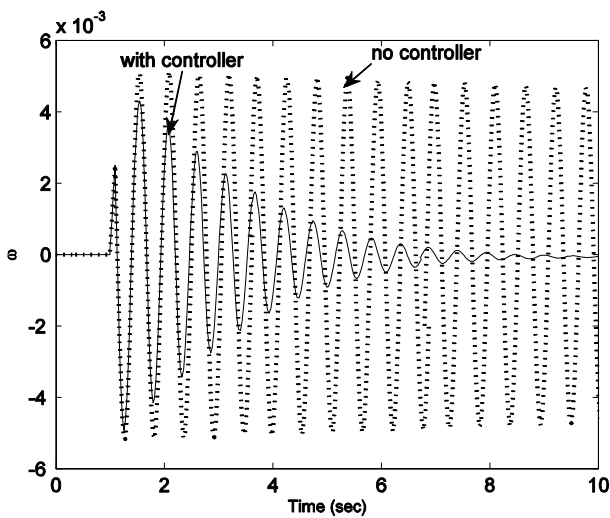


Fig. 18. Rotor Speed response with and without damping controller  $\delta_1$  at  $P_e = 0.2$  pu.

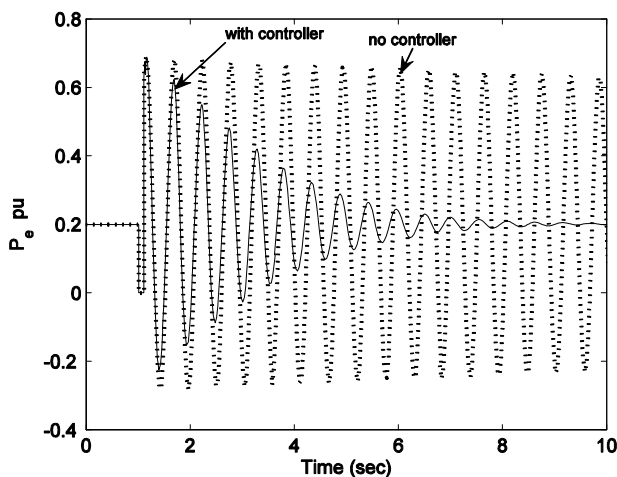


Fig. 19. Electrical Power response with and without damping controller  $\delta_1$  at  $P_e = 0.2$  pu

respectively in the presence of the damping controller  $\delta_1$ . The settling time is around 9.5 sec

which is more compared to the settling times when the damping controllers  $m_1$  and  $m_2$  are used at the two different operating points  $P_e = 0.2$  pu and  $P_e = 0.8$  pu.

### 5.2.4 Damping Controller $\delta_2$

Table 9 gives the eigenvalues when the damping controller  $\delta_2$  is placed in the power system. As observed during the operating point  $P_e = 0.8$  pu, this controller also does not contribute to any damping during the operating point  $P_e = 0.2$  pu as seen in Table 9. This is also verified from the responses of rotor speed and electrical power in Fig. 20 and Fig. 21 respectively. The controller does not help in mitigating the power system oscillations. Thus damping controller  $\delta_2$  is not suitable for improving the damping of the oscillation mode.

Table 9: Eigenvalues of the linearized SMIB at operating point  $P_e = 0.2$  pu with damping controller  $\delta_2$

Eigenvalues	Damping Ratio	Frequency
0	-	0
-100.2	1	0
$-0.027141 \pm j11.736$	0.0023127	1.8678
-0.00078018	1	0
-0.062618	1	0
-0.10615	1	0
$-0.24777 \pm j0.049733$	0.98044	0.0079153

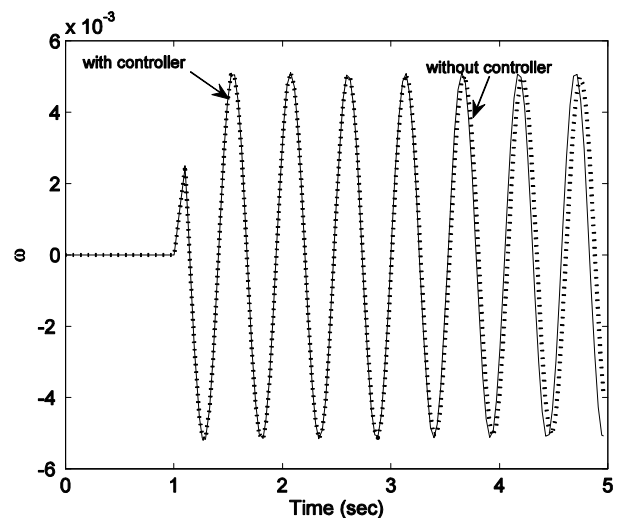


Fig. 20. Rotor Speed response with and without damping controller  $\delta_2$  at  $P_e = 0.2$  pu.

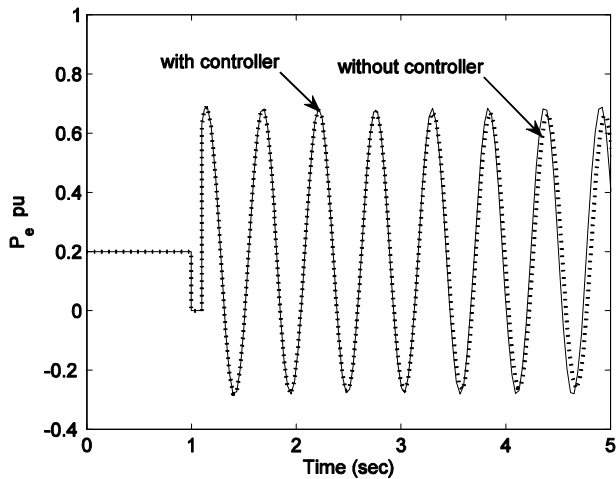


Fig. 21. Electrical Power response with and without damping controller  $\delta_2$  at  $P_e = 0.2$  pu

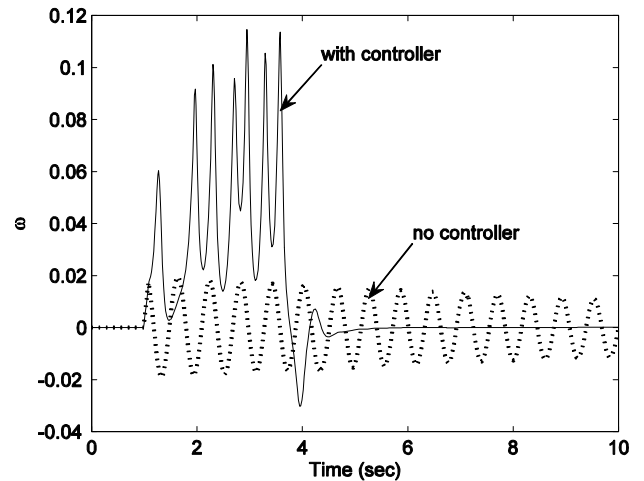


Fig. 22. Rotor Speed response with and without damping controller  $m_1$  at  $P_e = 1.4$  pu.

### 5.3 Operating point $P_e = 1.4$ pu (heavy load condition)

The damping controller performance of the power system is observed for the operating point  $P_e = 1.4$  pu i.e at heavy load condition with various damping controllers.

#### 5.3.1 Damping Controller $m_1$

The eigenvalues of the power system at  $P_e = 1.4$  pu with the damping controller  $m_1$  is given in Table 10. It appears that the damping controller  $m_1$  contributes negative damping at heavy load conditions as observed from Table 10. The oscillation mode is forced into the RHS of the S - plane. But upon the non linear simulation of the system with this controller  $m_1$ , we observe a peculiarity in the responses of the rotor speed and electrical power as shown in Fig. 22 and Fig. 23

Table 10: Eigenvalues of the linearized SMIB at operating point  $P_e = 1.4$  pu with damping controller  $m_1$

Eigenvalues	Damping Ratio	Frequency
0	-	0
-100.19	1	0
$2.6187 \pm j9.2251$	-0.27308	1.4682
-8.79	1	0
-0.81499	1	0
-0.097471	1	0
6.4304e-005	-1	0

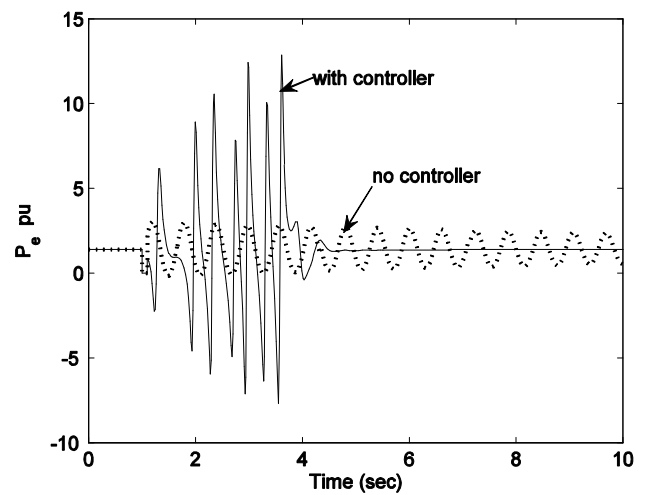


Fig. 23. Electrical Power response with and without damping controller  $m_1$  at  $P_e = 1.4$  pu.

respectively. The oscillation seems to increase in amplitude with high peak overshoots as if leading the system to instability reflecting the eigenvalues computed in Table 10. But at time 4.5 sec the oscillation suddenly are mitigated. This unusual nature of the damping controller  $m_1$  providing excessive damping at light load condition, providing damping at heavy load condition with high peak values and requirement of higher gain value to provide the required damping makes it unreliable for damping the power system oscillations consistently for all operating conditions.

#### 5.3.2 Damping Controller $m_2$

Table 11 represents the eigenvalues of the power system with the damping controller  $m_2$ . At heavy

load condition the controller provides a damping about 5.7%. The oscillations in the rotor speed and

Table 11: Eigenvalues of the linearized SMIB at operating point  $P_e = 1.4$  pu with damping controller  $m_2$

Eigenvalues	Damping Ratio	Frequency
0	-	0
-99.847	1	0
$-0.6271 \pm j10.91$	0.057388	1.7363
-11.039	1	0
-0.71301	1	0
-0.099809	1	0
6.4304e-005	-1	0

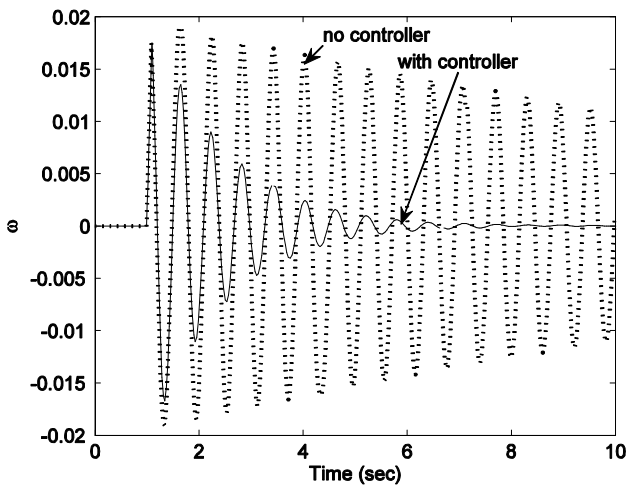


Fig. 24. Rotor Speed response with and without damping controller  $m_2$  at  $P_e = 1.4$  pu.

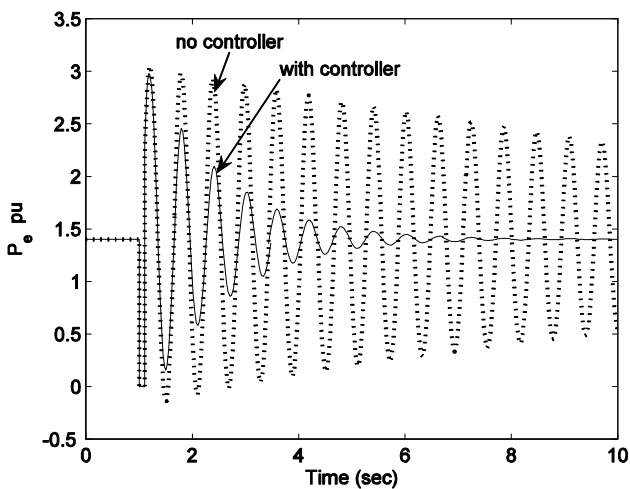


Fig. 25. Electrical Power response with and without damping controller  $m_2$  at  $P_e = 1.4$  pu.

electrical power is shown in Fig. 24 and Fig. 25 respectively. The damping controller  $m_2$  dampens the oscillations at about 7.5 sec for heavy load condition. This damping controller  $m_2$  provides sufficient damping at lighter load condition  $P_e = 0.2$  pu and nominal load condition  $P_e = 0.8$  pu. However, its performance in heavy load condition  $P_e = 1.4$  pu does not meet the designed requirement of achieving the damping ratio of 0.1 although it mitigates the oscillation consistently.

### 5.3.3 Damping Controller $\delta_1$

The eigenvalues of the system with the damping controller  $\delta_1$  is shown in Table 12. The damping controller  $\delta_1$  contributes slightly to the oscillation mode of interest and it also introduces another set of

Table 12: Eigenvalues of the linearized SMIB at operating point  $P_e = 1.4$  pu with damping controller  $\delta_1$

Eigenvalues	Damping Ratio	Frequency
0	-	0
-116.91	1	0
$-27.566 \pm j96.088i$	0.27576	15.293
$-0.87469 \pm j9.8899$	0.088099	1.574
-0.69493	1	0
-0.10006	1	0
6.4304e-005	-1	0

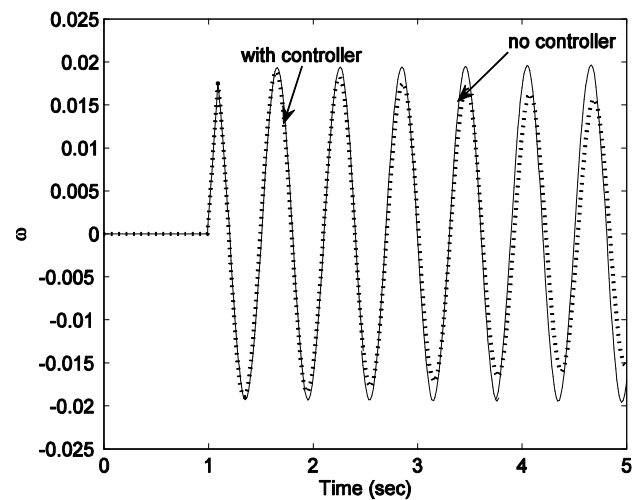


Fig. 26. Rotor Speed response with and without damping controller  $\delta_1$  at  $P_e = 1.4$  pu.

complex eigenvalues, though it has sufficient damping ratio. However the responses obtained from the nonlinear simulation as shown in Fig. 26 and Fig. 27 for rotor speed and electrical power output respectively indicate the ineptness of this controller to provide damping compared to the other damping controllers  $m_1$  and  $m_2$ . The responses indicate that the controller is ineffective in damping the oscillations at heavy load conditions.

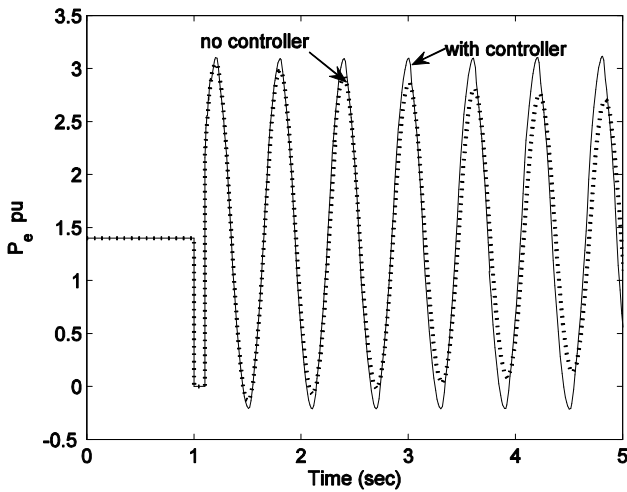


Fig. 27. Electrical Power response with and without damping controller  $\delta_1$  at  $P_e = 1.4$  pu.

**5.3.4 Damping Controller  $\delta_2$**

The damping controller  $\delta_2$  is not a suitable signal for damping as can be observed from Table 13 where the eigenvalues of oscillation mode are shifted to RHS of S-plane making the system unstable. This is also seen in Fig 28 and 29 that the controller does not provide any damping.

Table 13: Eigenvalues of the linearized SMIB at operating point  $P_e = 1.4$  pu with damping controller  $\delta_2$

Eigenvalues	Damping Ratio	Frequency
0	-	0
-99.873	1	0
$0.02401 \pm j9.9107$	-0.0024226	1.5773
-0.75652	1	0
-0.14535	1	0
-0.10615	1	0
-0.083081	1	0
6.4306e-005	-1	0

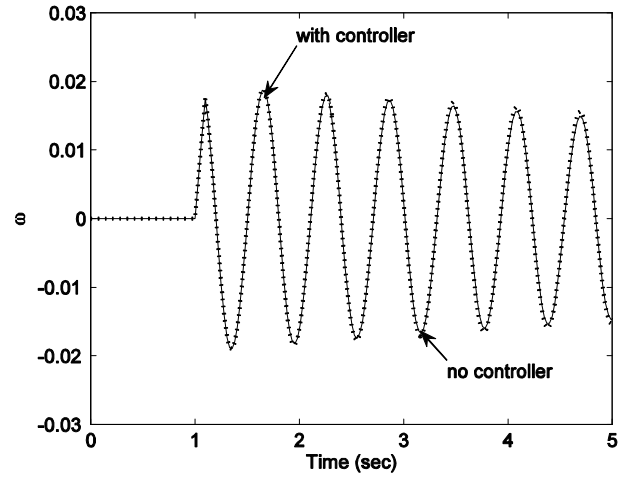


Fig. 28. Rotor Speed response with and without damping controller  $\delta_2$  at  $P_e = 1.4$  pu.

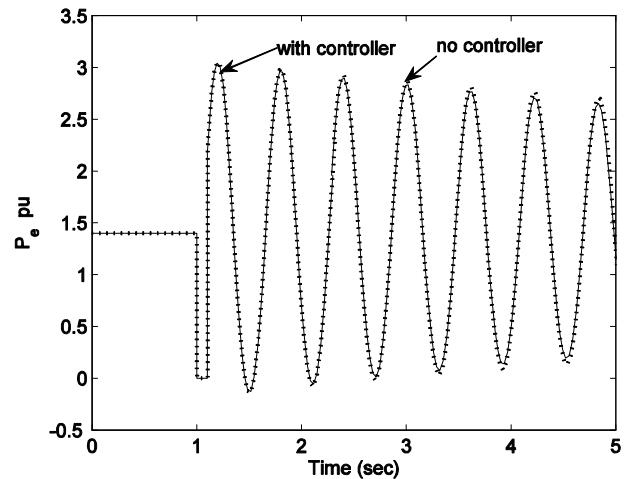


Fig. 29. Electrical Power response with and without damping controller  $\delta_2$  at  $P_e = 1.4$  pu.

From the analysis we have deduced that the controller  $\delta_2$  is inept in providing damping to the power system oscillations.  $m_1$  and  $m_2$  prove to be suitable input signals on which the damping function can be added. However the damping controller  $m_2$  is more efficient as the required damping is provided at minimum control cost, and it provides consistent damping throughout the varying operating conditions. This is also proved with the controllability index given in Table 14; from we can observe that the input signal  $m_2$  is the most efficient signal for damping as it has higher value of controllability index compared to other input signals.

Table 14: Controllability indices with different IPFC controllable parameters

Input signal	Controllability index
$m_1$	0.0170
$\delta_1$	0.0055
$m_2$	0.1560
$\delta_2$	0.0079

Furthermore, if the operating condition where the IPFC damping controller is least effective is selected for the design of damping controller then it becomes more effective in damping at other operating conditions indicating its robustness. As we have seen, the damping controller  $m_2$  is least effective at heavy load condition comparatively, and also the damping ratio of the concerned oscillation mode is the least at the operating condition of  $P_e = 1.4$  pu as indicated in Table 15. Consequently the damping controller is designed at the operating point  $P_e = 1.4$  pu and its performance at varying operating conditions is observed in Fig. 30. The results of the eigenanalysis with damping controller  $m_2$ , designed at the operating point  $P_e = 1.4$  pu, at different operating conditions are shown in Table 16. It is observed that the controller provides damping without sharp drops or increases in the damping contribution with various operating conditions

Table 15: Oscillation modes at various operating conditions

Op. Pt.	Eigenvalues without damping		
	Eigenvalues	Damping ratio	Frequency
0.2	$-0.031219 \pm j12.275$	0.0025433	1.9536
0.8	$-0.09782 \pm j11.514$	0.0084952	1.8325
1.4	$-0.016734 \pm j11.009$	0.00152	1.7521

Table 16: Oscillation modes at various operating conditions with damping controller  $m_2$  designed at  $P_e = 1.4$  pu

Op. Pt.	Eigenvalues with damping $m_2$		
	Eigenvalues	Damping ratio	Frequency
0.2	$-2.6316 \pm j12.503$	0.20596	1.99
0.8	$-2.1822 \pm j11.669$	0.18382	1.8573
1.4	$-1.1397 \pm j10.965$	0.10338	1.7451

making the damping controller  $m_2$  more robust and effective. Fig. 30 shows the rotor speed response with the damping controller  $m_2$  at different load conditions. It is noted that the oscillations are mitigated at a faster rate with lighter load conditions which validates the results of Table 16.

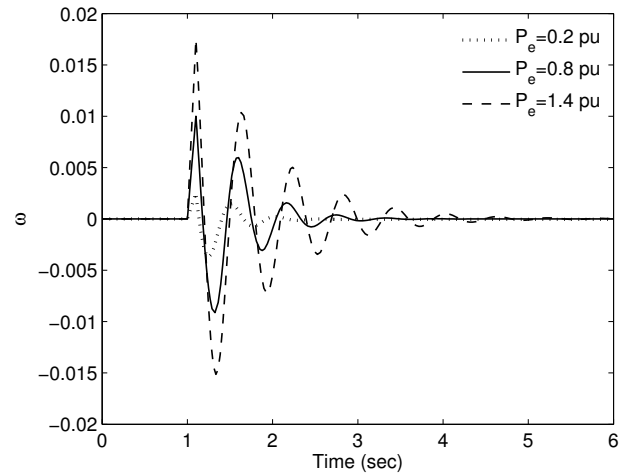


Fig. 30. Rotor Speed response with controller  $m_2$  with varying operating conditions

The effect of the IPFC damping controller  $m_2$  is also verified during a step variation of 0.01 pu in mechanical power input  $P_m$ . Fig. 31 shows the response of the electrical power when the disturbance is given at 1.0 sec. The effect of the damping controller  $m_2$  designed at the two operating conditions  $P_e = 0.8$  pu and at  $P_e = 1.4$  pu is compared during this disturbance.

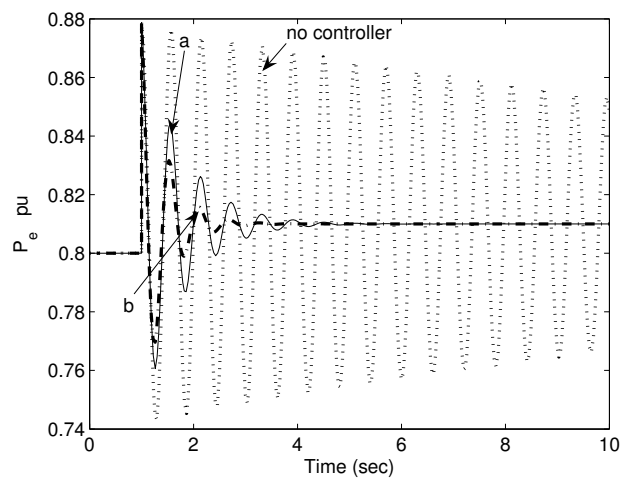


Fig. 31. Electrical Power response without damping controller and with damping controller  $m_2$  designed at (a)  $P_e = 0.8$  pu (b)  $P_e = 1.4$  pu

It is clearly seen that the damping controller  $m_2$  designed at the operating point  $P_e = 1.4$  pu gives better damping as the settling time is at 3 sec. It improves the performance by 55% in comparison with the controller designed at  $P_e = 0.8$  pu. Thus the controller is more robust when designed at the operating point at which the damping ratio of the oscillation mode is minimum or where it is least effective to ensure to effectiveness at other operating conditions. The operating point and the input signal play a significant role in damping the power system oscillations.

## 6 Conclusion

In this paper the non linear model of the IPFC has been developed and the extended linearized Phillips-Heffron model of a single machine infinite bus power system incorporated with IPFC is established. The parameters of the IPFC damping controller is determined using the phase compensation method based on the linearized model. The relative effectiveness of the input control signals  $\Delta m_1$ ,  $\Delta \delta_1$ ,  $\Delta m_2$  and  $\Delta \delta_2$  has been examined on example power system subjected to various disturbances. Investigations revealed that control signal  $\Delta m_2$  is the most efficient of the input control signals to be used for damping in the power system whereas the control signal  $\Delta \delta_2$  is inefficient in providing the damping. It is found that the IPFC damping controller is more robust over various operating conditions when the controller is designed at appropriate operating condition. The effectiveness and robustness of the IPFC damping controller is validated through eigenanalysis and non linear simulation. The authors are further investigating the additional damping provided by the proposed IPFC based damping controller in a multi-machine power system incorporated with IPFC.

### References:

- [1] F.P. DeMello and C. Concordia, Concepts of Synchronous Machine Stability as Affected by Excitation Control, *IEEE Transactions on Power Apparatus and Systems*, Vol. PAS-88, 1969, pp. 316-329.
- [2] E.V. Larsen and D.A. Swann, Applying Power System Stabilizers, Parts I - 111, *IEEE Transactions on Power Apparatus and Systems*, Vol. PAS-100, 1981, pp. 3017-3046.
- [3] J. H. Chow and J. J. Sanchez-Gasca, Pole-placement design of power System Stabilizers, *IEEE T-PWRS*, Vo1.4, 1989.
- [4] R. Sadikovic, P. Korba and G. Andersson, Application of FACTS Devices for Damping of Power System Oscillations, *IEEE PowerTech 2005*, Russia, June 2005.
- [5] P. K. Dash, S. Mishra, G. Panda, Damping Multimodal Power System Oscillation Using a Hybrid Fuzzy Controller for Series Connected FACTS Devices, *IEEE Transactions on Power Systems*, Vol. 15, No. 4, November 2000, pp. 1360 – 1366.
- [6] H. F. Hang, Design of SSSC Damping Controller to Improve Power System Oscillation Stability, *IEEE* 1999.
- [7] N. Tambey and M. L. Kothari, Damping of Power System Oscillation with Unified Power Flow Controller, *IEE Proc. Gener. Trans. Distib.* Vol. 150, No. 2, March 2003, pp. 129 – 140.
- [8] A. Kazemi and F. Mahamnia, Improving of Transient Stability of Power Systems by Supplementary Controllers of UPFC using different Fault Conditions, *WSEAS Transaction on Power Systems*, Issue 7, Vol. 3, July 2008, pp. 547-556.
- [9] S. N. Dhurvey and V. K. Chandrakar, Performance Comparison of UPFC in Coordination and Optimized POD and PSS on Damping of Power System Oscillations, *WSEAS Transaction on Power Systems*, Issue 5, Vol. 3, May 2008, pp. 287-299.
- [10] N. G. Hingorami, L.Gyugyi, *Understanding FACTS: Concepts and Technology of Flexible AC Transmission system*, IEEE Press, 1999
- [11] Y. H. Song and A. T. Johns, *Flexible AC Transmission systems*, IEE Power and Energy series 30, 1999.
- [12] M. Ahmadzadeh, S. S. Mortazavi, A. Saeedian, A Novel Method of coordinating PSSs and FACTS Devices in Power System stability Enhancement, *WSEAS Transaction on Power Systems* Issue 5, Vol. 4, May 2009, pp. 177-188.
- [13] L. Gyugyi, K. K. Sen, and C. D. Schauder, The interline power flow controller concept: A new approach to power flow management in transmission systems, *IEEE Trans. Power Del.*, Vol. 14, No. 3, Jul. 1999, pp. 1115–1123.
- [14] X. Wei, J. H. Chow, B. Fardanesh, Ahdel-Aty Edris, A common modeling framework of voltage-sourced converters for loadflow, sensitivity, and dispatch analysis, *Power Engineering Society General Meeting*, IEEE Vol. 4, July 2003, pp. 13-17.
- [15] J. Zhang, A. Yokoyama, A Comparison between the UPFC and the IPFC in Optimal

- [16] Power Flow Control and Power Flow Regulation, *38th North American Power Symposium, NAPS 2006*, Sept. 2006, pp. 339–345.
- [17] Wei, X.; Chow, J. H.; Fardanesh, B.; Edris, A.A, A dispatch strategy for an interline power flow controller operating at rated capacity, *Power Systems Conference and Exposition, IEEE PES*, 10-13 Oct. 2004, Vol.3, pp. 1459 - 1466.
- [18] J. Chen, T. T. Lie, D. M. Vilathgamuwa, Basic control of interline power flow controller, *Power Engineering Society Winter Meeting, IEEE Volume 1*, 27-31 Jan. 2002, Vol.1, pp. 521 – 525.
- [19] J. Chen, T. T. Lie, D. M. Vilathgamuwa, Design of an interline power flow controller, 14th PSCC, Sevilla, 24-28 June 2002.
- [20] A. Kazemi, E. Karimi, The Effect of Interline Power Flow Controller (IPFC) on Damping Inter-area Oscillations in the Interconnected Power Systems, *Industrial Electronics, 2006 IEEE International Symposium*, Vol. 3, July 2006, pp. 1911 – 1915.
- [21] A. Nabavi-Niaki, M. R. Irvani, Steady-state and dynamic models of unified power flow controller (UPFC) for power system studies, *IEEE Trans. Power Systems*, Vol. 11, No. 4, Nov. 1996, pp. 1937-1943.
- [22] H. F. Wang, M. Li, and F. J. Swift, FACTS-based stabilizer designed by the phase compensation method. Part I and II, *Proceedings of APSCOM-97*, Hong Kong, 1997, pp. 638-649.

## Appendix

### Appendix A

The parameters of the single machine infinite bus power system are as follows (in pu except where indicated):

$$\begin{array}{lll}
 H = 4.0s., & D = 0.0, & T'_{d0} = 5.044s., \\
 x_d = 1.0, & x_q = 0.6, & x'_d = 0.3,
 \end{array}$$

$$\begin{array}{lll}
 x_t = 0.01, & x_{t1} = 0.015, & x_{t2} = 0.015, \\
 x_{L1} = 0.05, & x_{L2} = 0.05, & K_A = 10.0, \\
 T_A = 0.01s., & v_{dc0} = 225KV, & P_{e0} = 0.8, \\
 V_{b0} = 1.0, & V_t = 1.02.
 \end{array}$$

### Appendix B

$K$  constants at the operating point of  $P_e = 0.8$  pu

$$\begin{array}{lll}
 K_1 = 3.166416, & K_2 = 0.323807 & K_3 = 3.043796 \\
 K_4 = 0.066681 & K_5 = -0.104002 & K_6 = -0.001198 \\
 K_7 = 0.002149 & K_8 = -0.009759 & K_9 = 0.000035 \\
 K_{pv} = 0.123469 & K_{qv} = -0.004512 & K_{vv} = 0.012725 \\
 K_{pm1} = 1.497362 & & K_{p\delta1} = -0.008114 \\
 K_{pm2} = 1.578447 & & K_{p\delta2} = -0.017687 \\
 K_{qm1} = -0.285734 & & K_{q\delta1} = -0.015464 \\
 K_{qm2} = -0.031945 & & K_{q\delta2} = -0.144520 \\
 K_{vm1} = 0.129343 & & K_{v\delta1} = 0.000640 \\
 K_{vm2} = 0.165458 & & K_{v\delta2} = 0.028441 \\
 K_{cm1} = -0.898796 & & K_{c\delta1} = 0.005237 \\
 K_{cm2} = 0.034733 & & K_{c\delta2} = -0.053150
 \end{array}$$

### Appendix C

Damping controller designed at  $P_e = 0.8$  pu

$$T_w = 10 \text{ sec}$$

Damping controller  $m_1$

$$K_{dc} = 182.12, T_1 = 0.057312, T_2 = 0.13174, n = 1$$

Damping controller  $m_2$

$$K_{dc} = 15.235, T_1 = 0.083781, T_2 = 0.090121, n = 1$$

Damping controller  $\delta_1$

$$K_{dc} = 5.0117, T_1 = 0.73539, T_2 = 0.010267, n = 2$$

Damping controller  $\delta_2$

$$K_{dc} = 34420, T_1 = 0.00080155, T_2 = 9.4198, n = 2$$

# Interline Power Flow Controller (IPFC) Based Damping Controllers for Damping Low Frequency Oscillations in a Power System

Alivelu M. Parimi *Student Member IEEE*, Irraivan Elamvazuthi and Nordin Saad

**Abstract**— The Interline Power Flow Controller (IPFC) is a voltage-source-converter (VSC)-based flexible ac transmission system (FACTS) controller which can inject a voltage with controllable magnitude and phase angle at the line-frequency thereby providing compensation among multiple transmission lines. In this paper, the use of the IPFC based controller in damping of low frequency oscillations is investigated. An extended Heffron-Phillips model of a single machine infinite bus (SMIB) system installed with IPFC is established and used to analyze the damping torque contribution of the IPFC damping control to the power system. The potential of various IPFC control signals upon the power system oscillation stability is investigated using a controllability index. Simulation results using Matlab Simulink demonstrate the effectiveness of IPFC damping controllers on damping low frequency oscillations.

## I. INTRODUCTION

THE present day interconnected power system consists of a great number of generators being connected together through a high-voltage long transmission network, supplying power to loads through lower-voltage distribution systems. The phenomenon that is of great concern in the planning and operation of interconnected power systems is the low frequency electromechanical oscillations. These oscillations are the consequence of the dynamical interactions between the generator groups. The oscillations associated with groups of generators when oscillating against each other are called inter-area modes and having frequencies in the range 0.1 to 0.8 Hz, whereas the oscillations, associated with a single generator oscillating against the rest of the system, are called local modes and normally have frequencies in the range of 0.7 to 2.0 Hz [1]. These low frequency oscillations constrain the capability of power transmission, threaten system security and damage the efficient operation of the power system [2-3]. For this reason, the use of controllers to provide better damping to the power system oscillations is of utmost importance to maintain power stability.

In the last decade, the flexible ac transmission systems (FACTS) devices have been progressively developed to deal with the above control objectives [4]. A stream of voltage source converter (VSC) based FACTS devices, [5], and [6] such as Static Compensator (STATCOM), Static Synchronous Series Compensators (SSSC), and Unified Power Flow Controller (UPFC) have been successfully

applied in damping power system oscillations [7-14].

Interline power flow controller (IPFC) is the latest generation of FACTS controllers [15]. It is the combination of two or more SSSCs which are coupled via a common DC link. With this scheme, IPFC has the capability to provide an independently controllable reactive series compensation for each individual line and also to transfer real power between the compensated lines. There has been growing interest recently in studying the IPFC modeling [16], its basic function to control power flow among transmission lines [17] and oscillation damping [18]. Kazemi and Karimi proposed a PI supplementary damping controller for the IPFC for damping inter-area oscillations [18]. However, the controller parameters are not optimized. Further, no effort had been made to identify the most suitable control parameter. A supplementary PID damping controller was proposed in [19], but the performance degraded due to the system nonlinearity and complexity.

Therefore, in this paper, the linearised Heffron-Phillips model of a single machine infinite bus (SMIB) power system installed with an IPFC is first established. It is of same form as that of the unified model presented in [20-22] for UPFC. Phase compensation method [23] is applied for the design of IPFC damping controllers based on the established linearized model. The relative effectiveness of modulating alternative IPFC control parameters for damping power system oscillations at the nominal point of the system is examined. The controllability index is used to determine the most effective output control signal among ( $m_1, \theta_1, m_2, \text{ and } \theta_2$ ) from the damping controller.

## II. MODEL OF THE SYSTEM STUDIED

A single machine infinite bus (SMIB) system installed with IPFC is considered for the analysis of stability. Fig. 1. shows the generator connected to the infinite bus through the two parallel transmission lines. The static excitation system, model type IEEE-ST1A, has been considered. PSS is not taken into account in the power system. A simple IPFC is incorporated into the system, which consists of two, three phase GTO based voltage source converters (VSC's), each providing a series compensation for the two lines. The converters are linked together at their dc terminals and connected to the transmission lines through their series coupling transformers. This configuration allows the control of real and reactive power flow in line 1. For the series converter in line 2, it is assumed that active power flow constraint is used while reactive power flow is relaxed.

Manuscript received on July 15, 2008.

Alivelu M. Parimi, Irraivan Elamvazuthi, and Nordin Saad are with Universiti Teknologi PETRONAS, Bandar Seri Iskandar, Tronoh, Perak, Malaysia. (e-mails: alivelu\_manga@utp.edu.my; irraivan\_elamvazuthi@petronas.com.my, nordiss@petronas.com.my).

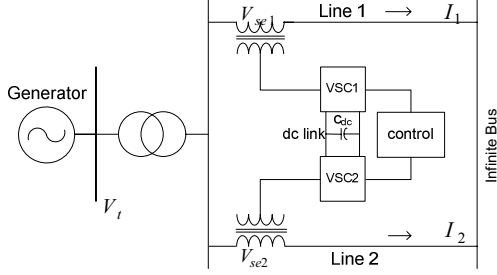


Fig. 1: SMIB system installed with an IPFC.

The system data and the initial operating conditions of the system are as follows:

- Generator:  $M=2H=8.0$  MJ/MVA  $D=0$   $T'_{do}=5.044s$   
 $x_d=1.0pu$   $x_q=0.6pu$   $x'_d=0.3pu$   
Excitation system :  $K_a=50$   $T_a=0.05s$   
Transmission line :  $x_{L1}=x_{L2}=x_L=0.5 pu$   
Transformers :  $x_t=0.15pu$   $x_{t1}=x_{t2}=0.1 pu$   
Operating condition:  $P=0.8$   $Q=0.1958$   $V_t=1.0 pu$   
 $V_b=1.0pu$   $f=60 Hz$   
IPFC parameters :  $m_1=0.15$ ,  $m_2=0.1$ .  
 $V_{dc}=2 pu$ ,  $C_{dc}=1 pu$

#### A. Power system Non Linear Dynamic Model

A non-linear dynamic model of the system is derived by neglecting the resistances of all the components of the system (generator, transformer, transmission lines and series converter transformers) and the transients of the transmission lines and transformers of the IPFC. The IPFC considered is based on pulse width modulation. The non-linear dynamic model of the power system in Fig. 1 is

$$\dot{\delta} = \omega_0(\omega - 1) \quad (1)$$

$$\dot{\omega} = \frac{P_m - P_e - P_D}{M} \quad (2)$$

$$\dot{E}'_q = \frac{(-E_q + E_{fd})}{T'_{do}} \quad (3)$$

$$\dot{E}_{fd} = \frac{-E_{fd} + K_a(V_{ref} - V_t)}{T_a} \quad (4)$$

$$\dot{V}_{dc} = \frac{3m_1}{4C_{dc}} (\cos \theta_1 I_{1d} + \sin \theta_1 I_{1q}) + \frac{3m_2}{4C_{dc}} (\cos \theta_2 I_{2d} + \sin \theta_2 I_{2q}) \quad (5)$$

Where  $\delta$ , is the rotor angle of synchronous generator in radians,  $\omega$  is rotor speed in rad/sec,  $V_t$  is the terminal voltage of the generator,  $E'_q$  is generator internal voltage,  $E_{fd}$  is the generator field voltage,  $V_{dc}$  is the voltage at DC link. More details are given in Appendix I. The voltages injected by the IPFC converters in d-q coordinates are obtained as follows:

$$V_{se1d} = -x_{t1}I_{1q} + \frac{V_{dc}}{2} m_1 \cos \theta_1$$

$$V_{se1q} = x_{t1}I_{1d} + \frac{V_{dc}}{2} m_1 \sin \theta_1$$

$$V_{se2d} = -x_{t2}I_{2q} + \frac{V_{dc}}{2} m_2 \cos \theta_2,$$

$$V_{se2q} = x_{t2}I_{2d} + \frac{V_{dc}}{2} m_2 \sin \theta_2$$

$$V_{se i} = V_{se id} + jV_{se iq} = V_{se i} e^{j\theta_i} \quad (6)$$

where  $V_{se i}$ ,  $i=1, 2$  is the complex controllable series injected voltage,  $x_{t1}$  and  $x_{t2}$  are the reactance's of the transformers in line 1 and 2.

#### B. Power System Linear Model

The linear Heffron-Phillips model of SMIB system installed with IPFC is obtained by linearizing the non linear model around an operating condition, which is obtained from power flow analysis [24]. The linearized model obtained is given as:

$$\Delta \dot{\omega} = \frac{(\Delta P_m - \Delta P_e - D\Delta \omega)}{M} \quad (7)$$

$$\Delta \dot{\delta} = \omega_0 \Delta \omega \quad (8)$$

$$\Delta \dot{E}'_q = \frac{-\Delta E_q + \Delta E_{fd}}{T'_{do}} \quad (9)$$

$$\Delta \dot{E}_{fd} = \frac{-\Delta E_{fd} + K_a(\Delta V_{ref} - \Delta V_t)}{T_a} \quad (10)$$

$$\Delta \dot{V}_{dc} = K_7 \Delta \delta + K_8 \Delta E'_q - K_9 \Delta V_{dc} + K_{cm1} \Delta m_1 + K_{c\theta1} \Delta \theta_1 + K_{cm2} \Delta m_2 + K_{c\theta2} \Delta \theta_2 \quad (11)$$

where

$$\Delta P_e = K_1 \Delta \delta + K_2 \Delta E'_q + K_{pv} \Delta V_{dc} + K_{pm1} \Delta m_1 + K_{p\theta1} \Delta \theta_1 + K_{pm2} \Delta m_2 + K_{p\theta2} \Delta \theta_2 \quad (12)$$

$$\Delta E_q = K_4 \Delta \delta + K_3 \Delta E'_q + K_{qv} \Delta V_{dc} + K_{qm1} \Delta m_1 + K_{q\theta1} \Delta \theta_1 + K_{qm2} \Delta m_2 + K_{q\theta2} \Delta \theta_2 \quad (13)$$

$$\Delta V_t = K_5 \Delta \delta + K_6 \Delta E'_q + K_{vv} \Delta V_{dc} + K_{vm1} \Delta m_1 + K_{v\theta1} \Delta \theta_1 + K_{vm2} \Delta m_2 + K_{v\theta2} \Delta \theta_2 \quad (14)$$

The model has 28 K-constants. These constants are functions of system parameters and the initial operating condition.

#### C. State space Model

In state-space representation, the power system can be modeled as

$$\dot{X} = AX + BU \quad (15)$$

where the state vector and control vector are as follows:

$$X = [\Delta \delta \quad \Delta \omega \quad \Delta E'_q \quad \Delta E_{fd} \quad \Delta V_{dc}]^T$$

$$U = [\Delta m_1 \quad \Delta \theta_1 \quad \Delta m_2 \quad \Delta \theta_2]^T \quad (16)$$

The system matrix and control matrix are:

$$A = \begin{bmatrix} 0 & \omega_o & 0 & 0 & 0 \\ -\frac{K_1}{M} & -\frac{D}{M} & -\frac{K_2}{M} & 0 & -\frac{K_{pv}}{M} \\ \frac{K_4}{T'_{do}} & 0 & \frac{K_3}{T'_{do}} & \frac{1}{T'_{do}} & -\frac{K_{qv}}{T'_{do}} \\ -\frac{K_a K_5}{T_a} & 0 & -\frac{K_a K_6}{T_a} & -\frac{1}{T_a} & -\frac{K_a K_{vv}}{T_a} \\ K_7 & 0 & K_8 & 0 & -K_9 \end{bmatrix}$$

$$B = \begin{bmatrix} 0 & 0 & 0 & 0 \\ -\frac{K_{pm1}}{M} & -\frac{K_{p\theta1}}{M} & -\frac{K_{pm2}}{M} & -\frac{K_{p\theta2}}{M} \\ -\frac{K_{qm1}}{T'_{do}} & -\frac{K_{q\theta1}}{T'_{do}} & -\frac{K_{qm2}}{T'_{do}} & -\frac{K_{q\theta2}}{T'_{do}} \\ -\frac{K_a K_{vm1}}{T_a} & -\frac{K_a K_{v\theta1}}{T_a} & -\frac{K_a K_{vm2}}{T_a} & -\frac{K_a K_{v\theta2}}{T_a} \\ K_{cm1} & K_{c\theta1} & K_{cm2} & K_{c\theta2} \end{bmatrix}$$

and  $\Delta m_1$  is the deviation in pulse width modulation index  $m_1$  of voltage series converter 1 in line 1. By controlling  $m_1$ , the magnitude of series injected voltage in line 1 can be controlled.  $\Delta m_2$  is the deviation in pulse width modulation index  $m_2$  of voltage series converter 2 in line 2. By controlling  $m_2$ , the magnitude of series injected voltage in line 2 can be controlled.  $\Delta \theta_1$  is the deviation in phase angle of the injected voltage  $V_{se1}$ .  $\Delta \theta_2$  is the deviation in phase angle of the injected voltage  $V_{se2}$ .

### III. DESIGN OF IPFC DAMPING CONTROLLERS

To improve the damping of low frequency oscillations the damping controllers are provided to produce the additional damping torque. The speed deviation  $\Delta \omega$  is considered as the input to the damping controllers which reflects the swings on the machines and lines of interest. As such, the output of the controller is in phase with the speed deviation.

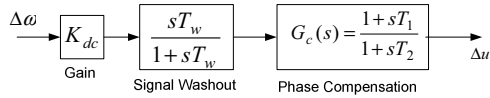


Fig. 2: Structure of IPFC based damping controller.

The structure of IPFC based damping controller is shown in Fig. 2. It consists of gain, signal washout and phase compensation blocks. The optimum parameters of the damping controller are obtained using the phase compensation technique [22]. The design is presented in Appendix II. The time constants of the phase compensator are chosen such that the phase angle of the system is fully compensated. For the nominal operating condition, the

magnitude and phase angle of transfer function,  $\Delta P_e / \Delta U$ , will be computed for  $s = j\omega_n$ . The gain setting of the damping controller is chosen to achieve the required damping ratio of 0.1. As observed from (16) there are four choices of input signals ( $m_1, \theta_1, m_2, \text{ and } \theta_2$ ) of the IPFC to modulate. The signal which can achieve effective damping control at minimum control cost will be the most efficient. This selection is made at open loop condition before installation of damping controller. The concept of controllability index is used to select the most suitable IPFC control parameter from the damping controller for modulation [25].

### IV. SIMULATION RESULTS

The effectiveness of IPFC damping controllers on damping low frequency oscillations is demonstrated using Matlab simulink. First, the system is simulated without IPFC. The K-constants are computed as given in table I. The system is simulated using these values and the change in rotor speed ( $\Delta \omega$ ) response is obtained, by making 1% step increase in  $P_m$  i.e.  $\Delta P_m = 0.01$ , as shown in Fig. 3. The response clearly indicates that the system is unstable.

TABLE I  
K-CONSTANTS FOR THE SYSTEM WITHOUT IPFC

$K_1 = 0.8674$	$K_4 = -0.2854$	$K_7 = 0.8674$
$K_2 = 1.0192$	$K_5 = -0.0994$	$K_8 = 1.0192$
$K_3 = 0.7143$	$K_6 = 0.5179$	$K_9 = 0.7143$

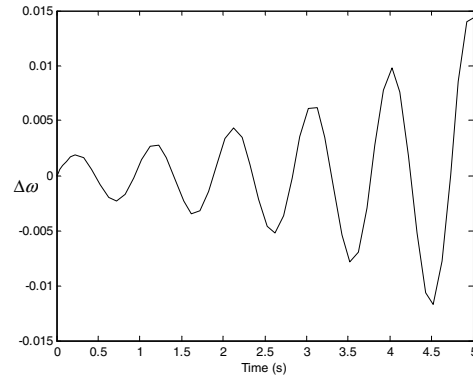


Fig. 3: Rotor speed deviation without IPFC

The system is incorporated with IPFC. Load flow analysis is performed to obtain the operating point which is given as follows:

$$P_e = 0.9000, \quad Q = 0.1958, \quad V_l = 1.02$$

$$V_b = 1, \quad V_{se1} = 0.3795, \quad V_{do} = 0.4311$$

$$V_{q0} = 0.9244, \quad I_{d0} = 0.5469, \quad I_{q0} = 0.7185$$

$$\delta_0 = 7.6056^\circ, \quad \theta_{10} = 71.5651^\circ, \quad \theta_{20} = 7.7250^\circ$$

The system is linearized about this operating point. The

K-constants for the system installed with IPFC, are computed as follows:

$$\begin{aligned}
K_1 &= 2.0552 & K_2 &= 0.0413 & K_3 &= 0.7333 \\
K_4 &= 0 & K_5 &= 0.0185 & K_6 &= 0.6001 \\
K_7 &= -0.0885 & K_8 &= -0.1088 & K_9 &= 7.6663 \times 10^{-4} \\
K_{pv} &= 0.0672 & K_{qv} &= -0.0087 & K_{vv} &= -0.0116 \\
K_{pm1} &= 0.0552 & K_{p\theta1} &= 0.0376 & K_{pm2} &= 0.2530 \\
K_{p\theta2} &= -0.0045 & K_{qm1} &= -0.0326 & K_{q\theta1} &= 0.0010 \\
K_{qm2} &= 0.0056 & K_{q\theta2} &= 0.0033 & K_{vm1} &= -0.0360 \\
K_{v\theta1} &= -0.0029 & K_{vm2} &= -0.0038 & K_{v\theta2} &= -0.0021 \\
K_{cm1} &= 7.6663 \times 10^{-4} & K_{c\theta1} &= 0.0672 & K_{cm2} &= -0.0087 \\
& & & & K_{c\theta2} &= -0.0116
\end{aligned}$$

The eigenvalues corresponding to oscillatory modes of the system are computed as given in table II. From the table II, we observe that the system consists of both local modes and inter area modes. The inter area modes are sufficiently damped, whereas, the local modes are lightly damped.

TABLE II  
EIGENVALUES OF THE SYSTEM

Eigenvalues	Damping ratio of oscillatory modes	Natural frequency of oscillations (Hz)
$-0.0032 \pm 9.8410j$	0.0003	1.5662
$-10.0698 \pm 4.5122j$	0.9126	0.7181
-0.0000291	1.0000	0

For the nominal operating point, the natural frequency of oscillation  $\omega_n$  is equal to  $9.8410j$  rad/sec. This mode is responsible for the low frequency oscillation of around 1.5 Hz with very less damping of 0.0003. The damping controllers are designed to provide the additional damping. The parameters of the controllers are computed assuming a damping ratio ( $\xi$ ) of 0.1. The gain and phase angle of  $G_c(s)$  for the various inputs are computed and given in table III.

TABLE III  
MAGNITUDE AND PHASE ANGLE OF THE TRANSFER FUNCTION

$G_c(s)$	$ G_c(s) $	$\angle G_c(s)$
$\Delta P_e / \Delta m_1$	0.055447	$-1.5426^\circ$
$\Delta P_e / \Delta \theta_1$	0.037634	$-0.89511^\circ$
$\Delta P_e / \Delta m_2$	0.25303	$-0.042285^\circ$
$\Delta P_e / \Delta \theta_2$	0.0044907	$-179.98^\circ$

It can be seen that the phase angle of the system for the control parameter  $\Delta \theta_2$  is near to  $-180^\circ$ , therefore the system becomes unstable when the controller ( $\Delta \theta_2$ ) is used. This controller is not considered in further investigations. Table-

IV shows the parameters of the remaining three alternative damping controllers computed at the nominal operating point.

TABLE IV  
PARAMETERS OF THE IPFC DAMPING CONTROLLERS

	K	$T_1$
Damping controller $\Delta m_1$	276.44	0.10439
Damping controller $\Delta \theta_1$	411.91	0.10321
Damping controller $\Delta m_2$	62.183	0.10169

Fig. 4 shows the response of  $\Delta \omega$  with the three alternative damping controllers. The response of  $\Delta \omega$  is obtained with a step perturbation of  $\Delta P_m = 0.01$ . Fig.4 shows the responses are identical which indicates that any of the IPFC damping controllers, provide satisfactory performance at the nominal operating point.

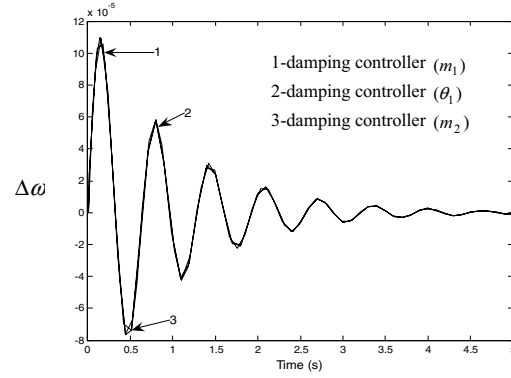


Fig. 4: Dynamic response for  $\Delta \omega$  with different damping controllers.

However, in order to select the most effective IPFC control signal for damping, the controllability index is computed. The index is computed for the electromechanical mode ( $9.8410j$  rad/sec) to be damped taking into account all the control signals one at a time. Table V gives the computed values of the indices.

TABLE V  
CONTROLLABILITY INDICES WITH DIFFERENT IPFC CONTROLLABLE PARAMETERS

IPFC Control Parameters	Controllability index
$\Delta m_1$	0.17974
$\Delta m_2$	0.8202
$\Delta \theta_1$	0.12194
$\Delta \theta_2$	0.014551

Table V reveals that the controllability index corresponding to IPFC control parameter  $\Delta m_2$ , is highest and that of  $\Delta \theta_2$ , is insignificant compared to the other

control parameters. Hence,  $\Delta u = \Delta m_2$  is the best selection for the design of the IPFC damping controller since the minimum control cost (the lowest gain) is needed to provide the required damping (as also observed in table 3). From now on, the damping controllers based on  $\Delta m_2$  shall be denoted as damping controller  $\Delta m_2$ . Fig. 5 shows the dynamic response of the system with and without the damping controller  $\Delta m_2$ .

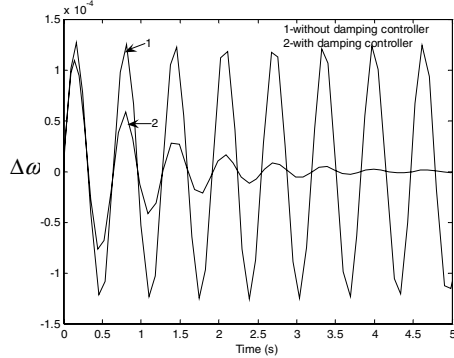


Fig. 5: Rotor speed deviation for  $D=0$ , with and without damping controller

The dynamic performance of the system is further examined considering a case in which two damping controllers operate simultaneously. Fig. 6 shows the dynamic response for  $\Delta\omega$  with damping controller  $\Delta m_1$ ,  $\Delta m_2$  and simultaneous operation of both the controllers (dual controller).

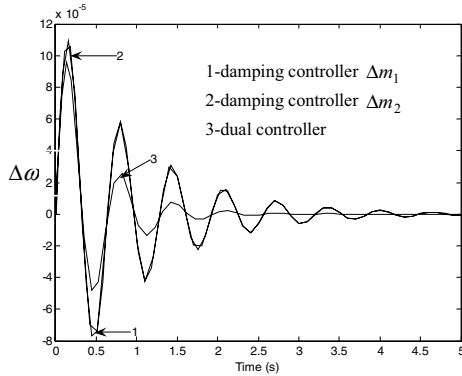


Fig. 6: Dynamic response with different damping controllers.

It is observed that the dynamic response of the system has improved with the use of dual controllers, and thus, more effective than individual controllers.

## V. CONCLUSIONS

The linearized modified Heffron-Phillips model of a single machine infinite bus system installed with IPFC has been established. The linearized model is applied to study

the effect of alternative IPFC damping controllers on oscillation damping. Controllability index is utilized to determine the most effective damping control signal for the design of IPFC damping controller. From the study it is revealed that the IPFC control signal  $\Delta m_2$  is the most effective. However, the dual damping controller which modulates the control signals  $\Delta m_1$  and  $\Delta m_2$  is more effective in providing significant damping torque.

## APPENDIX I

$$\begin{aligned}
 P_e &= P_1 + P_2 = V_{td}I_{td} + V_{tq}I_{tq} \\
 E_q &= E'_q + (X_d - X'_d)I_{td} = E'_q + (X_d - X'_d)(I_{1d} + I_{2d}) \\
 V_t &= V_{td} + jV_{tq}; \quad I_t = I_{td} + jI_{tq} \\
 V_{td} &= X_q I_{tq}; V_{tq} = E'_q - X'_d I_{td} \\
 I_{td} &= (I_{1d} + I_{2d}); \quad I_{tq} = (I_{1q} + I_{2q}) \\
 I_{1d} &= x_{11d}E'_q + \frac{1}{2}(x_{12d} - x_{11d})v_{dc}m_2 \sin \theta_2 \\
 &\quad - \frac{1}{2}x_{12d}v_{dc}m_1 \sin \theta_1 - x_{11d}v_b \cos \delta \\
 I_{2d} &= x_{21d}E'_q + \frac{1}{2}(x_{22d} - x_{21d})v_{dc}m_2 \sin \theta_2 \\
 &\quad - \frac{1}{2}x_{22d}v_{dc}m_1 \sin \theta_1 - x_{21d}v_b \cos \delta \\
 I_{1q} &= \frac{1}{2}(x_{11q} + x_{12q})v_{dc}m_2 \cos \theta_2 - \frac{1}{2}(x_{12q})v_{dc}m_1 \cos \theta_1 \\
 &\quad + x_{11q}v_b \sin \delta \\
 I_{2q} &= \frac{1}{2}(x_{21q} + x_{22q})v_{dc}m_2 \cos \theta_2 - \frac{1}{2}(x_{22q})v_{dc}m_1 \cos \theta_1 \\
 &\quad + x_{21q}v_b \sin \delta \\
 \begin{bmatrix} x_{11d} & x_{12d} \\ x_{21d} & x_{22d} \end{bmatrix} &= \begin{bmatrix} x'_d + x_t & x'_d + x_t + x_{t2} + x_{L2} \\ x_{t1} + x_{L1} & -(x_{t2} + x_{L2}) \end{bmatrix}^{-1} \\
 \begin{bmatrix} x_{11q} & x_{12q} \\ x_{21q} & x_{22q} \end{bmatrix} &= \begin{bmatrix} x_d + x_t & x_d + x_t + x_{t2} + x_{L2} \\ -(x_{t1} + x_{L1}) & (x_{t2} + x_{L2}) \end{bmatrix}^{-1}
 \end{aligned}$$

$V_t$  : Terminal voltage of generator

$M = 2H$  : is the inertia constant

$P_D = D(\omega - 1)$ ,  $D$ : Damping coefficient

$T'_{do}$  : Open circuit d-axis time constant in sec

$K_a$  : AVR gain,

$T_a$  : Time constant of AVR in sec

$P_e$  : Electrical power of the generator

$P_m$  : Mechanical power input to the generator

$V_{ref}$  : Reference voltage

$C_{dc}$  : DC link capacitor

$m_1$  : Modulation index of VSC 1

$m_2$  : Modulation index of VSC 1



# Damping of Inter Area Oscillations Using Interline Power Flow Controller Based Damping Controllers

Alivelu M. Parimi\*, Irraivan Elamvazuthi\*\* and Nordin Saad\*\*\*

Universiti Teknologi PETRONAS, Tronoh, Perak, Malaysia.

Email: \*alivelu\_manga@utp.edu.my

\*\* irraivan\_elamvazuthi@petronas.com.my

\*\*\* nordiss@petronas.com.my

**Abstract**—This paper investigates the effect of Interline Power Flow Controller (IPFC), an advanced Flexible AC Transmission System (FACTS) controller, in damping low frequency oscillations via supplementary control. For this purpose, a modified linearised Phillips-Heffron model for a Single machine Infinite Bus (SMIB) system installed with IPFC is established, and the power oscillation damping controller is designed. The effect of this damping controller on the system, subjected to wide variations in loading conditions and system parameters, is investigated. Results of simulation investigations in Matlab are presented to validate the proposed approach.

**Keywords**—IPFC; inter area oscillation; damping controller

## I. INTRODUCTION

Today's heavily loaded and stressed power transmission networks exhibit complex dynamic system behavior. They are continually exposed to sudden, small and large, disturbances in load, generation and transmission network configuration. As such the appearance of low frequency electromechanical oscillations in the interconnected power systems is a reasonably frequent phenomenon. Growing oscillations eventually lead to loss of synchronism in a power system causing either damage or making the parallel operation infeasible. In this context, damping devices are imperative for the modern power systems to improve system stability and suppress undesirable oscillations. The electromechanical oscillations are usually in the range between 0.1 and 2 Hz [1]. The oscillations in the range 0.1 to 0.8 Hz are called inter-area modes which are associated among groups of generators or groups of plants. Oscillations associated with a single generator or more in an area with respect to the rest of the system are called local modes having frequencies in the range 0.8 to 2.0 Hz.

In recent years, Flexible AC Transmission System (FACTS) controllers are found to be more capable of handling power flow control, transient stability and oscillation damping enhancement as reported in [2-6]. Researchers have presented design of FACTS-based stabilizers for SVC, TCSC, TCPS, and Unified Power Flow Controller (UPFC) in [7]. Interline Power Flow Controller (IPFC) is an advanced voltage sourced converter based FACTS controller [8] which employs a number of dc to ac converters each providing a series compensation for a different line. The converters are

linked together at their dc terminals and connected to the ac systems through their series coupling transformers. The IPFC allows to simultaneously and independently inject, over each transmission line, a controllable series voltage which enables to equalize both real and reactive power flow between the lines; transfer power demand from overload to under loaded lines; compensate against resistive line voltage drops and the corresponding reactive power demand; increase the effectiveness of the overall compensating system for dynamic disturbances. Though the primary function of the IPFC is to control power flow on a given line, it can also be utilized for damping power system oscillations by judiciously applying a damping controller.

A supplementary PID damping controller along with power flow control was proposed in [9], but the performance is degraded due to nonlinearity of the system. The effect of IPFC on damping inter-area oscillations with a PI damping controller, with electrical power as input, was proposed by Kazemi [10]. However, the parameters of the controller are not optimized. In the view of this, the main purpose of this paper is to extend the design of damping controllers for UPFC previously proposed by the authors [5, 11] to IPFC. Adopting similar techniques, the modified linearized Phillips-Heffron model for a single machine infinite bus (SMIB) system with IPFC is derived. Thereafter, an IPFC based power oscillation damping controller is designed. The performance of the damping controller under wide variations in loading conditions and in system parameters (equivalent line reactance) is investigated.

## II. SYSTEM INVESTIGATED

A single machine infinite bus system installed with IPFC as shown in Fig. 1 is considered.

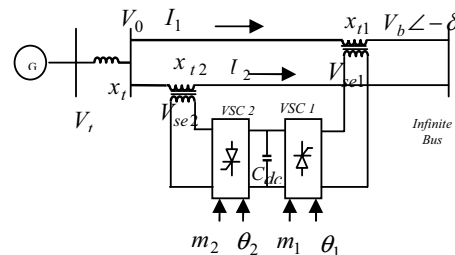


Figure 1. IPFC installed in a SMIB system

The IPFC is installed on the two parallel transmission lines. The IPFC is assumed to be based on pulse width modulation (PWM) converters.

#### A. Non Linear Dynamic Model of the System with IPFC

A non-linear dynamic model of the system is derived by neglecting the resistances of all the components of the system (generator, transformer, transmission lines, and series converter transformers); the transients of the transmission lines and transformers of the IPFC. The non-linear dynamic model of the system using IPFC is derived as follows

$$\dot{\delta} = \omega_0(\omega - 1) \quad (1)$$

$$\dot{\omega} = \frac{P_m - P_e - P_D}{M} \quad (2)$$

$$\dot{E}'_q = \frac{(-E_q + E_{fd})}{T'_{do}} \quad (3)$$

$$\dot{E}_{fd} = \frac{-E_{fd} + K_a(V_{ref} - V_t)}{T_a} \quad (4)$$

$$\dot{V}_{dc} = \frac{3m_1}{4C_{dc}}(\cos\theta_1 I_{1d} + \sin\theta_1 I_{1q}) + \frac{3m_2}{4C_{dc}}(\cos\theta_2 I_{2d} + \sin\theta_2 I_{2q}) \quad (5)$$

where

$\delta$  : Rotor angle of synchronous generator in radians

$\omega$  : Rotor speed in rad/sec

$V_t$  : Terminal voltage of generator

$M = 2H$  : is the inertia constant

$P_D = D(\omega - 1)$ ,  $D$ : Damping coefficient

$T'_{do}$  : Open circuit d-axis time constant in sec

$K_a$  : AVR gain,

$T_a$  : Time constant of AVR in sec

$P_e$  : Electrical power of the generator

$P_m$  : Mechanical power input to the generator

$\dot{E}'_q$  : Generator internal voltage

$E_{fd}$  : Generator field voltage

$V_{ref}$  : Reference voltage

$V_{dc}$  : Voltage at DC link

$C_{dc}$  : DC link capacitor

$m_1$  : Modulation index of VSC 1

$m_2$  : Modulation index of VSC 2

$\theta_1$  : Phase angle of series converter 1 voltage

$\theta_2$  : Phase angle of series converter 2 voltage

$I_{1d}$  : d-axis current in line 1

$I_{1q}$  : q-axis current in line 1

$I_{2d}$  : d-axis current in line 2

$I_{2q}$  : q-axis current in line 2

The equivalent controllable injected voltage source magnitude and angle of the series converter are constrained by :

$$V_{sei}^{\min} \leq V_{sei} \leq V_{sei}^{\max} \quad (6)$$

$$-\pi \leq \theta_i \leq \pi$$

where  $i=1, 2$ ; and  $V_{sei}^{\min}, V_{sei}^{\max}$  are the minimal and maximal voltage limits of  $V_{sei}$ , respectively [12].

According to the principle of IPFC, the operating constraint representing the active power exchange ( $PE$ ) between or among the converters via the common DC link is given by:

$$PE = \sum_i P_{sei} = 0 \quad (i=1,2) \quad (7)$$

where  $P_{sei} = \text{Re}(V_{sei} I_{sei}^*)$  ( $i=1,2$ ),  $I_{sei}^*$  is the conjugate of  $I_{sei}$  [12]. General pulse width modulator is used for the VSC's. The voltages injected by the IPFC converters in d-q coordinates are obtained as follows:

$$V_{se1d} = -x_{t1} I_{1q} + \frac{v_{dc}}{2} m_1 \cos \theta_1$$

$$V_{se1q} = x_{t1} I_{1d} + \frac{v_{dc}}{2} m_1 \sin \theta_1$$

$$V_{se2d} = -x_{t2} I_{2q} + \frac{v_{dc}}{2} m_2 \cos \theta_2$$

$$V_{se2q} = x_{t2} I_{2d} + \frac{v_{dc}}{2} m_2 \sin \theta_2$$

$$V_{sei} = V_{seid} + jV_{seiq} = V_{sei} e^{j\theta_i} \quad (8)$$

where  $x_{t1}$  and  $x_{t2}$  are the reactance's of the transformers in line 1 and 2.

#### B. Linear Dynamic Model (Modified Heffron-Phillips Model of an SMIB System including IPFC) in State Space form

A linear dynamic model is obtained by linearising the non linear model (1) to (5) around an operating condition which is obtained from power flow analysis. The linearised model in state space form is obtained as

$$\dot{X} = AX + BU \quad (9)$$

$$\text{where } X = [\Delta\delta \quad \Delta\omega \quad \Delta E'_q \quad \Delta E_{fd} \quad \Delta V_{dc}]^T$$

$$A = \begin{bmatrix} 0 & \omega_o & 0 & 0 & 0 \\ -\frac{K_1}{M} & -\frac{D}{M} & -\frac{K_2}{M} & 0 & -\frac{K_{pv}}{M} \\ \frac{K_4}{T'_{do}} & 0 & -\frac{K_3}{T'_{do}} & \frac{1}{T'_{do}} & -\frac{K_{qv}}{T'_{do}} \\ -\frac{K_a K_5}{T_a} & 0 & -\frac{K_a K_6}{T_a} & \frac{1}{T_a} & -\frac{K_a K_{vv}}{T_a} \\ K_7 & 0 & K_8 & 0 & -K_9 \end{bmatrix}$$

$$B = \begin{bmatrix} 0 & 0 & 0 & 0 \\ \frac{K_{pm1}}{M} & \frac{K_{p\theta1}}{M} & \frac{K_{pm2}}{M} & \frac{K_{p\theta2}}{M} \\ -\frac{K_{qm1}}{T'_{do}} & -\frac{K_{q\theta1}}{T'_{do}} & -\frac{K_{qm2}}{T'_{do}} & -\frac{K_{q\theta2}}{T'_{do}} \\ -\frac{K_a K_{vm1}}{T_a} & -\frac{K_a K_{v\theta1}}{T_a} & -\frac{K_a K_{vm2}}{T_a} & -\frac{K_a K_{v\theta2}}{T_a} \\ K_{cm1} & K_{c\theta1} & K_{cm2} & K_{c\theta2} \end{bmatrix}$$

The control vector  $u$  is defined as follows:

$$U = [\Delta m_1 \quad \Delta \theta_1 \quad \Delta m_2 \quad \Delta \theta_2]^T \quad (10)$$

where

$\Delta m_1$  : Deviation in pulse width modulation index  $m_1$  of voltage series converter 1 in line 1. By controlling  $m_1$ , the magnitude of series injected voltage in line 1 can be controlled.

$\Delta m_2$  : Deviation in pulse width modulation index  $m_2$  of voltage series converter 2 in line 2. By controlling  $m_2$ , the magnitude of series injected voltage in line 2 can be controlled.

$\Delta \theta_1$  : Deviation in phase angle of the series injected voltage  $V_{se1}$ .

$\Delta \theta_2$  : Deviation in phase angle of the series injected voltage  $V_{se2}$ .

Fig. 2 shows the modified Phillips-Heffron transfer function model of the system incorporating IPFC. The model has 28 constants similar to SMIB model with UPFC [5]. These constants are functions of system parameters and the initial operating condition. It should be noted that  $K_p, K_q, K_v$  and  $K_c$  in Fig. 2 are the row vectors defined as

$$K_p = [K_{pm1} \quad K_{p\theta1} \quad K_{pm2} \quad K_{p\theta2}]$$

$$K_q = [K_{qm1} \quad K_{q\theta1} \quad K_{qm2} \quad K_{q\theta2}]$$

$$K_v = [K_{vm1} \quad K_{v\theta1} \quad K_{vm2} \quad K_{v\theta2}]$$

$$K_c = [K_{cm1} \quad K_{c\theta1} \quad K_{cm2} \quad K_{c\theta2}] \quad (11)$$

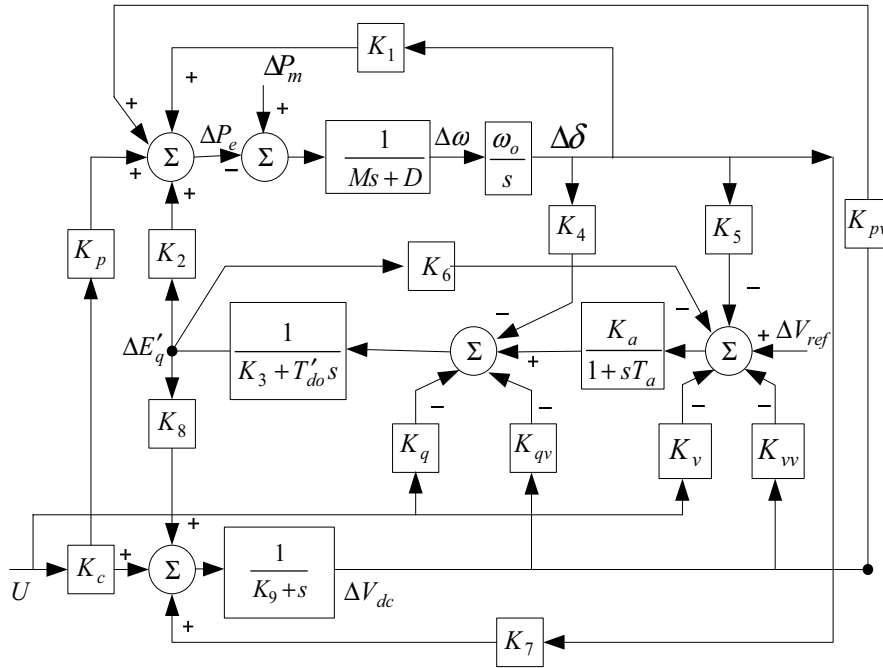


Figure 2. Modified Heffron-Phillips model of SMIB system with IPFC

### C. Computation of Constants of the Power System

The initial d-q axes voltage and current components computed for the nominal operating point ( $P_e = 0.8$  p.u.,  $Q_e = 0.4$  p.u.,  $V_t = 1.0$ ,  $V_b = 1.0$  p.u.) are as follows:

$$\begin{aligned} V_{do} &= 0.3610 & V_{qo} &= 0.9326 \\ I_{do} &= 0.6618 & I_{qo} &= 0.6017 \\ \delta_o &= 53.1301^\circ & V_{se1o} &= 0.1328 \\ \theta_{1o} &= 71.565^\circ & \theta_{2o} &= 4.44^\circ \end{aligned}$$

The system parameters are given in appendix. The data is required for computing the constants of the system model. The constants for the nominal condition are as follows

$$\begin{aligned} K_1 &= 0.9617 & K_2 &= 0.0295 & K_3 &= 0.8577 \\ K_4 &= -4.515 \times 10^{-8} & K_5 &= 0.0066 & K_6 &= 0.7861 \\ K_7 &= 0.0032 & K_8 &= -0.0074 & K_9 &= -2.641 \times 10^{-5} \\ K_{pv} &= 0.0563 & K_{qv} &= 3.62e-4 & K_{vv} &= -0.0026 \\ K_{pm1} &= 0.1169 & K_{p\theta1} &= 0.0042 & K_{pm2} &= 0.1064 \\ K_{p\theta2} &= -0.0056 & K_{qm1} &= -0.0043 & K_{q\theta1} &= 0.0026 \\ K_{qm2} &= 0.0082 & K_{q\theta2} &= 0.0016 & K_{vm1} &= -0.0212 \\ K_{v\theta1} &= 0.0017 & K_{vm2} &= 0.0188 & K_{v\theta2} &= -0.0013 \\ K_{cm1} &= -2.64 \times 10^{-5} & K_{c\theta1} &= 0.0563 & K_{cm2} &= 3.62 \times 10^{-4} \\ & & & & K_{c\theta2} &= -0.0026 \end{aligned}$$

### D. Design of Damping Controllers

The damping controllers are designed to provide an additional electrical torque in phase with the speed deviation. The speed deviation  $\Delta\omega$  is considered as the input to the damping controller whose output is used to modulate the controlled parameter  $m_2$  which controls the series voltage injected in line 2. It is assumed that, for the series converter in line 2, the active power flow control constraint is used while the reactive power flow constraint is relaxed. The structure of IPFC based damping controller is shown in Fig. 3. It consists of gain, signal washout and phase compensation blocks.

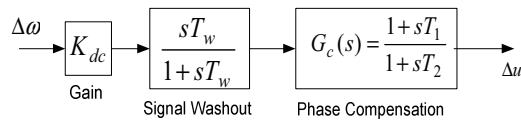


Figure 3. Structure of IPFC based damping controller

The parameters of the damping controller are determined using the phase compensation technique [13]. The magnitude and phase angle of transfer

function,  $\Delta P_e / \Delta m_2$  is computed for  $s = j\omega_n$  at

nominal operating condition where  $\omega_n = \sqrt{\frac{K_1 \omega_0}{M}}$ . The

gain setting of the damping controller is chosen to achieve required damping ratio equal to 0.5. The time constants computed to compensate the phase angle of the transfer function  $\Delta P_e / \Delta m_2$  for the system at  $s = 6.7314i$  are  $T_1 = 0.1478s$  and  $T_2 = 0.1493s$ . The gain setting  $K_{dc}$  is equal to 511.0965. The value of  $T_w$  (the washout filter time constant) is chosen as 20s which should be high enough to pass low frequency oscillations unchanged. Then, the dynamic performance of the system is investigated with the designed controller while varying the loading conditions and the equivalent line reactance  $x_e$  over the range of  $\pm 20\%$  from its nominal value considering a step perturbation  $\Delta P_m = 0.01$  p.u.

### III. RESULTS AND DISCUSSION

To examine the effect of IPFC based damping controller on the system, simulations are performed using Matlab simulink on the system, first without IPFC and then, with IPFC and damping controller. The K-constants for the system without IPFC are computed which are given as follows:

$$\begin{aligned} K_1 &= 0.2884 & K_2 &= 0.7385 & K_3 &= 0.8467 \\ K_4 &= -1744 & K_5 &= -0.1706 & K_6 &= 0.7182 \end{aligned}$$

Using these values the Phillips-Heffron linear model of the single machine infinite bus without IPFC is simulated in Matlab. The response of change in speed  $\Delta\omega$  for the system when there is no IPFC is given in Fig 4. which indicates the system is unstable and requires additional damping to sustain the oscillation.

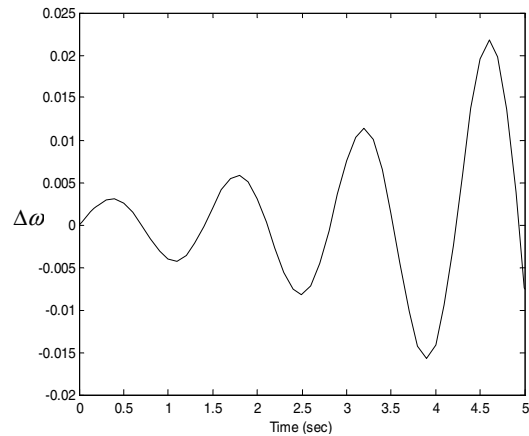


Figure 4. Dynamic response for  $\Delta\omega$  without IPFC

The system is incorporated with IPFC and the operating point is obtained from load flow. The K-constants are computed using the system parameters and initial operating point, as given in section C and the system is simulated. The response of  $\Delta\omega$  for the system with the IPFC based damping controller

included is shown in Fig 5. It shows the damping controller provides satisfactory performance at the nominal operating condition. The robustness of the damping controller designed at the nominal operating point is examined by varying the loading conditions of the system. The load condition of the system is varied from  $P_e = 0.1$  to  $P_e = 1.0$ . The dynamic responses of the system are obtained for each loading condition.

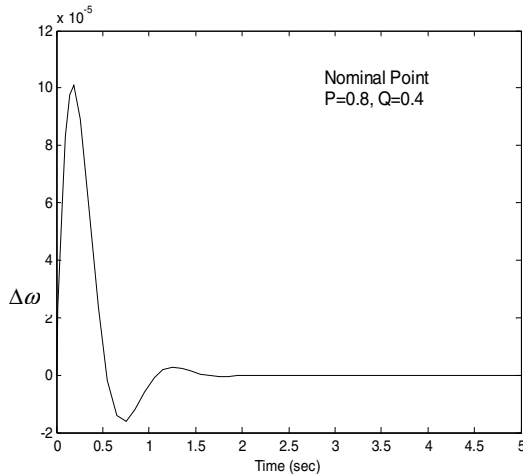


Figure 5. Dynamic response for  $\Delta\omega$  with the IPFC based damping controller

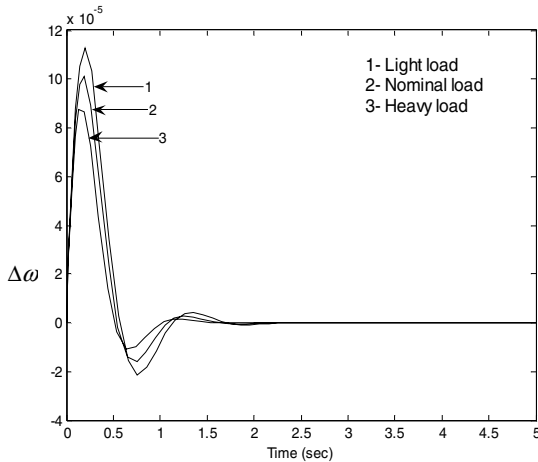


Figure 6. Dynamic response for  $\Delta\omega$  with the IPFC based damping controller for different loading conditions

Fig 6, shows the dynamic responses of  $\Delta\omega$  for  $P_e = 0.2$  (light loading),  $P_e = 0.8$  (nominal loading) and  $P_e = 1.0$  (heavy loading). It can be seen that the responses are similar in terms of settling time which indicates that the damping controller provides satisfactory performance under wide variation in loading conditions. The performance of the damping controller is further investigated with variation in equivalent reactance  $x_e$ . Fig. 7 shows the dynamic performance of the system for variation in  $x_e$  for  $\pm 20\%$  from the nominal value.

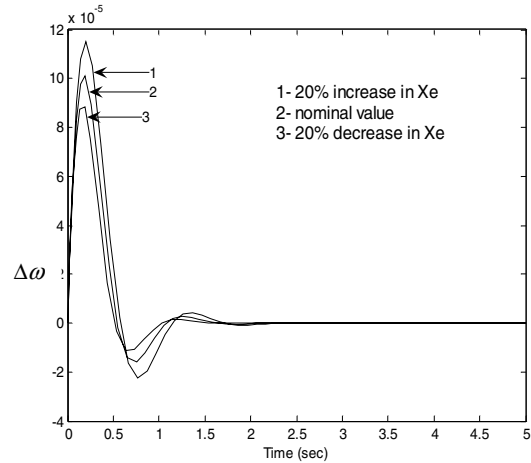


Figure 7. Dynamic response for  $\Delta\omega$  with the IPFC based damping controller for different variations in  $x_e$

The damping controller provides a satisfactory response even with variation in equivalent reactance  $x_e$ .

#### IV. CONCLUSION

The effectiveness of the IPFC based damping controller has been investigated in damping low frequency oscillations. Dynamic simulations results have emphasized that the damping controller which modulates the control signal  $m_2$  provides satisfactory dynamic performance under wide variations in loading condition and system parameters. Further work will be carried on applying the controller design for a multi-machine system.

#### REFERENCES

- [1] P. Kundur, *Power System Stability and Control*. Mc Graw-Hill, New York, 1994.
- [2] R. Sadikovic, P. Korba and G. Andersson, "Application of FACTS Devices for Damping of Power System Oscillations," *IEEE PowerTech 2005*, Russia, June 2005.
- [3] P.K.Dash, S.MishraA, G.Panda, "Damping Multimodal Power System Oscillation Using a Hybrid Fuzzy Controller for Series Connected FACTS Devices," *IEEE Transactions on Power Systems*, Vol. 15, No. 4, November 2000, pp. 1360 – 1366.
- [4] H.F. Hang, "Design of SSSC Damping Controller to Improve Power System Oscillation Stability," *IEEE* 1999.
- [5] N.Tambey and M.L.Kothari, "Damping of Power System Oscillation with Unified Power Flow Controller," *IEE Proc. Gener. Trans. Distrib.* Vol. 150, No. 2, March 2003, pp. 129 – 140.
- [6] N.G. Hingorami, L.Gyugyi, *Understanding FACTS: Concepts and Technology of Flexible AC Transmission system*, IEEE Press, 1999
- [7] Y.H. Song and A.T. Johns, *Flexible AC Transmission systems*, IEE Power and Energy series 30, 1999.
- [8] L.Gyugyi, K.K.Sen, C.D.Schauder, "The Interline Power FlowController Concept: A New Approach to Power Flow Management in Transmission Systems," *IEEE Transactions on Power Delivery*, Vol. 14, No. 3, July 1999, pp. 1115 – 1123.
- [9] J. Chen, T.T. Lie, D.M. Vilathgamuwa, "Design of Interline Power Flow Controller," 14<sup>th</sup> PSCC, Sevilla, June 2002.
- [10] Kazemi, A.; Karimi, E., "The Effect of Interline Power Flow Controller (IPFC) on Damping Inter-area Oscillations in the Interconnected Power Systems," *Industrial Electronics*, 2006

*IEEE International Symposium*, Volume 3, July 2006, pp. 1911 – 1915.

- [11] H.F. Wang. "Applications of Modelling UPFC into Multimachine Power Systems," *IEE Proceedings-C*, vol 146, no 3, May 1999, pp. 306.
- [12] X.-P. Zhang, "Modelling of the interline power flow controller and the generalised unified power flow controller in Newton power flow", *Generation, Transmission and Distribution, IEE Proceedings*-Volume 150, Issue 3, May 2003 pp. 268 – 274.
- [13] Yao-Nan Yu, *Electric Power System Dynamics*, Academic Pres, Inc, London, 1983.

#### APPENDIX

The nominal parameters and the operating condition of the system are given as follows:

Generator:  $M = 2H = 8.0 \text{ MJ/MVA}$   $D = 0$ ,  $T'_{do} = 5.044s$

$$X_d = 0.1, X_q = 0.6, X'_d = 0.3$$

Excitation system:  $K_a = 50$ ,  $T_a = 0.05$

Transformer :  $x_{t1} = 1.0 \text{ p.u.}$ ,  $x_{t1} = x_{t2} = x_l = 0.01$

$$x_{t1} = x_{t2} = 0.2, x_e = 1.0 + (0.01 + 0.2)/2$$

Operating Condition:  $P_e = 0.8 \text{ p.u.}$ ,  $Q_e = 0.4 \text{ p.u.}$

$$V_b = 1.0 \text{ p.u.}, V_t = 1.0$$

IPFC parameters:  $m_1 = 0.15$ ,  $m_2 = 0.1$

Parameters of DC link:  $V_{dc} = 2 \text{ p.u.}$ ,  $C_{dc} = 1 \text{ p.u.}$

# Dynamic Modeling of Interline Power Flow Controller for Small Signal Stability

Alivelu M. Parimi, Nirod C. Sahoo, Irraivan Elamvazuthi, Nordin Saad  
Electrical and Electronics Department  
Universiti Teknologi PETRONAS,  
Tronoh 31750, Perak, Malaysia.

**Abstract**—This paper addresses the formulation of the non-linear dynamic model of the power system installed with Interline Power Flow Controller (IPFC). The linearized model for both single-machine infinite-bus and multi-machine power system installed with IPFC is developed and incorporated into the Phillips-Heffron model. These models lay the foundation for small signal stability studies of the power system using IPFC. The application of the models is demonstrated for a Multi-machine power system.

**Keywords**—IPFC; power system modelling; Phillips-Heffron model

## I. INTRODUCTION

The Interline Power Flow Controller (IPFC) belongs to the converter-based FACTS Controllers, representing the new generation of transmission controllers, employing the self commutated, voltage-sourced converters (VSC). An IPFC consists of a number of VSCs linked together at their dc terminals. Each VSC injects a controllable ac voltage to its respective transmission line providing series compensation [1, 2], whilst the common dc link facilitates the transfer of real power flow among the transmission lines. Thus, real power is transferred from overloaded to under-loaded lines and increases the capacity of the transmission lines. The IPFC simultaneously compensates multiple transmission lines by equalizing the real and reactive power flows in between the lines. IPFC also provides voltage control, improves transient stability, and enhances oscillation damping. Recently, modelling of IPFC and its various control functions has come under intensive investigation. Work has been established to model the IPFC into the power systems in a steady-state mode of operation for load flow studies and power flow control [3-5]. Control strategies for damping improvement such as supplementary PI controller or lead lag controller had been suggested for IPFC in [6-9]. These controllers were designed based on linear models of single machine infinite bus (SMIB) power system installed with IPFC. Studies on this system reveal good damping characteristics of IPFC. However, modelling of the IPFC into a multi-machine power system (MMPS) for small signal stability is very limited. The small signal stability analysis based on eigenvalue technique is suitable for planning and operation of the power systems, to examine the problems associated with oscillations and to mitigate the power system oscillations using various control methods [10]. The Phillips-Heffron model of the power system with the FACTS device is suitable for

understanding of system damping in the area of small perturbation stability. It presents an insight into the operation of the damping control of the FACTS device and is useful in studying the small signal stability of the power system.

In this view, the non-linear dynamic model of a power system installed with an IPFC is initially developed. Further, the linearized Phillips-Heffron model is modified to include the FACTS device, IPFC, which is utilized to perform the small signal stability analysis. Consequently, in the following sections the non-linear model of SMIB power system and MMPS installed with IPFC is developed. Then the small signal linearized Phillips-Heffron model of these systems is derived. The linearized model of a power system with an IPFC obtained, is in similar form to that of the unified Phillips-Heffron model presented in [11-14] for other FACTS devices such as, Static VAR Compensator (SVC), Thyristor-Controlled Series Compensator (TCSC), Thyristor-Controlled Phase Shifter (TCPS) and Unified Power Flow Controller (UPFC) for single machine and multi-machine power systems. On the basis of linearized system model, the IPFC controllers are designed and their effect is investigated on oscillation stability.

## II. SINGLE MACHINE INFINITE BUS POWER SYSTEM

A SMIB system installed with IPFC as shown in Fig. 1 is considered. The IPFC is installed on the two parallel transmission lines through series transformers. The IPFC consists of two VSCs which are linked together at the dc link.

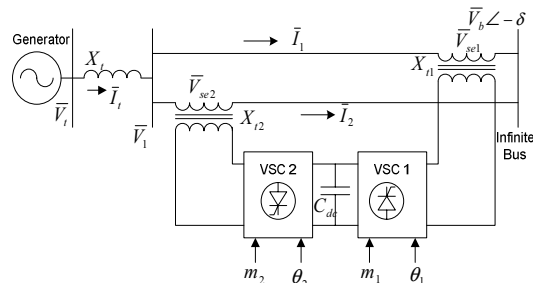


Figure 1. IPFC installed in a SMIB system

The voltages injected by the IPFC converters are given by [7, 8]:

$$\bar{V}_{se1} = \frac{v_{dc}}{2} m_1 e^{j\theta_1}, \quad \bar{V}_{se2} = \frac{v_{dc}}{2} m_2 e^{j\theta_2} \quad (1)$$

where  $v_{dc}$  is the voltage at DC link,  $m_1$  and  $m_2$  are the modulation indices of VSC 1 and 2,  $\theta_1$  and  $\theta_2$  are the phase angles of series converter 1 and 2. The dc capacitor voltage is given by

$$\dot{v}_{dc} = \frac{3m_1}{4C_{dc}}(i_{1d} \cos \theta_1 + i_{1q} \sin \theta_1) + \frac{3m_2}{4C_{dc}}(i_{2d} \cos \theta_2 + i_{2q} \sin \theta_2) \quad (2)$$

where,  $C_{dc}$  is the dc link capacitor,  $i_{1d}$  and  $i_{2d}$  are the d-axis currents in line 1 and 2,  $i_{1q}$  and  $i_{2q}$  are the q-axis current in line 1 and 2 respectively. From the Fig. 1 we obtain,

$$\bar{V}_t = jx_t \bar{I}_t + \bar{V}_1 \quad (3)$$

$$\begin{aligned} \bar{V}_1 &= jx_{t1} \bar{I}_1 + \bar{V}_{se1} + jx_{L1} \bar{I}_1 + \bar{V}_b \\ &= jx_{t2} \bar{I}_2 + \bar{V}_{se2} + jx_{L2} \bar{I}_2 + \bar{V}_b \end{aligned} \quad (4)$$

where,  $x_{t1}$  and  $x_{t2}$  are the reactance of the transformers in line 1 and 2 respectively and  $x_{L1}$  and  $x_{L2}$  are the reactance of the transmission line 1 and 2 respectively. Solving (3) and (4) we get the currents in d-q axis as follows:

$$\begin{aligned} i_{1d} &= x_{11d} E'_q + \frac{1}{2}(x_{12d} - x_{11d})v_{dc} m_2 \sin \theta_2 \\ &\quad - \frac{1}{2}x_{12d} v_{dc} m_1 \sin \theta_1 - x_{11d} v_b \cos \delta \end{aligned} \quad (5)$$

$$\begin{aligned} i_{2d} &= x_{21d} E'_q + \frac{1}{2}(x_{22d} - x_{21d})v_{dc} m_2 \sin \theta_2 \\ &\quad - \frac{1}{2}x_{22d} v_{dc} m_1 \sin \theta_1 - x_{21d} v_b \cos \delta \end{aligned} \quad (6)$$

$$\begin{aligned} i_{1q} &= \frac{1}{2}(x_{11q} + x_{12q})v_{dc} m_2 \cos \theta_2 \\ &\quad - \frac{1}{2}(x_{12q})v_{dc} m_1 \cos \theta_1 + x_{11q} v_b \sin \delta \end{aligned} \quad (7)$$

$$\begin{aligned} i_{2q} &= \frac{1}{2}(x_{21q} + x_{22q})v_{dc} m_2 \cos \theta_2 \\ &\quad - \frac{1}{2}(x_{22q})v_{dc} m_1 \cos \theta_1 + x_{21q} v_b \sin \delta \end{aligned} \quad (8)$$

where,  $x_{11d} = x_{tL2} / x_{\Sigma 1}$ ,  $x_{12d} = (x'_{dt} + x_{tL2}) / x_{\Sigma 1}$

$$x_{21d} = x_{tL1} / x_{\Sigma 1}, \quad x_{22d} = -x'_{dt} / x_{\Sigma 1}$$

$$x_{11q} = x_{tL2} / x_{\Sigma 2}, \quad x_{12q} = -(x'_{qt} + x_{tL2}) / x_{\Sigma 2}$$

$$x_{21q} = x_{tL1} / x_{\Sigma 2}, \quad x_{22d} = -x'_{qt} / x_{\Sigma 2}$$

$$x_{tL2} = x_{t2} + x_{L2}, \quad x'_{dt} = x'_d + x_t$$

$$x_{tL1} = x_{t1} + x_{L1}, \quad x'_{qt} = x_q + x_t$$

$$x_{\Sigma 1} = (x'_{dt} \cdot x_{tL2}) + (x'_{dt} + x_{tL2})(x_{tL1})$$

$$x_{\Sigma 2} = (x'_{qt} \cdot x_{tL2}) + (x'_{qt} + x_{tL2})(x_{tL1})$$

#### A. Non-linear model of Single Machine Infinite Bus

The non-linear dynamic model of the power system incorporated with IPFC is derived as follows [7 - 9]:

$$\dot{\delta} = \omega_o(\omega - 1)$$

$$\dot{\omega} = (P_m - P_e - P_D) / M$$

$$\dot{E}'_q = (-E_q + E_{fd}) / T'_{do}$$

$$\dot{E}_{fd} = (-E_{fd} + K_a(V_{ref} - V_t)) / T_a \quad (9)$$

where  $\delta$  is the rotor angle of synchronous generator in radians,  $\omega$  is the rotor speed in rad/sec,  $V_t$  is the terminal voltage of generator,  $M (= 2H)$  is the inertia constant,  $P_D = D(\omega - 1)$ ,  $D$  is the damping coefficient,  $T'_{do}$  is the open circuit d-axis time constant in sec,  $K_a$  is the AVR gain,  $T_a$  is the time constant of AVR in sec,  $P_e$  is the electrical power of the generator,  $P_m$  is the mechanical power input to the generator,  $E'_q$  is the generator internal voltage,  $E_{fd}$  is the generator field voltage,  $V_{ref}$  is the reference voltage,

#### B. Linearized Model of an SMIB System including IPFC in State Space form

A linear dynamic model is obtained by linearizing the non-linear model (9) around an operating condition which is obtained from power flow analysis. The linearized model in state space form is obtained as ,

$$\dot{X} = AX + BU \quad (10)$$

where,  $X = [\Delta\delta \quad \Delta\omega \quad \Delta E'_q \quad \Delta E_{fd} \quad \Delta V_{dc}]^T$

$$A = \begin{bmatrix} 0 & \omega_o & 0 & 0 & 0 \\ -\frac{K_1}{M} & -\frac{D}{M} & -\frac{K_2}{M} & 0 & -\frac{K_{pv}}{M} \\ -\frac{K_4}{T'_{do}} & 0 & -\frac{K_3}{T'_{do}} & \frac{1}{T'_{do}} & -\frac{K_{qv}}{T'_{do}} \\ -\frac{K_a K_5}{T_a} & 0 & -\frac{K_a K_6}{T_a} & -\frac{1}{T_a} & -\frac{K_a K_{vv}}{T_a} \\ K_7 & 0 & K_8 & 0 & -K_9 \end{bmatrix}$$

$$B = \begin{bmatrix} 0 & 0 & 0 & 0 \\ -\frac{K_{pm1}}{M} & -\frac{K_{p\theta1}}{M} & -\frac{K_{pm2}}{M} & -\frac{K_{p\theta2}}{M} \\ -\frac{K_{qm1}}{T'_{do}} & -\frac{K_{q\theta1}}{T'_{do}} & -\frac{K_{qm2}}{T'_{do}} & -\frac{K_{q\theta2}}{T'_{do}} \\ -\frac{K_a K_{vm1}}{T_a} & -\frac{K_a K_{v\theta1}}{T_a} & -\frac{K_a K_{vm2}}{T_a} & -\frac{K_a K_{v\theta2}}{T_a} \\ K_{cm1} & K_{c\theta1} & K_{cm2} & K_{c\theta2} \end{bmatrix}$$

The control vector  $u$  is defined as follows:

$$U = [\Delta m_1 \quad \Delta \theta_1 \quad \Delta m_2 \quad \Delta \theta_2]^T \quad (11)$$

where,  $\Delta m_1$  ( $\Delta m_2$ ) is the deviation in pulse width modulation index  $m_1$  ( $m_2$ ) of voltage series converter 1 (2) in line 1 (2). By controlling  $m_1$  ( $m_2$ ), the magnitude of series injected voltage in line 1 (2) can be controlled.  $\Delta \theta_1$  ( $\Delta \theta_2$ ) is the deviation in phase angle of the series injected voltage  $V_{se1}$  ( $V_{se2}$ ).

Fig. 2 shows the modified Phillips-Heffron model of the power system with IPFC. The model has 28 constants which are functions of system parameters and the initial operating condition. It should be noted that  $K_p, K_q, K_v$  and  $K_c$  in Fig. 2 are the row vectors defined as

$$K_p = [K_{pm1} \quad K_{p\theta1} \quad K_{pm2} \quad K_{p\theta2}]$$

$$K_q = [K_{qm1} \quad K_{q\theta1} \quad K_{qm2} \quad K_{q\theta2}]$$

$$K_v = [K_{vm1} \quad K_{v\theta1} \quad K_{vm2} \quad K_{v\theta2}]$$

$$K_c = [K_{cm1} \quad K_{c\theta1} \quad K_{cm2} \quad K_{c\theta2}] \quad (12)$$

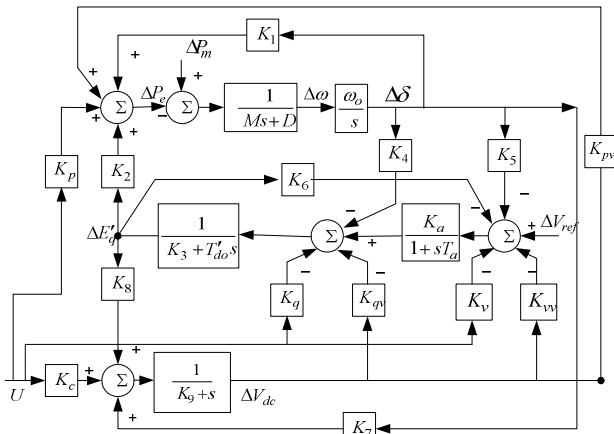


Figure 2. Phillips Heffron model of SMIB with IPFC

### III. MULTI-MACHINE POWER SYSTEM

Without loss of generality, we assume that in an  $n$  machine power system, an IPFC is installed on the branches 4-2 and 4-3, as shown in Fig. 3. For developing the dynamic model of the system, the network is

represented by taking out the buses connecting the lines in which IPFC is installed.

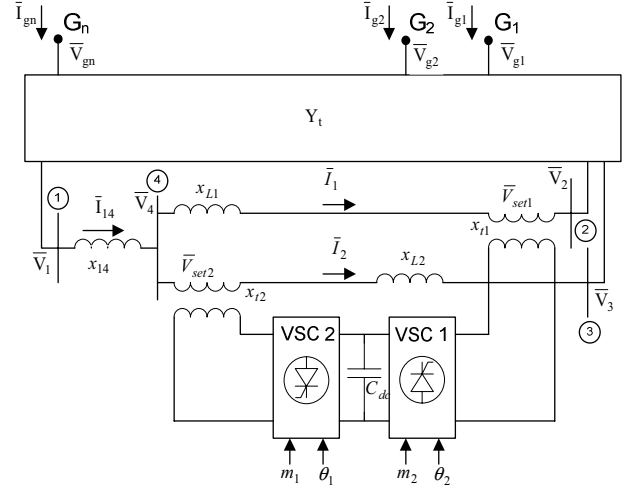


Figure 3. An  $n$ -machine power system installed with an IPFC

The network admittance  $\bar{Y}_l$  is formed before the IPFC has been installed, keeping  $n$  generator nodes along with the nodes 1-4. The equation of the network is given by:

$$\begin{bmatrix} 0 \\ 0 \\ 0 \\ 0 \\ \bar{I}_g \end{bmatrix} = \begin{bmatrix} \bar{Y}_{11} & \bar{Y}_{12} & \bar{Y}_{13} & \bar{Y}_{14} & \bar{Y}_{15} \\ \bar{Y}_{21} & \bar{Y}_{22} & \bar{Y}_{23} & \bar{Y}_{24} & \bar{Y}_{25} \\ \bar{Y}_{31} & \bar{Y}_{32} & \bar{Y}_{33} & \bar{Y}_{34} & \bar{Y}_{35} \\ \bar{Y}_{41} & \bar{Y}_{42} & \bar{Y}_{43} & \bar{Y}_{44} & \bar{Y}_{45} \\ \bar{Y}_{51} & \bar{Y}_{52} & \bar{Y}_{53} & \bar{Y}_{54} & \bar{Y}_{55} \end{bmatrix} \begin{bmatrix} \bar{V}_1 \\ \bar{V}_2 \\ \bar{V}_3 \\ \bar{V}_4 \\ \bar{V}_g \end{bmatrix} \quad (13)$$

where,

$$\bar{I}_g = [\bar{I}_{g1} \quad \bar{I}_{g2} \quad \dots \quad \bar{I}_{gn}]^T$$

$$\bar{V}_g = [\bar{V}_{g1} \quad \bar{V}_{g2} \quad \dots \quad \bar{V}_{gn}]^T$$

With the installation of IPFC between the branches 4-2 and 4-3, the network equations are modified as follows:

$$\bar{I}_{14} = \bar{I}_1 + \bar{I}_2$$

$$\bar{Y}'_{11} \bar{V}_1 + \bar{I}_{14} + \bar{Y}_{15} \bar{V}_g = 0$$

$$\bar{Y}'_{22} \bar{V}_2 - \bar{I}_1 + \bar{Y}_{25} \bar{V}_g = 0$$

$$\bar{Y}'_{33} \bar{V}_3 - \bar{I}_2 + \bar{Y}_{35} \bar{V}_g = 0$$

$$\bar{Y}_{51} \bar{V}_1 + \bar{Y}_{52} \bar{V}_2 + \bar{Y}_{53} \bar{V}_3 + \bar{Y}_{55} \bar{V}_g = \bar{I}_g \quad (14)$$

where,  $\bar{Y}'_{11} = \bar{Y}_{11} - y_{14}$ ,  $\bar{Y}'_{22} = \bar{Y}_{22} - y_{24}$ ,  $\bar{Y}'_{33} = \bar{Y}_{33} - y_{34}$

From Fig. 3 we have,

$$\bar{V}_1 = jx_{14} \bar{I}_{14} + \bar{V}_4$$

$$\begin{aligned}\bar{V}_4 &= jx_{L1}\bar{I}_1 + \bar{V}_{se1} + \bar{V}_2 \\ &= jx_{L2}\bar{I}_2 + \bar{V}_{se2} + \bar{V}_3\end{aligned}\quad (15)$$

where,  $\bar{V}_{se1} = jxt_1\bar{I}_1 + \bar{V}_{se1}$ ,  $\bar{V}_{se2} = jxt_2\bar{I}_2 + \bar{V}_{se2}$

Substituting (1) in (15) and solving for currents we obtain,

$$\begin{aligned}\bar{I}_1 &= \frac{1}{x_\Sigma} [-j(x_{L2} + x_{t2})\bar{V}_1 + j(x_{14} + x_{L2} + x_{t2})\bar{V}_2 \\ &\quad - jx_{14}\bar{V}_3 + j(x_{14} + x_{L2} + x_{t2})\bar{V}_{se1} - jx_{14}\bar{V}_{se2}]\end{aligned}\quad (16)$$

$$\begin{aligned}\bar{I}_2 &= \frac{1}{x_\Sigma} [-j(x_{L1} + x_{t1})\bar{V}_1 - jx_{14}\bar{V}_2 + j(x_{14} + x_{L1} \\ &\quad + x_{t1})\bar{V}_3 - jx_{14}\bar{V}_{se1} + j(x_{14} + x_{L1} + x_{t1})\bar{V}_{se2}]\end{aligned}\quad (17)$$

where,  $x_\Sigma = x_{14}(x_{L2} + x_{t2}) + (x_{L1} + x_{t1})(x_{14} + x_{L2} + x_{t2})$   
Substituting (16-17) in (14) and deleting nodes 1-4 we obtain,

$$\bar{\mathbf{I}}_g = \bar{\mathbf{Y}}_g \bar{\mathbf{V}}_g + \bar{\mathbf{Y}}_{se1} \bar{\mathbf{V}}_{se1} + \bar{\mathbf{Y}}_{se2} \bar{\mathbf{V}}_{se2}\quad (18)$$

where,

$$\begin{aligned}\bar{\mathbf{Y}}_g &= \bar{\mathbf{Y}}_{55} - [\bar{\mathbf{Y}}_{51} \quad \bar{\mathbf{Y}}_{52} \quad \bar{\mathbf{Y}}_{53}] \mathbf{Y}'_t^{-1} \begin{bmatrix} \bar{\mathbf{Y}}_{15} \\ \bar{\mathbf{Y}}_{25} \\ \bar{\mathbf{Y}}_{35} \end{bmatrix} \\ \bar{\mathbf{Y}}_{se1} &= -[\bar{\mathbf{Y}}_{51} \quad \bar{\mathbf{Y}}_{52} \quad \bar{\mathbf{Y}}_{53}] \mathbf{Y}'_t^{-1} \begin{bmatrix} j(x_{L2} + x_{t2})/x_\Sigma \\ -j(x_{L2} + x_{t2} + x_{14})/x_\Sigma \\ j(x_{14})/x_\Sigma \end{bmatrix} \\ \bar{\mathbf{Y}}_{se2} &= -[\bar{\mathbf{Y}}_{51} \quad \bar{\mathbf{Y}}_{52} \quad \bar{\mathbf{Y}}_{53}] \mathbf{Y}'_t^{-1} \begin{bmatrix} j(x_{L1} + x_{t1})/x_\Sigma \\ j(x_{14})/x_\Sigma \\ -j(x_{14} + x_{L1} + x_{t1})/x_\Sigma \end{bmatrix} \\ \mathbf{Y}'_t &= \begin{bmatrix} \bar{Y}'_{11} - & & \\ \frac{j(x_{L1} + x_{t1} + x_{L2} + x_{t2})}{x_\Sigma} & \frac{j(x_{L2} + x_{t2})}{x_\Sigma} & \frac{j(x_{L1} + x_{t1})}{x_\Sigma} \\ \frac{j(x_{L2} + x_{t2})}{x_\Sigma} & \frac{\bar{Y}'_{22} -}{x_\Sigma} & \frac{j(x_{14})}{x_\Sigma} \\ \frac{j(x_{L1} + x_{t1})}{x_\Sigma} & \frac{j(x_{14})}{x_\Sigma} & \frac{\bar{Y}'_{33} -}{x_\Sigma} \end{bmatrix}\end{aligned}$$

#### A. Nonlinear model of the multi-machine power system installed with IPFC

The nonlinear model of the multi-machine power system with IPFC, is developed as follows:

$$\dot{\boldsymbol{\delta}} = \boldsymbol{\omega}_0 \boldsymbol{\omega}$$

$$\dot{\boldsymbol{\omega}} = \mathbf{M}^{-1}(\mathbf{P}_m - \mathbf{P}_e - \mathbf{D}\boldsymbol{\Delta}\boldsymbol{\omega})$$

$$\dot{\mathbf{E}}'_q = \mathbf{T}'_{d0}{}^{-1}(-\mathbf{E}'_q - (\mathbf{X}_D - \mathbf{X}'_D)\mathbf{I}_D + \mathbf{E}_{fd})$$

$$\dot{\mathbf{E}}_{fd} = \mathbf{T}_A^{-1}(-\mathbf{E}_{fd} + \mathbf{K}_A(\mathbf{V}_{ref} - \mathbf{V}_T))\quad (19)$$

where,

$$\mathbf{P}_e = \mathbf{I}_Q \mathbf{V}_{TQ} + \mathbf{I}_D \mathbf{V}_{TD}, \quad \mathbf{V}_{TD} = \mathbf{X}_Q \mathbf{I}_Q,$$

$$\mathbf{V}_{TQ} = \dot{\mathbf{E}}'_q - \mathbf{X}'_D \mathbf{I}_D$$

$$\boldsymbol{\delta} = [\delta_1 \quad \delta_2 \quad \dots \quad \delta_n]^T, \quad \boldsymbol{\omega} = [\omega_1 \quad \omega_2 \quad \dots \quad \omega_n]^T,$$

$$\mathbf{E}'_q = [E'_{q1} \quad E'_{q2} \quad \dots \quad E'_{qn}]^T,$$

$$\mathbf{E}_{fd} = [E_{fd1} \quad E_{fd2} \quad \dots \quad E_{fdn}]^T,$$

$$\mathbf{I}_D = [I_{d1} \quad I_{d2} \quad \dots \quad I_{dn}]^T,$$

$$\mathbf{I}_Q = [I_{q1} \quad I_{q2} \quad \dots \quad I_{qn}]^T,$$

$$\mathbf{V}_{TD} = [V_{t1d} \quad V_{t2d} \quad \dots \quad V_{tnd}]^T,$$

$$\mathbf{V}_{TQ} = [V_{t1q} \quad V_{t2q} \quad \dots \quad V_{tnq}]^T, \quad V_{Ti} = \sqrt{V_{tid}^2 + V_{tiq}^2},$$

$$\mathbf{M} = \text{diag}(2H_i), \quad \mathbf{D} = \text{diag}(D_i), \quad \mathbf{T}'_{d0} = \text{diag}(T'_{d0i}),$$

$$\mathbf{X}_D = \text{diag}(x_{di}), \quad \mathbf{X}_Q = \text{diag}(x_{qi}), \quad \mathbf{X}'_D = \text{diag}(x'_{di})$$

and,  $i=1,2 \dots n$ ,  $n$  is the number of generators.

The terminal voltage of the generators for the  $n$  machine power system can also be expressed in the common coordinates as [15]:

$$\bar{\mathbf{V}}_g = \bar{\mathbf{E}}'_q - j\mathbf{X}'_D \bar{\mathbf{I}}_g - j(\mathbf{X}_Q - \mathbf{X}'_D) \bar{\mathbf{I}}_Q\quad (20)$$

Substituting (20) in (18) we get,

$$\bar{\mathbf{I}}_g = \bar{\mathbf{Y}}_d (\bar{\mathbf{E}}'_q - j(\mathbf{X}_Q - \mathbf{X}'_D) \bar{\mathbf{I}}_Q + \bar{\mathbf{Y}}_A \bar{\mathbf{V}}_{se1} + \bar{\mathbf{Y}}_B \bar{\mathbf{V}}_{se2})\quad (21)$$

where,

$$\bar{\mathbf{Y}}_d = [\bar{\mathbf{Y}}^{-1}_g + j\mathbf{X}'_D]^{-1}, \quad \bar{\mathbf{Y}}_A = \bar{\mathbf{Y}}^{-1}_g \bar{\mathbf{Y}}_{se1}, \quad \bar{\mathbf{Y}}_B = \bar{\mathbf{Y}}^{-1}_g \bar{\mathbf{Y}}_{se2}$$

In d-q axis form the generator currents (21) can be expressed as

$$\bar{I}_{Gi} = \bar{I}_{gi} e^{j\delta_i}$$

$$\begin{aligned}\bar{I}_{Gi} &= \sum_{j=1}^n \bar{Y}_{dij} [E'_{qj} e^{j(90^\circ + \delta_i - \delta_j)} + (x'_{qj} - x'_{dj}) \times \\ &\quad e^{j(\delta_i - \delta_j)} + \bar{Y}_{Aj} \bar{V}_{se1} e^{j(\delta_i)} + \bar{Y}_{Bj} \bar{V}_{se2} e^{j(\delta_i)}]\end{aligned}\quad (22)$$

Denoting

$$\bar{Y}_{dij} = Y_{dij} e^{j(\beta_{dij})}, \quad \bar{Y}_{Aj} = Y_{Aj} e^{j(\beta_{Aj})},$$

$$\bar{Y}_{Bj} = Y_{Bj} e^{j(\beta_{Bj})}$$

$$I_{di} = \text{real}(\bar{I}_{Gi}), I_{qi} = \text{imag}(\bar{I}_{Gi})$$

$$\begin{aligned} \delta_{dij} &= \delta_i - \delta_j + \beta_{dij}, \\ \delta_{Aij} &= \delta_i + \beta_{dij} + \beta_{Aj} + \theta_1, \\ \delta_{Bij} &= \delta_i + \beta_{dij} + \beta_{Bj} + \theta_2 \end{aligned}$$

$$\bar{I}_{di} = \sum_{j=1}^n Y_{dij} \left[ -E'_{qj} \sin \delta_{dij} + (x_{qj} - x'_{dj}) \cos \delta_{dij} I_{qj} + Y_{Aj} V_{se1} \cos \delta_{Aij} + Y_{Bj} V_{se2} \cos \delta_{Bij} \right] \quad (23)$$

$$\bar{I}_{qi} = \sum_{j=1}^n Y_{dij} \left[ E'_{qj} \cos \delta_{dij} + (x_{qj} - x'_{dj}) \sin \delta_{dij} I_{qj} + Y_{Aj} V_{se1} \sin \delta_{Aij} + Y_{Bj} V_{se2} \sin \delta_{Bij} \right] \quad (24)$$

### B. Linearised Model of an Multi-machine Power System including IPFC in State Space form

The linear dynamic model of the multi-machine power system with IPFC is obtained by linearizing the non-linear equations (2, 19, 23, and 24) around an operating point of the power system. The modified Phillips Heffron model of the multi-machine power system installed with IPFC along with the capacitor dynamics in state space form is as follows:

$$\begin{bmatrix} \Delta \dot{\delta} \\ \Delta \dot{\omega} \\ \Delta \dot{E}'_q \\ \Delta \dot{E}_{fd} \\ \Delta \dot{V}_{dc} \end{bmatrix} = \begin{bmatrix} \mathbf{0} & \omega_o \mathbf{I} \\ -\mathbf{M}^{-1} \mathbf{K}_1 & -\mathbf{M}^{-1} \mathbf{D} \\ -\mathbf{T}'_{do}{}^{-1} \mathbf{K}_4 & \mathbf{0} \\ -\mathbf{T}'_a{}^{-1} \mathbf{K}_a \mathbf{K}_5 & \mathbf{0} \\ \mathbf{K}_7 & \mathbf{0} \end{bmatrix} \begin{bmatrix} \Delta \delta \\ \Delta \omega \\ \Delta E'_q \\ \Delta E_{fd} \\ \Delta V_{dc} \end{bmatrix} + \begin{bmatrix} \mathbf{0} & \mathbf{0} & \mathbf{0} \\ -\mathbf{M}^{-1} \mathbf{K}_2 & \mathbf{0} & -\mathbf{M}^{-1} \mathbf{K}_{pv} \\ -\mathbf{T}'_{do}{}^{-1} \mathbf{K}_3 & \mathbf{T}'_{do}{}^{-1} & -\mathbf{T}'_{do}{}^{-1} \mathbf{K}_{qv} \\ -\mathbf{T}'_a{}^{-1} \mathbf{K}_a \mathbf{K}_6 & -\mathbf{T}'_a{}^{-1} & -\mathbf{T}'_a{}^{-1} \mathbf{K}_a \mathbf{K}_{vv} \\ \mathbf{K}_8 & \mathbf{0} & -\mathbf{K}_9 \end{bmatrix} \begin{bmatrix} \Delta \delta \\ \Delta \omega \\ \Delta E'_q \\ \Delta E_{fd} \\ \Delta V_{dc} \end{bmatrix} + \begin{bmatrix} \mathbf{0} & \mathbf{0} \\ -\mathbf{M}^{-1} \mathbf{K}_{pm1} & -\mathbf{M}^{-1} \mathbf{K}_{p01} \\ -\mathbf{T}'_{do}{}^{-1} \mathbf{K}_{qm1} & -\mathbf{T}'_{do}{}^{-1} \mathbf{K}_{q01} \\ -\mathbf{T}'_a{}^{-1} \mathbf{K}_a \mathbf{K}_{vm1} & -\mathbf{T}'_a{}^{-1} \mathbf{K}_a \mathbf{K}_{v01} \\ \mathbf{K}_{cm1} & \mathbf{K}_{c01} \end{bmatrix} \begin{bmatrix} \Delta m_1 \\ \Delta \theta_1 \\ \Delta m_2 \\ \Delta \theta_2 \end{bmatrix} \quad (25)$$

Fig. 4 shows the block diagram of Phillips Heffron model of a multi-machine system including IPFC. In this model,  $\Delta \delta, \Delta \omega, \Delta E'_q, \Delta E_{fd}$  are  $n$  dimensional vectors,  $\mathbf{K}_1 - \mathbf{K}_6$  are  $n \times n$  matrices and

$$\begin{aligned} \mathbf{K}_p &= [\mathbf{K}_{pm1} \quad \mathbf{K}_{p00} \quad \mathbf{K}_{pm2} \quad \mathbf{K}_{p00}] \\ \mathbf{K}_q &= [\mathbf{K}_{qm1} \quad \mathbf{K}_{q00} \quad \mathbf{K}_{qm2} \quad \mathbf{K}_{q00}] \\ \mathbf{K}_v &= [\mathbf{K}_{vm1} \quad \mathbf{K}_{v00} \quad \mathbf{K}_{vm2} \quad \mathbf{K}_{v00}] \\ \mathbf{K}_c &= [\mathbf{K}_{cm1} \quad \mathbf{K}_{c00} \quad \mathbf{K}_{cm2} \quad \mathbf{K}_{c00}] \end{aligned} \quad (26)$$

The elements of the above vectors are  $n$  dimensional column vectors. All the constants of the model are functions of the system parameters and operating condition.

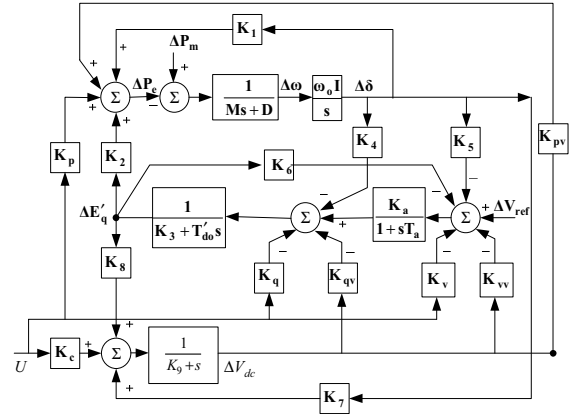


Figure 4. Modified Heffron-Phillips model of  $n$ -machine system with IPFC installed

## IV. SYSTEM INVESTIGATED

A three machine example power system [13] shown in Fig 5 is considered for MMPS analysis. An IPFC is installed into the two parallel transmission lines through the transformers between bus 3 and bus 1. The parameters of the system are given in the Appendix.

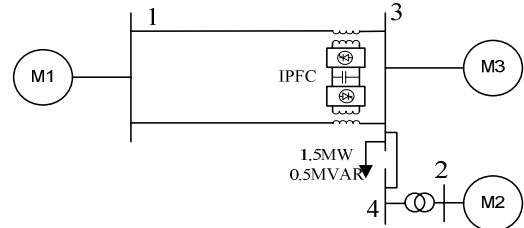


Figure 5. Three-machine, power system installed with IPFC

A generalized load flow program based on Newton technique with embedded IPFC [16] has been developed to obtain steady state operating point. For this initial condition the system equations are linearized and the constants of the system model are computed. The study focuses on the improvement in rotor angle oscillation damping. Table 1 shows the oscillation modes computed from the linearized system. The system has one inter area mode where all machines oscillate together, and one local area modes where machine 2 and 3 oscillate against each other which is determined using the participation factors [10].

TABLE I.  
OSCILLATION MODES

Multi-machine system	Local mode	Inter area mode
With no IPFC and no PSS	0.0146 - 6.7033i	-0.0020 + 3.9599i
Damping	0.0022	0.0005
Frequency	1.0669	0.6302
With PSS at machine 3	-0.6686 + 6.4833i	-0.0868 + 3.9289i
Damping	0.1026	0.0221
Frequency	1.0319	0.6253
IPFC along with PSS at machine 3	-0.6993 + 6.9322i	-0.1151 + 4.0879i
Damping	0.1004	0.0281
Frequency	1.1033	0.6506
IPFC installed with damping controller along with PSS at machine 3	-0.6996 + 6.9269i	-0.4912 + 4.1193i
Damping	0.1005	0.1184
Frequency	1.1024	0.6556

The oscillation modes have very low damping. PSS is installed at machine 3, which is designed based on the linearized system to increase the damping ratio to 0.1, using phase compensation technique. The PSS is able to sufficiently increase the damping of the modes as observed from the table. However the damping ratio of the inter area modes is still less. The IPFC is now installed in the power system. We observe that in the presence of the IPFC there is no significant change in the damping of the oscillation modes. The damping controller having a lead lag structure [9] is designed using phase compensation technique based on the Phillips Heffron model to increase the damping of the inter area mode. The IPFC based controller improves the damping of the inter area modes without effecting the local mode as shown in the Table 1.

## V. CONCLUSION

The mathematical modeling of the power system installed with IPFC is outlined in this paper. A dynamic model for both SMIB and multi-machine power system is developed. Further the procedure for formulation of the extended Phillips Heffron model of the power system installed with IPFC for these systems have been established. The model also includes the dc capacitor dynamics. The developed formulation is general and the models are applicable for small signal stability analysis. The application of the model for small signal stability analysis is using eigenvalue analysis is demonstrated for a three machine power system. The IPFC based controller, designed based on the linearized model of the power system, significantly improves the damping of the concerned oscillation modes.

## REFERENCES

[1] L.Gyugyi, K. K. Sen, C. D. Schauder, "The Interline Power FlowController Concept: A New Approach to Power Flow Management in Transmission Systems," *IEEE Transactions on Power Delivery*, vol. 14, No. 3, July 1999, pp. 1115 – 1123.

[2] N. G. Hingorami, L. Gyugyi, *Understanding FACTS: Concepts and Technology of Flexible AC Transmission system*, IEEE Press, 1999.

[3] X. Wei, J. H. Chow, B. Fardanesh, A. A. Edris, "A common modeling framework of voltage-sourced converters for loadflow,

sensitivity, and dispatch analysis," *Power Engineering Society General Meeting*, IEEE Vol. 4, July 2003, pp. 13-17.

[4] J. Zhang, A. Yokoyama, "A Comparison between the UPFC and the IPFC in Optimal Power Flow Control and Power Flow Regulation," *38th North American Power Symposium, NAPS 2006*, Sept. 2006, pp. 339–345.

[5] X. Wei, J. H. Chow, B. Fardanesh, A. A. Edris, "A dispatch strategy for an interline power flow controller operating at rated capacity," *Power Systems Conference and Exposition, IEEE PES*, 10-13 Oct. 2004, Vol.3, pp. 1459 - 1466.

[6] A. Kazemi, E. Karimi, "The Effect of Interline Power Flow Controller (IPFC) on Damping Inter-area Oscillations in the Interconnected Power Systems," *Industrial Electronics, 2006 IEEE International Symposium*, Volume 3, July 2006, pp. 1911-1915.

[7] A. M. Parimi, I. Elamvazuthi, N. Saad, "Damping of inter area oscillations using Interline Power Flow Controller based damping controllers," *IEEE 2<sup>nd</sup> International Power and Energy Conference*, 2008. 1-3 Dec. 2008, pp. 67 – 72.

[8] A. M. Parimi, I. Elamvazuthi, N. Saad, N, "Interline Power Flow Controller (IPFC) based damping controllers for damping low frequency oscillations in a power system," *IEEE International Conference on Sustainable Energy Technologies*, 24-27, Nov. 2008, pp. 334 – 339.

[9] A. M. Parimi, I. Elamvazuthi, N. Saad, "Interline Power Flow Controller Application for Low Frequency Oscillations Damping" *WSEAS Transactions on Systems*, Issue 5, Vol. 9, May 2010.

[10] P. Kundur, *Power System Stability and Control*. Mc Graw-Hill, New York, 1994.

[11] H. F. Wang, F. J. Swift, and M. Li, "An unified model for the analysis of FACTS devices in damping power system oscillations Part I: Single-machine Infinite-bus power systems," *IEEE Trans. on Power Delivery*, Vol. 12, No. 2, April 1997.

[12] H. F. Wang, F. J. Swift, and M. Li, "An unified model for the analysis of FACTS devices in damping power system oscillations Part II: Multimachine power systems," *IEEE Trans. on Power Delivery*, Vol. 13, No. 4, October 1998.

[13] H. F. Wang, "An unified model for the analysis of FACTS devices in damping power system oscillations Part III: Unified Power Flow Controller," *IEEE Trans. on Power Delivery*, Vol. 15, No. 3, July 2000.

[14] H. F. Wang, "Applications of modeling UPFC into multi-machine power systems," *IEE proc. – C*, Vol. 146, NO. 3, pp.306-312, May 1999.

[15] Y. N. Yu, *Electric Power System Dynamics*, Academic Press. Inc, London, 1983.

[16] X. P. Zhang, "Modelling of the interline power flow controller and the generalised unified power flow controller in Newton power flow", *Generation, Transmission and Distribution, IEE Proceedings-Volume 150*, Issue 3, May 2003 pp. 268 – 274.

## APPENDIX

Parameters of the three machine power system (in p.u except where indicated) .

Generator:  $H_1 = 20.09s$ ,  $H_2 = 20.09s$ ,  $H_3 = 11.8s$

$D_1 = D_2 = D_3 = 0$ ,

$T'_{d01} = 7.5s$ ,  $T'_{d02} = 7.5s$ ,  $T'_{d03} = 4.7s$ ,

$x_{d1} = 0.19$ ,  $x_{d2} = 0.19$ ,  $x_{d3} = 0.41$ ,

$x_{q1} = 0.163$ ,  $x_{q2} = 0.163$ ,  $x_{q3} = 0.33$ ,

$x'_{d1} = 0.0765$ ,  $x'_{d2} = 0.0765$ ,  $x'_{d3} = 0.173$

Exciter :  $K_{a1} = K_{a3} = 20$ ,  $K_{a2} = 100$ ,

$T_{a1} = T_{a3} = 0.05s$ ,  $T_{a2} = 0.01s$

Transmission lines:  $Z_{13} = j1.2$  for each line,

$Z_{24} = j0.03$ ,  $Z_{34} = j0.03$

# Transient Stability Enhancement and Power Flow Control in a Multi-Machine Power System Using Interline Power Flow Controller

Alivelu. M. Parimi, Nirod. C. Sahoo, Irraivan Elamvazuthi, and Nordin Saad  
 Department of Electrical and Electronic Engineering  
 Universiti Teknologi PETRONAS  
 Tronoh 31750, Perak, Malaysia

**Abstract**—In this paper, the nonlinear dynamic model of a typical multi-machine power system incorporated with Interline Power Flow Controller (IPFC) has been developed. The oscillation modes with low damping ratio are identified from the eigenvalue analysis of the linearized Phillips-Heffron model. A power oscillation damping controller has been designed for the IPFC using phase compensation technique to enhance the transient stability of the system. Additional power flow controllers have also been incorporated into the system, to control the power flow demand in the transmission lines on which the IPFC is connected. The performance of the designed IPFC controllers has been assessed by simulation studies on a multi-machine system for power flow demand control as well as overall power system damping.

**Keywords**—IPFC; multi-machine power system; Phillips-Heffron model; damping control.

## I. INTRODUCTION

The Interline Power Flow Controller (IPFC) is a converter-based FACTS Controller, representing the new generation of transmission controllers. It employs self commutated, voltage-sourced converters (VSC). An IPFC can consist of a number of VSCs linked together at their common dc terminals. Each VSC injects a controllable ac voltage to its respective transmission line for series compensation [1, 2]. The dc link facilitates real power flow among the transmission lines enabling real power transfer from overloaded to under-loaded lines. The IPFC provides simultaneous compensation for multiple transmission lines by real and reactive power flow control in the lines. It also provides voltage control, improves transient stability, and enhances oscillation damping. Recently, modelling of IPFC and its various control functions have undergone rigorous research. In [3-5], the steady state model of IPFC with the power system is developed for load flow studies and power flow control. Control strategies with the help of supplementary PI (proportional-integral) controller or lead-lag controller for damping enhancement are suggested in [6-9]. These controllers were designed based on linear models of single machine infinite bus (SMIB) power system installed with IPFC. However, studies on modeling of IPFC in a multi-machine power system [10] for stability analysis are very limited. The stability analysis based on eigenvalue

technique is suitable for planning and operation of the power systems, to examine the problems associated with oscillations and to mitigate the power system oscillations using various control methods [11]. The Phillips-Heffron model of power system with the FACTS (Flexible AC Transmission System) device is suitable for understanding of system damping for small perturbation stability.

In this paper, the nonlinear dynamic model of a multi-machine power system installed with an IPFC is developed. Further, the linearized Phillips-Heffron model is modified to include IPFC; this model is of similar structure as that of the unified Phillips-Heffron model presented in [12-15]. This Phillips-Heffron model is utilized for investigating small signal stability analysis by identifying the oscillation modes with low damping ratio. Based on this analysis and the linearized model, an oscillation damping controller has been designed for the IPFC using phase compensation technique. This supplementary controller is added to the standard power flow demand controllers used for the IPFC. The efficacy of the overall control architecture has been evaluated by eigenvalue analysis as well as computer simulation experiments.

The paper is organized as follows. Section 2 presents the development of nonlinear and linearized models of a typical multi-machine power system incorporated with an IPFC. In Section 3, the details of damping controller and power flow controllers are provided. The simulation results and analysis are presented in Section 4. Section 5 concludes the paper.

## II. MULTI-MACHINE POWER SYSTEM WITH IPFC

A typical installation of IPFC in a multi-machine system is shown in Fig. 1. It is assumed that an IPFC is installed on the branches  $i-j$  and  $i-k$ . The network admittance  $\bar{Y}_i$  is formed before the IPFC has been installed, keeping  $n$  generator nodes along with the nodes  $i, j$  and  $k$ . The network equation is given by:

$$\begin{bmatrix} 0 \\ 0 \\ 0 \\ \bar{\mathbf{I}}_G \end{bmatrix} = \begin{bmatrix} \bar{Y}_{ii} & \bar{Y}_{ij} & \bar{Y}_{ik} & \bar{\mathbf{Y}}_{iG} \\ \bar{Y}_{ji} & \bar{Y}_{jj} & \bar{Y}_{jk} & \bar{\mathbf{Y}}_{jG} \\ \bar{Y}_{ki} & \bar{Y}_{kj} & \bar{Y}_{kk} & \bar{\mathbf{Y}}_{kG} \\ \bar{\mathbf{Y}}_{Gi} & \bar{\mathbf{Y}}_{Gj} & \bar{\mathbf{Y}}_{Gk} & \bar{\mathbf{Y}}_{GG} \end{bmatrix} \begin{bmatrix} \bar{V}_i \\ \bar{V}_j \\ \bar{V}_k \\ \bar{\mathbf{V}}_G \end{bmatrix} \quad (1)$$

where,  $\bar{\mathbf{I}}_{\mathbf{G}} = [\bar{I}_{g1}, \dots, \bar{I}_{gn}]^T$  and  $\bar{\mathbf{V}}_{\mathbf{G}} = [\bar{V}_{g1}, \dots, \bar{V}_{gn}]^T$ .

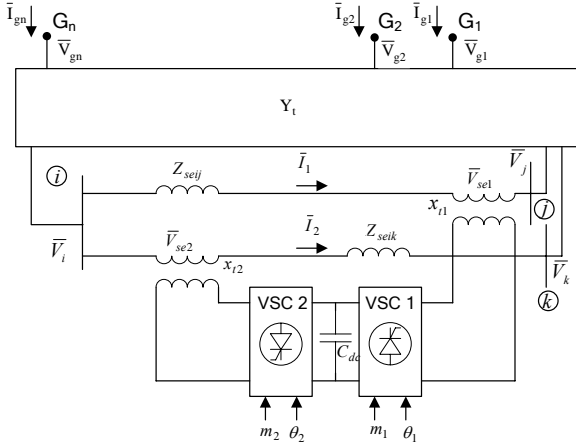


Figure 1. An n-machine power system installed with an IPFC

With the installation of IPFC between the branches  $i-j$  and  $i-k$ , the network equations are modified as:

$$\bar{Y}'_{ii} \bar{V}_i + \bar{I}_1 + \bar{I}_2 + \bar{\mathbf{Y}}_{i\mathbf{G}} \bar{\mathbf{V}}_{\mathbf{G}} = 0 \quad (2)$$

$$\bar{Y}'_{jj} \bar{V}_j - \bar{I}_1 + \bar{Y}'_{jk} \bar{V}_k + \bar{\mathbf{Y}}_{j\mathbf{G}} \bar{\mathbf{V}}_{\mathbf{G}} = 0 \quad (3)$$

$$\bar{Y}'_{kj} \bar{V}_j + \bar{Y}'_{kk} \bar{V}_k - \bar{I}_2 + \bar{\mathbf{Y}}_{k\mathbf{G}} \bar{\mathbf{V}}_{\mathbf{G}} = 0 \quad (4)$$

$$\bar{\mathbf{Y}}_{\mathbf{G}i} \bar{V}_i + \bar{\mathbf{Y}}_{\mathbf{G}j} \bar{V}_j + \bar{\mathbf{Y}}_{\mathbf{G}k} \bar{V}_k + \bar{\mathbf{Y}}_{\mathbf{G}\mathbf{G}} \bar{\mathbf{V}}_{\mathbf{G}} = \bar{\mathbf{I}}_{\mathbf{G}} \quad (5)$$

where  $\bar{Y}'_{ii} = \bar{Y}_{ii} - y_{ij} - y_{ik}$ ,  $\bar{Y}'_{jj} = \bar{Y}_{jj} - y_{ji}$  and  $\bar{Y}'_{kk} = \bar{Y}_{kk} - y_{ki}$ . From Fig. 1, the currents in the IPFC branches can be written as:

$$\bar{I}_1 = \bar{V}_i - \bar{V}_{se1} - \bar{V}_j / \bar{Z}_{seij} \quad (6)$$

$$\bar{I}_2 = \bar{V}_i - \bar{V}_{se2} - \bar{V}_k / \bar{Z}_{seik} \quad (7)$$

Substituting the currents (6) and (7), into (2-4) the IPFC buses voltages  $\bar{V}_i, \bar{V}_j, \bar{V}_k$ , can be written in matrix form as follows:

$$\begin{bmatrix} \bar{V}_i \\ \bar{V}_j \\ \bar{V}_k \end{bmatrix} = -\bar{Y}_t^{-1} \begin{bmatrix} -1/\bar{Z}_{seij} & -1/\bar{Z}_{seik} \\ -1/\bar{Z}_{seij} & 0 \\ 0 & -1/\bar{Z}_{seik} \end{bmatrix} \begin{bmatrix} \bar{V}_{se1} \\ \bar{V}_{se2} \end{bmatrix} + \begin{bmatrix} \bar{Y}_{i\mathbf{G}} \\ \bar{Y}_{j\mathbf{G}} \\ \bar{Y}_{k\mathbf{G}} \end{bmatrix} \bar{\mathbf{V}}_{\mathbf{G}} \quad (8)$$

where,

$$\bar{Y}_t = \begin{bmatrix} \bar{Y}'_{ii} + 1/\bar{Z}_{seij} + 1/\bar{Z}_{seik} & -1/\bar{Z}_{seij} & -1/\bar{Z}_{seik} \\ -1/\bar{Z}_{seij} & \bar{Y}'_{jj} + 1/\bar{Z}_{seij} & \bar{Y}'_{jk} \\ -1/\bar{Z}_{seik} & \bar{Y}'_{jk} & \bar{Y}'_{kk} + 1/\bar{Z}_{seik} \end{bmatrix}$$

Substituting the voltages  $\bar{V}_i, \bar{V}_j, \bar{V}_k$ , from (8) into (5) and eliminating them the generator currents can be written as the follows:

$$\bar{\mathbf{I}}_{\mathbf{G}} = \bar{\mathbf{Y}}_{\mathbf{G}} \bar{\mathbf{V}}_{\mathbf{G}} + \bar{\mathbf{Y}}_{se1} \bar{V}_{se1} + \bar{\mathbf{Y}}_{se2} \bar{V}_{se2} \quad (9)$$

where,

$$\bar{\mathbf{Y}}_{\mathbf{G}} = \bar{\mathbf{Y}}_{\mathbf{G}\mathbf{G}} - \begin{bmatrix} \bar{\mathbf{Y}}_{\mathbf{G}i} & \bar{\mathbf{Y}}_{\mathbf{G}j} & \bar{\mathbf{Y}}_{\mathbf{G}k} \end{bmatrix} \mathbf{Y}_t^{-1} \begin{bmatrix} \bar{\mathbf{Y}}_{i\mathbf{G}} \\ \bar{\mathbf{Y}}_{j\mathbf{G}} \\ \bar{\mathbf{Y}}_{k\mathbf{G}} \end{bmatrix}$$

$$\bar{\mathbf{Y}}_{se1} = -\begin{bmatrix} \bar{\mathbf{Y}}_{\mathbf{G}i} & \bar{\mathbf{Y}}_{\mathbf{G}j} & \bar{\mathbf{Y}}_{\mathbf{G}k} \end{bmatrix} \mathbf{Y}_t^{-1} \begin{bmatrix} 1/\bar{Z}_{seij} \\ -1/\bar{Z}_{seij} \\ 0 \end{bmatrix}$$

$$\bar{\mathbf{Y}}_{se2} = -\begin{bmatrix} \bar{\mathbf{Y}}_{\mathbf{G}i} & \bar{\mathbf{Y}}_{\mathbf{G}j} & \bar{\mathbf{Y}}_{\mathbf{G}k} \end{bmatrix} \mathbf{Y}_t^{-1} \begin{bmatrix} 1/\bar{Z}_{seik} \\ 0 \\ -1/\bar{Z}_{seik} \end{bmatrix}$$

#### A. Nonlinear model of the multi-machine power system installed with IPFC

The nonlinear dynamic model of the multi-machine power system with IPFC is developed as follows:

$$\dot{\boldsymbol{\delta}} = \boldsymbol{\omega}_o (\boldsymbol{\omega} - \mathbf{1}) \quad (10)$$

$$\dot{\boldsymbol{\omega}} = \mathbf{M}^{-1} (\mathbf{P}_m - \mathbf{P}_e - \mathbf{D}\boldsymbol{\omega}) \quad (11)$$

$$\dot{\mathbf{E}}'_q = \mathbf{T}'_{d0}{}^{-1} (-\mathbf{E}'_q - (\mathbf{X}_D - \mathbf{X}'_D) \mathbf{I}_D + \mathbf{E}_{fd}) \quad (12)$$

$$\dot{\mathbf{E}}_{fd} = \mathbf{T}_A^{-1} (-\mathbf{E}_{fd} + \mathbf{K}_A (\mathbf{V}_{ref} - \mathbf{V}_T)) \quad (13)$$

$$\dot{V}_{dc} = \frac{3m_1}{4C_{dc}} (i_{1d} \cos \theta_1 + i_{1q} \sin \theta_1) + \frac{3m_2}{4C_{dc}} (i_{2d} \cos \theta_2 + i_{2q} \sin \theta_2) \quad (14)$$

where  $\mathbf{P}_e = \mathbf{I}_Q \mathbf{V}_{TQ} + \mathbf{I}_D \mathbf{V}_{TD}$ ,  $\mathbf{V}_{TD} = \mathbf{X}_Q \mathbf{I}_Q$ ,

$$\mathbf{V}_{TQ} = \dot{\mathbf{E}}'_q - \mathbf{X}'_D \mathbf{I}_D, \boldsymbol{\delta} = [\delta_1 \dots \delta_n]^T,$$

$$\boldsymbol{\omega} = [\omega_1 \dots \omega_n]^T, \mathbf{E}'_q = [E'_{q1} \dots E'_{qn}]^T,$$

$$\mathbf{E}_{fd} = [E_{fd1} \dots E_{fdn}]^T, \mathbf{I}_D = [I_{d1} \dots I_{dn}]^T,$$

$$\mathbf{I}_Q = [I_{q1} \dots I_{qn}]^T, \mathbf{V}_{TD} = [V_{td1} \dots V_{tdn}]^T,$$

$$\mathbf{V}_{TQ} = [V_{tq1} \dots V_{tqn}]^T, V_{Ti} = \sqrt{V_{uid}^2 + V_{uq}^2},$$

$$\mathbf{M} = \text{diag}(2H_i), \mathbf{D} = \text{diag}(D_i), \mathbf{T}'_{d0} = \text{diag}(T'_{d0i}),$$

$$\mathbf{X}_D = \text{diag}(x_{di}), \mathbf{X}_Q = \text{diag}(x_{qi}), \mathbf{X}'_D = \text{diag}(x'_{di})$$

and,  $i=1,2,\dots,n$ ,  $n$  is the number of generators.

The terminal voltage of the generators for the  $n$ - machine power system in the common coordinates is [16]:

$$\bar{\mathbf{V}}_g = \mathbf{e}^{j(\pi/2 - \delta)} \bar{\mathbf{E}}'_q - j\mathbf{X}'_D \bar{\mathbf{I}}_{\mathbf{G}} - j(\mathbf{X}_Q - \mathbf{X}'_D) \mathbf{e}^{-j\delta} \bar{\mathbf{I}}_{\mathbf{G}} \quad (15)$$

$$\bar{\mathbf{I}}_g = \bar{\mathbf{Y}}_d (\bar{\mathbf{E}}'_q - j(\mathbf{X}_Q - \mathbf{X}'_D) \bar{\mathbf{I}}_{\mathbf{G}} + \bar{\mathbf{Y}}_A \bar{V}_{se1} + \bar{\mathbf{Y}}_B \bar{V}_{se2}) \quad (16)$$

where,  $\bar{\mathbf{Y}}_d = [\bar{\mathbf{Y}}^{-1}_g + j\mathbf{X}'_D]^{-1}$ ,  $\bar{\mathbf{Y}}_A = \bar{\mathbf{Y}}^{-1}_g \bar{\mathbf{Y}}_{se1}$ , and

$\bar{\mathbf{Y}}_B = \bar{\mathbf{Y}}^{-1} \mathbf{g} \bar{\mathbf{Y}}_{se2}$ . In d-q axis form, the generator currents are:

$$\bar{I}_{Gi} = \bar{I}_{gi} e^{j\delta_i} \quad (17)$$

$$\bar{I}_{Gi} = \sum_{j=1}^n \bar{Y}_{di j} \left[ E'_{qj} e^{j(90^\circ + \delta_i - \delta_j)} + (x_{qj} - x'_{dj}) \times \dots \right. \\ \left. e^{j(\delta_i - \delta_j)} + \bar{Y}_{Aj} \bar{V}_{se1} e^{j(\delta_i)} + \bar{Y}_{Bj} \bar{V}_{se2} e^{j(\delta_i)} \right] \quad (18)$$

Denoting  $\bar{Y}_{di j} = Y_{di j} e^{j(\beta_{dij})}$ ,  $\bar{Y}_{Aj} = Y_{Aj} e^{j(\beta_{Aj})}$ ,

$$\bar{Y}_{Bj} = Y_{Bj} e^{j(\beta_{Bj})}, I_{di} = \text{real}(\bar{I}_{Gi}), I_{qi} = \text{imag}(\bar{I}_{Gi})$$

$$\delta_{dij} = \delta_i - \delta_j + \beta_{dij}, \quad \delta_{Aij} = \delta_i + \beta_{dij} + \beta_{Aj} + \theta_1, \\ \delta_{Bij} = \delta_i + \beta_{dij} + \beta_{Bj} + \theta_2,$$

$$\bar{I}_{di} = \sum_{j=1}^n Y_{di j} \left[ -E'_{qj} \sin \delta_{dij} + (x_{qj} - x'_{dj}) \cos \delta_{dij} I_{qj} \right. \\ \left. + Y_{Aj} V_{se1} \cos \delta_{Aij} + Y_{Bj} V_{se2} \cos \delta_{Bij} \right] \quad (19)$$

$$\bar{I}_{qi} = \sum_{j=1}^n Y_{di j} \left[ E'_{qj} \cos \delta_{dij} + (x_{qj} - x'_{dj}) \sin \delta_{dij} I_{qj} \right. \\ \left. + Y_{Aj} V_{se1} \sin \delta_{Aij} + Y_{Bj} V_{se2} \sin \delta_{Bij} \right] \quad (20)$$

### B. Linearised Model of an Multi-machine Power System including IPFC in State Space form

The linear dynamic model of the multi-machine power system with IPFC is obtained by linearizing the non-linear equations around a steady state operating point of the power system. The modified Phillips Heffron model of the multi-machine power system installed with IPFC along the capacitor dynamics in state space form is as follows:

$$\begin{bmatrix} \Delta \dot{\delta} \\ \Delta \dot{\omega} \\ \Delta \dot{\mathbf{E}}'_q \\ \Delta \dot{\mathbf{E}}'_{fd} \\ \Delta \dot{V}_{dc} \end{bmatrix} = \begin{bmatrix} \mathbf{0} & \omega_0 \mathbf{I} \\ -\mathbf{M}^{-1} \mathbf{K}_1 & -\mathbf{M}^{-1} \mathbf{D} \\ -\mathbf{T}'_{do}{}^{-1} \mathbf{K}_4 & \mathbf{0} \\ -\mathbf{T}'_a{}^{-1} \mathbf{K}_a \mathbf{K}_5 & \mathbf{0} \\ \mathbf{K}_7 & \mathbf{0} \end{bmatrix} \begin{bmatrix} \Delta \delta \\ \Delta \omega \\ \Delta \mathbf{E}'_q \\ \Delta \mathbf{E}'_{fd} \\ \Delta V_{dc} \end{bmatrix} \\ + \begin{bmatrix} \mathbf{0} & \mathbf{0} & \mathbf{0} \\ -\mathbf{M}^{-1} \mathbf{K}_2 & \mathbf{0} & -\mathbf{M}^{-1} \mathbf{K}_{pv} \\ -\mathbf{T}'_{do}{}^{-1} \mathbf{K}_3 & \mathbf{T}'_{do}{}^{-1} & -\mathbf{T}'_{do}{}^{-1} \mathbf{K}_{qv} \\ -\mathbf{T}'_a{}^{-1} \mathbf{K}_a \mathbf{K}_6 & -\mathbf{T}'_a{}^{-1} & -\mathbf{T}'_a{}^{-1} \mathbf{K}_a \mathbf{K}_{vv} \\ \mathbf{K}_8 & \mathbf{0} & -\mathbf{K}_9 \end{bmatrix} \begin{bmatrix} \Delta \delta \\ \Delta \omega \\ \Delta \mathbf{E}'_q \\ \Delta \mathbf{E}'_{fd} \\ \Delta V_{dc} \end{bmatrix} \\ + \begin{bmatrix} \mathbf{0} & \mathbf{0} \\ -\mathbf{M}^{-1} \mathbf{K}_{pm1} & -\mathbf{M}^{-1} \mathbf{K}_{p\theta1} \\ -\mathbf{T}'_{do}{}^{-1} \mathbf{K}_{qm1} & -\mathbf{T}'_{do}{}^{-1} \mathbf{K}_{q\theta1} \\ -\mathbf{T}'_a{}^{-1} \mathbf{K}_a \mathbf{K}_{vm1} & -\mathbf{T}'_a{}^{-1} \mathbf{K}_a \mathbf{K}_{v\theta1} \\ \mathbf{K}_{cm1} & \mathbf{K}_{c\theta1} \end{bmatrix} \begin{bmatrix} \Delta m_1 \\ \Delta \theta_1 \\ \Delta m_2 \\ \Delta \theta_2 \end{bmatrix}$$

$$\begin{bmatrix} \mathbf{0} & \mathbf{0} \\ -\mathbf{M}^{-1} \mathbf{K}_{pm2} & -\mathbf{M}^{-1} \mathbf{K}_{p\theta2} \\ -\mathbf{T}'_{do}{}^{-1} \mathbf{K}_{qm2} & -\mathbf{T}'_{do}{}^{-1} \mathbf{K}_{q\theta2} \\ -\mathbf{T}'_a{}^{-1} \mathbf{K}_a \mathbf{K}_{vm2} & -\mathbf{T}'_a{}^{-1} \mathbf{K}_a \mathbf{K}_{v\theta2} \\ \mathbf{K}_{cm2} & \mathbf{K}_{c\theta2} \end{bmatrix} \begin{bmatrix} \Delta m_1 \\ \Delta \theta_1 \\ \Delta m_2 \\ \Delta \theta_2 \end{bmatrix} \quad (21)$$

In this model,  $\Delta \delta, \Delta \omega, \Delta \mathbf{E}'_q, \Delta \mathbf{E}'_{fd}$  are  $n$ -dimensional vectors,  $\mathbf{K}_1 - \mathbf{K}_6$  are  $n \times n$  matrices. The other vector elements are  $n$ -dimensional column vectors. All the constants of the model are functions of the system parameters and operating condition.

## III. CONTROLLERS FOR IPFC

The IPFC is installed with three separate controllers. They are: (1) Power flow controller, (ii) DC voltage regulator, and (iii) Power Oscillation Damping controller.

### A. Power Flow Controller

The power flow controller regulates the power in the transmission lines. The structure of the PI-type power flow controller is shown in Fig. 2.

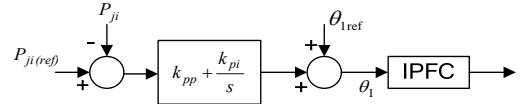


Figure 2. Power flow controller

The controller regulates real power in the transmission line 1 to the specified value of  $P_{ji(ref)}$  in the system. The real power can be controlled by varying the phase angle  $\theta_1$  of the series injected voltage of VSC 1. Generally the input signal  $m_1$  can also be used to regulate the active power of the transmission line, however, the range in which  $m_1$  ( $0 \leq m_1 \leq 1$ ) can be regulated is narrower than that of  $\theta_1$  ( $0 \leq \theta_1 \leq 360^\circ$ ). Modulating the input signal  $\theta_1$ , the currents in both the transmission lines are controlled, as they are function of  $\theta_1$ . Thus, the active and reactive powers in both the lines are modulated. Similar to the structure of Fig. 2, two more power flow controllers are also placed in the system to the control the reactive power in line 1 and real power in line 2.

### B. DC Voltage Regulator

The DC voltage regulator functions by controlling the exchange of active power between the two VSCs and the power system. It has to ensure that the net exchange of real power is zero. This is achieved by maintaining constant voltage across the capacitor. The DC voltage regulator is of PI type as shown in Fig. 3.

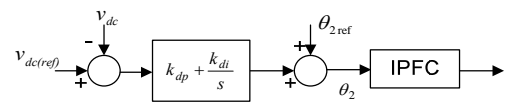


Figure 3. DC voltage regulator

As this regulator is responsible for converting the same amount of real power to replace the power drained by the

VSC-1 through the DC link, the regulator is used to modulate the input signal  $\theta_2$ , the phase angle of the injected voltage of VSC 2. In the Fig. 3  $v_{dc(ref)}$  is the reference voltage. Since the currents flowing in the transmission lines are function of  $\theta_2$ , this controller make sure the net active power exchanged is zero.

### C. Power Oscillation Damping Controller

Since the FACTS device is incorporated on the transmission lines it is more appropriate to select a signal, given to the damping controller, in its vicinity. Usually the local input signals are always preferred, such as the active or reactive power flow through FACTS device. As such the error signal between the set point and the measured signal of the active power flow will be taken as the input to the damping controller as shown in Fig. 4. The design of the damping controller is based on phase compensation technique such that its output is in phase with the real power flow deviation. This active power has been obtained from the line on which the VSC of IPFC has been installed. The structure of the damping controller is given in Fig. 5. The most suitable control signal for providing additional damping is determined from the controllability index computed from the linearized model [17]. It is observed that the input signal  $m_1$  has the highest value, an indicator for the best signal to provide damping.

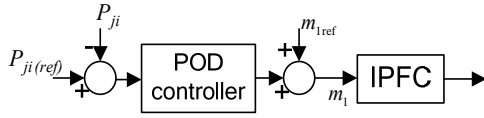


Figure 4. Power oscillation damping controller

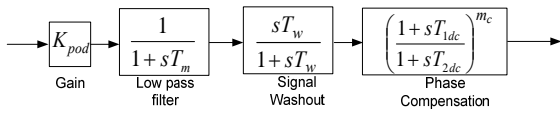


Figure 5. Structure of the damping controller

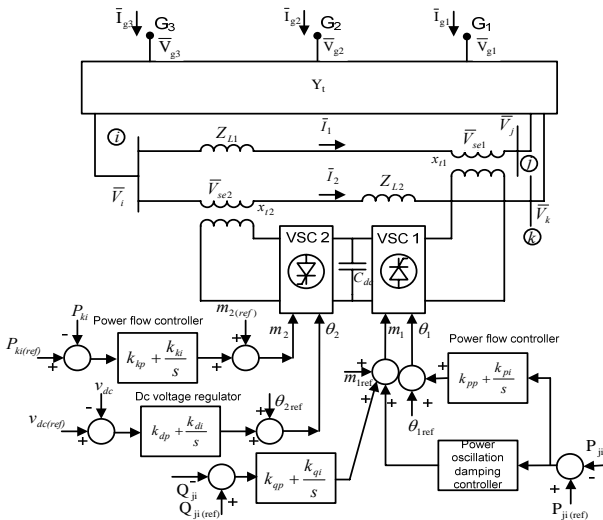


Figure 6. Multi-machine system with IPC and its controllers

The complete IPFC based multi-machine power system with all the controllers in place is shown in Fig. 6.

## IV. SIMULATION RESULTS

A three machine example power system [18] shown in Fig 7 is considered for computer simulation experiments. An IPFC is installed in the branches 7-5 and 7-8.

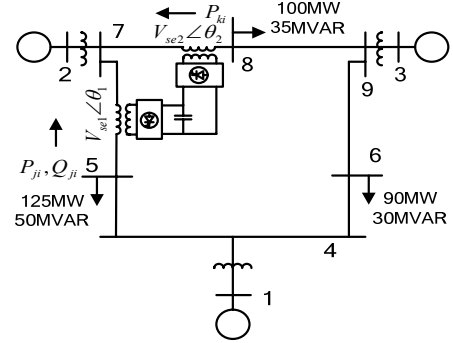


Figure 7. Three-machine power system installed with IPFC

A generalized load flow program based on Newton technique with embedded IPFC [19] has been developed to obtain steady state operating point. For this initial condition the system equations are linearized and the constants of the system model are computed. Table 1 gives the eigenvalues of the system from which the participation factors of all the eigenvalues are computed. It is revealed that the oscillation modes 4&5, 6&7 have the least damping ratio contributed by machine 3 and 2, respectively. In order to increase the damping ratio, PSS is installed in the system for machine 2 and 3. The eigenvalues of the systems with PSS are shown in Table 2. It is seen that the damping ratios of the concerned modes have increased. However, there is still a pair of eigenvalues having a damping ratio less than 0.1. This can be increased by means of the IPFC POD controller. The most suitable signal for providing additional damping is determined from the controllability index computed from the linearized model [17]. Table 3 shows the controllability indices. It is observed that the input signal  $m_1$  has the highest index, an indicator for best signal for damping.

TABLE I. EIGENVALUES OF THE SYSTEM

No.	Eigenvalues	Damping ratio	Frequency	Dominant states
1	-19.3	1	0	$E_{fd3}$
2	-17.1802	1	0	$E_{fd2}$
3	-15.6798	1	0	$E_{fd1}$
4,5	$-0.3009 \pm j11.2735$	0.0267	1.7942	$\delta_3 \omega_3$
6,7	$-0.2933 \pm j 8.1607$	0.0359	1.2988	$\delta_2 \omega_2$
8	-4.4731	1	0	$E'_{q1}$
9	-2.7315	1	0	$E'_{q2}$
10	-0.6816	1	0	$E'_{q3}$
11,12	$-0.0174 \pm j 0.2109$	0.0823	0.0336	$\delta_1 \omega_1$
13	-0.0196	1	0	$v_{dc}$

TABLE II. EIGENVALUES WITH PSS

Eigenvalues	Damping ratio	Frequency	Dominant states
-54.1642	1	0	
-26.8454	1	0	
$-22.1998 \pm j10.1872$	0.9089	1.6213	
$-15.7747 \pm j 5.8177$	0.9382	0.9259	
-15.6979	1	0	
$-1.1200 \pm j 10.7658$	0.1035	1.7134	$\delta_3 \omega_3$
$-0.6599 \pm j 8.3559$	0.0787	1.3299	$\delta_2 \omega_2$
-4.4747	1	0	
-2.5057	1	0	
$-0.5183 \pm j 0.2606$	0.8934	0.0415	
$-0.0455 \pm j 0.0864$	0.4654	0.0138	
-0.0198	1	0	
-0.1	1	0	

TABLE III. CONTROLLABILITY INDICES

Input signal	Controllability index
$\Delta m_1$	0.0201
$\Delta \theta_1$	0.0036
$\Delta m_2$	0.0070
$\Delta \theta_2$	0.0040

With the IPFC controllers in place, the performance evaluation of the designed controllers is carried out by computer simulation studies under various disturbance conditions. The results are shown below.

### A. Step Change in Mechanical Power Input

A disturbance in the form of a 1% step change of in mechanical power input to machine 2 is applied. The IPFC controllers control the power flow in the lines to damp out the oscillations. The transient responses, shown in Fig. 8, highlight the efficacy of controllers.

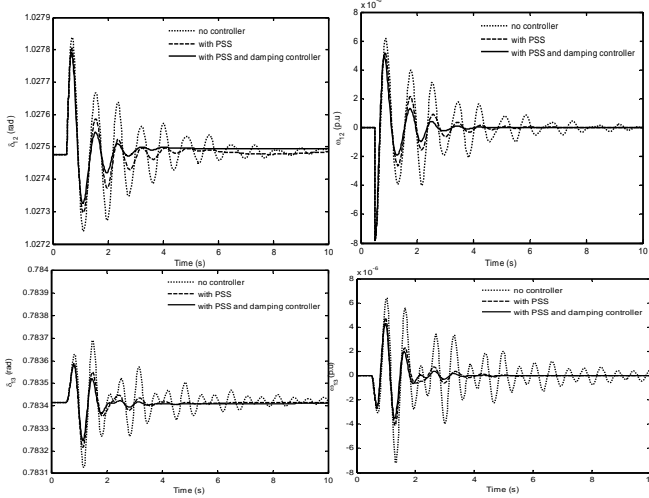


Figure 8. Relative rotor angle and rotor speed deviations with respect to machine 1 for mechanical power input change in machine 2

### B. Three-phase Fault

A three-phase fault of 100 ms duration is simulated near bus 9 (at the end of line 6-9). The dynamic responses of the system states are shown in Fig. 9. This again establishes the elegance of the proposed IPFC controllers under a severe disturbance.

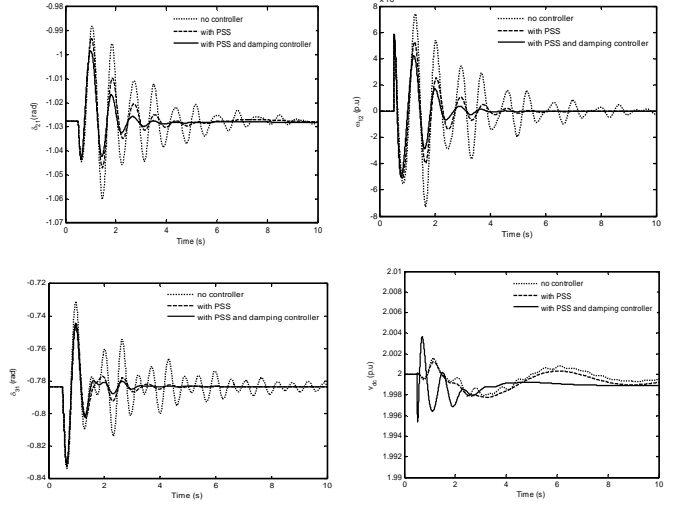


Figure 9. Relative rotor angle and rotor speed deviations (with respect to machine 1) and capacitor voltage transient response for 3-phase fault

### C. Change in Power Flow Reference

The power flow in the lines can be controlled by IPFC by change of reference set point. This is verified by changing the reference power flow in line 5-7 by 1%. The test results are delineated in Fig. 10.

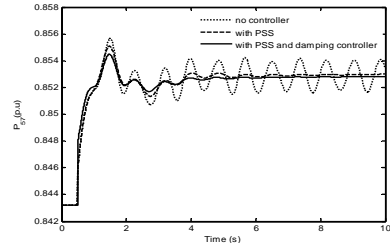


Figure 10. Dynamic response for real power flow in line 5-7 with a change in reference power flow

## V. CONCLUSION

The nonlinear model of multi-machine power system with IPFC is developed. The linearized Phillips-Heffron model is formulated. The modes having low damping ratio are found by eigenvalue analysis. The IPFC POD controller is designed using the phase compensation method to increase the damping of the concerned oscillation mode. The power flow controllers and DC voltage controller are incorporated to regulate the power flow and to maintain DC link voltage. The effectiveness of the IPFC controllers are validated through nonlinear simulations of the power system subjected to various disturbances. The IPFC based POD controller and PSS ensure reliable damping of the low frequency oscillations in the multi-machine power system with IPFC.

## REFERENCES

- [1] L.Gyugyi, K. K. Sen, C. D. Schauder, "The Interline Power FlowController Concept: A New Approach to Power Flow Management in Transmission Systems," *IEEE Transactions on Power Delivery*, vol. 14, No. 3, July 1999, pp. 1115 – 1123.
- [2] N. G. Hingorami, L. Gyugyi, *Understanding FACTS: Concepts and Technology of Flexible AC Transmission system*, IEEE Press, 1999.
- [3] X. Wei, J. H. Chow, B. Fardanesh, A. A. Edris, "A common modeling framework of voltage-sourced converters for loadflow, sensitivity, and dispatch analysis," *Power Engineering Society General Meeting*, IEEE Vol. 4, July 2003, pp. 13-17.
- [4] J. Zhang, A. Yokoyama, "A Comparison between the UPFC and the IPFC in Optimal Power Flow Control and Power Flow Regulation," *38th North American Power Symposium, NAPS 2006*, Sept. 2006, pp. 339–345.
- [5] X. Wei, J. H. Chow, B. Fardanesh, A. A. Edris, "A dispatch strategy for an interline power flow controller operating at rated capacity," *Power Systems Conference and Exposition, IEEE PES*, 10-13 Oct. 2004, Vol.3, pp. 1459 - 1466.
- [6] A. Kazemi, E. Karimi, "The Effect of Interline Power Flow Controller (IPFC) on Damping Inter-area Oscillations in the Interconnected Power Systems," *Industrial Electronics, 2006 IEEE International Symposium*, Volume 3, July 2006, pp. 1911-1915.
- [7] A. M. Parimi, I. Elamvazuthi, N. Saad, "Damping of inter area oscillations using Interline Power Flow Controller based damping controllers," *IEEE 2<sup>nd</sup> International Power and Energy Conference*, 2008. 1-3 Dec. 2008, pp. 67 – 72.
- [8] A. M. Parimi, I. Elamvazuthi, N. Saad, N, "Interline Power Flow Controller (IPFC) based damping controllers for damping low frequency oscillations in a power system," *IEEE International Conference on Sustainable Energy Technologies*, 24-27, pp. 334 – 339, Nov. 2008.
- [9] A. M. Parimi, I. Elamvazuthi, N. Saad, "Interline Power Flow Controller Application for Low Frequency Oscillations Damping" *WSEAS Transactions on Systems*, Issue 5, Vol. 9, May 2010.
- [10] A. M. Parimi, N. C. Sahoo, I. Elamvazuthi, N. Saad, N, "Dynamic modeling of Interline Power Flow Controller for small signal stability" *IEEE International Conference on Power and Energy*, 2010, pp. 583 – 588.
- [11] P. Kundur, *Power System Stability and Control*. Mc Graw-Hill, New York, 1994.
- [12] H. F. Wang, F. J. Swift, and M. Li, "An unified model for the analysis of FACTS devices in damping power system oscillations Part I: Single-machine Infinite-bus power systems," *IEEE Trans. on Power Delivery*, Vol. 12, No. 2, April 1997.
- [13] H. F. Wang, F. J. Swift, and M. Li, "An unified model for the analysis of FACTS devices in damping power system oscillations Part II: Multimachine power systems," *IEEE Trans. on Power Delivery*, Vol. 13, No. 4, October 1998.
- [14] H. F. Wang, "An unified model for the analysis of FACTS devices in damping power system oscillations Part III: Unified Power Flow Controller," *IEEE Trans. on Power Delivery*, Vol. 15, No. 3, July 2000.
- [15] H. F. Wang, "Applications of modeling UPFC into multi-machine power systems," *IEE proc. – C*, Vol. 146, NO. 3, pp.306-312, May 1999.
- [16] Y. N. Yu, *Electric Power System Dynamics*, Academic Press. Inc, London, 1983.
- [17] E. V. Larsen, J. S. Gasca, and J. H. Chow, "Concepts for design of FACTS controllers to damp power swings," *IEEE Trans. on Power System*, vol. 10, no. 2, pp. 948-956, May 1995.
- [18] P. W. Sauer and M. A. Pai, *Power System Dynamics and Stability*. New Jersey: Prentice-Hall, Inc., 1998.
- [19] X. P. Zhang, "Modelling of the interline power flow controller and the generalised unified power flow controller in Newton power flow", *Generation, Transmission and Distribution, IEE Proceedings-Volume 150, Issue 3, May 2003* pp. 268 – 274.

## APPENDIX

### Nomenclature:

$\delta$  is the rotor angle in electric radians,  $\omega$  is generator rotor speed in p.u.,  $\omega_0 = 2\pi f$  in rad/s,  $V_t$  is the terminal voltage in p.u.,  $\dot{E}'_q$  is internal quadrature-axis voltage in p.u.,  $E_{fd}$  is the field voltage in p.u,  $v_{dc}$  is the voltage at DC link in p.u,  $M = 2H$ ,  $H$  is the inertia constant in p.u.,  $P_m$  is the mechanical input in p.u,  $P_e$  is the electrical output in p.u,  $D$  is the damping coefficient,  $x_d, x'_d$  are the d-axis reactance and d-axis transient reactance in p.u,  $T'_{do}$  is the open circuit d axis time constant in sec,  $I_d, I_q$  are the direct and quadrature axis components of stator current in p.u,  $V_{td}, V_{tq}$  are the d, and q axis components of terminal voltage in p.u.,  $T_a$  and  $K_a$  are time constant and gain of voltage regulator.  $v_{dc}$  is the capacitor voltage of the DC link of the IPFC.  $m_1$  and  $m_2$  are the modulation indices of VSC 1 and 2,  $\theta_1$  and  $\theta_2$  are the phase angles of series converter 1 and 2.  $C_{dc}$  is the dc link capacitor,  $i_{1d}$  and  $i_{1q}$  are the d-q axis components of current  $\bar{I}_1$  in line  $i-j$  and  $i_{2d}$  and  $i_{2q}$  the d-q axis components of  $\bar{I}_2$  in line  $i-k$  respectively.

### PSS structure and parameters:

the structure of PSS is given in Fig. 11. The parameters are designed by phase compensation method and are given in the following table.

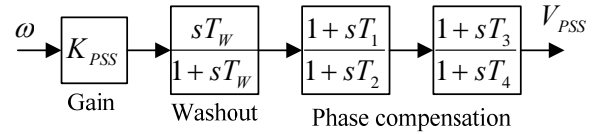


Figure 11. Power system stabilizer

TABLE IV. PARAMETERS OF THE PSS

PSS	Gain	$T_1$	$T_2$	$T_3$	$T_4$
Machine 2	1.8807	0.3002	0.0492	0.3002	0.0492
Machine 3	3.5843	0.3001	0.0243	0.3001	0.0243

### IPFC Controller Parameters:

The parameters of the IPFC controllers are  $k_{pp} = 5$ ,  $k_{pi} = 25$ ,  $k_{qp} = 0.06$ ,  $k_{qi} = 0.007$ ,  $k_{kp} = 0.01$ ,  $k_{ki} = 0.01$ ,  $k_{dp} = 10$  and  $k_{di} = 20$ . The parameters of the POD controller are  $k_{dc} = 0.3554$ ,  $T_w = 10s$ ,  $T_m = 0.01s$ ,  $T_1 = 0.20058$ ,  $T_2 = 0.071407$ , and  $m_c = 1$ .